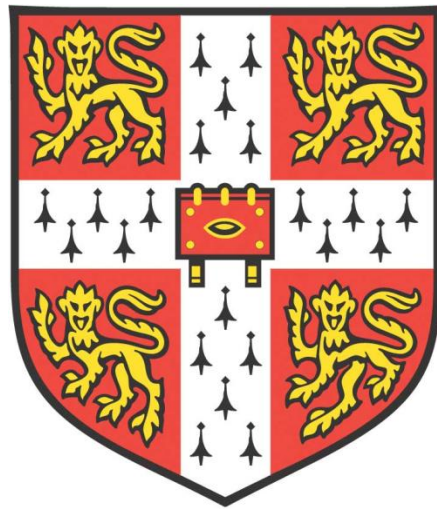


PHOSPHATE STARVATION ALTERS  
CALCIUM SIGNALLING IN ROOTS OF  
*ARABIDOPSIS THALIANA*



**Elsa Matthus**

**Churchill College**

**Transport Group**

**Department of Plant Sciences**

**University of Cambridge**

**This dissertation is submitted for the degree of Doctor of Philosophy**

**September 2018**



*To plants*

## DECLARATION

This dissertation is the result of my own work and includes nothing which is the outcome of work done in collaboration except as specified in the text.

It is not substantially the same as any that I have submitted, or, is being concurrently submitted for a degree or diploma or other qualification at the University of Cambridge or any other University or similar institution except as declared in the Preface and specified in the text. I further state that no substantial part of my dissertation has already been submitted, or, is being concurrently submitted for any such degree, diploma or other qualification at the University of Cambridge or any other University or similar institution except as specified in the text.

A handwritten signature in black ink, appearing to read 'Elsa Matthus', written in a cursive style.

Elsa Matthus

September 2018



## SUMMARY

Low bioavailability of phosphate (P) due to low concentration and high immobility in soils is a key limiting factor in crop production. Application of excess amounts of P fertilizer is costly and by no means sustainable, as world-wide P resources are finite and running out. To facilitate the breeding of crops adapted to low-input soils, it is essential to understand the consequences of P deficiency. The second messenger calcium ( $\text{Ca}^{2+}$ ) is known to signal in plant development and stress perception, and most recently its direct role in signalling nutrient availability and deficiency has been partially elucidated. The use of  $\text{Ca}^{2+}$  as a signal has to be tightly controlled, as  $\text{Ca}^{2+}$  easily complexes with P groups and therefore is highly toxic to cellular P metabolism. It is unknown whether  $\text{Ca}^{2+}$  signals P availability or whether signalling is altered under P starvation conditions.

The aim of this PhD project was to characterise the use of  $\text{Ca}^{2+}$  ions, particularly cytosolic free  $\text{Ca}^{2+}$  ( $[\text{Ca}^{2+}]_{\text{cyt}}$ ), in stress signalling by P-starved roots of the model plant *Arabidopsis thaliana*. The hypothesis was that under P starvation and a resulting decreased cellular P pool, the use of  $[\text{Ca}^{2+}]_{\text{cyt}}$  may have to be restricted to avoid cytotoxic complexation of  $\text{Ca}^{2+}$  with limited P groups. Employing a range of genetically encoded  $\text{Ca}^{2+}$  reporters in *Arabidopsis*, P starvation but not nitrogen starvation was found to strongly dampen the root  $[\text{Ca}^{2+}]_{\text{cyt}}$  increases evoked by mechanical, salt, osmotic, and oxidative stress as well as by extracellular nucleotides. The strongly altered root  $[\text{Ca}^{2+}]_{\text{cyt}}$  response to extracellular nucleotides was shown to manifest itself during seedling development under chronic P deprivation, but could be reversed by P resupply. Fluorescent imaging elucidated that P-starved roots showed a normal  $[\text{Ca}^{2+}]_{\text{cyt}}$  response to extracellular nucleotides at the apex, but a strongly dampened  $[\text{Ca}^{2+}]_{\text{cyt}}$  response in distal parts of the root tip, correlating with high reactive oxygen species (ROS) levels induced by P starvation. Excluding iron, as well as P, rescued the altered  $[\text{Ca}^{2+}]_{\text{cyt}}$  response, and restored ROS levels to those seen under nutrient-replete conditions. P availability was not signalled through  $[\text{Ca}^{2+}]_{\text{cyt}}$ . In another part of this PhD project, a library of 77 putative  $\text{Ca}^{2+}$  channel mutants was compiled and screened for aberrant root hair growth under P starvation conditions. No mutant line showed aberrant root hair growth.

These results indicate that P starvation strongly affects stress-induced  $[\text{Ca}^{2+}]_{\text{cyt}}$  modulations. The data generated in this thesis further understanding of how plants can integrate nutritional and environmental cues, adding another layer of complexity to the use of  $\text{Ca}^{2+}$  as a signal transducer.



## ACKNOWLEDGEMENTS

Thank you, Cambridge, it's been amazing. A huge thank you to my supervisor Dr. Julia Davies, for giving me the space to work and think and tinker at the Department of Plant Sciences, and for showing me the incredible world of ion channels and membranes. Thank you very much to the BBSRC DTP scheme for funding my PhD project.

Thank you to my second supervisor Prof. Alex Webb for support and discussion. Thank you Katie, Amirah, Stéphanie, Limin, Zhizhong and Adeeba, for having taught me and worked alongside me in the Transport Group. Tea times and pub times with you and the whole Lab 201 crew, including Carmen, Laura, Hyun-ju, Gareth, Lukas, Tim, Jun and Matt, have been one of my favourite things about Cambridge! The Department of Plant Sciences has been very kind and supportive, and I would like to thank Annie, Barbara, Christine, Dik, Greg, Del, Pawel, Seb, Simon, Emma and Nigel at the PGF, for taking such good care of me, my plants and my coffee needs. Thank you Francis Darwin, for having been there at some point, and thank you Enid MacRobbie, for having paved the way.

Thank you Prof. Alex Costa and Gandolfo, Uni Milan, for lessons in microscopy and coffee. Thank you Helen Scott, Uni Oxford, for discussing plant growth medium with me. Thank you Dr. Benjamin Kilian and Luigi Guarino at the Crop Trust, for letting me PIPS. My way to Cambridge was signposted by Prof. Stephan Clemens (Uni Bayreuth) giving a political talk about plant research, and Prof. Michael Frei (Uni Bonn) showing me the world of plant nutrition. Thank you.

Thank you to Kayla Friedman and Malcolm Morgan, University of Cambridge, for producing a Word thesis template.

Churchill College has shaped my Cambridge experience very much; a big thank you to Athene Donald for running things and writing a blog, to Rebecca, Annie and the porter crew, Ian and the kitchen crew, the MCR community and the Vicious Penguin for being full of new friends. Huge thanks to the Ultimate Frisbee community, for countless hours of flying discs in rain and sunshine, and pub sessions afterwards, all in the Spirit of the Game. Hot on defence, cool on offense.

I shared a quaint, beige house with Phibi and also Chrilih and Frabi, who are the finest housemates ever. Having had you guys, and science talks and picnics in the garden and endless game and crumble nights, has given my life in Cambridge a home.

Finally, 'thank you' seems too small a word compared to what I would like to say to my family and friends for all their support. Biggest thank you, mum, for pots of honey and knowing Alles ist in dir and Happy & Donna. Einen großen Dank an meine Omas, für all ihre Unterstützung und Päckchen voller Schokolade und Schnaps. And thank you Ben, for making me calm at present and excited for the future.

# CONTENTS

<b>1 Introduction</b> .....	<b>1</b>
<b>1.1 Plant phosphate nutrition and homeostasis</b> .....	<b>1</b>
1.1.1 <i>Food security and the ‘phosphate problem’ in agriculture</i> .....	1
1.1.2 <i>P uptake, translocation and storage</i> .....	4
1.1.3 <i>Impact of P deficiency on plant root growth and metabolism</i> .....	8
1.1.4 <i>P sensing and molecular responses to P deficiency</i> .....	9
<b>1.2 Calcium – macronutrient with structural and signalling roles</b> .....	<b>12</b>
1.2.1 <i>Ca<sup>2+</sup> uptake, translocation and storage on whole plant level</i> .....	13
1.2.2 <i>Ca<sup>2+</sup> uptake and translocation on a cellular level</i> .....	13
1.2.3 <i>Ca<sup>2+</sup> channels localizing to the plasma membrane</i> .....	15
1.2.4 <i>Ca<sup>2+</sup> channels and uniporters localizing to organellar membranes</i> .....	17
1.2.5 <i>Ca<sup>2+</sup> storage on a cellular level</i> .....	18
1.2.6 <i>Ca<sup>2+</sup> as a signal transducer of abiotic and biotic stress signalling</i> .....	19
1.2.7 <i>Ca<sup>2+</sup> as direct signal transducer in nutrient stress signalling</i> .....	20
1.2.8 <i>Decoding of stress-specific Ca<sup>2+</sup> signatures</i> .....	21
1.2.9 <i>Quantification and visualization of Ca<sup>2+</sup> in vivo using genetically encoded reporters</i> .....	23
<b>1.3 The relationship of phosphate and calcium</b> .....	<b>26</b>
1.3.1 <i>Calcium phosphates were recently also described in plants</i> .....	27
<b>1.4 Working hypothesis and experimental approaches</b> .....	<b>27</b>
<b>2 Material and Methods</b> .....	<b>29</b>
<b>2.1 Plant material</b> .....	<b>29</b>
<b>2.2 Plant growth conditions</b> .....	<b>30</b>
2.2.1 <i>General propagation conditions</i> .....	30
2.2.2 <i>General sterile growth conditions</i> .....	30
2.2.3 <i>Plant growth on Murashige and Skoog growth medium</i> .....	30
2.2.4 <i>Transfer experiments</i> .....	32
2.2.5 <i>Growth conditions for root hair screen</i> .....	32
<b>2.3 Root system architecture quantification and image analysis</b> .....	<b>33</b>
<b>2.4 Extracellular ATP quantification</b> .....	<b>33</b>
<b>2.5 Confocal microscopy using ANNI-GFP lines</b> .....	<b>34</b>
<b>2.6 Root [Ca<sup>2+</sup>]<sub>cyt</sub> measurements by aequorin luminescence</b> .....	<b>34</b>

2.6.1	<i>Sample preparation and coelenterazine incubation</i>	34
2.6.2	<i>Luminescence quantification using a plate reader</i>	35
2.6.3	<i>Luminescence quantification using a luminometer</i>	36
2.6.4	<i>Abiotic stress treatments</i>	36
2.6.5	<i>Pharmacological inhibitor treatments</i>	37
<b>2.7</b>	<b>Root <math>[Ca^{2+}]_{cyt}</math> measurements by ratiometric YC3.6 reporter</b>	<b>38</b>
2.7.1	<i>Sample preparation and superfusion set-up</i>	38
2.7.2	<i>Inverted fluorescence microscopy</i>	38
2.7.3	<i>Stress treatment</i>	38
2.7.4	<i>YC3.6 image analysis using ImageJ Fiji</i>	39
<b>2.8</b>	<b>Root <math>[Ca^{2+}]_{cyt}</math> measurements by intensimetric GCaMP3 reporter</b>	<b>39</b>
2.8.1	<i>Sample preparation and set-up</i>	39
2.8.2	<i>Microscopy of GCaMP3-expressing plants</i>	40
2.8.3	<i>GCaMP3 Image analysis using ImageJ Fiji</i>	40
<b>2.9</b>	<b>Histological staining</b>	<b>41</b>
2.9.1	<i>Intracellular ROS staining</i>	41
2.9.2	<i>Callose staining</i>	41
<b>2.10</b>	<b>Genotyping of <i>Arabidopsis</i> mutant lines</b>	<b>42</b>
2.10.1	<i>Manual genomic DNA extraction</i>	42
2.10.2	<i>High-throughput genomic DNA extraction</i>	42
2.10.3	<i>Polymerase chain reaction (PCR)</i>	43
<b>2.11</b>	<b>Bioinformatic resources and statistical analysis</b>	<b>44</b>
<b>3</b>	<b>Phosphate Starvation alters Calcium Signalling in <i>ARABIDOPSIS</i> roots</b>	<b>46</b>
<b>3.1</b>	<b>Introduction</b>	<b>46</b>
3.1.1	<i>Abiotic stress perception involves <math>Ca^{2+}</math> ion fluxes</i>	46
3.1.2	<i>The involvement of <math>Ca^{2+}</math> fluxes in nutrient deficiencies – unknown for P starvation</i>	51
3.1.3	<i>Experimental approaches and aims</i>	51
<b>3.2</b>	<b>Results</b>	<b>53</b>
3.2.1	<i>Phosphate starvation inhibits primary root growth</i>	53
3.2.2	<i>Phosphate starvation induces root hair growth – independent of non-functional single putative <math>Ca^{2+}</math> channels</i>	55
3.2.3	<i>Phosphate-starved root tips show an altered <math>[Ca^{2+}]_{cyt}</math> response to a range of abiotic stresses</i>	57

3.2.4 Phosphate-starved root tips show an altered $[Ca^{2+}]_{cyt}$ response to extracellular nucleotides.....	64
3.2.5 Phosphate-starved root tips tend to respond less to mechanical stimulation	78
3.2.6 Nitrogen starvation leads to primary root length reduction.....	80
3.2.7 Nitrogen starvation does not dampen the $[Ca^{2+}]_{cyt}$ signature in response to abiotic stresses .....	81
3.2.8 Overall aequorin luminescence levels are comparable between nutrient conditions.....	87
3.2.9 Phosphate-starved root tips still accumulate extracellular ATP .....	90
3.2.10 Proteins potentially involved in shaping the altered $[Ca^{2+}]_{cyt}$ in phosphate-starved root tips .....	92
3.2.11 The altered $[Ca^{2+}]_{cyt}$ response under phosphate starvation occurs during development .....	101
3.2.12 The altered $[Ca^{2+}]_{cyt}$ response under phosphate starvation is reversible .	107
3.2.13 Iron availability alters the primary root length of phosphate-starved roots .....	116
3.2.14 Exclusion of iron rescues the altered $[Ca^{2+}]_{cyt}$ response of phosphate-starved root tips .....	119
3.2.15 Under phosphate starvation, increasing the iron levels in the growth medium does not alter the $[Ca^{2+}]_{cyt}$ response further .....	122
3.2.16 Excluding iron from otherwise nutrient-replete roots only slightly affects their $[Ca^{2+}]_{cyt}$ response to extracellular ATP.....	125
3.2.17 The dampened $[Ca^{2+}]_{cyt}$ response is due to a phosphate x iron interaction, not to iron toxicity alone .....	128
3.2.18 Exclusion of copper does not rescue the altered $[Ca^{2+}]_{cyt}$ response of phosphate starved roots .....	131
3.2.19 $[Ca^{2+}]_{cyt}$ does not seem to signal P availability.....	133
<b>3.3 Discussion.....</b>	<b>135</b>
3.3.1 Considerations on aequorin as reporter.....	135
3.3.2 Phosphate starvation dynamically alters the $[Ca^{2+}]_{cyt}$ response to extracellular ATP, which was dependent on DORN1 but not ANNEXIN1.....	137
3.3.3 Phosphate-starved roots still accumulate low levels of extracellular ATP .	139
3.3.4 Iron-availability is linked to the phosphate-starvation induced altered $[Ca^{2+}]_{cyt}$ response .....	140

3.3.5 Phosphate availability does not seem to be signalled through immediate $[Ca^{2+}]_{\text{cyt}}$ modulations .....	142
<b>3.4 Conclusions and future work .....</b>	<b>144</b>
<b>4 Deconstructing the cytosolic free calcium response to extracellular ATP in roots .....</b>	<b>147</b>
<b>4.1 Introduction .....</b>	<b>147</b>
4.1.1 Extracellular ATP as a danger signal .....	147
4.1.2 Extracellular ATP triggers movement of $Ca^{2+}$ ions .....	149
4.1.3 Signalling network in response to extracellular ATP perception .....	151
4.1.4 Experimental approaches and aims .....	153
<b>4.2 Results .....</b>	<b>155</b>
4.2.1 The $[Ca^{2+}]_{\text{cyt}}$ response to extracellular ATP comes mainly from the root tip .....	155
4.2.2 The eATP-induced multi-phasic $[Ca^{2+}]_{\text{cyt}}$ increase maps to different regions of the root tip .....	159
4.2.3 The spatially distinct $[Ca^{2+}]_{\text{cyt}}$ responses to extracellular ATP can be generated independently of each other .....	174
4.2.4 The increase of intracellular ROS is dependent on an interplay of phosphate and iron levels .....	188
4.2.5 The secondary $[Ca^{2+}]_{\text{cyt}}$ response to extracellular ATP is sensitive to pharmacological alterations of cellular redox status .....	194
4.2.6 Callose deposition is dependent on iron, but not phosphate, availability ...	200
<b>4.3 Discussion .....</b>	<b>205</b>
4.3.1 On whole plant level, root tip tissue responds most strongly to eATP .....	205
4.3.2 On root tip level, eATP triggers distinct $[Ca^{2+}]_{\text{cyt}}$ responses that vary in time and space .....	205
4.3.3 The $Ca^{2+}$ reporters paint an overall similar picture, but differ in sensitivity .....	208
4.3.4 The two distinct increases in $[Ca^{2+}]_{\text{cyt}}$ can be generated independently of each other – a ‘wave’ component is likely but requires further analysis .....	209
4.3.5 The secondary response is linked to ROS signalling, and lost when the root tissue is primed by ROS overload .....	211
4.3.6 Absolute levels of callose deposition do not correlate with the secondary response to eATP .....	212
4.3.7 Conclusions and Future work .....	214



<b>5 Discussion</b> .....	<b>216</b>
<b>5.1 Phosphate starvation dampens root tips' <math>[Ca^{2+}]_{cyt}</math> response to abiotic stresses</b> .....	<b>216</b>
<b>5.2 Phosphate-starved root tips lack the response to extracellular ATP in the distal     root tip</b> .....	<b>220</b>
<b>5.3 Molecular identities of plasma membrane <math>Ca^{2+}</math> channels and transporters     remain largely unknown</b> .....	<b>224</b>
<b>5.4 Linking P and <math>Ca^{2+}</math> is difficult, and direct links are scarce</b> .....	<b>226</b>
<b>5.5 Concluding remarks and future work</b> .....	<b>227</b>
<b>6 References</b> .....	<b>229</b>
<b>7 Appendices</b> .....	<b>276</b>
<b>Appendix I</b> .....	<b>277</b>
<b>Appendix II</b> .....	<b>282</b>
<b>Appendix III</b> .....	<b>287</b>
<b>Appendix IV</b> .....	<b>289</b>
<b>Appendix V</b> .....	<b>292</b>
<b>Appendix VI</b> .....	<b>295</b>

## LIST OF TABLES

<b>Table 1:</b> Details of the genetically encoded $\text{Ca}^{2+}$ -sensors used in this thesis.....	25
<b>Table 2:</b> Nutrient modifications of half MS medium relevant for particular deficiency growth condition. ....	32
<b>Table 3:</b> Analysed parameters of the $[\text{Ca}^{2+}]_{\text{cyt}}$ response of differently aged phosphate-starved root tips to 1 mM eATP.....	106
<b>Table 4:</b> Mean signal intensities of phosphate- and iron-starved primary root tips stained for intracellular reactive oxygen species.....	193

## LIST OF FIGURES

<b>Figure 1:</b> The ‘phosphate problem’ .....	3
<b>Figure 2:</b> Schematic of phosphate and calcium uptake and transport across the root as explained in the text. ....	7
<b>Figure 3:</b> Trialling different barriers to allow localized application of treatment solution in a simple plate-based horizontal set-up. ....	40
<b>Figure 4:</b> Primary root lengths of phosphate-starved <i>Arabidopsis thaliana</i> plants.....	54
<b>Figure 5:</b> Root hair growth of phosphate-starved <i>Arabidopsis</i> wild type plants. ....	56
<b>Figure 6:</b> Schematic representation of aequorin-based $[Ca^{2+}]_{cyt}$ time-courses and analysis as presented in this thesis. ....	58
<b>Figure 7:</b> The $[Ca^{2+}]_{cyt}$ response of phosphate-starved root tips to salt and osmotic stress. ....	60
<b>Figure 8:</b> The $[Ca^{2+}]_{cyt}$ response of phosphate-starved root tips to oxidative stress. ....	63
<b>Figure 9:</b> The $[Ca^{2+}]_{cyt}$ response of phosphate-starved root tips to mechanical stimulation and a phosphate source. ....	65
<b>Figure 10:</b> The $[Ca^{2+}]_{cyt}$ response of phosphate-starved root tips to extracellular ATP. ....	69
<b>Figure 11:</b> The $[Ca^{2+}]_{cyt}$ response of phosphate-starved root tips to a non-hydrolysable ATP analogue.....	73
<b>Figure 12:</b> The $[Ca^{2+}]_{cyt}$ response of phosphate-starved root tips to extracellular ADP.....	77
<b>Figure 13:</b> The $[Ca^{2+}]_{cyt}$ response of phosphate-starved root tips to mechanical stimulation.....	79
<b>Figure 14:</b> Nitrogen starvation alters root architecture of <i>Arabidopsis</i> . ....	80
<b>Figure 15:</b> The $[Ca^{2+}]_{cyt}$ response of nitrogen-starved root tips to salt and osmotic stress. ....	82
<b>Figure 16:</b> The $[Ca^{2+}]_{cyt}$ response of nitrogen-starved root tips to oxidative stress. ....	84
<b>Figure 17:</b> The $[Ca^{2+}]_{cyt}$ response of nitrogen-starved root tips to extracellular ATP....	86
<b>Figure 18:</b> Luminescence counts of compiled aequorin experiments.....	89

<b>Figure 19:</b> Quantification of extracellular ATP in root bathing medium of phosphate-starved roots. ....	91
<b>Figure 20:</b> The $[Ca^{2+}]_{cyt}$ response of phosphate-starved <i>dorn1-1</i> mutants to extracellular ATP. ....	94
<b>Figure 21:</b> The $[Ca^{2+}]_{cyt}$ response of phosphate-starved <i>ann1</i> mutants to extracellular ATP. ....	96
<b>Figure 22:</b> <i>ANNEXIN1</i> gene expression in phosphate-starved root tips. ....	99
<b>Figure 23:</b> ANNEXIN1 protein expression in phosphate-starved root tips. ....	100
<b>Figure 24:</b> Primary root lengths of 5-, 6-, 7- and 10-day old phosphate-starved <i>Arabidopsis</i> . ....	102
<b>Figure 25:</b> The $[Ca^{2+}]_{cyt}$ response of phosphate-starved root tips of different age to extracellular ATP. ....	105
<b>Figure 26:</b> Primary root lengths of <i>Arabidopsis</i> transferred to differing phosphate growth conditions during development. ....	109
<b>Figure 27:</b> The $[Ca^{2+}]_{cyt}$ response of short-term phosphate-resupplied <i>Arabidopsis</i> root tips to extracellular ATP. ....	112
<b>Figure 28:</b> The $[Ca^{2+}]_{cyt}$ response of short-term phosphate-starved <i>Arabidopsis</i> root tips to extracellular ATP. ....	114
<b>Figure 29:</b> Primary root lengths of <i>Arabidopsis</i> grown on varying levels of phosphate and iron. ....	118
<b>Figure 30:</b> The $[Ca^{2+}]_{cyt}$ response of phosphate- and iron-starved root tips to extracellular ATP. ....	121
<b>Figure 31:</b> The effect of Fe excess on the $[Ca^{2+}]_{cyt}$ response of phosphate-starved root tips to extracellular ATP. ....	124
<b>Figure 32:</b> The $[Ca^{2+}]_{cyt}$ response of iron-starved root tips to extracellular ATP. ....	127
<b>Figure 33:</b> The effect of excess iron levels on the $[Ca^{2+}]_{cyt}$ response of root tips to extracellular ATP. ....	130
<b>Figure 34:</b> The $[Ca^{2+}]_{cyt}$ response of copper- and phosphate-starved root tips to extracellular ATP. ....	132

<b>Figure 35:</b> The $[Ca^{2+}]_{cyt}$ response of phosphate-starved whole seedlings to phosphate re-supply. ....	134
<b>Figure 36:</b> The $[Ca^{2+}]_{cyt}$ response of phosphate-starved leaves, whole roots and excised root tips to extracellular ATP. ....	158
<b>Figure 37:</b> Spatial dynamics of the $[Ca^{2+}]_{cyt}$ response of phosphate-starved root tips to extracellular ATP using a ratiometric reporter. ....	163
<b>Figure 38:</b> Kymographs of the $[Ca^{2+}]_{cyt}$ response to extracellular ATP of phosphate-starved root tips. ....	165
<b>Figure 39:</b> The $[Ca^{2+}]_{cyt}$ response to extracellular ATP in specific regions of phosphate-starved root tips using a ratiometric reporter. ....	167
<b>Figure 40:</b> Spatial dynamics of the $[Ca^{2+}]_{cyt}$ response of phosphate-starved root tips to extracellular ATP using an intensimetric reporter. ....	172
<b>Figure 41:</b> The $[Ca^{2+}]_{cyt}$ response to extracellular ATP in specific regions of phosphate-starved root tips using an intensimetric reporter. ....	173
<b>Figure 42:</b> The $[Ca^{2+}]_{cyt}$ response of phosphate-starved intact or cut root tips to extracellular ATP. ....	177
<b>Figure 43:</b> The $[Ca^{2+}]_{cyt}$ response to extracellular ATP in specific regions of intact and cut root tips using an intensimetric reporter. ....	180
<b>Figure 44:</b> The $[Ca^{2+}]_{cyt}$ response of roots to locally applied extracellular ATP, first applied to the tip then to the elongation zone. ....	185
<b>Figure 45:</b> The $[Ca^{2+}]_{cyt}$ response of roots to locally applied extracellular ATP, first applied to the elongation zone then to the tip. ....	186
<b>Figure 46:</b> Distribution of intracellular reactive oxygen species in phosphate- and iron-starved primary root tips. ....	191
<b>Figure 47:</b> Fluorescence intensity from intracellular reactive oxygen species staining along phosphate- and iron-starved primary roots. ....	192
<b>Figure 48:</b> The effect of a more reduced cellular redox state on the $[Ca^{2+}]_{cyt}$ response of phosphate-starved root tips to extracellular ATP. ....	196
<b>Figure 49:</b> The effect of inhibiting ROS production on the $[Ca^{2+}]_{cyt}$ response of phosphate-starved root tips to extracellular ATP. ....	199

<b>Figure 50:</b> Callose distribution in phosphate- and iron-starved primary root tips. ....	203
<b>Figure 51:</b> Quantification of callose distribution in phosphate- and iron-starved primary root tips. ....	204
<b>Figure 52:</b> Components involved in signalling extracellular ATP in the root tip of <i>Arabidopsis</i> as investigated in this thesis.....	221

## LIST OF ABBREVIATIONS AND ACRONYMS

(v/v)	volume per volume
(w/v)	weight per volume
[Ca <sup>2+</sup> ] <sub>cyt</sub>	cytosolic free calcium ion
ADP	adenosine 5'-diphosphate
AMP	adenosine 5'-monophosphate
ANN1	Annexin1
ATP	adenosine 5'-triphosphate
bp	base pair
Ca <sup>2+</sup>	calcium ion
CaM	calmodulin
Ca-P	calcium phosphate
CBL	calcineurin B-like protein
CDPK	calcium-dependent protein kinase
CFP	cyan fluorescent protein
CIPK	CBL-interacting protein kinase
CM-H <sub>2</sub> DCFDA	2', 7'-dichlorodihydrofluorescein diacetate
CNGC	cyclic nucleotide-gated channel
cpVenus	circular permutation yellow fluorescent protein variant
Cu <sup>2+</sup>	copper ion
DMSO	dimethyl sulfoxide
DNA	deoxyribonucleic acid
DORN1	<u>D</u> oes not <u>R</u> espond to <u>N</u> ucleotides1
DPI	diphenyleneiodonium
DTT	dithiothreitol
eATP	extracellular adenosine 5'-triphosphate
EMS	ethyl methanesulfonate
ER	endoplasmatic reticulum
Fe	iron
FRET	Förster resonance energy transfer
<i>g</i>	G-force
GCaMP3	single wavelength Ca <sup>2+</sup> reporter
gDNA	genomic DNA
GFP	green fluorescent protein

GLR	glutamate receptor-like
H <sub>2</sub> O	water
H <sub>2</sub> O <sub>2</sub>	hydrogen peroxide
InsP <sub>3</sub>	inositol triphosphate
IS	imaging solution
K <sup>+</sup>	potassium ion
kb	kilobase
MCA	calcium channel ( <u>mid1-complementing activity</u> )
med	medium
MES	2-(N-morpholino)ethanesulfonic
Mg <sup>2+</sup>	magnesium ion
MS	Murashige and Skoog nutrient medium
MSL	<u>MscS-like</u> gene family
NaCl	sodium chloride
NES-YC3.6	<u>nuclear export signal</u> (cytosolic localized) <u>yellow cameleon 3.6</u>
N <sub>liq</sub>	liquid nitrogen
NRT1.1	nitrate transporter 1.1
OSCA	reduced hyperosmolality-induced [ <u>Ca</u> <sup>2+</sup> ] <sub>cyt</sub> increase
P	phosphate
P-acid	phosphoric acid
PCR	polymerase chain reaction
PM	plasma membrane
ROI	region of interest
ROS	reactive oxygen species
sec	second
SEM	standard error of mean
T-DNA	transfer DNA
TPC1	<u>Two Pore Channel</u> 1
Tris	Tris base, 2-amino-2-(hydroxymethyl)-1,3-propanediol
YC3.6	<u>Yellow Cameleon 3.6</u>
YFP	yellow fluorescent protein
γ-ATP	adenosine 5'-[γ-thio]triphosphate tetralithium



## LIST OF APPENDICES

Appendix I.....	277
Appendix II.....	282
Appendix III.....	287
Appendix IV.....	289
Appendix V.....	292
Appendix VI.....	295



# 1 INTRODUCTION

## 1.1 Plant phosphate nutrition and homeostasis

### 1.1.1 Food security and the ‘phosphate problem’ in agriculture

Globally, an estimated 815 million people suffer from hunger and malnutrition (FAO, State of Food Security and Nutrition, 2017). The projected population growth from currently 7.5 billion to 10 billion in 2050 will intensify the problem (FAO, 2017). The 20<sup>th</sup> century has seen the ‘Green Revolution’ and dramatic increases in yield, using new crop varieties, manufactured fertilizers, pesticides and herbicides, as well as modern agricultural technologies. However, this Revolution has failed to deliver productivity in sustainable ways. To achieve ‘Zero Hunger’ (Sustainable Development Goal 2, United Nations, 2015) moving forward, food production needs to increase, whilst being environmentally and socially sustainable. More and nutritious food needs to be produced on less land using lower inputs, whilst being resilient to threats such as climate change and degraded soils. This ‘Evergreen Revolution’ will need to increase productivity without ecological and social harm (Swaminathan, 2000).

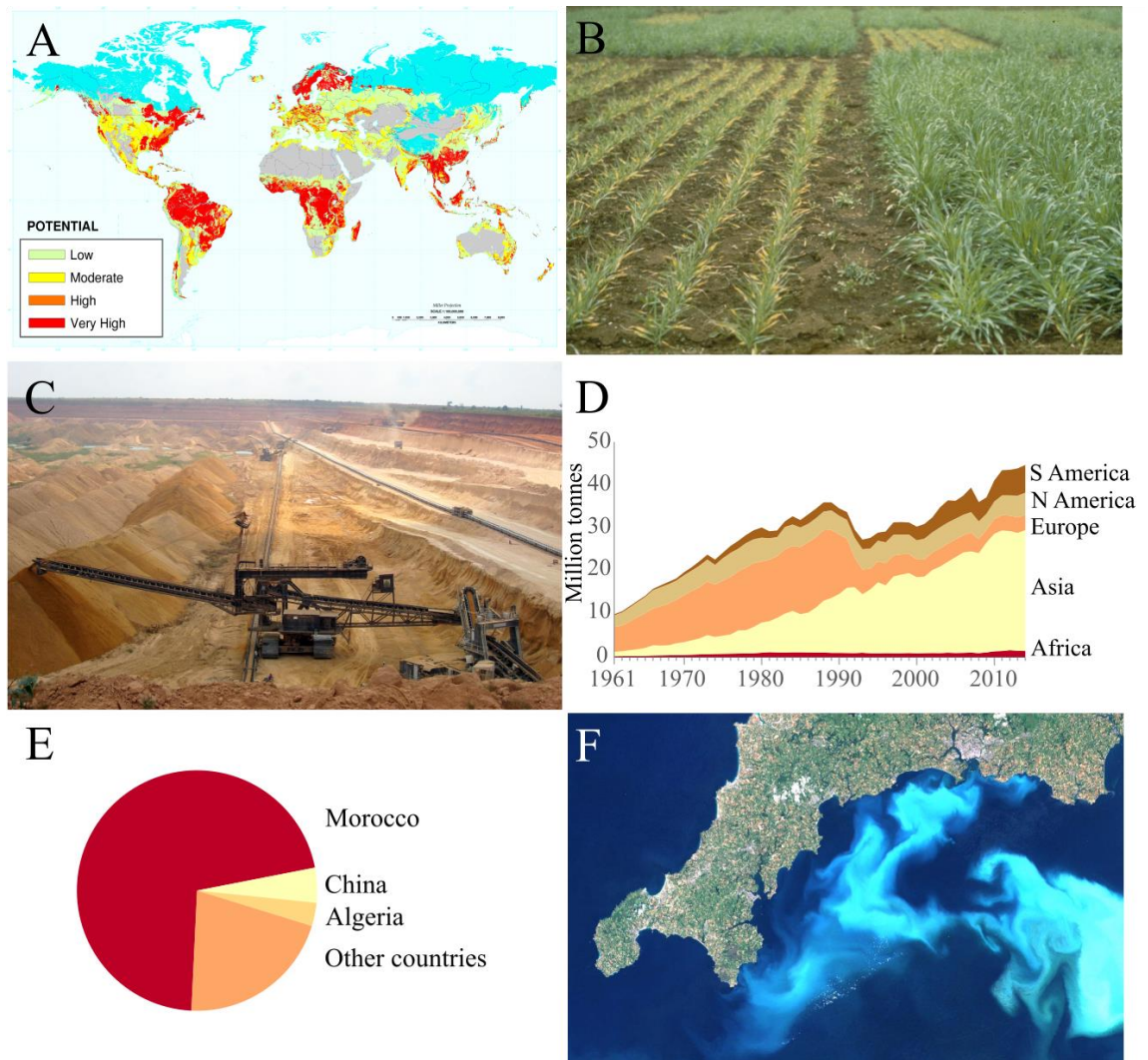
Phosphorus is one of the most limiting nutrients for plant growth in agriculture. Its ionic form phosphate ( $\text{PO}_4^{3-}$ , P) is a key macronutrient in metabolic processes, playing central roles in cell membranes, DNA, RNA and proteins, protein phosphorylations as well as signalling and energy transport molecules, most notably adenosine 5'- triphosphate (ATP) (Westheimer, 1987; Hunter, 2012; Fernández-García *et al.*, 2017). Whilst plants require high cellular P concentrations in the millimolar range, soil P concentrations are

low and in the micromolar range (Raghothama, 1999; Werner *et al.*, 2017). The little P that occurs in soil is heterogeneously spread, immobile and has a low bioavailability, as it readily complexes with aluminium or iron in acidic soils, and calcium in alkaline soils (Cole *et al.*, 1953; Wang *et al.*, 2012; Werner *et al.*, 2017). This scarcity of P most dramatically affects the crop yield of small-scale farmers in developing countries who generally work on the least productive arable land and cannot afford costly fertilizer (Raghothama, 1999; Nachtergaele *et al.*, 2009; Kochian, 2012). In high-input agricultural systems, low soil P status is overcome by application of excessive amounts of P fertilizer, with on average less than 10 percent's being utilized by crops (Sylvester-Bradley *et al.*, 2016).

In contrast to the geochemical nitrogen (N) cycle, where N enters the ecosystem through biological N<sub>2</sub> fixation and is thus available to plants, the soil P concentration depends solely on the mineral composition of parental rock. P fertilizer is mined from phosphate rock. The main use of all globally mined rock phosphate is as fertilizer in agriculture (over 87 % in 2014, FAO STAT). The consumption of P fertilizer has increased more than four-fold since the 1960s. Globally, over 47 million tonnes are consumed per year (FAO STAT, last data entry 2014). World resources of rock phosphate include the currently mined high-grade type, as well as off-shore and lower-grade rock phosphate which are currently untapped due to being economically and ecologically unsustainable (Gilbert, 2009; United States Geological Survey, 2018). Mined rock phosphate reserves have been predicted to run out within 50 – 125 years, as almost no recycling of applied fertilizer takes place (Cordell *et al.*, 2009; Gilbert, 2009). On the contrary, fertilizer run-off from fields into water bodies adds another dimension to the 'phosphate problem', as eutrophication leads to harmful algal bloom and hypoxia (Vörösmarty *et al.*, 2010; Bouwman *et al.*, 2017). Making rock phosphate an explosive socioeconomic issue is its uneven occurrence across the globe (Obersteiner *et al.*, 2013), with Morocco and Western Sahara sitting on 71 percent of estimated global rock phosphate reserves (China: 5 %, Algeria: 3 %, remaining countries: 21 %; United States Geological Survey 2018). See Figure 1 for a summary of the 'phosphate problem'.

Closing yield gaps and dismissing nutrient overuse is deemed achievable (Mueller *et al.*, 2012). However, moving towards a more sustainable use of P fertilizer in future agricultural practice without compromising yields will need to see changes on political, socioeconomic and agricultural levels. Of major importance for the latter is the generation of high-yielding crop varieties for low-input systems (Lynch, 2007). To do so, we need

to understand the relationship between plants and soil P, as well as the impact of lower P levels on plant growth. In the following section, aspects involved in overall plant P metabolism and signalling will be summarized. The focus will be on plant roots, as roots are the point of contact with soil, and responsible for nutrient uptake.



**Figure 1:** The ‘phosphate problem’. (A) Globally, phosphate (P) availability in soils is low, with regions in red showing high P retention potential. (B) Plant growth, and ultimately crop yield, is affected by P scarcity (shown here is a wheat field, with P-deficient wheat plants on the left, P-sufficient plants on the right). (C) Rock phosphate is invasively mined for fertilizer, for example in a mine in Togo, and (D) fertilizer consumption has increased drastically since the 1960’s (Million tonnes consumed by regions per year). (E) Most rock phosphate reserves are estimated to localize to Morocco. (F) Increased P run-off into waterways leads to environmental problems, such as algal bloom off the Devon and Cornwall coast. Sources: A - USDA-NRCS Soil Science Division, Phosphorus retention potential map, B – Peter Wall, Cimmyt, C – Wikicommons, D – FAOSTAT, E – US Geological Survey Phosphate Rock 2018, F – Wikicommons.

### 1.1.2 P uptake, translocation and storage

Plants can take up and assimilate inorganic phosphate ( $\text{PO}_4^{3-}$ ,  $\text{H}_2\text{PO}_4^-$  or  $\text{HPO}_4^{2-}$ , referred to as P hereafter) (Raghothama, 1999; Marschner, 2012; Srivastava *et al.*, 2018). Soil solution contains very low levels of plant available P (low micromolar range), whereas the cellular P pool is maintained at much higher levels (5 – 20 mM; Raghothama, 1999; Marschner, 2012). Cytosolic P concentrations are difficult to measure and therefore debated (Kanno, Cuyas, *et al.*, 2016), however they are reported to be within the range of 1 – 10 mM (Mukherjee *et al.*, 2015; Versaw and Garcia, 2017). To maintain this steep gradient between extra- and intracellular P, P can be taken up directly from the soil or indirectly through association with beneficial mycorrhizal fungi (Javot *et al.*, 2007; Kobae and Hata, 2010; Sawers *et al.*, 2017). In both cases, P needs to be transported across the plant cell plasma membrane against its electrochemical gradient (low apoplastic [P], high cytosolic [P]). This is facilitated by phosphate transport proteins which are well studied in numerous plant species (reviewed by Młodzińska and Zboińska, 2016; Srivastava *et al.*, 2018). In the non-mycorrhizal model plant *Arabidopsis thaliana* these are encoded by the PHOSPHATE TRANSPORTER (PHT) family. PHT1 subfamily are energy-driven, proton-coupled  $\text{H}_2\text{PO}_4^-$  symporters in the plasma membrane (PM) with different affinities for P (PHT1, first reported by Muchhal, Pardo and Raghothama, 1996; reviewed by Młodzińska and Zboińska, 2016; Srivastava *et al.*, 2018). Expectedly, proton co-transport resulted in acidification of the cytoplasm, as was shown during P uptake in *Catharanthus roseus* cell cultures and root hairs of the aquatic plant *Limnium stoloniferum* (Ullrich and Novacky, 1990; Sakano *et al.*, 1992). Uptake of P across the PM can lead to a quick and transient depolarization of the membrane potential of plant cells (*i.e.* the membrane potential becoming more positive), indicating influx of overall positive charge consistent with a  $\text{H}^+$ : P stoichiometry of more than 1 (Ullrich and Novacky, 1990; Dunlop and Gardiner, 1993).

In *Arabidopsis*, PHT1;1 and PHT1;4 are responsible for up to 75 % of P uptake, and are localized to the root tip (Shin *et al.*, 2004). Tracer experiments using radio-labelled  $^{33}\text{P}$  showed that the root cap and root tip more generally play major roles in P uptake. The root cap alone absorbed circa 20 % of total P despite its small surface area (Kanno, Arrighi, *et al.*, 2016). Depending on cellular P demand, the abundance and composition of PHTs is altered, modulating the affinity and capacity of the overall transport system (Ayadi *et al.*, 2015). Due to redundancy and overlapping expression patterns, some debate exists around unique functions and localization of the individual transporters

(summarized by Nussaume *et al.*, 2011; Młodzińska and Zboińska, 2016; Srivastava *et al.*, 2018). An accessory, endoplasmic reticulum- (ER) localized protein, called PHOSPHATE TRANSPORTER TRAFFIC FACILITATOR1 (PHF), was shown to facilitate correct ER-export and PM-targeting of the PHT1;1 transporter (Gonzalez *et al.*, 2005). Some PHT1 transporters display dual affinity for P, indicating that posttranslational regulation adds another level of regulatory complexity (Ayadi *et al.*, 2015). The potato phosphate transporter StPT2 has been shown to localize to the outer PM domain of epidermal cells, indicating that polar localization of transporters further directs P flux from soil into root (Gordon-Weeks *et al.*, 2003; Barberon and Geldner, 2014).

Once P is taken up across the PM into the cytosol, organellar P pools need to be replenished dynamically to satisfy metabolic demand, whereas the vacuole acts as a storage compartment for P. Members of the PHT2/4, PHT3 and PHT4 subfamilies transport P across the plastid, mitochondrial and Golgi membrane, respectively (Versaw and Garcia, 2017). Sufficient plastid P is further regulated by PLASTIDIC PHOSPHATE TRANSLOCATOR proteins (pPTs), exchanging triose-P for P (Knappe, 2003; Lee *et al.*, 2014). Mitochondrial P supply for ATP synthesis is regulated through MITOCHONDRIAL PHOSPHATE TRANSPORTER (MPT, Jia *et al.*, 2015). The recently discovered VACUOLAR PHOSPHATE TRANSPORTER1 (VPT1, also named PHT5;1) imports P across the tonoplast (Jinlong Liu *et al.*, 2015; Liu *et al.*, 2016).

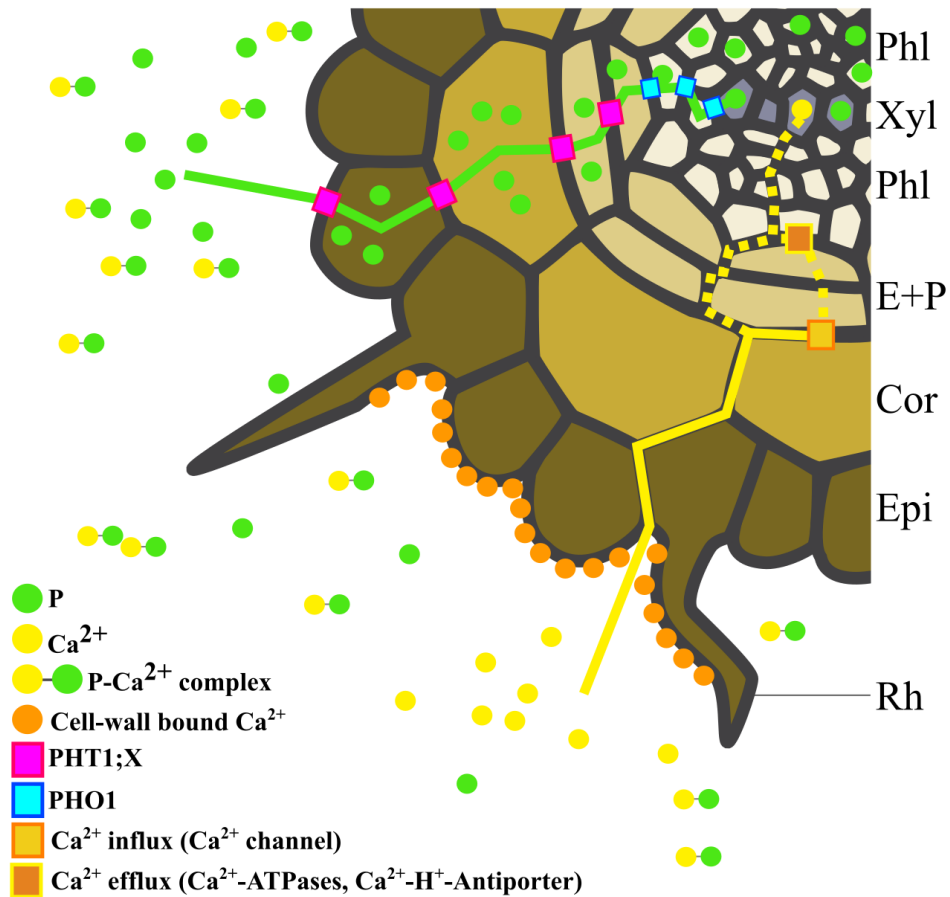
Intercellular, long-distance root-to-shoot transport of P occurs mainly in the xylem (Marschner, 2012). A major player in root-to-shoot translocation is PHO1, which loads P from root pericycle cells into xylem vessels (Poirier *et al.*, 1991; Hamburger *et al.*, 2002). PHO1 protein was found to mostly locate to the Golgi, to some extent to vesicular structures of unknown identity and to the PM upon P supply (Arpat *et al.*, 2012). Recently, PHO1 was found to be specifically expressed in unsubserved 'passage cells', specialized endodermal cells that have been suggested to act as a 'nutrient funnel' from outer into inner root cell layers (Andersen *et al.*, 2018). To date it is unclear if PHO1 exports P directly *via* PM transport and/or through exocytosis of loaded vesicles, possibly linking intra- and intercellular P transport (Arpat *et al.*, 2012; also see Figure 2 for a schematic of P uptake across the root).

Root P uptake and transport to sink tissues such as the shoot occurs within minutes. Rice seedling roots were shown to translocate radio-labelled  $^{32}\text{P}$  within 15 minutes along the whole plant (bulk  $^{32}\text{P}$  remained in the root, 5 % had moved to the shoot, Kobayashi *et al.*,

2013). Using a higher resolution approach and 43-day old *Arabidopsis*, the velocity of  $^{32}\text{P}$  in the shoot was calculated to be  $> 6$  cm per hour (Sugita *et al.*, 2016). Few studies have considered a diurnal regulation of P uptake and translocation. In tomatoes, P uptake took place dominantly during the night compared to all other nutrients and was independent of water uptake and transpiration rate (Terabayashi *et al.*, 1991; Marschner 2012). Similarly,  $^{32}\text{P}$  uptake into the root was accelerated during the night in *Lotus* (Yamawaki *et al.*, 2011). The same study found that  $^{32}\text{P}$  translocation from root to shoot was almost absent during the night but occurred during the day (Yamawaki *et al.*, 2011). The chloroplast P importers, PHT2;1 and PHT4;1, have been annotated to be under circadian control, with their expression peaking around dawn (Covington and Harmer, 2007). Increased translocation between cellular compartments is likely needed to satisfy P demand in photosynthesis during the day (Haydon *et al.*, 2011, 2015). In general, a trend to P uptake during the night, and P translocation during the day emerges.

The vacuole is the primary storage compartment for P in vegetative tissue (Bielecki, 1973; Yang *et al.*, 2017). Due to a more positive membrane potential on the inside of the tonoplast, ten times more P could be accumulated in the vacuole relative to the cytosol (Versaw and Garcia, 2017). Fluctuations in external P levels can therefore lead to significant changes in vacuolar P levels, whilst cytosolic P levels are well buffered (Rebeille *et al.*, 1983; Mimura *et al.*, 1996; Pratt *et al.*, 2009). In contrast to fungi and algae, which store P in long chains called polyphosphate, higher plants store most P in the same form as required, as inorganic phosphate, in their vegetative tissue (reviewed by Yang *et al.*, 2017). P can be remobilized and redistributed through the plant *via* the phloem (Marschner, 2012). This nutrient cycling occurs during developmental processes, *e.g.* during senescence and seed-loading (Mimura *et al.*, 1996; Nagarajan *et al.*, 2011). In seeds, P is mainly stored as phytate (phytic acid with cations such as  $\text{Ca}^{2+}$ ,  $\text{Fe}^{3+}$ ,  $\text{K}^+$ ,  $\text{Mg}^{2+}$ ,  $\text{Mn}^{2+}$ ,  $\text{Zn}^{2+}$ , Bielecki, 1973; Marschner, 2012). During germination, phytate is hydrolysed into P and inositol to nurture the emerging seedling.





**Figure 2:** Schematic of phosphate and calcium uptake and transport across the root as explained in the text. P (green dots) occurs in low concentration in soil, particularly in alkaline soils complexed with Ca<sup>2+</sup> (green-yellow dots). P is taken up mostly symplastically into cells (green solid line) through proteins of the P transporter family (PHT1;X, pink box) and loaded into xylem for long-distance transport *via* PHO1 (blue box). P can be redistributed in the plant *via* the phloem. P uptake seems to predominate during the night. Ca<sup>2+</sup> (yellow dots) is abundant in most soils, and extracellular concentrations are high, where Ca<sup>2+</sup> is being non-metabolically accumulated in the cell wall through binding to negatively charged groups (exemplified by orange dots). Ca<sup>2+</sup> transport across the root occurs mainly in the apoplast (solid yellow line), but some symplastic passage is necessary (dashed yellow line) to cross endodermal cells impregnated by the Casparian strip. Ca<sup>2+</sup> long-distance transport *via* the xylem is dependent on transpiration rate. Ca<sup>2+</sup> shows very low phloem mobility. Phl – phloem, Xyl – xylem, E+P – endodermis and pericycle, Cor – cortex, Epi – epidermis, Rh – root hair; drawing is not to scale. Root cross section template downloaded from figshare.com.

### 1.1.3 Impact of P deficiency on plant root growth and metabolism

P deficiency leads to profound changes in plant metabolism and growth. When P is limited, plants show an array of adaptive responses to increase exploration of the soil, uptake and use of P. On a systemic level, growth slows. Root growth is favoured over shoot growth, indicative of maximizing soil exploration and thus nutrient uptake (Gruber *et al.*, 2013). In addition, root system architecture is remodelled which has been well described in many crop species, such as barley, maize, rice and tomato, as well as *Arabidopsis* (Péret *et al.*, 2014). Multi-component nutrient studies found P to be the predominant nutrient controlling primary root length (Gruber *et al.*, 2013; Kellermeier *et al.*, 2014). Primary root growth stops, through inhibition of both cell proliferation in the meristematic zone and cell expansion in the elongation zone (Williamson *et al.*, 2001; Sánchez-Calderón *et al.*, 2005; Svistoonoff *et al.*, 2007; Balzergue *et al.*, 2017). In many cases, lateral root formation is favoured (Williamson *et al.*, 2001; Nacry *et al.*, 2005), with lateral roots of bean, maize, rice and *Arabidopsis* becoming shallower to explore P-rich topsoil layers (Lynch and Brown, 2001; Bai *et al.*, 2013; Huang *et al.*, 2018). Strikingly, fine root hairs increase in length and density in many plant species, likely to increase overall root surface area for nutrient uptake whilst investing little energy (Foehse and Jungk, 1983; Bates and Lynch, 1996; Gahoonia *et al.*, 1997; Ma *et al.*, 2001; Mueller and Schmidt, 2004; Haling *et al.*, 2013; Bhosale *et al.*, 2018). Another adaptation to P scarce conditions, seen particularly in plant species evolved on highly weathered soils, is the formation of so called ‘cluster roots’, rootlets of extremely high density (reviewed by Lambers, Martinoia and Renton, 2015). Besides increasing P uptake, P is recycled throughout the plant body, *e.g.* from older to younger leaves, as well as from shoot-to-root *via* the phloem to satisfy P demand. Roots exude organic acids to acidify the rhizosphere and thus to solubilize P-containing minerals, as well as secreting acid phosphatases to release P from organic substrates (Diatloff *et al.*, 2004; Mukherjee *et al.*, 2015; Wang and Liu, 2018).

The majority of plant species enter a beneficial symbiosis with root-associated fungi, in which the fungus delivers P through its extensive hyphal system, and receives plant assimilated carbon in return. Association can occur extracellularly, classified as ectomycorrhizal fungi (reviewed by Tedersoo *et al.*, 2010), or intracellularly through arbuscular mycorrhizal fungi of the phylum Glomeromycota (reviewed by Choi *et al.*, 2018). The latter unload P across the periarbuscular membrane into the fungus/plant interface, to be taken up by plant cells *via* P transporters belonging to the MtPT4/OsPT11

type, characterized in *Medicago truncatula* and rice respectively (Paszkowski *et al.*, 2002; Javot *et al.*, 2007; Kobae and Hata, 2010). In addition, P transport does not only occur from fungus to plant, but was also shown to move from a ‘source’ plant through an associated fungus into a ‘donor’ plant, establishing inter-plant connectivity (Eason *et al.*, 1991). Recently, diverse endophytic fungi and root microbiota have been shown to modulate P stress responses, even in plants that do not establish mycorrhizal symbiosis such as *Arabidopsis* (Hiruma *et al.*, 2016; Castrillo *et al.*, 2017).

On a cellular level, it has long been known that P deficiency leads to a lower cellular P level and cytosolic P can drop within minutes of starvation (Duff *et al.*, 1989; Pratt *et al.*, 2009). The organic P pools - DNA, RNA, P-esters and phospholipids - are known to have different turnover times, with DNA’s being the most stable, phospholipids turning over within hours, and P-esters turning over within seconds to minutes (Bielecki, 1973), allowing for remodelling of P distribution within cells. Cellular ATP and GTP levels drop sharply after onset of P deficiency, *e.g.* shown in *Catharanthus roseus* and sycamore cell culture (Shimano and Ashihara, 2006; Gout *et al.*, 2014). Overall, P deficiency triggers a shift to alternative metabolic pathways which consume less P (Duff *et al.*, 1989; Plaxton and Tran, 2011; Pant *et al.*, 2015). Phosphorylated metabolites decrease (Pant *et al.*, 2015). Phospholipids are remodelled into sulfo- and glycolipids, restricted to the cytoplasmic leaflet of the PM (Andersson *et al.*, 2005; Tjellstrom *et al.*, 2010; Nakamura, 2013; Okazaki *et al.*, 2013). Despite PM remodelling, no significant change in overall membrane potential seems to occur under P deficiency (Mimura *et al.*, 1998; Dindas *et al.*, 2018).

#### 1.1.4 P sensing and molecular responses to P deficiency

Plants monitor internal as well as external P status, which involves systemic or local signalling events, respectively. A myriad of molecular players functioning in the P deficiency response have been described in recent years. In general, changes in root system architecture have been found to be controlled locally by P supply, whereas activity of P uptake and distribution was found to be under systemic control (reviewed by Abel, 2017).

Local P supply is sensed by the root tip, irrespective of the P status of the shoot (Svistoonoff *et al.*, 2007; Thibaud *et al.*, 2010). Mutant studies uncovered a response module, consisting of the transcription factor SENSITIVE TO PROTON TOXICITY1

(STOP1) and its target ALUMINIUM-ACTIVATED MALATE TRANSPORTER1 (ALMT1), a malate channel, as well as LOW PHOSPHATE ROOT1 (LPR1), a cell wall targeted ferroxidase, LPR2 and PHOSPHATE DEFICIENCY RESPONSE (PDR2), a P5-type ATPase with unknown substrate that governs the inhibition of primary root growth upon root tip contact with low external P (Svistonoff *et al.*, 2007; Ticconi *et al.*, 2009; Balzergue *et al.*, 2017). In the elongation zone, STOP1 stimulates the expression of *ALMT1*, which in turn results in ALMT1-mediated malate efflux into the apoplast (Balzergue *et al.*, 2017). Malate alters Fe chelation and activity of the LPR1-PDR2 module (Balzergue *et al.*, 2017). Fe accumulates, which in turn triggers reactive oxygen species (ROS) production, cell wall stiffening and callose (1,3- $\beta$ -glucan) deposition, significantly decreasing symplastic communication and cell elongation (Müller *et al.*, 2015; Hoehenwarter *et al.*, 2016; Balzergue *et al.*, 2017). Callose deposits have in general been described as major regulators of plasmodesmal permeability, mostly for biotic stress responses (Kauss, 1985; Xu *et al.*, 2017). Callose deposition occurs rapidly (within 10 minutes), but is a reversible process (Kauss, 1985). Once cell-to-cell communication is impaired, movement of transcription factors such as SCARE CROW, involved in root patterning, or SHORT ROOT, involved in maintenance of the stem cell niche, are less mobile (Ticconi *et al.*, 2009; Müller *et al.*, 2015; Balzergue *et al.*, 2017). In the meristem, the LPR1-PDR2 module leads to an inhibition of cell division that is STOP1- and ALMT1-independent (Balzergue *et al.*, 2017).

Once a change in external P levels has been detected, the systemic P status is signalled and sensed through multiple networks of signalling molecules. P itself likely acts as a signal, independent of its function as a nutrient, as the non-metabolic analogue phosphite suppressed P deficiency responses (Ticconi *et al.*, 2001). Long non-coding RNAs and microRNAs, such as microRNA399, are induced under P deficiency and were found to be shoot-to-root mobile (Bari *et al.*, 2006; Pant *et al.*, 2008; Yuan *et al.*, 2016). Sugars are described as another shoot-derived systemic signal, as malfunctioning of photosynthesis under P limitation leads to less sugars' being transported into the roots (Hammond and White, 2011). A wide range of hormonal signals such as ethylene, auxin, strigolactone and gibberellin play prominent roles under P deficiency, acting in intricate networks (reviewed by *e.g.* Chien *et al.*, 2018). For example, strigolactone levels in roots of *Arabidopsis* and rice have been shown to increase under P starvation conditions (Umehara *et al.*, 2010; Kohlen *et al.*, 2011), leading to changes in root system architecture such as stimulating root hair outgrowth (Kapulnik, Delaux, *et al.*, 2011). Strigolactone's

involvement in root hair elongation was further found to be co-regulated by ethylene, but independent of the promoting growth effect of auxin (Kapulnik, Resnick, *et al.*, 2011). Auxin transport from the root apex into the differentiation zone was recently found to be a major regulator of P starvation-induced root hair outgrowth in *Arabidopsis* and rice (Bhosale *et al.*, 2018; Giri *et al.*, 2018).

On a transcriptional level, PHOSPHATE STARVATION RESPONSE1 (PHR1) has been described as a master regulator. PHR1 is a MYB transcription factor, and alongside its homologues PHR-like (PHL), was found to regulate most genes that were induced upon P deficiency (Rubio *et al.*, 2001; Bustos *et al.*, 2010; Sun *et al.*, 2016). For example, PHR1 controls the transcription of microRNA399 (Bari *et al.*, 2006). PHR1 further regulates FERRITIN1 (FER1), establishing a first genetic link between P and Fe nutrition (Bournier *et al.*, 2013). Cross-talk with other nutrients such as nitrate, zinc and sulphate are involved in signal read out (Briat *et al.*, 2015; Medici *et al.*, 2015). Interestingly, Fe and N transporters, namely IRT1 and NRT1.1, have recently been described to function as ‘transceptors’, *i.e.* transporting ions as well as sensing the nutritional status like a receptor (Bouguyon *et al.*, 2015; Dubeaux *et al.*, 2018). For P nutrition, the yeast transporter PHO84 has been described as a transceptor (Popova *et al.*, 2010). Unequivocal proof for a plant P transceptor however is missing. In *Arabidopsis*, P deficiency led to upregulation of PHTs, increasing P uptake (Ayadi *et al.*, 2015; Z. Q. Wang *et al.*, 2018). Downstream P translocation through PHO1 was recently shown to be upregulated under P starvation conditions, through the degradation of the PHO1-repressor, transcription factor WRKY6 (Ye *et al.*, 2018).

Post-transcriptionally, P deficiency led to dynamic changes in global DNA methylation patterns, recently shown for both rice and *Arabidopsis* (Secco *et al.*, 2015; Yong-Villalobos *et al.*, 2015). Using cell-free extract from *Arabidopsis* seedlings, P deficiency altered gene silencing *via* inhibition of DICER-LIKE3 (DCL3), whereas small interfering RNA production through DCL3 was rescued by P re-addition *in vitro* (Seta *et al.*, 2017). Chromatin modifications through the activity of HISTON DEACETYLASE19 (HDA19) controlled epidermal cell elongation, root hair density and membrane lipid remodelling under P deficiency (Chen *et al.*, 2015).

A common attribute of P-responsive genetic elements across the eukaryotes is the occurrence of SPX domains, sensing intracellular P status (named after *SYG1*, *PHO81* and *XPR1*, the first three identified *SPX* gene members, reviewed by Liu *et al.*, 2018). These domains are either part of a more complex protein, as found for example in PHO1

and VPT1, or occur as independent, single-domain proteins (Duan *et al.*, 2008; Puga *et al.*, 2014; Jinlong Liu *et al.*, 2015; Wild *et al.*, 2016). For example, SPX1 protein binds to PHR1, preventing the transcription of PHR1 target genes and as such the expression of deficiency genes under P-sufficient conditions (Duan *et al.*, 2008; Puga *et al.*, 2014). Recently it has been shown that SPX domains interact with P-containing ligands, but with little specificity and selectivity for P itself. Inositol P (InsP) rather than P was found to be important in SPX-dependent PHO1-mediated P homeostasis (Wild *et al.*, 2016). HDA19 regulates SPX expression transcriptionally (Chen *et al.*, 2015).

A signal transducer of widespread action is  $\text{Ca}^{2+}$ . Its involvement in P sensing and modulation of plant responses to P deficiency has been hypothesized (Chiou and Lin, 2011; Lin *et al.*, 2014), however to date no known study has reported the use of  $\text{Ca}^{2+}$  as a signalling ion in the context of P deficiency responses.

## 1.2 Calcium – macronutrient with structural and signalling roles

Calcium is an essential macronutrient for plant growth and development. The calcium ion,  $\text{Ca}^{2+}$ , has a structural and growth regulatory role, as well as acting as a signal transducer (Hirschi, 2004). In general, its structural role in macromolecules is determined by its capacity to coordinate through stable but reversible linkages (Marschner, 2012). Through cross-linkage of pectins, it stabilizes cell walls (Kinzel, 1989). Through cross-linkage of P groups in phospholipids and carboxylic groups in proteins, it equally stabilizes membranes (Kinzel, 1989).  $\text{Ca}^{2+}$  has also been shown to regulate cell extension and secretory processes, most notably the polar growth of single cell systems such as root hairs and pollen tubes (Bibikova *et al.*, 1997; Felle and Hepler, 1997; Véry and Davies, 2000; Ketelaar *et al.*, 2008). On a cellular level, the same mechanism can be observed as to what occurs in soils:  $\text{Ca}^{2+}$  forming stable complexes with P. Therefore, to avoid cytotoxicity, levels of cytosolic free  $\text{Ca}^{2+}$  ( $[\text{Ca}^{2+}]_{\text{cyt}}$ ) have to be maintained at low levels to guarantee a functioning metabolism (Edel and Kudla, 2015; Verkhatsky and Parpura, 2015). In the following, plant  $\text{Ca}^{2+}$  nutrition will be briefly summarized, to enable a comparison with P nutrition. Then, its role as a signal transducer will be described in more detail.

### 1.2.1 Ca<sup>2+</sup> uptake, translocation and storage on whole plant level

The negatively charged groups in the cell wall (carboxylic groups, R.COO<sup>-</sup>) attract cations from the soil solution, easily leading to the accumulation of Ca<sup>2+</sup> in a non-metabolic way (Marschner, 2012; Barberon and Geldner, 2014; see Figure 2 for a schematic). A high proportion of total plant Ca<sup>2+</sup> therefore localizes to the apoplast and cell wall (Marschner, 2012). Movement through the outer layers of the root has been described to occur through the apoplast (White and Broadley, 2003). It has however been under debate if Ca<sup>2+</sup> is *exclusively* transported through the apoplast before its being loaded into the xylem for long-distance transport, or whether Casparian strip and suberized endodermal cells require Ca<sup>2+</sup> loading into the symplast (Ferguson and Clarkson, 1976; White, 2001; Baxter *et al.*, 2009; Marschner, 2012). Only recently it has been shown that suberized endodermal cells indeed block apoplastic Ca<sup>2+</sup> movement, indicative of a symplastic passage of Ca<sup>2+</sup> through non-suberized cells (Li *et al.*, 2017).

Most Ca<sup>2+</sup> taken up by the root is shuttled to the shoot (Conn and Gilliam, 2010). This transport occurs in the xylem, where Ca<sup>2+</sup> is mostly chelated with organic acids such as malate and citrate (Marschner, 2012). The speed of Ca<sup>2+</sup> translocation directly depends on water uptake and transpiration rate and therefore occurs mainly during the day (Terabayashi *et al.*, 1991; Marschner, 2012). Ca<sup>2+</sup> has a very low mobility in the phloem, posing the problem that it cannot be redistributed, and might accumulate at terminal sites of the transpiration stream (Conn and Gilliam, 2010; Tang and Luan, 2017). Plants have been shown to accumulate Ca<sup>2+</sup> in trichomes or store away Ca-oxalates in the apoplast to manage excess Ca<sup>2+</sup> (Fink, 1991; White and Broadley, 2003; Franceschi and Nakata, 2005).

### 1.2.2 Ca<sup>2+</sup> uptake and translocation on a cellular level

Ca<sup>2+</sup>'s entering the symplast is risky as, within the cytosol, Ca<sup>2+</sup> is easily cytotoxic. This is due to Ca<sup>2+</sup>'s (i) readily complexing with cellular P groups, such as ATP, and (ii) competing with magnesium for binding sites, which overall disturbs cellular metabolism (Hepler and Wayne, 1985; Sanders, Brownlee and Harper, 1999; Marschner, 2012; Edel and Kudla, 2015; Verkhatsky and Parpura, 2015). Therefore, early on in the evolution of life that based its metabolism on P-rich molecules, Ca<sup>2+</sup> entry into the cytosol had to be tightly regulated to maintain a low concentration of [Ca<sup>2+</sup>]<sub>cyt</sub>, resulting in a large machinery of influx and efflux proteins, as well as Ca<sup>2+</sup>-binding proteins which decrease

the activity of cytosolic  $\text{Ca}^{2+}$  (Hodgkin and Keynes, 1957; Conn and Gilliam, 2010; Demidchik *et al.*, 2018).

Whilst apoplastic  $\text{Ca}^{2+}$  levels are easily within millimolar range, levels of  $[\text{Ca}^{2+}]_{\text{cyt}}$  are maintained within 50 - 200 nanomolar (Felle, 1988; Sanders *et al.*, 1999; Stael *et al.*, 2012; Costa *et al.*, 2018). To facilitate such low  $[\text{Ca}^{2+}]_{\text{cyt}}$  levels, auto-inhibited  $\text{Ca}^{2+}$ -ATPases (ACAs) and ER  $\text{Ca}^{2+}$ -ATPases (ECAs) transport  $\text{Ca}^{2+}$  out of the cytosol into the apoplast and organelles (Boursiac and Harper, 2007; Aslam *et al.*, 2017; Costa *et al.*, 2017). Additionally, on the vacuolar membrane,  $\text{Ca}^{2+}$ - $\text{H}^{+}$ -antiporters ( $\text{Ca}^{2+}$  exchanger, CAX) have been described (Hirschi *et al.*, 1996; Cheng *et al.*, 2005). Both  $\text{Ca}^{2+}$ -ATPases and  $\text{Ca}^{2+}$ - $\text{H}^{+}$ -antiporter move  $\text{Ca}^{2+}$  against its electrochemical gradient, and consume ATP, either directly ( $\text{Ca}^{2+}$ -ATPases) or indirectly (CAX). Measurement of organellar  $[\text{Ca}^{2+}]$  levels is challenging, but has become more accessible through the advent of genetically encoded  $\text{Ca}^{2+}$  reporters (summarized by Costa *et al.*, 2018, see section 1.2.9 for introduction to  $\text{Ca}^{2+}$  reporters). Organellar  $\text{Ca}^{2+}$  levels are finely tuned, *e.g.* up to 500 nM was found in the thylakoid lumen, which is 3 – 5 times higher than what was found in the chloroplast stroma of *Arabidopsis* (Sello *et al.*, 2018). Mitochondrial matrix, ER lumen, Golgi lumen and peroxisome lumen are all compartments with reported free  $\text{Ca}^{2+}$  concentration well above  $[\text{Ca}^{2+}]_{\text{cyt}}$  (Stael *et al.*, 2012; Costa *et al.*, 2018).

The return flow down the electrochemical gradient and across membranes occurs *via* different kinds of ion channel or uniporter proteins (reviewed by Swarbreck *et al.*, 2013; Demidchik *et al.*, 2018). By definition, channels exhibit a higher turnover rate than uniporters, and  $\text{Ca}^{2+}$  channels were found capable of transporting more than 1 million ions *per second* (Tsien *et al.*, 1987). This implies that only a few proteins within a given membrane are required to influence cellular physiology significantly and need to be tightly regulated. Functional characterization of channel proteins has proven very difficult, as with any transmembrane proteins, and is further complicated by their low abundance. Channel characteristics and genetic basis have been elucidated using pharmacological treatment, electrophysiological approaches, phenotypic screens or by exploiting sequence similarity to animal, bacterial or yeast  $\text{Ca}^{2+}$  channels.

Using patch-clamp technique and other electrophysiological approaches, much progress has been made by demonstrating that, at the PM, such channels can be variously activated by voltage, as well as be voltage independent (Swarbreck *et al.*, 2013). Hyperpolarization-activated  $\text{Ca}^{2+}$  channels (HACCs) are triggered by the PM potential's becoming more negative, depolarization-activated  $\text{Ca}^{2+}$  channels (DACCs) are opened if the PM potential



becomes more positive (Swarbreck *et al.*, 2013). Accordingly, voltage-independent  $\text{Ca}^{2+}$  channels (VICCs) would be capable of transporting  $\text{Ca}^{2+}$  at any given membrane voltage. Taken together, the membrane harbours an arsenal of protein complexes which would allow for regulated  $\text{Ca}^{2+}$  flux at any given membrane potential (Swarbreck *et al.*, 2013). Channels can be further regulated by signalling events/molecules, such as cyclic AMP/GMP, phosphorylation and reactive oxygen species (Yoshioka *et al.*, 2006; Demidchik *et al.*, 2009; Richards *et al.*, 2014). The direct or indirect activation of such signalling intermediates is often challenging to determine. Further complicating the issue is the fact that specificity of a given channel protein for a species of ions might be low, resulting in transport of mixed ionic content, *e.g.* “ $\text{Ca}^{2+}$  permeable, non-selective cation channel” might refer to a channel capable of transporting  $\text{Ca}^{2+}$ , whilst moving other cations such as  $\text{K}^+$  to various degrees (Véry and Davies, 2000). Therefore, to find the genetic basis plus its involvement in  $\text{Ca}^{2+}$  flux plus a phenotype for a given channel is challenging, and evidence for most candidates is scant (Swarbreck *et al.*, 2013).

### 1.2.3 $\text{Ca}^{2+}$ channels localizing to the plasma membrane

Through sequence similarity with known  $\text{Ca}^{2+}$  channels from other evolutionary lineages, the genetic basis of some HACCs, DACCs and VICCs has been identified in plants. The cyclic nucleotide-gated channels (CNGCs; Kohlen *et al.*, 1999; Leng *et al.*, 1999) and glutamate receptor-like (GLRs; Lam *et al.*, 1998; Chiu *et al.*, 2002) channels bear some structural similarities to their animal counterparts, and form conventional, membrane-spanning channel proteins. *Arabidopsis* possesses large gene families coding for CNGCs and GLRs, with 20 members each (Mäser *et al.*, 2001; Chiu *et al.*, 2002). Size of gene families varies greatly depending on plant species, *e.g.* 11 CNGCs have been annotated for the *Ricinus communis* genome, whilst wheat was recently found to contain as many as 47 CNGCs genes (Saand *et al.*, 2015; Guo *et al.*, 2018). The same variation in size has been reported for GLRs. Tree species of Rosaceae (pear, plum, peach) were recently annotated to harbour between 34 to 40 GLR genes in their genome, including a subfamily absent in *Arabidopsis* and Brassicales in general (Chen *et al.*, 2016). It has further been shown that different GLRs can form heteromultimeric complexes, adding another level of diversity to the observed  $\text{Ca}^{2+}$  channel behaviours (Price and Okumoto, 2013). Both CNGCs and GLRs are found mostly at the PM and shown to be activated by intracellular cyclic nucleotides and extracellular amino acids, respectively (Michard *et al.*, 2011; Vincill *et al.*, 2012; Kong *et al.*, 2016). Both CNGCs and GLRs are involved in abiotic

and biotic stress perception, as well as in general plant ion homeostasis. For example, *Arabidopsis* CNGC2 was reported to be involved in pathogen resistance, and overall  $\text{Ca}^{2+}$  homeostasis (Clough *et al.*, 2000; Chan *et al.*, 2008; Chaiwongsar *et al.*, 2009). *Arabidopsis* CNGC10 was found to regulate the response to both fungal attack and salt stress (Vadassery *et al.*, 2009; Jin *et al.*, 2014), whilst CNGC14 has recently been described to govern the root gravitropic response, as well as auxin-dependent root hair growth (Shih *et al.*, 2015; Zhang *et al.*, 2017; Dindas *et al.*, 2018). Outside *Arabidopsis*, the role of CNGCs is being elucidated, with *e.g.* wheat CNGC14 and CNGC16 being strongly induced upon pathogen perception (Guo *et al.*, 2018). GLRs are similarly involved in a range of responses, such as *Arabidopsis* GLR3.7's being prominently involved in pollen tube growth, and tolerance to high salt levels during germination (Michard *et al.*, 2011; Cheng *et al.*, 2016). Tomato GLR1.1 and GLR3.5 were found hypersensitive to  $\text{Na}^+$  and  $\text{K}^+$  stress, through controlling  $\text{Ca}^{2+}$  uptake and homeostasis (Aouini *et al.*, 2012).

More recently, annexins have been described as capable of forming  $\text{Ca}^{2+}$ -permeable channels. Annexins are ubiquitous, small amphipathic proteins able to bind to membrane phospholipids (reviewed by Davies, 2014). Eight annexins are found in *Arabidopsis* (Jami *et al.*, 2012), with ANNEXIN1's (ANN1) being the best studied member of the family. In contrast to canonical channel proteins, which localize exclusively to membranes, annexins occur both within the cytosol as well as inserting into bilayer membranes, thus establishing ionic transport (Laohavisit *et al.*, 2012). Recruitment to the membrane would allow rapid and quantitative response to external stimuli. ANN1-dependent  $\text{Ca}^{2+}$  transport across the root plasma membrane is activated by reactive oxygen species (Laohavisit *et al.*, 2012; Richards *et al.*, 2014).

$\text{Ca}^{2+}$  is known to play an important role in mechanosensing (Braam and Davis, 1990; Knight *et al.*, 1991, 1992; Legué *et al.*, 1997; Kiegle, *et al.*, 2000; Monshausen *et al.*, 2009) and it has long been postulated that mechanically-gated ion channels could be involved (Braam and Davis, 1990; Ding and Pickard, 1993). Candidates for  $\text{Ca}^{2+}$ -permeable mechanosensitive channels have been described based on sequence similarity to their bacterial homologues, as the Mechanosensitive channels of small conductance (MscS) are well-studied in *Escherichia coli* (Kung *et al.*, 2010). In *Arabidopsis*, the MscS-like gene family (MSL) has 10 members, mostly localizing to the PM (Haswell and Meyerowitz, 2006; Haswell *et al.*, 2008; Hamilton *et al.*, 2015). MSL channels are mainly described to function as anion channels (Kurusu *et al.*, 2013; Hamilton *et al.*, 2015),

however they have also been shown to moderately transport  $\text{Ca}^{2+}$  (Haswell *et al.*, 2008), thus their role in  $[\text{Ca}^{2+}]_{\text{cyt}}$  requires further studies.

Another family of mechanosensitive and  $\text{Ca}^{2+}$ -permeable channel proteins comprises the MCAs (mid1-complementing activity). MCA1 was named after it was found to complement the *mid1* yeast mutant, which lacks a putative  $\text{Ca}^{2+}$  channel (Nakagawa *et al.*, 2007). MCA1 and MCA2 proteins are localized to the PM, permit influx of  $\text{Ca}^{2+}$  upon mechanical stimulation, and are involved in cold sensing (Mori *et al.*, 2018). The MCA proteins are likely to be unique to land plants (Nakagawa *et al.*, 2007). From their structure it is likely that they are a component of a channel complex (Yamanaka *et al.*, 2010).

Most recently, two independent studies described another family of *Arabidopsis* mechanosensitive  $\text{Ca}^{2+}$  channels, responding to osmotic shock. The hyperosmolality gated  $\text{Ca}^{2+}$ -permeable channel was named ‘reduced hyperosmolality-induced  $[\text{Ca}^{2+}]_{\text{cyt}}$  increase’ (OSCA, Yuan *et al.*, 2014) or ‘Calcium permeable Stress-gated cation Channel1’ (CSC1, Hou *et al.*, 2014). OSCA1/CSC1 localized to the PM, and transported various cations including  $\text{Ca}^{2+}$  (Hou *et al.*, 2014; Yuan *et al.*, 2014). Closure of the channel seemed dependent on  $\text{Ca}^{2+}$  (Hou *et al.*, 2014). Mutants of OSCA1/CSC1 showed impaired  $\text{Ca}^{2+}$  fluxes in response to osmotic stimuli in guard cells and roots (Hou *et al.*, 2014; Yuan *et al.*, 2014). The family of OSCA/CSC comprises 15 members in *Arabidopsis*, and 11 members in rice (Yuan *et al.*, 2014; Li *et al.*, 2015). Gene expression of 10 out of 11 rice *OSCA* genes was found to be regulated by osmotic stress, indicating a conserved role of OSCAs across plant species (Li *et al.*, 2015).

#### 1.2.4 $\text{Ca}^{2+}$ channels and uniporters localizing to organellar membranes

Besides PM localization, some members of the CNGC and GLR family have been reported to localize to organellar membranes. For example, *Arabidopsis* CNGC19 and CNGC20 localized to the tonoplast (Yuen and Christopher, 2013). Splicing variants of GLR3.5 were shown to be targeted to either inner mitochondrial membrane, or plastid membrane (Teardo *et al.*, 2015), whilst GLR3.4 localized to both plasma and plastid membrane (Teardo *et al.*, 2011). ANN1 has been identified in the membrane of ER, vacuole, mitochondria and chloroplasts (Davies, 2014). MSL1 localized to the inner mitochondrial membrane (Lee *et al.*, 2016), MSL2 and MSL3 localized to the plastid envelope (Haswell and Meyerowitz, 2006).

As mitochondrial  $\text{Ca}^{2+}$  dynamics in animals are regulated through a mitochondrial calcium uniporter complex (MCUC), the search was on to find a similar complex in plants. Based on sequence similarity, a similar complex has recently been starting to be elucidated in plants. MICU, named after its animal counterpart and with one member in *Arabidopsis*, was found to localize to the mitochondrial membrane and regulate mitochondrial free  $\text{Ca}^{2+}$  dynamics (Wagner *et al.*, 2015). MICU mutants showed higher resting concentrations of free  $\text{Ca}^{2+}$  in the mitochondrial matrix, indicating MICUs involvement in  $\text{Ca}^{2+}$  homeostasis in the mitochondria, whilst no impact was seen on  $[\text{Ca}^{2+}]_{\text{cyt}}$  responses (Wagner *et al.*, 2015). Recently it has then been shown that the Mitochondrial Calcium Uniporter (MCU) was the component responsible for  $\text{Ca}^{2+}$ -permeability, named AtMCU1 in *Arabidopsis*, being regulated by MICU (Teardo *et al.*, 2017). MCU1 equally localizes to the mitochondrial membrane, and is highly expressed in root tissue (Teardo *et al.*, 2017).

The ‘slow vacuolar’  $\text{Ca}^{2+}$  channel is encoded by the *Two Pore Channel* gene (*TPC1*), with one member described in *Arabidopsis*, functioning as a homodimer (Peiter *et al.*, 2005; Guo *et al.*, 2016). TPC1 was shown to be voltage dependent and requires cytosolic  $\text{Ca}^{2+}$  for activation – the more cytosolic  $\text{Ca}^{2+}$ , the easier to activate (Guo *et al.*, 2016). As TPC1 shows low  $\text{Ca}^{2+}$  selectivity and ambiguous phenotypes, its function is still under debate as the protein knock-out led to few striking phenotypes considering its supposedly important role as tonoplast  $\text{Ca}^{2+}$  channel (Ranf *et al.*, 2008; Stael *et al.*, 2012; Swarbreck *et al.*, 2013). Nonetheless, TPC1 has been described to govern the propagation of ‘ $\text{Ca}^{2+}$  waves’ upon salt perception in roots of *Arabidopsis* (W.-G. Choi *et al.*, 2014; Evans *et al.*, 2016).

### 1.2.5 $\text{Ca}^{2+}$ storage on a cellular level

The vacuole is often considered the main  $\text{Ca}^{2+}$  intracellular store to sequester excess  $\text{Ca}^{2+}$  (Marschner, 2012; Stael *et al.*, 2012; Schönknecht, 2013; Costa, Navazio and Szabo, 2018). This assumption is based on the large volume vacuoles have compared to cytosol and other cellular organelles (up to 90 % of total cell volume, Costa, Navazio and Szabo, 2018); and high vacuolar  $\text{Ca}^{2+}$  concentrations measured in leaf tissue. For example, 12 mM free  $\text{Ca}^{2+}$  and up to 80 mM total  $\text{Ca}^{2+}$  were measured in *Arabidopsis* leaf vacuoles (Conn and Gilliam, 2010; Conn *et al.*, 2011). Interestingly, the few studies that quantified root vacuolar  $\text{Ca}^{2+}$  reported much lower accumulation of  $\text{Ca}^{2+}$  in vacuoles of

all root cell types, *e.g.* 1.5 mM free Ca<sup>2+</sup> in maize roots, 0.2 mM in roots of red beet (Felle, 1988; Pérez *et al.*, 2008). This is likely an effect of little Ca<sup>2+</sup> being taken up into the symplast of root cells, but Ca<sup>2+</sup> rather being transported *via* the transpiration stream into shoot tissue (also see section 1.2.1).

### 1.2.6 Ca<sup>2+</sup> as a signal transducer of abiotic and biotic stress signalling

Ca<sup>2+</sup> ions serve as second messengers which transduce a primary signalling event. The steep Ca<sup>2+</sup> gradient between cytosol and neighbouring apoplast and organelles sets the scene for the use of Ca<sup>2+</sup> as a signal: flux of comparably few ions are needed to evoke a large concentration difference in compartments of low [Ca<sup>2+</sup>], such as the cytosol. This movement of Ca<sup>2+</sup> needs to occur transiently, to avoid cytotoxicity. The modulation of intracellular Ca<sup>2+</sup> has been termed ‘Ca<sup>2+</sup> signature’, and can differ in duration, amplitude, frequency and spatial occurrence (Williamson and Ashley, 1982; Hetherington *et al.*, 1997; McAinsh and Pittman, 2009; Dodd *et al.*, 2010). Importantly, it is observed that specific Ca<sup>2+</sup> signatures are elicited in response to a multitude of biotic and abiotic stresses. It is deduced that the kinetics of the Ca<sup>2+</sup> transients encode information, which can be decoded intracellularly and translated into intracellular response. Hence, one type of signalling ion, Ca<sup>2+</sup>, can transduce different messages.

Modulation of [Ca<sup>2+</sup>]<sub>cyt</sub> has been described for many abiotic stresses, including mechanostimulation, salt, osmotic and drought stress, oxidative and wounding stress, temperature stress and perception of extracellular purine nucleotides (Knight *et al.*, 1991; Knight, Trewavas and Knight, 1996; Legué *et al.*, 1997; Demidchik *et al.*, 2003; Rentel and Knight, 2004; Monshausen *et al.*, 2009; Choi *et al.*, 2014; Storti *et al.*, 2018; for a review see Wilkins *et al.*, 2016). Oscillations of [Ca<sup>2+</sup>]<sub>cyt</sub> are tightly linked to circadian rhythms (Johnson *et al.*, 1995; Dodd *et al.*, 2006). A large body of work has uncovered the effect of abiotic and biotic stresses on [Ca<sup>2+</sup>]<sub>cyt</sub> transients and oscillations in guard cells, regulating stomatal aperture and as such temperature response or defence against pathogens (McAinsh and Pittman, 2009). See Chapter 3, section 3.1.1, for a more detailed introduction to rapid Ca<sup>2+</sup> signalling events upon perception of mechanostimulation, salt, osmotic and oxidative stress. See Chapter 4, section 4.1.2, for a more detailed introduction to Ca<sup>2+</sup>'s involvement in extracellular nucleotide signalling.

Perception of biotic signals equally involves early modulation in [Ca<sup>2+</sup>]. Both pathogen-induced immunity responses as well as establishment of symbiosis rely on similar, but

distinct initial signalling components: cell-surface receptors to perceive the specific biotic signalling molecules, and  $\text{Ca}^{2+}$  fluxes to transduce the stimuli (reviewed by Zipfel and Oldroyd, 2017). The focus has been on nuclear  $[\text{Ca}^{2+}]$  oscillations. As beneficial symbioses respectively lead to better nitrogen (N) and P nutrition of the plant, the signalling role of  $\text{Ca}^{2+}$  in these cases can be seen as indirectly involved in plant nutrition.

### 1.2.7 $\text{Ca}^{2+}$ as direct signal transducer in nutrient stress signalling

Besides  $\text{Ca}^{2+}$  involvement in mycorrhizal symbiosis and bacterial nodulation, it is only recently that a possible direct role of  $\text{Ca}^{2+}$  in nutrient stress signalling has been investigated, likely owing to its being technically challenging and nutrition being very complex (Wilkins *et al.*, 2016). Three scenarios of direct  $\text{Ca}^{2+}$  involvement are theoretically conceivable: (i) the use of  $\text{Ca}^{2+}$  to signal availability of a given nutrient, (ii) the use of  $\text{Ca}^{2+}$  to signal absence of a given nutrient, or (iii) alteration of the  $\text{Ca}^{2+}$  signature as a function of nutrient deficiency/toxicity and subsequent altered stress perception.

In the case of nitrate, starved *Arabidopsis* roots have been shown to respond through a monophasic transient increase of  $[\text{Ca}^{2+}]_{\text{cyt}}$  to a re-supply of nitrate, which was dependent on the nitrate transporter NRT1.1 (Riveras *et al.*, 2015). Another study using *Arabidopsis* mesophyll protoplasts found a more prolonged increase of  $[\text{Ca}^{2+}]_{\text{cyt}}$  upon nitrate re-addition, and an increased nuclear  $[\text{Ca}^{2+}]$  (Liu *et al.*, 2017).

Recently,  $\text{K}^+$  deficiency was found to trigger two distinct  $[\text{Ca}^{2+}]_{\text{cyt}}$  elevations within the *Arabidopsis* root, the first response occurring within 1 to 4 minutes, and the second response from 18 to 32 hours after onset of  $\text{K}^+$  deficiency (Behera *et al.*, 2017). The first increase may reflect the effect of lowering external  $\text{K}^+$  on epidermal PM potential, as this should hyperpolarize the voltage and promote  $\text{Ca}^{2+}$  influx. Indeed, hyperpolarizing PM potential of *Arabidopsis* root epidermal protoplasts by lowering external  $\text{K}^+$  supported higher  $[\text{Ca}^{2+}]_{\text{cyt}}$  (Demidchik *et al.*, 2002).

Magnesium ( $\text{Mg}^{2+}$ ) is - besides  $\text{Ca}^{2+}$  - the most abundant divalent cation in plants, and mostly described as having an antagonistic relationship with cellular  $\text{Ca}^{2+}$  (reviewed by Tang and Luan, 2017). Recently, it was found that  $[\text{Ca}^{2+}]_{\text{cyt}}$  signalling were necessary for vacuolar  $\text{Mg}^{2+}$  detoxification in a high  $\text{Mg}^{2+}$  environment (Tang *et al.*, 2015).

In the case of the microelement boron (B), a transient rise in  $[\text{Ca}^{2+}]_{\text{cyt}}$  in response to deprivation has yet to be reported (Gonzalez-Fontes *et al.*, 2014; Wilkins *et al.*, 2016).

However, in bean, B deprivation led to a release of membrane-bound  $\text{Ca}^{2+}$  into the apoplast within minutes, and B starvation-induced gene expression was reliant on external  $\text{Ca}^{2+}$  availability in tobacco, indicating some involvement of  $\text{Ca}^{2+}$  (Mühling *et al.*, 1998; Koshiba *et al.*, 2010). B deprivation led to an increase of baseline  $[\text{Ca}^{2+}]_{\text{cyt}}$  in *Arabidopsis*, however over the course of hours (reported for 6 and 24 h after onset of B-deprivation, Quiles-Pando *et al.*, 2013).

Microelements iron (Fe) and copper (Cu) have been reported to induce transient increases in  $[\text{Ca}^{2+}]_{\text{cyt}}$  of various dynamics in marine diatoms, marine algae and higher plants (Falciatore *et al.*, 2000; González *et al.*, 2010; Rodrigo-Moreno *et al.*, 2013). However, as both Fe and Cu play dual roles within metabolism – being essential for the functioning of a number of enzymes, but leading to production of oxidative stress if in excess – the increase of  $[\text{Ca}^{2+}]_{\text{cyt}}$  after addition of Fe or Cu might be due to oxidative stress rather than perception of nutrient availability (Richards *et al.*, 2015; Wilkins *et al.*, 2016). Intriguingly, a study using tobacco cell cultures, found that high (and physiologically toxic) Cu concentrations were found to elicit an increase in  $[\text{Ca}^{2+}]_{\text{cyt}}$  that was independent of ROS production but rather dependent on PM thiol groups (Inoue *et al.*, 2005).

### 1.2.8 Decoding of stress-specific $\text{Ca}^{2+}$ signatures

Stress perception triggers particular  $\text{Ca}^{2+}$  signatures, as well as changes in other signalling molecules, such as reactive oxygen species and lipid signalling molecules. Together, these molecules induce the stress response of plants (see Chapter 3 and Chapter 4 for more details on the interplay of various, stress-triggered signalling molecules). Differences in observed  $\text{Ca}^{2+}$  signatures have long been hypothesized to encode information, and evidence is accumulating that modulations in  $[\text{Ca}^{2+}]$  are sufficient and necessary to elicit specific downstream responses such as gene expression changes (Whalley *et al.*, 2011; Whalley and Knight, 2013; J. Liu *et al.*, 2015; Lenzoni *et al.*, 2017). However, the lag-time between the transient, often short-lived  $\text{Ca}^{2+}$  signature, and downstream responses such as transcriptional changes easily obscure causative relationships. Much progress has been made in recent years in both elucidating the vast array of gene families encoding  $\text{Ca}^{2+}$ -binding elements, as well as their interaction in decoding a  $\text{Ca}^{2+}$  signature into an appropriate response.

Perception of intracellular changes in  $[\text{Ca}^{2+}]$  is made possible by the ability of proteins to bind  $\text{Ca}^{2+}$  through  $\text{Ca}^{2+}$ -binding motifs, followed by a conformational change (McAinsh

and Pittman, 2009). Large numbers of genes have been annotated as capable of  $\text{Ca}^{2+}$ -binding, *i.e.* around two percent of all genes in *Arabidopsis* (Vaz Martins *et al.*, 2013).  $\text{Ca}^{2+}$ -dependent protein kinases (CDPKs) have been summarized as primary responders (Bender *et al.*, 2018; Costa *et al.*, 2018). Calmodulins (CaMs), calmodulin-like proteins (CMLs) and calcineurin B-like proteins (CBLs) are secondary signal relays (Lenzoni *et al.*, 2017; Bender *et al.*, 2018). Specificity is conceivable through variable binding affinity, location, plus the high number of potential interactions and binding complexes (Lenzoni *et al.*, 2017). Different  $\text{Ca}^{2+}$  signatures have been shown to regulate transcription *via* the induction of specific transcription factors (Whalley and Knight, 2013). For a particular group of transcription factors, the calmodulin-binding transcription activators (CAMTAs), mathematical modelling elucidated that  $\text{Ca}^{2+}$  increases, and binding to CaM and CAMTA non-linearly amplified the initial signal, indicating a complex and often counter-intuitive relationship (J. Liu *et al.*, 2015). Taking an immunity response as example, the number of  $\text{Ca}^{2+}$  binding sites of the CaMs involved, as well as the CaM-binding sites in downstream molecular elements such as the CAMTAs were shown to give rise to a high number of potential outcomes, together funnelling a specific  $\text{Ca}^{2+}$  signature into transcriptional changes relevant to the primary stress (Lenzoni *et al.*, 2017). Interestingly, the time needed to return to steady-state  $\text{Ca}^{2+}$  levels was found to be quantitatively relevant for the transcriptional response (Lenzoni *et al.*, 2017).

With regards to nutritional stress, a number of  $\text{Ca}^{2+}$  signal decoding protein networks have been described. For example, CDPK10, CDPK30 and CDPK32 were described as master regulators in the response to nitrate re-supply, activating a large number of transcription factors and thus amplifying the nitrate-induced  $\text{Ca}^{2+}$  cue (Liu *et al.*, 2017). High  $\text{Mg}^{2+}$  levels and subsequent detoxification of  $\text{Mg}^{2+}$  into the vacuole relied on  $\text{Ca}^{2+}$  binding to CBL2 and CBL3, and their interaction with four CBL-interacting protein kinases (CIPK; CIPK3, CIPK9, CIPK23, CIPK26; Tang *et al.*, 2015). Interestingly, CIPK23 has also been reported by multiple other studies to be involved in nutritional signalling: CIPK23 has been shown to activate the major root  $\text{K}^+$  transporter AKT1 in *Arabidopsis* and rice (Cheong *et al.*, 2007; Li *et al.*, 2014), as well as the high-affinity  $\text{K}^+$  transporter HAK5 (Ragel *et al.*, 2015). CIPK23 was found to inhibit ammonium transport (Straub *et al.*, 2017), whilst on the other hand converting the nitrate transporter NRT1.1 through phosphorylation from a low- to high-affinity transport system when nitrate was scarce (Ho *et al.*, 2009). Most recently, CIPK23 was found to phosphorylate the Fe transporter IRT1, inducing its self-degradation under metal toxic conditions (Dubeaux *et*



*al.*, 2018). Hence, CIPK23 is a central hub in integrating root responses to nutrient availability, and unveils complex and multi-functional signalling networks integrating nutrient status. Little evidence suggests  $\text{Ca}^{2+}$  decoders to signal in P nutrition. Through an *in silico* screen and experimental validation of candidate genes, knock-out of a similar network of CBL-CIPKs (CBL1, CIPK2, CIPK14) was recently found to act as negative regulators of growth under P starvation (Linn *et al.*, 2017). However, this was based on longer term growth studies rather than immediate ( $\text{Ca}^{2+}$ ) responses to an acute stress. Overall, the role of  $\text{Ca}^{2+}$ -signalling networks, including appropriate decoder proteins, likely plays a much larger role than has been investigated so far.

### 1.2.9 Quantification and visualization of $\text{Ca}^{2+}$ *in vivo* using genetically encoded reporters

Visualizing and quantifying the dynamics of  $\text{Ca}^{2+}$  ions *in planta* is challenging. Historically, this was first achieved through the use of microinjection and  $\text{Ca}^{2+}$ -specific dyes such as Quin2 and fura-2 (Tsien *et al.*, 1982; Grynkiewicz *et al.*, 1985). Even though ground-breaking, these set-ups were biased through invasive dye-loading procedures, low throughput, and artefacts introduced by the dyes themselves (Costa *et al.*, 2018). The use of genetically-encoded  $\text{Ca}^{2+}$  indicators (GECIs) has since revolutionised the  $\text{Ca}^{2+}$  field.  $\text{Ca}^{2+}$  dynamics can be monitored *in vivo* with high resolution and sensitivity, without much handling of the material, and – depending on the reporter protein – over long time courses. The GECIs differ in sensitivity and affinity for  $\text{Ca}^{2+}$ , as well as other characteristics such as pH-sensitivity and quantum yield, and can be expressed in different cell types or subcellular organelles. Together with modern imaging technology, single-cell analysis has become feasible (Costa *et al.*, 2013a). In the following, the three GECIs used in this thesis will be introduced, covering some of the major GECI types: aequorin, Yellow Cameleon 3.6 (YC3.6) and GCaMP3.

The most prominent  $\text{Ca}^{2+}$  reporter is aequorin, isolated originally from the bioluminescent jellyfish *Aequorea victoria* (Shimomura *et al.*, 1962; Shimomura, 1995). Once transformed cells express the (apo)aequorin protein, it can be reconstituted through exogenous application of its prosthetic group coelenterazine (Shimomura *et al.*, 1990; Knight *et al.*, 1991). Upon  $\text{Ca}^{2+}$  binding, the reconstituted protein undergoes a conformational change which leads to the production of luminescence. Photon emission measurements allow determination of free  $\text{Ca}^{2+}$  concentrations in cellular compartments (Knight *et al.*, 1991). Advantages of aequorin include its insensitivity to changes in pH,



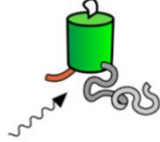

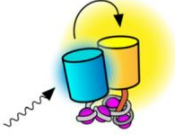
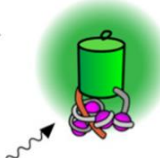
its high signal-to-noise ratio, and that no damaging illumination of the sample is necessary, thus samples can be measured for long time intervals (Brini, 2008; Marti *et al.*, 2013, also see Table 1). In *Arabidopsis*, aequorin has been targeted to various cellular compartments, such as the cytosol, tonoplast, nucleus, chloroplast and mitochondria (Knight *et al.*, 1991, 1996; Mehlmer *et al.*, 2012; Sello *et al.*, 2018); or specific tissues within the root and shoot (Kiegle *et al.*, 2000; Dodd *et al.*, 2006; Marti *et al.*, 2013). Aequorin has also been successfully transformed into other plant species such as *Physcomitrella patens*, tomato, wheat and rice (Moyen *et al.*, 1998; Nagel-Volkmann *et al.*, 2009; Finka *et al.*, 2012; Y. Zhang *et al.*, 2015).

One of the major drawbacks of aequorin is its low amount of emitted light, necessitating highly sensitive photon-counting equipment and complete occlusion of the sample. Hence, only low spatial resolution within the sampled tissue is possible, and emitted light is averaged over a cell population. Advances in the field of fluorescent ratiometric  $\text{Ca}^{2+}$  reporter proteins have enabled a higher spatial resolution, as signal read-out is not dependent on underlying amounts of reporter protein, but rather a ratio shift of the emitted signal output. One particular group, the cameleon proteins (for example Yellow Cameleon 3.6; YC3.6), are based on variants of the green fluorescent protein (GFP). These cameleons are Förster Resonance Energy Transfer (FRET)-based indicator proteins, consisting of a cyan and yellow fluorescent protein (CFP and YFP). These moieties are connected through a  $\text{Ca}^{2+}$ -binding calmodulin and the calmodulin-binding protein M13 (Miyawaki *et al.*, 1997; Nagai *et al.*, 2004).  $\text{Ca}^{2+}$  binding to calmodulin leads to a conformational change, which brings together the YFP and CFP. This decrease in distance allows energy to be transferred, *i.e.* in the scenario of CFP excitation, the binding of  $\text{Ca}^{2+}$  would decrease the distance between CFP and YFP, transferring energy onto YFP, and leading to an increase of YFP over CFP emission (Miyawaki *et al.*, 1997, see Table 1 for a schematic). Fluorescence microscopy allows for high spatial resolution, down to single-cell analysis (Costa and Kudla, 2015). As the signal read-out fully relies on ratio shift, these proteins are not hampered by actual protein expression levels of the cell, and are highly suitable for conditions where protein expression might be affected (Costa *et al.*, 2018). These cameleon sensors are available with different sensitivities for  $\text{Ca}^{2+}$  and can be expressed in different subcellular compartments such as the cytosol, nucleus, chloroplast and ER (Krebs *et al.*, 2012; Loro *et al.*, 2012, 2016; Bonza *et al.*, 2013; Costa *et al.*, 2017). Different plant species, such as rice and most recently the moss

*Physcomitrella patens*, have been successfully transformed with cameleon proteins (Behera *et al.*, 2015; Storti *et al.*, 2018).

Disadvantages of these ratiometric probes are the low throughput and the need for highly advanced microscopes (*e.g.* with beam splitter to separate YFP and CFP emission). Fluorescent probes for simple microscopy set-ups, *i.e.* based on single wavelength emission only, have more recently been designed and are available as plant-compatible constructs such as the GCaMP3 series (Tian *et al.*, 2009; Vincent *et al.*, 2017). GCaMP3 is based on a single permuted green fluorescent protein (cpGFP), and fluorescence intensity increases upon binding to  $\text{Ca}^{2+}$  and is used as direct read-out (see Table 1).

**Table 1:** Details of the genetically encoded  $\text{Ca}^{2+}$ -sensors used in this thesis. Cartoons were modified after P. Koldenkova and Nagai (2013). Pink dots represent bound  $\text{Ca}^{2+}$ , arrows indicate excitation light. The  $\text{Ca}^{2+}$ -bound states are in all reporter constructs reversible. References: Kendall *et al.*, 1992; Brini *et al.*, 1995; Nagai *et al.*, 2004; Tian *et al.*, 2009; Akerboom *et al.*, 2012; Krebs *et al.*, 2012.

	<b>Aequorin</b>	<b>YC3.6</b>	<b>GCaMP3</b>
<b>Reporter type</b>	bioluminescent	ratiometric	intensiometric
<b>Excitation / Emission [nm]</b>	noEx / Em 465	Ex 440 / Em 480/530	Ex 488 / Em 515
<b><i>In vitro</i> <math>K_D</math> for <math>\text{Ca}^{2+}</math></b>	7.2 -13 $\mu\text{M}$	250 nM	405 - 660 nM
<b>References</b>	Kendall <i>et al.</i> , 1992,; Brini <i>et al.</i> , 1995	Nagai <i>et al.</i> , 2004; Krebs <i>et al.</i> , 2012	Tian <i>et al.</i> , 2009; Akerboom <i>et al.</i> , 2012
<b><math>\text{Ca}^{2+}</math> not bound</b>			
<b><math>\text{Ca}^{2+}</math> bound</b>			

### 1.3 The relationship of phosphate and calcium

Recent years have seen major advances in the two fields of  $\text{Ca}^{2+}$  signalling and P starvation research. Molecular players in response to P starvation have been elucidated in plants, with signalling networks being formed by hormones, other nutrients and transcriptional and translational feedback loops. Similarly,  $\text{Ca}^{2+}$  signalling research has been resolved to single-cell level using a palette of GECIs as  $\text{Ca}^{2+}$  reporters and superior imaging techniques. However, the two fields have not yet been directly connected.  $\text{Ca}^{2+}$  has been hypothesized to signal in P starvation responses (Chiou and Lin, 2011; Chien *et al.*, 2018), but few studies have made connections between P nutrition and  $\text{Ca}^{2+}$  signalling.

Some P-starvation studies reported  $\text{Ca}^{2+}$ -associated proteins to be differentially expressed. For example, P-starved *Brachypodium distachyon* showed up-regulated expression of a few CDPKs amongst a number of other kinases (Zhao *et al.*, 2018), hence there is no dominant ' $\text{Ca}^{2+}$  fingerprint'. In tomato roots, a  $\text{Ca}^{2+}$ -ATPase was found to be highly upregulated under P starvation (Muchhal *et al.*, 1997). Intracellular  $\text{Ca}^{2+}$  levels were not quantified, but membrane damage and leakage were reasoned to trigger higher  $[\text{Ca}^{2+}]_{\text{cyt}}$  influx and thus higher  $\text{Ca}^{2+}$ -ATPase activity (Muchhal *et al.*, 1997). One of the most direct links between  $\text{Ca}^{2+}$  and P homeostasis was described for vacuolar  $\text{Ca}^{2+}/\text{H}^{+}$  transporter knock-out mutants, *cax1* and *cax3* in *Arabidopsis* (Liu *et al.*, 2011). The mutant lines took up more P, and had subsequent higher P content in leaves, suggesting a role of the  $\text{Ca}^{2+}/\text{H}^{+}$  transport system in P homeostasis (Liu *et al.*, 2011). For the unconventional  $\text{Ca}^{2+}$  channel proteins of the annexin family, ANNEXIN 1 was found to be the protein of highest abundance in P-starved roots (Lan *et al.*, 2012). This was recently corroborated by another study quantifying proteomic response in whole seedlings of *Arabidopsis*, and reporting higher abundance of ANNEXIN1, 2 and 4 (Z. Q. Wang *et al.*, 2018).

P and  $\text{Ca}^{2+}$  have an exceptional relationship, as they easily form tight complexes. Calcium phosphate (Ca-P) complexation occurs in neutral to alkaline soils, and similar complexation would occur in cells at physiological pH (Cole, 1953; Edel and Kudla, 2015; Verkhatsky and Parpura, 2015). Therefore, early during the evolution of life, a sophisticated machinery of  $\text{Ca}^{2+}$  regulating transport and buffer proteins evolved to maintain low cytosolic free  $\text{Ca}^{2+}$  levels, giving rise to the use of  $\text{Ca}^{2+}$  as a signalling ion (Verkhatsky and Parpura, 2015). Plants struggle to accumulate P in necessary amounts

to sustain metabolism. To avoid precipitation of precious P with  $\text{Ca}^{2+}$ ,  $\text{Ca}^{2+}$  follows different uptake dynamics and is stored in different tissue compared to P (see Figure 2).

### 1.3.1 Calcium phosphates were recently also described in plants

Through consumption of primary P-accumulators (plants), animals can afford to ‘spend’ more P, and use the benefits arising from stable Ca-P complexes. Bones and teeth are composed mainly of Ca-Ps, in the case of humans representing 99 % of total body  $\text{Ca}^{2+}$  (Plattner and Verkhatsky, 2015). However, animals employ a complex endocrine system to regulate blood  $\text{Ca}^{2+}$  and P levels and subsequent bone formation which only exists in vertebrates, and thus little can be learnt about the regulation of Ca-Ps in plants (Bouillon and Suda, 2014).

Compared to animal Ca-P skeletons, algae evolved carbonate biomineralization whilst in some vascular plants, such as grasses, epidermal cells became stabilized by silica-based minerals (Knoll, 2003). Only recently, the first report of Ca-Ps in higher plants was reported (Ensikat *et al.*, 2016). Trichomes of the South-American rock nettle family *Loasaceae* were found to contain Ca-Ps as structural fortification (Ensikat *et al.*, 2016). Since then, Ca-Ps were similarly found in the trichomes of a diverse range of higher plant species of the order Malpighiales, Rosales, Boraginales, and Brassicales – including *Arabidopsis* (Weigend *et al.*, 2017; Mustafa *et al.*, 2018). Ca-Ps were found to replace or co-localize with silica in trichome tips and cell walls, indicating biomineralization patterns to be more complex than so far assumed. To date, no mechanism is known that guides and regulates Ca-P formation in plants.

## 1.4 Working hypothesis and experimental approaches

The involvement of the second messenger  $\text{Ca}^{2+}$  in signalling nutrient availability and deficiency has been partially elucidated. However, to date no study has apparently investigated its involvement in signalling under P starvation conditions. In light of the particular relationship of  $\text{Ca}^{2+}$  and P, this PhD thesis investigates the following hypothesis:

In plants, P starvation changes the use of  $\text{Ca}^{2+}$  as signalling ion.

The overall aim of this PhD thesis was to test if and how the use of cytosolic free  $\text{Ca}^{2+}$  ( $[\text{Ca}^{2+}]_{\text{cyt}}$ ) were altered in P-starved roots of the model plant *Arabidopsis thaliana*, and subsequently dissect the underlying molecular components.

To this end, genetically encoded reporters of  $[\text{Ca}^{2+}]_{\text{cyt}}$  (aequorin, NES-YC3.6, GCaMP3) were employed to quantify the  $[\text{Ca}^{2+}]_{\text{cyt}}$  response of P-starved roots to a range of abiotic stresses (mechanical stimulation, salt, osmotic and oxidative stress), extracellular nucleotides and a P source. As a test for specificity, N-starved roots were challenged with similar stresses. Iron and copper availability in P starvation conditions were tested for involvement in modulating the stress-induced  $[\text{Ca}^{2+}]_{\text{cyt}}$  responses, as well as employing receptor and  $\text{Ca}^{2+}$  channel mutants to test for their involvement in shaping the  $[\text{Ca}^{2+}]_{\text{cyt}}$  responses under P starvation.

Provided that  $[\text{Ca}^{2+}]_{\text{cyt}}$  responses were altered as a consequence of P starvation, the underlying molecular components of an exemplary treatment, *i.e.* extracellular ATP, would be dissected. Pharmacological treatments, physical manipulation, and histological staining of stress markers would delineate the components of a root  $[\text{Ca}^{2+}]_{\text{cyt}}$  response, and determine how these are altered under P starvation. To further identify the genetic basis of  $\text{Ca}^{2+}$  channels involved in root growth particularly under P starvation conditions, such as root hair elongation, a collection of putative  $\text{Ca}^{2+}$  channel mutants in *Arabidopsis* was compiled, and this mutant library was screened for a P starvation-induced root hair phenotype.

Taken together, this work will elucidate how P starvation influences the use of  $\text{Ca}^{2+}$  as signalling ion, and more generally enhance our understanding of how nutrition affects the root signalling landscape.

## 2 MATERIAL AND METHODS

### 2.1 Plant material

All *Arabidopsis thaliana* (from here on, *Arabidopsis*) lines were in the Col-0 ecotype background unless otherwise stated and transformed with (apo)aequorin as a cytosolic free calcium ( $[Ca^{2+}]_{\text{cyt}}$ ) reporter where indicated. Transformations had been performed previously by laboratory members such that (apo)aequorin was constitutively expressed under the 35S-CaMV promoter (Knight *et al.*, 1991). Lines at the T3 generation or onwards were used. If not indicated otherwise, all seed material used was from laboratory stock and had been genotyped previously. Lines expressing the ratiometric cameleon sensor in the cytosol and under control of the *UBIQUITIN10* promoter (NES-YC3.6, Krebs *et al.*, 2012) were a gift from Alex Costa's group (University of Milan). Lines expressing the intensimetric 35S::GCaMP3 construct in the cytosol (Tian *et al.*, 2009) were a gift from Dale Sanders' group (John Innes Centre, Norwich).

*Arabidopsis* containing stably transformed green fluorescent protein (GFP)-tagged *ANNEXIN1* constructs were previously generated by Siân Richards (University of Cambridge). In the first, GFP was fused to a long version (2 kilo bases upstream of the coding region) promoter of *ANN1* ( $LP_{ANN1}::sGFP$ ), to visualize gene expression of *ANN1*. In the second, GFP was fused to the same *ANN1* promoter as well as the coding region of *ANN1* ( $LP_{ANN1}::ANN1-sGFP$ ), designed to visualize localization of ANN1 protein. Both constructs were transformed in *ann1* mutant lines of Col-0 background.

A library of putative calcium channel mutants was compiled (see Appendix I for complete list of mutant lines, including their bioinformatics annotations; see Appendix II for details

of origin of seed stock). In total, 100 mutant lines were sourced from the Nottingham *Arabidopsis* Stock Centre (NASC), other laboratories and own laboratory stock. Mutagenized lines were derived from SALK T-DNA library (Alonso *et al.*, 2003), SAIL T-DNA library (Syngenta *Arabidopsis* Insertion Library), GABI-Kat library (Kleinboelting *et al.*, 2012), WiscDsLox T-DNA library (Woody *et al.*, 2007), T-DNA-tag library (Kazusa DNA Research Institute), TILLING mutant library (Till *et al.*, 2003), Agrikola RNAi library (Hilson *et al.*, 2004), ethyl methane sulfonate (EMS) mutagenized *Arabidopsis* population (Yu *et al.*, 1998). Out of 100 received mutant lines, 74 single mutants and 3 higher order mutants could be employed for root hair growth analysis (as they were genotyped homozygous for the mutation, germinated well and set seeds).

## 2.2 Plant growth conditions

### 2.2.1 General propagation conditions

All plant material was propagated in the Plant Growth Facilities (PGF) of the Plant Sciences Department, University of Cambridge. Plants were grown on Levington's F2 compost, containing the systemic insecticide imidacloprid (Fargro Limited). *Arabidopsis* plants were grown until seed maturity under long-day conditions (16 h light / 8 h dark) in a growth room (200  $\mu\text{mol m}^{-2} \text{s}^{-1}$  light intensity, 20°C, 60 % relative humidity).

### 2.2.2 General sterile growth conditions

*Arabidopsis* seeds were surface sterilized by rinsing briefly with 70 % (v/v) ethanol, then sterile distilled water, shaking for 5 minutes in sterilizing solution (10 % (v/v) sodium hypochlorite solution (Fisher Chemicals), 0.01 % (v/v) Triton X-100 (Sigma-Aldrich)), and then rinsed five times using sterile distilled water.

### 2.2.3 Plant growth on Murashige and Skoog growth medium

Standard half strength Murashige and Skoog growth medium with vitamins (Duchefa), 'half MS', contained: 9.4 mM KNO<sub>3</sub>, 0.75 mM MgSO<sub>4</sub>, 1.5 mM CaCl<sub>2</sub>, 10.3 mM NH<sub>4</sub>NO<sub>3</sub>, 0.625 mM KH<sub>2</sub>PO<sub>4</sub>, 0.055  $\mu\text{M}$  CoCl<sub>2</sub>, 0.05  $\mu\text{M}$  CuSO<sub>4</sub>, 50  $\mu\text{M}$  H<sub>3</sub>BO<sub>3</sub>, 2.5  $\mu\text{M}$  KI, 50  $\mu\text{M}$  MnSO<sub>4</sub>, 0.52  $\mu\text{M}$  Na<sub>2</sub>MoO<sub>4</sub>, 15  $\mu\text{M}$  ZnSO<sub>4</sub>, 50  $\mu\text{M}$  FeNaEDTA, vitamins: 13.3  $\mu\text{M}$  glycine, 277.5  $\mu\text{M}$  myo-inositol, 2  $\mu\text{M}$  nicotinic acid, 1.2  $\mu\text{M}$  pyridoxine HCl,



0.15  $\mu\text{M}$  thiamine HCl. This standard half MS comprised the full phosphate, ‘full P’, and full nitrogen, ‘full N’, growth condition. A custom-made MS medium without P was used for ‘zero P’ conditions (Duchefa, DU1072) or without N for ‘zero N’ conditions (PhytoTechnology Laboratories, M531). KCl was used to substitute for missing potassium ( $\text{K}^+$ ) whenever P ( $\text{KH}_2\text{PO}_4$ ) or N ( $\text{KNO}_3$ ) were excluded (Table 2). As the N-free medium was not available including vitamins, MS vitamin x 1000 stock solution (Sigma-Aldrich, M7150) was added to ‘zero N’ medium to the same final concentration as described above. For all growth conditions requiring modified iron (Fe) or copper (Cu) content, half MS medium was prepared from stock solutions and vitamins were supplied from the MS vitamin x 1000 stock (Table 2).

*Arabidopsis* seeds were sown aseptically and grown vertically on medium in square petri dishes (12 cm x 12 cm, Greiner Bio-One), with 12 seeds per plate. In general, each plate contained *circa* 100 ml of half MS, with varying P / N / Fe / Cu as stated in the individual experiments. Medium was prepared using distilled water, without sucrose addition. The pH of the media was adjusted to pH 5.6 using dilute KOH / HCl, before 0.8 % (w/v) agar (Bacto agar, BD Biosciences) was added and the medium was autoclaved. Plates were dried for 55 – 60 min under sterile air to ensure equal humidity. Plates were sealed using micropore tape (3M) to allow for gas exchange. All seeds were stratified at 4°C and in darkness for 2 to 3 days prior to cultivation under long-day conditions (16 h light / 8 h dark) in a growth chamber with 78  $\mu\text{mol m}^{-2} \text{s}^{-1}$  light intensity, at 23°C (PERCIVAL, CLF Plant Climatics).

The nomenclature used in this thesis, *e.g.* ‘zero P’ and ‘zero N’, reflects the nutrient content of the growth medium rather than the nutrients available to the plant, as all seeds would have nutrients stored. Further, the agar used introduced mineral traces (BD Bacto agar typical analysis: P < 0.005 %, nitrate < 0.005 %, Fe 0.002 %, Cu < 0.001 %; Difco™ & BBL™ Manual, 2<sup>nd</sup> Edition). The programme Geochem EZ (Shaff *et al.*, 2010) was employed to calculate the ion activities in the nutrient solutions used, and determine possible complexations (also see Chapter 3, section 3.2.13 onwards).

**Table 2:** Nutrient modifications of half MS medium relevant for particular deficiency growth condition. ‘Label’ includes names used in different experimental chapters (separated by dash). KCl was added to substitute for missing potassium.

Growth condition	Label	P [mM]	N [mM]	KCl [mM]	Fe [ $\mu$ M]	Cu [ $\mu$ M]
Control/ no deficiency	full P / full N / full P_full Fe	0.625	19.7	0	50	0.05
P deficiency	zero P / zero P_full Fe / zero P_full Cu	0	19.7	0.625	50	0.05
	medium P	0.1	19.7	0.525	50	0.05
N deficiency	zero N	0.625	0	9.4	50	0.05
P / Fe deficiency	full P_zero Fe	0.625	19.7	0	0	0.05
	full free P_full free Fe	0.626	19.7	0	55.35	0.05
	full P_excess Fe	0.625	19.7	0	100	0.05
	zero P_zero Fe	0	19.7	0.625	0	0.05
	zero P_low Fe	0	19.7	0.625	10	0.05
	zero P_excess Fe	0	19.7	0.625	100	0.05
P / Cu deficiency	zero P_zero Cu	0	19.7	0.625	50	0

## 2.2.4 Transfer experiments

For transfer experiments, *Arabidopsis* plants expressing (apo)aequorin were grown as described in section 2.2.3 on sterile half MS agar plates. After eight days of growth, seedlings were aseptically transferred using ethanol-cleaned forceps to: (i) Plates containing the same growth condition (*e.g.*, full P to full P = transfer control); (ii) plates containing the opposite growth condition (*e.g.*, full P to zero P) or; (iii) not transferred (= no transfer control). Plants were then grown further in standard growth cabinet conditions. Plants were used for cytosolic free calcium measurements on day 11 as described in section 2.6.

## 2.2.5 Growth conditions for root hair screen

To screen *Arabidopsis* mutants for a root hair phenotype, different growth conditions were trialled based on growth conditions found in the literature (see Appendix III for more details). To aid microscopy, the use of Phytigel as a gelling agent proved requisite. Therefore, the composition of the growth medium had to be adjusted, and the following protocol was used (adapted after Bates and Lynch, 1996; Datta, Prescott and Dolan, 2015). *Arabidopsis* seeds, pooled from multiple plants of the same genotype, were sown

aseptically and grown vertically on medium in square petri dishes (12 cm x 12 cm, Greiner Bio-One), with 4 seeds per genotype per plate (12 seeds per plate in total). The growth medium was half strength Johnson medium ('half Johnson'), containing 3 mM KNO<sub>3</sub>, 0.5 mM MgSO<sub>4</sub>, 2 mM Ca(NO<sub>3</sub>)<sub>2</sub>, 25 µM KCl, 12.5 µM H<sub>3</sub>BO<sub>3</sub>, 1 µM MnSO<sub>4</sub>, 1 µM ZnSO<sub>4</sub>, 0.25 µM CuSO<sub>4</sub>, 0.25 µM (NH<sub>4</sub>)<sub>6</sub>Mo<sub>7</sub>O<sub>24</sub>, 25 µM FeEDTA, 1 % (w/v) sucrose, 2.5 mM MES. This was adjusted to pH 5.7 using KOH, before 0.5 % (w/v) Phytigel (Sigma-Aldrich) was added and the medium was autoclaved. The 'full P' condition of half Johnson medium contained 1 mM NH<sub>4</sub>H<sub>2</sub>PO<sub>4</sub>. The 'zero P' condition of half Johnson medium contained 0 mM P, and 1 mM (NH<sub>4</sub>)<sub>2</sub>SO<sub>4</sub> was added to substitute for missing N.

### 2.3 Root system architecture quantification and image analysis

To determine primary root (PR) length, number and length of lateral roots (LR), plants grown vertically on plates were scanned using a Perfection V300 Photo scanner (Epson) with 300 dots per inch (dpi) resolution, saving the images in .tiff format. The software ImageJ (Abràmoff *et al.*, 2004) and plugin NeuronJ (Meijering *et al.*, 2004) were used to trace root length.

To measure root hair length and density, 6-day old plants were imaged on a stereo microscope M165FC (Leica), capturing the first cm of the root tip. Plants grown on the edge of the plate were not considered for analysis. Images were saved in .tiff format. Using the Grid plugin in ImageJ, the images were divided into 1 mm segments. Using the NeuronJ plugin, root hair length was quantified by measuring the 10 longest, fully expanded root hairs within a 1 mm segment, 4-5 mm away from the root tip, with 5 root hairs on either side. Root hair density was determined by counting all root hairs with clear tips within the same 1 mm segment (Bates and Lynch, 1996; Yi *et al.*, 2010; Stetter *et al.*, 2015).

### 2.4 Extracellular ATP quantification

To determine extracellular ATP accumulated by roots (eATP), 11-day old *Arabidopsis* Col-0 seedlings (grown as described in section 2.2.3) were tested in sterile, 6-well plates (Corning Costar, Sigma-Aldrich) containing 1 ml of autoclaved liquid half MS, containing full or zero P to maintain prior growth conditions of the seedlings, pH adjusted to 5.6 using Tris / MES, and tilted at 30° from the horizontal. Per well, the roots of 4

seedlings were submerged into the medium, whilst the shoots stood upright into the air. Without touching the roots, a sample (100  $\mu$ l) of the medium surrounding the roots was taken immediately after transfer of the seedlings. Seedlings were left in light and at room temperature for 1 hour, before the next medium sample (at 60 minutes) was taken. All samples were flash frozen in  $N_{liq}$  and stored at  $-80^{\circ}C$  until quantification. ATP concentration in the roots' bathing medium was determined using the ATP Determination Kit (Life Technologies) following the standard protocol. The assay is based on the enzyme luciferase's requirement for ATP in producing light. The resulting luminescence was detected using the plate reader FLUOstar OPTIMA (BMG Labtech). Each sample was measured in 2 technical replicates. Fresh weight of the roots was recorded after drying them quickly on filter paper and separating roots from shoots.

## 2.5 Confocal microscopy using *ANN1*-GFP lines

*Arabidopsis* lines expressing the  $LP_{ANN1}::sGFP$  or  $LP_{ANN1}::ANN1-sGFP$  were grown on half MS medium containing full or zero P (as described in section 2.2.2 and 2.2.3). Roots of 10-day old seedlings were placed between microscopy slides (2.5 cm x 7.5 cm) and cover glass (22 x 50 mm), in a drop of control solution (autoclaved liquid half MS medium including vitamins and 1.175 mM MES (Sigma), pH adjusted to pH 5.6 using Tris base (Sigma), and maintaining prior growth condition, *i.e.* full or zero P levels). Root tips were imaged on a Leica SP5 DM6000B confocal microscope, using a x 10 (HC PL APO 10x / 0.4 CS) or x 20 objective (HC PL APO 20x / 0.7). GFP was excited at 488 nm using an argon laser, set to 30 % laser power. GFP fluorescence emission was measured at 502 to 540 nm. Throughout the experiments the settings were kept constant (pinhole: 101.35  $\mu$ m, gain set to 652 (for x 10 objective) or 690 (for x 20 objective), line average set to 8, and speed of scanning to 400 Hz). Bright field images were also taken of every imaged root section.

## 2.6 Root $[Ca^{2+}]_{cyt}$ measurements by aequorin luminescence

### 2.6.1 Sample preparation and coelenterazine incubation

Excised whole roots or root tips (1 cm) of Col-0 seedlings expressing the cytosolic free  $Ca^{2+}$  reporter protein (apo)aequorin were used (Knight *et al.*, 1991). If not otherwise stated, the plate reader was used for luminescence quantification for which sample tissue

was prepared as follows. Excised whole roots or root tips of 10-day old seedlings were incubated in 100  $\mu$ l incubation medium containing 10  $\mu$ M coelenterazine (NanoLight Technology) overnight, in darkness and at room temperature, with one leaf or root or root tip being placed per well in white 96-well plates (Greiner Bio-One), covered tightly with aluminium foil. Tissue was assayed on day 11. The coelenterazine incubation medium comprised autoclaved liquid half MS medium including vitamins and the same nutrient concentrations (*i.e.*, varying P / N / Fe / Cu concentrations) as the plants were grown on. This was to maintain prior growth conditions during the whole assay. The incubation medium further contained 1.175 mM MES (Sigma), the pH was set to 5.6 using Tris base (Sigma) solution. Coelenterazine aliquots were dissolved in methanol before being carried over into the incubation medium. The final methanol concentration was 0.2 % (v/v) methanol. All work involving coelenterazine was carried out in green light.

For luminometer experiments (stated in corresponding experiments), sample tissue was prepared as described above, with the adjustments of using whole seedlings, placed into 3.5 ml tubes (55 mm x 12 mm, Sarstedt) containing 500  $\mu$ l of 10  $\mu$ M coelenterazine (NanoLight Technology) in incubation medium. On the morning of the assay (day 11), coelenterazine containing solution was replaced with 500  $\mu$ l fresh incubation medium (without coelenterazine, maintaining full and zero P growth conditions). Samples were left to acclimatize after the washing step for 30 to 45 minutes before starting the assay.

### 2.6.2 Luminescence quantification using a plate reader

After overnight incubation, the plate containing root tissue was uncovered and inserted into a bioluminescence plate reader (FLUOstar OPTIMA, BMG Labtech). Per well, luminescence was recorded every second for 200 seconds. Baseline luminescence was recorded for 35 seconds, before injecting 100  $\mu$ l of different treatment solutions (see section 2.6.4) with an injection speed of 150  $\mu$ l / second. Changes in luminescence signal were monitored for 120 seconds, before injecting 100  $\mu$ l discharge solution (final concentration: 10 % (v/v) ethanol, 1 M CaCl<sub>2</sub>) and monitoring for a further 45 seconds. The gain of the plate reader was adjusted to render the photon counting detector as sensitive as possible, without saturating it. Gain settings were kept constant between corresponding experiments. As the relationship between luminescence and Ca<sup>2+</sup> concentration is temperature dependent, the plate reader was set to constant 25°C (Knight

*et al.*, 1997). For a time course of  $n$  time points, cytosolic free  $\text{Ca}^{2+}$  concentrations were calculated according to the following formula

$$-\log[\text{Ca}^{2+}]_{\text{cyt}} = a \times \left[ -\log\left(\frac{L_c}{L_t}\right) \right] + b$$

with  $L_c$  = luminescence count per second at time point  $n$  (background luminescence subtracted);  $L_t$  = total luminescence counts;  $a = 0.3326$ ;  $b = 5.559$  (Knight *et al.*, 1997).

### 2.6.3 Luminescence quantification using a luminometer

For longer time-course and higher sensitivity luminescence measurements, a photon-counting luminometer (photomultiplier tube 9899A) was employed to quantify aequorin-derived luminescence (stated in corresponding experiments). The luminometer was cooled to  $-20^\circ\text{C}$  with a FACT50 housing (Electron Tubes), and controlled using the EV6 Counter/Timer Software. Tubes containing whole, coelenterazine-reconstituted seedlings were placed into the holder, and left to acclimatize from handling for *circa* 5 minutes, or until baseline luminescence was stable. Luminescence was recorded every second for in total 1100 seconds. Baseline luminescence was recorded for at least 150 seconds, before manual treatment applications (500  $\mu\text{l}$ ) were performed using a 1-ml light-tight syringe (Terumo), attached to a luer needle (26 g x 75 mm). Changes in luminescence signal were monitored for 850 seconds, before 500  $\mu\text{l}$  of discharge solution was injected (final concentration: 10 % (v/v) ethanol, 1 M  $\text{CaCl}_2$ ) and monitoring for a further 100 seconds. Cytosolic free  $\text{Ca}^{2+}$  concentrations were determined as described in section 2.6.2.

### 2.6.4 Abiotic stress treatments

Coelenterazine-reconstituted, (apo)aequorin-expressing roots of *Arabidopsis* were challenged with a variety of abiotic stresses. Treatment solutions comprised autoclaved liquid half MS medium corresponding to prior growth conditions, to maintain the same nutrient conditions throughout the assay (from here on referred to as ‘control solution’, and essentially the same as the liquid medium used for incubation, see section 2.6.1, but excluding coelenterazine). The liquid medium further contained 1.175 mM MES (Sigma), pH was set to 5.6 using Tris base solution (Sigma). Application of this control solution was further used as a control treatment for mechanical stimulation induced by application of any of the treatment solutions described below.

On the plate reader, test treatments were applied in varying concentrations containing: Adenosine 5'-triphosphate disodium salt trihydrate (ATP, Melford); adenosine 5'-diphosphate disodium salt dehydrate (ADP, Melford); non-hydrolyzable ATP-analogue adenosine 5'-[ $\gamma$ -thio]triphosphate tetralithium salt ( $\gamma$ -ATP, Sigma); phosphoric acid (Thermo Fisher); NaCl (Thermo Fisher); osmotic control for NaCl treatments, D-sorbitol (Sigma-Aldrich); hydrogen peroxide ( $H_2O_2$ , Sigma). The accompanying ions ( $Na^+$  for ATP and ADP;  $Li^+$  for  $\gamma$ -ATP) were previously shown in our laboratory not to confound the response (Demidchik *et al.*, 2009). Test treatments were prepared at double strength, as in the well, a 1:2 dilution led to the desired final concentration of the treatment. On the plate reader, treatment volume was 100  $\mu$ l, applied with a pump speed of 150  $\mu$ l / second. A Vapro5520 osmometer (Wescor) was used to measure the osmolality of the NaCl and D-sorbitol treatment solutions.

For the luminometer, test treatments applied were a high P-source (5 mM  $KH_2PO_4$ , in control solution background) or a solution containing equivalent  $[K^+]$  to control for any  $K^+$  applied with  $KH_2PO_4$  (5 mM KCl, in control solution background).

### 2.6.5 Pharmacological inhibitor treatments

Coelenterazine-reconstituted, (apo)aequorin-expressing roots of *Arabidopsis* were pre-incubated with either diphenyleneiodonium chloride (DPI, Merck / Calbiochem), or 1,4 – dithiothreitol (DTT, Life Technologies). DPI is a cell membrane-permeable, irreversible inhibitor of NADPH-Oxidases (Bolwell and Wojtaszek 1997). Powdered DPI was dissolved in dimethyl sulfoxide (DMSO) for a stock solution, further diluted in control solution background (see section 2.6.4) to a final concentration of 100  $\mu$ M (final DMSO content: 0.63 % (v/v)) and used to pre-incubate root tissue for 30 minutes. Control roots were incubated in an equal DMSO concentration, without DPI. After 30 minutes, DPI / DMSO was washed off, and root tissue re-suspended in control solution before conducting the assay as described in section 2.6.2.

DTT is known as a potent reducing agent, maintaining accessible protein thiol groups in reduced states (Carmack 1968, Demidchik 2009). Powdered DTT was dissolved in sterile distilled water for a 100 mM stock solution, further diluted in control solution background (see section 2.6.4) to a final concentration of 2 mM and used to pre-incubate root tissue for 30 minutes. DTT was kept in the well during the assay.

Root tissue pre-treated with DPI or DTT were challenged with ATP treatment (or corresponding control solution background) only.

## 2.7 Root $[Ca^{2+}]_{cyt}$ measurements by ratiometric YC3.6 reporter

### 2.7.1 Sample preparation and superfusion set-up

Förster resonance energy transfer (FRET) microscopy was carried out in the laboratory of Alex Costa, University of Milan, Italy. Ten-day old *Arabidopsis* seedlings, grown on half MS (0.8 % bactoagar, pH 5.6, no sucrose) and expressing a cytosolic cameleon sensor (NES-YC3.6; Krebs *et al.*, 2012) were mounted into a custom-built superfusion chamber (Behera and Kudla, 2013), stabilized with wetted cotton wool and continuously superfused with imaging solution (IS; 5mM KCl, 10 mM CaCl<sub>2</sub>, 10 mM MES, set to pH 5.8 using Tris) using an EconoPump system (BioRad) with a tube diameter of 0.8 mm and a speed of 0.9 ml / minute. The shoots were not submerged but propped onto the cotton wool. Seedlings were left to acclimatize to constant superfusion for 10 - 15 minutes, before starting the experiment.

### 2.7.2 Inverted fluorescence microscopy

NES-YC3.6-expressing plants were imaged using a Ti-E widefield inverted fluorescence microscope (Nikon) with a Nikon Plan Fluor 4x 0.13 dry objective. The samples were excited at 440 nm using a Prior Lumen 200 PRO fluorescent light source (Prior Scientific). Images were collected with an ORCA-D2 Dual CCD camera (Hamamatsu). Exposure time was 250 ms with 4 x 4 binning. Images were acquired every five seconds for up to 30 minutes. The software NIS Elements AR 4.0 (Nikon) was used to control the microscope, light source and camera.

### 2.7.3 Stress treatment

Upon the start of an experiment, seedlings were imaged for two minutes whilst superfusing IS. Stress treatment (1 mM ATP, in IS background) was then superfused through the system for three minutes before changing back to IS without ATP.



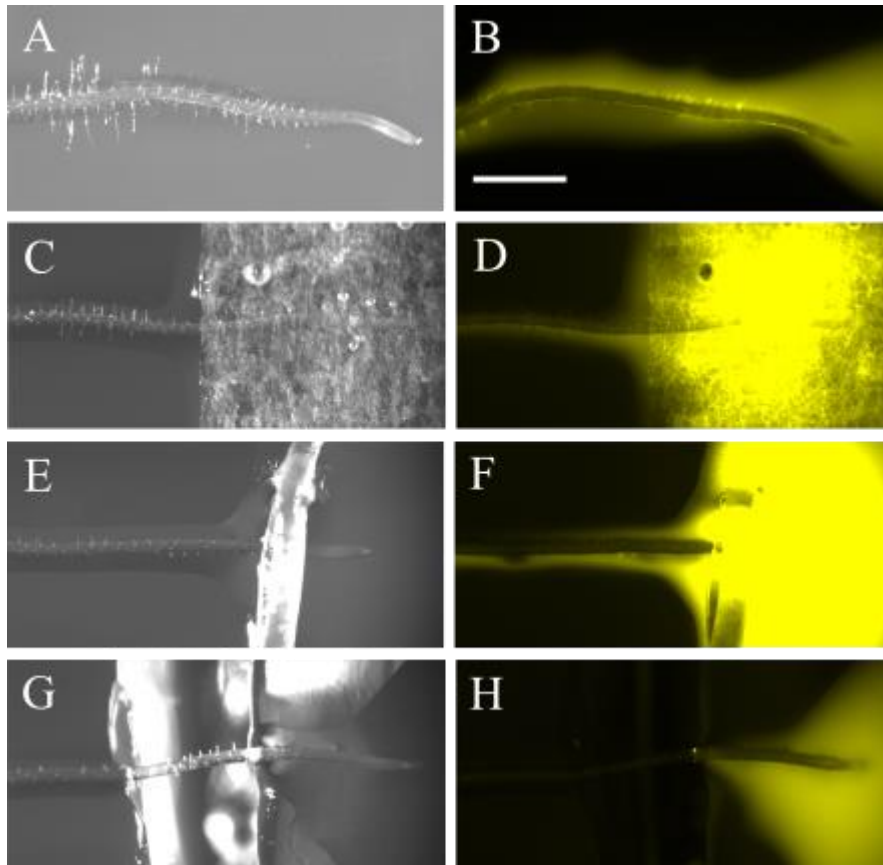
### 2.7.4 YC3.6 image analysis using ImageJ Fiji

ImageJ Fiji was used to process the cpVenus and CFP signal intensities. Using the ‘ROI Manager’ tool, each root sample was individually fitted with regions of interest (ROI) which covered comparable areas (size and location, determined as distance from the root tip). Z-axis profiles were plotted for each channel and used to calculate the FRET raw ratios (cpVenus / CFP). Background signal was subtracted.

## 2.8 Root $[Ca^{2+}]_{cyt}$ measurements by intensiometric GCaMP3 reporter

### 2.8.1 Sample preparation and set-up

Ten- to 11-day old *Arabidopsis* seedlings grown on half MS (0.8 % bactoagar, pH 5.6, no sucrose) and expressing the 35S::GCaMP3 reporter in the cytosol were used for experiments (Tian *et al.*, 2009; Vincent *et al.*, 2017). Seedlings remained on horizontal growth medium plates for the entire experiment, facilitating minimal handling and local application of treatment solution (compared to injection and perfusion set-up for aequorin and YC3.6 assays, respectively). Treatment solution (1 mM ATP) was in control solution background (containing respective full or zero P, further containing 1.175 mM MES, set to pH 5.6 using Tris, as for treatment solutions in aequorin trials, see section 2.6.4). Control solution without ATP was used as a control for any mechanical stimulation during treatment application. Treatment was applied as a 3  $\mu$ l drop to the root tip. A fluorescein solution (20  $\mu$ M, gift from Philip Mair, Biochemistry Department), was applied to test for capillary spread along the root and was monitored using a GFP-specific emission spectrum. The applied solution was found to spread within < 1.5 seconds along the imaged root section (Figure 3). Different barrier set-ups were therefore trialled to allow a defined local application of treatment (see Figure 3), of which a gap in the agar proved most successful in preventing spread of treatment solution. Whenever a localized application of treatment solution was required, root tips were placed across a gap in the agar.



**Figure 3:** Trialling different barriers to allow localized application of treatment solution in a simple plate-based horizontal set-up. Brightfield images (A, C, E, G) and GFP-emission (B, D, F, H) depict the spread of a fluorescein-containing solution along the root if applied to the root tip without barrier (A, B), if applied to KimWipe square placed over root tip (C, D), applied to the root tip with Vaseline barrier across root (E, F) and applied to the root tip with the root being placed over a gap in the agar (G, H). Scale bar in B: 1 mm.

### 2.8.2 Microscopy of GCaMP3-expressing plants

GCaMP3-expressing *Arabidopsis* plants were imaged on a Stereo microscope M205 FA (Leica), with a DFC365FX camera (Leica) and a Sola SE365 light source (Lumencor), which allowed excitation at 470/40 nm and using a GFP-ET filter collected emission at 525/50 nm, with a 500 ms exposure time, a gain of 2.0 and 30 x magnification. The software LAS X (Leica) was used to control the microscope, light source and camera.

### 2.8.3 GCaMP3 Image analysis using ImageJ Fiji

ImageJ Fiji was used to process the GCaMP3 GFP signal intensities. Using the ‘ROI Manager’ tool, each root sample was individually fitted with regions of interest (ROI)

which covered comparable areas (size and location, determined as distance from the root tip). Z-axis profiles were plotted for each ROI, and background signal was subtracted.

## 2.9 Histological staining

### 2.9.1 Intracellular ROS staining

To stain intracellular ROS (reactive oxygen species), the membrane-permeable dye CM-H<sub>2</sub>DCFDA (2', 7'-dichlorodihydrofluorescein diacetate, Thermo Fisher) was used at a final concentration of 20  $\mu$ M. A 50  $\mu$ g aliquot of the dye was dissolved in dimethyl sulfoxide (DMSO) to give a 10 mM stock, and further diluted in assay medium (0.1 mM KCl, 0.1 mM CaCl<sub>2</sub>, 1.175 mM MES, set to pH 6.0 using Tris, adapted from Foreman *et al.*, 2003). Work was carried out in the dark as the dye is light sensitive. Ten- to 11-day old *Arabidopsis* Col-0 seedlings grown on half MS (0.8 % bactoagar, pH 5.6, no sucrose, with varying P and Fe concentrations) were incubated in 20  $\mu$ M CM-H<sub>2</sub>DCFDA for one hour (in the dark and at 4°C to inhibit activity of extracellular esterases), before seedlings were gently washed in fresh assay medium and placed back onto plates containing half MS medium matching their prior nutrient growth condition. Plants acclimatized in light for one hour before being imaged on the plates under a stereo microscope, M205FA (Leica, see section 2.8.2). The GFP-ET filter allowed excitation at 470/40 nm and collected emission at 525/50 nm, with a 400 ms exposure time, light intensity of 70 %, a gain of 2.0 and 50 x magnification. ImageJ Fiji software was used to trace each root using the line tool (line width: 10) in combination with the 'plot profile' function which reports signal intensity along the root (Reyt *et al.*, 2015). For each root, three lines were drawn (from root tip shoot wards through centre of root, from root tip shoot wards along the upper side of the root, from root tip shoot wards along the lower part of the root), and the intensity profiles averaged to report an overall average per root (Reyt *et al.*, 2015).

### 2.9.2 Callose staining

Callose deposition was stained using aniline blue. Ten- to 11-day old *Arabidopsis* Col-0 seedlings grown on half MS (0.8 % bactoagar, pH 5.6, no sucrose, with varying P and Fe concentrations) were incubated in 0.01 % (w/v) aniline blue (BDH Chemicals) in a background medium of 150 mM K<sub>2</sub>HPO<sub>4</sub> (Fisher Chemicals) in distilled water, pH 9, for 1.5 hours in the dark and at room temperature (after Schenk and Schikora, 2015).

Seedlings were gently washed in distilled water, and placed into a drop of 60 % (v/v) glycerol on microscopy slides (2.5 cm x 7.5 cm) and cover glass (22 x 50 mm). Root tips were imaged under a stereo microscope, M205FA (Leica, see section 2.8.2). Samples were excited at 358 nm and a UV-filter (Leica # 10447415) allowed emission collection at 461 nm, with a 1.5 second exposure time, light intensity of 100 %, gain of 2.0 and x 50 magnification. ImageJ Fiji software was used to process the captured images. As aniline-stained callose deposition results in small but distinct spots, which are difficult to quantify, presence or absence in the root tip (0 – 500 µm) and elongation zone (1000 – 1500 µm) was scored, to relate callose deposition to regions of intracellular ROS hotspots (for more details, see Chapter 4, Figure 51).

## 2.10 Genotyping of *Arabidopsis* mutant lines

### 2.10.1 Manual genomic DNA extraction

One leaf per *circa* 2-week old seedling grown on half MS medium (0.8 % bactoagar, pH 5.6, no sucrose) was placed in a sterile 1.5 ml Eppendorf tube and flash frozen in liquid nitrogen ( $N_{liq}$ ). Using  $N_{liq}$ -cooled micropestles, each sample was ground and 400 µl of genomic DNA (gDNA) extraction buffer added (200 mM Tris-HCl pH 7.5, 250 mM NaCl, 25 mM ethylenediaminetetraacetic acid (EDTA), 0.5 % (v/v) sodium dodecyl sulfate (SDS), in autoclaved distilled water). Samples were vortexed to further disrupt the tissue, before being centrifuged for 7.5 minutes at full speed (14 000 *g*). The supernatant (*circa* 300 µl) was pipetted off and into new, sterile Eppendorf tubes containing an equal amount of ice-cold isopropanol, quickly vortexed, and left at -20°C for 10 to 15 minutes to precipitate the gDNA. Samples were centrifuged for 5 minutes at 14 000 *g* before removing supernatant and drying the gDNA (by opening the Eppendorf lids) at room temperature for 15-30 minutes. The pelleted gDNA was resuspended in 25 – 40 µl autoclaved distilled water, before checking DNA concentration and quality on a NanoDrop 2000 Spectrophotometer (Thermo Fisher).

### 2.10.2 High-throughput genomic DNA extraction

One leaf per *circa* 2-week old seedling was harvested into 8-strip 1.2 ml collection tubes (Alpha Laboratories), adding one 3 mm-glass bead per tube, and 200 µl of gDNA extraction buffer without SDS (see section 2.10.1 for extraction buffer details). The 8-

strip tubes were fitted into 96-sample adapters of the TissueLyzerII (Qiagen), which was used to disrupt the sample tissue with 2 cycles at 20 Hz, turning the plates in between the cycles to ensure homogenous tissue disruption. Samples were pulse-centrifuged in a Sorvall Legend RT Plus centrifuge (Thermo Fisher), before adding 200 µl of gDNA extraction buffer with 1% (v/v) SDS. Samples were centrifuged for 7 minutes (3000 rcf, 4°C), before transferring 200 µl supernatant per sample into the wells of a storage plate (0.8 ml, Thermo Fisher), containing 200 µl isopropanol. Samples were left at -20°C for 10 minutes up to overnight, before centrifuging for 35 minutes (3000 rcf, 4°C). Supernatant was poured off, plates blotted dry with paper towel, the pelleted gDNA washed with 150 µl 70% ethanol, pulse-spinned upside down to remove excess ethanol and dried at room temperature for 20-30 minutes. The pelleted gDNA was resuspended in 75 µl autoclaved distilled water, before checking DNA concentration and quality on a NanoDrop 2000 Spectrophotometer (Thermo Fisher).

### 2.10.3 Polymerase chain reaction (PCR)

Gene-specific primers were designed using the Signal Salk T-DNA Primer Design tool powered by the Genome Express Browser Server ([signal.salk.edu/tdnaprimers.2.html](http://signal.salk.edu/tdnaprimers.2.html)). Resulting primer sequences were checked for specificity using the Primer Blast tool ([www.ncbi.nlm.nih.gov/tools/primer-blast/](http://www.ncbi.nlm.nih.gov/tools/primer-blast/)) powered by the National Centre for Biotechnology Information (NCBI). For a complete list of genotyping primers, including T-DNA insertion specific primers, see Appendix II. Corresponding wild type gDNA samples were run alongside every T-DNA-mutant to be analysed. A *Taq* DNA Polymerase ('Eco-Taq', produced and purified in the Department of Plant Sciences) was used for PCR reactions at the following concentrations: 1 x Taq reaction buffer (20 mM (NH<sub>4</sub>)<sub>2</sub>SO<sub>4</sub>, 75 mM Tris-HCl pH 8.8, 2 mM MgCl<sub>2</sub>, 0.01 % (v/v) Tween-20), 200 µM deoxynucleotide mix (Bioline), 0.1 µM forward and reverse primer (Sigma-Aldrich), 0.5 U *Taq* DNA Polymerase, and 1 µl of extracted gDNA in a total volume of 20 µl autoclaved distilled water. PCRs were run on a ProFlex PCR system (Thermo Fisher), using the following hot-start programme: Heat lid to 105°C; initial denaturation step (2 min, 95°C); 35 cycles of denaturation (30 sec, 95°C), annealing (30 sec, 58-63°C depending on amplicon of interest), elongation (1 min, 72°C); a final elongation step (10 min, 72°C), cooling the reaction to 4°C (10 min), and holding at 15 - 20°C until stopping the run. PCR products were checked using gel electrophoresis (Sub-Cell GT electrophoresis cell with a PowerPac300 power source, BioRad). Samples were run on

0.8 – 1 % (w/v) agarose (Melford) gels in 1 x Tris-Acetate EDTA background (TAE, diluted from 50 x stock: 2 M Tris, 1 M glacial acetic acid, 50 mM EDTA). Five times concentrated DNA loading buffer (BioLine) was added at a final concentration of 1 x to each sample, and DNA was stained using SYBR Safe DNA gel stain (Invitrogen). Hyperladder 1kb (BioLine) was used to estimate size of amplicons. Gel electrophoresis was run at 90 mV, and resulting band separation imaged under UV light on an InGenious 3 imaging system (Syngene).

## 2.11 Bioinformatic resources and statistical analysis

A list of putative genes for Ca<sup>2+</sup> channels in *Arabidopsis* was compiled, according to the following criteria: (i) Include experimentally confirmed Ca<sup>2+</sup> channels reported for *Arabidopsis*; (ii) include all members of their gene family; (iii) include all genes belonging to gene ontology term “Ca<sup>2+</sup> channel activity” (GO:0005262, defined as: “enables the facilitated diffusion of a calcium ion (by an energy-independent process) involving passage through a transmembrane aqueous pore or channel without evidence for a carrier mediated mechanism”). Candidates were checked for site of expression and prioritized if expressed in the root (particularly root hairs), pollen tube or ‘not annotated’, to avoid false negatives (site of expression was assessed through araport.org and previous studies (Talke *et al.*, 2003; Gobert *et al.*, 2006; Jones *et al.*, 2006; Brady *et al.*, 2007; Deal and Henikoff, 2010; Bruex *et al.*, 2012; Lan *et al.*, 2013; Becker *et al.*, 2014; Kellermeier *et al.*, 2014; L. Huang *et al.*, 2017)).

Using publicly available bioinformatic resources and previous studies, the genes were checked for reported change of expression under low P (Lin *et al.*, 2011; Kellermeier *et al.*, 2014), in response to gravity vector or mechanical stimulation (Kimbrough *et al.*, 2004), their co-expression with genes of interest with regards to P starvation and root hair growth using the atted.jp co-expression database (Obayashi *et al.*, 2014), proteomic changes upon P starvation (Lan *et al.*, 2012), and membrane-localized protein-protein interaction using the MIND database (Jones *et al.*, 2014a). See Appendix I for a full list of putative Ca<sup>2+</sup> channels.

All statistical analyses were performed using the open-source software R (www.r-project.org, version 3.5.1) in a R studio environment. The R packages ‘dplyr’ and ‘tidyr’ were used to arrange data. The package ‘MESS’ was used to calculate area under the curve. See Figure 6 for details on analysis of aequorin-derived data. A Student’s *t*-test or

ANOVA was used to test for statistically significant differences, using a significance threshold of  $p < 0.05$ . A Tukey HSD *post-hoc* test was employed to determine differences among the groups. A 95% family-wise confidence level was applied.

R was used to plot data, using the package ‘ggplot2’. The default boxplot design (as implemented in R, after Tukey) was used to display the data spread, using an underlying ‘jitterplot’ to display individual data points. In the boxplot, the thick middle line denotes the median, separating the upper and lower half of the data; the hinges (box outline) denote median of the upper and the lower half of the data, respectively; the bars denote entirety of data excluding outliers; outliers are depicted by individual points outside the boxplot bars. The free graphic software Inkscape ([www.inkscape.org](http://www.inkscape.org), version 0.92.2) was used for figure design.

# 3 PHOSPHATE STARVATION ALTERS CALCIUM SIGNALLING IN *ARABIDOPSIS* ROOTS

## 3.1 Introduction

### 3.1.1 Abiotic stress perception involves Ca<sup>2+</sup> ion fluxes

In the field, plants are exposed to a multitude of external stresses, such as mechanical stimulation, salt, drought and oxidative stress and wounding. Stress perception and translation into adequate plant responses are fundamental to optimal plant growth and ultimately, survival. On a cellular level, much progress has been made in uncovering networks of signalling molecules that translate extra- into intracellular clues. Fluxes of Ca<sup>2+</sup> ions across membranes have been shown to play a major role (see Chapter 1, section 1.2.6 onwards, for a more thorough introduction to Ca<sup>2+</sup> as a second messenger, and Chapter 4, section 4.1.2, for a more thorough introduction to extracellular nucleotide signalling). In the following, abiotic stresses used as tools to elicit Ca<sup>2+</sup> fluxes will be briefly introduced, and the main questions for the for the involvement of Ca<sup>2+</sup> signalling in P starvation will be outlined.



**Mechanical stress** has long been known to rapidly trigger the influx of  $\text{Ca}^{2+}$  ions into cells of tobacco and *Arabidopsis* (Knight *et al.*, 1991, 1992; V Legué *et al.*, 1997). The resulting  $[\text{Ca}^{2+}]_{\text{cyt}}$  signatures were shown to vary depending on the tissue affected and the stimulus perceived (V Legué *et al.*, 1997; Monshausen *et al.*, 2009; Shih *et al.*, 2014). *Arabidopsis* root epidermal cells from the elongation and mature zone showed a localized extracellular alkalinisation (increase of pH) within seconds of touch stimulus, whereas a transient acidification occurred intracellularly (Monshausen *et al.*, 2009). Two extracellular ROS bursts occurred within less than a minute upon touch perception (Monshausen *et al.*, 2009). Both pH change and ROS production were dependent on an initial increase in  $[\text{Ca}^{2+}]_{\text{cyt}}$  (Monshausen *et al.*, 2009). Widespread transcriptional changes were reported within minutes of mechanostimulation (Kimbrough *et al.*, 2004).  $\text{Ca}^{2+}$ -associated genes such as Calmodulin-like (CML) 12 and CML24 were strongly upregulated (Braam and Davis, 1990). A PM-localized receptor-like kinase, FERONIA, was found necessary for the full  $[\text{Ca}^{2+}]_{\text{cyt}}$  and pH response upon a bending stimulus, as well as induction of touch-related genes, *e.g.* CML12 and CML24 (Shih *et al.*, 2014).

Early on, the existence of mechanoresponsive  $\text{Ca}^{2+}$ -permeable channels was deduced and to date, several PM-localized mechanosensitive  $\text{Ca}^{2+}$ -permeable channels have been identified *in planta*, including MCA1 and MCA2 (Nakagawa *et al.*, 2007; Yamanaka *et al.*, 2010), the MSL family with ten members (Haswell and Meyerowitz, 2006; Haswell *et al.*, 2008; Hamilton *et al.*, 2015) and most recently, the hyperosmolality-gated  $\text{Ca}^{2+}$ -permeable channel OSCA1 / CSC1 with 15 family members in *Arabidopsis* (Hou *et al.*, 2014; Yuan *et al.*, 2014; see Chapter 1 section 1.2.3 and 1.2.4 for a more detailed introduction to putative  $\text{Ca}^{2+}$  channels). Understanding the molecular components involved in mechanosensing is however hampered by the fact that disturbing the function of those channel proteins mostly led to very mild phenotypes, possibly due to genetic redundancy. Recently, an embryo lethal phenotype has been described for a transmembrane protein, Defective Kernell1 (DEK1), which was necessary for a mechanically activated  $\text{Ca}^{2+}$  flux in *Arabidopsis* protoplasts, (Tran *et al.*, 2017). If DEK1 forms a mechanosensitive  $\text{Ca}^{2+}$  channel itself or rather is associated with another channel is however unknown (Tran *et al.*, 2017).

**Salt and osmotic stress** have also been shown to lead to dynamic increases in  $[\text{Ca}^{2+}]_{\text{cyt}}$ , reported for many plant species including tobacco, *Arabidopsis*, rice and most recently the moss *Physcomitrella patens* (Knight *et al.*, 1997; Kiegle, C. Moore, *et al.*, 2000; Moore *et al.*, 2002; Tracey *et al.*, 2008; Laohavisit *et al.*, 2013; W.-G. Choi *et al.*, 2014;

X. Zhang *et al.*, 2015; Y. Zhang *et al.*, 2015; F. Huang *et al.*, 2017; Storti *et al.*, 2018). Hyperosmotic stress is defined as a higher solute concentration outside compared to inside the cells (occurring during *e.g.* drought and salt stress), and *vice versa* for hypoosmotic stress (occurring in *e.g.* waterlogged soils). Salt stress is composed of a hyperosmotic component as well as toxicity through excess Na<sup>+</sup> and Cl<sup>-</sup> ion accumulation (Maathuis, 2014).

Monitoring whole-tissue [Ca<sup>2+</sup>]<sub>cyt</sub> did initially not show marked differences between response to salt and osmotic stress (Knight *et al.*, 1997), cell-type specific targeting of aequorin however resolved different responses (Kiegle *et al.*, 2000). A pronounced [Ca<sup>2+</sup>]<sub>cyt</sub> response to both salt and osmotic stress occurred in the epi- and endodermis, but to a lesser extent in the pericycle upon osmotic stress (Kiegle *et al.*, 2000). Local salt treatment of root tissue led to the propagation of a [Ca<sup>2+</sup>]<sub>cyt</sub> signal along the roots' endodermis and cortex, to areas not in direct contact with the stress (W.-G. Choi *et al.*, 2014). The experimental bathing medium and hence the PM's voltage was found to strongly influence the [Ca<sup>2+</sup>]<sub>cyt</sub> response to salt and osmotic treatment (Tracey *et al.*, 2008). PM-Ca<sup>2+</sup> channel blockers (lanthanides) dampened, but did not abolish, the [Ca<sup>2+</sup>]<sub>cyt</sub> response upon salt and mannitol in both *Arabidopsis* and rice roots, indicating that both extracellular and intracellular Ca<sup>2+</sup> stores operate in the response, as well as other signalling events besides Ca<sup>2+</sup> transducing the message (Knight *et al.*, 1997; Tracey *et al.*, 2008; Y. Zhang *et al.*, 2015). Other signalling molecules rapidly increasing upon salt perception were extracellular ATP and ROS (Miller *et al.*, 2009; Dark *et al.*, 2011; Ma *et al.*, 2012). ROS formation in the roots was dependent on the NADPH-oxidases D and F (Ma *et al.*, 2012). Inositol triphosphate (InsP<sub>3</sub>)-dependent [Ca<sup>2+</sup>]<sub>cyt</sub> microdomains were found adjacent to the tonoplast, suggesting the vacuole as intracellular source and InsP<sub>3</sub> as a signal transducer upon osmotic stress (Knight *et al.*, 1997). The ER, which is described as another major Ca<sup>2+</sup> source in cells, did not show a decrease in [Ca<sup>2+</sup>], but only a rapid increase upon salt perception, excluding the ER as (major) Ca<sup>2+</sup> source upon salt stress (Bonza *et al.*, 2013).

Particularly for salt stress, the initial [Ca<sup>2+</sup>]<sub>cyt</sub> increase has been linked to downstream changes in gene expression (W.-G. Choi *et al.*, 2014). Most prominently, the Salt Overly Sensitive (SOS) pathway has been dissected, in which the PM-localized CBL4 (or SOS3) senses the salt-dependent increase in [Ca<sup>2+</sup>]<sub>cyt</sub>, and has been shown to interact with CIPK24 (SOS2) (Liu *et al.*, 2000). The CBL/CIPK complex then phosphorylates and thus

activates the PM  $\text{Na}^+/\text{H}^+$  antiporter (SOS1), which enhances  $\text{Na}^+$  efflux from the cytosol (Shi *et al.*, 2000; Quintero *et al.*, 2011).

As  $\text{Na}^+$  entry depolarizes the epidermal PM voltage (Maathuis, 2014), voltage-dependent and independent PM  $\text{Ca}^{2+}$ -permeable channels have been implicated in response to salt stress (Wilkins *et al.*, 2016). So far, knocking out individual single channel proteins has not led to major inhibition of the rapidly triggered  $[\text{Ca}^{2+}]_{\text{cyt}}$  fluxes, thus the genetic identity of channel proteins underlying the trans-PM and trans-endomembrane  $\text{Ca}^{2+}$  flux upon salt perception remain unknown. TPC1 has been implicated in governing vacuolar  $\text{Ca}^{2+}$  release upon salt stimulus, however it showed a delayed rather than an inhibited  $\text{Ca}^{2+}$  response (W.-G. Choi *et al.*, 2014). ANN1 was found to be responsible for the ROS-activated  $[\text{Ca}^{2+}]_{\text{cyt}}$  component of salt stress perception, consistent with ANN1's role as a  $\text{Ca}^{2+}$ -permeable channel activated by extracellular ROS (Laohavisit *et al.*, 2012, 2013). As osmotic stress is easily linked to mechanical stress – through increase or decrease of turgor – ion channels activated could be mechano-regulated. Indeed, OSCA1 showed a strongly dampened  $\text{Ca}^{2+}$  influx in response to hyperosmotic stress (Yuan *et al.*, 2014). Trans-PM  $\text{Ca}^{2+}$  influx upon hypoosmotic stress was shown to be mediated by MCA proteins, in rice, tobacco and *Arabidopsis* (Kurusu *et al.*, 2012; Kamano *et al.*, 2015).

**Oxidative stress** can occur as a *bona fide* stress in the field (*e.g.* through exposure to high concentrations of ozone), and oxidative signalling (in the form of ROS) has been mentioned as a component of the above described mechanical and osmotic stresses. Both reactive oxygen as well as reactive nitrogen species (ROS, RNS, respectively) occur in diverse, often short-lived forms of which most are difficult to quantify, and of which ROS are the better studied (Halliwell and Whiteman, 2004; Richards *et al.*, 2015). In plants, ROS can be produced enzymatically *via* specialized NADPH-Oxidases, in which intracellular NADPH oxidation is translated into extracellular  $\text{H}_2\text{O}_2$  production (Foreman *et al.*, 2003; Miller *et al.*, 2009; Magnani *et al.*, 2017). Transition metals, such as iron and copper, non-enzymatically catalyse the formation of intra- and extracellular reactive species, *e.g.* hydroxyl radicals, and thus have to be tightly regulated (Kehrer, 2000; Ravet *et al.*, 2009; Richards *et al.*, 2015).

Perception of ROS rapidly triggers an increase in  $[\text{Ca}^{2+}]_{\text{cyt}}$  (Price *et al.*, 1994; Rentel and Knight, 2004; Evans *et al.*, 2005). The response has been shown to vary depending on the type of ROS, *e.g.* *Arabidopsis* root tissue responded differently to ozone and hydrogen peroxide ( $\text{H}_2\text{O}_2$ ; Evans *et al.*, 2005), or hydroxyl radicals and  $\text{H}_2\text{O}_2$  (Demidchik, Shabala, *et al.*, 2003). PM-localized  $\text{Ca}^{2+}$  channels in *Arabidopsis* root tissue showed a decreasing

sensitivity to extracellular H<sub>2</sub>O<sub>2</sub> the more mature the epidermal cells tested, but independently of age, epidermal cells always responded more readily to H<sub>2</sub>O<sub>2</sub> than cortex cells (Demidchik *et al.*, 2007). Recently, transmembrane aquaporins were shown to facilitate transport of extracellular H<sub>2</sub>O<sub>2</sub> into cells, so far however only reported for leaf, and not root, cells of *Arabidopsis* (Tian *et al.*, 2016; Rodrigues *et al.*, 2017). A receptor for H<sub>2</sub>O<sub>2</sub> encoded by a PM-localized leucine rich repeat receptor-like kinase, GHR1 (guard cell hydrogen peroxide resistant 1), was described in *Arabidopsis* guard cells (Hua *et al.*, 2012). GHR1 was shown to be ubiquitously expressed, including in roots (Wu *et al.*, 2016), studies so far have however focussed to characterize GHR1 in leaf tissue only (Hua *et al.*, 2012; Devireddy *et al.*, 2018).

Early work to characterize the PM Ca<sup>2+</sup> channel(s) involved focussed on guard cells, and showed H<sub>2</sub>O<sub>2</sub>-activated PM Ca<sup>2+</sup> flux in *Arabidopsis* (Pei *et al.*, 2000). Since then, it was demonstrated that ROS equally regulated channel-activity in root cells of *Arabidopsis* and pea (Demidchik, Shabala, *et al.*, 2003; Foreman *et al.*, 2003; Zepeda-Jazo *et al.*, 2011). ANN1 was shown to form redox-regulated Ca<sup>2+</sup>-permeable pores in the PM of root epidermal cells (Laohavisit *et al.*, 2012). The genetic identity of the ROS-activated conventional Ca<sup>2+</sup> channels remains unknown.

**Extracellular nucleotides**, such as extracellular ATP (eATP), are known to consistently trigger strong [Ca<sup>2+</sup>]<sub>cyt</sub> increases in plant tissue (Demidchik, Nichols, *et al.*, 2003; Tanaka *et al.*, 2010; J. Choi, Tanaka, Cao, *et al.*, 2014). The receptor for eATP, mutants of which completely lack the eATP-induced [Ca<sup>2+</sup>]<sub>cyt</sub> response, has only recently been characterised in plants (Does Not Respond to Nucleotides1 (DORN1); Choi, Tanaka, Cao, *et al.*, 2014). DORN1 protein localizes to the plasma membrane (Choi, Tanaka, Liang, *et al.*, 2014) and is expressed throughout the root, with highest levels of expression found in the quiescent centre and columella root cap cells, as well as in the endodermis and cortex cells of the elongation zone (Birnbaum *et al.*, 2003; Nawy *et al.*, 2005; Brady *et al.*, 2007; J. Choi, Tanaka, Liang, *et al.*, 2014). Signalling networks upon eATP perception will be introduced in more detail in Chapter 4 (see section 4.1.1 onwards).

### 3.1.2 The involvement of $\text{Ca}^{2+}$ fluxes in nutrient deficiencies – unknown for P starvation

Besides their role in abiotic stress perception (for details on  $\text{Ca}^{2+}$ 's role in biotic stress perception see Chapter 1, section 1.2.6), fluxes of  $\text{Ca}^{2+}$  have more recently also been shown to play a role in nutrient sensing. For nitrate-starved *Arabidopsis* root and leaf tissue, there is strong evidence for nitrate-resupply's eliciting rapid modulations in  $[\text{Ca}^{2+}]_{\text{cyt}}$ , followed by an increase in nuclear  $[\text{Ca}^{2+}]$  (Riveras *et al.*, 2015; Liu *et al.*, 2017). Potassium ( $\text{K}^+$ ) deficiency triggered rapid and more delayed changes in  $[\text{Ca}^{2+}]_{\text{cyt}}$  (Behera *et al.*, 2017). As altering the  $[\text{K}^+]$  however strongly affects the PM voltage (Demidchik *et al.*, 2002), it is unknown to what extent this is an effect of mis-regulated PM voltage over direct sensing of nutrient availability. Vacuolar magnesium ( $\text{Mg}^{2+}$ ) detoxification relied on  $[\text{Ca}^{2+}]_{\text{cyt}}$  signalling (Tang *et al.*, 2015). For boron (B), prolonged deprivation was shown to increase  $[\text{Ca}^{2+}]_{\text{cyt}}$ , however so far no short-term  $[\text{Ca}^{2+}]_{\text{cyt}}$  modulation has been reported (Mühling *et al.*, 1998; Quiles-Pando *et al.*, 2013). Iron (Fe) and copper ( $\text{Cu}^{2+}$ ) addition led to rapid increases in  $[\text{Ca}^{2+}]_{\text{cyt}}$  in marine diatoms, marine algae and *Arabidopsis*, however owing to their redox-active role it is difficult to discern their nutritional role from their involvement in generating oxidative stress (Falciatore *et al.*, 2000; González *et al.*, 2010; Rodrigo-Moreno *et al.*, 2013).

Even though P, alongside nitrogen (N) and  $\text{K}^+$ , is one of the major nutrients limiting plant growth when limited in availability, the involvement of  $[\text{Ca}^{2+}]_{\text{cyt}}$  signalling in P nutrition is currently unknown. A role for  $[\text{Ca}^{2+}]_{\text{cyt}}$  in P nutrition is particularly intriguing given the special relationship P and  $\text{Ca}^{2+}$  have; they easily complex, which evolutionary dictated low  $[\text{Ca}^{2+}]_{\text{cyt}}$  to guarantee a functioning P-based metabolism (see Chapter 1, section 1.3 for a more detailed dissection of the problem). The involvement of  $[\text{Ca}^{2+}]_{\text{cyt}}$  in P nutrient sensing has been implied but not resolved (Chiou and Lin, 2011; Lin *et al.*, 2014; Chien *et al.*, 2018). Both the effect of P starvation on  $[\text{Ca}^{2+}]_{\text{cyt}}$  signalling, as well as the involvement of  $[\text{Ca}^{2+}]_{\text{cyt}}$  in transducing P availability, are unknown.

### 3.1.3 Experimental approaches and aims

To elucidate the role of  $[\text{Ca}^{2+}]_{\text{cyt}}$  in P nutrition, *Arabidopsis* wild type plants, ubiquitously expressing the  $\text{Ca}^{2+}$  reporter aequorin in the cytosol, were starved of P. In general, half MS medium was used as the standard growth medium, and nutrient content was modified according to the experimental question, *e.g.* altering P levels (see Chapter 2, section 2.2.3,

for further details). Root system architecture was quantified to assess the impact of the altered ionic composition of the growth medium on plant growth. Root tissue was used for the analysis of  $[Ca^{2+}]_{cyt}$  responses, particularly root tip tissue, as roots in general are the first site of contact with nutrients in the soil, and the root tip was found to be predominantly responsible for P uptake (Kanno, Arrighi, *et al.*, 2016).

First, the  $[Ca^{2+}]_{cyt}$  response of aequorin-expressing P-starved root tips to abiotic stresses (mechanical, osmotic and salt, oxidative stress and extracellular nucleotide signalling molecules) was tested. P-starvation could potentially affect the  $[Ca^{2+}]_{cyt}$  response by either increasing or decreasing the use of  $Ca^{2+}$  upon stress perception, or not alter its use at all. Given the fact that  $Ca^{2+}$  easily complexes with P-groups, it could be conceived that in P-limited conditions, and an overall decreased cellular P-pool, the use of  $Ca^{2+}$  might be restricted to contain its cytotoxic effects.

Secondly, to test the specificity of the  $[Ca^{2+}]_{cyt}$  response of P-starved root tissue to abiotic stress treatments, (apo)aequorin-expressing *Arabidopsis* plants were also starved of N and root tissue subjected to stress treatments. As it is known that Fe-availability affects P-starvation responses of *Arabidopsis*, including remodelling of the root system (see Chapter 1, section 1.1.4 for an introduction), Fe levels were modified in addition to varying P levels, to test how the described Fe-P interaction might influence the  $[Ca^{2+}]_{cyt}$  response.  $Cu^{2+}$ -deprived *Arabidopsis* plants were then used to test for the specificity of this Fe-P relationship.

Finally, P-starved *Arabidopsis* aequorin-expressing plants were resupplied with a high P-pulse, to test if  $[Ca^{2+}]_{cyt}$  were involved in perception of P availability. Both a transient increase of  $[Ca^{2+}]_{cyt}$ , as reported for nitrate resupply ((Riveras *et al.*, 2015; Liu *et al.*, 2017), as well as a transient decrease of  $[Ca^{2+}]_{cyt}$  upon P resupply are theoretically conceivable to act as a signalling event.

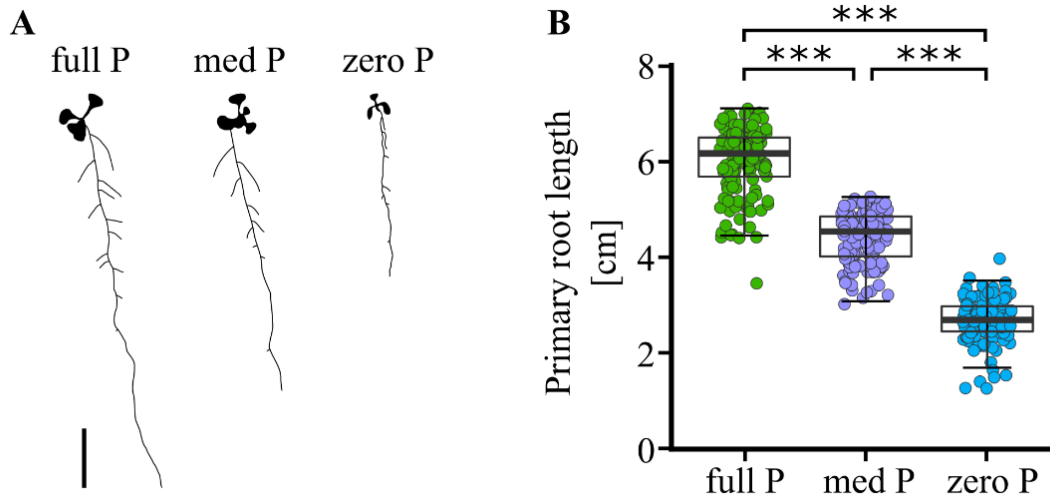
Overall, these experimental approaches should enable answering the following questions:

- Is the  $[Ca^{2+}]_{cyt}$  response to abiotic stresses altered under P starvation?
- If so, is this effect specific to P starvation?
- What other components are involved in shaping the  $[Ca^{2+}]_{cyt}$  response under P starvation (*e.g.* proteins involved, developmental aspects, links to Fe nutrition)?
- Is P availability signalled through modulations in  $[Ca^{2+}]_{cyt}$ ?

## 3.2 Results

### 3.2.1 Phosphate starvation inhibits primary root growth

To study the effect of P starvation on the free cytosolic calcium ( $[Ca^{2+}]_{cyt}$ ) signature, *Arabidopsis thaliana* Col-0 roots constitutively expressing cytosolic (apo)aequorin were grown under different P regimes. Seedlings were germinated and grown on half-strength Murashige & Skoog medium (half MS), with varying P concentrations: full P: 0.625 mM P, medium P: 0.1 mM P, zero P: 0 mM P. Roots grown on these P regimes differed in primary root length, with primary root growth being inhibited by decreasing P supply (Figure 4A). Seedlings grown on full P showed a primary root length of  $6.01 \pm 0.06$  cm (mean  $\pm$  standard error of means (SEM), 5 independent trials,  $n = 142 - 144$  individual roots measured per growth condition, Figure 4B), medium P roots were significantly shorter than full P roots ( $4.42 \pm 0.04$  cm, Analysis of variance (ANOVA) with *post-hoc* Tukey test:  $p$ -value  $< 0.001$ , Figure 4B). Zero P roots were significantly shorter than medium P roots ( $2.69 \text{ cm} \pm 0.04 \text{ cm}$ ,  $p$ -value  $< 0.001$ ).



**Figure 4:** Primary root lengths of phosphate-starved *Arabidopsis thaliana* plants. Col-0 were grown on gel-based nutrient medium with varying P concentrations: full P (0.625 mM  $\text{PO}_4^{3-}$ ), medium P (med P, 0.1 mM  $\text{PO}_4^{3-}$ ) or zero P (0 mM  $\text{PO}_4^{3-}$ ). On day 10, plants were scanned and primary root length was quantified using the ImageJ NeuronJ Plugin. (A) Representative root system architecture of 10-day old seedlings, scale bar indicates 1 cm. (B) Primary root lengths of  $n = 142 - 144$  individual seedlings per growth condition, data from 5 independent trials. Boxplot thick middle line denotes median. Analysis of variance (ANOVA) with *post-hoc* Tukey Test was used to assess statistical differences. Significance levels ( $p$ -value): \*\*\* ( $< 0.001$ ).



### 3.2.2 Phosphate starvation induces root hair growth – independent of non-functional single putative Ca<sup>2+</sup> channels

*Mutant genotyping and root hair phenotyping was carried out in collaboration with Dr. Zhizhong Song, Ludong University, China*

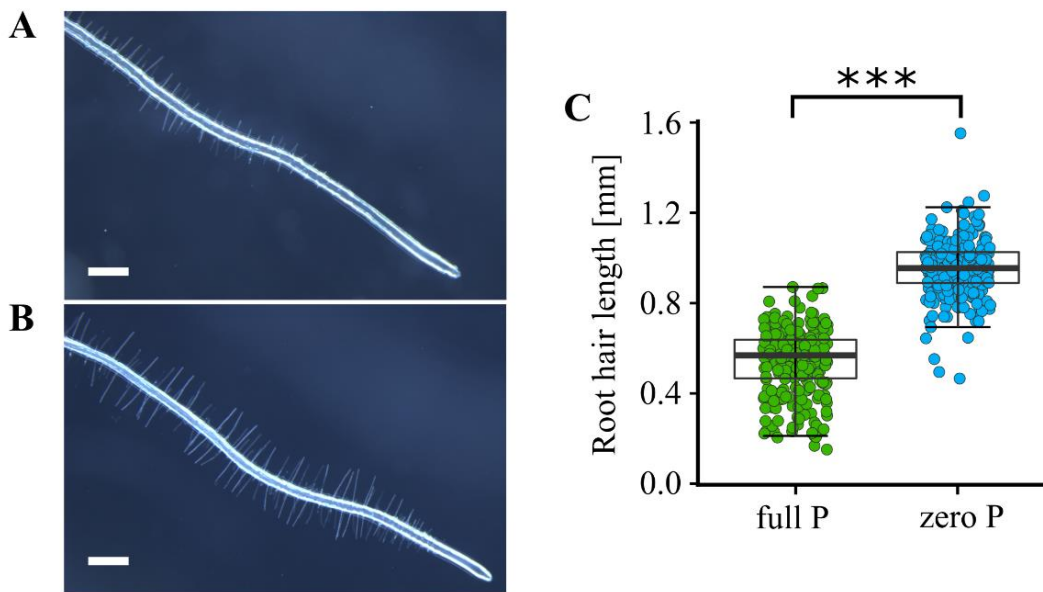
Another root system architectural trait linked to P starvation is the increased length of root hairs (Foehse and Jungk, 1983; Bates and Lynch, 1996; Ma *et al.*, 2001; Haling *et al.*, 2013; Bhosale *et al.*, 2018). As [Ca<sup>2+</sup>]<sub>cyt</sub> oscillations and gradients are involved in governing polar root hair growth (Bibikova *et al.*, 1997; Monshausen *et al.*, 2008), mediated by PM localized Ca<sup>2+</sup> channels (Véry and Davies, 2000), it was of passing interest to test for involvement of putative Ca<sup>2+</sup> channel genes in root hair growth under P starvation conditions. In short, a suite of *Arabidopsis* lines defective in putative Ca<sup>2+</sup> channels was compiled and genotyped (see Chapter 2, section 2.1 and 2.11, for details of compilation, and Appendix I for putative Ca<sup>2+</sup> channel details; see section 2.10 and Appendix II for details on genotyping and the individual mutant lines). Different root hair growth conditions were trialled (based on relevant previous studies, Appendix III), and optimal growth conditions for the current laboratory conditions chosen (see Chapter 2, section 2.2.5, and Appendix III).

In total, 74 single mutants and 3 higher-order mutant lines were screened for a root hair phenotype under both full and zero P growth conditions. As for some gene models more than one allele was included, this mutant library covered 61 unique gene models. Each mutant was grown with its respective paired wild type. Primary root lengths were scored as a measure of how the mutation might affect overall root growth and potentially bias root hair scoring (Appendix IV). All mutants showed primary root lengths within a range that was comparable to their respective wild types. Quantification of root hairs (for details see Chapter 2, section 2.3) showed significantly elongated root hairs under P starvation conditions (compare Figure 5A and B). Under nutrient-replete conditions, wild types grew mean root hair lengths ( $\pm$  SEM) of  $0.55 \pm 0.01$  mm (data of 6 independent trials,  $n = 251 - 236$  individual roots per growth condition, Figure 5C). Under P starvation conditions, wild types had mean root hair lengths of  $0.95 \pm 0.01$  mm (Figure 5C).

However, all mutant lines showed considerable root hair outgrowth, and within the range scored for their respective wild types (Appendix V). Only one mutant allele, *glr3.7-2*, displayed impaired root hair growth. This mutant phenotype did however not manifest itself in another line (which technically was annotated as being the same line), *glr3.7-1*,

and was later shown to be independent of the mutation found in the *GLR3.7* gene, but linked to another T-DNA insertion within the genome (Prof. Alex Costa, personal communication).

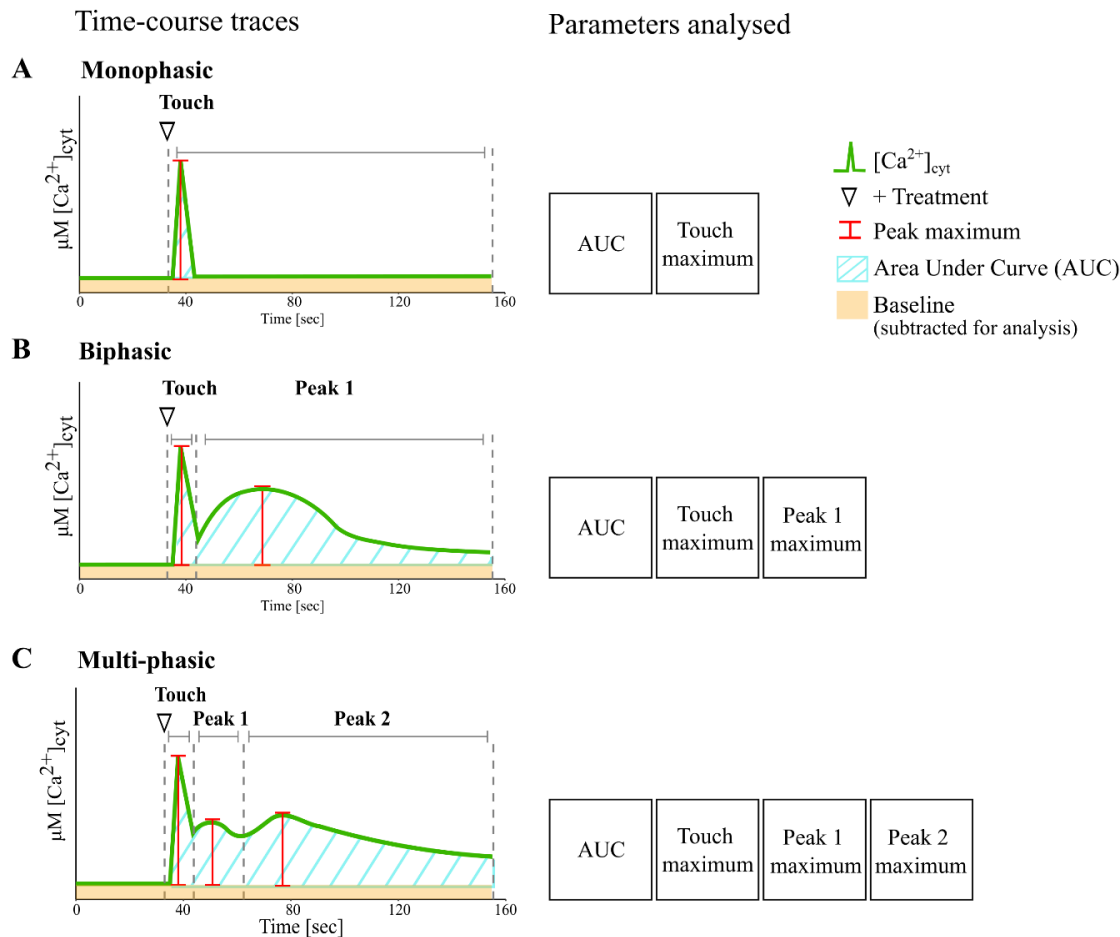
Overall, this indicated that the knock-out of single genes within large gene families did not cause a root hair phenotype, likely due to genetic redundancy (see Chapter 1, section 1.2.3 onwards for an introduction to  $\text{Ca}^{2+}$  channel families).



**Figure 5:** Root hair growth of phosphate-starved *Arabidopsis* wild type plants. As part of screening putative  $\text{Ca}^{2+}$  channel mutants for a root hair phenotype, paired *Arabidopsis* wild type were grown alongside. Root tips of 6-day old seedlings were imaged under a stereomicroscope, shown are representative images for plants grown on (A) full phosphate conditions (full P, 1 mM  $\text{PO}_4^{3-}$ ) and (B) zero phosphate conditions (zero P, 0 mM  $\text{PO}_4^{3-}$ ), scale bar: 1 mm. Root hair lengths were analysed by measuring the 10 longest root hairs (5 on either side of the root) within a 1 mm window, 4-5 mm from the apical tip, using the ImageJ NeuronJ plugin. (C) Measured root hair lengths of  $n = 236 - 251$  individual wild type roots per growth condition, data from 6 independent trials. In boxplot, thick line denotes median, dots display individual data points (= mean root hair length of a single root). A Welch two sample  $t$ -test was used to assess statistical differences. Significance levels ( $p$ -value): \*\*\* ( $< 0.001$ ).

### 3.2.3 Phosphate-starved root tips show an altered $[Ca^{2+}]_{cyt}$ response to a range of abiotic stresses

To test if stress-induced  $[Ca^{2+}]_{cyt}$  signatures were altered in P-starved roots, *Arabidopsis* Col-0 roots constitutively expressing cytosolic (apo)aequorin were P-starved and subsequently challenged with different abiotic stresses. Mechanical, salt, osmotic and redox stress were applied in the form of control solution application, NaCl, sorbitol and  $H_2O_2$  treatment, respectively. To account for differences in root size due to varying P growth conditions (see Figure 4), excised root tips of equal length (1 cm) were used for the aequorin assays. Single root tips were challenged with application of control solution, or stress treatments in control solution background. Changes in  $[Ca^{2+}]_{cyt}$  were recorded every second over a time-course of in total 155 seconds, before discharging all remaining reconstituted aequorin (for more details, see Chapter 2, section 2.6.2). Figure 6 defines the wording used throughout this thesis to describe  $[Ca^{2+}]_{cyt}$  time-course traces and analysed parameters. Traces of individual samples were analysed for peak maxima (= maximum of peak height with average baseline subtracted), and area under the curve (= integrated area under the curve with average baseline subtracted). Peak maxima report the maximal increase of  $[Ca^{2+}]_{cyt}$  in response to a treatment. Area under the curve (AUC) is an estimate of the  $[Ca^{2+}]_{cyt}$  mobilised during  $[Ca^{2+}]_{cyt}$  response to a treatment. Different stresses result in overall monophasic, biphasic and multi-phasic  $[Ca^{2+}]_{cyt}$  signatures originating from the cell population of the tissue used (see schematic in Figure 6).

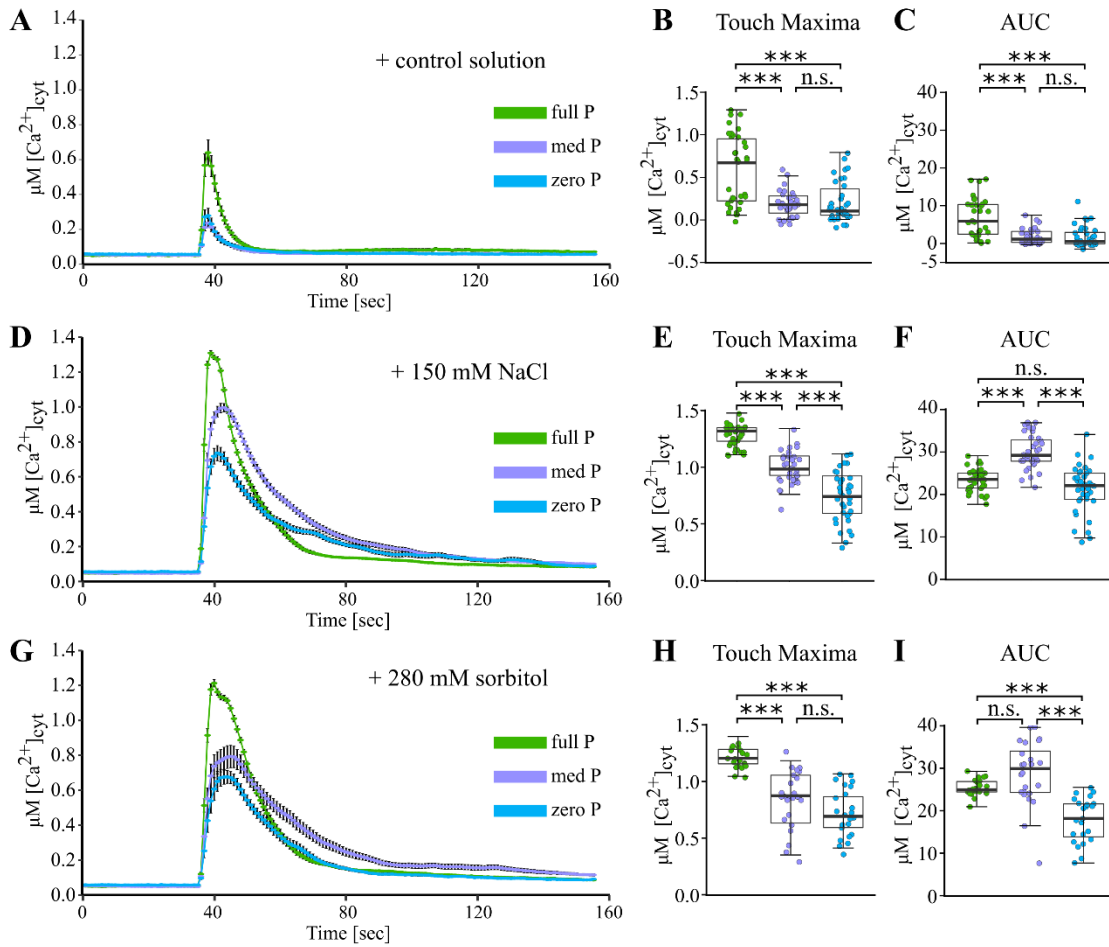


**Figure 6:** Schematic representation of aequorin-based  $[Ca^{2+}]_{cyt}$  time-courses and analysis as presented in this thesis. Mean time-course traces are plotted for (A) monophasic responses (control solution application; NaCl, sorbitol treatment), (B) biphasic responses ( $H_2O_2$  treatment) and (C) multi-phasic responses (ATP, ADP,  $\gamma$ -ATP treatments). Traces from individual samples were baseline-subtracted prior to analysis (baseline = mean of 0 – 35 second measurements prior to application of treatment solution). Analysed parameters include area under the curve (AUC, totalled over 35 – 155 seconds) and maxima of specific peaks occurring within set phases as indicated by grey dashed lines ((A) Touch Maximum: 35 – 155 seconds; (B) Touch Maximum: 35 – 49 seconds, Peak 1 Maximum: occurring in 50 – 155 seconds; (C) Touch Maximum: 35 - 41 seconds, Peak 1 Maximum: 42 - 63 seconds, Peak 2 Maximum: 64 - 155 seconds).

In a first set of experiments, P-starved root tips were challenged with salt and osmotic stress. Stress treatments were prepared to be osmotically equivalent, represented by 150 mM NaCl and 280 mM sorbitol. Application of control solution was used to quantify the response of root tips to mechanical stimulation without any further stress treatment addition. Application of control solution led to an immediate and monophasic  $[Ca^{2+}]_{\text{cyt}}$  response in root tips from all P growth conditions (Figure 7A), with return to pre-stimulus levels approximately 20 seconds after treatment application. Control solution response was variable, but overall full P roots responded with a stronger increase in  $[Ca^{2+}]_{\text{cyt}}$  (mean touch maxima  $\pm$  SEM:  $0.6 \pm 0.07 \mu\text{M}$ ) compared to medium P ( $0.2 \pm 0.03 \mu\text{M}$ ) and zero P ( $0.24 \pm 0.04 \mu\text{M}$ ) root tips. Both parameters analysed, touch maximum (Figure 7B) and area under the curve (Figure 7C), were highly significantly greater in full P root tips compared to medium and zero P root tips ( $p$ -value  $< 0.001$ , analysis of variance (ANOVA) with *post-hoc* Tukey Test,  $n = 31 - 36$  individual root tips per growth condition from 3 independent trials). There was no significant difference between medium and zero P root tips ( $p = 0.875$  (touch maxima),  $p = 0.968$  (AUC)).

Application of 150 mM NaCl led to a significantly higher  $[Ca^{2+}]_{\text{cyt}}$  response (Figure 7D) compared to control solution treatment irrespective of P growth condition ( $p < 0.001$ ;  $n = 35 - 36$  root tips). Full P roots showed significantly higher touch maxima ( $1.29 \pm 0.02 \mu\text{M}$ ,  $p$ -value  $< 0.001$ ) than medium P root tips ( $1.0 \pm 0.02 \mu\text{M}$ ), which in turn responded significantly more strongly than zero P root tips ( $0.74 \pm 0.03 \mu\text{M}$ ,  $p < 0.001$ , Figure 7E). With regards to area under the curve, the  $[Ca^{2+}]_{\text{cyt}}$  response to NaCl was more prolonged in medium P root tips, resulting in a significantly higher area under the curve than full P root tips ( $p < 0.001$ , Figure 7F), even though the touch maxima was lower.

Treatment with 280 mM sorbitol led to a similarly strong response as was seen in NaCl-treated root tips, with full P root tips responding significantly more strongly ( $1.21 \pm 0.02 \mu\text{M}$ ) than medium and zero P root tips ( $0.84 \pm 0.05 \mu\text{M}$ ;  $0.72 \pm 0.04 \mu\text{M}$ ,  $p < 0.001$ ,  $n = 22 - 24$ , Figure 7H). For all P growth conditions, response to sorbitol was significantly higher than to control solution ( $p < 0.001$ ). As was seen for NaCl treatment, medium P root tips showed a more prolonged response to sorbitol than full and zero P root tips, resulting in an area under the curve not statistically significantly different from full P root tips ( $p = 0.113$ , Figure 7I). Zero P root tips show a significantly lower area under the curve compared to full and medium P root tips ( $p < 0.001$ , Figure 7I). Comparing NaCl and sorbitol treatment with the respective P growth conditions, neither touch maxima nor area under the curve were significantly different ( $p > 0.05$ ).



**Figure 7:** The  $[Ca^{2+}]_{cyt}$  response of phosphate-starved root tips to salt and osmotic stress. Col-0 aequorin-expressing seedlings were grown on full, medium (med) or zero P (green, purple, blue trace respectively). Root tips (1 cm) of 11-day old seedlings were challenged with treatments applied at 35 seconds, and  $[Ca^{2+}]_{cyt}$  was measured for 155 seconds. (A) Mechanical stimulation (control solution); time course trace represents mean  $\pm$  standard error of mean (SEM) from 3 independent trials, with  $n = 31 - 36$  root tips averaged per data point. Time course data were analysed for (B) touch maxima and (C) area under the curve (AUC), both baseline-subtracted, with each dot representing an individual data point (see Figure 6 for details). Boxplot middle line denotes median. (D-F) Responses to 150 mM NaCl (3 independent trials,  $n = 35 - 36$  root tips). (G-I) Responses to 280 mM sorbitol (3 independent trials,  $n = 22 - 24$  root tips). Analysis of variance (ANOVA) with *post-hoc* Tukey Test was used to assess statistical differences. Significance levels (*p*-values): \*\*\* ( $<0.001$ ), \*\* ( $<0.01$ ), \* ( $<0.05$ ), n.s. (not significant).

In a second set of experiments, root tips were challenged with oxidative stress in the form of hydrogen peroxide, H<sub>2</sub>O<sub>2</sub>. Stress treatments were 1 mM and 5 mM H<sub>2</sub>O<sub>2</sub> in control solution background. Application of control solution alone led to an immediate and monophasic [Ca<sup>2+</sup>]<sub>cyt</sub> response (Figure 8A), as was seen previously. However, in this set of experiments, response to control solution mostly did not differ between roots grown on different P conditions. The area under the curve was not significantly different between full P and zero P, as well as full P and medium P root tips ( $p > 0.05$ ,  $n = 24$  individual root tips per growth condition from 3 independent trials, Figure 8B). Medium P root tips showed a significantly higher area under the curve than zero P root tips ( $p = 0.003$ , Figure 8B). The maximum touch response to control solution did not differ between root tips grown on different P concentrations (full P:  $0.29 \pm 0.06 \mu\text{M}$ , medium P:  $0.30 \pm 0.04 \mu\text{M}$ , zero P:  $0.21 \pm 0.04 \mu\text{M}$ ,  $p > 0.05$  for all comparisons, Figure 8C).

Application of H<sub>2</sub>O<sub>2</sub> led to an overall biphasic increase in [Ca<sup>2+</sup>]<sub>cyt</sub> for both 1 and 5 mM H<sub>2</sub>O<sub>2</sub>. The immediate touch response was followed by a more prolonged increase in [Ca<sup>2+</sup>]<sub>cyt</sub> which peaked within approximately 30 seconds of onset, then slowly decreased without returning fully to pre-stimulus baseline levels within the timeframe monitored (Figure 8D, H).

Application of 1 mM H<sub>2</sub>O<sub>2</sub> led to significantly more [Ca<sup>2+</sup>]<sub>cyt</sub> being mobilised in full P root tips compared to medium and zero P root tips ( $p \leq 0.002$ , Figure 8E). Medium P root tips mobilised significantly more [Ca<sup>2+</sup>]<sub>cyt</sub> than zero P root tips ( $p = 0.001$ , Figure 8E). Touch maxima did not differ between full, medium and zero P root tips treated with 1 mM H<sub>2</sub>O<sub>2</sub> (full P:  $0.40 \pm 0.07 \mu\text{M}$ , medium P:  $0.34 \pm 0.03 \mu\text{M}$ , zero P:  $0.28 \pm 0.05 \mu\text{M}$ ,  $n = 23 - 24$  root tips per growth condition,  $p \geq 0.228$ , Figure 8F). Compared to control solution application, 1 mM H<sub>2</sub>O<sub>2</sub> did not lead to higher touch maxima in all three P regimes ( $p \geq 0.7$ ). The subsequent, prolonged increase in [Ca<sup>2+</sup>]<sub>cyt</sub> however was significantly lower in zero P root tips, compared to both full and medium P root tips (full P:  $0.39 \pm 0.01 \mu\text{M}$ , medium P:  $0.39 \pm 0.01 \mu\text{M}$ , zero P:  $0.26 \pm 0.01 \mu\text{M}$ ,  $p < 0.001$ , Figure 8G).

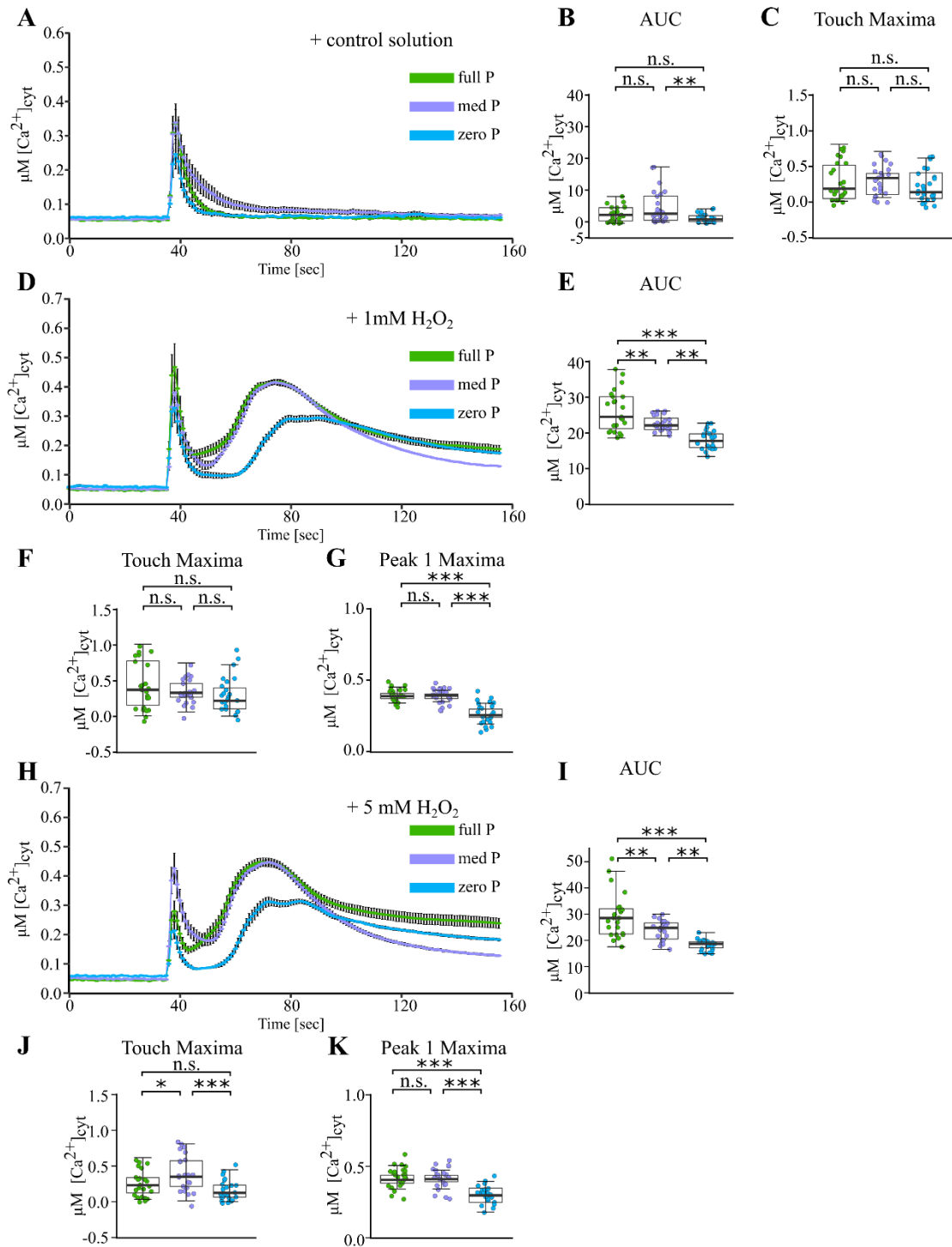
Increasing the treatment H<sub>2</sub>O<sub>2</sub> concentration to 5 mM resulted in a pattern of [Ca<sup>2+</sup>]<sub>cyt</sub> response that was very similar to 1 mM H<sub>2</sub>O<sub>2</sub> treatments (Figure 8H). Again, full P root tips mobilised significantly more [Ca<sup>2+</sup>]<sub>cyt</sub> than medium P and zero P root tips, as quantified by area under the curve ( $p \leq 0.003$ , Figure 8I). Medium P root tips in turn mobilised significantly more [Ca<sup>2+</sup>]<sub>cyt</sub> than zero P root tips ( $p = 0.004$ , Figure 8I). In contrast to treatment with 1 mM H<sub>2</sub>O<sub>2</sub> however, medium P root tips showed a higher

touch maximum ( $0.39 \pm 0.05 \mu\text{M}$ ,  $p \leq 0.34$ ) compared to full and zero P root tips (full P:  $0.25 \pm 0.03 \mu\text{M}$ , zero P:  $0.16 \pm 0.03 \mu\text{M}$ ,  $n = 22 - 24$  root tips per growth condition, Figure 8J). Touch maxima of full and zero P root tips did not differ significantly ( $p = 0.26$ ). Compared to control solution application, 5 mM  $\text{H}_2\text{O}_2$  did not lead to higher touch maxima in all three P regimes ( $p \geq 0.9$ ). As was seen for 1 mM  $\text{H}_2\text{O}_2$  treatment, the subsequent  $[\text{Ca}^{2+}]_{\text{cyt}}$  response was similarly high in full P and medium P root tips (Peak 1 maxima: full P:  $0.42 \pm 0.07 \mu\text{M}$ , medium P:  $0.41 \pm 0.03 \mu\text{M}$ ,  $p = 0.98$ ), but significantly dampened in zero P root tips ( $0.29 \pm 0.01 \mu\text{M}$ ,  $p < 0.001$ , Figure 8K).

When comparing control solution treatment to 1 mM and 5 mM  $\text{H}_2\text{O}_2$  stress treatment, touch maxima were not significantly different, regardless of P growth condition ( $p \geq 0.7$  for all comparisons). Unsurprisingly,  $\text{H}_2\text{O}_2$  treatment led to an overall significantly larger area under the curve in all P regimes, compared to control solution treatment ( $p < 0.001$ ).

When comparing 1 mM to 5 mM  $\text{H}_2\text{O}_2$  stress treatments, the  $[\text{Ca}^{2+}]_{\text{cyt}}$  response did not differ regardless of P growth condition ( $p \geq 0.3$ ). Peak maxima and area under the curve were very similar between 1 mM and 5 mM  $\text{H}_2\text{O}_2$  treatment, indicating that the root tips could not sense an increase in  $\text{H}_2\text{O}_2$  concentration, possibly because 1 mM  $\text{H}_2\text{O}_2$  already triggered the maximal  $[\text{Ca}^{2+}]_{\text{cyt}}$  stress response.





**Figure 8:** The [Ca<sup>2+</sup>]<sub>cyt</sub> response of phosphate-starved root tips to oxidative stress. Col-0 aequorin-expressing seedlings were grown on full, medium (med) or zero P (green, purple, blue trace respectively). Root tips (1 cm) of 11-day old seedlings were challenged with treatments applied at 35 seconds, and [Ca<sup>2+</sup>]<sub>cyt</sub> was measured for 155 seconds. (A) Mechanical stimulation (control solution); time course trace represents mean ± standard error of mean (SEM) from 3 independent trials, with n = 24 individual root tips averaged per data point. Time course data were analysed for (B) area under the curve (AUC) and (C) touch maxima, both baseline-subtracted, with each

dot representing an individual data point (see Figure 6 for details). Boxplot middle line denotes median. (D-G) Responses to 1 mM H<sub>2</sub>O<sub>2</sub> (3 independent trials, n = 23 – 24 root tips). (H-K) Responses to 5 mM H<sub>2</sub>O<sub>2</sub> (3 independent trials, n = 22 – 24 root tips). Analysis of variance (ANOVA) with *post-hoc* Tukey Test was used to assess statistical differences. Significance levels (*p*-values): \*\*\* (<0.001), \*\* (<0.01), \* (<0.05), n.s. (not significant).

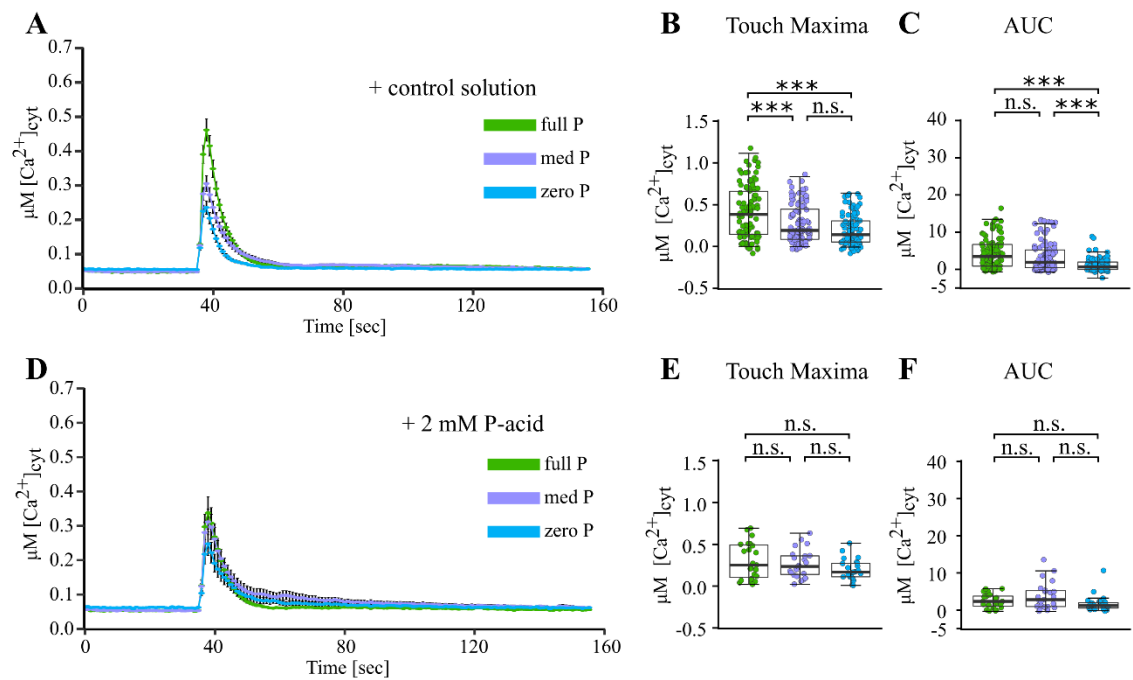
### 3.2.4 Phosphate-starved root tips show an altered [Ca<sup>2+</sup>]<sub>cyt</sub> response to extracellular nucleotides

P-starved, aequorin-expressing root tips were next challenged with the extracellular nucleotides ATP and ADP. ATP carries two hydrolysable P groups, ADP carries one, which might increase P availability in any solution if added as a treatment. As it was unknown how P-starved root tips respond to P resupply, an initial control experiment was therefore carried out to test if the P available from hydrolysis of ATP and ADP would trigger any [Ca<sup>2+</sup>]<sub>cyt</sub> response. To equal the maximum P available from a 1 mM ATP solution, a 2 mM phosphoric acid (P-acid) treatment solution was prepared in control solution background and used to treat root tips grown on different P conditions.

In this set of experiments, application of control solution again led to an immediate and monophasic [Ca<sup>2+</sup>]<sub>cyt</sub> response (Figure 9A). On average, the maximal [Ca<sup>2+</sup>]<sub>cyt</sub> increase was significantly higher in full P root tips, compared to medium and zero P root tips (Touch maxima: full P: 0.42 ± 0.03 μM, medium P: 0.27 ± 0.02 μM, zero P: 0.20 ± 0.02 μM, data from 11 independent trials, n = 90 - 97 individual root tips per growth condition, *p* < 0.001 for both comparisons, Figure 9B). Medium and zero P root tips showed a comparable touch maximum (*p* = 0.112, Figure 9B). The area under the curve was not significantly different between full and medium P root tips (*p* = 0.159), but significantly larger in full and medium P root tips compared to zero P root tips (*p* < 0.001, Figure 9C).

Application of a 2 mM P-acid solution led to a [Ca<sup>2+</sup>]<sub>cyt</sub> signature comparable to control solution treatment (Figure 9D), as the increase in [Ca<sup>2+</sup>]<sub>cyt</sub> was immediate and monophasic. Touch maxima of the root tips were as follows: full P: 0.30 ± 0.05 μM, medium P: 0.27 ± 0.04 μM, zero P: 0.2 ± 0.03 μM (data from 3 independent trials, n = 22 – 23 individual root tips), implying a trend of lowered touch response in zero P root tips. However, as data were variable (see individual data points in Figure 9E), neither touch maxima (Figure 9E) nor area under the curve (Figure 9F) were significantly different between the different P growth regimes (*p* > 0.05).

Comparing 2 mM P-acid treatment (in control solution background) to the respective control solution treatments did not show any significant differences for both touch maxima and area under the curve, regardless of P growth condition ( $p \geq 0.883$ ). This indicates that addition of a 2 mM P pulse to root tips does not evoke a different response than adding control solution alone. Therefore, ATP and ADP stress treatments could be carried out, reasoning that hydrolysed P from purine nucleotides would not interfere with the response of P-starved root tips.



**Figure 9:** The  $[Ca^{2+}]_{cyt}$  response of phosphate-starved root tips to mechanical stimulation and a phosphate source. Col-0 aequorin-expressing seedlings were grown on full, medium (med) or zero P (green, purple, blue trace respectively). Root tips (1 cm) of 11-day old seedlings were challenged with treatments applied at 35 seconds, and  $[Ca^{2+}]_{cyt}$  was measured for 155 seconds. (A) Mechanical stimulation (control solution); time course trace represents mean  $\pm$  standard error of mean (SEM) from 11 independent trials, with  $n = 90 - 97$  individual root tips averaged per data point. Time course data were analysed for (B) touch maxima and (C) area under the curve (AUC), both baseline-subtracted, with each dot representing an individual data point (see Figure 6 for details). Boxplot middle line denotes median. (D-F) Responses to 2 mM phosphoric acid (P-acid, 3 independent trials,  $n = 22 - 23$  root tips). Analysis of variance (ANOVA) with *post-hoc* Tukey Test was used to assess statistical differences. Significance levels ( $p$ -values): \*\*\* ( $<0.001$ ), \*\* ( $<0.01$ ), \* ( $<0.05$ ), n.s. (not significant).

In the next set of experiments, (apo)aequorin expressing wild type *Arabidopsis* seedlings were again P-starved, and root tips challenged with different concentrations of ATP (0.1 mM and 1 mM). Regardless of the concentration, ATP treatment led to a multi-phasic  $[Ca^{2+}]_{\text{cyt}}$  signature in control root tips (grown on full P). ATP application triggered an immediate increase in  $[Ca^{2+}]_{\text{cyt}}$ , similar in shape as seen for mechanical stimulation treatments previously. After approximately 15 seconds, this initial ‘touch’ response was superseded by a secondary increase and subsequent decrease, appearing as a peak for approximately 20 seconds (‘peak 1’), before another increase and decrease of  $[Ca^{2+}]_{\text{cyt}}$  defined another peak (‘peak 2’, Figure 10A, F). Most distinctively, this multi-phasic  $[Ca^{2+}]_{\text{cyt}}$  response was found to be dampened in P-starved root tips, with zero P grown root tips showing a reduced peak 1 and missing peak 2 (Figure 10A, F).

Application of 0.1 mM ATP led to the most  $[Ca^{2+}]_{\text{cyt}}$  being mobilised in full P grown root tips, showing a significantly larger area under the curve compared to medium P and zero P root tips (data from 6 individual trials,  $n = 34 - 36$  root tips per growth condition,  $p < 0.001$ , Figure 10B). Medium P root tips in turn showed a significantly larger area under the curve than zero P root tips ( $p < 0.001$ ). Full P root tips showed a variable touch response, however mean ( $0.59 \pm 0.06 \mu\text{M}$ ) full P touch maxima were significantly higher than medium P ( $0.4 \pm 0.05 \mu\text{M}$ ,  $p < 0.01$ ) and zero P root tips ( $0.23 \pm 0.04 \mu\text{M}$ ,  $p < 0.001$ , Figure 10C). With regards to peak 1 maxima, 0.1 mM ATP treatment led to a maximal and similar response of  $0.29 \pm 0.02 \mu\text{M}$  in full P and  $0.28 \pm 0.02 \mu\text{M}$  in medium P root tips ( $p = 0.684$ , Figure 10D). Zero P grown root tips showed strongly dampened peak 1 maxima ( $0.16 \pm 0.01 \mu\text{M}$ ), responding significantly different than full and medium P root tips ( $p < 0.001$ , Figure 10D). Most strikingly, peak 2 maxima differed strongly between the three P growth conditions. Full P roots showed a strong response, with mean peak 2 maxima of  $0.24 \pm 0.03 \mu\text{M}$ . Medium P root tips responded significantly less ( $0.15 \pm 0.01 \mu\text{M}$ ,  $p < 0.001$ , Figure 10E). Zero P root tips arguably did not show any increase of  $[Ca^{2+}]_{\text{cyt}}$  in the peak 2 phase analysed, but rather a ‘leak through’ of peak 1 (Figure 10A), with maximum mean  $[Ca^{2+}]_{\text{cyt}}$  of  $0.09 \pm 0.004 \mu\text{M}$ , being significantly lower than full and medium P root tips ( $p < 0.001$ , Figure 10E).

Application of 1 mM ATP led to a very similar  $[Ca^{2+}]_{\text{cyt}}$  response as was seen for 0.1 mM ATP application (data from 5 independent trials,  $n = 27 - 45$  root tips per growth condition). Full P root tips responded strongest, with three distinct peaks of  $[Ca^{2+}]_{\text{cyt}}$  (Figure 10F). Medium P root tips again showed a dampened  $[Ca^{2+}]_{\text{cyt}}$  signature, but with three distinct peaks of  $[Ca^{2+}]_{\text{cyt}}$  increase and decrease (Figure 10F). Zero P root tips again

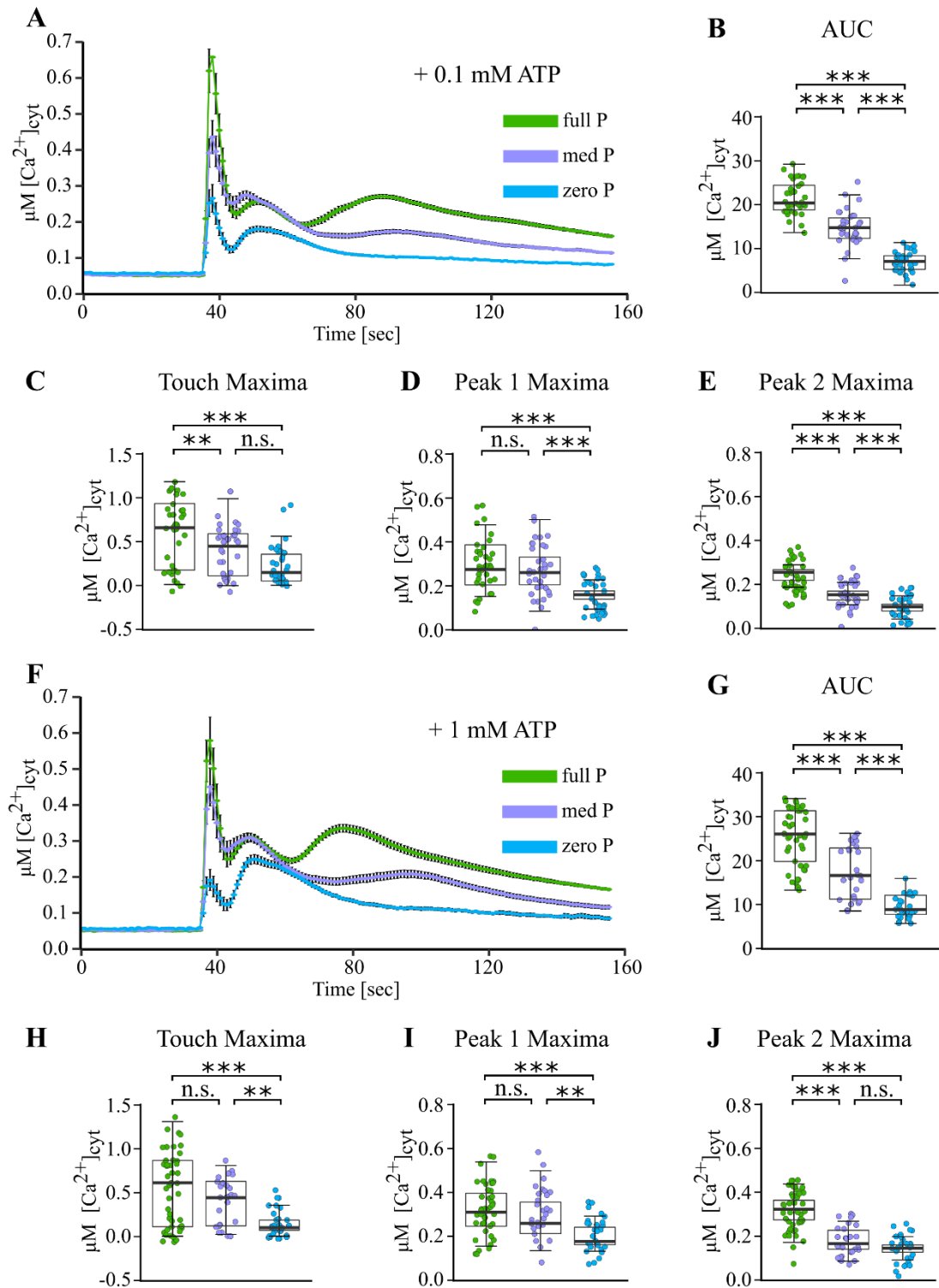
showed a dampened peak 1, and missed peak 2 (Figure 10F). Overall, the area under the curve was significantly larger in full P root tips compared to medium and zero P root tips ( $p < 0.001$ , Figure 10G). Medium P root tips had a larger area under the curve compared to zero P root tips ( $p < 0.001$ , Figure 10G). Full P root tips responded to 1 mM ATP application with mean touch maxima of  $0.54 \pm 0.06 \mu\text{M}$ , due to the spread of the data this was similar to the response of medium P root tips ( $0.40 \pm 0.05 \mu\text{M}$ ,  $p = 0.203$ , Figure 10H). Zero P root tips showed significantly lower touch maxima ( $0.15 \pm 0.02 \mu\text{M}$ ,  $p \leq 0.009$ , Figure 10H). The subsequent increase of  $[\text{Ca}^{2+}]_{\text{cyt}}$  was not significantly different in amplitude compared between full P and medium P root tips (peak 1 maxima full P:  $0.32 \pm 0.02 \mu\text{M}$ , medium P:  $0.29 \pm 0.02 \mu\text{M}$ ,  $p = 0.259$ , Figure 10I). Peak 1 maxima in zero P root tips were significantly lower ( $0.2 \pm 0.01 \mu\text{M}$ ) compared to full and medium P root tips ( $p \leq 0.001$ , Figure 10I). For peak 2 maxima, full P root tips responded significantly stronger ( $0.31 \pm 0.01 \mu\text{M}$ ) than medium ( $0.18 \pm 0.01 \mu\text{M}$ ) and zero P ( $0.15 \pm 0.01 \mu\text{M}$ ) root tips ( $p < 0.001$ , Figure 10J). Medium P and zero P grown root tips did not differ in their peak 2 maxima – as mentioned for 0.1 mM ATP treatment, this is likely to reflect a ‘leak through’ of peak 1 in zero P root tips, rather than an actual increase of  $[\text{Ca}^{2+}]_{\text{cyt}}$  within that phase.

Comparing ATP treatments with their respective control solution treatments (see Figure 9A-C) did not show any difference in touch maxima between 0.1 mM ATP treatment and control solution treatment ( $p \geq 0.123$ ), or 1 mM ATP treatment and control solution treatment respectively ( $p \geq 0.473$ ). This indicates that the initial touch response is due to mechanical stimulation, but independent of an ATP response.

To delineate if an increase of ATP concentration led to an increase in  $[\text{Ca}^{2+}]_{\text{cyt}}$  response, the two ATP treatments were compared within their P regimes (*e.g.* full P 0.1 mM ATP *versus* full P 1 mM ATP treatment). No difference could be seen between touch maxima ( $p = 0.999$ ), which agrees with the finding that this initial response is due to mechanical stimulation, and thus independent of ATP perception. Further, peak 1 maxima did not show a difference between 0.1 and 1 mM ATP in all P growth conditions ( $p \geq 0.977$ ). It was only for peak 2 maxima that increasing the ATP concentration ten-fold from 0.1 mM to 1 mM ATP led to a stronger response in full P and zero P root tips ( $p < 0.001$ ). Medium P root tips did not show a significantly increased response to higher ATP treatment ( $p = 0.128$ ). With regards to area under the curve, only full P root tips mobilised more  $[\text{Ca}^{2+}]_{\text{cyt}}$  in response to 1 mM ATP compared to 0.1 mM ATP ( $p < 0.001$ ). Medium P root tips and

zero P root tips did not show a ATP concentration-dependent significant increase in area under the curve ( $p = 0.366$ ,  $p = 0.329$  respectively).

Overall, P-starvation led to a dampening of the ATP-induced  $[Ca^{2+}]_{\text{cyt}}$  signature in medium P root tips, and a dampening (peak 1) as well as knock-out of a defined  $[Ca^{2+}]_{\text{cyt}}$  increase (peak 2) in zero P root tips. Only full P root tips overall responded to an increase in ATP concentration (determined by area under the curve), *i.e.* medium and zero P grown root tips did not mobilize more  $[Ca^{2+}]_{\text{cyt}}$  when increasing the ATP treatment from 0.1 mM to 1 mM. Increasing the ATP concentration ten-fold did not lead to stronger peak 1 maxima irrespective of P growth condition, but did increase peak 2 maxima in full P and zero P root tips. It needs to be stressed that the analysis of peak 2 maxima for zero P root tips might be hampered by the fact that zero P root tips did not show a defined increase and decrease within the phase analysed, but rather only a decrease of the preceding peak 1. This might bias absolute values of peak 2 maxima quantified and mask the missing response of zero P root tips in that phase.



**Figure 10:** The  $[Ca^{2+}]_{cyt}$  response of phosphate-starved root tips to extracellular ATP. Col-0 aequorin-expressing seedlings were grown on full, medium (med) or zero P (green, purple, blue trace respectively). Root tips (1 cm) of 11-day old seedlings were challenged with treatments applied at 35 seconds, and  $[Ca^{2+}]_{cyt}$  was measured for 155 seconds. (A) Stress treatment of 0.1 mM ATP; time course trace represents mean  $\pm$  standard error of mean (SEM) from 6 independent trials, with n = 34 - 36 individual root tips averaged per data point. Time course data were analysed

for (B) area under the curve (AUC), (C) touch maxima, (D) peak 1 maxima and (E) peak 2 maxima, all baseline-subtracted, with each dot representing an individual data point (see Figure 6 for details). Boxplot middle line denotes median. (F-G) Responses to 1 mM ATP (5 independent trials, n = 27 - 45 root tips per growth condition). Analysis of variance (ANOVA) with *post-hoc* Tukey Test was used to assess statistical differences. Significance levels (*p*-values): \*\*\* (<0.001), \*\* (<0.01), \* (<0.05), n.s. (not significant).

Next, it was interesting to test if the observed altered  $[Ca^{2+}]_{cyt}$  response of P-starved root tips in response to ATP treatment were dependent on ATP hydrolysis. Both hydrolysis, as well as hydrolytic products (such as ADP) could be direct effectors in the observed ATP response. First, a non-hydrolysable analogue of ATP was used to dissect any effect due to the mechanism of ATP hydrolysis. Adenosine 5'-[ $\gamma$ -thio]triphosphate tetralithium ( $\gamma$ -ATP) is one of the non-hydrolysable ATP analogues available. It is easily water soluble, and could therefore be prepared in control solution background as was done with standard ATP treatments.

As with ATP,  $\gamma$ -ATP was applied to (apo)aequorin expressing *Arabidopsis* Col-0 root tips, grown on full, medium and zero P growth medium. Two concentrations were tested, 0.1 mM and 1 mM  $\gamma$ -ATP (Figure 11). The  $[Ca^{2+}]_{cyt}$  response of root tips was very similar to what was seen upon ATP treatment. Upon application of 0.1 mM  $\gamma$ -ATP, the overall  $[Ca^{2+}]_{cyt}$  mobilised was significantly different between all P regimes, with full P root tips showing the largest area under the curve, and zero P root tips showing the smallest area under the curve ( $p < 0.001$ , data from 3 independent trials, n = 22 – 23 root tips per growth condition, Figure 11B). The touch maxima of full P root tips were variable, but their means were significantly higher ( $p < 0.01$ ) than medium and zero P grown root tips, which did not differ in touch maxima (touch maxima: full P:  $0.51 \pm 0.07 \mu M$ , medium P:  $0.27 \pm 0.04 \mu M$ , zero P:  $0.27 \pm 0.04 \mu M$ , Figure 11C). The same pattern was observed for peak 1 maxima, with full P root tips responding significantly stronger ( $p < 0.001$ ) than medium and zero P root tips, which responded similarly (peak 1 maxima: full P:  $0.31 \pm 0.02 \mu M$ , medium P:  $0.19 \pm 0.01 \mu M$ , zero P:  $0.16 \pm 0.01 \mu M$ , Figure 11D). For peak 2 maxima, significant differences between all P regimes were observed ( $p < 0.001$  for all comparisons, Figure 11E). Full P roots showed the highest mean  $[Ca^{2+}]_{cyt}$  response ( $0.21 \pm 0.01 \mu M$ ), medium P root tips a moderate  $[Ca^{2+}]_{cyt}$  response ( $0.13 \pm 0.01 \mu M$ ), and zero P root tips the lowest  $[Ca^{2+}]_{cyt}$  response ( $0.09 \pm 0.01 \mu M$ , Figure 11E).



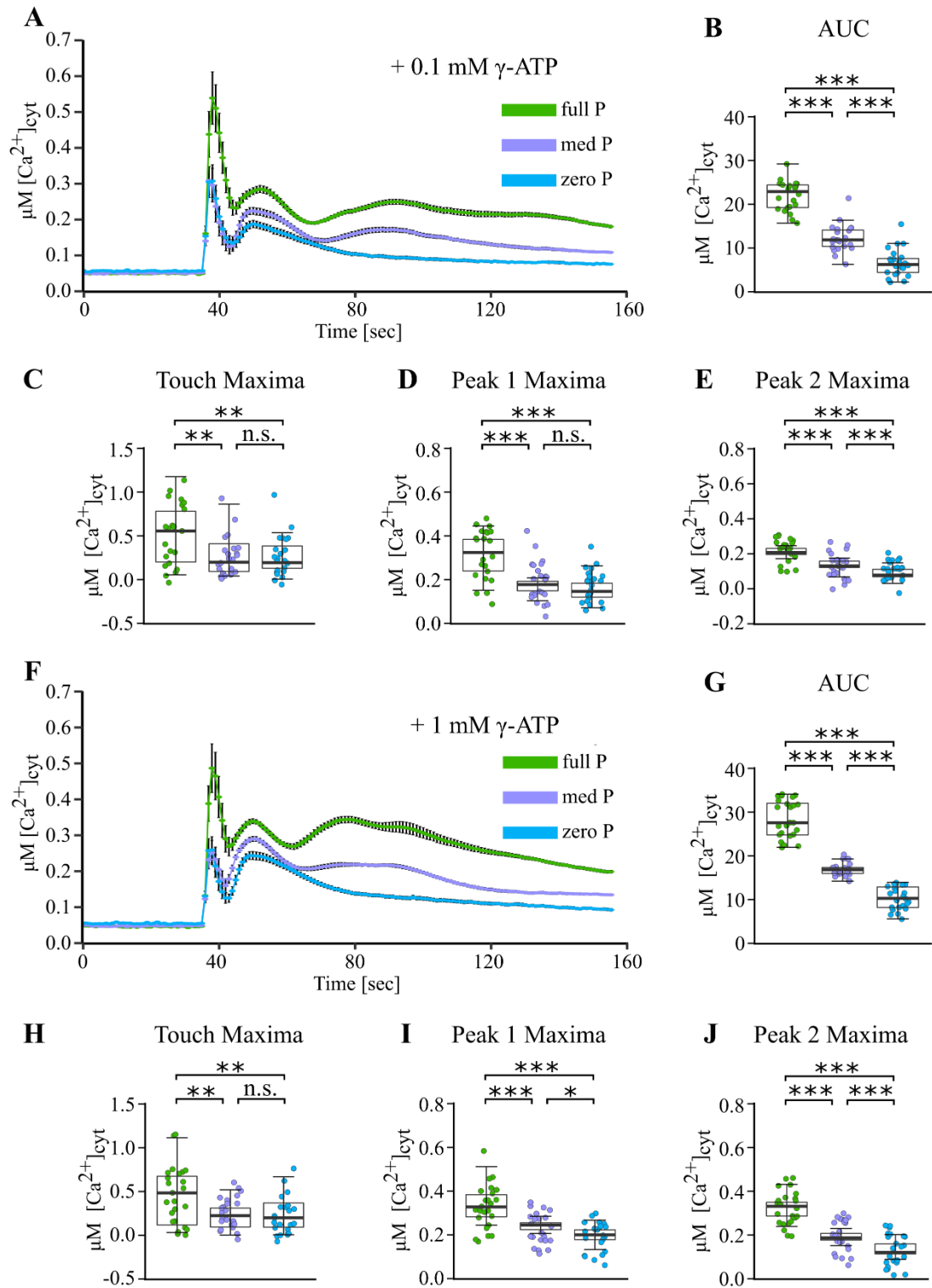
Increasing the  $\gamma$ -ATP concentration ten-fold, to 1 mM, led to a similar pattern of the  $[\text{Ca}^{2+}]_{\text{cyt}}$  response (Figure 11F). The area under the curve was significantly different between all P grown root tips, with full P root tips showing the largest area under the curve, and zero P root tips the smallest ( $p < 0.001$  in all comparisons, data from 3 independent trials, with  $n = 23 - 24$  root tips per growth condition, Figure 11G). Touch maxima were significantly higher ( $p \leq 0.01$ ) in full P root tips ( $0.46 \pm 0.07 \mu\text{M}$ ) compared to medium ( $0.23 \pm 0.03 \mu\text{M}$ ) and zero P root tips ( $0.23 \pm 0.04 \mu\text{M}$ , Figure 11H). This was the same pattern as was observed upon 0.1 mM  $\gamma$ -ATP treatment. Peak 1 maxima were significantly higher ( $p < 0.001$ ) in full P root tips ( $0.35 \pm 0.02 \mu\text{M}$ ) compared to medium ( $0.25 \pm 0.01 \mu\text{M}$ ) and zero P root tips ( $0.2 \pm 0.01 \mu\text{M}$ , Figure 11I). Peak 2 maxima differed significantly ( $p < 0.001$  for all comparisons), with full P root tips showing the strongest response ( $0.33 \pm 0.01 \mu\text{M}$ ) compared to medium ( $0.19 \pm 0.004 \mu\text{M}$ ) and zero P root tips ( $0.14 \pm 0.01 \mu\text{M}$ , Figure 11J). Again, this was the same pattern as observed upon 0.1 mM  $\gamma$ -ATP treatment.

Comparing  $\gamma$ -ATP treatments with their respective control solution treatments (see Figure 9A-C) did not show any difference in touch maxima between 0.1 mM  $\gamma$ -ATP treatment and control solution treatment ( $p \geq 0.996$ ), or 1 mM  $\gamma$ -ATP treatment and control solution treatment respectively ( $p \geq 0.999$ ), regardless of P regime. This corroborates what was seen with ATP treatment, and suggests that the initial touch response is due to mechanical stimulation, but independent of  $\gamma$ -ATP perception.

To characterize if an increase of  $\gamma$ -ATP concentration led to a difference in  $[\text{Ca}^{2+}]_{\text{cyt}}$  response, the response of root tips to 0.1 mM and 1 mM  $\gamma$ -ATP was compared. For both touch maxima and peak 1 maxima, there were no differences between 0.1 mM and 1 mM  $\gamma$ -ATP treatment ( $p \geq 0.891$ ), regardless of P regime. Peak 2 maxima were significantly higher in response to 1mM  $\gamma$ -ATP ( $p < 0.001$ ) for all P growth conditions. Overall, this led to a significant larger area under the curve for full P and medium P root tips in response to 1mM  $\gamma$ -ATP compared to 0.1 mM  $\gamma$ -ATP ( $p \leq 0.003$ ). Zero P root tips did also show an increase of area under the curve, when increasing the  $\gamma$ -ATP concentration to 1 mM, this difference was however not significant ( $p = 0.07$ ).

To answer the initial question – if the hydrolysis of ATP played a role in the observed  $[\text{Ca}^{2+}]_{\text{cyt}}$  responses – ATP and  $\gamma$ -ATP treatments were compared within respective P growth conditions. None of the parameters analysed (area under the curve, touch maxima, peak 1 maxima, peak 2 maxima) showed any significant difference when comparing 0.1 mM ATP and 0.1 mM  $\gamma$ -ATP, as well as 1 mM ATP and 1 mM  $\gamma$ -ATP ( $p$ -values were

in the range of 0.125 – 0.999). This suggests that (i) the  $[Ca^{2+}]_{cyt}$  response observed in full P root tips (= control root tips) was independent of ATP hydrolysis, and (ii) that ATP hydrolysis did not play a role in the dampened and altered  $[Ca^{2+}]_{cyt}$  response observed in P-starved root tips.



**Figure 11:** The  $[Ca^{2+}]_{cyt}$  response of phosphate-starved root tips to a non-hydrolysable ATP analogue. Col-0 aequorin-expressing seedlings were grown on full, medium (med) or zero P (green, purple, blue trace respectively). Root tips (1 cm) of 11-day old seedlings were challenged with treatments applied at 35 seconds, and  $[Ca^{2+}]_{cyt}$  was measured for 155 seconds. (A) Stress treatment of 0.1 mM  $\gamma$ -ATP; time course trace represents mean  $\pm$  standard error of mean (SEM) from 3 independent trials, with  $n = 22 - 23$  individual root tips averaged per data point. Time

course data were analysed for (B) area under the curve (AUC), (C) touch maxima, (D) peak 1 maxima and (E) peak 2 maxima, all baseline-subtracted, with each dot representing an individual data point (see Figure 6 for details). Boxplot middle line denotes median. (F-G) Responses to 1 mM  $\gamma$ -ATP (3 independent trials, n = 23 - 24 root tips per growth condition). Analysis of variance (ANOVA) with *post-hoc* Tukey Test was used to assess statistical differences. Significance levels (*p*-values): \*\*\* (<0.001), \*\* (<0.01), \* (<0.05), n.s. (not significant).

In the next set of experiments, the effect of the purine nucleotide ADP on the  $[Ca^{2+}]_{\text{cyt}}$  response of P-starved, (apo)aequorin expressing *Arabidopsis* Col-0 plants was investigated. Two different concentrations of ADP, 0.1 mM and 1 mM, were prepared in control solution background and applied to root tips. Treatment with ADP led to a similar  $[Ca^{2+}]_{\text{cyt}}$  signature as was seen upon ATP and  $\gamma$ -ATP treatment – a multi-phasic response, which could be divided into three distinct phases (touch, peak 1, peak 2), with P-starved root tips showing an altered signature (Figure 12A, F).

Application of 0.1 mM ADP triggered the strongest  $[Ca^{2+}]_{\text{cyt}}$  response in full P root tips, which showed a significantly higher area under the curve compared to medium and zero P root tips ( $p < 0.001$ , Figure 12B). Medium P root tips in turn responded significantly more strongly than zero P root tips ( $p < 0.001$ , Figure 12B). The initial response to 0.1 mM ADP, quantified as mean touch maxima, were similar between the three P growth conditions (full P:  $0.38 \pm 0.07 \mu\text{M}$ , medium P:  $0.32 \pm 0.04 \mu\text{M}$ , zero P:  $0.3 \pm 0.04 \mu\text{M}$ ,  $p \geq 0.582$ , Figure 12C). With regards to peak 1 maxima, full and medium P root tips responded similarly ( $0.26 \pm 0.01 \mu\text{M}$ ,  $0.26 \pm 0.02 \mu\text{M}$ , respectively,  $p = 0.985$ , Figure 12D). Zero P root tips showed significantly dampened peak 1 maxima ( $0.16 \pm 0.01 \mu\text{M}$ ) compared to full and medium P root tips ( $p < 0.001$ , Figure 12D). With regards to peak 2 maxima, full P root tips responded significantly more strongly ( $0.27 \pm 0.01 \mu\text{M}$ ) than medium P root tips ( $0.19 \pm 0.01 \mu\text{M}$ ,  $p < 0.001$ ), which in turn responded significantly more strongly than zero P root tips ( $0.1 \pm 0.01 \mu\text{M}$ ,  $p < 0.001$ , Figure 12E).

Increasing the ADP concentration ten-fold to 1 mM led to a similar  $[Ca^{2+}]_{\text{cyt}}$  pattern as was observed upon application of 0.1 mM ADP (Figure 12F). Again, area under the curve was largest for full P, intermediate for medium P and smallest for zero P root tips ( $p < 0.001$  for all comparisons, Figure 12G). Touch maxima in response to 1 mM ADP were not different between the P growth conditions (full P:  $0.39 \pm 0.06 \mu\text{M}$ , medium P:  $0.28 \pm 0.05 \mu\text{M}$ , zero P:  $0.30 \pm 0.05 \mu\text{M}$ ,  $p \geq 0.268$ , Figure 12H). Peak 1 maxima were comparable between full P ( $0.30 \pm 0.02 \mu\text{M}$ ) and medium P ( $0.28 \pm 0.01 \mu\text{M}$ ,  $p = 0.7$ ,

Figure 12I) root tips. Zero P root tips however showed significantly lower peak 1 maxima compared to full and medium P root tips ( $p < 0.01$ , Figure 12I). Peak 2 maxima were significantly different between all P growth conditions, with full P root tips exhibiting the strongest response ( $0.34 \pm 0.01 \mu\text{M}$ ), medium P root tips responding intermediately ( $0.24 \pm 0.01 \mu\text{M}$ ) and zero P root tips the lowest ( $0.15 \pm 0.01 \mu\text{M}$ ,  $p < 0.001$  for all comparisons, Figure 12K). As mentioned for ATP and  $\gamma$ -ATP treatment experiments: zero P root tips did not show a defined peak (increase and decrease of  $[\text{Ca}^{2+}]_{\text{cyt}}$ ) with the phase, where peak 2 maxima were easily determined for full and medium P root tips. The value reported for zero P root tips might rather be a trailing off of peak 1.

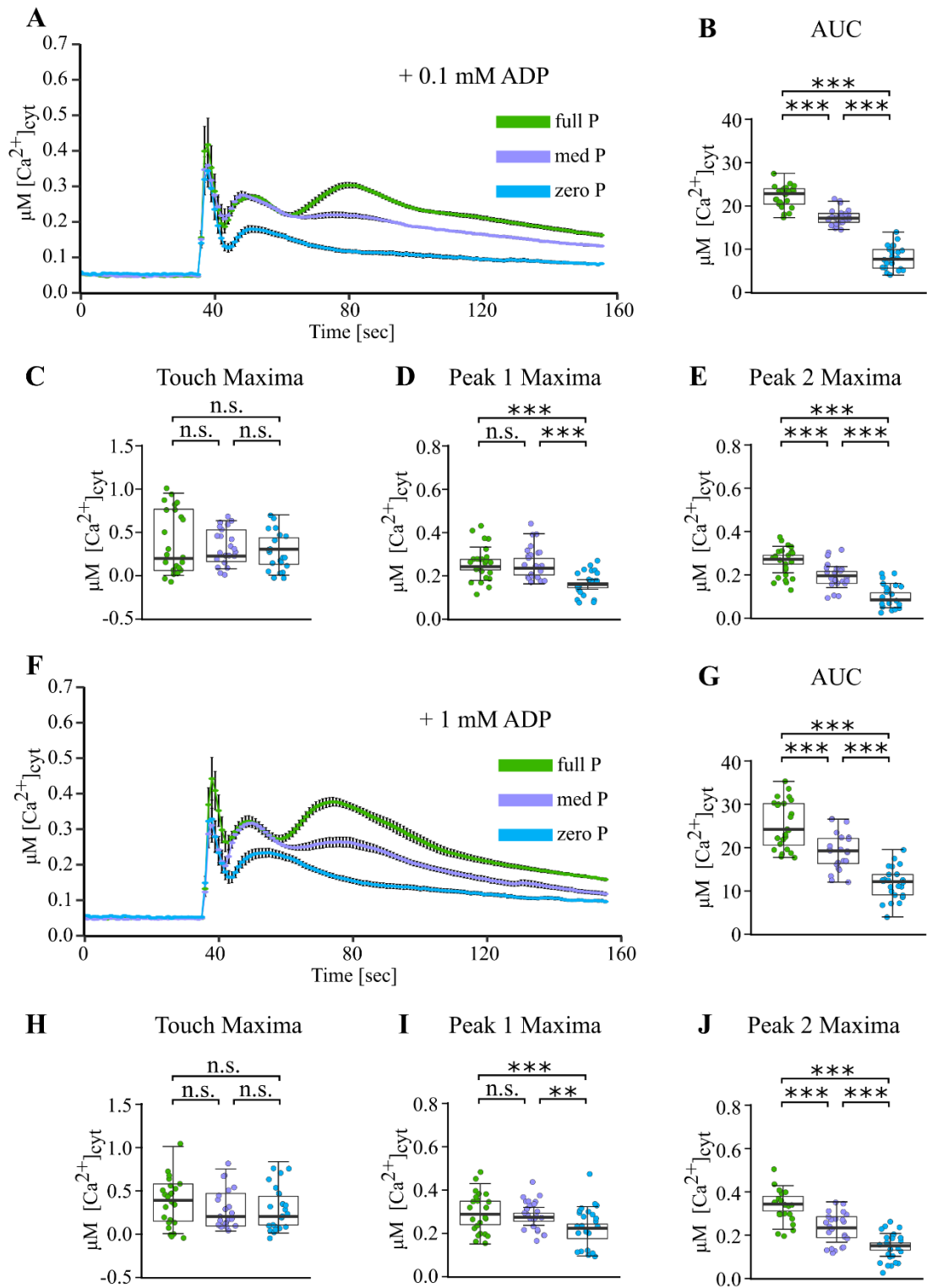
Comparing both 0.1 mM and 1 mM ADP treatments with their respective control solution treatments (see Figure 9A-C) showed very similar maximal touch responses, regardless of P growth condition ( $p \geq 0.534$  for all comparisons). This corroborates the observations described above for ATP and  $\gamma$ -ATP treatments, *i.e.* the ‘touch response’ being attributable to mechanical stimulation but not to a response to purinergic molecules. ADP in all cases mobilized significantly more  $[\text{Ca}^{2+}]_{\text{cyt}}$  compared to control solution application, when comparing area under the curves for all P growth conditions ( $p < 0.001$  for all comparisons).

To understand if roots responded differently to a ten-fold increase in ADP concentration, their  $[\text{Ca}^{2+}]_{\text{cyt}}$  response to 0.1 mM and 1 mM ADP treatment was compared. Regardless of P growth condition, touch maxima and peak 1 maxima did not show a significant difference between 0.1 mM and 1 mM ADP treatment ( $p$ -values in the range of 0.355 – 0.999 for all comparisons). Peak 2 maxima however were significantly higher when treating root tips with 1 mM ADP, for all P growth conditions ( $p \leq 0.001$  for all comparisons). Overall, 1 mM ADP led to a significantly larger area under the curve in zero P grown root tips ( $p = 0.027$ ), whereas medium P root tips did not show a larger area under the curve ( $p = 0.901$ ). Full P grown root tips did show an overall larger area under the curve in response to the higher ADP treatment of 1 mM, the difference was however not significant ( $p = 0.078$ ).

To answer the initial question, if any hydrolytic product were involved in shaping the  $[\text{Ca}^{2+}]_{\text{cyt}}$  signature when challenging roots with ATP treatment, ADP and ATP treatments were compared. Comparing 0.1 mM ADP with 0.1 mM ATP, and 1 mM ADP with 1 mM ATP treatments showed that there was no significant difference between touch maxima and peak 1 maxima ( $p$ -values in the range of 0.061 – 0.999 for all comparisons). It was only for peak 2 maxima and subsequently, area under the curve, that differences were

observed, depending on P growth condition: Full P grown root tips showed a significantly stronger response to 0.1 mM ADP compared to 0.1 mM ATP ( $p = 0.011$ ). However, this difference was lost when higher concentrations (1 mM) of both ATP and ADP were applied ( $p = 0.348$ ). No difference of area under the curve was observed in full P grown root tips, comparing low ADP to low ATP, and high ADP to high ATP treatment ( $p \geq 0.960$ ). Medium P grown root tips showed the most pronounced difference between ADP and ATP treatment: 0.1 mM ADP treatment evoked significantly higher peak 2 maxima compared to 0.1 mM ATP treatment ( $p < 0.001$ ), the same was observed when comparing 1 mM ADP treatment to 1 mM ATP treatment ( $p < 0.001$ ). This subsequently resulted in a significantly smaller area under the curve in medium P grown root tips treated with 0.1 mM ATP compared to 0.1 mM ADP ( $p = 0.014$ ). However, the area under the curve in response to 1 mM ATP and 1 mM ADP in medium P root tips was similar ( $p = 0.847$ ). Zero P grown root tips did not show a difference in response to low ATP and low ADP, or high ATP and high ADP treatment ( $p \geq 0.628$ ).

Taken together, ADP application to root tips triggered a very similar  $[Ca^{2+}]_{\text{cyt}}$  response to what was observed for ATP treatment. Furthermore, P-starvation led to a similarly dampened  $[Ca^{2+}]_{\text{cyt}}$  response to ADP, as well as an altered  $[Ca^{2+}]_{\text{cyt}}$  signature with regards to peak 2. A ten-fold increase in ADP concentration (0.1 mM to 1 mM) did not affect analysed touch maxima or peak 1 maxima, it did however increase the downstream peak 2.



**Figure 12:** The  $[Ca^{2+}]_{cyt}$  response of phosphate-starved root tips to extracellular ADP. Col-0 aequorin-expressing seedlings were grown on full, medium (med) or zero P (green, purple, blue trace respectively). Root tips (1 cm) of 11-day old seedlings were challenged with treatments applied at 35 seconds, and  $[Ca^{2+}]_{cyt}$  was measured for 155 seconds. (A) Stress treatment of 0.1 mM ADP; time course trace represents mean  $\pm$  standard error of mean (SEM) from 3 independent trials, with  $n = 22 - 24$  individual root tips averaged per data point. Time course data were

analysed for (B) area under the curve (AUC), (C) touch maxima, (D) peak 1 maxima and (E) peak 2 maxima, all baseline-subtracted, with each dot representing an individual data point (see Figure 6 for details). Boxplot middle line denotes median. (F-G) Responses to 1 mM ADP (3 independent trials,  $n = 23 - 24$  root tips per growth condition). Analysis of variance (ANOVA) with *post-hoc* Tukey Test was used to assess statistical differences. Significance levels ( $p$ -values): \*\*\* ( $<0.001$ ), \*\* ( $<0.01$ ), \* ( $<0.05$ ), n.s. (not significant).

### 3.2.5 Phosphate-starved root tips tend to respond less to mechanical stimulation

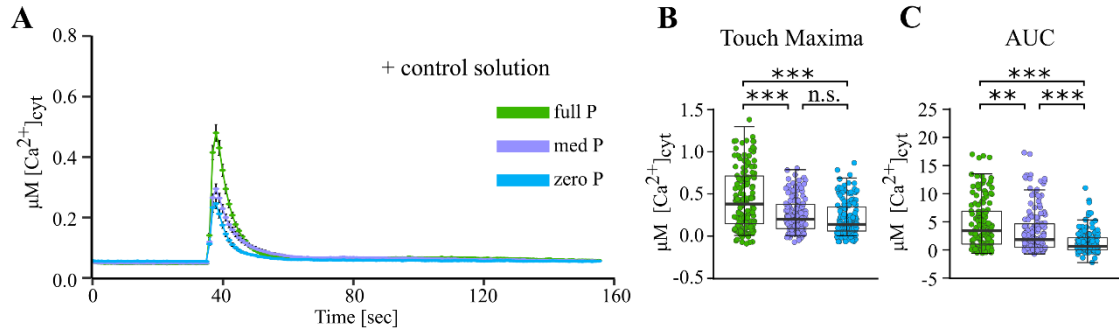
In previous experiments, a trend was observed that the amplitude of the touch response was linked to the P growth condition, *i.e.* full P root tips showing a stronger  $[Ca^{2+}]_{cyt}$  response to mechanical stimulation, and zero P root tips showing a weaker response. However, the response was variable *e.g.*, full P root tips showing a wide range of weak to strong responses to mechanical stimulation. In some sets of experiments, this response was significantly different between P regimes (see control treatments run together with NaCl, sorbitol, and purine nucleotide experiments (Figure 7, Figure 9). In other experiments, root tips grown on different P growth conditions did not show a significant difference in response to mechanical stimulation (even though the trend was there, see  $H_2O_2$  experiments, Figure 8).

To gain a clearer picture, control solution treatments of individual experiments were compiled to increase statistical power (18 independent trials,  $n = 150 - 155$  individual root tips per P growth condition, Figure 13). Application of control solution clearly evoked a stronger mean  $[Ca^{2+}]_{cyt}$  response in full P grown root tips ( $0.44 \pm 0.03 \mu M$ ), compared to medium P ( $0.26 \pm 0.02 \mu M$ ) and zero P root tips ( $0.21 \pm 0.02 \mu M$ ,  $p < 0.001$  for both comparisons, Figure 13A, B). Medium and zero P grown root tips did not show a significant difference in touch maxima ( $p = 0.185$ , Figure 13B). With regards to area under the curve, full P root tips mobilized significantly more  $[Ca^{2+}]_{cyt}$  compared to medium and zero P root tips ( $p \leq 0.01$ , Figure 13C). In contrast to touch maxima, medium P root tips showed a significantly larger area under the curve compared to zero P root tips, as their response was prolonged ( $p < 0.001$ , Figure 13C).

Taken together, this indicates that P starvation influences the ability of root tips to respond to mechanical stimulation. As the response to mechanical stimulation was varied, even in



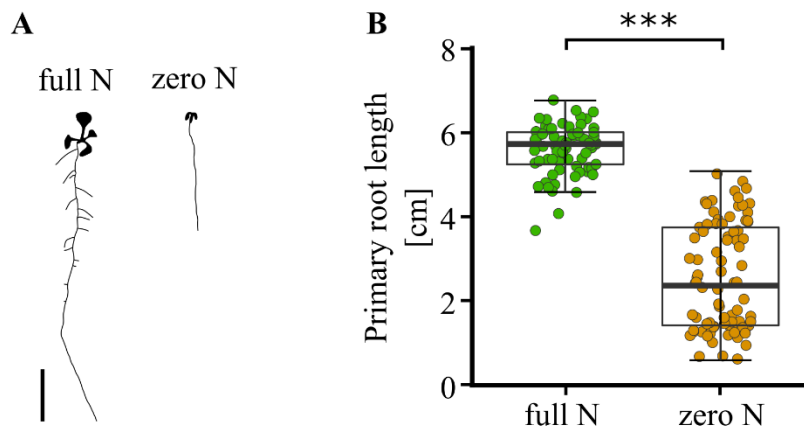
nutrient-sufficient conditions (= full P), this difference could be observed as a trend in smaller sets of experiments, gaining statistical significance when increasing sample size.



**Figure 13:** The  $[Ca^{2+}]_{cyt}$  response of phosphate-starved root tips to mechanical stimulation. *Arabidopsis* Col-0 aequorin-expressing seedlings were grown on full, medium (med) or zero P (green, purple, blue trace respectively). Root tips (1 cm) of 11-day old seedlings were challenged with treatments applied at 35 seconds, and  $[Ca^{2+}]_{cyt}$  was measured for 155 seconds. (A) Mechanical stimulation by application of control solution; time course trace represents mean  $\pm$  standard error of mean (SEM) from 18 compiled independent trials, with n = 150 – 155 individual root tips averaged per data point. Time course data were analysed for (B) area under the curve (AUC) and (C) touch maxima, all baseline-subtracted, with each dot representing an individual data point (see Figure 6 for details). Boxplot middle line denotes median. Analysis of variance (ANOVA) with *post-hoc* Tukey Test was used to assess statistical differences. Significance levels (*p*-values): \*\*\* (<0.001), \*\* (<0.01), \* (<0.05), n.s. (not significant).

### 3.2.6 Nitrogen starvation leads to primary root length reduction

Next, it was of interest to test if the dampened  $[Ca^{2+}]_{\text{cyt}}$  response described above were specific to P nutrition, or a general starvation response. Therefore, (apo)aequorin expressing *Arabidopsis* Col-0 plants were starved of nitrogen (N). To induce N starvation, seedlings were germinated and grown on half MS, containing either standard amounts of N ('full N': 19.7 mM N total), or no N ('zero N': 0 mM N). The full N condition is the same as the full P condition reported earlier (both are standard half MS). Starving seedlings of N led to severely stunted plants, which strongly differed in root architecture, as quantified after 10 days of growth (Figure 14A). N-starved seedlings appeared overall more fragile than P-starved seedlings. Mean primary root lengths of seedlings grown on full N conditions were  $5.6 \pm 0.07$  cm (data from 3 independent trials,  $n = 76 - 88$  individual root tips per growth condition, Figure 14B). N-starved primary roots were significantly shorter ( $2.5 \pm 0.13$  cm,  $p < 0.001$ , Welch two sample  $t$ -test, Figure 14B). N-starvation thus led to primary roots that were comparable in length to P-starved roots ( $p = 0.203$ , see Figure 4 for zero P primary root lengths).



**Figure 14:** Nitrogen starvation alters root architecture of *Arabidopsis*. Col-0 was grown on gel-based nutrient medium with varying N concentrations: full N (19.7 mM N) or zero N (0 mM N). On day 10, plants were scanned and primary root length was quantified using the ImageJ NeuronJ Plugin. (A) Representative root system architecture of 10-day old seedlings, scale bar: 1 cm. (B) Primary root lengths of  $n = 76 - 88$  individual seedlings per growth condition, data from 3 independent trials. Boxplot thick middle line denotes median. Welch two-sample  $t$ -test was used to assess statistical differences. Significance levels ( $p$ -value): \*\*\* ( $<0.001$ ).

### 3.2.7 Nitrogen starvation does not dampen the $[Ca^{2+}]_{cyt}$ signature in response to abiotic stresses

In a first set of experiments, N-starved roots were challenged with salt and osmotic stress. To account for differences in root size between full and zero N roots, 1 cm of root tip was used for the assays, as was done for P starvation experiments. As salt stress has a major osmotic component, an osmotic treatment was run alongside the salt treatment. The osmotic treatment, 280 mM sorbitol, was prepared to be osmotically equivalent to the salt stress treatment of 150 mM NaCl.

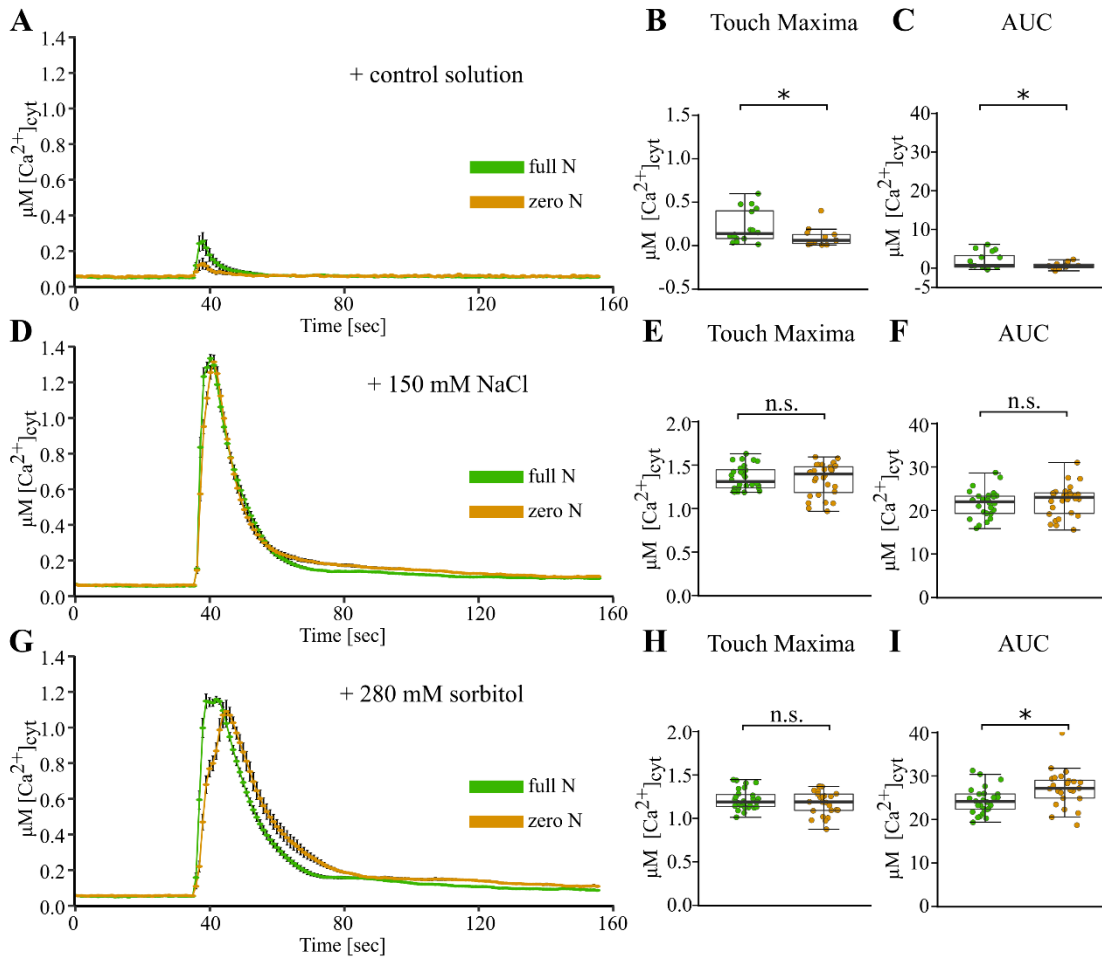
To control for mechanical stimulation due to application of treatment solutions, control solution was applied to full and zero N root tips, resulting in an immediate increase of  $[Ca^{2+}]_{cyt}$  (data of 3 independent experiments, with  $n = 13 - 16$  individual root tips per growth condition, Figure 15A). Full N root tips showed slight but significantly higher touch maxima ( $0.21 \pm 0.05 \mu M$ ) than zero N root tips ( $0.1 \pm 0.03 \mu M$ , ANOVA with *post-hoc* Tukey test:  $p = 0.04$ , Figure 15B). Equally, the area under the curve was significantly larger in full N root tips compared to zero N root tips ( $p = 0.049$ , Figure 15C).

Application of 150 mM NaCl led to an immediate, strong and monophasic increase in  $[Ca^{2+}]_{cyt}$ , returning to baseline levels within approximately 40 seconds ( $n = 28$  individual root tips per growth condition, Figure 15D). Full and zero N root tips responded very similarly with regards to touch maxima (full N:  $1.35 \pm 0.03 \mu M$ , zero N:  $1.3 \pm 0.04 \mu M$ ,  $p = 0.7$ , Figure 15E) as well as area under the curve ( $p = 0.43$ , Figure 15F).

Application of 280 mM sorbitol led to a similar  $[Ca^{2+}]_{cyt}$  signature as was seen in response to salt treatment: an immediate, strong and monophasic response, returning to baseline levels within approximately 40 seconds ( $n = 24 - 27$  individual root tips per growth condition, Figure 15G). The touch maxima of full and zero N root tips were similar (full N:  $1.22 \pm 0.02 \mu M$ , zero N:  $1.18 \pm 0.03 \mu M$ ,  $p = 0.246$ , Figure 15H). However, zero N root tips overall mobilised more  $[Ca^{2+}]_{cyt}$ , as their response to sorbitol was slightly prolonged (quantified as area under the curve,  $p = 0.01$ , Figure 15I).

Compared with control solution application, salt and osmotic stress led in all parameters analysed to a significantly stronger  $[Ca^{2+}]_{cyt}$  response, regardless of N growth condition ( $p < 0.001$  for all comparisons). Comparing salt to osmotic stress treatment, full N root tips did not show a significant difference in touch maxima or area under the curve ( $p = 0.068$ ,  $p = 0.582$ , respectively). Zero N root tips showed significantly lower touch maxima

in response to sorbitol compared to salt treatment ( $p < 0.001$ ), but no difference in area under the curve ( $p = 0.137$ ).

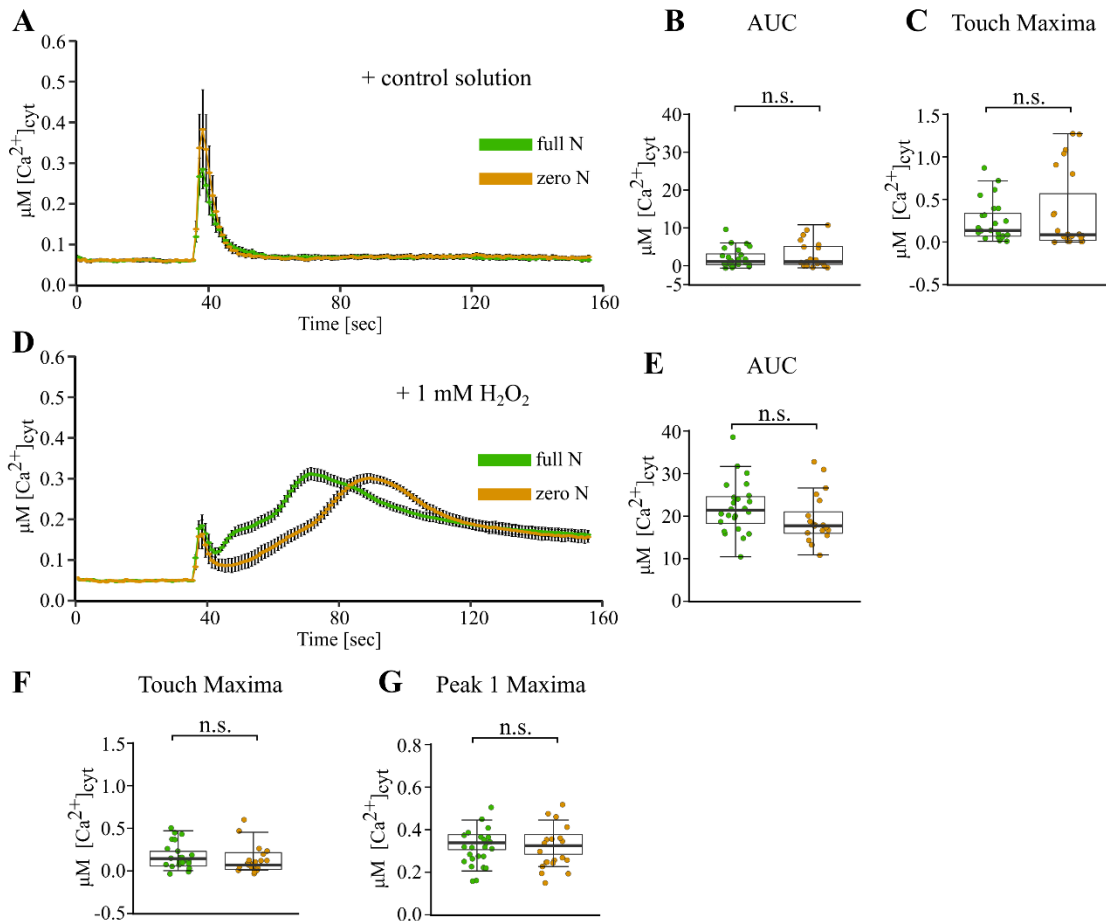


**Figure 15:** The  $[Ca^{2+}]_{cyt}$  response of nitrogen-starved root tips to salt and osmotic stress. Col-0 aequorin-expressing seedlings were grown on full N or zero N (green, beige trace respectively). Root tips (1 cm) of 11-day old seedlings were challenged with treatments applied at 35 seconds, and  $[Ca^{2+}]_{cyt}$  was measured for 155 seconds. (A) Application of control solution; time course trace represents mean  $\pm$  standard error of mean (SEM) from 3 independent trials, with  $n = 13 - 16$  individual root tips averaged per data point. Time course data were analysed for (B) touch maxima (AUC) and (C) area under the curve (AUC), all baseline-subtracted, with each dot representing an individual data point (see Figure 6 for details). Boxplot middle line denotes median. (D-F) Responses to 150 mM NaCl (3 independent trials,  $n = 28$  individual root tips per growth condition). (G-I) Responses to 280 mM sorbitol (3 independent trials,  $n = 24 - 27$  individual root tips per growth condition). Analysis of variance (ANOVA) with *post-hoc* Tukey Test was used to assess statistical differences. Significance levels ( $p$ -values): \*\*\* ( $<0.001$ ), \*\* ( $<0.01$ ), \* ( $<0.05$ ), n.s. (not significant).

In a second set of experiments, N-starved root tips were challenged with oxidative stress in the form of 1 mM H<sub>2</sub>O<sub>2</sub> (data from 3 independent trials, Figure 16). Application of control solution led to similar areas under the curves between full and zero N root tips ( $p = 0.418$ ,  $n = 23 - 24$  individual root tips per growth condition, Figure 16B). Equally, touch maxima did not differ significantly, as especially the response in zero N root tips was variable (full N:  $0.24 \pm 0.05 \mu\text{M}$ , zero N:  $0.34 \pm 0.1 \mu\text{M}$ ,  $p = 0.373$ , Figure 16C).

Application of 1 mM H<sub>2</sub>O<sub>2</sub> triggered a biphasic [Ca<sup>2+</sup>]<sub>cyt</sub> response, where an immediate touch response was followed by a prolonged increase in [Ca<sup>2+</sup>]<sub>cyt</sub> of approximately 50 seconds, which then started to decrease but did not reach pre-treatment baseline levels within the time monitored ( $n = 20 - 24$  individual root tips per growth condition, Figure 16D). The overall mobilised [Ca<sup>2+</sup>]<sub>cyt</sub> was not significantly different between full and zero N root tips ( $p = 0.118$ , Figure 16E). Similarly, touch maxima (full N:  $0.18 \pm 0.3 \mu\text{M}$ , zero N:  $0.15 \pm 0.4 \mu\text{M}$ ,  $p = 0.537$ , Figure 16F) and peak 1 maxima (full N:  $0.33 \pm 0.2 \mu\text{M}$ , zero N:  $0.32 \pm 0.2 \mu\text{M}$ ,  $p = 0.984$ , Figure 16G) did not differ between the N growth conditions. Even though the amplitude of the [Ca<sup>2+</sup>]<sub>cyt</sub> response was similar between full and zero N root tips, it was striking that zero N root tips significantly lagged behind in their prolonged ('peak 1') response to 1 mM H<sub>2</sub>O<sub>2</sub>. Zero N root tips reached peak 1 maxima on average 17 seconds later than full N root tips (timing of peak 1 maxima, given as seconds after start of experiment: full N:  $74.4 \pm 3.2$  seconds, zero N:  $91.5 \pm 3.4$  seconds,  $p = 0.001$  (as determined by Welch two sample *t*-test)).

Comparing 1 mM H<sub>2</sub>O<sub>2</sub> and control solution application, touch maxima were highly variable and therefore not significantly different, regardless of N regime ( $p \geq 0.763$ ). On the other hand, 1 mM H<sub>2</sub>O<sub>2</sub> mobilised significantly more [Ca<sup>2+</sup>]<sub>cyt</sub> overall than did control solution treatment, regardless of N growth condition (area under the curve:  $p < 0.001$ ).



**Figure 16:** The [Ca<sup>2+</sup>]<sub>cyt</sub> response of nitrogen-starved root tips to oxidative stress. Col-0 aequorin-expressing seedlings were grown on full or zero N (green, beige trace respectively). Root tips (1 cm) of 11-day old seedlings were challenged with treatments applied at 35 seconds, and [Ca<sup>2+</sup>]<sub>cyt</sub> was measured for 155 seconds. (A) Mechanical stimulation (control solution); time course trace represents mean ± standard error of mean (SEM) from 3 independent trials, with n = 23 - 24 individual root tips averaged per data point. Time course data were analysed for (B) area under the curve (AUC) and (C) touch maxima, both baseline-subtracted, with each dot representing an individual data point (see Figure 6 for details). Boxplot middle line denotes median. (D-G) Responses to 1 mM H<sub>2</sub>O<sub>2</sub> (3 independent trials, n = 20 - 24 root tips). Analysis of variance (ANOVA) with *post-hoc* Tukey Test was used to assess statistical differences. Significance levels (*p*-values): \*\*\* (<0.001), \*\* (<0.01), \* (<0.05), n.s. (not significant).

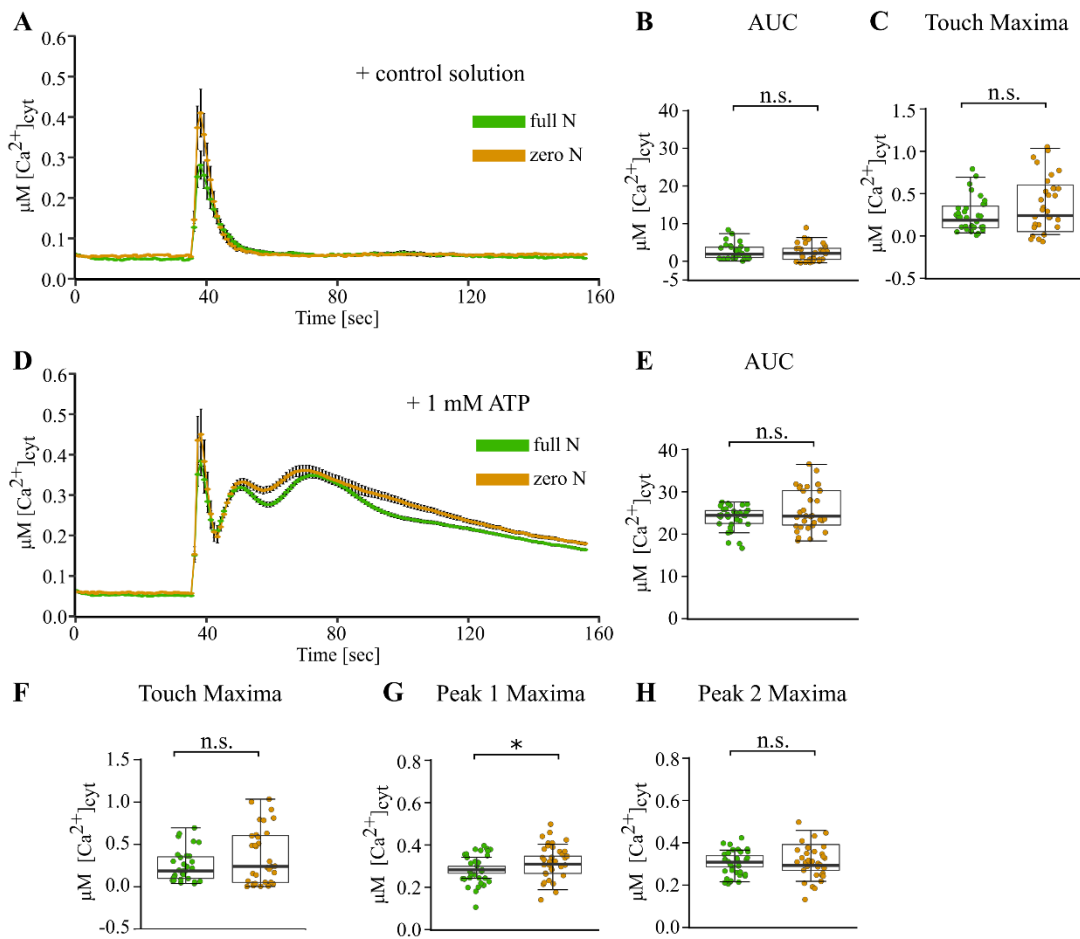
In a last set of experiments using N-starved root tips, these were treated with 1 mM extracellular ATP (data from 3 independent trials, Figure 17). Application of control solution again led to an immediate and monophasic increase in [Ca<sup>2+</sup>]<sub>cyt</sub> (n = 31 - 32 individual root tips per growth condition, Figure 17A). Full and zero N root tips responded similarly, with no significant difference between their areas under the curve

( $p = 0.662$ , Figure 17B). Touch maxima were variable, especially in zero N root tips, but not significantly different (full N:  $0.25 \pm 0.3 \mu\text{M}$ , zero N:  $0.37 \pm 0.6 \mu\text{M}$ ,  $p = 0.08$ , Figure 17C).

Application of 1 mM ATP led to a multi-phasic  $[\text{Ca}^{2+}]_{\text{cyt}}$  signature, without any apparent difference between the response of full and zero N root tips ( $n = 33 - 34$  individual root tips per growth condition, Figure 17D). Zero N root tips showed a more variable area under the curve, but on average mobilised comparable amounts of  $[\text{Ca}^{2+}]_{\text{cyt}}$  compared with full N root tips ( $p = 0.05$ , Figure 17E). Touch maxima (full N:  $0.34 \pm 0.04 \mu\text{M}$ , zero N:  $0.40 \pm 0.06 \mu\text{M}$ ,  $p = 0.362$ , Figure 17F) and peak 2 maxima (full N:  $0.31 \pm 0.01 \mu\text{M}$ , zero N:  $0.32 \pm 0.01 \mu\text{M}$ ,  $p = 0.336$ , Figure 17H) did not differ depending on the N-status of the root tips. Only peak 1 maxima showed a significant difference, as zero N root tips responded slightly, but significantly, more strongly (full N:  $0.28 \pm 0.01 \mu\text{M}$ , zero N:  $0.32 \pm 0.01 \mu\text{M}$ ,  $p = 0.021$ , Figure 17G).

Comparing control solution treatment with 1 mM ATP treatment showed no difference for the initial touch maxima ( $p \geq 0.539$ ), regardless of N regime. With regards to total  $[\text{Ca}^{2+}]_{\text{cyt}}$  mobilized, ATP treatment led to a significantly larger area under the curve than control solution treatment in both full and zero N root tips ( $p < 0.001$ ).

Taken together, the response of N-starved root tips to NaCl, sorbitol,  $\text{H}_2\text{O}_2$  and ATP resembled that of N-sufficient root tips. This was an interesting finding, as N-starved seedlings looked poorly, even more so than P-starved root tips.



**Figure 17:** The  $[Ca^{2+}]_{cyt}$  response of nitrogen-starved root tips to extracellular ATP. Col-0 aequorin-expressing seedlings were grown on full N or zero N (green, beige trace respectively). Root tips (1 cm) of 11-day old seedlings were challenged with treatments applied at 35 seconds, and  $[Ca^{2+}]_{cyt}$  was measured for 155 seconds. (A) Mechanical stimulation (control solution); time course trace represents mean  $\pm$  standard error of mean (SEM) from 3 independent trials, with  $n = 31 - 32$  individual root tips averaged per data point. Time course data were analysed for (B) area under the curve (AUC) and (C) touch maxima, both baseline-subtracted, with each dot representing an individual data point (see Figure 6 for details). Boxplot middle line denotes median. (D-H) Responses to 1 mM eATP (3 independent trials,  $n = 33 - 34$  individual root tips per growth condition). Analysis of variance (ANOVA) with *post-hoc* Tukey Test was used to assess statistical differences. Significance levels ( $p$ -values): \*\*\* ( $<0.001$ ), \*\* ( $<0.01$ ), \* ( $<0.05$ ), n.s. (not significant).



### 3.2.8 Overall aequorin luminescence levels are comparable between nutrient conditions

All experiments shown so far were based on the use of (apo)aequorin as reporter construct. In this construct, the aequorin gene is under the control of a 35S-promoter, leading to constitutively high aequorin protein expression in the cytosol of all cell types. Differences of aequorin protein levels between individual plant samples are controlled for by ‘discharging’ all available aequorin in any given sample at the end of each experiment (see Chapter 2, section 2.6.2). This allows normalization of the  $[Ca^{2+}]_{\text{cyt}}$  stress response with overall ‘ability’ of the given sample to respond to the stress, based on total luminescence counts as a proxy for aequorin levels.

However, nutrient starvation conditions might alter (a) aequorin expression and / or (b) reconstitution of (apo)aequorin with its co-factor coelenterazine, as coelenterazine uptake across the plasma membrane might differ. This could potentially bias the  $[Ca^{2+}]_{\text{cyt}}$  signature. Initial trials were therefore re-examined for levels of total aequorin luminescence signal, to appraise the use of this particular reporter construct in nutrient starvation experiments (for its other characteristics, see Chapter 1, section 1.2.9). Individual root tips were found to support varying levels of aequorin discharge, as determined by total luminescence counts, but to similar levels when overall comparing P starvation conditions (Figure 18).

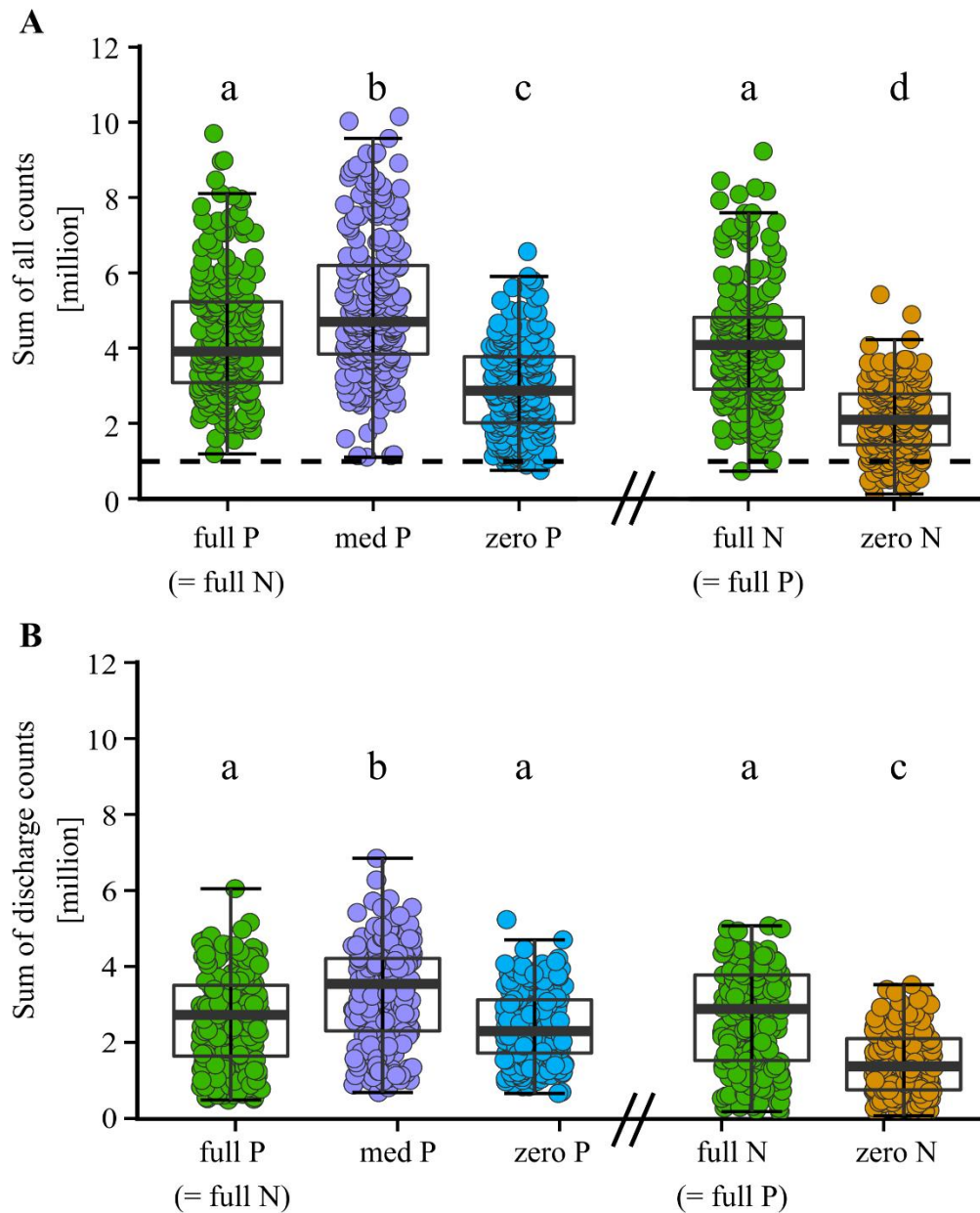
When finishing a larger body of experimental trials, overall aequorin discharge levels were compiled from root tips challenged with control solution and test solutions (Figure 18). Root tip aequorin discharge levels were assessed with two parameters: (i) ‘sum of all counts’, the overall luminescence signal including ‘discharged’ aequorin (Figure 18A), and (ii) sum of discharge counts, the luminescence signal occurring 4 seconds after application of discharge solution (Figure 18B). Four seconds was the time frame in which, after application of discharge solution, the major luminescence response of all remaining available aequorin occurred. This was taken as a proxy of how much coelenterazine-reconstituted aequorin could have been available for previous stress response during treatment application.

With regards to total luminescence counts (‘sum of all counts’), full P and full N grown root tips showed the strongest response, and were not significantly different from each other ( $p = 0.847$ ). This was as expected as full P / full N were both standard half MS, nutrient replete conditions. Medium P root tips showed higher, zero P root tips lower total

luminescence counts ( $p < 0.001$ ). Zero N root tips showed the lowest total luminescence signal, significantly lower than all other nutrient conditions ( $p < 0.001$ ). Mean sum of all counts were as follows (mean  $\pm$  SEM, in million counts) for compiled P-starvation trials: full P:  $4.3 \pm 0.1$ , medium P:  $5.1 \pm 0.1$ , zero P:  $2.9 \pm 0.07$  and for compiled N-starvation trials: full N:  $4.1 \pm 0.1$ , zero N:  $2.1 \pm 0.06$  (data from 19 independent trials, with  $n = 211 - 231$  individual root tips per growth condition, Figure 18A). A total luminescence count of one million had been used in laboratory practice as an acceptable threshold for a 'strong' luminescence signal when selecting lines after aequorin-transformation. All growth conditions barring some samples of zero N root tips were above this threshold (see dashed black line, Figure 18A), indicating strong luminescence signal.

Considering a smaller window of luminescence signal, namely the immediate seconds after discharge application, showed a similar picture. Full P, full N and also zero P root tips showed no significant difference (in million counts: full P:  $2.6 \pm 0.08$ , full N:  $2.7 \pm 0.09$ , zero P:  $2.4 \pm 0.06$ ,  $p \geq 0.149$ , Figure 18B). Medium P root tips again showed a significantly stronger signal ( $3.3 \pm 0.09$ ,  $p < 0.001$ ). Zero N root tips showed the lowest immediate discharge response ( $1.5 \pm 0.06$ ,  $p < 0.001$  compared to all other conditions, Figure 18B).

Overall, this indicates that nutrient conditions did affect aequorin discharge levels. However, the luminescence signal of all root tips was still considerably strong. As this study is particularly interested in the response of P-starved roots, with N-starved root tips showing similarly shaped  $[Ca^{2+}]_{\text{cyt}}$  signatures compared to nutrient-replete plants, the use of aequorin as  $[Ca^{2+}]_{\text{cyt}}$  reporter was considered acceptable.



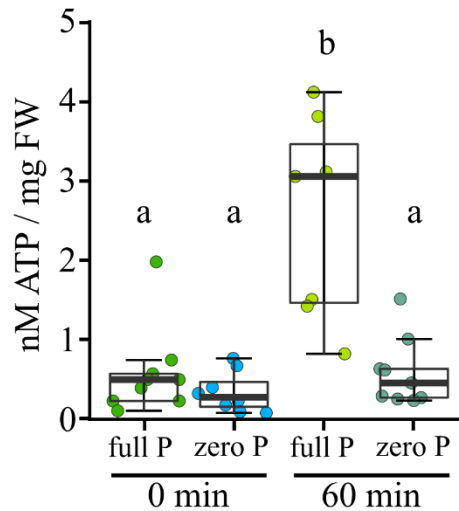
**Figure 18:** Luminescence counts of compiled aequorin experiments. (A) Sum of all counts (in million), each dot representing total luminescence counts of one individual root tip sample as monitored within 200 seconds, including stress treatment application and ‘discharge’ of all remaining, reconstituted aequorin. Data were compiled if belonging to P-starvation experimental series (zero, medium (med), full P; green, purple, blue trace respectively, on the left) or N-starvation experimental series (full, zero N; green, beige trace respectively, on the right). Full P and full N are both standard half MS growth condition. Data from 19 independent trials,  $n = 211 - 230$  individual root tip samples per growth condition. Boxplot middle line denotes median. (B) As A, but only considering luminescence counts immediately (4 seconds) after application of discharge solution. Analysis of variance (ANOVA) with *post-hoc* Tukey Test was used to assess statistical differences. Different lower-case letters describe groups of significant statistical difference ( $p < 0.05$ ), same letters indicate no statistical significance ( $p > 0.05$ ).

### 3.2.9 Phosphate-starved root tips still accumulate extracellular ATP

As it was unknown if P-starved plants still employ eATP as a P-costly signalling molecule, the capacity of P-starved root tips to accumulate eATP in the extracellular space was investigated. To do so, the roots of full P and zero P whole seedlings were placed into control solution bathing medium (containing respective full or zero P concentrations, see Chapter 2 section 2.4 for further details). Samples of bathing medium close to the root were taken immediately after immersion (0 min) and after a prolonged period of immersion in the bathing medium (60 min). Concentrations of ATP in these samples were determined using a luciferase-assay. To normalize for differences in root size, ATP concentrations were then calculated relative to root biomass (Figure 19).

Immediately after immersion, full P roots supported mean concentrations of  $0.58 \pm 0.19$  nM ATP per mg root fresh weight (root mg FW, data of 3 independent trials,  $n = 7 - 9$  individual samples per growth condition), zero P roots supported  $0.34 \pm 0.09$  nM per root mg FW, which was not significantly different ( $p = 0.999$ , Figure 19). After one hour of keeping the roots in the medium, full P roots showed significantly more ATP ( $2.6 \pm 0.49$  nM ATP per root mg FW) than zero P roots ( $0.59 \pm 0.14$  nM ATP per root mg FW,  $p < 0.001$ , Figure 19). Even though the mean eATP accumulation of zero P roots was slightly higher after 60 minutes compared to 0 minutes, the difference between the two time points was not significant ( $p = 0.999$ ).

As this technique cannot take the effect of hydrolysed ATP into account, the following can be concluded: full P roots accumulated higher amounts of eATP in their surrounding assay medium, and / or showed a lower rate of eATP hydrolysis than zero P roots. Extracellular ATP could be detected in the assay medium of zero P root tips, indicating that P-starved roots still accumulated some eATP. However, whether lower eATP accumulation is due to less efflux, and / or higher rate of ATP hydrolysis remains to be determined.



**Figure 19:** Quantification of extracellular ATP in root bathing medium of phosphate-starved roots. Col-0 seedlings were grown on full or zero P. Roots of 11-day old seedlings were submerged into control solution (roots of four seedlings per sample), with shoots not touching the bathing medium. Bathing medium samples were taken immediately (0 min) after placing the seedlings into the bathing medium, and after 60 minutes. ATP concentrations of these samples were analysed using a luciferase assay, with two technical replicates per sample. Each dot represents the mean of two technical replicates per biological sample. Boxplot middle line denotes median. Data from 3 independent trials, with  $n = 7 - 9$  individual samples per growth condition. Analysis of variance (ANOVA) with *post-hoc* Tukey Test was used to assess statistical differences. Different lower-case letters describe groups of significant statistical difference ( $p < 0.05$ ), same letters indicate no statistical significance ( $p > 0.05$ ).

### 3.2.10 Proteins potentially involved in shaping the altered $[Ca^{2+}]_{\text{cyt}}$ in phosphate-starved root tips

To understand if - under P starvation - roots rely on the same mechanistic components to perceive eATP as under P-sufficient conditions, aequorin-expressing *dorn1-1* mutant lines were grown on full and zero P conditions. Root tips (1 cm) were challenged with control solution, as control for mechanical stimulation occurring in the assay, or 1 mM ATP in control solution background, as the eATP treatment (Figure 20).

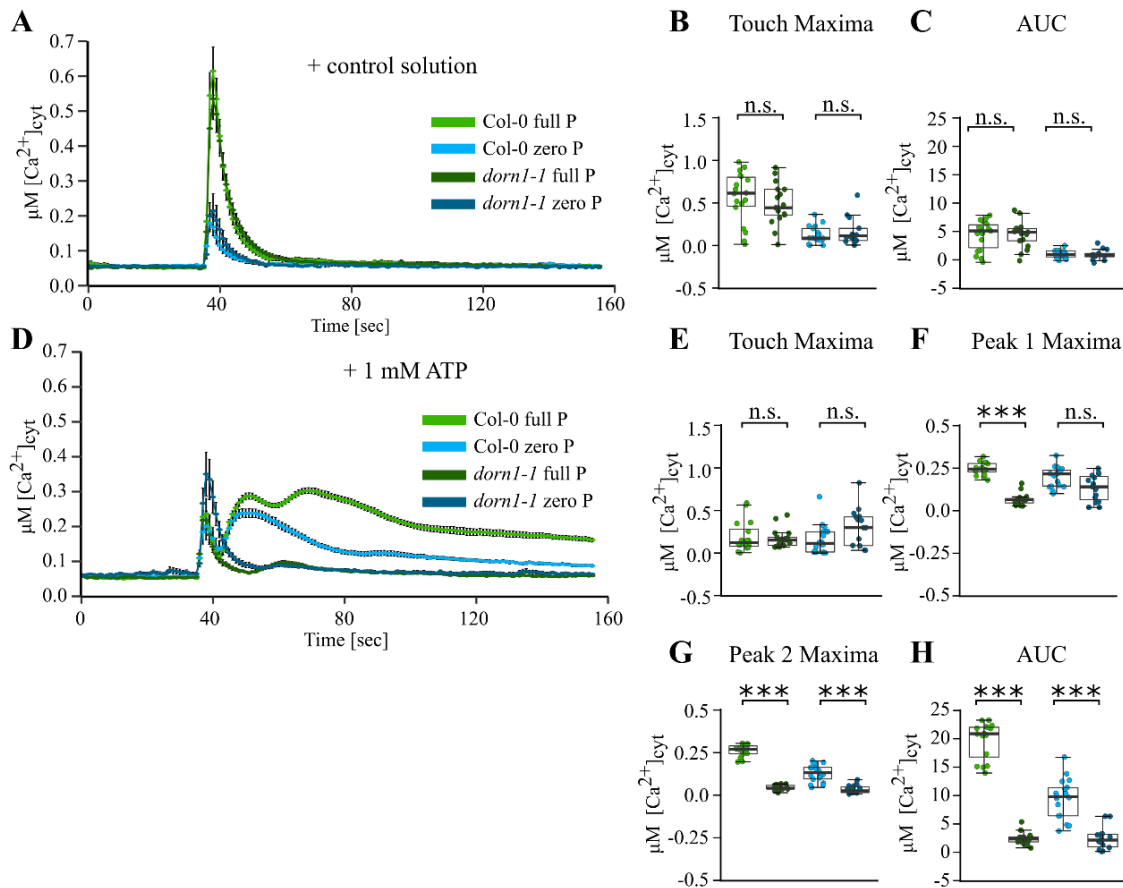
Control solution application led to an immediate and monophasic  $[Ca^{2+}]_{\text{cyt}}$  response in both Col-0 as well as *dorn1-1* mutant plants (data from 3 independent trials,  $n = 13 - 18$  individual root tips per growth condition and genotype, Figure 20A). The maximal  $[Ca^{2+}]_{\text{cyt}}$  increase was higher in full P root tips (Col-0:  $0.57 \pm 0.07 \mu\text{M}$ , *dorn1-1*:  $0.49 \pm 0.06 \mu\text{M}$ ) than in zero P root tips (Col-0:  $0.13 \pm 0.03 \mu\text{M}$ , *dorn1-1*:  $0.17 \pm 0.05 \mu\text{M}$ , Figure 20B), however it did not differ between the genotypes with respect to the two P conditions ( $p \geq 0.928$ ). Equally, the area under the curve did not differ between Col-0 and *dorn1-1* in response to mechanical stimulation (Figure 20C).

Application of 1 mM eATP led to a multi-phasic response in  $[Ca^{2+}]_{\text{cyt}}$  in Col-0 root tips grown on full P, and the characteristically altered  $[Ca^{2+}]_{\text{cyt}}$  response of zero P root tips ( $n = 16 - 18$  individual root tips per growth condition and genotype, Figure 20D). In *dorn1-1* root tips however, only an initial touch response was observed, without any further strong  $[Ca^{2+}]_{\text{cyt}}$  increases as seen in wild type root tips (Figure 20D). Touch maxima were not significantly different between wild type and *dorn1-1*, neither for full nor zero P conditions (Col-0: full P:  $0.19 \pm 0.05 \mu\text{M}$ , zero P:  $0.16 \pm 0.04 \mu\text{M}$ ; *dorn1-1*: full P:  $0.17 \pm 0.03 \mu\text{M}$ , zero P:  $0.3 \pm 0.06 \mu\text{M}$ ;  $p \geq 0.424$ , Figure 20E). Peak 1 maxima were significantly higher in wild type root tips grown on full P ( $0.25 \pm 0.01 \mu\text{M}$ ) compared to *dorn1-1* ( $0.07 \pm 0.01 \mu\text{M}$ ,  $p < 0.001$ , Figure 20F). Zero P root tips however showed no significant difference in peak 1 maxima between wild type ( $0.2 \pm 0.01 \mu\text{M}$ ) and *dorn1-1* ( $0.13 \pm 0.02 \mu\text{M}$ ,  $p = 0.212$ , Figure 20F), even though the  $[Ca^{2+}]_{\text{cyt}}$  response was a much more defined peak in wild type than in *dorn1-1* (see Figure 20D). This is likely due to the bias introduced into analysis of peak 1 maxima, as *dorn1-1* touch response was slightly more prolonged, ‘leaking’ into the phase analysed for peak 1 maxima (see Figure 6 for analysis details). Wild type peak 2 maxima were dependent on P conditions (full P:  $0.26 \pm 0.01 \mu\text{M}$ , zero P:  $0.13 \pm 0.01 \mu\text{M}$ ), as has been reported earlier (for more details see Figure 10). Independent of P-regime, *dorn1-1* however showed

significantly lower peak 2 maxima than wild type (full P:  $0.05 \pm 0.001 \mu\text{M}$ , zero P:  $0.03 \pm 0.01 \mu\text{M}$ ,  $p < 0.001$  for both comparisons), as no  $[\text{Ca}^{2+}]_{\text{cyt}}$  response to ATP was observed (Figure 20G). Overall, wild type root tips mobilized more  $[\text{Ca}^{2+}]_{\text{cyt}}$  than *dorn1-1* independent of P growth condition ( $p < 0.001$  for both comparisons, Figure 20H).

It should be pointed out that in response to eATP, a very slight  $[\text{Ca}^{2+}]_{\text{cyt}}$  increase of approximately 15 seconds can be observed in *dorn1-1* root tips, independent of P growth condition (see Figure 20D). This is more of a response than previously reported (J. Choi, Tanaka, Cao, *et al.*, 2014), where whole seedlings of *dorn1-1* did not show even the slightest response to ATP.

Taken together, both wild type and *dorn1-1* root tips responded to mechanical stimulation. However, *dorn1-1* mutant lines showed an overall impaired response to eATP, independent of P regime. This indicates that the perception of eATP is dependent on DORN1 under P replete and starvation conditions, and no alternative ATP-perception comes into effect under P starvation.



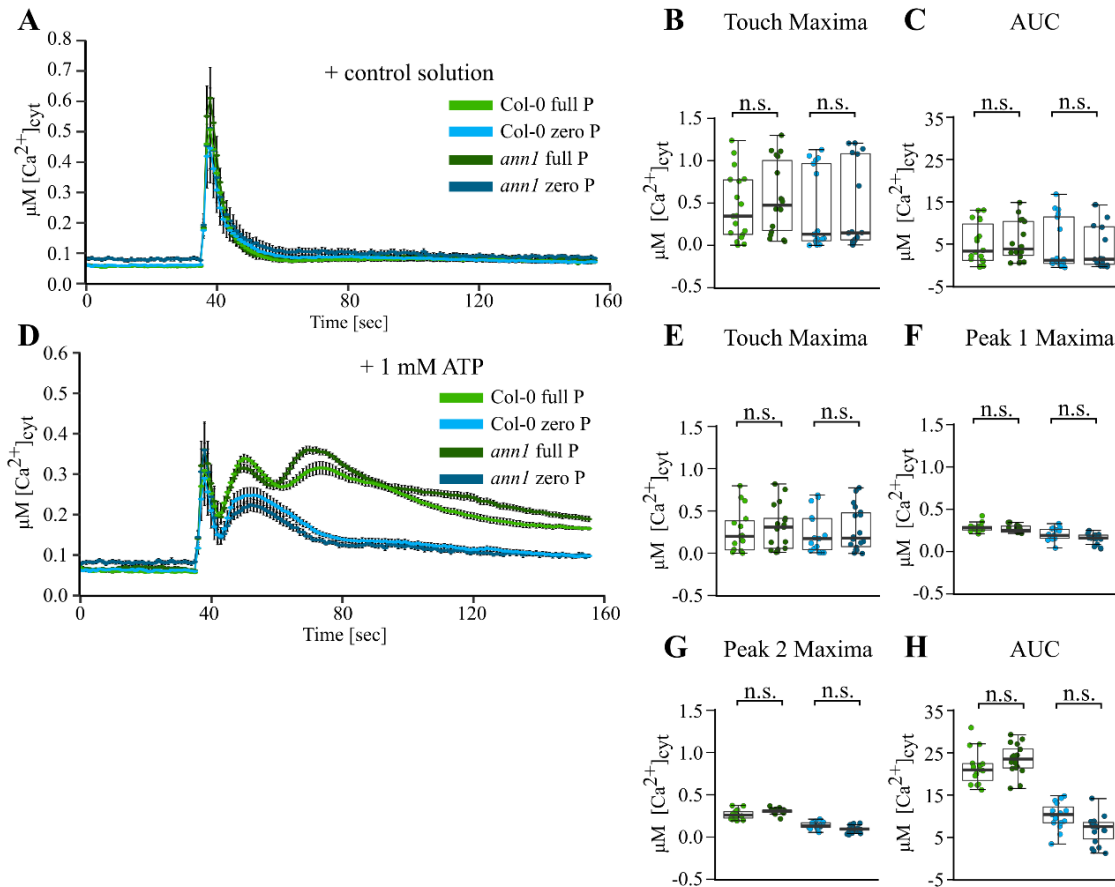
**Figure 20:** The  $[Ca^{2+}]_{cyt}$  response of phosphate-starved *dorn1-1* mutants to extracellular ATP. Col-0 and *dorn1-1* mutant, both expressing aequorin, were grown on full, or zero P (green, blue trace respectively, light colours for Col-0, dark colours for *dorn1-1*). Root tips (1 cm) of 11-day old seedlings were challenged with treatments applied at 35 seconds, and  $[Ca^{2+}]_{cyt}$  was measured for 155 seconds. (A) Application of control solution; time course trace represents mean  $\pm$  standard error of mean (SEM) from 3 independent trials, with  $n = 13 - 18$  individual root tips averaged per data point. Time course data were analysed for (B) touch maxima and (C) area under the curve (AUC), all baseline-subtracted, with each dot representing an individual data point (see Figure 6 for details). Boxplot middle line denotes median. (D-H) Responses to 1 mM eATP (3 independent trials,  $n = 16 - 18$  individual root tips per growth condition and genotype). Analysis of variance (ANOVA) with *post-hoc* Tukey Test was used to assess statistical differences. Significance levels (*p*-values): \*\*\* ( $<0.001$ ), \*\* ( $<0.01$ ), \* ( $<0.05$ ), n.s. (not significant).



Next, the potential involvement of ANNEXIN1 (ANN1) protein in the regulation of the  $[Ca^{2+}]_{cyt}$  signature under P starvation was investigated. As ANN1 was reported to be up-regulated by P starvation, this might correlate with the observed alteration of the eATP-induced  $[Ca^{2+}]_{cyt}$  response in P-starved root tips. This would imply ANN1's acting as a negative regulator of the eATP-induced  $[Ca^{2+}]_{cyt}$  response. To test if ANN1 up-regulation was indeed the causative factor, aequorin-expressing lines with a non-functional ANN1 protein, *ann1*, were grown on full and zero P and challenged with eATP. Knock-out of *ANN1* should rescue the dampened  $[Ca^{2+}]_{cyt}$  response of zero P root tips, back to a multi-phasic response as seen in full P.

Application of control solution, as a control for mechanical stimulation, led to an immediate and monophasic, as well as variable,  $[Ca^{2+}]_{cyt}$  response in both wild type and *ann1* mutant root tips (Figure 21A). Neither touch maxima (Col-0: full P:  $0.46 \pm 0.09 \mu\text{M}$ , zero P:  $0.40 \pm 0.11 \mu\text{M}$ , *ann1*: full P:  $0.56 \pm 0.1 \mu\text{M}$ , zero P:  $0.45 \pm 0.09 \mu\text{M}$ ) nor area under the curve were significantly different with regards to the *ann1* mutation ( $p \geq 0.989$  for all comparisons, Figure 21B, C).

Application of 1 mM ATP treatment led to a multi-phasic  $[Ca^{2+}]_{cyt}$  response in full P root tips, and an altered  $[Ca^{2+}]_{cyt}$  signature in zero P root tips (Figure 21D). However, this was observed in both wild type and *ann1* mutant. Touch maxima did not differ significantly between wild type and mutant, regardless of growth condition (Col-0: full P:  $0.27 \pm 0.07 \mu\text{M}$ , zero P:  $0.25 \pm 0.06 \mu\text{M}$ , *ann1*: full P:  $0.31 \pm 0.06 \mu\text{M}$ , zero P:  $0.29 \pm 0.06 \mu\text{M}$ ,  $p = 0.999$ , Figure 21E). Peak 1 maxima did also not show any significant difference between wild type and *ann1* (Col-0: full P:  $0.29 \pm 0.01 \mu\text{M}$ , zero P:  $0.20 \pm 0.02 \mu\text{M}$ , *ann1*: full P:  $0.27 \pm 0.01 \mu\text{M}$ , zero P:  $0.16 \pm 0.02 \mu\text{M}$ ,  $p \geq 0.963$ , Figure 21F). Under full P, the *ann1* mutant line showed a slightly stronger peak 2 response, however not significantly different to the wild type response ( $p = 0.061$ , Figure 21G). Under P starvation conditions, both *ann1* and wild type showed an altered peak 2 response, and lower peak 2 maxima compared to full P root tips (peak 2 maxima as follows: Col-0: full P:  $0.27 \pm 0.02 \mu\text{M}$ , zero P:  $0.10 \pm 0.01 \mu\text{M}$ , *ann1*: full P:  $0.31 \pm 0.01 \mu\text{M}$ , zero P:  $0.14 \pm 0.01 \mu\text{M}$ , Figure 21G). Overall, wild type and *ann1* mobilized comparable levels of  $[Ca^{2+}]_{cyt}$ , quantified as area under the curve, dependent of P regime ( $p \geq 0.390$ , Figure 21H). Taken together, *ann1* mutant responded very similarly to wild type, both in full and zero P growth conditions. Hence, the knock-out of functional ANN1 protein did not rescue the altered  $[Ca^{2+}]_{cyt}$  signature in response to eATP treatment.



**Figure 21:** The  $[\text{Ca}^{2+}]_{\text{cyt}}$  response of phosphate-starved *ann1* mutants to extracellular ATP. Col-0 and *ann1* mutant, both expressing aequorin, were grown on full, or zero P (green, blue trace respectively, light colours for Col-0, dark colours for *ann1*). Root tips (1 cm) of 11-day old seedlings were challenged with treatments applied at 35 seconds, and  $[\text{Ca}^{2+}]_{\text{cyt}}$  was measured for 155 seconds. (A) Application of control solution; time course trace represents mean  $\pm$  standard error of mean (SEM) from 3 independent trials, with  $n = 17 - 18$  individual root tips averaged per data point. Time course data were analysed for (B) touch maxima and (C) area under the curve (AUC), all baseline-subtracted, with each dot representing an individual data point (see Figure 6 for details). Boxplot middle line denotes median. (D-H) Responses to 1 mM eATP (3 independent trials,  $n = 15 - 18$  individual root tips per growth condition and genotype). Analysis of variance (ANOVA) with *post-hoc* Tukey Test was used to assess statistical differences. Significance levels ( $p$ -values): \*\*\* ( $<0.001$ ), \*\* ( $<0.01$ ), \* ( $<0.05$ ), n.s. (not significant).

Complementary to the aequorin-based study of ANN1 involvement, its localization and – roughly – its abundance were estimated using GFP-fused reporter lines. These lines had been produced by Siân Richards (University of Cambridge). Two constructs were available for fluorescence microscopy. In the first construct, a soluble GFP (sGFP), was fused to a long version (2 kilo bases upstream of the coding region) promoter of *ANN1*. This promoter-sGFP fusion was designed to visualize *ANN1* gene expression (hereafter labelled as LP<sub>ANN1</sub>::sGFP). In a second construct, the same *ANN1* promoter as well as the coding region of *ANN1* was fused to sGFP. This promoter-coding region-sGFP fusion was designed to visualize localization of ANN1 protein (hereafter labelled as LP<sub>ANN1</sub>::ANN1-sGFP).

To visualize both *ANN1* gene expression as well as ANN1 protein localization, both GFP constructs were used and plants were grown on full and zero P. Ten-day old seedlings were imaged using a confocal microscope, with particular focus on the root tip of seedlings, to enable comparison with aequorin data.

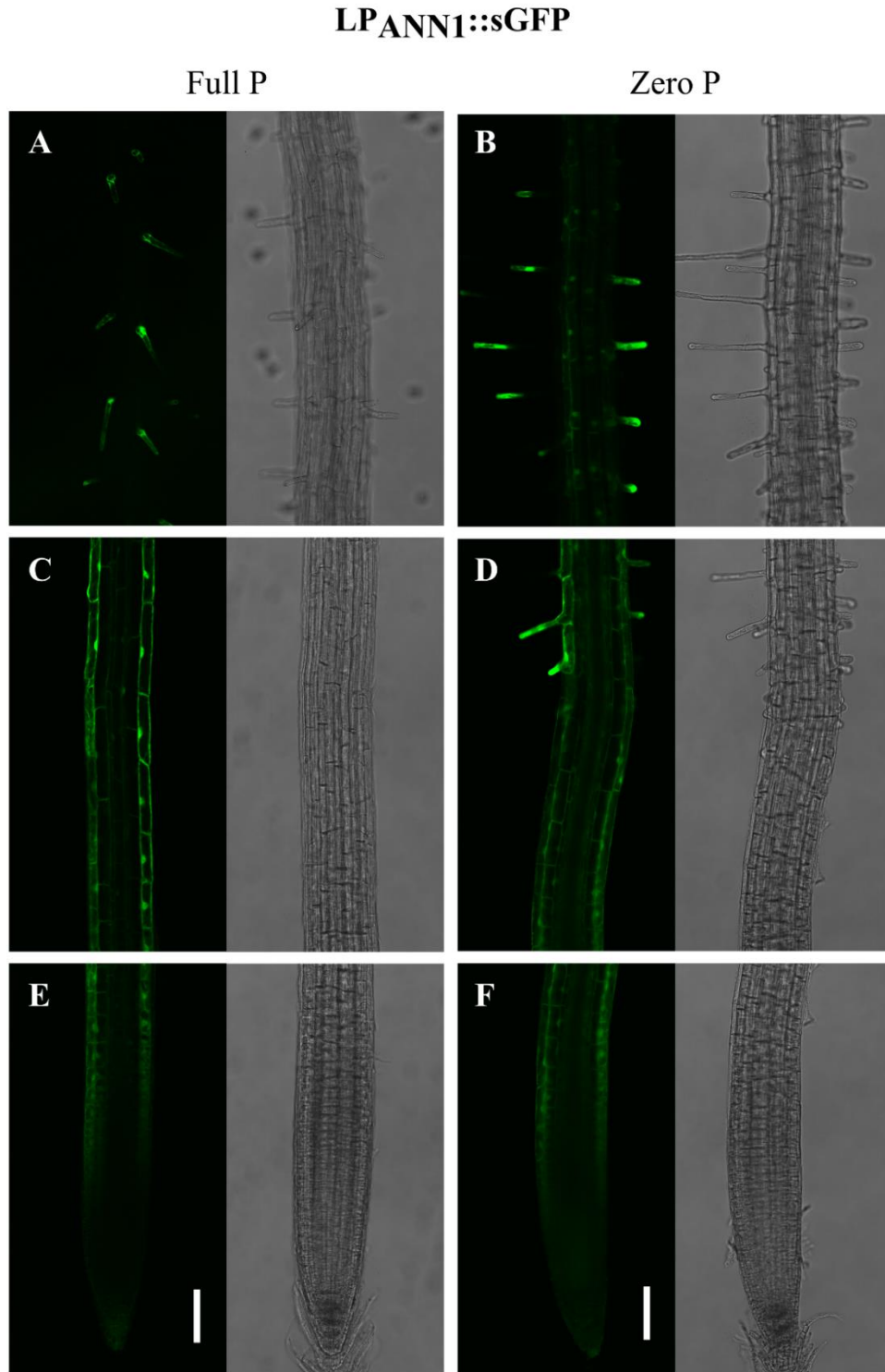
In full P roots, *ANN1* gene expression, visualized using the LP<sub>ANN1</sub>::sGFP line, was found throughout the root (data from 2 experiments, representative images shown in Figure 22A, C, E). The signal was particularly strong in root hairs (Figure 22A) and the epidermis (Figure 22C). Within the epidermis, expression was localized to cytosol and nucleus (Figure 22C). There was weak to no expression in the first approximately 200  $\mu$ M of the root tip (Figure 22E). This followed exactly the pattern as described before (Siân Richards, PhD thesis).

When starving LP<sub>ANN1</sub>::sGFP seedlings of P, localization of *ANN1* gene expression was very similar to what was seen under full P growth conditions. A strong signal was found throughout the root, particularly in root hairs and within the epidermis (Figure 22B, D). As was seen under full P conditions, there was no signal in the immediate root tip (Figure 22F).

The ANN1-protein fusion (LP<sub>ANN1</sub>::ANN1-sGFP) showed a signal mostly comparable with what was seen for *ANN1* gene expression. Under full P conditions, the translational GFP-fusion was easily detectable throughout the root (Figure 23A, C, E). The signal was strong in root hairs, where it occurred in aggregates (Figure 23A). As was seen with the gene expression construct, the epidermis showed a stronger signal compared with the other cell layers (Figure 23C). However, the signal did not localize to the nucleus, was patchier and, as was seen in root hairs, appeared in aggregates (Figure 23C). In contrast

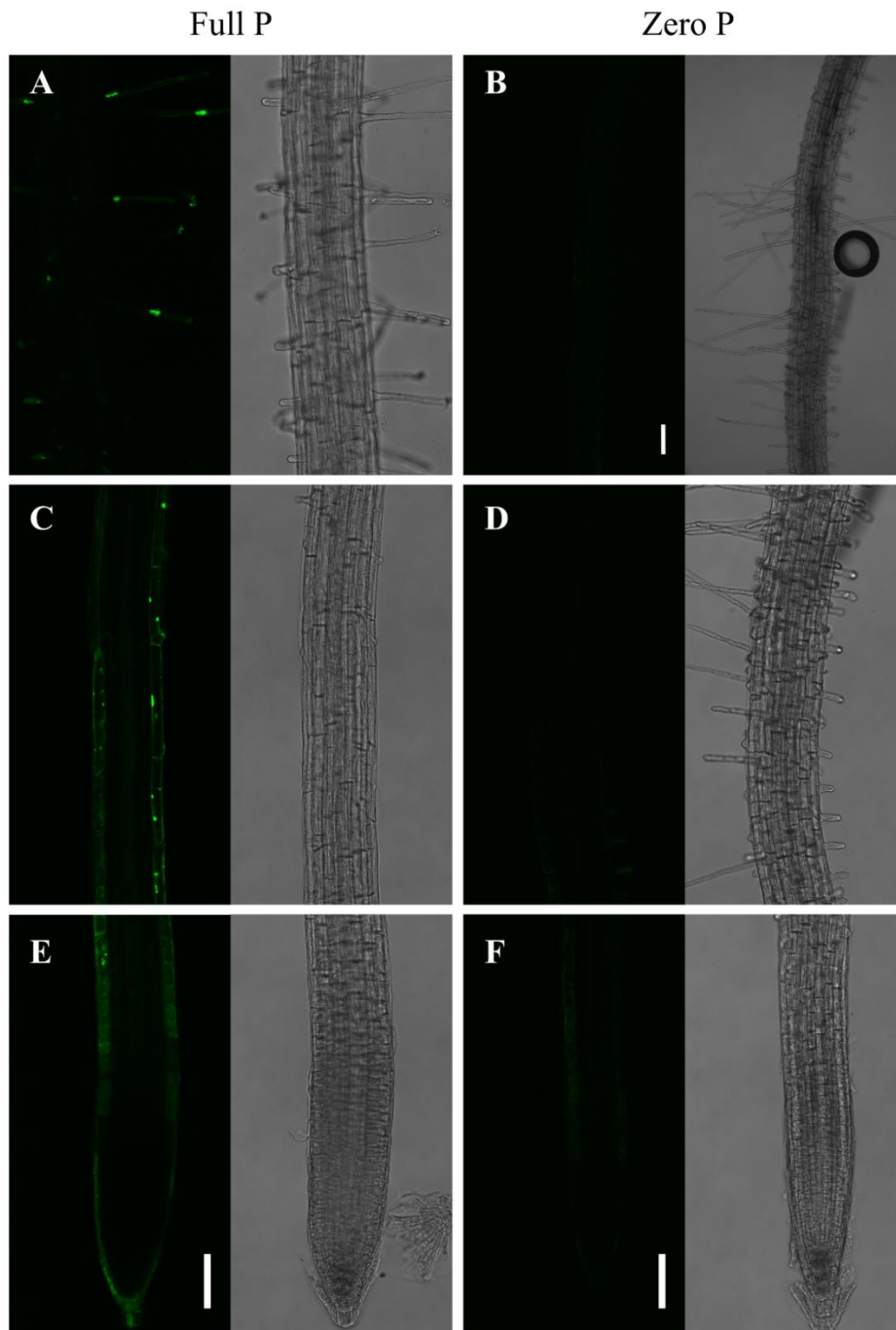
to *ANN1* gene expression, the translational construct was also found in the immediate root tip, where it occurred in the outermost cell layer, and cells of the root cap (Figure 23E). This localization of the ANN1 protein-GFP fusion construct was as described previously (Siân Richards, PhD thesis). Additionally, it was found previously that the aggregates in root hairs and epidermal cells moved over time, possibly indicating cytoskeleton association or cytoplasmic streaming (Siân Richards, PhD thesis).

Growing seedlings of the LP<sub>ANN1</sub>::ANN1-sGFP construct on zero P, led to an overall much lower and diffuse signal of ANN1 protein expression (Figure 23B, D, F). This was unexpected, as previous studies reported the up-regulation of ANN1 protein under P starvation conditions (Lan *et al.*, 2012; Z. Q. Wang *et al.*, 2018).



**Figure 22:** *ANNEXIN1* gene expression in phosphate-starved root tips. Ten-day old *Arabidopsis* roots, expressing the LP<sub>ANN1</sub>::sGFP construct, were grown on full P (A, C, E) or zero P (B, D, F). Images were captured using a confocal microscope, with each sample being shown as GFP-channel and corresponding bright field image. Representative images from 2 independent experiments. Scale bar: 100  $\mu$ m.

**LP<sub>ANN1</sub>::ANN1-sGFP**

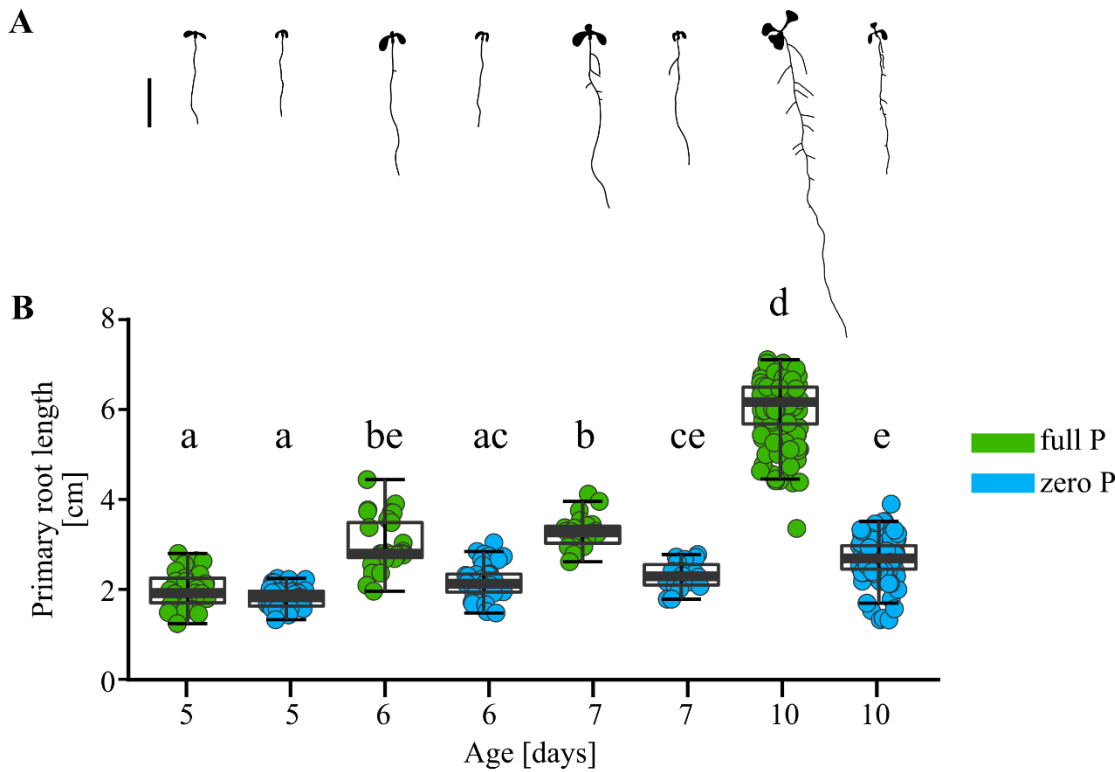


**Figure 23:** ANNEXIN1 protein expression in phosphate-starved root tips. Ten-day old *Arabidopsis* roots, expressing the LP<sub>ANN1</sub>::ANN1-sGFP construct, were grown on full P (A, C, E) or zero P (B, D, F). Images were captured using a confocal microscope, with each sample being shown as GFP-channel and corresponding bright field image. Representative images from 2 independent experiments. Scale bar: 100  $\mu$ m (please note the different magnification for (B) only).

### 3.2.11 The altered $[Ca^{2+}]_{\text{cyt}}$ response under phosphate starvation occurs during development

To delineate if the dampening of  $[Ca^{2+}]_{\text{cyt}}$  response occurred early or later in root development, Col-0 (apo)aequorin-expressing seedlings were grown on full or zero P for 6, 7, or 8 days, to be then challenged with eATP, and compared to the response of 11-day old root tips.

To track root development, plants grown on plates were scanned prior to preparation for aequorin assays (hence on day 5, 6, 7 and 10 of growth), and primary root lengths were quantified (data from 3 independent trials for 5-, 6-, and 7-day old seedlings,  $n = 18 - 39$  individual roots scored per growth condition and age; and data from 5 independent trials for 10-day old seedlings,  $n = 142 - 144$  individual roots scored per growth condition, Figure 24). In general, plants grown on the full P condition showed a strong increase in root length over the time period monitored, whilst P-starved plants showed only a minor increase in root length (see Figure 24A for representative images). On day 5, full P primary roots were already slightly longer than zero P root tips, this difference was however not significant (mean primary root length  $\pm$  SEM: full P:  $1.99 \pm 0.08$  cm, zero P:  $1.83 \pm 0.04$  cm,  $p = 0.908$ , Figure 24B). Already in 6-day old plants, the root length was significantly different between full and zero P grown plants (full P:  $2.99 \pm 0.11$  cm, zero P:  $2.18 \pm 0.07$  cm,  $p < 0.001$ , Figure 24B). This difference became even more pronounced in 7-day old plants (full P:  $3.27 \pm 0.08$  cm, zero P:  $2.31 \pm 0.07$  cm,  $p < 0.001$ , Figure 24B), and most pronounced in 10-day old plants (full P:  $6.01 \pm 0.06$  cm, zero P:  $2.69 \pm 0.04$  cm,  $p < 0.001$ , Figure 24B, also see Figure 4 for 10-day old root lengths only). P-starved, 10-day old plants had, on average, root lengths comparable to 6-day old plants grown on full P ( $p = 0.08$ ).



**Figure 24:** Primary root lengths of 5-, 6-, 7- and 10-day old phosphate-starved *Arabidopsis*. Col-0 expressing (apo)aequorin was grown on gel-based nutrient medium with varying P concentrations: full P (0.625 mM  $\text{PO}_4^{3-}$ , in green) or zero P (0 mM  $\text{PO}_4^{3-}$ , in blue). On day 5, 6, 7 or 10, plants were scanned and primary root length was quantified using the ImageJ NeuronJ Plugin. (A) Representative root system architecture of differently aged seedlings (corresponding to subjacent labelling in (B)), scale bar indicates 1 cm. (B) Primary root lengths of 5-, 6- and 7-day old seedlings (data from 3 independent trials,  $n = 18 - 39$  individual seedlings per growth condition) and 10-day old seedlings (data from 5 independent trials,  $n = 142 - 144$  individual seedlings per growth condition, same data as shown in Figure 4). Boxplot thick middle line denotes median. Analysis of variance (ANOVA) with *post-hoc* Tukey Test was used to assess statistical differences. Different lower-case letters describe groups of significant statistical difference ( $p < 0.001$ ), same letters indicate no statistical significance ( $p > 0.05$ ).

For luminometric determination of the  $[\text{Ca}^{2+}]_{\text{cyt}}$  response, root tips (1 cm) of differently aged plants were challenged with 1 mM eATP treatment (data of 6-, 7-, 8-day old root tips from 3 independent experiments,  $n = 13 - 16$  individual root tips per growth condition and age; data for 11-day old root tips from 5 independent experiments,  $n = 29 - 45$  individual root tips per growth condition, Figure 25). The additional ‘day’ relative to root length determinations reflects the post-harvest preparation time for luminometry. Six-day old root tips showed a multi-phasic response to eATP, for both full and zero P grown root



tips. An immediate touch response was followed by two defined increases of  $[Ca^{2+}]_{\text{cyt}}$  (Figure 25A). Already on day 6, the  $[Ca^{2+}]_{\text{cyt}}$  response was however dampened in zero P root tips. On day 7, the shape of the  $[Ca^{2+}]_{\text{cyt}}$  signature started to change shape in zero P root tips, with peak 2 starting to decrease (Figure 25B), being fully knocked down after 8 days (Figure 25C).

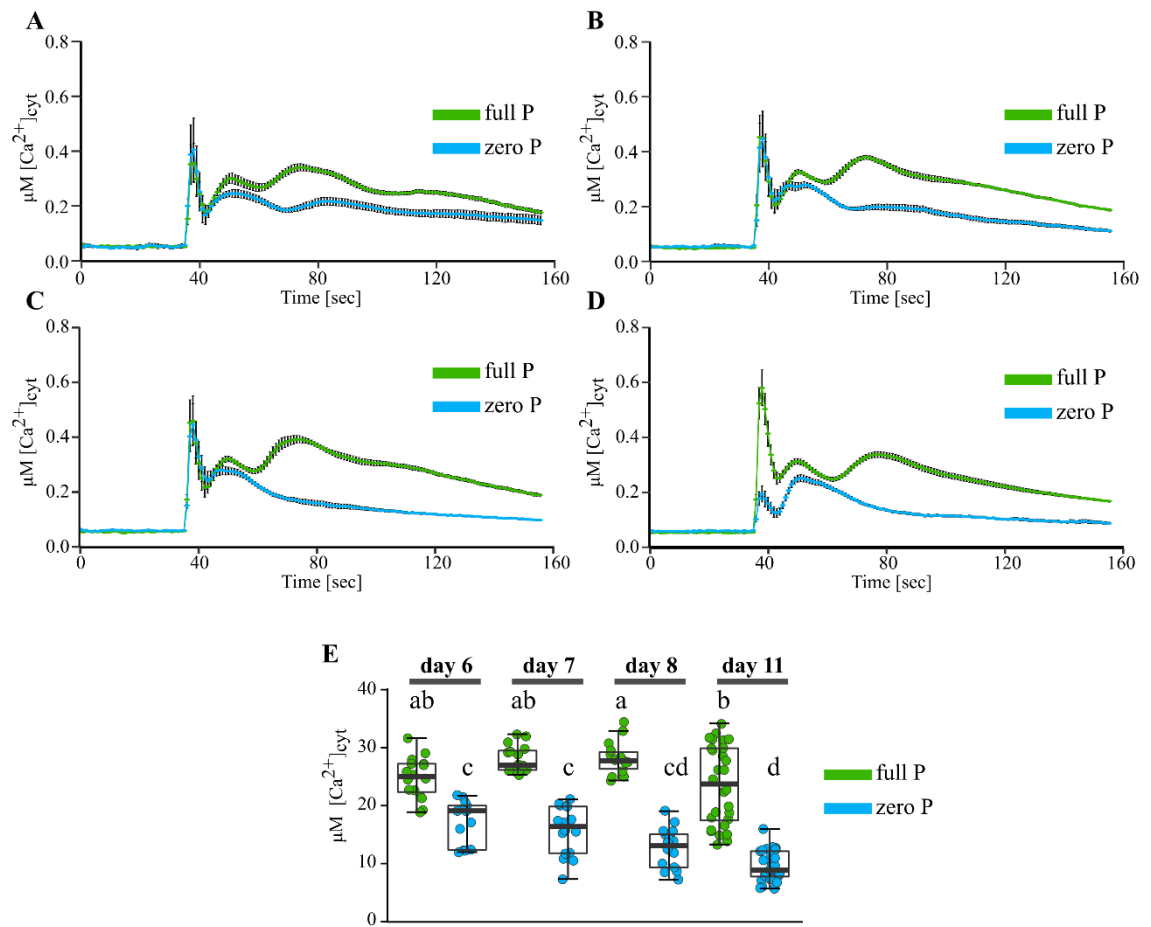
The pattern can be summarized as follows: touch maxima are not significantly different ( $p > 0.05$ ) in 6-, 7- and 8-day old root tips when comparing full and zero P root tips (see Table 3 for mean  $[Ca^{2+}]_{\text{cyt}}$  response  $\pm$  SEM). Only in 11-day old material, touch maxima were significantly lower in zero P root tips ( $p < 0.001$ ). The same was observed for peak 1 maxima (not significantly different between P growth conditions in 6-, 7- and 8-day old root tips ( $p > 0.05$ ), but significantly lower in 11-day old zero P root tips ( $p < 0.001$ )). Peak 2 maxima however were strongly dampened already in 6-day old P-starved, and all older, root tips ( $p < 0.001$ ). Overall, eATP mobilised significantly more  $[Ca^{2+}]_{\text{cyt}}$  in full P root tips, as approximated by area under the curve, compared to zero P root tips, independent of age (see Figure 25E for an overview). In full P root tips, the area under the curve remained similar when comparing the response of differently aged root tips (Figure 25E). In zero P root tips, the area under the curve was similar between 6-, 7- and 8-day old root tips, however significantly decreased in 11-day old root tips ( $p < 0.001$ , Figure 25E).

To exactly pin-point when during development peak 2 is ‘lost’ in zero P root tips, peak 2 maxima of differently aged zero P root tips were compared. Peak 2 maxima of 6- and 7-day old root tips were very similar ( $p = 0.93$ ). Comparing 6-day peak 2 maxima to 8- or 11-day peak 2 maxima of zero P root tips showed a much lower response, however not quite significant ( $p = 0.06$  for both comparisons). Peak 2 maxima between 7-, 8- and 11-day old zero P root tips were very similar ( $p = 0.52 - 0.99$ ).

Taken together, this indicates that P starvation led to a dampening of the eATP-induced  $[Ca^{2+}]_{\text{cyt}}$  response already in young seedlings (= 6 days after germination on zero P medium). Initially, P-starved root tips still showed a multi-phasic  $[Ca^{2+}]_{\text{cyt}}$  response to eATP, which was however altered 6 to 7 days after germination. After 11 days of P starvation, all parameters quantified – touch maxima, peak 1 maxima, peak 2 maxima and area under the curve – were strongly reduced in zero P root tips.

Lastly, the  $[Ca^{2+}]_{\text{cyt}}$  response of differently aged seedlings (Figure 25) was considered in light of their primary root lengths (Figure 24). To clarify: root lengths of 5-day old

seedlings would relate to the  $[Ca^{2+}]_{cyt}$  response of 6-day old seedlings (as aequorin-assay included an overnight incubation step, and 'age in days' defines the number of days since germination). This relation might introduce an error term, however, excised root tips incubated overnight would not grow as they would in the same time on an intact root. Hence, 5-day old primary roots grown on P-sufficient and P-deficient medium were similar in length (Figure 24B), and showed a multi-phasic response to eATP treatment (Figure 25A). However, the  $[Ca^{2+}]_{cyt}$  response was already dampened in zero P root tips. From 6 days onward (for root length measurements, Figure 24B, relating to '7-day old'  $[Ca^{2+}]_{cyt}$  measurements, Figure 25B), zero P roots were significantly shorter than full P grown roots, and also lost the multi-phasic  $[Ca^{2+}]_{cyt}$  response to eATP. This suggests that P-starvation early on dampened the  $[Ca^{2+}]_{cyt}$  response to eATP, without altering the dynamics of the response. Only later on, the  $[Ca^{2+}]_{cyt}$  dynamics were altered in P-starved root tips, occurring simultaneously with primary root growth inhibition.



**Figure 25:** The  $[\text{Ca}^{2+}]_{\text{cyt}}$  response of phosphate-starved root tips of different age to extracellular ATP. Col-0 aequorin-expressing seedlings were grown on full or zero P (green, blue trace respectively). Root tips (1 cm) of (A) 6-day, (B) 7-day, (C) 8-day or (D) 11-day aged seedlings were challenged with 1 mM eATP applied at 35 seconds, and  $[\text{Ca}^{2+}]_{\text{cyt}}$  was measured for 155 seconds. Time course trace represents mean  $\pm$  standard error of mean (SEM) from 3 - 5 independent trials, with  $n = 13 - 45$  individual root tips averaged per data point. Time course data were analysed for (E) area under the curve (AUC), see Table 3 for means  $\pm$  SEM of touch maxima, peak 1 maxima, peak 2 maxima, area under the curve, all baseline-subtracted, (see Figure 6 for details). Boxplot middle line in (E) denotes median. Analysis of variance (ANOVA) with *post-hoc* Tukey Test was used to assess statistical differences. Different lower-case letters describe groups of significant statistical difference ( $p < 0.001$ ), same letters indicate no statistical significance ( $p > 0.05$ ).

**Table 3:** Analysed parameters of the  $[Ca^{2+}]_{cyt}$  response of differently aged phosphate-starved root tips to 1 mM eATP. Primary data are shown in Figure 25. See Figure 6 for details of analysis.

<b>Growth condition</b>	full P	full P	full P	full P	zero P	zero P	zero P	zero P
<b>Treatment</b>	1mM ATP	1mM ATP	1mM ATP	1mM ATP	1mM ATP	1mM ATP	1mM ATP	1mM ATP
<b>Age [days]</b>	<b>6</b>	<b>7</b>	<b>8</b>	<b>11</b>	<b>6</b>	<b>7</b>	<b>8</b>	<b>11</b>
Baseline mean	0.05	0.05	0.05	0.05	0.05	0.05	0.05	0.05
± SEM	0.002	0.002	0.002	0.001	0.004	0.003	0.003	0.002
Touch maxima mean	0.32	0.42	0.42	0.54	0.37	0.40	0.40	0.15
± SEM	0.072	0.083	0.087	0.061	0.102	0.099	0.071	0.024
Peak 1 maxima mean	0.26	0.31	0.31	0.32	0.24	0.27	0.26	0.20
± SEM	0.013	0.006	0.010	0.015	0.019	0.026	0.027	0.009
Peak 2 maxima mean	0.31	0.35	0.36	0.31	0.19	0.17	0.14	0.15
± SEM	0.011	0.007	0.011	0.010	0.011	0.010	0.008	0.006
Area under the curve mean	24.7	27.9	28.2	25.4	17.2	15.7	12.6	9.6
± SEM	0.9	0.6	0.8	0.9	1.0	1.0	0.9	0.5
<b>n</b>	16	16	14	45	13	16	16	29

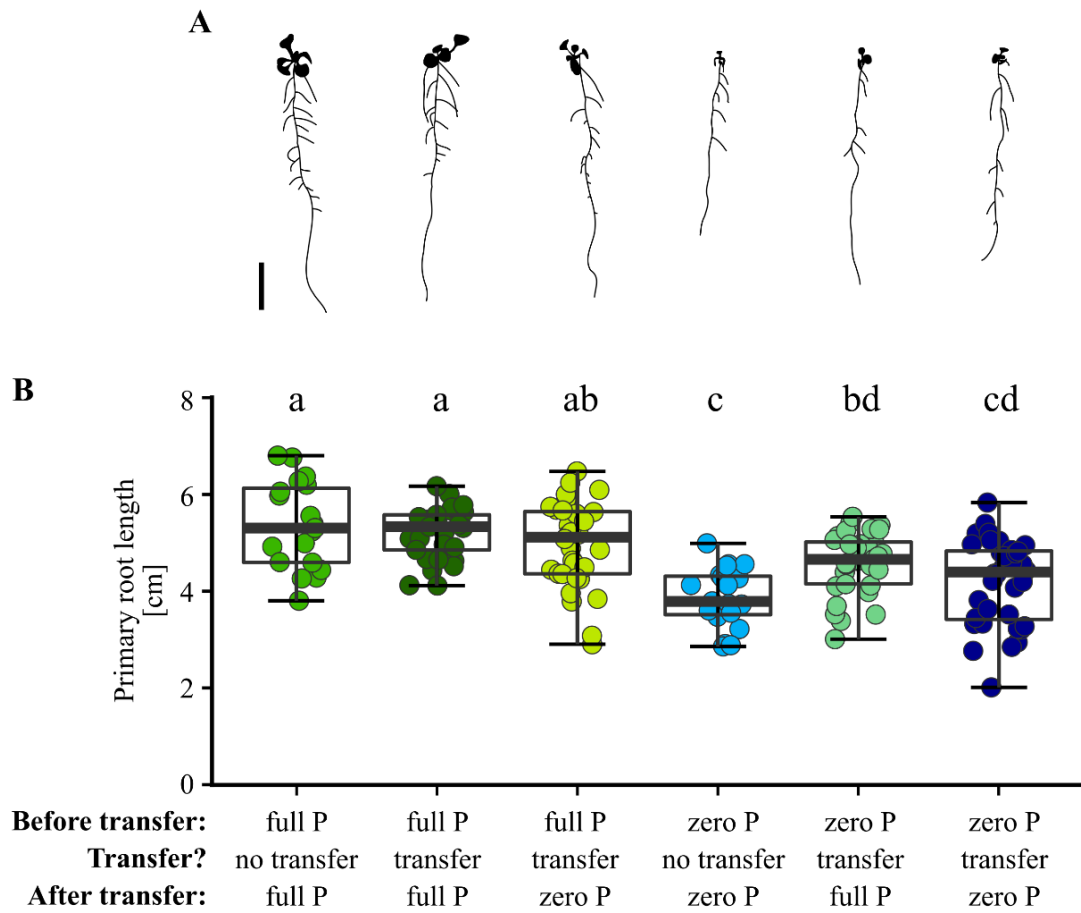
### 3.2.12 The altered $[Ca^{2+}]_{\text{cyt}}$ response under phosphate starvation is reversible

In the previous experiment it was shown that the altered  $[Ca^{2+}]_{\text{cyt}}$  response to eATP in P-starved root tips correlated with the onset of primary root growth inhibition during development. So far, all experiments shown examined root tissue that was germinated and grown under *chronic* P-replete or P-deficient conditions. To further characterize the developmental mechanism underlying the altered  $[Ca^{2+}]_{\text{cyt}}$  signature, it was of interest to examine if short-term P deprivation or P resupply could impair or rescue the  $[Ca^{2+}]_{\text{cyt}}$  signature, respectively.

To this end, a transfer experiment was designed in which (apo)aequorin-expressing *Arabidopsis* Col-0 seedlings were first germinated on either full or zero P growth medium. After 8 days, the seedlings were (i) not transferred, (ii) transferred to the same growth condition (*e.g.* full P to full P, representing a transfer control) or (iii) transferred to the opposite growth condition (*e.g.* full P to zero P). Plants were then grown for a further 2 days, before scanning the plants on day 10 (after germination), and preparing them for subsequent luminometric analysis on day 11 (see Chapter 2, section 2.6.1 for further details). Day 8 was chosen as the transfer day for two reasons: 8-day old plants already showed a severely altered  $[Ca^{2+}]_{\text{cyt}}$  signature (see Figure 25C) if grown on zero P; and if transferred on day 8 (rather than day 9), plants could be grown for a considerable time to recover from any transfer stress, and still be prepared on day 10 and assayed on day 11, making the data comparable to the majority of aequorin assays reported in this thesis.

Plants grown on such variable P conditions were scanned on day 10, and their primary root lengths were scored (data from 3 independent trials,  $n = 19 - 36$  individual plants scored per growth condition, Figure 26). By eye, plants grown initially on full P showed a much larger root and shoot biomass than plants grown initially on zero P (see Figure 26A for representative seedling architectures). Primary roots of non-transferred full P grown plants were on average ( $\pm$  SEM)  $5.36 \pm 0.21$  cm long, whereas zero P grown plants had significantly short roots ( $3.87 \pm 0.14$  cm,  $p < 0.001$ , Figure 26B). Transferring plants from full P to full P for 2 days of growth did not significantly change their primary root length ( $5.20 \pm 0.1$  cm,  $p = 0.983$ , Figure 26B). Transferring plants from full P to zero P slightly decreased their primary root length to  $4.96 \pm 0.16$  cm, however this difference was not significant ( $p = 0.454$ ). Transferring plants from zero P to a full P growth

condition stimulated primary root growth, and roots were significantly longer ( $4.58 \pm 0.11$  cm) than grown on zero P alone ( $p = 0.016$ ). Plants transferred from zero P to zero P showed an intermediate primary root length ( $4.19 \pm 0.15$  cm), as it was not significantly different to both non-transferred P-starved roots and transferred and P-resupplied roots ( $p = 0.677$  and  $p = 0.260$ , respectively). Plants that were transferred to the opposite growth medium, *i.e.* full P to zero P, and zero P to full P, had root lengths comparable to each other ( $p = 0.322$ ). Overall, this indicated that a 2-day resupply or depletion of P manifested itself to some extent at the level of primary root length.



**Figure 26:** Primary root lengths of *Arabidopsis* transferred to differing phosphate growth conditions during development. Col-0 expressing (apo)aequorin was grown on gelled nutrient medium with varying P: full P (0.625 mM  $\text{PO}_4^{3-}$ ) or zero P (0 mM  $\text{PO}_4^{3-}$ ). On day 8, plants were either (i) not transferred, (ii) transferred to the same growth conditions (e.g. full P to full P) or (iii) transferred to the opposite growth conditions (e.g. full P to zero P). On day 10 (= 2 days after transfer), plants were scanned and primary root length was quantified using the ImageJ NeuronJ Plugin. (A) Representative root system architecture of differently grown seedlings (corresponding to subjacent labelling in (B)), scale bar indicates 1 cm. (B) Primary root lengths of differently grown seedlings, see labelling for transfer conditions (data from 3 independent trials, n = 19 - 36 individual seedlings per growth condition). Boxplot thick middle line denotes median. Analysis of variance (ANOVA) with *post-hoc* Tukey Test was used to assess statistical differences. Different lower-case letters describe groups of significant statistical difference ( $p < 0.05$ ), same letters indicate no statistical significance ( $p > 0.05$ ).

With regards to  $[Ca^{2+}]_{\text{cyt}}$  dynamics, it was first investigated if short-term resupply of P to initially P-starved plants could rescue the impaired  $[Ca^{2+}]_{\text{cyt}}$  signature. Three growth conditions were considered: zero P grown plants without transfer, zero P to zero P transferred plants, and zero P to full P transferred plants. As in previous experiments, 1 cm excised root tips were used for the assays, challenging them with control solution (to control for mechanical stimulation) or 1 mM eATP treatment (in control solution background).

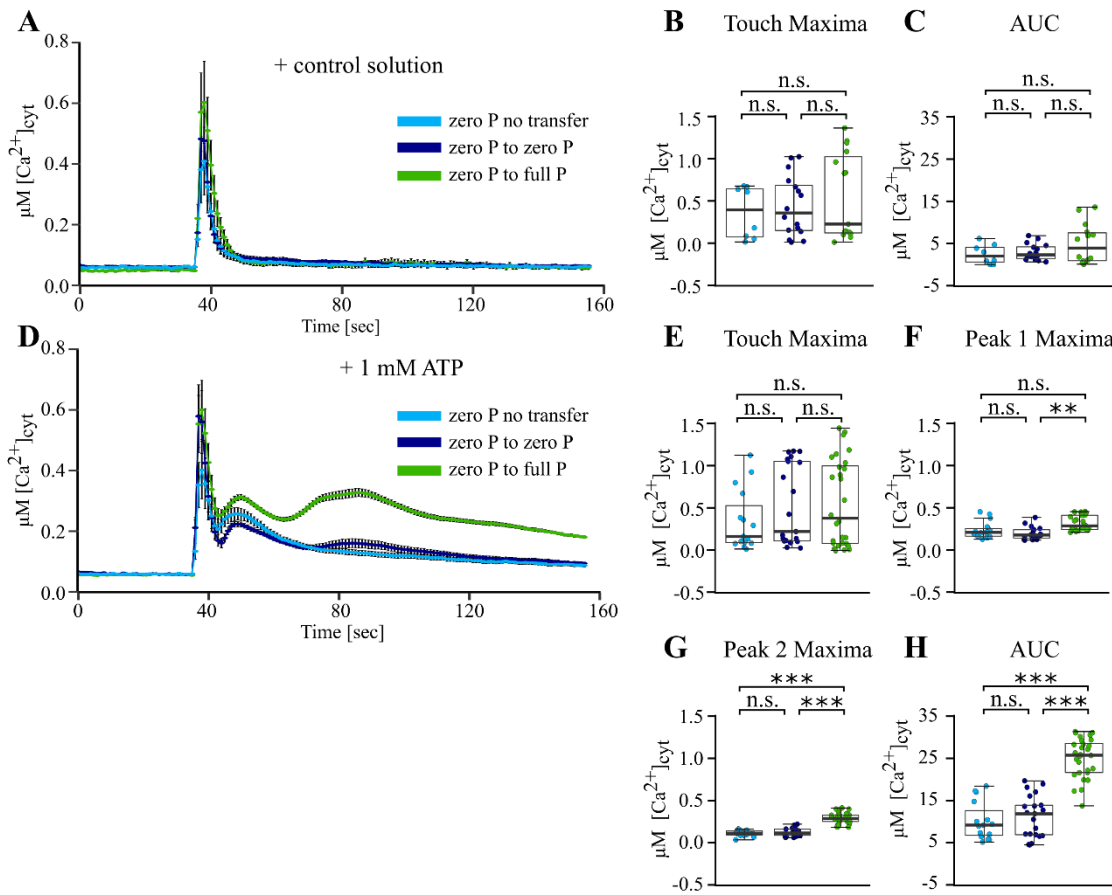
Application of control solution led to an immediate and monophasic increase in  $[Ca^{2+}]_{\text{cyt}}$  (data from 3 independent trials,  $n = 8 - 15$  individual root tips per growth condition, Figure 27A). The response was very similar between all three growth conditions, *i.e.* roots grown on zero P and then transferred to full or zero P, or not transferred at all. Neither touch maxima (Figure 27B) nor area under the curve (Figure 27C) were significantly different between the three growth conditions ( $p \geq 0.995$  for all comparisons).

Application of 1 mM eATP treatment showed the characteristically altered  $[Ca^{2+}]_{\text{cyt}}$  signature in non-transferred zero P root tips (data from 3 independent trials,  $n = 15 - 28$  individual root tips per growth condition, Figure 27D). Most interestingly though, transfer of zero P grown plants to both zero P or full P rescued the  $[Ca^{2+}]_{\text{cyt}}$  signature, albeit to varying degrees (Figure 27D). It was re-assuring to find that transferring zero P grown plants to full P rescued the  $[Ca^{2+}]_{\text{cyt}}$  signature back to dynamics normally observed in full P grown root tips – the response to eATP was multi-phasic, with each increase in  $[Ca^{2+}]_{\text{cyt}}$  being clearly defined.

The initial touch response to eATP treatment was highly variable, and touch maxima did not differ significantly between the different growth conditions (mean touch maxima in  $\mu\text{M } [Ca^{2+}]_{\text{cyt}} \pm \text{SEM}$ : zero P no transfer:  $0.35 \pm 0.09 \mu\text{M}$ , zero P to full P:  $0.56 \pm 0.1 \mu\text{M}$ , zero P to zero P:  $0.52 \pm 0.1 \mu\text{M}$ ,  $p \geq 0.998$ , Figure 27E). Peak 1 maxima were similar between root tips of non-transferred zero P grown plants and plants that had been transferred to zero P (zero P no transfer:  $0.24 \pm 0.1 \mu\text{M}$ , zero P to zero P:  $0.19 \pm 0.02 \mu\text{M}$ ,  $p \geq 0.285$ , Figure 27F). However, root tips of plants that had been transferred to full P showed significantly higher peak 1 maxima than when transferred to zero P (zero P to full P:  $0.32 \pm 0.02 \mu\text{M}$ ,  $p = 0.003$ , Figure 27F). This pattern was even more pronounced when considering peak 2 maxima, where root tips of plants that had been transferred from zero to full P showed drastically higher peak 2 maxima (zero P to full P:  $0.29 \pm 0.01 \mu\text{M}$ ,  $p < 0.001$  for both comparisons, Figure 27G). Interestingly, root tips that had been transferred from zero P to zero P, showed a small but defined increase during peak 2



phase (see purple trace in Figure 27D). However, the magnitude of this response was not significantly different compared to non-transferred zero P grown root tips which did not show any appreciable  $[Ca^{2+}]_{\text{cyt}}$  increase during the same period ( $p = 0.999$ , Figure 27G). Overall, and compared to growing plants on zero P only (with and without transfer), P resupply led to a significantly higher mobilisation of  $[Ca^{2+}]_{\text{cyt}}$  in response to eATP treatment (quantified as area under the curve,  $p < 0.001$  for both comparisons, Figure 27H).



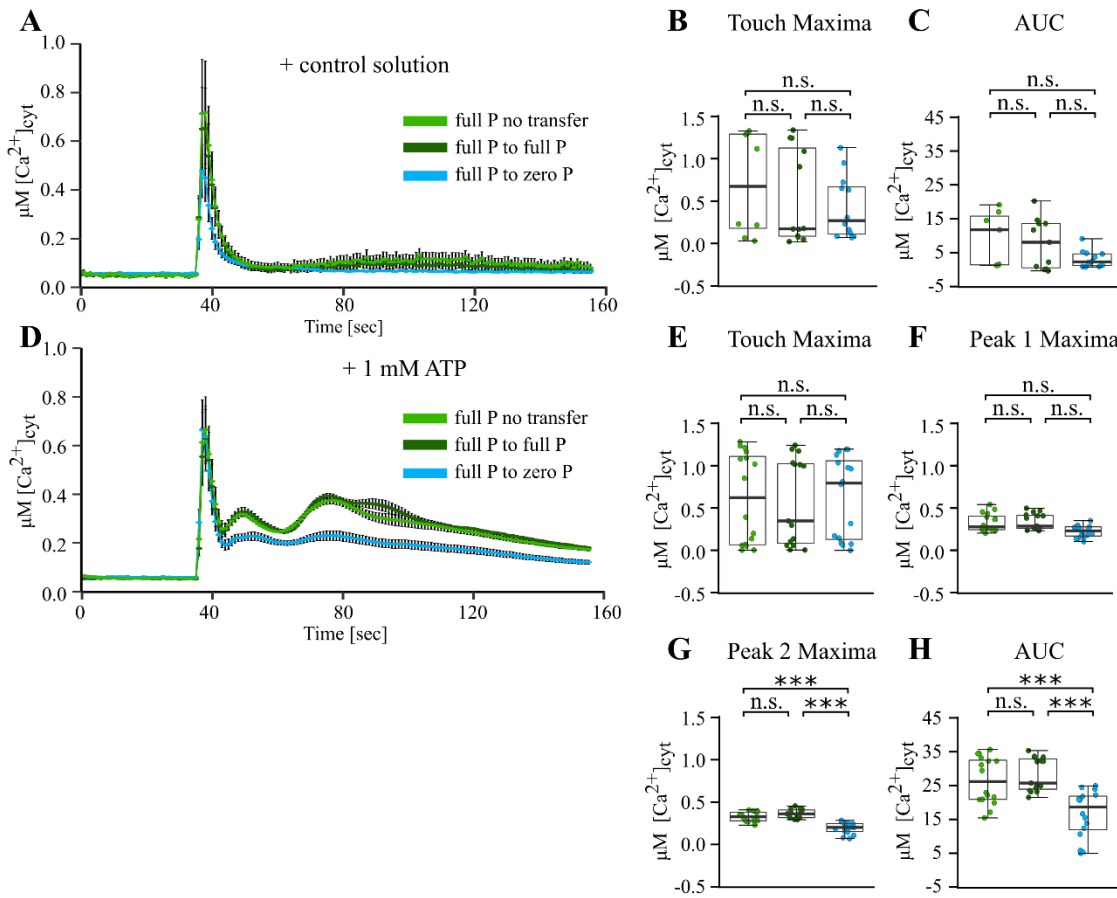
**Figure 27:** The  $[Ca^{2+}]_{cyt}$  response of short-term phosphate-resupplied *Arabidopsis* root tips to extracellular ATP. Col-0 expressing aequorin was grown on zero P for 8 days, when plants were either (i) not transferred ('zero P no transfer'), (ii) transferred to zero P growth medium ('zero P to zero P'), or (iii) transferred to full P growth medium ('zero P to full P'). Root tips (1 cm) of 11-day old seedlings were challenged with treatments applied at 35 seconds, and  $[Ca^{2+}]_{cyt}$  was measured for 155 seconds. (A) Application of control solution; time course trace represents mean  $\pm$  standard error of mean (SEM) from 3 independent trials, with  $n = 8 - 15$  individual root tips averaged per data point. Time course data were analysed for (B) touch maxima and (C) area under the curve (AUC), all baseline-subtracted, with each dot representing an individual data point (see Figure 6 for details). Boxplot middle line denotes median. (D-H) Responses to 1 mM eATP (3 independent trials,  $n = 15 - 28$  individual root tips per growth condition). Analysis of variance (ANOVA) with *post-hoc* Tukey Test was used to assess statistical differences. Significance levels (*p*-values): \*\*\* (<0.001), \*\* (<0.01), \* (<0.05), n.s. (not significant).

Secondly, it was investigated if a short-term deprivation of initially full P-grown plants would affect the  $[Ca^{2+}]_{\text{cyt}}$  response to eATP treatment. To this end, plants were initially grown on full P growth medium, until day 8, when plants were either not transferred, transferred from full P to full P, or transferred from full P to zero P. Excised root tips (1 cm) were used in the assays, and treated with control solution (to control for mechanical stimulation) or 1 mM eATP treatment (in control solution background).

Control solution application led to an immediate and monophasic increase in  $[Ca^{2+}]_{\text{cyt}}$ , which was in general highly variable, and overall not significantly different between the three growth conditions (data from 3 independent trials,  $n = 8 - 13$  individual root tips per growth condition, Figure 28A). Neither touch maxima nor area under the curve showed any significant differences ( $p \geq 0.12$  for all comparisons, Figure 28B and C).

Application of 1 mM eATP treatment led to the typical multi-phasic response in non-transferred full P grown root tips (data from 3 independent trials,  $n = 15 - 16$  individual root tips per growth condition, Figure 28D). Root tips that had been transferred from full P to full P showed a multi-phasic response very similar to non-transferred full P root tips. However, the response was less synchronous than what was normally observed, leading to a small additional bump when overall averaging the time-course data (see dark green trace in Figure 28D). Transferring plants from full P to zero P, led to a substantial dampening of the overall  $[Ca^{2+}]_{\text{cyt}}$  response (light blue trace in Figure 28D).

Quantifying the response to eATP showed variable touch maxima which were overall not significantly different between the growth conditions ( $p = 0.999$  for all comparisons, Figure 28E). Peak 1 maxima were lower in full P to zero P transferred root tips ( $0.22 \pm 0.02 \mu\text{M}$ ) compared to non-transferred full P grown root tips ( $0.33 \pm 0.03 \mu\text{M}$ ) and full P to full P transferred root tips ( $0.34 \pm 0.03 \mu\text{M}$ ), however, this difference was not significant ( $p = 0.189$  and  $p = 0.104$ , respectively, Figure 28F). The difference was however highly significant when examining peak 2 maxima: full P transferred to zero P root tips showed much lower peak 2 maxima ( $0.19 \pm 0.02 \mu\text{M}$ ), compared to non-transferred full P root tips ( $0.33 \pm 0.01 \mu\text{M}$ ) and full P transferred to full P root tips ( $0.36 \pm 0.01 \mu\text{M}$ ,  $p < 0.001$  for both comparisons, Figure 28G). The latter two did not differ in their peak 2 maxima ( $p = 0.726$ ). Overall, root tips that had been transferred from full P to zero P mobilised significantly less  $[Ca^{2+}]_{\text{cyt}}$  in response to eATP, compared to growing plants on full P growth medium for the entire time (as quantified by area under the curve,  $p < 0.001$  for both comparisons, Figure 28H).



**Figure 28:** The  $[Ca^{2+}]_{cyt}$  response of short-term phosphate-starved *Arabidopsis* root tips to extracellular ATP. Col-0 expressing aequorin was grown on full P for 8 days, when plants were either (i) not transferred ('full P no transfer'), (ii) transferred to full P growth medium ('full P to full P'), or (iii) transferred to zero P growth medium ('full P to zero P'). Root tips (1 cm) of 11-day old seedlings were challenged with treatments applied at 35 seconds, and  $[Ca^{2+}]_{cyt}$  was measured for 155 seconds. (A) Application of control solution; time course trace represents mean  $\pm$  standard error of mean (SEM) from 3 independent trials, with  $n = 8 - 13$  individual root tips averaged per data point. Time course data were analysed for (B) touch maxima and (C) area under the curve (AUC), all baseline-subtracted, with each dot representing an individual data point (see Figure 6 for details). Boxplot middle line denotes median. (D-H) Responses to 1 mM eATP (3 independent trials,  $n = 15 - 16$  individual root tips per growth condition). Analysis of variance (ANOVA) with *post-hoc* Tukey Test was used to assess statistical differences. Significance levels (*p*-values): \*\*\* ( $<0.001$ ), \*\* ( $<0.01$ ), \* ( $<0.05$ ), n.s. (not significant).

Taken together, both a short-term P resupply as well as P deprivation significantly altered the  $[Ca^{2+}]_{cyt}$  dynamics triggered by eATP perception. Resupplying P to P-starved plants rescued their otherwise dampened  $[Ca^{2+}]_{cyt}$  response to eATP treatment (Figure 27). *Vice versa*, depriving initially nutrient replete plants of P led to a significantly dampened  $[Ca^{2+}]_{cyt}$  response to eATP (Figure 28).

To fully acknowledge to what extent this short-term P resupply or deprivation affected the root tips, the response of initially P-starved and initially P-replete root tips was compared (*i.e.* comparing data shown in Figure 27 and Figure 28).

P resupply (the transfer of initially zero P grown plants to full P growth medium) rescued the  $[Ca^{2+}]_{cyt}$  response to eATP almost in every aspect, when compared to full P grown non-transferred or full P to full P transferred plants. Area under the curve, touch maxima and peak 1 maxima were similar ( $p \geq 0.731$  for all comparisons). Peak 2 maxima were similar when comparing zero P to full P transferred root tips with full P grown root tips that had not been transferred ( $p = 0.447$ ). Compared to root tips that had been transferred from full P to full P, however, zero P to full P transferred root tips showed significantly lower peak 2 maxima ( $p < 0.001$ ).

P deprivation (the transfer of initially full P grown plants to zero P growth medium) dampened the  $[Ca^{2+}]_{cyt}$  response to eATP, to a comparable extent as to what was observed for the touch maxima and peak 1 maxima of non-transferred zero P grown root tips, as well as zero P to zero P transferred root tips ( $p \geq 0.896$  for all comparisons). Even though the  $[Ca^{2+}]_{cyt}$  response of short-term P-deprived root tips was dampened during peak 2 phase, it was still significantly higher than peak 2 maxima observed for non-transferred zero P root tips, and zero P to zero P transferred root tips ( $p \leq 0.002$  for both comparisons). The area under the curve was thus larger in full P to zero P transferred root tips compared to non-transferred zero P grown root tips ( $p = 0.037$ ). Compared to zero P to zero P transferred root tips, this difference was not significant ( $p = 0.083$ ).

### 3.2.13 Iron availability alters the primary root length of phosphate-starved roots

The assays described so far used a defined length of root, 1 cm of root tip, to control for difference in size of full P and zero P grown primary roots (also see Figure 4). Therefore, the finding that Fe exclusion alleviated the P starvation-induced inhibition of primary root growth was considered as a useful tool to (i) starve roots of P whilst (ii) maintaining similar primary root lengths between nutrient-replete and depleted plants.

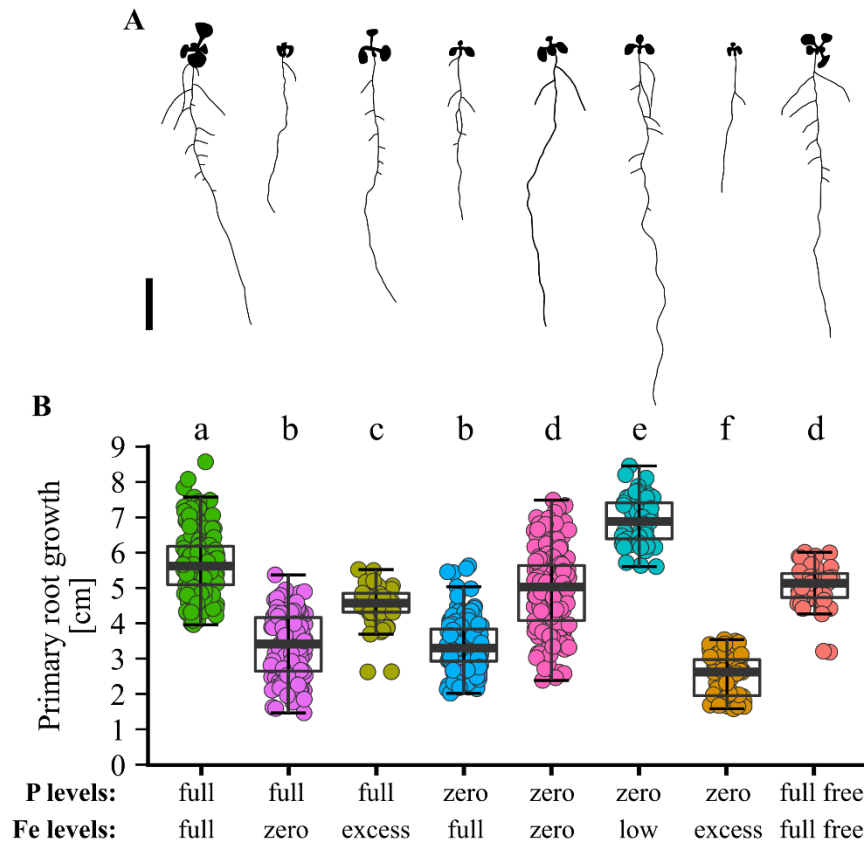
In general, standard half MS growth medium contains 50  $\mu\text{M}$  Fe. This implies that both the full P and zero P growth condition described so far both contained standard levels of Fe, *i.e.* 50  $\mu\text{M}$ . Therefore, to test the influence of Fe on primary root growth and ultimately  $[\text{Ca}^{2+}]_{\text{cyt}}$  signature, in addition to varying P levels, aequorin-expressing *Arabidopsis* seedlings were grown in a number of Fe exclusion and addition scenarios.

In short, P and Fe levels were modified in a standard half MS growth medium background. In the following, ‘full’ always refers to standard half MS nutrient levels, *i.e.* full P = 0.625 mM P, full Fe = 50  $\mu\text{M}$  Fe. ‘Zero’ refers to exclusion of the nutrient from the growth medium, *i.e.* zero P = 0 mM P, zero Fe = 0  $\mu\text{M}$  Fe. ‘Low Fe’ indicates levels of 10  $\mu\text{M}$  Fe. For the ‘excess Fe’ condition, twice the amount normally found in half MS was added, *i.e.* 100  $\mu\text{M}$ .

As modifying the amount of one species of ions in a complex solution easily affects the availability of the remaining ions, ion activities in solution were estimated using the chemical speciation program GEOCHEM-EZ (Shaff *et al.*, 2010). According to this software, both P and Fe complex with each other in solution as well as with many of the other ions, leading to overall lower levels of available free P and free Fe than would be assumed from the absolute concentrations alone. Thus, in solutions containing ‘full P’, a small fraction of P (0.74 %) is estimated to be complexed with Fe, leading to less available free P and free Fe. In solutions without P, ‘zero P’, no such complexation would occur, leading to slightly elevated levels of free Fe compared to the P-containing solution. To test if this slight increase in free Fe could be responsible for the altered  $[\text{Ca}^{2+}]_{\text{cyt}}$  signature reported for zero P grown root tips, the composition of the growth medium was adjusted in such a way that a full P solution would have the same free Fe levels as were estimated for a zero P solution. Thus, the ‘full free P\_full free Fe’ condition reported below contained 0.626 mM P and 55.35  $\mu\text{M}$  Fe (see Chapter 2 section 2.2.3 for further details).

After 10 days of growth on varying P and Fe conditions, plants were scanned and the primary root length was quantified. The interplay of P and Fe led to very distinct shoot and root systems (representative seedlings architectures are shown in Figure 29A). Primary root lengths were strongly affected by the different growth conditions (data from 3 – 8 independent trials,  $n = 48 - 169$  individual seedlings scored per growth condition, Figure 29B). Nutrient-replete conditions (full P\_full Fe) showed a mean primary root length ( $\pm$  SEM) of  $5.68 \pm 0.07$  cm. Almost all other modifications of P and Fe levels led to shorter primary roots, except zero P\_low Fe (Figure 29B). In the following, growth conditions are ordered, starting with the growth condition that led to the shortest mean primary roots ('<' indicating a statistically significant difference of  $p < 0.05$ ; ', ' indicating no statistically significant difference): zero P\_excess Fe ( $2.52 \pm 0.07$  cm) < zero P\_full Fe ( $3.38 \pm 0.06$  cm), full P\_zero Fe ( $3.39 \pm 0.07$  cm) < full P\_excess Fe ( $4.51 \pm 0.08$  cm) < zero P\_zero Fe ( $4.94 \pm 0.09$  cm), full free P\_full free Fe ( $5.05 \pm 0.07$  cm) < full P\_full Fe ( $5.68 \pm 0.07$  cm) < zero P\_low Fe ( $6.90 \pm 0.08$  cm).

In a full P background, excluding Fe (full P\_zero Fe) as well as including excess amounts of Fe (full P\_excess Fe) led to a reduction in primary root length. In a zero P background, the exclusion of Fe (zero P\_zero Fe) rescued the primary root length of P-starved roots almost back to nutrient-replete levels. This corroborated previous studies (Ward *et al.*, 2008; Müller *et al.*, 2015). Strikingly, plants grown without P and low levels of Fe (zero P\_low Fe) showed primary roots even longer than nutrient replete plants. Increasing Fe levels to  $50 \mu\text{M}$  or  $100 \mu\text{M}$  in a zero P background (zero P\_full Fe, zero P\_excess Fe, respectively) however led to severely stunted primary roots. Increasing the availability of free Fe (in a full P background (full free P\_full free Fe)) to levels estimated to occur in zero P\_full Fe, led to on average shorter primary roots than quantified for control conditions (full P\_full Fe), however within very much the same range (Figure 29B).



**Figure 29:** Primary root lengths of *Arabidopsis* grown on varying levels of phosphate and iron. Col-0 expressing (apo)aequorin was grown on gelled nutrient medium with varying P and Fe concentrations: full P (0.625 mM  $\text{PO}_4^{3-}$ , in green) or zero P (0 mM  $\text{PO}_4^{3-}$ , in blue). On day 10, plants were scanned and primary root length was quantified using the ImageJ NeuronJ Plugin. (A) Representative root system architecture of seedlings grown on varying P and Fe levels (corresponding to subjacent labelling in (B)), scale bar: 1 cm. (B) Primary root lengths (data from 3 - 8 independent trials,  $n = 48 - 169$  individual seedlings per growth condition). Boxplot thick middle line denotes median. Analysis of variance (ANOVA) with *post-hoc* Tukey Test was used to assess statistical differences. Different lower-case letters describe groups of significant statistical difference ( $p < 0.05$ ), same letters indicate no statistical significance ( $p > 0.05$ ).

In the following sections, plants grown on these different combinations of P and Fe were analysed for their eATP-induced  $[\text{Ca}^{2+}]_{\text{cyt}}$  response.



### 3.2.14 Exclusion of iron rescues the altered $[Ca^{2+}]_{\text{cyt}}$ response of phosphate-starved root tips

As described above (section 3.2.13), (apo)aequorin-expressing *Arabidopsis* Col-0 was grown on varying levels of P and Fe, in otherwise half MS growth medium background. For a first set of experiments, seedlings were grown on nutrient replete conditions (full P\_full Fe), as well as zero P conditions with full or decreased Fe levels (zero P\_full Fe, zero P\_low Fe, zero P\_zero Fe). To test for their  $[Ca^{2+}]_{\text{cyt}}$  response to eATP treatment, root tips (1 cm) of 11-day old seedlings were challenged with control solution, to account for mechanical stimulation, or 1 mM eATP (in control solution background).

Control solution application led to an immediate and monophasic increase in  $[Ca^{2+}]_{\text{cyt}}$  (data from 3 - 6 independent trials, n = 11 - 35 individual root tips per data point, Figure 30A). The touch maxima were highly variable, and there was no difference between touch maxima between the four growth conditions ( $p > 0.05$ , Figure 30B). The area under the curve was however significantly higher in full P\_full Fe root tips, compared to zero P\_low Fe and zero P\_zero Fe root tips ( $p > 0.05$ , Figure 30C).

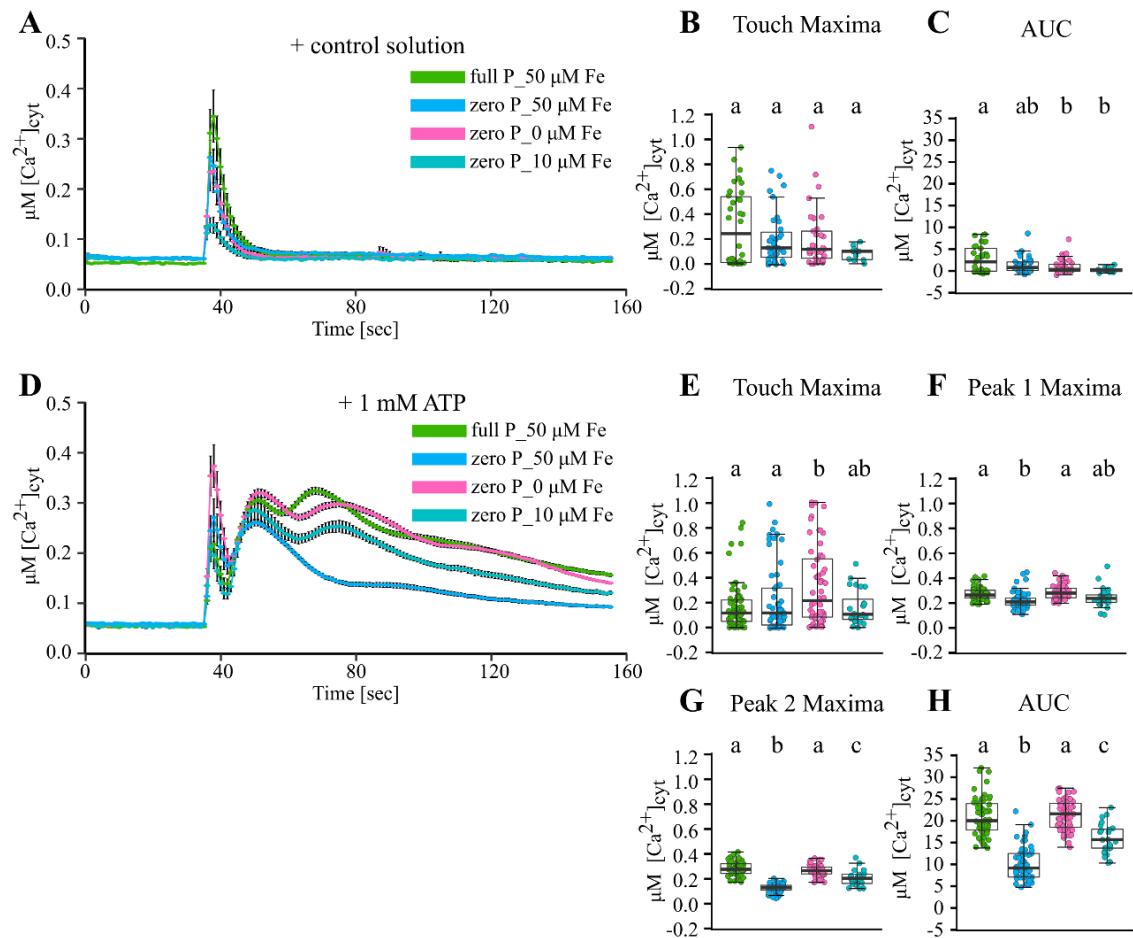
Application of 1 mM eATP led to a multi-phasic response in full P\_full Fe grown root tips, but most strikingly also in zero P\_zero Fe grown root tips (data from 3 – 6 independent trials, n = 24 – 61 individual root tips per growth condition, Figure 30D). Zero P\_full Fe root tips showed the characteristic knock-out of peak 2. Zero P\_low Fe grown root tips showed a dampened  $[Ca^{2+}]_{\text{cyt}}$  response, but with a defined peak 2. Touch maxima were similar in all conditions, but slightly higher in zero P\_zero Fe grown root tips, however variable (Figure 30E). Peak 1 maxima were significantly lower in zero P\_full Fe, compared to full P\_full Fe and zero P\_zero Fe grown root tips ( $p < 0.05$ , Figure 30F). This trend was amplified for peak 2 maxima: full P\_full Fe and zero P\_zero Fe grown root tips did not differ in their response ( $p = 0.56$ ), a low Fe concentration (zero P\_low Fe) however already dampened the response significantly ( $p < 0.001$ ). Increasing the Fe concentration in P-starvation background (zero P\_full Fe grown root tips) significantly decreased peak 2 maxima ( $p < 0.001$ , Figure 30G).

Overall, this led to a similar area under the curve in full P\_full Fe and zero P\_zero Fe grown root tips ( $p = 0.999$ , Figure 30H). In contrast, zero P\_low Fe grown root tips showed a significantly decreased area under the curve ( $p < 0.001$ ). Zero P\_full Fe grown

root tips had a significantly lower area under the curve than all other growth conditions ( $p < 0.001$ ).

Taken together, these data demonstrated that the altered eATP-induced  $[Ca^{2+}]_{cyt}$  response of P-starved root tips could be rescued by decreasing or fully excluding Fe from the growth medium. The induction of yet another nutrient deficiency (Fe deficiency) overcame the dampened  $[Ca^{2+}]_{cyt}$  response seen in P-starved roots, leading to a  $[Ca^{2+}]_{cyt}$  response similar to nutrient replete roots.

Relating these observed  $[Ca^{2+}]_{cyt}$  responses (Figure 30) to quantified primary root lengths (Figure 29) showed no clear pattern. For example, zero P\_low Fe grew longer primary roots than full P\_full Fe, but showed a lower, more intermediate,  $[Ca^{2+}]_{cyt}$  response to eATP.



**Figure 30:** The  $[Ca^{2+}]_{cyt}$  response of phosphate- and iron-starved root tips to extracellular ATP. Col-0 aequorin-expressing seedlings were grown on standard half MS growth medium, full P<sub>full</sub> Fe (green trace), zero P<sub>full</sub> Fe (blue trace), zero P<sub>low</sub> Fe (pink trace) or zero P<sub>zero</sub> Fe (turquoise trace). Root tips (1 cm) of 11-day old seedlings were challenged with treatments applied at 35 seconds, and  $[Ca^{2+}]_{cyt}$  was measured for 155 seconds. (A) Application of control solution; time course trace represents mean  $\pm$  standard error of mean (SEM) from 3 - 6 independent trials, with n = 11 - 35 individual root tips averaged per data point. Time course data were analysed for (B) touch maxima and (C) area under the curve (AUC), all baseline-subtracted, with each dot representing an individual data point (see Figure 6 for details). Boxplot middle line denotes median. (D-H) Responses to 1 mM eATP (3 - 6 independent trials, n = 24 - 61 root tips per growth condition). Analysis of variance (ANOVA) with *post-hoc* Tukey Test was used to assess statistical differences. Different lower-case letters describe groups of significant statistical difference ( $p < 0.05$ ), same letters indicate no statistical significance ( $p > 0.05$ ).

### 3.2.15 Under phosphate starvation, increasing the iron levels in the growth medium does not alter the $[Ca^{2+}]_{cyt}$ response further

To test if an *increase* of Fe concentration in the growth medium of P-starved root tips could further dampen the  $[Ca^{2+}]_{cyt}$  response, a set of experiments was carried out where roots were grown on zero P growth medium with excess Fe added (100  $\mu$ M Fe, which is double the amount found in standard half MS medium). The  $[Ca^{2+}]_{cyt}$  response of these root tips (1 cm excised root tip) was compared to nutrient-replete root tips (full P\_full Fe) and P-starved root tips with standard amounts of Fe (zero P\_full Fe, containing 50  $\mu$ M Fe). Eleven-day old root tips were treated with control solution, to control for mechanical stimulation, or 1 mM eATP solution (in control solution background).

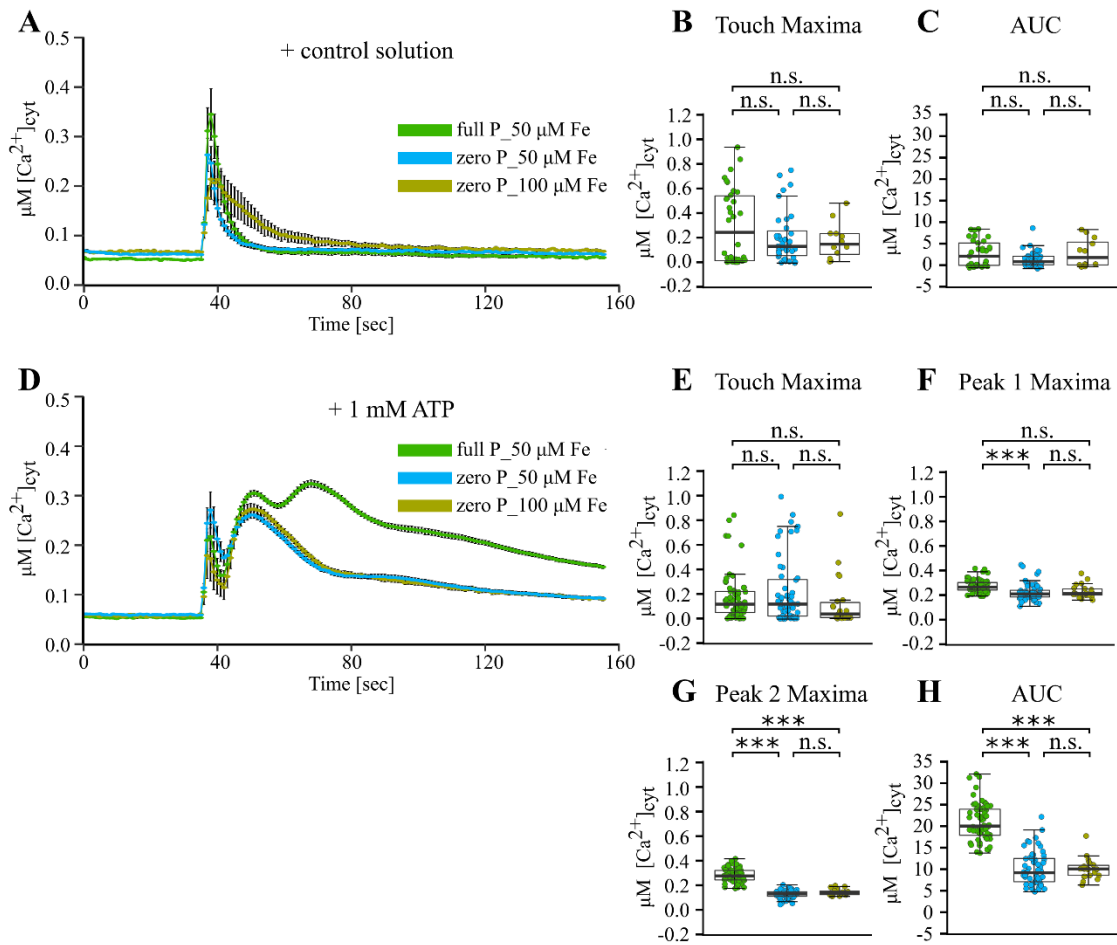
Application of control solution led to an immediate and monophasic increase in  $[Ca^{2+}]_{cyt}$  in root tips of all three growth conditions (data from 3 – 6 independent trials,  $n = 12 - 35$  individual root tips per growth condition, Figure 31A). Some samples of zero P\_excess Fe grown root tips showed a slightly prolonged response to control solution (see larger than usual error bars on olive coloured trace, Figure 31A). However, neither touch maxima nor area under the curve were significantly different between the growth conditions (touch maxima:  $p \geq 0.645$  for all comparisons, Figure 31B, area under the curve:  $p \geq 0.223$  for all comparisons, Figure 31C).

Treatment with 1 mM eATP solution led to the characteristic multi-phasic  $[Ca^{2+}]_{cyt}$  response in nutrient-replete plants (green trace in Figure 31D), and a dampened  $[Ca^{2+}]_{cyt}$  response in zero P\_full Fe root tips, with peak 2's being absent (blue trace in Figure 31D). Excess Fe, as in root tips grown on zero P\_excess Fe (olive-coloured trace in Figure 31D), led to a  $[Ca^{2+}]_{cyt}$  response very similar to root tips grown on half the amount of Fe (zero P\_full P). Touch maxima in response to 1 mM eATP application were varied in all three growth conditions, but not significantly different between the three growth conditions ( $p \geq 0.879$  for all comparisons, Figure 31E). Peak 1 maxima already showed a difference in response between full P\_full Fe (mean  $\mu$ M  $[Ca^{2+}]_{cyt} \pm$  SEM:  $0.28 \pm 0.01 \mu$ M) and zero P\_full Fe root tips ( $0.22 \pm 0.01 \mu$ M,  $p < 0.001$ , Figure 31F). However, the response of zero P\_excess Fe root tips was more intermediate ( $0.23 \pm 0.01 \mu$ M), and not significantly different from neither full P\_full Fe root tips ( $p = 0.082$ ) or zero P\_full Fe root tips ( $p = 0.999$ , Figure 31F).

However, the subsequent increase in  $[Ca^{2+}]_{cyt}$  ('peak 2') was completely absent in the P-starved root tips, regardless of whether 50  $\mu$ M or 100  $\mu$ M Fe had been added. This led to

full P\_full Fe root tips showing significantly higher peak 2 maxima ( $0.28 \pm 0.01 \mu\text{M}$ ) compared to zero P\_full Fe ( $0.13 \pm 0.01 \mu\text{M}$ ,  $p < 0.001$ ) or zero P\_excess Fe ( $0.14 \pm 0.01 \mu\text{M}$ ,  $p < 0.001$ ) root tips (Figure 31G). This pattern resulted in an overall significantly higher area under the curve in full P\_full Fe root tips, compared to both zero P\_full Fe and zero P\_excess Fe root tips ( $p < 0.001$  for both comparisons, Figure 31H).

Overall, doubling the Fe concentration (from  $50 \mu\text{M}$  to  $100 \mu\text{M}$ ), whilst starving *Arabidopsis* plants of P, led to an even more stunted primary root (Figure 29). However, the  $[\text{Ca}^{2+}]_{\text{cyt}}$  response to eATP was not further altered overall between the two Fe conditions in the P-starvation background.



**Figure 31:** The effect of Fe excess on the  $[\text{Ca}^{2+}]_{\text{cyt}}$  response of phosphate-starved root tips to extracellular ATP. Col-0 aequorin-expressing seedlings were grown on standard half MS growth medium, full P\_full Fe (green trace), zero P\_full Fe (blue trace) or zero P\_excess Fe (olive trace). Root tips (1 cm) of 11-day old seedlings were challenged with treatments applied at 35 seconds, and  $[\text{Ca}^{2+}]_{\text{cyt}}$  was measured for 155 seconds. (A) Application of control solution; time course trace represents mean  $\pm$  standard error of mean (SEM) from 3 - 6 independent trials, with  $n = 12 - 35$  individual root tips averaged per data point. Time course data were analysed for (B) touch maxima and (C) area under the curve (AUC), all baseline-subtracted, with each dot representing an individual data point (see Figure 6 for details). Boxplot middle line denotes median. (D-H) Responses to 1 mM eATP (3 - 6 independent trials,  $n = 22 - 61$  root tips per growth condition). Analysis of variance (ANOVA) with *post-hoc* Tukey Test was used to assess statistical differences. Significance levels (*p*-values): \*\*\* ( $<0.001$ ), \*\* ( $<0.01$ ), \* ( $<0.05$ ), n.s. (not significant).

### 3.2.16 Excluding iron from otherwise nutrient-replete roots only slightly affects their $[Ca^{2+}]_{cyt}$ response to extracellular ATP

Next, it was of interest to investigate the effect of both Fe exclusion and Fe addition on P-replete roots. In a first set of experiments, (apo)aequorin expressing *Arabidopsis* Col-0 plants were grown on growth medium containing standard levels of P but no Fe (full P\_zero Fe). Eleven-day old excised root tips (1 cm) were challenged with control solution, or 1 mM eATP treatment (in control solution background), and their response was compared to full P\_full Fe and zero P\_full Fe grown root tips.

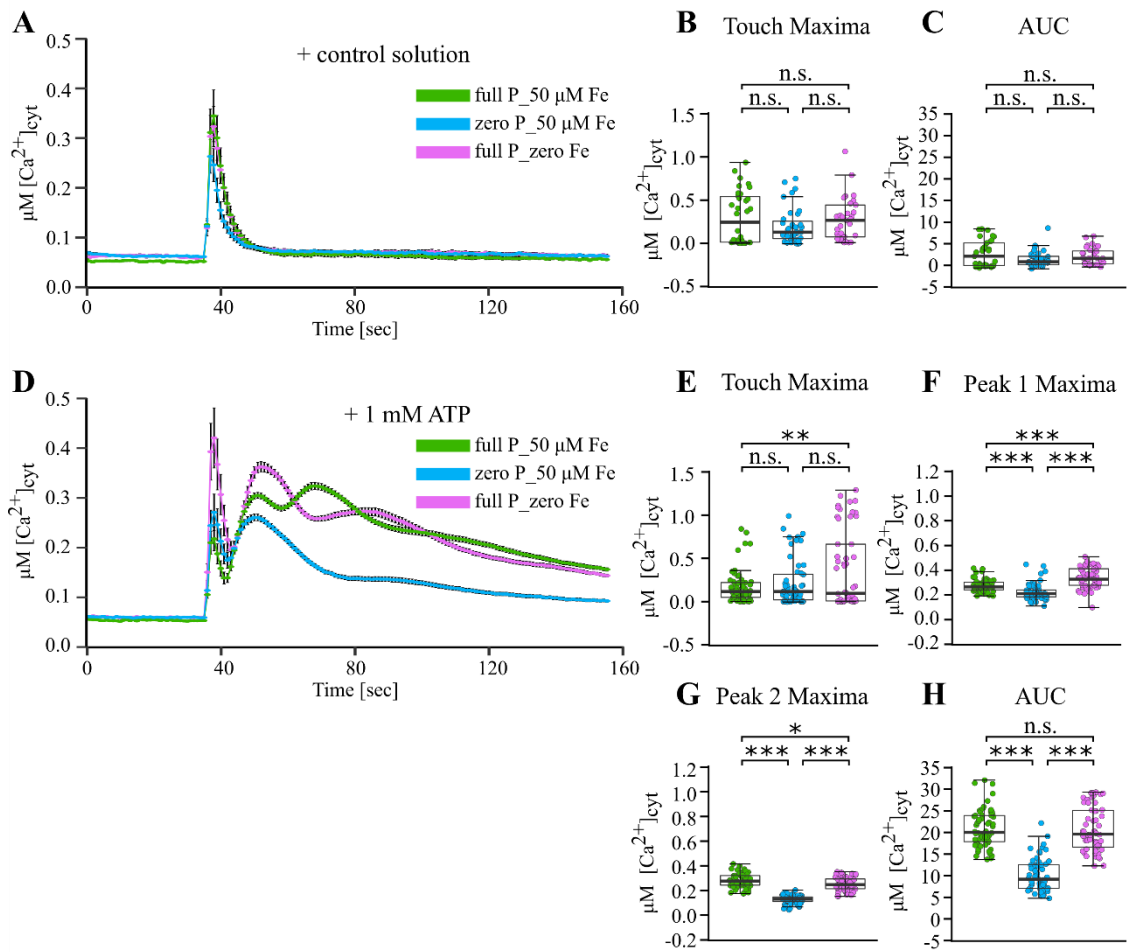
Application of control solution, to control for mechanical stimulation imposed during the assay, led to an immediate and monophasic increase in  $[Ca^{2+}]_{cyt}$  in all three growth conditions examined (data from 3 - 6 independent trials,  $n = 33 - 35$  individual root tips per growth condition, Figure 32A). The  $[Ca^{2+}]_{cyt}$  increase was similar in all growth conditions, and neither touch maxima nor area under the curve differed ( $p \geq 0.223$  for all comparisons, Figure 32B and C).

Treatment with 1 mM eATP led to the characteristic multi-phasic  $[Ca^{2+}]_{cyt}$  response in nutrient-replete plants (full P\_full Fe), which was strongly knocked down in P-starved root tips (zero P\_full Fe, data from 3 - 6 independent trials,  $n = 33 - 61$  individual root tips per growth condition, Figure 32D). Fe-starved root tips (full P\_zero Fe) showed a  $[Ca^{2+}]_{cyt}$  signature more similar to nutrient-replete root tips: multi-phasic, but with slightly different dynamics (pink trace in Figure 32D). With regards to touch maxima, the responses were variable, but overall full P\_zero Fe root tips responded significantly more strongly than full P\_full Fe root tips ( $p = 0.006$ ), however not more strongly than zero P\_full Fe root tips ( $p = 0.13$ , Figure 32E). The amplitude of the subsequent  $[Ca^{2+}]_{cyt}$  response was however very dissimilar, with peak 1 maxima being lowest in zero P\_full Fe root tips (mean  $\mu M [Ca^{2+}]_{cyt} \pm SEM: 0.22 \pm 0.01 \mu M$ ), intermediate in full P\_full Fe root tips ( $0.28 \pm 0.01 \mu M$ ), and highest in full P\_zero Fe root tips ( $0.34 \pm 0.01 \mu M$ ,  $p < 0.001$  for all comparisons, Figure 32F). With regards to peak 2 maxima, zero P\_full Fe root tips showed almost no increase in  $[Ca^{2+}]_{cyt}$ , and thus had the lowest peak 2 maxima ( $0.13 \pm 0.01 \mu M$ ,  $p < 0.001$  compared to both other growth conditions). Full P\_zero Fe root tips showed significantly lower peak 2 maxima ( $0.26 \pm 0.01 \mu M$ ) compared to full P\_full Fe root tips ( $0.28 \pm 0.01 \mu M$ ), *i.e.* the pattern observed for peak 1 for those two growth conditions was reversed ( $p = 0.044$ , Figure 32G). Strikingly, exclusion of Fe (*i.e.*, in full P\_zero Fe root tips) delayed the maximal increase during peak 2 phase by more

than 10 seconds (compare green to pink trace, Figure 32G). Considering overall amounts of  $[Ca^{2+}]_{\text{cyt}}$  mobilised in response to 1 mM eATP treatment, Fe-starved (full P\_zero Fe) root tips showed a comparable area under the curve to nutrient-replete (full P\_full Fe) root tips ( $p = 0.999$ , Figure 32H). P-starved (zero P\_full Fe) root tips showed a significantly lower area under the curve compared to both full P\_full Fe and full P\_zero Fe root tips ( $p < 0.001$  for both comparisons, Figure 32H).

Relating the observed  $[Ca^{2+}]_{\text{cyt}}$  signatures of Fe-starved root tips to quantified primary root lengths allowed the following observation: Fe-starved plants had primary root lengths similar to P-starved primary roots, but much shorter than nutrient-replete plants (Figure 29). However, Fe-starved root tips showed a similarly strong response to eATP treatment as did nutrient-replete root tips (Figure 32D - H). Taken together, it can be concluded that (i) Fe-starvation only slightly interfered with the  $[Ca^{2+}]_{\text{cyt}}$  response to eATP compared to P-starvation, and (ii) that primary root length was not the determining factor in the knock-down of the  $[Ca^{2+}]_{\text{cyt}}$  response.





**Figure 32:** The  $[Ca^{2+}]_{cyt}$  response of iron-starved root tips to extracellular ATP. Col-0 aequorin-expressing seedlings were grown on standard half MS growth medium, full P\_full Fe (green trace), zero P\_full Fe (blue trace) or full P\_zero Fe (pink trace). Root tips (1 cm) of 11-day old seedlings were challenged with treatments applied at 35 seconds, and  $[Ca^{2+}]_{cyt}$  was measured for 155 seconds. (A) Application of control solution; time course trace represents mean  $\pm$  standard error of mean (SEM) from 3 - 6 independent trials, with  $n = 33 - 35$  individual root tips averaged per data point. Time course data were analysed for (B) touch maxima and (C) area under the curve (AUC), all baseline-subtracted, with each dot representing an individual data point (see Figure 6 for details). Boxplot middle line denotes median. (D-H) Responses to 1 mM eATP (3 - 6 independent trials,  $n = 33 - 61$  root tips per growth condition). Analysis of variance (ANOVA) with *post-hoc* Tukey Test was used to assess statistical differences. Significance levels ( $p$ -values): \*\*\* ( $<0.001$ ), \*\* ( $<0.01$ ), \* ( $<0.05$ ), n.s. (not significant).

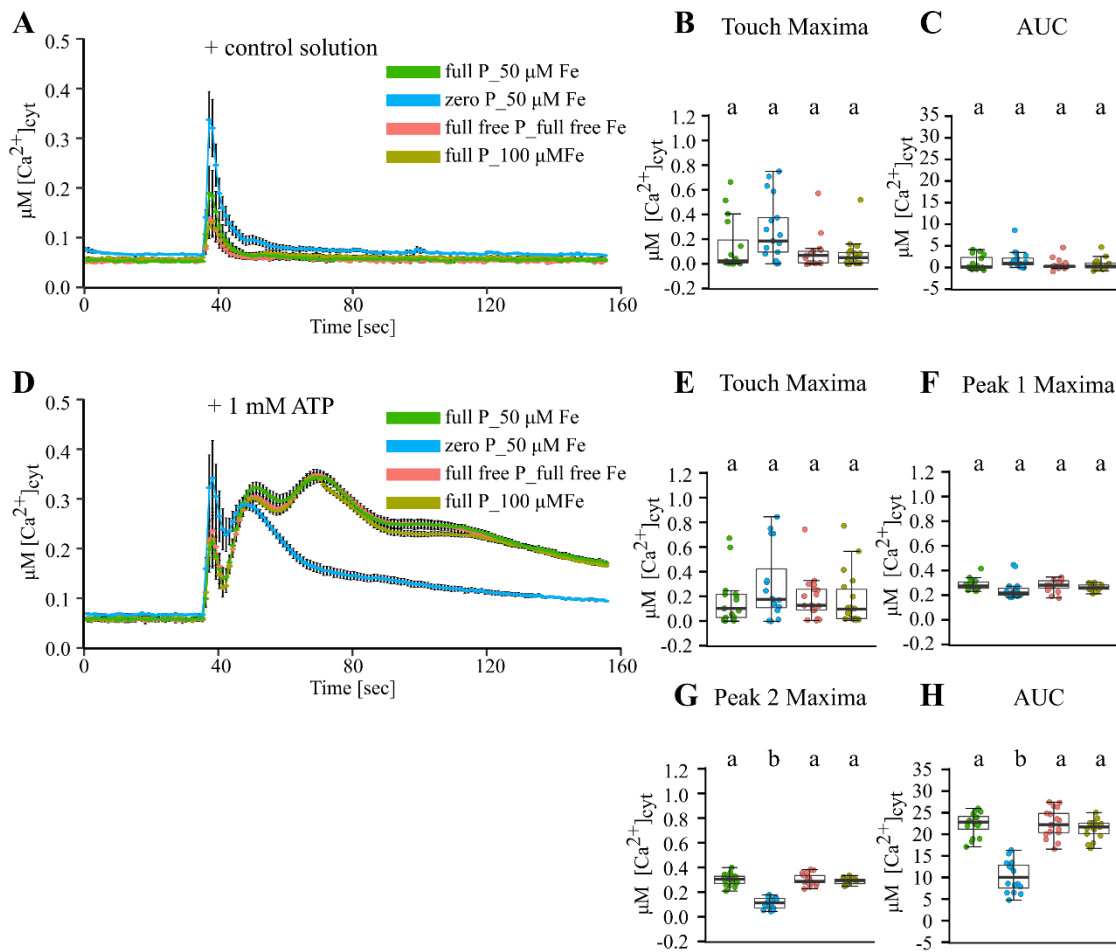
### 3.2.17 The dampened $[Ca^{2+}]_{\text{cyt}}$ response is due to a phosphate x iron interaction, not to iron toxicity alone

In the next set of experiments, the effect of excess Fe on the  $[Ca^{2+}]_{\text{cyt}}$  response of nutrient-replete roots was examined. To this end, (apo)aequorin-expressing *Arabidopsis* Col-0 plants were grown on medium containing replete levels of P, but increased Fe levels. Growth medium with two increased Fe levels were used. First, absolute Fe levels were increased to twice the strength found in standard half MS growth medium (*i.e.* increased from 50  $\mu\text{M}$  to 100), named ‘full P\_excess Fe’. Secondly, free Fe levels were increased, to mimic availability of free Fe estimated to occur in zero P\_full Fe growth medium (see Chapter 2, section 2.2.3 and Table 2 for more details on ionic composition of growth medium). This meant translating free Fe levels from zero P\_full Fe medium into a full P-background, and was linked to also adjusting free P levels to what was estimated for standard P-replete medium. This modified medium was named ‘full free P\_full free Fe’, containing 0.626 mM P and 55.35  $\mu\text{M}$  Fe (see Chapter 2, section 2.2.3 for more details). To compare these increased Fe growth media to standard Fe growth medium, plants were also grown under full P\_full Fe and zero P\_full Fe conditions. Excised root tips (1 cm) of 11-day old plants were used for the assay, treated with control solution or 1 mM eATP treatment (in control solution background).

Application of control solution led to an immediate and monophasic increase in  $[Ca^{2+}]_{\text{cyt}}$  (data from 3 trials,  $n = 16 - 17$  individual root tips per growth condition, Figure 33A). In zero P\_full Fe root tips, some samples showed a slightly prolonged  $[Ca^{2+}]_{\text{cyt}}$  response, which when averaged led to a small bump (see blue trace in Figure 33A). Besides, all four growth conditions did not show significant differences with regards to touch maxima ( $p \geq 0.151$  for all comparisons, Figure 33B) or area under the curve ( $p \geq 0.518$  for all comparisons, Figure 33C).

Compared to control solution, treatment with 1 mM eATP solution triggered a strong, multi-phasic  $[Ca^{2+}]_{\text{cyt}}$  response in all root tips grown on full P, regardless of the Fe level, and a much weaker  $[Ca^{2+}]_{\text{cyt}}$  response in P-starved root tips (data from 3 trials,  $n = 16 - 18$  individual root tips per growth condition, Figure 33D). Both touch response and peak 1 response were similar between all growth conditions (touch maxima:  $p \leq 0.783$  for all comparisons, Figure 33E; peak 1 maxima:  $p \geq 0.348$  for all comparisons, Figure 33F). The subsequent  $[Ca^{2+}]_{\text{cyt}}$  response, termed peak 2, was strongly impaired in P-starved root tips (peak 2 maxima  $\pm$  SEM:  $0.11 \pm 0.01 \mu\text{M}$ ,  $p < 0.001$  compared to all other three

growth conditions). Most interestingly, increasing the Fe concentration, both in the full P\_excess Fe and full free P\_full free Fe versions of growth medium, showed peak 2 maxima very similar to root tips grown on standard nutrient medium, *i.e.* full P\_full Fe (peak 2 maxima  $\pm$  SEM: full P\_full Fe:  $0.30 \pm 0.01 \mu\text{M}$ , full P\_excess Fe:  $0.29 \pm 0.01 \mu\text{M}$ , full free P\_full free Fe:  $0.30 \pm 0.01 \mu\text{M}$ ,  $p \geq 0.956$  for all comparisons, Figure 33G). Overall, this led to very similar levels of  $[\text{Ca}^{2+}]_{\text{cyt}}$  being mobilised in all full P growth conditions, regardless of Fe levels ( $p \geq 0.862$  for all comparisons), all of which were significantly higher than P-starved root tips ( $p < 0.001$  for all comparisons, Figure 33H). Taken together, increasing the Fe concentration did not alter the  $[\text{Ca}^{2+}]_{\text{cyt}}$  response of *Arabidopsis* root tips to eATP. In addition, the full free P\_full free Fe growth condition allowed testing of the hypothesis that Fe rather than P effected the dampened  $[\text{Ca}^{2+}]_{\text{cyt}}$  response seen in P-starved root tips. However, as it did *not* affect the  $[\text{Ca}^{2+}]_{\text{cyt}}$  response, it can be concluded that the  $[\text{Ca}^{2+}]_{\text{cyt}}$  response to eATP observed in P-starved root tips is not merely due to a slightly higher availability of Fe in the growth medium.



**Figure 33:** The effect of excess iron levels on the  $[Ca^{2+}]_{cyt}$  response of root tips to extracellular ATP. Col-0 aequorin-expressing seedlings were grown on standard half MS growth medium, full P<sub>full</sub> Fe (green trace), zero P<sub>full</sub> Fe (blue trace), full free P<sub>full</sub> free Fe (red trace) or full P<sub>excess</sub> Fe (beige trace). Root tips (1 cm) of 11-day old seedlings were challenged with treatments applied at 35 seconds, and  $[Ca^{2+}]_{cyt}$  was measured for 155 seconds. (A) Application of control solution; time course trace represents mean  $\pm$  standard error of mean (SEM) from 3 independent trials, with n = 16 - 17 individual root tips averaged per data point. Time course data were analysed for (B) touch maxima and (C) area under the curve (AUC), all baseline-subtracted, with each dot representing an individual data point (see Figure 6 for details). Boxplot middle line denotes median. (D-H) Responses to 1 mM eATP (3 independent trials, n = 16 - 18 root tips per growth condition). Analysis of variance (ANOVA) with *post-hoc* Tukey Test was used to assess statistical differences. Different lower-case letters describe groups of significant statistical difference ( $p < 0.05$ ), same letters indicate no statistical significance ( $p > 0.05$ ).

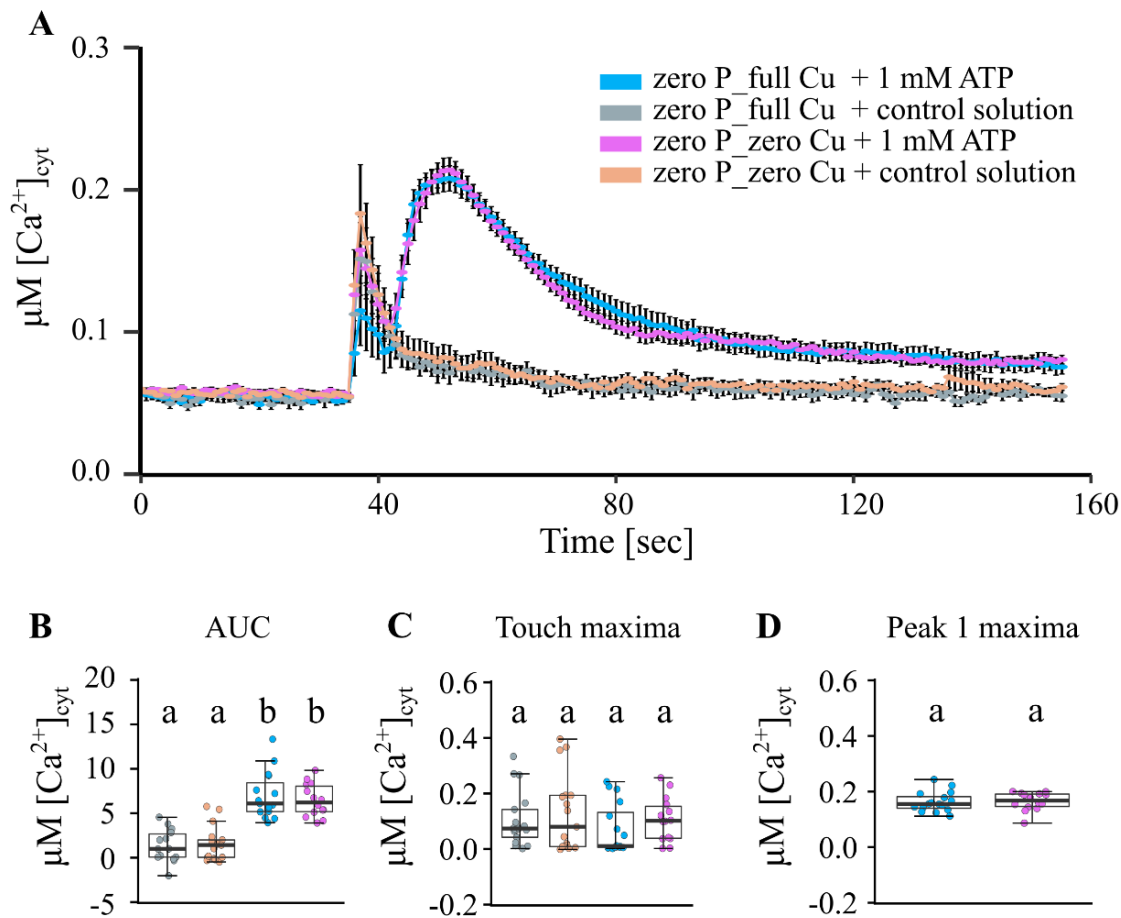
### 3.2.18 Exclusion of copper does not rescue the altered $[Ca^{2+}]_{\text{cyt}}$ response of phosphate starved roots

*This experiment was designed by EM but carried out by Nicholas Doddrell, Part II student, University of Cambridge*

To test if not only Fe, but also the availability of another reactive transition metal could similarly rescue the dampened  $[Ca^{2+}]_{\text{cyt}}$  response, the involvement of copper ( $Cu^{2+}$ ) was investigated. *Arabidopsis* was therefore starved as before of P (zero P, 0 mM P), additionally,  $Cu^{2+}$  levels were varied, to either contain ‘full Cu’ (standard half MS levels, 0.05  $\mu\text{M } Cu^{2+}$ ) or ‘zero Cu’ (0  $\mu\text{M } Cu^{2+}$ ). Seedlings grown under these conditions grew comparably, *i.e.* the primary root length did not differ significantly (mean primary root length (cm)  $\pm$  SEM: zero P\_full Cu:  $3.24 \pm 0.08$  cm; zero P\_zero Cu:  $3.48 \pm 0.14$  cm,  $p = 0.152$  as determined by Welch two sample *t*-test, data from 3 independent trials, with  $n = 38 - 89$  individual root lengths scored per growth condition).

Excised 11-day old root tips (1 cm) grown under these conditions were then challenged with control solution (to control for mechanical stimulation occurring during the assay) or 1 mM eATP treatment solution (in control solution background, maintaining P and  $Cu^{2+}$  levels, Figure 34). Application of control solution led to an immediate and monophasic increase in  $[Ca^{2+}]_{\text{cyt}}$ , treatment with 1 mM eATP led to the characteristic touch response followed by a single increase (‘peak 1’) in  $[Ca^{2+}]_{\text{cyt}}$  (Figure 34A), as has been reported so far for P-starved root tips. However, no difference could be observed between root tips grown with  $Cu^{2+}$  (zero P\_full Cu) or without  $Cu^{2+}$  (zero P\_zero Cu) (compare blue and pink trace in Figure 34A). Upon application of control solution, the variation in  $Cu^{2+}$  did not lead to a different area under the curve or touch maxima ( $p \geq 0.927$  for both comparisons, Figure 34B and C). Treatment with 1 mM eATP did mobilize more  $[Ca^{2+}]_{\text{cyt}}$  than control solution alone, but no difference could be observed between root tips grown on full Cu or zero Cu, in a zero P background, for all relevant parameters analysed ( $p \geq 0.79$  for all comparisons, area under the curve (Figure 34B), touch maxima (Figure 34C) and peak 1 maxima (Figure 34D)).

Taken together, exclusion of  $Cu^{2+}$  from the growth medium did not rescue the dampened  $[Ca^{2+}]_{\text{cyt}}$  response of P-starved roots to eATP. This indicates that the dampening of the response is specifically linked to Fe availability, and not a general effect of availability or absence of transition metals as exemplified by  $Cu^{2+}$  availability.



**Figure 34:** The  $[Ca^{2+}]_{\text{cyt}}$  response of copper- and phosphate-starved root tips to extracellular ATP. Col-0 aequorin-expressing seedlings were grown on modified half MS growth medium: zero P\_full Cu (blue and grey trace) or zero P\_zero Cu (pink and light pink traces). Root tips (1 cm) of 11-day old seedlings were challenged with treatments applied at 35 seconds, and  $[Ca^{2+}]_{\text{cyt}}$  was measured for 155 seconds. (A) Application of control solution (grey and light pink trace) or 1 mM eATP treatment (blue and pink trace); time course trace represents mean  $\pm$  standard error of mean (SEM) from 3 independent trials, with  $n = 14 - 17$  individual root tips averaged per data point. Time course data were analysed for (B) area under the curve (AUC), (C) touch maxima, and (D) peak 1 maxima, all baseline-subtracted, with each dot representing an individual data point (see Figure 6 for details). Boxplot middle line denotes median. Analysis of variance (ANOVA) with *post-hoc* Tukey Test was used to assess statistical differences. Different lower-case letters describe groups of significant statistical difference ( $p < 0.05$ ), same letters indicate no statistical significance ( $p > 0.05$ ).

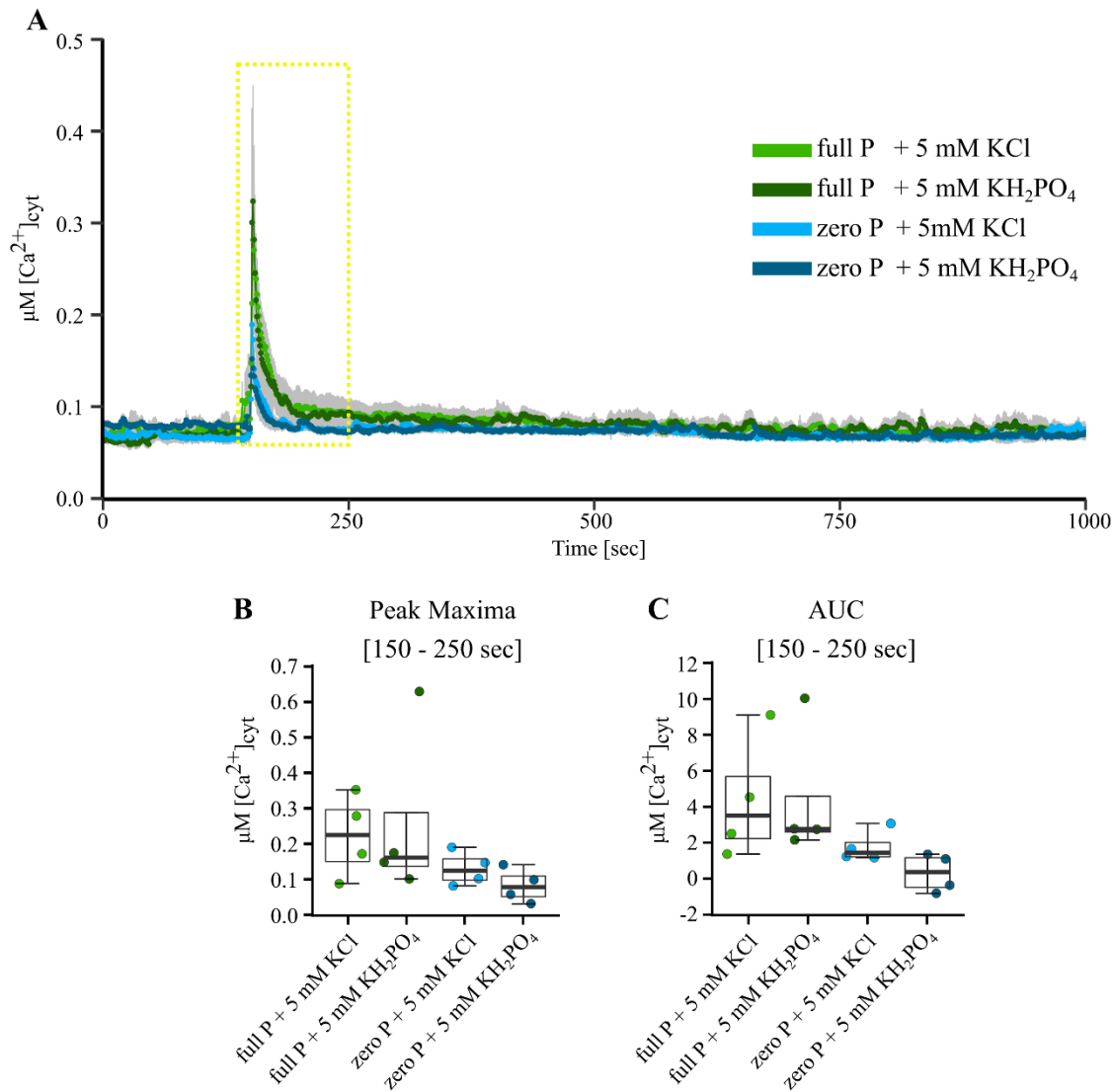
### 3.2.19 $[Ca^{2+}]_{\text{cyt}}$ does not seem to signal P availability

In P nutrition, it is unknown if  $[Ca^{2+}]_{\text{cyt}}$  (or any organellar free  $Ca^{2+}$  pool) signals P availability. More particularly, it is unknown if P re-supply is signalled through modulations of  $[Ca^{2+}]_{\text{cyt}}$ .

Initially, it was planned to design an experiment similar to what Riveras *et al.* (2015) carried out for nitrate-starved roots; starve aequorin-expressing *Arabidopsis* seedlings of P, then monitor the  $[Ca^{2+}]_{\text{cyt}}$  response of roots to re-addition of a P-source, with particular focus on touch maxima. However, in the course of this thesis it became apparent that this set-up was not applicable for P-starved roots as P-starvation led to a lowered touch response (Figure 13) which would bias any analysis of touch maxima. Furthermore, application of a 2 mM P source (phosphoric acid, at pH 5.6, Figure 9) did not lead to any differences in  $[Ca^{2+}]_{\text{cyt}}$  response compared to control solution application, in both medium and zero P grown root tips. P-sources in the soil are generally described to be in the micromolar range (Raghothama, 1999; Werner *et al.*, 2017), thus 2 mM P addition (see Figure 9) would already be considered a high [P] stimulus.

However, P re-supply could trigger  $[Ca^{2+}]_{\text{cyt}}$  modulations downstream of the initial touch response. For example, P re-supply and uptake could trigger a longer-term decrease or increase of  $[Ca^{2+}]_{\text{cyt}}$ . Therefore, aequorin-expressing, individual whole seedlings of *Arabidopsis* were grown on full or zero P medium, challenged with a high P source, 5 mM  $KH_2PO_4$ , and monitored for a longer time period of approximately 16 minutes (1000 seconds) using a luminometer (see Chapter 2, section 2.6.3). A 5 mM KCl treatment was used to control for the effect of  $K^+$  addition as part of the  $KH_2PO_4$  treatment.

Application of both  $KH_2PO_4$  or KCl treatment solution led to an immediate and monophasic increase in  $[Ca^{2+}]_{\text{cyt}}$  (data from 2 independent trials, with  $n = 4$  individual whole seedlings per growth condition and treatment, Figure 35A). The initial window of response (150 – 250 seconds, see yellow box in Figure 35A) was analysed for peak maxima and area under the curve. The trend was that full P seedlings showed a stronger  $[Ca^{2+}]_{\text{cyt}}$  response than zero P seedlings, with little difference observed between  $KH_2PO_4$  and KCl treatment (Figure 35B, C). As replicate number was low, no statistical test was carried out.



**Figure 35:** The  $[\text{Ca}^{2+}]_{\text{cyt}}$  response of phosphate-starved whole seedlings to phosphate re-supply. Col-0 aequorin-expressing seedlings were grown on full P (green traces) or zero P (blue traces). Eleven-day old whole seedlings were challenged with treatments applied at 150 seconds, and  $[\text{Ca}^{2+}]_{\text{cyt}}$  was measured for in total 1000 seconds in a luminometer before application of a discharge solution. (A) Application of 5 mM  $\text{KH}_2\text{PO}_4$  or 5 mM KCl; time course trace represents mean  $\pm$  standard error of mean (SEM) from 2 independent trials, with  $n = 4$  individual whole seedlings averaged per data point. Time course data were analysed for (B) touch maxima (150 – 250 seconds, see yellow dashed box in (A)) and (C) area under the curve (AUC, 150 – 250 seconds, see yellow dashed box in (A)), all baseline-subtracted, with each dot representing an individual data point. Boxplot middle line denotes median. Due to low replicate number, no statistical test was carried out.



### 3.3 Discussion

#### 3.3.1 Considerations on aequorin as reporter

Limitations of the aequorin  $\text{Ca}^{2+}$  reporter aequorin used here are (i) prolonged incubation times to reconstitute aequorin, (ii) excision of sample tissue if a defined region rather than whole seedlings were to be investigated, and (iii) injection of treatment solutions eliciting a mechanical stimulation. These aspects will be discussed in the following.

INCUBATION - Bioluminescence generation of aequorin upon  $\text{Ca}^{2+}$  binding relies on (apo)aequorin's being reconstituted with its prosthetic group coelenterazine. This requires a prolonged incubation of sample tissue in coelenterazine-containing solution which can affect the downstream ability of the sample tissue to respond through dissimilar uptake of coelenterazine between individual samples. In addition, the assay bathing medium was found to strongly influence the  $[\text{Ca}^{2+}]_{\text{cyt}}$  response (reported for whole seedlings and osmotic stress treatment, Tracey *et al.*, 2008), as the ionic composition would influence the PM resting potential.

A proxy for how much aequorin is available to react with  $\text{Ca}^{2+}$  (and thus was successfully reconstituted with coelenterazine) is the total level of 'discharge', *i.e.* the maximal luminescence generated upon saturation of all reconstituted aequorin with high  $[\text{Ca}^{2+}]$ . As nutrient starvation might influence both the level of aequorin protein, as well as the uptake levels of coelenterazine (*e.g.* through altered membrane composition), the discharge levels of N- and P-starved root tips were compared. Discharge levels varied between the nutrient growth conditions, but except for some N-starved root tips, were found to be above an acceptable threshold (over 1 million total luminescence counts) and thus considered suitable for  $[\text{Ca}^{2+}]_{\text{cyt}}$  analysis.

Previous studies employing the aequorin reporter mostly used water (*e.g.* Knight *et al.*, 1991; Riveras *et al.*, 2015; Lenzoni, Liu and Knight, 2017) or a low  $\text{Ca}^{2+}$  and low  $\text{K}^+$  bathing medium with set pH (*e.g.* Demidchik *et al.*, 2003; Laohavisit *et al.*, 2012; Richards *et al.*, 2014). Bathing medium containing *e.g.* 10 mM  $\text{CaCl}_2$  and 0.1 mM KCl, *i.e.* higher  $[\text{Ca}^{2+}]$  than  $[\text{K}^+]$ , would constitute a more hyperpolarizing bathing medium and would set the PM resting potential to approximately -135 to -150 mV (Demidchik *et al.*, 2002). However, both incubation in plain water or low-solute medium would quickly induce nutrient deficiencies, as it has been shown that nutrient deficiency can be perceived rapidly, *e.g.* P deprivation led to cell wall stiffening within 30 minutes,

inhibited root cell elongation within less than 2 hours (Balzergue *et al.*, 2017), and global transcriptomic changes were apparent after 1 hour of P starvation (earliest time point tested, Lin *et al.*, 2011). To study the particular effect of P-starvation, without confounding effects of other short-term nutrient deprivations, the bathing medium used in this thesis was therefore designed to maintain prior growth conditions, *i.e.* constituted a nutrient rich half MS liquid medium with or without P, N, *etc.*. Standard half MS medium has a  $K^+ : Ca^{2+}$  ratio of approximately 12.5:1.5, *i.e.* lower  $[Ca^{2+}]$  than  $[K^+]$ . This constitutes a depolarizing medium which would indicate a PM resting potential around -85 mV (Demidchik *et al.*, 2002). P starvation was shown to not alter the PM potential further (Mimura *et al.*, 1998; Dindas *et al.*, 2018). Taken together, the bathing medium used for aequorin assays in this thesis, but not P starvation *per se*, would depolarize the PM resting potential which could ultimately alter ion channel activity upon stress perception.

EXCISION - Previous studies employing aequorin often assayed the response of whole seedlings to stress treatments (Knight *et al.*, 1991; Tanaka *et al.*, 2010; J. Choi, Tanaka, Cao, *et al.*, 2014; Chen *et al.*, 2017). If the response of a specific tissue / organ were to be investigated, excised root / shoot tissue or protoplasts were employed (Demidchik, Nichols, *et al.*, 2003; Rentel and Knight, 2004; Richards *et al.*, 2014). The results presented here were based on using excised root tips (apical 1 cm) for aequorin assays, for the following reasons. First, the root tip has been shown to be highly sensitive to stress perception (Demidchik *et al.*, 2007; Weerasinghe *et al.*, 2009; Costa *et al.*, 2013b). Secondly, the root tip was shown to play a dominant role in P nutrition, both in P sensing and uptake (Svistoonoff *et al.*, 2007; Kanno *et al.*, 2016; reviewed by Abel, 2017). And lastly, P starvation profoundly inhibited primary root growth, which is well documented in the literature (Sánchez-Calderón *et al.*, 2005; Svistoonoff *et al.*, 2007; Balzergue *et al.*, 2017). The data presented here showed 10-day old, P-replete seedlings to have more than twice the primary root length compared to chronically P-starved seedlings (approximately 6 cm *versus* 2.7 cm). Monitoring the averaged  $[Ca^{2+}]_{\text{cyt}}$  response of whole seedlings or whole roots would have constituted a bias due to large differences in deployed sample tissue. To control for differences in root size, a defined length of root tissue of interest was used for the assays (1 cm of apical root tip). Whilst this might reduce the error, it is unlikely to fully exclude the bias as P starvation was shown to change the cellular patterning: The overall root meristem size was reduced, epidermal cells were found to be smaller, whilst the number of cortex cells increased, ultimately influencing and increasing

outgrowth of root hairs (Ma *et al.*, 2001; Williamson *et al.*, 2001; Cederholm and Benfey, 2015; Balzergue *et al.*, 2017; Janes *et al.*, 2018).

An error source introduced by excision of root tips would be acute physical damage. As wounding is known to induce a stress response, including *e.g.* ATP exudation, ROS production and downstream changes in gene expression (Demidchik *et al.*, 2009; Dark *et al.*, 2011; J. Choi, Tanaka, Cao, *et al.*, 2014), excised tissue will likely be ‘primed’ differently to intact tissue. Particularly with regards to eATP perception, it is unclear how previous exposure to wounding-induced eATP might dampen or enhance any subsequent ATP application.

INJECTION - Plate-reader based quantification of aequorin-derived luminescence necessitated the injection of treatment solutions, which elicited a  $[Ca^{2+}]_{cyt}$  response due to mechanical stimulation alone. To dissect this ‘touch response’ from the effect of abiotic stress responses, every experiment was complemented with control solution application to estimate the effect of mechanical stimulation. Salt and osmotic stress triggered a  $[Ca^{2+}]_{cyt}$  response which overlaid any response due to mechanical stimulation. In  $H_2O_2$  and extracellular nucleotide (ATP, ADP,  $\gamma$ -ATP) treatments, there was however an immediate  $[Ca^{2+}]_{cyt}$  response similar in dynamics to the  $[Ca^{2+}]_{cyt}$  response triggered by application of control solution alone. Indeed, comparing these initial responses between control solution and stress treatments showed no difference, indicating that the initial ‘touch response’ was due to mechanical stimulation and was not further modulated due to  $H_2O_2$  and extracellular nucleotide perception.

To overcome the described limitations of the set-up used for  $[Ca^{2+}]_{cyt}$  determinations in this Chapter, a set-up using (i) intact plants and (ii) superfusion rather than injection of treatment solutions would be preferable. This can be achieved by using microscopy-based  $Ca^{2+}$  reporter in a perfusion set-up. Such a system will be employed and discussed in Chapter 4.

### 3.3.2 Phosphate starvation dynamically alters the $[Ca^{2+}]_{cyt}$ response to extracellular ATP, which was dependent on DORN1 but not ANNEXIN1

Chronic P-starvation already showed a dampening of ATP-induced  $[Ca^{2+}]_{cyt}$  response in 6-day old seedlings, whilst the  $[Ca^{2+}]_{cyt}$  dynamics (distinct touch response, followed by peak 1 and peak 2) were still similar to P-replete root tips. Only after 7 to 8 days of P-starvation was the characteristic change in  $[Ca^{2+}]_{cyt}$  signature (dampened touch response,

followed by peak 1, but peak 2 absent) found to occur. This suggested that P deprivation gradually affects the  $[Ca^{2+}]_{cyt}$  response, rather than tilting a single on/off switch.

Transferring P-starved seedlings to P-containing growth medium (for 3 days) significantly reversed the initially dampened  $[Ca^{2+}]_{cyt}$  response to eATP back to P-replete levels. *Vice versa*, subjecting P-replete plants to 3 days of P starvation significantly dampened the  $[Ca^{2+}]_{cyt}$  response to eATP. Taken together, this indicated that P availability dynamically modulates the  $[Ca^{2+}]_{cyt}$  response to eATP.

To elucidate molecular components involved in the changed  $[Ca^{2+}]_{cyt}$  response to eATP of P-starved root tips, mutants of DORN1 and ANNEXIN1 were tested. Independent of P availability, the eATP receptor DORN1 was found necessary for all eATP-induced  $[Ca^{2+}]_{cyt}$  changes in root tips, which corroborated previous findings in whole seedlings (J. Choi, Tanaka, Cao, *et al.*, 2014). Further, the involvement of ANNEXIN1 was tested. ANN1 had been reported to govern  $Ca^{2+}$  influx across the PM (Laohavisit *et al.*, 2009, 2012) and was particularly highly upregulated upon P starvation (Lan *et al.*, 2012; Z. Q. Wang *et al.*, 2018). ANN1's upregulation upon P starvation would imply its acting as a negative regulator of the eATP-induced  $[Ca^{2+}]_{cyt}$  response, and knock-out of ANN1 should potentially rescue the dampened  $[Ca^{2+}]_{cyt}$  response of P-starved root tips. However, knock-out of ANN1 had no effect on the  $[Ca^{2+}]_{cyt}$  response in the conditions used. Using GFP-tagged constructs, localization studies of ANN1 gene expression and ANN1 protein agreed with previous findings with regards to distribution in P-replete roots (Siân Richards, unpublished). Under P-starvation, ANN1 gene was expressed to similar levels as in nutrient-replete roots, and equally distributed within the root, with the strongest expression occurring in epidermal and root hair cells. However, ANN1 protein abundance was found to be diminished in P-starved root tips, contrary to what had been expected based on previous studies (Lan *et al.*, 2012; Z. Q. Wang *et al.*, 2018). This could be due to differences in growth conditions, *e.g.* both studies used a transfer set-up in which plants were grown on nutrient-replete conditions for 7 days, before being transferred to low P for 3 days (Lan *et al.*, 2012) or 7 days (Z. Q. Wang *et al.*, 2018). In addition, both studies used different complex nutrient compositions, with added sucrose ('*Arabidopsis thaliana* salts', Lan *et al.*, 2012; or half-strength Hoagland solution, Z. Q. Wang *et al.*, 2018).

### 3.3.3 Phosphate-starved roots still accumulate low levels of extracellular ATP

Low levels of extracellular ATP (eATP) have been shown to be essential for optimal plant growth (S.-Y. Kim *et al.*, 2006; Clark *et al.*, 2010). Furthermore, elevations of eATP are described to occur during stress perception (Weerasinghe *et al.*, 2009; Dark *et al.*, 2011), potentially reaching millimolar concentrations of eATP close to site of PM rupture / wounding. Upon mechanical stimulation, nanomolar concentrations of eATP could be determined in bathing medium surrounding roots (approximately 60 nM 1 minute after mechanical stimulation (Weerasinghe *et al.*, 2009), or 80 nM measured 15 minutes after mechanical stimulation (Dark *et al.*, 2011).

The use of P-rich signalling molecules - ATP containing 3 labile P groups, ADP containing 2 labile P groups – might however be constrained in P-limited conditions. Onset of P-starvation has reliably been shown to induce a rapid intracellular drop in P-rich molecules (including nucleotides), substitution of membrane phospholipids with glyco-/sulpholipids, and in general a switch to alternative metabolic pathways consuming less P (Duff *et al.*, 1989; Andersson *et al.*, 2005; Shimano and Ashihara, 2006; Pratt *et al.*, 2009; Nakamura, 2013; Okazaki *et al.*, 2013; Pant *et al.*, 2015). Therefore, it was interesting to test if chronic P starvation altered the use of extracellular ATP as signalling molecule.

Extracellular ATP in bathing medium surrounding P-replete and P-starved roots was quantified using a luciferase-dependent method, as has been employed by previous studies (Weerasinghe *et al.*, 2009; Dark *et al.*, 2011). These previous studies reported absolute ATP values (in nM) for a set number of seedlings. As seedlings grown on full or zero P showed strong differences in growth, comparison between individual seedlings would have been biased, and quantified [eATP] was therefore normalized for root fresh weight. In doing so, it was revealed that both full P and zero P grown roots showed similar baseline [eATP] baseline levels, directly after transfer to the bathing medium. eATP levels were in the low nanomolar range, similar to what had been reported previously (Weerasinghe *et al.*, 2009; Dark *et al.*, 2011). After 60 minutes, bathing medium sampled at similar positions close to the root tip showed a five-fold increase of [eATP] in full P grown roots, whereas zero P grown roots did not quite double the amount of [eATP] surrounding their roots. This indicates that P-starved roots sustain some eATP levels.

However, the assay was limited in that it did not allow taking ATP hydrolysis into account, and further might be hindered by diluting exuded ATP in bathing medium, rather than sampling at the site of eATP exudation (between PM and cell wall). In a similar set-up, the  $t_{1/2}$  of ATP breakdown in the bathing medium was determined to be 180 min (Weerasinghe *et al.*, 2009). This is likely to be an underestimate, as it does not consider the higher activity of cell wall-localized hydrolytic enzyme compared to the diluted bathing medium. Nevertheless, it *does* show that ATP hydrolysis occurs within the time frame of 60 minutes (as sampled in this thesis) and thus likely contorts the absolute values reported here. Therefore, it can be concluded that zero P grown roots still accumulate some eATP, however to lower levels than P-replete roots. If this were due to lower efflux or a higher rate of ATP hydrolysis in P-starved roots remains to be determined.

### 3.3.4 Iron-availability is linked to the phosphate-starvation induced altered $[Ca^{2+}]_{cyt}$ response

Excluding P from growth medium has been shown to lead to excess Fe accumulation in *Arabidopsis* roots (Hirsch *et al.*, 2006; Ward *et al.*, 2008). As removing Fe from the growth medium, in addition to P, restored primary root growth, it has been hypothesized that root growth inhibition is an effect of Fe toxicity rather than P starvation (Ward *et al.*, 2008). To test how Fe availability affected the dampened  $[Ca^{2+}]_{cyt}$  signature, and if it were due to Fe toxicity rather than P starvation, root tips grown on different P and Fe levels were challenged with eATP.

In this thesis excluding Fe from the growth medium as well as P restored *Arabidopsis* primary root growth, in agreement with what had been reported previously (Ward *et al.*, 2008; Müller *et al.*, 2015; Balzergue *et al.*, 2017). Fe availability furthermore strongly modulated the  $[Ca^{2+}]_{cyt}$  signature in response to 1 mM eATP. Exclusion of Fe, as well as P (zero P\_zero Fe), almost fully restored the ATP-induced  $[Ca^{2+}]_{cyt}$  signature in both amplitude and dynamics. Low levels of Fe (10  $\mu$ M instead of 50  $\mu$ M Fe, zero P\_low Fe) relieved the impaired  $[Ca^{2+}]_{cyt}$  signature of P-starved root tips in response to eATP, but to a lesser extent. At the other end of the scale, increasing the Fe levels from 50  $\mu$ M to 100  $\mu$ M Fe in a zero P background (zero P\_excess Fe) did not further dampen the observed  $[Ca^{2+}]_{cyt}$  signature.

As this could indeed support the idea that Fe toxicity, rather than P starvation, was responsible for the dampened  $[Ca^{2+}]_{cyt}$  signature, Fe availability in a P-replete background

was modified. Excluding Fe whilst maintaining sufficient P levels (full P<sub>zero</sub> Fe) overall showed a  $[Ca^{2+}]_{cyt}$  signature similar to nutrient replete plants, however more pronounced in the early response (peak 1), and slightly delayed during the later response (peak 2). Interestingly, the delay in peak 2 maximum was similar to what was seen in zero P<sub>zero</sub> Fe grown roots, indicating that Fe is involved in advancing maximal peak 2 responses.

Increasing the absolute amount of Fe (to twice its standard level: 100  $\mu$ M instead of 50  $\mu$ M, full P<sub>excess</sub> Fe), as well as adjusting the free Fe levels in accordance with the free P levels of the nutrient growth medium (full free P<sub>full</sub> free Fe, see section 3.2.13 for a thorough explanation) did not inhibit primary root growth to the extent observed in P-starved seedlings. It further did not *in the least* alter the  $[Ca^{2+}]_{cyt}$  response to eATP. This strongly suggest that an interaction between P starvation and Fe availability, and not Fe toxicity alone, alters the  $[Ca^{2+}]_{cyt}$  signature in response to eATP. This endorses previous findings, where increased Fe levels (500  $\mu$ M) also led to Fe depositions in P-replete *Arabidopsis* roots. The studies cited above focus on Fe overaccumulation under low P conditions, and on the redox active role of Fe in generating ROS overload, eventually leading to cell wall stiffening and inhibition of cell elongation (Ward *et al.*, 2008; Müller *et al.*, 2015; Hoehenwarter *et al.*, 2016; Balzergue *et al.*, 2017). However, it was not tested if the ROS overload was specific to Fe accumulation, or could at least in part be mediated by another redox active element such as copper ( $Cu^{2+}$ ). To test, if the dampened  $[Ca^{2+}]_{cyt}$  signature of P-starved roots could equally be rescued by exclusion of  $Cu^{2+}$ , 11-day old root tips starved of P and  $Cu^{2+}$  were challenged with eATP. Excluding  $Cu^{2+}$  from the growth medium did *not* rescue the  $[Ca^{2+}]_{cyt}$  response to eATP, indicating that Fe overaccumulation in low P conditions was indeed the causative factor. However, as  $Cu^{2+}$  is required in much smaller amounts than Fe for plant growth (in absolute terms being 1000 x lower, as standard half-strength MS contains only 0.05  $\mu$ M  $Cu^{2+}$ , and 50  $\mu$ M Fe), it is possible that within the time frame monitored here no severe  $Cu^{2+}$  deficiency was induced. However, it is unlikely that  $Cu^{2+}$  availability influences the  $[Ca^{2+}]_{cyt}$  signature similar to what has been reported for Fe, as excluding Fe from zero P medium fully rescued the  $[Ca^{2+}]_{cyt}$  signature even though it would still contain standard levels of  $Cu^{2+}$ . In addition, it has been reported that excluding Fe from growth medium led to increased accumulation of  $Cu^{2+}$  in 9-day old *Arabidopsis* and 7-day old cucumber leaves (Ward *et al.*, 2008; Waters and Armbrust, 2013). If  $Cu^{2+}$  were involved in generating ROS, similar to Fe, its effect should be *pronounced* in Fe-free medium. Instead, Fe-free medium showed a  $[Ca^{2+}]_{cyt}$  signature comparable to nutrient-replete root tips.

### 3.3.5 Phosphate availability does not seem to be signalled through immediate $[Ca^{2+}]_{\text{cyt}}$ modulations

For nitrate-starved roots, it has been shown that nitrate resupply triggered a rapid increase in  $[Ca^{2+}]_{\text{cyt}}$  (Riveras *et al.*, 2015; Liu *et al.*, 2017). The initial discovery was done using a set-up similar to this thesis, *i.e.* aequorin-expressing *Arabidopsis* plants which were challenged with treatment solutions by injecting them onto the sample tissue (Riveras *et al.*, 2015). The reported  $[Ca^{2+}]_{\text{cyt}}$  response was thus primarily a response to mechanical stimulation due to injection, which was however shown to increase if nitrate was included into the treatment solution (Riveras *et al.*, 2015). Furthermore, this increased  $[Ca^{2+}]_{\text{cyt}}$  response was dependent on the nitrate transporter NRT1.1 (Riveras *et al.*, 2015). Accordingly, NRT1.1 has recently been described to function as a ‘transceptor’, *i.e.* as a transporter as well as a receptor of nitrate (Bouguyon *et al.*, 2015). For P nutrition, a transceptor has been characterized in yeast (Popova *et al.*, 2010), but if plants possess a similar P transceptor it remains to be identified.

To date, it has not been reported if  $[Ca^{2+}]_{\text{cyt}}$  is involved in signalling P availability. After resupply of P, P uptake has been described to occur within minutes, indicating that any signalling of P availability should occur within such a short time frame. Furthermore, P resupply to P-starved *Lemna gibba*, white clover and *Arabidopsis* root cells was shown to lead to a depolarization of the PM, *i.e.* the membrane potential becoming more positive (Ullrich-Eberius *et al.*, 1981; Dunlop and Gardiner, 1993; Dong *et al.*, 1999; Dindas *et al.*, 2018). The more P-starved the tissue and the higher the [P] applied, the stronger was the depolarization of the PM (Dunlop and Gardiner, 1993; Dong *et al.*, 1999; Dindas *et al.*, 2018). This depolarization could be the result of net positive charge entering the cell *via* a  $H^+$ -P symporter that translocates more  $H^+$  per cycle than P, rendering it electrogenic. It also potentially indicates opening of cation channels, including  $Ca^{2+}$ -permeable channels.

As the aequorin reporter was shown suitable to detect  $[Ca^{2+}]_{\text{cyt}}$  changes upon nutrient resupply, exemplified by Riveras *et al.* (2015), a similar approach was considered to test if P resupply would trigger modulations in  $[Ca^{2+}]_{\text{cyt}}$ . Both an increase or decrease in  $[Ca^{2+}]_{\text{cyt}}$  could occur. Application of control solution *maintaining* prior P conditions (*i.e.* applying control solution without P to zero P grown root tips) however showed that P-starved root tips responded differently to mechanical stimulation alone. The response to mechanical stimulation was variable, *e.g.* even nutrient replete plants showed a wide



range of response, from very small to very large increases in  $[Ca^{2+}]_{cyt}$ . This may be due to variation in the level of force experienced by receptive cells due to the different positioning of individual root tip samples in the well. When analysing a high number of biological replicates, P-starved root tips however responded significantly less to a mechanical stimulus. The mechanistic basis of this is unknown, but is likely to be a consequence of the P starvation induced changes such as altered membrane lipid composition and/or thickened and stiffened cell walls (Nakamura, 2013; Müller *et al.*, 2015; Balzergue *et al.*, 2017). Thus, using an altered touch response alone as read-out for any P-induced  $[Ca^{2+}]_{cyt}$  changes upon P resupply, as was done for nitrate resupply, would easily be biased.

Even if an altered touch response could not be used as a read-out, it was still feasible to test if P resupply would modulate  $[Ca^{2+}]_{cyt}$  beyond the initial touch response. As root tips were shown to be primarily responsible for P sensing and uptake (Svistonoff *et al.*, 2007; Kanno, Arrighi, *et al.*, 2016), they were initially used for P resupply experiments. However, application of a 2 mM P-source (applied as pH-buffered and dilute phosphoric acid) to root tips, and monitoring  $[Ca^{2+}]_{cyt}$  for 2 minutes after P resupply, showed no particular response over the usually observed response to mechanical stimulation.

Using a more sensitive system (luminometer instead of plate reader) and whole seedlings instead of excised root tips, a higher P dose (5 mM  $KH_2PO_4$ ) was applied. To control for additional  $K^+$  supplied with the treatment, a 5 mM KCl treatment was used. Seedlings were monitored for approximately 15 minutes after treatment application (as supplied P had been shown to translocate along whole rice plants within 15 minutes, Kobayashi *et al.*, 2013). However, no modulations in  $[Ca^{2+}]_{cyt}$  could be observed in this set-up either. This could be because (i)  $Ca^{2+}$  is not involved in signalling P availability, (ii) the  $Ca^{2+}$  fluxes are below the detection limit of the aequorin-luminometer set-up, or (iii) the  $Ca^{2+}$  fluxes occur within specific cells / specific cell types and are lost when averaging the response of all cells within a root tip / whole seedling, as is done when using ubiquitously expressed aequorin. It is unlikely that the P pulse was below the limit what plants might be capable of detecting, as P occurs sparingly within soil, but generally rather in micro- than millimolar concentrations (Raghothama, 1999).

Another aspect so far not considered in any study mentioning the involvement of  $[Ca^{2+}]_{cyt}$  in nutrient sensing, is a circadian regulation of both  $[Ca^{2+}]_{cyt}$  signalling and nutrient uptake. The few studies that tried to resolve diurnal P-uptake patterns reported a preferential P uptake during the night, independent of the transpiration stream

(Terabayashi *et al.*, 1991; Marschner, 2012). If this is a general pattern in all plant species remains to be determined, but it could suggest that nutrient sensing might also depend on the time of day. The experiments reported in this thesis were carried out between late morning until early afternoon. In the case of P, it would be very interesting to test its effect on  $[Ca^{2+}]_{cyt}$  with circadian resolution.

### 3.4 Conclusions and future work

It was shown that P starvation led to dampened, and overall altered  $[Ca^{2+}]_{cyt}$  signatures in *Arabidopsis* root tips in response to mechanical, oxidative, osmotic stress and extracellular nucleotides. This was specific to P starvation, as severe N starvation did not have the same effect.

P starvation was found to have a particularly strong effect on the  $[Ca^{2+}]_{cyt}$  response to eATP. However, P-starved roots were found to still accumulate detectable levels of eATP in extracellular bathing medium, indicating that even under chronic P starvation, baseline levels of eATP were to some extent maintained. Using a high (1 mM) eATP concentration as the standard test, Fe availability in combination with P nutrition was found to determine the  $[Ca^{2+}]_{cyt}$  response to eATP application. With the method used here, P-starved *Arabidopsis* root tips and whole seedlings did not respond to P resupply through modulations of  $[Ca^{2+}]_{cyt}$ . This suggests - but does not rule out - that P availability is not signalled through major changes of  $[Ca^{2+}]_{cyt}$ , in contrast to what has been shown for nitrate resupply.

Future work is needed to dissect the effect of P starvation on the root and shoot  $[Ca^{2+}]_{cyt}$  response to *biotic* stresses. Employing tissue- or organ-specific  $Ca^{2+}$  reporters, such as aequorin targeted to various root cell types, or a reporter suited for microscopy would facilitate dissection of specific responses. For studying the effect of P resupply on  $[Ca^{2+}]_{cyt}$ , the  $Ca^{2+}$  reporter would ideally be sensitive to even subtle changes of  $[Ca^{2+}]_{cyt}$  (such as the ultrasensitive Cameleon-Nano, Horikawa *et al.*, 2010; W.-G. Choi *et al.*, 2014), and targeted to epidermal root tip cells, shown to be pre-dominantly involved in P uptake and likely sensing (Kanno, Arrighi, *et al.*, 2016). Any circadian effect of P uptake, suggested to occur during the night, should be incorporated into the experimental design.

As excluding Fe from the growth medium was shown to relieve the dampened  $[Ca^{2+}]_{cyt}$  signature of P-starved root tips in response to eATP, whether Fe exclusion would also rescue the  $[Ca^{2+}]_{cyt}$  response to salt, osmotic and oxidative stress now needs to be

determined. Ideally, an atlas of nutrient deficiencies and their effect on  $[Ca^{2+}]_{\text{cyt}}$  could be generated.



# 4 DECONSTRUCTING THE CYTOSOLIC FREE CALCIUM RESPONSE TO EXTRACELLULAR ATP IN ROOTS

## 4.1 Introduction

### 4.1.1 Extracellular ATP as a danger signal

Adenosine 5'-triphosphate (ATP) is the primary carrier of energy in cells. In addition, it occurs extracellularly, where it has been shown to function as an important signalling molecule in animals and, more recently, also plants (Burnstock, 1972; Demidchik, Nichols, *et al.*, 2003; Tanaka *et al.*, 2010; J. Choi, Tanaka, Cao, *et al.*, 2014). Even though determinations of intracellular and extracellular ATP concentrations remain challenging, it has been reported that for both animals and plants, intracellular ATP is maintained at a surprisingly high level, occurring at millimolar levels where enzymatic reactions rely on micromolar concentrations (Traut, 1994; Napolitano and Shain, 2005; Patel *et al.*, 2017). In plant cells, cytosolic ATP levels in the low millimolar range have been reported, 0.5 – 1.3 mM using <sup>31</sup>-phosphorus nuclear magnetic resonance (Gout *et al.*, 1992, 2014), or approximately 2 mM based on ratiometric imaging (De Col *et al.*, 2017). Whilst the exact

mechanism of ATP release into the plant cell's extracellular space is still unknown, spontaneous release has been shown during growth and response to abiotic and biotic stimuli (Jeter *et al.*, 2004; S.-Y. Kim *et al.*, 2006; Song *et al.*, 2006; Weerasinghe *et al.*, 2009; Clark *et al.*, 2010; Dark *et al.*, 2011; Zhu *et al.*, 2017). Vesicular exocytosis or protein-mediated transport (through anion channels or ATP-binding cassette (ABC) transporters) are possible scenarios for release of intracellular ATP into the extracellular space, however at low concentrations (S.-Y. Kim *et al.*, 2006; Song *et al.*, 2006; Rieder and Neuhaus, 2011; Wu *et al.*, 2011). Physical damage of cellular membranes has been described to rapidly release high amounts of intracellular ATP into the extracellular space (Song *et al.*, 2006; Weerasinghe *et al.*, 2009; Dark *et al.*, 2011). Thus, extracellular ATP (eATP) has been termed a 'danger signal' (J. Choi, Tanaka, Liang, *et al.*, 2014). Basal levels of eATP are however needed for optimal plant growth, and both depletion and augmentation of eATP was shown to trigger plant stress responses (S.-Y. Kim *et al.*, 2006; Clark *et al.*, 2010; Chivasa *et al.*, 2013). With regards to roots, eATP levels within a certain range were found necessary for optimal root hair growth (7.25 – 25  $\mu\text{M}$  ATP or ADP would stimulate,  $\geq 150 \mu\text{M}$  would inhibit root hair growth; Clark *et al.*, 2010; Terrile *et al.*, 2010) and root gravity perception (Tang *et al.*, 2003; Haruta and Sussman, 2012; Yang *et al.*, 2015; Zhu *et al.*, 2017). Levels of eATP are controlled through ATP-hydrolysing ectoenzymes, most prominently apyrases (Wu *et al.*, 2007). Apyrases maintain eATP levels within the optimal range for cell growth and have furthermore been shown to play a role in phosphate homeostasis through scavenging of phosphate from ATP (Thomas *et al.*, 1999; Lim *et al.*, 2014). Considering that these enzymes were described to act extracellularly, it was unexpected to find the two apyrases of *Arabidopsis*, APY1 and APY2, localized to the Golgi (Chiu *et al.*, 2012; Schiller *et al.*, 2012). This dissent could potentially be explained by apyrases limiting the ATP loaded into Golgi-derived vesicles which ultimately serve as eATP source through PM fusion (discussed in Yang *et al.*, 2015).

Work on *Arabidopsis* protoplasts, *i.e.* a cell-wall free system, showed that eATP is perceived at the plant plasma membrane rather than cell wall (Demidchik *et al.*, 2009). Work on root hair cells showed that ATP as well as adenosine 5'diphosphate (ADP) addition caused depolarization of the PM (Lew and Dearnaley, 2000). Through a forward genetic screen, the receptor of eATP in plants was recently found to be a membrane-spanning, legume-like lectin receptor kinase, termed DOes not Respond to Nucleotides1 (DORN1; Choi, Tanaka, Cao, *et al.*, 2014). In an earlier study, this kinase had been

characterized as a regulatory component of the plasma membrane-cell wall continuum, important for pathogen resistance (Bouwmeester *et al.*, 2011). DORN1 was most specific towards ATP and ADP binding, with less affinity towards *e.g.* AMP, GTP, CTP and adenosine (J. Choi, Tanaka, Cao, *et al.*, 2014). It was found that DORN1 self-associates, which is enhanced upon eATP perception (Chen *et al.*, 2017). Most recently, it was reported that DORN1-mediated perception of eATP was necessary to induce plasma membrane  $K^+$  and  $Ca^{2+}$  fluxes in root epidermal protoplasts (L. Wang *et al.*, 2018). The genetic identities of the  $K^+$  and  $Ca^{2+}$  channels activated downstream of DORN1 remain unknown.

#### 4.1.2 Extracellular ATP triggers movement of $Ca^{2+}$ ions

One of the most immediate responses to eATP perception is the rapid movement of  $Ca^{2+}$  ions across membranes (see Chapter 1, section 1.2.6 onwards for an introduction to  $Ca^{2+}$  as a second messenger). In plants, eATP was first shown to lead to an increase of  $[Ca^{2+}]_{\text{cyt}}$  in *Arabidopsis* roots (Demidchik, Nichols, *et al.*, 2003). Using the  $Ca^{2+}$  reporter aequorin, which averages the  $Ca^{2+}$  signal of the assayed cell population, eATP was shown to trigger a dose-dependent, and characteristic multi-phasic  $[Ca^{2+}]_{\text{cyt}}$  response within seconds of application, lasting 5 to 10 minutes before returning to baseline levels (Demidchik *et al.*, 2003; Choi, Tanaka, Cao, *et al.*, 2014; also see Chapter 3, Figure 10). Non-synchronised single-cell oscillations were later described to be underlying this ‘averaged’ signal (Tanaka *et al.*, 2010; Krebs *et al.*, 2012). These single-cell oscillations were dependent on the presence of apyrases (Tanaka *et al.*, 2010). However, details about the origin of  $Ca^{2+}$ , as well as underlying signalling components in this overall multi-phasic response, are not well understood as spatial and temporal resolution are lacking. Excluding  $Ca^{2+}$  from the extracellular assaying solution and inhibiting plasma membrane  $Ca^{2+}$  channels were shown to abolish most of the  $[Ca^{2+}]_{\text{cyt}}$  response to eATP (Demidchik, Nichols, *et al.*, 2003; Loro *et al.*, 2016). This could indicate the apoplast as sole source of  $Ca^{2+}$ , but it does not rule out any downstream involvement of intracellular  $Ca^{2+}$  stores which might rely on an initial trigger of apoplastic  $Ca^{2+}$  flux (Demidchik, Nichols, *et al.*, 2003; Demidchik *et al.*, 2009). Inhibition of intracellular phospholipase C signalling was shown to affect only the later stages of  $[Ca^{2+}]_{\text{cyt}}$  signalling in response to eATP, leading the authors to conclude that both intracellular as well as apoplastic  $Ca^{2+}$  stores were involved in generating the later signal (Tanaka *et al.*, 2010).

Ca<sup>2+</sup> reporters targeted to various subcellular compartments uncovered links between cytosolic and organellar Ca<sup>2+</sup> dynamics upon eATP perception. These studies were not primarily interested in physiological eATP signalling, but used the reliable [Ca<sup>2+</sup>]<sub>cyt</sub> increase upon eATP treatment as a tool (Krebs *et al.*, 2012; Loro *et al.*, 2012, 2016; Bonza *et al.*, 2013). The ratiometric Ca<sup>2+</sup> reporter YC3.6 targeted to the plasma membrane reported differing Ca<sup>2+</sup> increases within one cell, suggested to represent hotspots of local Ca<sup>2+</sup> maxima (Krebs *et al.*, 2012). Targeting YC3.6 to the nucleus revealed non-synchronous oscillations in nuclear free [Ca<sup>2+</sup>] in response to eATP (Krebs *et al.*, 2012). These lagged behind the [Ca<sup>2+</sup>]<sub>cyt</sub> response by 7 minutes (Krebs *et al.*, 2012). Another nuclear targeted YC3.6 probe reported much faster Ca<sup>2+</sup> increases in response to eATP, similar in amplitude and kinetics to what was observed for [Ca<sup>2+</sup>]<sub>cyt</sub> increases (Loro *et al.*, 2012). Extracellular ATP treatment prompted [Ca<sup>2+</sup>] increases in mitochondria, plastids and ER (Loro *et al.*, 2012, 2016; Bonza *et al.*, 2013). Mitochondrial, plastid and ER increases in [Ca<sup>2+</sup>] were found to be strictly related to increases of [Ca<sup>2+</sup>]<sub>cyt</sub>, *i.e.* the larger the cytosolic increase, the larger the mitochondrial / plastid / ER increase (Loro *et al.*, 2012, 2016; Bonza *et al.*, 2013). Plastid and ER kinetics of Ca<sup>2+</sup> release to the cytosol were similar to what was observed for the determination of the cytosolic Ca<sup>2+</sup> response (Bonza *et al.*, 2013; Loro *et al.*, 2016). However, the return of mitochondrial Ca<sup>2+</sup> levels back to pre-stimulus baseline levels was much slower than what was observed for the cytosol, taking more than 20 minutes to return to pre-stimulus baseline levels (Loro *et al.*, 2012). As none of the organelle-targeted Ca<sup>2+</sup> reporters showed a decrease of [Ca<sup>2+</sup>] upon onset of the [Ca<sup>2+</sup>]<sub>cyt</sub> response, it was reasoned that the organelles examined so far do not function as the Ca<sup>2+</sup> source for the observed initial [Ca<sup>2+</sup>]<sub>cyt</sub> increases (*e.g.* Bonza *et al.*, 2013). However, the involvement of other organelles such as vacuole and Golgi remains to be tested.

So far, studies reporting changes in [Ca<sup>2+</sup>]<sub>cyt</sub> applied eATP treatment by total immersion or superfusion of the assayed tissue. This does not allow distinguishing between local or systemic effects of eATP perception. For example, it has been shown that locally applied salt treatment of *Arabidopsis* roots led to increases in [Ca<sup>2+</sup>]<sub>cyt</sub>, which propagated away and into areas of the plant that had not been in direct contact with the salt treatment, termed a ‘Ca<sup>2+</sup> wave’ (W.-G. Choi *et al.*, 2014). The same study found no such signal propagation upon mechanical stimulation, H<sub>2</sub>O<sub>2</sub> or cold treatment, and did not test for the response to eATP (W.-G. Choi *et al.*, 2014). Even though imaging of eATP-induced [Ca<sup>2+</sup>]<sub>cyt</sub> responses seemingly evoked the appearance of a Ca<sup>2+</sup> wave (noted by *e.g.* Loro



*et al.*, 2016), this conclusion cannot be reached when all tissue is immersed / superfused. Subsequent  $[Ca^{2+}]_{\text{cyt}}$  increases could merely be the result of direct cellular response delayed in time. Hence, it is unknown if eATP induces a  $Ca^{2+}$  wave which propagates away from locally treated areas.

#### 4.1.3 Signalling network in response to extracellular ATP perception

Besides immediate  $Ca^{2+}$  mobilisation, eATP was found to induce the action of multiple other signalling molecules. Extracellular ATP perception triggered the production of intra- and extracellular reactive oxygen species (ROS) in various plant tissues of *Medicago truncatula*, *Populus euphratica* and *Arabidopsis* (S.-Y. Kim *et al.*, 2006; Song *et al.*, 2006; Demidchik *et al.*, 2009; Sun *et al.*, 2012; Chen *et al.*, 2017). This response was found to be mostly specific to ATP (S.-Y. Kim *et al.*, 2006; Demidchik *et al.*, 2011) or ATP and ADP (Song *et al.*, 2006), but not AMP, adenosine or phosphate. The enzymes underlying the ROS production include plasma membrane NADPH oxidases (Foreman *et al.*, 2003; Song *et al.*, 2006; Demidchik *et al.*, 2009; Sun *et al.*, 2012). These would generate extracellular superoxide anion that could then be converted to  $H_2O_2$ . The current model is that the  $H_2O_2$  could then enter into the cytosol through aquaporins (Rodrigues *et al.*, 2017), to be detected as part of the intracellular ROS accumulation. However, the model does not yet explain how extracellular ADP can trigger extracellular superoxide anion production in *Arabidopsis* roots (measured with a non-permeable probe), yet does not elicit an increase in intracellular ROS (Demidchik *et al.*, 2009, 2011). The activation of NADPH oxidases in response to eATP appears to be downstream of plasma membrane channel-mediated  $Ca^{2+}$  flux (Demidchik, Shabala, *et al.*, 2003; Jeter *et al.*, 2004; Song *et al.*, 2006; Demidchik *et al.*, 2009). Recently, DORN1 was shown to co-localize with NADPH oxidase RBOHD in *Arabidopsis* leaves, phosphorylating RBOHD upon eATP recognition (Chen *et al.*, 2017).

Furthermore, eATP was shown to regulate the production of nitric oxide (NO). In *Salvia miltiorrhiza*, NO production was dose-dependent, with low eATP concentration (10-100  $\mu\text{M}$ ) inducing NO production, and higher eATP concentrations ( $> 100 \mu\text{M}$ ) decreasing NO levels (Wu and Wu, 2008). ATP-dependent NO production was dependent on  $Ca^{2+}$  fluxes across the PM (Wu and Wu, 2008). In tomato culture cells, NO production increased with increasing eATP concentrations, but the response saturated at 1 mM eATP treatment (Foresi *et al.*, 2007). In both studies, increases in NO concentration were

reported over the course of hours, limiting resolution with regards to immediate NO production upon perception of eATP. Action of phospholipase C (PLC) and diacylglycerol kinase (DGK) were found to be necessary components of eATP-induced NO production (Sueldo *et al.*, 2010).

Another signalling molecule shown to be triggered by eATP perception is phosphatidic acid (PA). PA is a lipid-derived molecule, generated through PLC or phospholipase D (PLD) and DGK action (Singh *et al.*, 2015). PA has been shown to lead to oxidative bursts in *Arabidopsis* leaf cells (Park *et al.*, 2004), however this has not yet been studied for eATP application. In tomato suspension culture cells, eATP induced the accumulation of PA, which did not occur upon ADP or AMP treatment, and did not rely on hydrolysis of ATP (Sueldo *et al.*, 2010). PA levels were analysed after 30 minutes of eATP treatment (Sueldo *et al.*, 2010). The authors suggested that PA accumulation occurred independently of any  $\text{Ca}^{2+}$  fluxes, however interpretation of the data is hindered due to low specificity of available pharmacological treatments (Sueldo *et al.*, 2010).

The concerted action of all these signalling molecules upon eATP perception was ultimately shown to result in changes in the level of gene expression and protein abundance. Early work on *Arabidopsis* showed eATP-dependent induction of *e.g.* mitogen-activated protein kinase genes (MAPKs, particularly *MPK3*, Jeter *et al.*, 2004; Demidchik *et al.*, 2009). Expression of the NADPH oxidase *RBOHD* was found to be induced 15 minutes after eATP treatment (Song *et al.*, 2006; Chen *et al.*, 2017). Using a microarray approach, the genes misregulated in a non-functional DORN1 background, and hence described to be eATP specific, showed a large overlap with wounding-response markers (J. Choi, Tanaka, Cao, *et al.*, 2014). However, overall eATP treatment led to low fold changes in all genes studied so far (Jeter *et al.*, 2004; J. Choi, Tanaka, Cao, *et al.*, 2014). Further, induced *RBOHD* gene expression did not translate into increased protein abundance (Chen *et al.*, 2017).

Overall, a range of signalling molecules are set in motion upon eATP perception, enabling the plant to respond. A linear connection can be drawn between a few, *e.g.* eATP increases  $[\text{Ca}^{2+}]_{\text{cyt}}$  which in turn induces ROS production through NADPH oxidases. However, a more complex network likely ties in all signalling events occurring upon eATP perception. Currently, our understanding of signalling networks is often hampered by low temporal and spatial resolution, *e.g.* staining procedures that require minutes or hours to report a signalling molecule, rather than seconds.

#### 4.1.4 Experimental approaches and aims

The aim of this Chapter is to further resolve the components underlying one of the most immediate responses to eATP perception in *Arabidopsis*: the eATP-induced  $[Ca^{2+}]_{cyt}$  response. Understanding the components of eATP signalling furthers elucidation of a multitude of signalling networks. The focus will be on deconstructing the rapid signalling events (within seconds to minutes), rather than long-term induced changes.

First, the origin of the multi-phasic response will be examined by using different root and shoot tissues of aequorin-expressing *Arabidopsis* plants. Next, to resolve if the  $[Ca^{2+}]_{cyt}$  increases that develop over time occur in spatially distinct locations of the root, fluorescence imaging of root tissue will be carried out. The ratiometric  $Ca^{2+}$  reporter YC3.6 as well as the intensimetric reporter GCaMP3 will be employed. Taken together, the tool set of aequorin, YC3.6 and GCaMP3, and their intrinsic properties, allow examination of the  $[Ca^{2+}]_{cyt}$  response in different set-ups (*e.g.* constant treatment *versus* superfusion, systemic *versus* local application of the eATP treatment). The use of multiple reporter constructs will further resolve if observed  $Ca^{2+}$  dynamics are due to construct limitations or physiologically relevant events. In many cases, P-starved roots will be used for the assays, to make use of the fact that P-starved root tips showed a significantly different  $[Ca^{2+}]_{cyt}$  response to eATP (also see Chapter 3, Figure 10).

Further, the involvement of ROS in generating the immediate  $[Ca^{2+}]_{cyt}$  response will be investigated, by using pharmacological inhibitor treatments. To correlate any rapidly occurring ROS signalling upon eATP perception to pre-treatment ROS levels, histochemical staining will be performed on roots altered in baseline ROS levels. A similar correlation will be carried out between immediate  $[Ca^{2+}]_{cyt}$  response and the occurrence of callose, a polysaccharide known to impair symplastic communication and thus limiting cell-to-cell signalling (see Chapter 1, section 1.1.4, for an introduction to callose deposition).

Previous studies have used a range of eATP concentrations as treatment, from as low as 3  $\mu$ M (Demidchik, Nichols, *et al.*, 2003) to 10 mM eATP (Cárdenas *et al.*, 2008), with concentrations most commonly used being in the range of 0.1 mM to 1 mM (*e.g.* Demidchik *et al.*, 2009; Tanaka *et al.*, 2010; Choi, Tanaka, Cao, *et al.*, 2014; Wang, Wilkins and Davies, 2018). Nano- to micromolar concentrations of eATP have been reported as basal levels, whilst rapid elevation to millimolar levels might occur during wounding and cell rupture. It is therefore not straightforward which concentration of

eATP should be considered a stress signal, and might depend on age and context of the assayed tissue. With regards to *Arabidopsis* root  $[Ca^{2+}]_{cyt}$  increases, these change only in amplitude when the treatment concentration is increased (also see Chapter 3, Figure 10, where 0.1 mM and 1 mM eATP were trialled). To provoke a clear phenotype, it was therefore decided to use 1 mM eATP treatment in the following experiments.

Overall, these experimental approaches should enable answering the following questions:

- What underlies the distinct  $[Ca^{2+}]_{cyt}$  increases in roots' response to eATP?
- Are the components of the  $[Ca^{2+}]_{cyt}$  response dependent on each other?
- What other signalling molecules are involved in modulating the eATP-induced  $[Ca^{2+}]_{cyt}$  response in roots?

## 4.2 Results

### 4.2.1 The $[Ca^{2+}]_{\text{cyt}}$ response to extracellular ATP comes mainly from the root tip

*Assays using whole root tissue were done in collaboration with Nicholas Doddrell, Part II student, University of Cambridge*

To check the ability of root and shoot tissue to respond to eATP in the present laboratory set-up, wild type *Arabidopsis* plants expressing (apo)aequorin were grown on full or zero P, and (i) excised individual leaves, (ii) excised individual whole roots or (iii) excised individual 1 cm root tips of 11-day old plants were challenged with 1 mM eATP treatment solution (Figure 36). As a control for the mechanical stimulation due to application of the treatment solution, control solution without eATP was applied (Figure 36). As a proxy for how much  $[Ca^{2+}]_{\text{cyt}}$  was mobilized in the different tissues, the area under the curves were analysed and compared.

To test the response of shoot tissue to eATP, individual excised leaves were used (3 independent trials,  $n = 15 - 19$  individual leaves, Figure 36A, B). Care was taken to sample true leaves and not cotyledons. Control solution application led to an immediate and monophasic increase in  $[Ca^{2+}]_{\text{cyt}}$ , in both full P- and zero P-grown leaves (Figure 36B). eATP treatment led to an equally immediate increase in  $[Ca^{2+}]_{\text{cyt}}$ , followed by a more prolonged increase in  $[Ca^{2+}]_{\text{cyt}}$  starting approximately 30 seconds after eATP application (Figure 36B). Overall, eATP treatment mobilized significantly more  $[Ca^{2+}]_{\text{cyt}}$  than control solution application, independent of P growth regime, as assessed by area under the curve (Analysis of variance (ANOVA) with *post-hoc* Tukey test:  $p \leq 0.014$ , Figure 36C). With regards to differences between P-sufficient and P-starved leaves, control solution application led to a very similar area under the curve ( $p = 0.999$ , Figure 36C). eATP treatment led to an overall significantly higher  $[Ca^{2+}]_{\text{cyt}}$  increase in full P- compared to zero P-grown leaves ( $p = 0.023$ , Figure 36C).

In whole roots, control solution application led to an immediate and monophasic increase in  $[Ca^{2+}]_{\text{cyt}}$  similar to what was observed in leaf tissue. The response to control solution application seemed dampened in zero P roots, however this effect was not significant between full and zero P grown roots ( $p = 0.08$ , data from 6 independent trials,  $n = 41 - 62$  individual whole roots, Figure 36E, F). In contrast to leaf tissue, eATP treatment of whole roots led to a more intricate  $[Ca^{2+}]_{\text{cyt}}$  response (Figure 36D, E). Overall, eATP

mobilized significantly more  $[Ca^{2+}]_{cyt}$  than control solution, independent of P growth condition ( $p < 0.001$ , Figure 36F). Further, eATP treatment triggered the characteristic multi-phasic increases in  $[Ca^{2+}]_{cyt}$  in full P whole roots (Figure 36E). In P-starved whole roots, the response to eATP was ‘missing’ the second, ATP-specific peak, and showed an overall significantly lower area under the curve compared to full P whole roots ( $p < 0.001$ , Figure 36E).

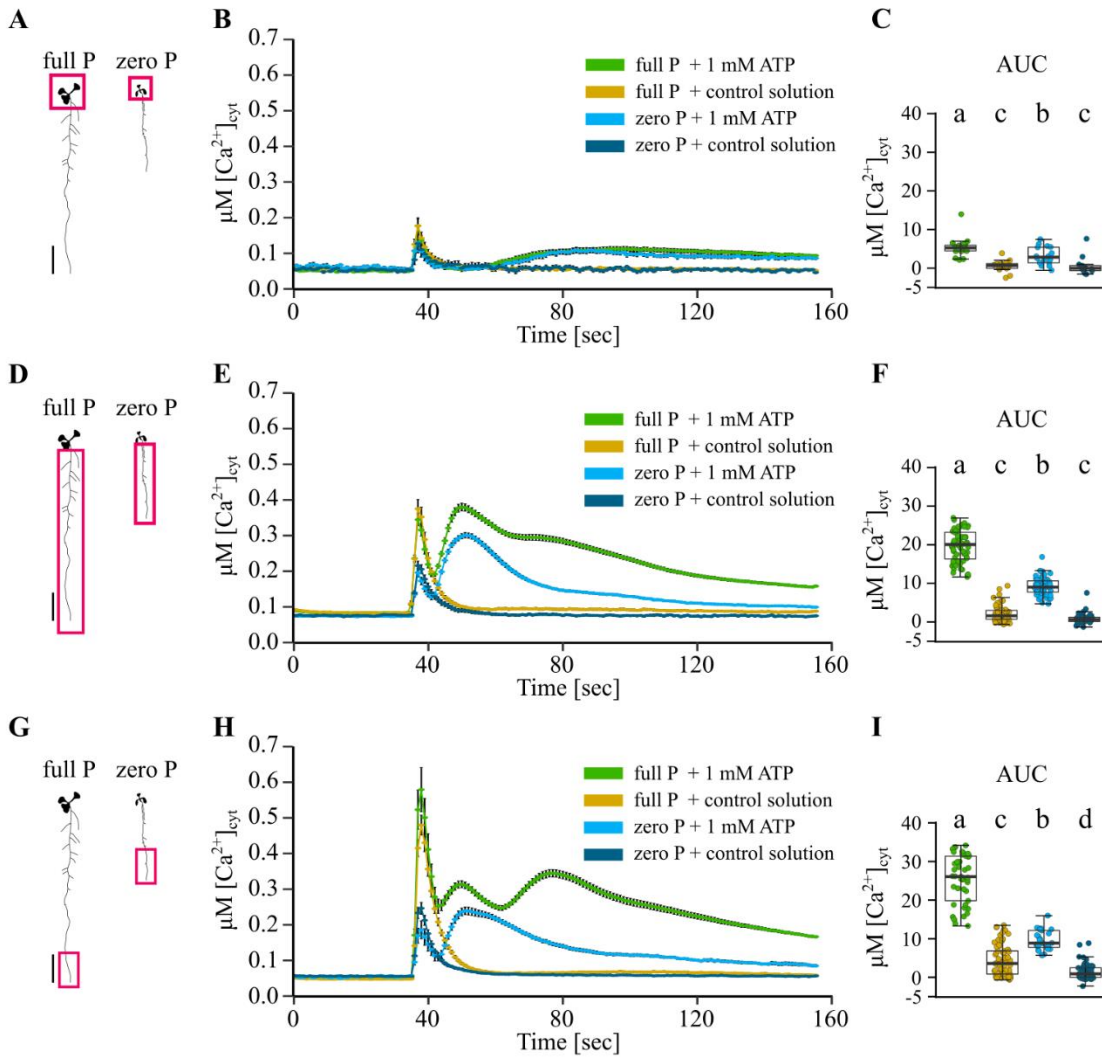
To narrow down the region within the root capable of responding to eATP, the root tip of the primary root was considered. The root tip has long been known for its sensitivity in perceiving and integrating cues from the environment (Darwin and Darwin, 1880). It comprises production of nascent cells, and their subsequent differentiation into specific cell types and elongation to final size (in the meristematic / differentiation / elongation zone, respectively). Using a determined size of this nascent tissue (1 cm), also allowed to control to some extent for differences in root size between P-replete and P-starved plants (Figure 36G). Therefore, excised 1 cm root tips were used for the assay (also see Chapter 3, Figure 10, for a more detailed analysis of the root tip response to eATP). The response of excised root tips to eATP was similar to what was observed in whole roots (9 independent trials,  $n = 29 - 75$  individual root tips, Figure 36H). Control solution application led to an immediate and monophasic  $[Ca^{2+}]_{cyt}$  response, which was significantly lower in zero P root tips compared to full P grown root tips ( $p < 0.001$ , Figure 36H, I). eATP treatment led to a significantly stronger  $[Ca^{2+}]_{cyt}$  response compared to control buffer treatment, regardless of P growth condition ( $p < 0.001$ , Figure 36H). Full P root tips showed a multi-phasic  $[Ca^{2+}]_{cyt}$  response to 1 mM eATP, zero P root tips showed a significantly dampened response to eATP (measured as area under the curve,  $p < 0.001$ , Figure 36I).

Finally, as a proxy for how much  $[Ca^{2+}]_{cyt}$  was mobilised in the different tissues, the areas under the curve were compared between leaves, whole roots and root. First, the response of full P grown tissue was considered. In response to control solution treatment, leaves and whole roots mobilized similar levels of  $[Ca^{2+}]_{cyt}$  ( $p = 0.836$ ), whereas the root tip mobilized significantly more  $[Ca^{2+}]_{cyt}$  than leaves and whole roots ( $p = 0.005$  and  $p = 0.038$ , respectively). eATP treatment led to a significantly higher area under the curve in whole roots than leaves ( $p < 0.001$ ). However, root tips in turn showed a significantly higher area under the curve compared to whole roots ( $p < 0.001$ ). Thus, 1 mM eATP treatment mobilized most  $[Ca^{2+}]_{cyt}$  in excised root tips.

Secondly, the response of zero P grown tissue was compared. Control solution application led to similar responses in leaves, whole roots and root tips ( $p = 0.999$  for all comparisons). eATP treatment led to a significantly lower area under the curve in zero P grown leaves, compared to whole roots and tips ( $p < 0.001$  for both comparisons). In contrast to full P grown tissue however, there was no significant difference of  $[Ca^{2+}]_{\text{cyt}}$  mobilized in whole roots compared to root tips ( $p = 0.999$ ).

Therefore, it can be confirmed that root tissue responds more strongly than shoot tissue to eATP (Tanaka *et al.*, 2010). Within root tissue, the root tip responded most strongly to eATP treatment in plants grown on standard half MS (= full P growth condition). P-starved roots still showed a stronger eATP response in root compared to shoot tissue, however the root tip showed a less pronounced  $[Ca^{2+}]_{\text{cyt}}$  response compared to whole root tissue. In the following experiments, the focus will therefore be on the root tips' response to eATP. Using P-starved root tips, which show an impaired response to eATP, will be used as a tool to dissect the overall eATP-induced mechanism.

(Please see Chapter 3 for a detailed dissection of the root tips' response to a non-hydrolysable ATP analogue (Figure 11) and ADP (Figure 12)).



**Figure 36:** The  $[Ca^{2+}]_{\text{cyt}}$  response of phosphate-starved leaves, whole roots and excised root tips to extracellular ATP. *Arabidopsis Col-0* aequorin-expressing seedlings were grown on full or zero P. Excised true leaves (A-C), whole roots (D-F) or root tips (1 cm; G-I) of 11-day old seedlings were challenged with treatments applied at 35 seconds, then  $[Ca^{2+}]_{\text{cyt}}$  was measured for 155 seconds. (A) Schematic of *Arabidopsis*, pink box depicts tissue sampled. (B) Response of excised leaves to 1 mM extracellular ATP treatment or mechanical stimulation (control solution); time course trace represents mean  $\pm$  standard error of mean (SEM) from 3 independent trials, with  $n = 15 - 19$  individual leaves averaged per data point. Time course data were baseline-subtracted and analysed for (C) area under the curve (AUC), with each dot representing an individual data point. Boxplot middle line denotes median. (D-F) Responses of excised whole roots to 1 mM ATP or control solution (6 independent trials,  $n = 41 - 62$  individual whole roots). (G-I) Responses of excised root tips (1 cm) to 1 mM ATP or control solution (9 independent trials,  $n = 29 - 75$  root tips). Analysis of variance (ANOVA) with *post-hoc* Tukey Test was used to assess statistical differences. Different lower-case letters describe groups of significant statistical difference ( $p < 0.05$ ), same letters indicate no statistical significance ( $p > 0.05$ ).



#### 4.2.2 The eATP-induced multi-phasic $[Ca^{2+}]_{\text{cyt}}$ increase maps to different regions of the root tip

*All NES-YC3.6 imaging was carried out in the laboratory of Prof. Alex Costa, University of Milan. Prof. Alex Costa and Fabrizio G. Doccia provided initial training and facilities.*

To overcome limitations of the aequorin reporter, another genetically encoded  $[Ca^{2+}]_{\text{cyt}}$  reporter was used to resolve the spatial occurrence of eATP-induced  $[Ca^{2+}]_{\text{cyt}}$  changes within the root tip. The ratiometric reporter Yellow Cameleon 3.6 was used as its cytosolic targeted version (NES-YC3.6, Krebs *et al.*, 2012). With this reporter,  $Ca^{2+}$  quantification relies on ratio changes between YFP and CFP fluorophore emission upon  $Ca^{2+}$  binding. Therefore, this ratiometric reporter requires a microscopy set-up capable of splitting the two output emissions. A research visit to Prof. Alex Costa's laboratory, University of Milan, was undertaken to use their microscopy facilities and be trained in the use of ratiometric reporters.

*Arabidopsis Col-0* wild type plants, expressing NES-YC3.6, were grown on full or zero P (same growth medium as used in aequorin trials). Ten-day old whole seedlings were mounted into a custom-built superfusion chamber, with the root sitting between a glass slide and wetted cotton wool, and therefore within the imaging field of an inverted microscope. The shoot was propped up on the cotton wool, reaching into the air (see Chapter 2, section 2.7 for a more detailed description). This set-up allowed the imaging of roots (i) without the need to excise the root, and (ii) whilst superfusing control or treatment solution interchangeably over the same sample (Behera and Kudla, 2013). Before starting an image acquisition time-course, samples were acclimatized to constant superfusion with control solution for at least 10 minutes, to recover from any stress induced by sample transfer to the chamber, and until baseline cpVenus / CFP levels were stable (false colour-coded as blue-green, Figure 37A). Constant superfusion with control solution did not elicit any cpVenus / CFP ratio changes, indicating that the superfusion system allowed application of a treatment without incurring a mechanical stimulation, which had been inevitable in aequorin assays. In addition, constant superfusion with control solution made the separate control solution application redundant.

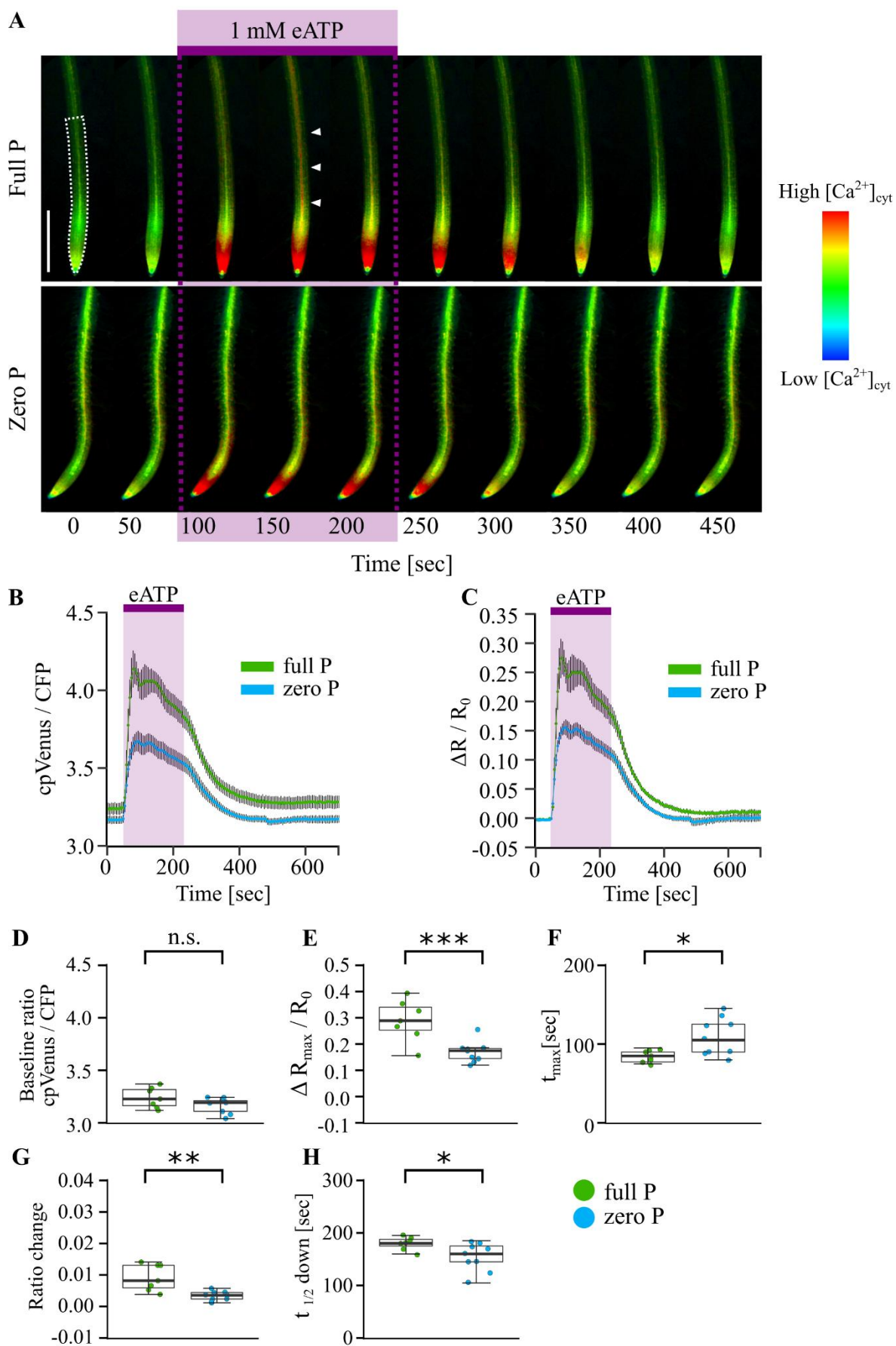
Changing the superfusion solution from control to 1 mM eATP solution led to a strong cpVenus / CFP ratio increase in the apical root tip of both full and zero P grown root tips (colour-coded by yellow-red, Figure 37A). This was then followed by a secondary ratio

increase, ‘shooting up’ within the longitudinal centre of full P grown roots (Figure 37A, upper panel, indicated by white triangles; see Appendix VI, movie 1, for a representative time series). This secondary response occurred to a lesser extent or was completely missing in zero P grown roots (Figure 37, lower panel; see Appendix VI, movie 2, for a representative time series). After three minutes of eATP treatment, the superfusion solution was changed back to the control solution. This washed out the eATP solution from the chamber, however, it cannot be determined exactly at which time point all eATP would have left the chamber. Once the eATP treatment was changed back to control, the cpVenus / CFP ratio returned back to pre-treatment baseline levels, taking slightly longer in full P than zero P roots (Figure 37A).

The acquired images could then be analysed for specific regions of interest (Roi). First, a Roi containing most of the root tip imaged (2.5 mm in length) was used to analyse the ‘whole root tip’ response (WR Roi, white dashed box in upper left image, Figure 37). Upon eATP application, the ratio changes in this WR Roi revealed a strong, possibly slightly bi-phasic, response in full P roots, peaking within 30 to 40 seconds (data from 3 independent trials,  $n = 7 - 9$  independent roots per growth condition, Figure 37B). Zero P root tips showed an equally immediate, but comparably lower ratio change in response to eATP treatment (Figure 37B). To account for differences in baseline ratios between full and zero P grown roots, the quantified cpVenus / CFP ratios were normalised with regards to their baseline levels ( $\Delta R / R_0 = (R - R_0) / R_0$ ; Figure 37C). Essentially, this normalisation approach takes differences in pre-treatment signal intensities into account and reveals the magnitude of response. As differences in baseline ratio levels were similar between the two growth conditions, the response pattern looked similar when comparing raw and normalized ratios (Figure 37B and C).

Quantitative raw and normalized ratios (as depicted in Figure 37B and C) could then be further analysed (analysis after Wagner *et al.*, 2015; Loro *et al.*, 2016, Figure 37D - H). Steady-state levels of cpVenus / CFP ratio prior to eATP application were found to be higher in full P WR Roi (mean cpVenus / CFP ratio  $\pm$  SEM:  $3.24 \pm 0.04$ ) than in zero P WR Roi ( $3.17 \pm 0.02$ ). However, this slight difference was not significant ( $p = 0.128$ , Figure 37D). Normalized ratio maxima, comparable to peak maxima reported for aequorin assays, were found to be significantly higher in full P compared to zero P WR Roi (mean  $\Delta R / R_0 \pm$  SEM: full P:  $0.29 \pm 0.03$ , zero P:  $0.17 \pm 0.01$ ,  $p = 0.006$ , Figure 37E). Full P grown root tips needed on average  $84.3 \pm 3$  seconds to reach the ratio maxima, whereas zero P grown root tips needed on average  $109.4 \pm 8$  seconds to

maximally respond (Figure 37F). Hence, full P root tips reached their maximal response significantly quicker than zero P grown root tips ( $p = 0.013$ , Figure 37F). This relationship can also be expressed as a ratio change (ratio maximum divided by time needed to reach ratio maximum), with full P grown root tips showing a significantly higher ratio change than zero P root tips (mean ratio change  $\pm$  SEM: full P:  $0.009 \pm 0.002$ , zero P:  $0.003 \pm 0.001$ ,  $p = 0.009$ , Figure 37G). In addition to analysing how quickly roots responded to an eATP treatment, it can further be analysed how quickly the response subsided. This is captured in how much time it takes to pass half-maximal ratio ( $t_{1/2}$  down [sec], Figure 37H). Full P grown root tips took on average  $180 \pm 4.5$  seconds until they reached half their maximal response, whereas zero P root tips took on average  $154 \pm 9.0$  seconds (Figure 37H). Thus, zero P root tips significantly more quickly recovered from their response to eATP compared to full P root tips ( $p = 0.026$ , Figure 37H). This parameterises the stronger and more prolonged response of full P grown roots (visualized in Figure 37A, and quantified in Figure 37B and C).

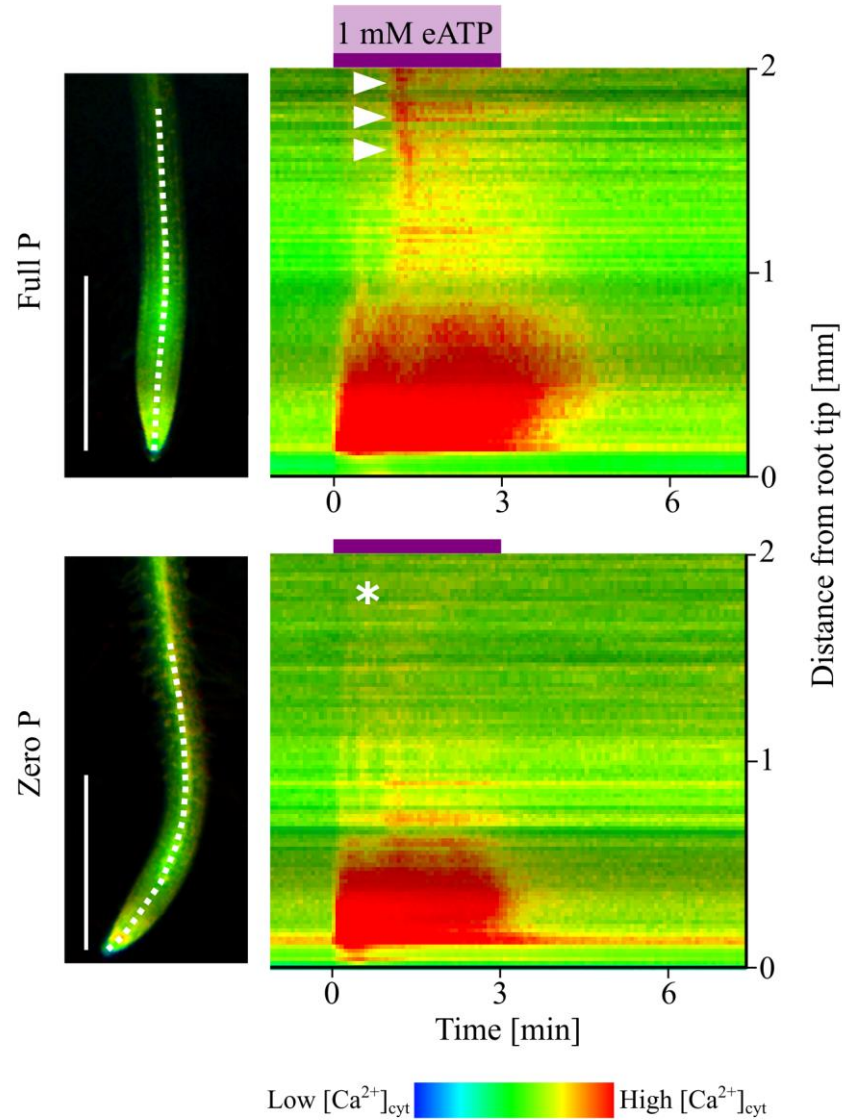


**Figure 37:** Spatial dynamics of the  $[Ca^{2+}]_{\text{cyt}}$  response of phosphate-starved root tips to extracellular ATP using a ratiometric reporter. *Arabidopsis* Col-0 expressing the cytosolic Yellow Cameleon 3.6 (NES-YC3.6) was grown on full or zero P. In a superfusion chamber, 10-day old seedlings were constantly superfused with control solution, before applying a 1 mM eATP treatment (applied during 50 – 230 second interval after start of image acquisition), followed by wash-out with control solution. (A) Ratiometric false-colour images from representative time series, background subtracted. Purple box indicates treatment with 1 mM eATP. White triangles highlight differences between the response of full and zero P root tips. Scale bar in upper left image: 1 mm. White dashed box in the upper left image indicates region of interest (2.5 mm root) plotted over time for (B) mean FRET ratio (cpVenus / CFP)  $\pm$  SEM and (C) normalized FRET ratio ( $\Delta R / R_0$ )  $\pm$  SEM, of full P (green trace) and zero P root tips (blue trace); data from 3 independent trials, with n = 7 - 9 individual root tips per growth condition. (D-H) Analysed kinetic parameters of data shown in (B) and (C), including (D) baseline cpVenus / CFP ratios preceding eATP treatment (mean of 50 seconds window before eATP application); (E) maximum normalized ratio after eATP treatment; (F) time needed to reach maximum ratio (in seconds); (G) ratio change upon eATP treatment (maximum ratio (as shown in (E)) per time needed to reach this maximum (as shown in (F))); and (H) time needed to reach half the maximum ratio, measured in seconds after maximum ratio was reached. In boxplots, each dot represents an individual data point, middle line denotes median. Analysis of variance (ANOVA) with *post-hoc* Tukey Test was used to assess statistical differences. Significance levels (*p*-values): \*\*\* (<0.001), \*\* (<0.01), \* (<0.05), n.s. (not significant).

From the YC3.6-based time series it became apparent that eATP treatment led to FRET ratio changes that were separated in time and space along the *Arabidopsis* root (Figure 37A; also see Appendix VI, movies 1 and 2). In particular, a secondary response to eATP ‘moved along’ the central part of the full P root, possibly aligning with the vasculature (marked by white triangles in the upper panel of Figure 37A). As the analysis of the whole root tip Roi did not differentiate between different regions within the roots, two efforts were undertaken to increase spatial resolution of the analysis: (i) visualizing the spatial position of ratio changes over time using the graphical features of a kymograph (Figure 38) and (ii) analysing more defined regions of interest along the longitudinal axis of the root (Figure 39).

First, for a graphical representation of the ratio changes upon eATP treatment, the NES-YC3.6 time series images were sliced along a defined line through the root longitudinal axis (see white dashed line in root micrographs on the left of Figure 38). This investigated axis ran from the apical root tip (0 mm) through the centre of the root towards the upper parts of the root (2 mm from root tip). The kymograph then displays the average intensity values for each position over time. Kymograph visual analysis was carried out for all roots sampled, the kymograph of a representative root grown on either full and zero P medium is shown (Figure 38). It was found that both full and zero P roots responded strongly to 1 mM eATP treatment in the apical root tip (false colour-coded in red, Figure 38). With a time-lag, full P roots then showed a secondary ratio increase further up the root (starting approximately 1 mm from the root tip, see white triangles in upper panel in Figure 38). This secondary response was lowered or completely missing in zero P grown roots (see white star in lower panel in Figure 38). Upon eATP wash-out, zero P roots more quickly returned to baseline FRET ratio levels (false colour-coded in green, Figure 38) than full P roots.

As the microscopy images were collected using a wide-field microscope (as opposed to a confocal microscope), the signal from all underlying cell layers were superimposed. Hence, no differentiation with regards to cell layers (*e.g.* epidermis, endodermis, *etc.*) could be made.



**Figure 38:** Kymographs of the  $[Ca^{2+}]_{\text{cyt}}$  response to extracellular ATP of phosphate-starved root tips. Quantitative ratiometric data (see Figure 37 for details) were used to generate kymographs of distinct regions along the root of full P- (top) and zero P- (bottom) grown root tips. On the left, white dashed line in root micrographs indicates region used for kymograph extraction, scale bar: 1 mm. On the right, kymographs depict temporal and spatial changes in  $[Ca^{2+}]_{\text{cyt}}$  in response to a 3-minute 1 mM eATP treatment (purple bar), preceded and followed by control solution superfusion. White triangles indicate increase in  $[Ca^{2+}]_{\text{cyt}}$  in full P root tips, which is missing in zero P root tips (marked by white star).

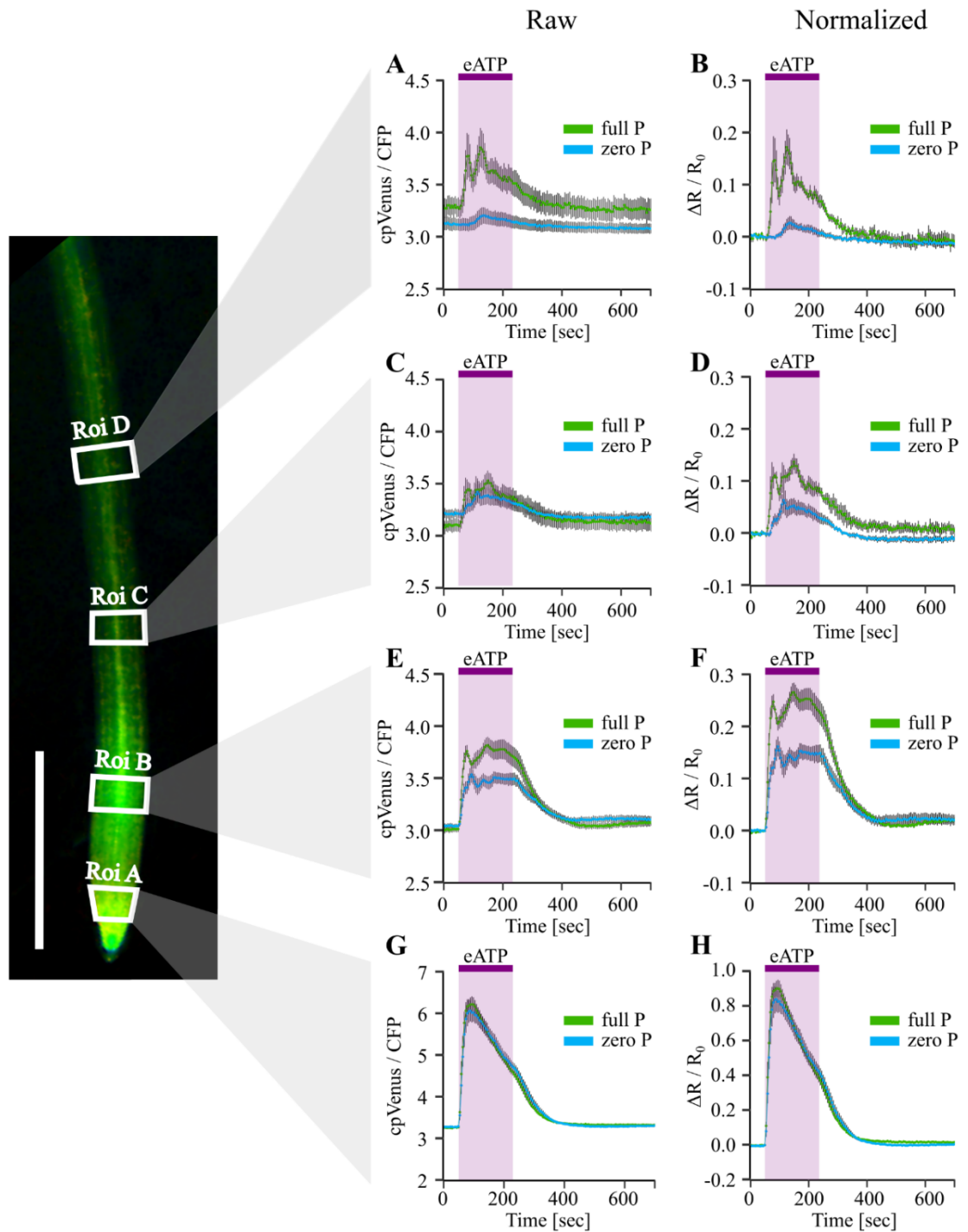
Secondly, the spatial occurrence of FRET ratio changes were investigated using defined regions of interest along the imaged root tip (Figure 39). The Rois were of equal height, tightly aligned with the individual root width and equally spaced with regards to the start of the root tip (white boxes in root micrograph on the left of Figure 39). Four different

Rois were designated, based on previous analysis of the whole root tip Roi and kymographs: Roi A – at the apical root tip, Roi B – at the upper end of the primary response region to eATP, circa 1 mm away from the root tip, Roi C – within the region of the secondary response, and at equal distance between Roi B and D, Roi D – at the end of the whole root tip Roi described earlier (2.5 mm away from the root tip), which was due to technical restriction of the imaging field.

As was visually depicted in the kymographs, superfusion with 1 mM eATP led to a strong and immediate ratio change in the apical root tip, Roi A (mean raw cpVenus /CFP ratios: Figure 39G; normalized  $\Delta R / R_0$ : Figure 39H). Interestingly, whilst superfusion with eATP was still on-going, the ratio already decreased. The response in Roi A was very similar between full and zero P-grown root tips. However, in Roi B a difference could be quantified between full and zero P-grown roots (Figure 39E and F). Full P root tips showed a stronger response to eATP, compared to zero P root tips. In Roi C, the response to eATP was low in both full and zero P root tips (Figure 39C), however still stronger in full P root tips when controlling for differences in baseline levels (Figure 39D). Furthest away from the root tip, in Roi D, the response to eATP was almost completely abolished in zero P root tips, whereas full P root tips still sustained a clear ratio increase upon eATP treatment (Figure 39A and B).

Taken together, analysing different regions within the first 2.5 mm of *Arabidopsis* YC3.6-expressing root tips revealed a strong spatial separation of the  $[Ca^{2+}]_{cyt}$  response to eATP. P-starved root tips were not generally impaired in responding to eATP, as their response to eATP was similar to P-replete root within the apical tip (Roi A). Only further up the root, where the secondary response to eATP occurred as visualized by kymograph and Roi D analysis, zero P roots showed a much weaker  $[Ca^{2+}]_{cyt}$  response to eATP than full P root tips.





**Figure 39:** The  $[Ca^{2+}]_{\text{cyt}}$  response to extracellular ATP in specific regions of phosphate-starved root tips using a ratiometric reporter. *Arabidopsis* Col-0 expressing the cytosolic Yellow Cameleon 3.6 (NES-YC3.6) were grown on full or zero P. In a superfusion chamber, 10-day old seedlings were constantly superfused with control solution, before applying a 1 mM eATP treatment (applied during 50 – 230 second interval after start of image acquisition), followed by wash-out with control solution. On the left, exemplary root tip with annotated regions of interest (‘Roi’, white boxes), analysed and plotted over time in A – H, scale bar: 1 mm. (A, B): Roi D; (C, D): Roi C; (E, F): Roi B; (G, H): Roi A. Purple boxes indicates treatment with 1 mM eATP.

(A, C, E, G) Mean FRET ratio (cpVenus / CFP)  $\pm$  SEM; (B, D, F, H) normalized FRET ratio ( $\Delta R / R_0$ )  $\pm$  SEM, of full P (green trace) and zero P root tips (blue trace). Data from 3 independent trials, with n = 7 - 9 individual root tips per growth condition.

To further validate what was found using the ratiometric NES-YC3.6 reporter, another  $[Ca^{2+}]_{\text{cyt}}$  reporter was employed. The intensiometric  $Ca^{2+}$  reporter GCaMP3 has been developed to have an increased baseline fluorescence and increased dynamic range upon  $Ca^{2+}$  binding, as well as being photostable (Tian *et al.*, 2009), and has recently been expressed in *Arabidopsis* (Vincent *et al.*, 2017). As  $Ca^{2+}$  binding leads to an increase of GFP signal, this single wavelength-based reporter promised ease of imaging using a less specific microscope set-up than was necessary for YC3.6 imaging, which necessitated an emission beam splitter. GCaMP3-expressing *Arabidopsis* plants could be trialled on a stereomicroscope equipped with a standard GFP-emission filter.

To make data comparable to YC3.6-derived results (Figure 37 - Figure 39), GCaMP3-expressing *Arabidopsis* wild type plants were grown on either full and zero P medium, and 10-day old seedlings were challenged with 1 mM eATP treatment (in control solution), or control solution (to account for mechanical stimulation due to treatment application). Compared to aequorin assays, no excision of root material and prolonged re-constitution with coelenterazine was necessary. Compared to both aequorin and YC3.6 assays, no submergence of the root tissue was employed (aequorin set-up: root tissue submerged in wells of 96-well plate; YC3.6 set-up: root tissue constantly superfused). Instead, GCaMP3-expressing seedlings were left on the agar-based growth medium they had grown on, which allowed minimal handling of the sample prior to microscopy. Treatment solutions were applied to the root tips as defined amounts using a pipette (see Chapter 2, section 2.8 for details).

Using a stereomicroscope equipped with a GFP-filter, GCaMP3-expressing intact root tips were left to acclimatize on the microscope stage until baseline fluorescence was stable, and then imaged over a time course of in total 250 seconds, with treatment solutions being applied at 20 seconds after start of image acquisition (Figure 40, also see Appendix VI, movies 3 – 6 for representative time series). eATP treatment led to a strong increase in GFP-fluorescence in the most apical regions of tips of both full and zero P grown roots (see representative images in Figure 40A). As the fluorescence signal

increase was strong upon eATP perception, care was taken to adjust imaging parameters to prevent image saturation and biasing downstream analysis.

Time course images were analysed, first for a ‘whole root tip’ region of interest (Roi), comparable in size to the whole root tip Roi analysed in YC3.6-derived data (2.5 mm in length, see white dashed box in upper left in Figure 40A). Fluorescence intensities showed a slight decrease upon treatment application (see time point 20 seconds, Figure 40B), due to slight shifts in focus due to treatment application. Application of control solution led to small increases in fluorescence intensity, whereas 1 mM eATP treatment led to strong increases in GFP signal, particularly in full P root tips (data from 3 independent trials, with  $n = 4 - 7$  individual roots per growth condition and treatment, Figure 40B). Zero P grown root tips showed a substantial, but lower signal increase upon eATP treatment. When correcting for differences in baseline fluorescence the pattern changed only slightly (Figure 40C). Data normalization was carried out as was done for YC3.6 data, which is the same procedure as described for GCaMP3-specific data processing ( $\Delta F / F_0 = (F - F_0) / F_0$ ;  $F$  – Fluorescence signal,  $F_0$  – baseline fluorescence signal; Vincent *et al.*, 2017). Normalized data were then further analysed with regards to maximal response upon treatment application ( $\Delta F_{\max} / F_0$ ; Figure 40D). Full P root tips showed a significant increase in intensity when treated with eATP compared to control buffer application (mean  $\Delta F_{\max} / F_0 \pm \text{SEM}$ : full P + 1 mM ATP:  $2.00 \pm 0.13$ , full P + control buffer:  $0.09 \pm 0.04$ ,  $p < 0.001$ , Figure 40D). Zero P root tips on average did show a higher response to eATP treatment than to control solution, but as the response was variable, the difference was not significant (zero P + 1 mM ATP:  $0.46 \pm 0.16$ , zero P + control solution:  $0.06 \pm 0.03$ ,  $p = 0.183$ , Figure 40D). There was no difference in the response to control solution when comparing full and zero P grown roots ( $p = 0.999$ ). Full P root tips showed a significantly higher increase in fluorescence upon eATP treatment, compared to zero P grown roots ( $p < 0.001$ ).

To assess spatial differences of the roots’ response to eATP, defined Rois along the root were analysed (Figure 41). These Rois were designed to be comparable with Rois analysed for YC3.6-based data. To make the analysis more efficient, the number of Rois was reduced, and the two most distinct Rois were analysed, labelled ‘Roi A’ and ‘Roi D’ (comparable to Roi A and Roi D in YC3.6 data; see white boxes on root micrograph on the left of Figure 41). GFP fluorescence intensity was found to slightly decrease upon treatment application in Roi A, whereas no decrease was observed at 20 seconds in Roi D (compare Figure 41A and D). This is due to the treatment being applied to the root tip

(Roi A region), which then slightly moves out of focus, whereas further up the root (Roi D region) no focus change occurs.

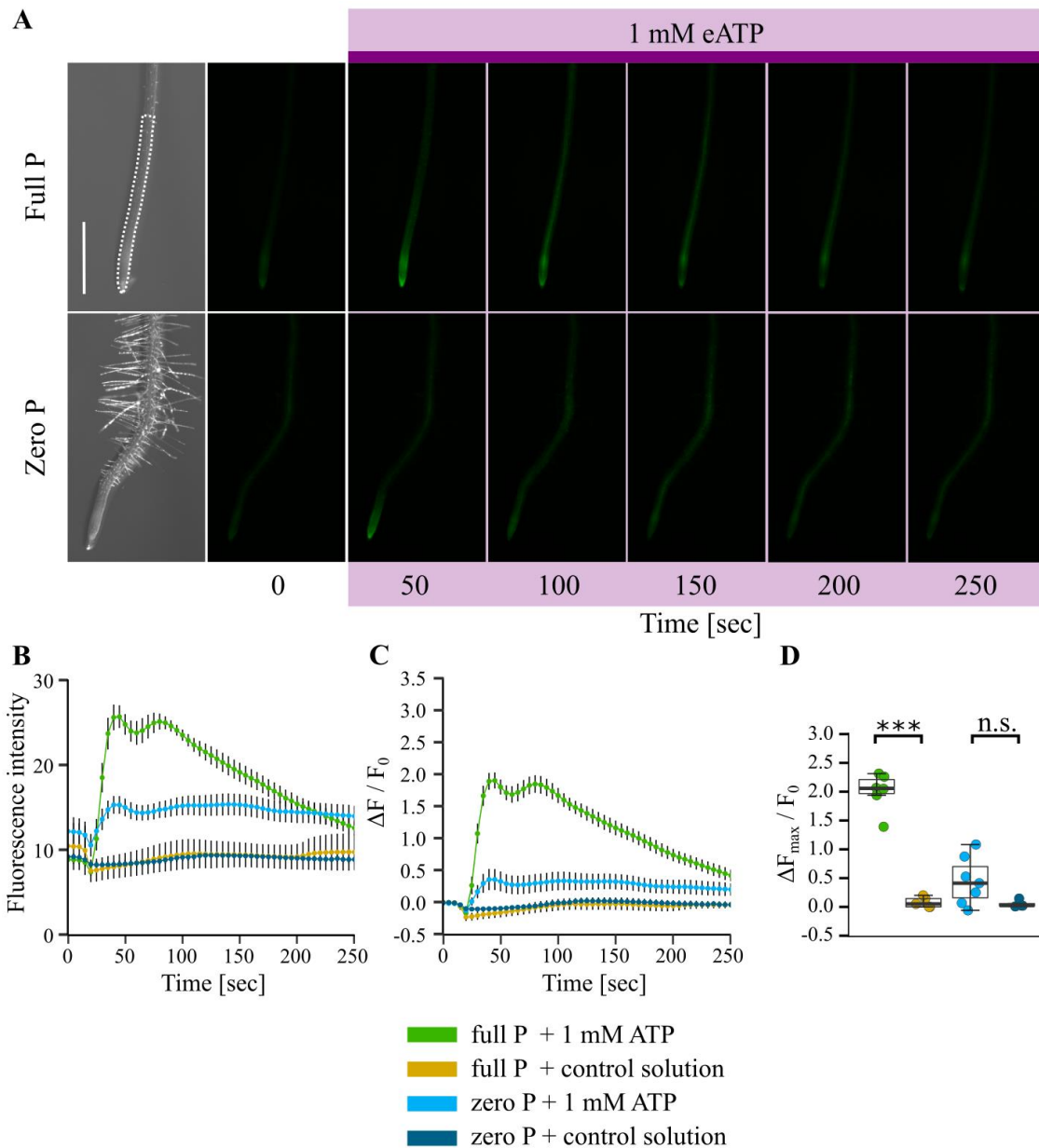
Most interestingly, the pattern of signal increase differed between the two Rois analysed. Control solution application led to little change in fluorescence, indicating that little mechanical stimulation occurred upon treatment application (Figure 41A, D, also see section 4.3.3 for a discussion of the probe's sensitivity). Full P root tips showed a very strong increase in GFP fluorescence upon treatment with 1 mM eATP, reaching its maximal amplitude within 10 seconds in the root tip apex (Roi A), and with a time lag of approximately 50 seconds further up the root (Roi D). Zero P grown root tips also responded to eATP treatment in the root tip apex (Roi A), however the response was different in shape compared to full P Roi A response. Where full P roots showed a defined peak in Roi A, the shape of response in zero P Roi A was that of a narrower peak, followed by a shoulder (compare green and light blue trace in Figure 41D). Further up the root, in Roi D, zero P root tips completely lacked any response to eATP treatment (Figure 41A). Controlling these raw fluorescence signals for differences in baseline levels (normalized fluorescence signal, Figure 41B, E) resulted in little change of pattern in Roi A, however the strong response in Roi D of full P roots became more pronounced.

The two Rois were further analysed by extracting fluorescence maxima for all treatments and growth conditions (Figure 41C, F). Not surprisingly, eATP treatment led to significantly higher fluorescence maxima in full P root Roi A compared to control treatment (full P + 1 mM ATP:  $2.11 \pm 0.14$ , full P + control:  $0.03 \pm 0.01$ ,  $p < 0.001$ , Figure 41F). Zero P root tips equally responded significantly more strongly to eATP than to control treatment in Roi A (zero P + 1 mM ATP:  $1.43 \pm 0.31$ , zero P + control:  $0.03 \pm 0.03$ ,  $p = 0.002$ , Figure 41F). No difference was observed when comparing control solution application between full and zero P root tips Roi A ( $p = 0.999$ ). Similarly, fluorescence maxima upon eATP were not significantly different in Roi A between full and zero P grown roots, even though full P root tips on average showed a stronger response ( $p = 0.118$ ).

Fluorescence maxima in Roi D of full P grown roots were significantly higher upon eATP treatment compared to control treatment (full P + 1 mM ATP:  $3.15 \pm 0.15$ , full P + control:  $0.07 \pm 0.02$ ,  $p < 0.001$ , Figure 41C). In Roi D of zero P grown root tips however, no difference was observed between eATP or control treatment (zero P + 1 mM ATP:  $0.25 \pm 0.11$ , zero P + control:  $0.05 \pm 0.02$ ,  $p = 0.58$ , Figure 41C). Full and zero P roots did not

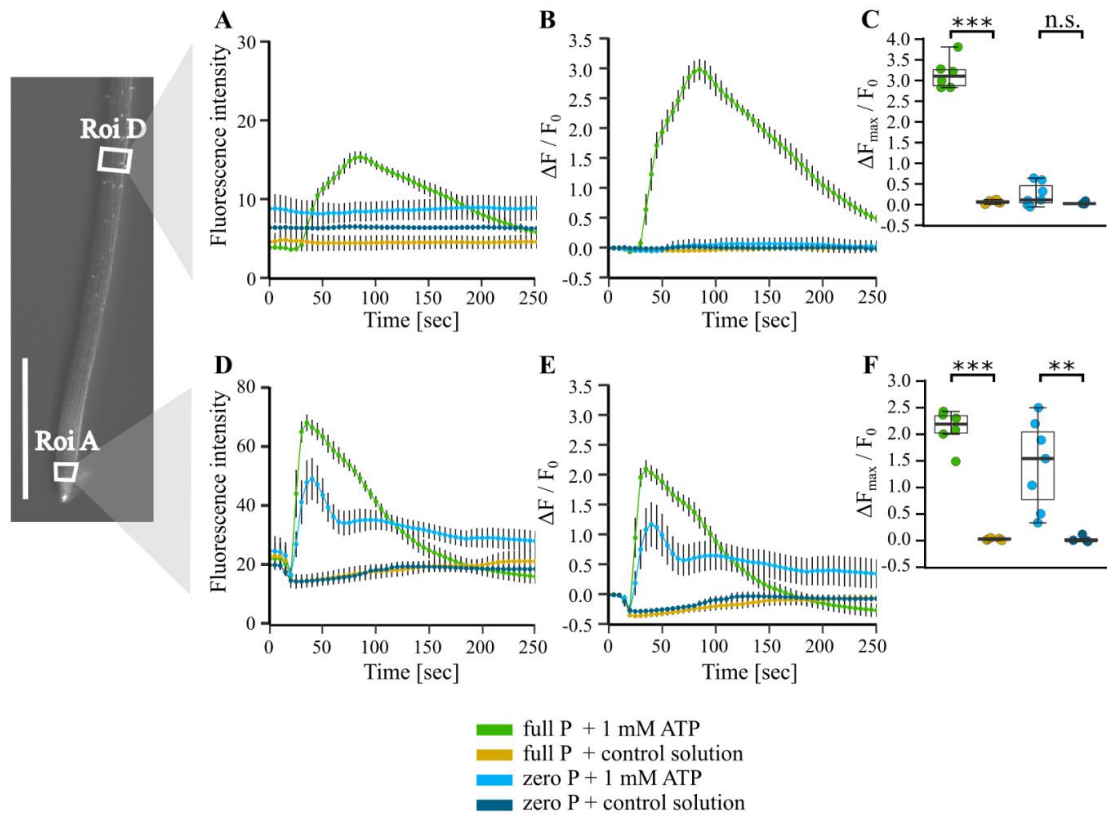
differ in their response to control in Roi D ( $p = 0.998$ ). Unsurprisingly, full P roots responded significantly more strongly than zero P roots in Roi D ( $p < 0.001$ ).

Taken together, the GCaMP3 reporter allowed for an easy-to-use imaging and quantification set-up to track changes in  $[Ca^{2+}]_{\text{cyt}}$ . In full P grown roots, treatment with 1 mM eATP led to spatially and temporarily distinct increases in  $[Ca^{2+}]_{\text{cyt}}$ , as quantified by changes in GFP-fluorescence. Zero P grown roots showed an ATP-specific  $[Ca^{2+}]_{\text{cyt}}$  in the root tip apex, however lacked any signal further up the root. These results were convincingly similar to those obtained using the YC3.6 reporter. These initial trials using intact GCaMP3 roots can therefore be used to further corroborate what was observed in YC3.6-expressing roots. However, being a single wavelength-based reporter, GCaMP3-based fluorescence signal is directly correlated with expressed protein level (*i.e.* more GCaMP3 protein, higher baseline fluorescence). Protein levels might be altered under nutrient starvation conditions, such as P-starvation. In the initial experiment reported here (Figure 40 and Figure 41), P-starved roots showed a clear fluorescence signal. Nevertheless, care should be taken when using GCaMP3 to compare between groups of potentially unequal protein expression. Due to its ease-of-use and resulting ease to manipulate, GCaMP3 is however very suitable when comparing within groups of *e.g.* the same nutrient growth condition (further discussed in section 4.3.3).



**Figure 40:** Spatial dynamics of the  $[Ca^{2+}]_{\text{cyt}}$  response of phosphate-starved root tips to extracellular ATP using an intensimetric reporter. *Arabidopsis* Col-0 expressing the cytosolic GCaMP3 was grown on either full or zero P medium. Ten-day old seedlings were treated with control or 1 mM eATP treatment solution, applied 20 seconds after start of image acquisition to the root tip of seedlings resting on gel-based growth medium, and imaged for in total 250 seconds. (A) Intensimetric false-colour images from representative time series of full and zero P grown roots treated with 1 mM eATP. Purple box indicates treatment with 1 mM eATP, scale bar in upper left image: 1 mm. White dashed box in upper left image indicates region of interest (2.5 mm root length) analysed and plotted over time for (B) mean GFP fluorescence intensity  $\pm$  SEM, background subtracted, (C) normalized GFP fluorescence ( $\Delta F / F_0$ )  $\pm$  SEM; data from 3 independent trials, with  $n = 4 - 7$  individual roots per growth condition and treatment. (D) Extracted normalized fluorescence maxima ( $\Delta F_{\max} / F_0$ ), each dot represents an individual data

point, middle line denotes median. Analysis of variance (ANOVA) with *post-hoc* Tukey Test was used to assess statistical differences. Significance levels (*p*-values): \*\*\* (<0.001), n.s. (not significant).



**Figure 41:** The  $[Ca^{2+}]_{\text{cyt}}$  response to extracellular ATP in specific regions of phosphate-starved root tips using an intensimetric reporter. *Arabidopsis* Col-0 expressing the cytosolic GCaMP3 was grown on full or zero P medium. Ten-day old seedlings were treated with control or 1 mM eATP treatment solution, applied 20 seconds after start of image acquisition to the root tip of seedlings resting on gel-based growth medium, and imaged for in total 250 seconds. On the left, exemplary root tip with annotated regions of interest ('Roi', white boxes), scale bar: 1 mm. (A, B): Roi D; (D, E): Roi A. (A, D) Mean GFP fluorescence intensity  $\pm$  SEM, background subtracted, and (B, E) normalized GFP fluorescence ( $\Delta F / F_0$ )  $\pm$  SEM; data from 3 independent trials, with  $n = 4 - 7$  individual roots per growth condition and treatment. (C, F) Extracted normalized fluorescence maxima ( $\Delta F_{\max} / F_0$ ), each dot represents an individual data point, middle line denotes median. Analysis of variance (ANOVA) with *post-hoc* Tukey Test was used to assess statistical differences. Significance levels (*p*-values): \*\*\* (<0.001), \*\* (<0.01), \* (<0.05), n.s. (not significant).

### 4.2.3 The spatially distinct $[Ca^{2+}]_{cyt}$ responses to extracellular ATP can be generated independently of each other

Extracellular ATP evokes a robust multi-phasic pattern of  $[Ca^{2+}]_{cyt}$  increase in *Arabidopsis* root tissue which has reliably been quantified using the luminescent aequorin reporter (Demidchik, Nichols, *et al.*, 2003; Tanaka *et al.*, 2010, also see Figure 36). Using the ratiometric  $Ca^{2+}$ -reporter YC3.6, it was shown in this Chapter that underlying this multi-phasic response were spatially separated hotspots of  $[Ca^{2+}]_{cyt}$  increase along the root (Figure 38, Figure 39). Interestingly, these responses were also separated in time, *i.e.* occurring in distinct phases after application of the eATP treatment, even though the eATP solution would envelop the assayed root tissue very rapidly. The question arose as to whether these two responses were dependent on each other and, if not, ultimately how the time difference could be explained.

First, it was investigated if the two distinct  $[Ca^{2+}]_{cyt}$  responses in full P roots were linked. More precisely, the role of the apical root tip (1 mm) in  $[Ca^{2+}]_{cyt}$  signal perception and generation upon eATP treatment was investigated. This part of the root tip showed the immediate and strong  $[Ca^{2+}]_{cyt}$  response in both full and zero P grown root tips. To this end, aequorin-expressing wild type *Arabidopsis* were grown on full and zero P growth medium. A defined size of root tissue was used for the assays (excised 1 cm of the primary root tip), to control for differences in root size between full and zero P grown plants. These root tips were either used in their intact form ('intact' = 1 cm of root tip), or the apical root tip was further cut off ('cut' = 1 cm of root tip missing approximately the first 1 mm of its apex). In preliminary trials it was also attempted to assay the 1 mm of apical root tip alone. However, handling of this delicate and small tissue proved problematic, and (due to limited tissue abundance) comparison of luminescence signal to intact root tips proved difficult. Therefore, the excised 1 mm root tip tissue was not assayed using the aequorin reporter (but later considered using the GCaMP3 reporter, see Figure 43).

Intact or cut root tips were challenged with control solution, to control for mechanical stimulation, or 1 mM eATP treatment solution (Figure 42). Application of control solution led to a monophasic and immediate increase in  $[Ca^{2+}]_{cyt}$  in all assayed root tips, however to different extents (Figure 42A). Intact root tips of full P grown roots responded significantly more strongly than when the apical tip was cut off (mean  $\mu M [Ca^{2+}]_{cyt}$  touch maxima  $\pm$  SEM: full P intact:  $1.14 \pm 0.08$ , full P cut:  $0.45 \pm 0.09$ ,  $p < 0.001$ , Figure 42B). However, this might be biased as fewer samples were run for intact full P root tips (see



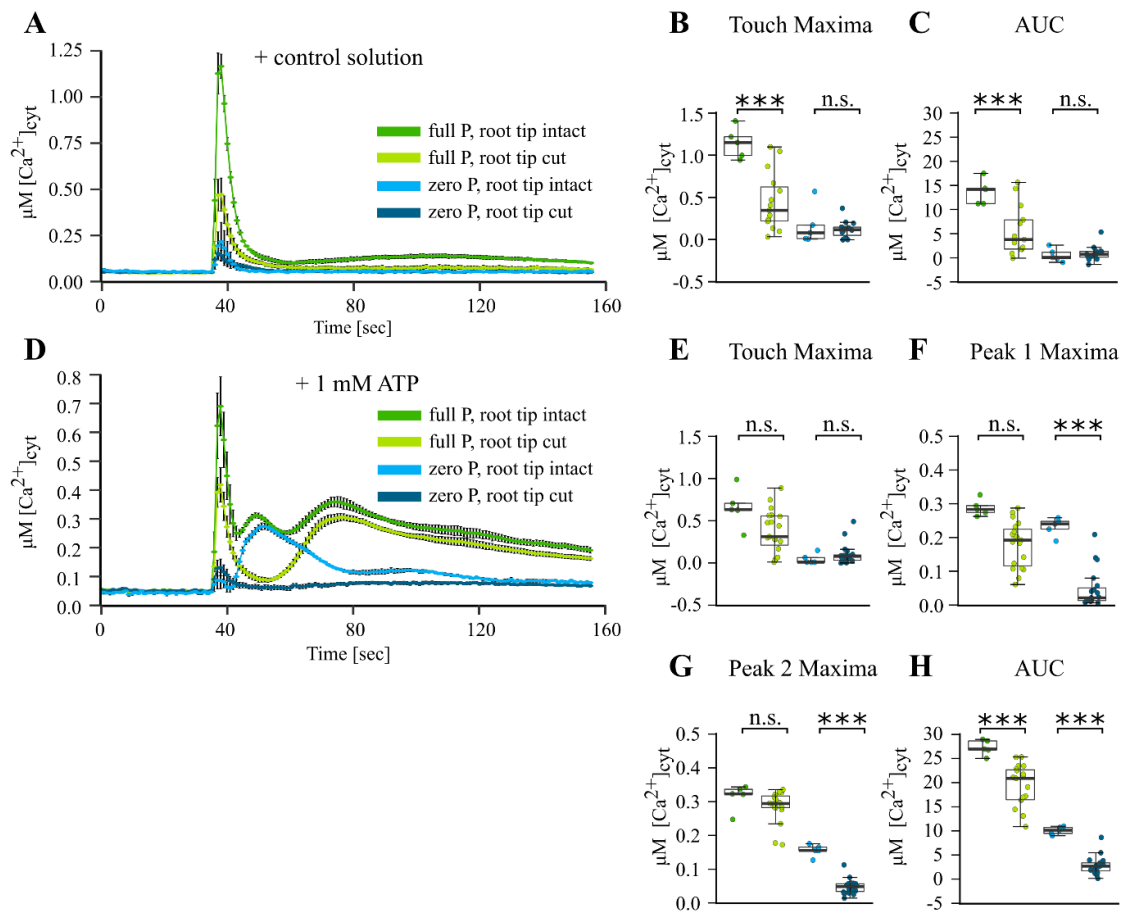
Chapter 3, Figure 13, for an in-depth analysis of the intact root tip response to mechanical stimulation). P-starved root tips responded less to mechanical stimulation than full P root tips, regardless of whether root tips were intact or cut (zero P intact:  $0.17 \pm 0.1$ , zero P cut:  $0.12 \pm 0.02$ ,  $p = 0.999$ , Figure 42B). The same pattern was observed when analysing area under the curve (full P intact versus cut root tips:  $p < 0.001$ , zero P intact versus cut root tips:  $p = 0.999$ , Figure 42C).

Upon application of 1 mM eATP, the difference between intact and cut root tips was however striking. As has been described before, intact root tips grown on full P showed the characteristic multi-phasic  $[Ca^{2+}]_{\text{cyt}}$  response of ‘touch’, ‘peak 1’ and ‘peak 2’ (see Chapter 3, Figure 6, for details on labelling and analysis). P-starved intact root tips showed a dampened  $[Ca^{2+}]_{\text{cyt}}$  signature, missing peak 2 (Figure 42D). When the apical 1 mm of root tip was cut off, however, this pattern changed drastically. Full P grown root tips still showed the initial sharp touch response, but lacked the characteristic peak 1. Instead,  $[Ca^{2+}]_{\text{cyt}}$  levels decreased to almost pre-treatment baseline levels, before showing another increase in  $[Ca^{2+}]_{\text{cyt}}$  which temporally aligned with peak 2 observed in intact root tips from full P plants. Zero P cut root tips showed a small  $[Ca^{2+}]_{\text{cyt}}$  increase upon 1 mM eATP treatment, without any further  $[Ca^{2+}]_{\text{cyt}}$  increases (Figure 42D). Quantification of these responses revealed no difference in perception of mechanical stimulation, regardless of the root tip being intact or cut (touch maxima: full P intact versus full P cut:  $p = 0.173$ , zero P intact versus zero P cut:  $p = 0.999$ ; Figure 42E). In full P roots, peak 1 maxima were on average much higher in intact than in cut root tips (full P intact:  $0.29 \pm 0.01$ , full P cut:  $0.18 \pm 0.02$ ), however this difference was not significant ( $p = 0.057$ , Figure 42F). This might be due to low sample size of intact root tips, and further might have been influenced by limitations of the analysis, *i.e.* the touch response ‘leaking’ into the phase analysed for peak 1 maxima. For zero P roots, intact root tips showed significantly higher peak 1 maxima compared to cut root tips (zero P intact:  $0.23 \pm 0.01$ , zero P cut:  $0.05 \pm 0.01$ ,  $p < 0.001$ , Figure 42F). Peak 2 maxima of full P root tips were slightly lower when the apical tip was cut off (full P intact:  $0.31 \pm 0.02$ , full P cut:  $0.29 \pm 0.01$ ), however, the difference was not significant ( $p = 0.586$ , Figure 42G). Zero P roots overall showed a much more dampened response than full P grown roots, however intact zero P root tips still responded significantly more strongly than zero P cut root tips (zero P intact:  $0.16 \pm 0.01$ , zero P cut:  $0.05 \pm 0.01$ ,  $p < 0.001$ , Figure 42G). Again, this might have been biased by the analysis windows, and peak 1 might have ‘leaked’ into the

analysis of peak 2 maxima, particularly having an impact on peak 2 maxima in zero P root tips.

Overall, less  $[Ca^{2+}]_{cyt}$  was mobilized upon eATP treatment in cut root tips, both in full and zero P grown roots (Figure 42H). The area under the curve was significantly larger in full P intact roots compared to cut roots ( $p < 0.001$ ), as well as in zero P intact roots compared to cut roots ( $p < 0.001$ , Figure 42C).

Taken together, cutting off the apical root tip (approximately 1 mm) drastically altered the  $[Ca^{2+}]_{cyt}$  signature upon eATP treatment. Both in full and zero P cut root tips, the characteristic  $[Ca^{2+}]_{cyt}$  increase termed peak 1 was absent. Full P root tips still showed a delayed response that temporarily aligned with what was normally observed in intact root tips as peak 2. However, temporal correlation would not necessarily imply that eATP provoked the same responses in intact and cut root tips, *i.e.* the underlying mechanism to generate  $[Ca^{2+}]_{cyt}$  influx could be different between intact and cut root tips. Further complicating the interpretation of the data was the fact that the aequorin-based assay did not allow spatial differentiation of the responses.



**Figure 42:** The  $[Ca^{2+}]_{\text{cyt}}$  response of phosphate-starved intact or cut root tips to extracellular ATP. *Arabidopsis* Col-0 aequorin-expressing seedlings were grown on full or zero P medium (green or blue traces). Intact root tips (1 cm) or cut root tips (1 cm of root tip with the apical 1 mm cut of) of 11-day old seedlings were challenged with treatments applied at 35 seconds, and  $[Ca^{2+}]_{\text{cyt}}$  was measured for 155 seconds. (A) Mechanical stimulation (control solution); time course trace represents mean  $\pm$  standard error of mean (SEM) from 2 independent trials, with  $n = 5$  individual intact root tips, and 3 independent trials, with  $n = 15$  individual cut root tips averaged per data point. Time course data were analysed for (B) touch maxima, (C) area under the curve (AUC), all baseline-subtracted, with each dot representing an individual data point (see Figure 6 for details). Boxplot middle line denotes median. (D-H) Responses to 1 mM eATP (data from 2 independent trials, with  $n = 5$  individual intact root tips, and 3 independent trials, with  $n = 19$  individual cut root tips). Analysis of variance (ANOVA) with *post-hoc* Tukey Test was used to assess statistical differences. Significance levels ( $p$ -values): \*\*\* ( $<0.001$ ), \*\* ( $<0.01$ ), \* ( $<0.05$ ), n.s. (not significant).

To investigate the spatial origin of the eATP-induced  $[Ca^{2+}]_{\text{cyt}}$  responses in severed root tips, the GCaMP3 reporter was employed. Plants expressing the GCaMP3 reporter could easily be manipulated prior to experimentation, *e.g.* apical root tip could be cut off and imaged together with the remaining distal root ‘stump’. This would allow resolution of the spatial response of cut root tips, which was not feasible in aequorin assays.

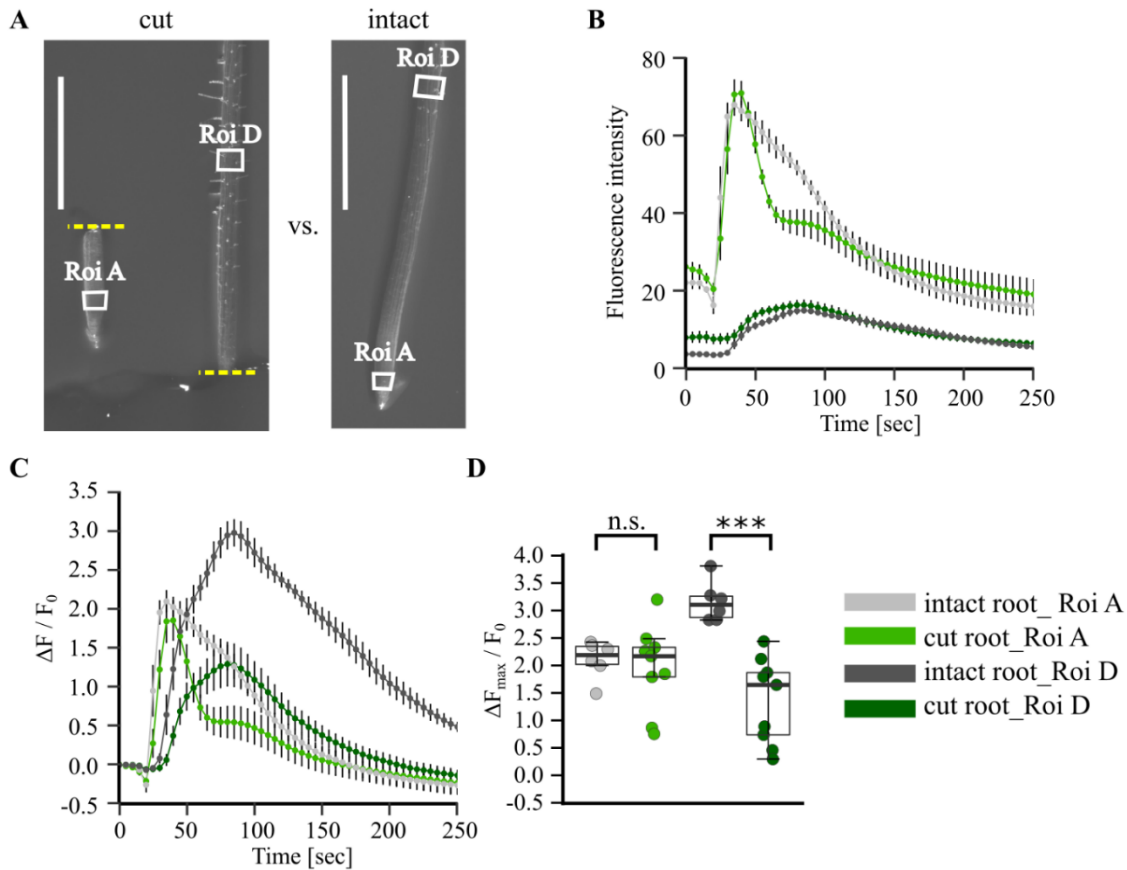
GCaMP3-expressing wild type *Arabidopsis* plants were grown on half MS medium (mostly labelled ‘full P’ in this thesis). Ten-day old plants used for microscopy were prepared in two ways: either without severing the root tip (‘intact’ roots) or by cutting the apical root tip off (‘cut’ roots, 0.8 – 1 mm cut off, Figure 43A). Cut off apical root tips were placed next to their respective distal root ‘stumps’, and left to recover for 5 to 10 minutes from this drastic manipulation before starting the assay. Both intact and cut roots rested on gel-based medium during the assay (see Chapter 2, section 2.8.1 for more details). Intact and cut roots were then treated with 1 mM eATP solution, applied to the intact root tip or severed root tip and stump simultaneously. Either way, the applied treatment would envelop all imaged root tissue in less than 1.5 seconds. Treatment was applied 20 seconds after start of image acquisition, and images were taken over a period of in total 250 seconds (see Appendix VI, movie 7, for a representative time series).

The response of intact GCaMP3-expressing roots to eATP treatment has been described in more detail previously (see Figure 40 and Figure 41). Hence, this section focusses on the response of cut root tips, and how it differs from the response of intact roots (Figure 43). To enable comparison between intact and cut roots, regions of interest (Roi) were designed to locate to equivalent positions along the root, measuring from (intact or cut of) start of the root tip, *i.e.* Roi A was positioned at the apical root tip, Roi D was positioned 2.5 mm from the apical root tip (see white boxes in Figure 43A).

Not surprisingly, baseline fluorescence levels were slightly elevated in cut roots due to previous wounding stress (see light and dark green traces in Figure 43B). Besides a slight decrease in fluorescence due to treatment application at 20 seconds, treatment with 1 mM eATP solution led to an immediate and strong increase in fluorescence intensity in Roi A of both intact and cut roots (Figure 43B). Interestingly, cut root tips exhibited a differently shaped response – instead of one defined peak (grey trace, intact roots), cut roots showed a much narrower peak, followed by a smaller shoulder (light green trace, compare in Figure 43B). This response indicated that some component of the eATP response went missing in cut roots. Furthermore, the ‘narrow peak and shoulder’ was reminiscent in shape as to what was observed for the eATP-response in zero P root Roi A (Figure 41D).

eATP treatment also triggered an increase in fluorescence signal in Roi D, however more gradual and delayed than the immediate response observed in Roi A (Figure 43B). Most interestingly, an increase of fluorescence in Roi D was observed even when the apical root tip was cut off. Moreover, both intact and cut roots showed responses that were aligned in time (compare dark green and dark grey traces in Figure 43B). It was further observed that, even though intact and cut roots ‘started’ their response from different pre-treatment baseline fluorescence levels, upon eATP treatment both reached the same absolute level of fluorescence.

When normalising for differences in baseline levels, the pattern described for Roi A changed little - the lower, more shouldered response in cut roots was preserved (Figure 43C). However, the amplitude of response in Roi D of intact roots proved to be on average twice as high as what was observed in Roi D of cut roots (Figure 43C). To quantify this difference, fluorescence maxima were extracted from normalised signal intensity traces ( $\Delta F_{\max} / F_0$ , Figure 43D). Although the kinetics of the response differed, maximal responses to eATP treatment were very similar in Roi A between intact and cut roots (mean  $\Delta F_{\max} / F_0 \pm \text{SEM}$ : intact roots:  $2.11 \pm 0.14$ , cut roots:  $1.97 \pm 0.26$ ,  $p = 0.975$ ). In contrast, intact roots showed a significantly higher magnitude of response in Roi D (intact roots:  $3.15 \pm 0.15$ , cut roots:  $1.36 \pm 0.26$ ,  $p < 0.001$ , Figure 43D).



**Figure 43:** The  $[Ca^{2+}]_{\text{cyt}}$  response to extracellular ATP in specific regions of intact and cut root tips using an intensimetric reporter. *Arabidopsis Col-0* expressing the cytosolic GCaMP3 were grown on half MS growth medium (full P). Primary roots of 10-day old seedlings were modified prior to the assays by either not severing the root ('intact root') or excising 0.8 – 1 mm of apical root tip ('cut root'). Root tips were then treated with 1 mM eATP treatment solution, applied 20 seconds after start of image acquisition to the root tip (and stump) of seedlings resting on gel-based growth medium, and imaged for in total 250 seconds. (A) Root micrographs depicting cut roots (yellow dashed line indicates site of cut, with root tip being placed next to root stump), and intact roots, including regions of interest used for analysis (Roi A, Roi D; indicated by white boxes), scale bar: 1 mm. (B) Mean GFP fluorescence intensity  $\pm$  SEM, background subtracted, and (C) normalized GFP fluorescence ( $\Delta F / F_0$ )  $\pm$  SEM; data from 3 independent trials, with  $n = 6 - 9$  individual roots per root modification. (D) Extracted normalized fluorescence maxima ( $\Delta F_{\max} / F_0$ ) of individual Rois, each dot represents an individual data point, middle line denotes median. Analysis of variance (ANOVA) with *post-hoc* Tukey Test was used to assess statistical differences. Significance levels ( $p$ -values): \*\*\* ( $<0.001$ ), \*\* ( $<0.01$ ), \* ( $<0.05$ ), n.s. (not significant).

To investigate any link between the spatially separated responses (the component missing in Roi D of cut roots, see above), it was therefore of interest to investigate the local *versus*

systemic effect of eATP perception and resulting  $[Ca^{2+}]_{\text{cyt}}$  signal. With regards to eATP perception, it is unknown if eATP leads to the propagation of a  $[Ca^{2+}]_{\text{cyt}}$  signal beyond the tissue that is in direct contact with the treatment solution. The experimental methods described so far did not allow a differentiation between local and systemic response to eATP, as aequorin, NES-YC3.6 and GCaMP3 set-ups relied on all root tissue being in contact with eATP treatment solution (aequorin: tissue was completely submerged in treatment solution; NES-YC3.6: superfusion of all root tissue with treatment solutions; GCaMP3 (shown so far): treatment solution rapidly spreading along the root due to capillary action).

Thus, an experiment was designed which allowed localized application of eATP treatment solution, whilst monitoring  $[Ca^{2+}]_{\text{cyt}}$  dynamics in (i) tissue that was in direct contact, and (ii) outside the tissue area being treated. GCaMP3-expressing plants were, as described for previous experiments, placed on gel-based growth medium to be imaged under a stereomicroscope. However, the roots were placed across a gap in the agar (approximately 1 mm gap). Cutting a gap in the agar was found to be the most reliable way to avoid spread of applied treatment solution along the whole root (see Chapter 2, Figure 3, for a comparison of trialled methods). Thus, the apical root tip (0.8 – 1 mm) rested on one side of the agar gap, allowing localized application of treatment solution to either the root tip or the elongation zone (see Figure 44A for an exemplary image of a root placed across an agar gap). The gap was supplied with liquid nutrient solution to avoid drying of the root placed across. Care was taken that the solution would not touch the roots, leading to a leak of applied treatment solution. Plant material used was 10 days old, and grown on full P or zero P growth medium.

Prepared seedlings were left to recover from any handling stress for 5 to 10 minutes, *i.e.* until baseline fluorescence levels were steady. Control solution or 1 mM eATP treatment solution was then applied to the apical root tip or the elongation zone. To test if the order of treated area would play a role in the observed response, two sets of experiments were conducted: (i) Roots were treated first at the root tip, and secondly in the elongation zone (Figure 44) or (ii) roots were first treated in the elongation zone, and secondly at the root tip (= reverse order). In both cases, the first treatment was applied 20 seconds after start of image acquisition, the subsequent treatment was applied at 295 seconds after start of image acquisition.

Regions of interest ('Roi') were designated to root regions comparable to intact and cut roots experiments described before, labelled as before 'Roi A' and 'Roi D' (Figure 41,

Figure 43). To test if any signal upon eATP perception were being propagated into the area not in contact with treatment solution (section of root that was placed across the gap), ‘Roi X’ was designated to the middle of the gap (see Figure 44A for a root micrograph with annotated Rois).

Applying 1 mM eATP treatment first to the root apex, and later to the elongation zone, revealed an immediate and strong fluorescence increase in the apex (Roi A, Figure 44B and E). Full P grown root fluorescence recovered back to pre-stimulus baseline levels in Roi A within approximately 180 seconds. Interestingly, the response showed a slight shoulder, which had been observed before in Roi A of cut, but not intact root tips (see Figure 43B). Roi A of zero P grown roots showed a similar amplitude of response, but different response kinetics as fluorescence levels did not return back to baseline within the timeframe monitored (Figure 44B and E). Application of control solution did not lead to any remarkable fluorescence increase (Figure 44B and E).

Most interestingly, Roi X which covered a root region that did not come in direct contact with any treatment solution, quickly showed a gradual increase in fluorescence upon eATP treatment of the root apex, in both full and zero P grown root tips (Figure 44C). As images were captured every 5 seconds, temporal resolution was low; an increase of fluorescence in Roi X was however detectable within approximately 5 to 20 seconds. The response was variable, but normalizing for differences in pre-stimulus baseline levels revealed that full P grown roots responded with a fairly strong fluorescence increase, and zero P grown root tips to a lesser extent (Figure 44F). This indicated that local application of eATP treatment to the apical root tip triggered a  $[Ca^{2+}]_{cyt}$  increase in tissue that did *not* come in contact with the treatment, travelling approximately 0.3 – 0.5 mm of untreated tissue before being monitored in Roi X (see Figure 44A for a schematic). No fluorescence increase in Roi X was seen upon control solution application, indicating that the response in Roi X is not due to mechanical stimulation, but rather is eATP-dependent (in the range that the GCaMP3 reporter is sensitive for  $[Ca^{2+}]_{cyt}$  changes, see section 4.3.3 for a discussion).

Monitoring the fluorescence response in the elongation zone (Roi D) showed no remarkable response in the initial 300 seconds, during which treatment was applied to the apical root tip, and only a slight, eATP-dependent raw fluorescence increase once treatment was applied to the elongation zone (Figure 44D). Most strikingly, when normalizing for differences in baseline fluorescence levels, full P grown roots showed an increase in fluorescence in Roi D upon treatment of the apical root tip (see green trace in



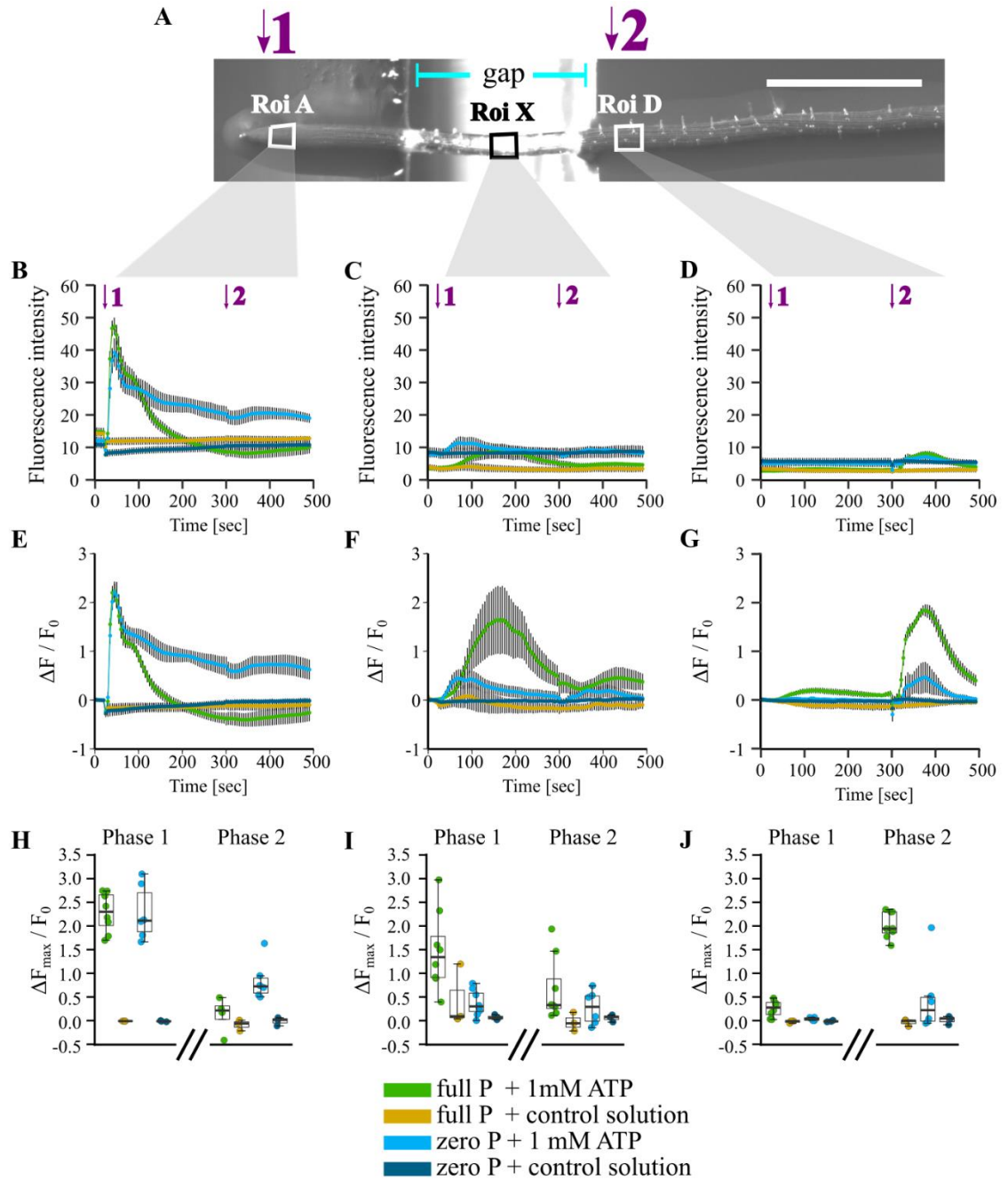
20 – 300 second window, Figure 44G and J). This would indicate that application of eATP to the apical root tip did not only trigger an increase in fluorescence signal in Roi X, but also in Roi D, essentially traversing approximately 2 mm of non-treated root tissue. Subsequent application of eATP to the elongation zone provoked a stronger increase in full P grown roots compared to zero P grown roots (Figure 44J). Control buffer application did not lead to any changes in fluorescence (Figure 44J).

Next, the same experimental set-up was employed but the treatment order reversed (*i.e.* the first treatment was applied to the elongation zone, the second treatment was applied to the root apex; see Figure 45A for a schematic). The pattern was very similar to what has been described above for the reversed order. Applying 1 mM eATP solution first to the elongation zone led to a strong response in full P roots, and a much dampened response in zero P roots within Roi D (Figure 45D, G, J). In the root section not in direct contact with treatment solution (Roi X), an increase of fluorescence was apparent in full P grown roots, whilst zero P roots showed a much lower response, comparable to what was observed for some samples upon control solution application (Figure 45C, F, I). Application of eATP to the root apex, at 295 seconds, led to a strong increase in fluorescence in Roi A, in both full P and zero P grown roots (Figure 45B, E, H). This response was very similar to the previous experiment, where the root apex was treated first with eATP solution (compare Figure 44B and Figure 45B). Interestingly, the response kinetics were conserved as well, *i.e.* both full and zero P grown roots showed a peak in fluorescence, followed by a smaller shoulder (Figure 44B and Figure 45B).

Overall, local application of eATP treatment in all root tissue and treatment order led to strong increases in fluorescence. When applying eATP to the root apex, there was no difference in response between roots grown on full or zero P. In the elongation zone, eATP treatment led to a stronger fluorescence increase in full P grown roots compared to zero P grown roots. Using this set-up, with the root being placed across a gap in the agar, it was possible to track any propagating signal into areas not in direct contact with eATP treatment. A gradual increase in fluorescence in Roi X could be detected almost instantly after the treatment was applied, with full P roots showing a stronger response compared to zero P roots. The response was however much more variable than what was observed in areas of direct eATP application. A fluorescence increase in Roi X was detected both after treatment application to the root apex and elongation zone. This indicates that the  $[Ca^{2+}]_{\text{cyt}}$  signal was capable of propagating both from the root apex shootwards, as well as from the elongation zone towards the apex. Care was taken to keep the root section,

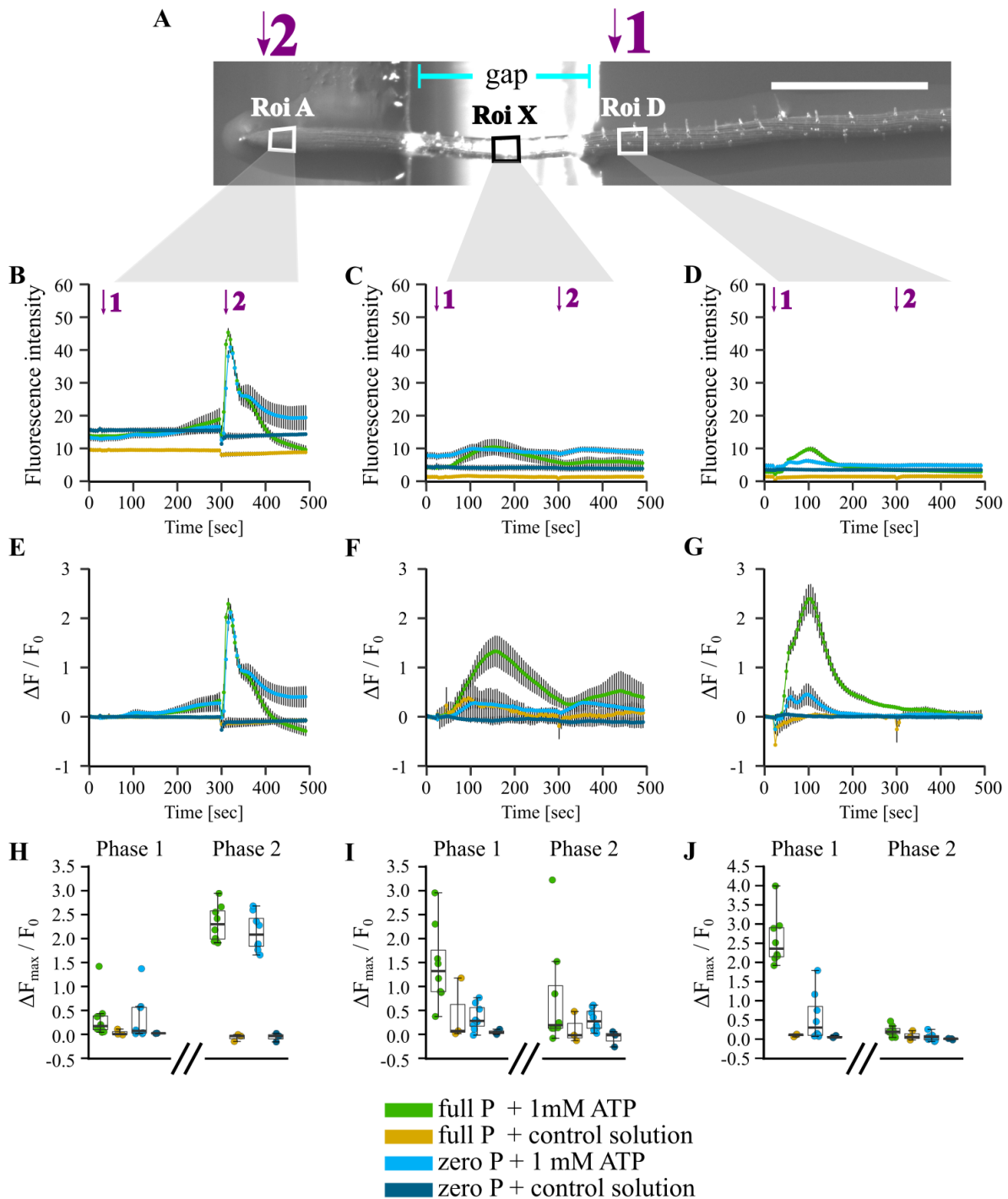
which was placed across the gap, humid. However, it should be taken into account that this section might still be primed differently than root tissue lying on agar, and influence any downstream response.

All experiments carried out to test the link between the spatially and temporarily distinct  $[Ca^{2+}]_{cyt}$  responses upon eATP perception can be summarized as follows. First, it was shown that detaching the root apex from the remaining root still led to two distinct  $[Ca^{2+}]_{cyt}$  responses in the apex and elongation zone when eATP was applied systemically. Secondly, local application of eATP treatment led to a strong response at the site of direct contact, but also triggered a systemic increase in  $[Ca^{2+}]_{cyt}$  outside the treated area. Intriguingly, this indicates that the two responses ('peak 1' and 'peak 2') mostly depend on direct contact with eATP containing solution, and can be generated independently of each other. Using the GCaMP3 reporter, some signal was shown to also occur systemically.



**Figure 44:** The  $[Ca^{2+}]_{\text{cyt}}$  response of roots to locally applied extracellular ATP, first applied to the tip then to the elongation zone. *Arabidopsis* Col-0 expressing cytosolic GCaMP3 was grown on full or zero P medium. Ten-day old seedlings were placed across a gap in the agar (see example root with annotated gap (A)); then treated with control or 1 mM eATP treatment solution, applied 20 seconds after start of image acquisition to the root tip (indicated by purple ‘1’ in (A)), and at 295 seconds to the elongation zone (indicated by purple ‘2’ in (A)), and imaged for in total 495 seconds. (A) Exemplary root tip with annotated regions of interest used for analysis (‘Roi’, white boxes), scale bar: 1 mm. (B, C, D) Mean GFP fluorescence intensity  $\pm$  SEM, background subtracted, and (E, F, G) normalized GFP fluorescence ( $\Delta F / F_0$ )  $\pm$  SEM; data from 3 independent trials, with  $n = 3$  individual roots for control treatments per growth condition, and  $n = 6 - 9$  individual roots per eATP treatment and growth condition. (H, I, J) Extracted normalized

fluorescence maxima ( $\Delta F_{\max} / F_0$ ), each dot represents an individual data point, middle line denotes median. Data shown in (B, E, H) represent Roi A; (C, F, I) represent Roi X; (D, G, J) represent Roi D.



**Figure 45:** The  $[Ca^{2+}]_{\text{cyt}}$  response of roots to locally applied extracellular ATP, first applied to the elongation zone then to the tip. *Arabidopsis* Col-0 expressing cytosolic GCaMP3 was grown on full or zero P medium. Ten-day old seedlings were placed across a gap in the agar (see example root with annotated gap (A)); then treated with control or 1 mM eATP treatment solution, applied

20 seconds after start of image acquisition to the elongation zone (indicated by purple '1' in (A)), and at 295 seconds to the root tip (indicated by purple '2' in (A)), and imaged for in total 495 seconds. (A) Exemplary root tip with annotated regions of interest used for analysis ('Roi', white boxes), scale bar: 1 mm. (B, C, D) Mean GFP fluorescence intensity  $\pm$  SEM, background subtracted, and (E, F, G) normalized GFP fluorescence ( $\Delta F / F_0$ )  $\pm$  SEM; data from 3 independent trials, with  $n = 3$  individual roots for control buffer treatments per growth condition, and  $n = 8$  individual roots per eATP treatment and growth condition. (H, I, J) Extracted normalized fluorescence maxima ( $\Delta F_{\max} / F_0$ ), each dot represents an individual data point, middle line denotes median. Data shown in (B, E, H) represent Roi A; (C, F, I) represent Roi X; (D, G, J) represent Roi D.

#### 4.2.4 The increase of intracellular ROS is dependent on an interplay of phosphate and iron levels

Next, the involvement of intracellular reactive oxygen species (ROS) was tested in generating and/or modulating the  $[Ca^{2+}]_{\text{cyt}}$  response to eATP. It had been reported that P starvation led to over-accumulation of Fe in particular regions of the root tip of wild type *Arabidopsis*, which in turn correlated with hotspots of ROS (Müller *et al.*, 2015; Reyt *et al.*, 2015; Hoehenwarter *et al.*, 2016; Balzergue *et al.*, 2017). Thus, P-starved roots were used as a tool to further delineate, and possibly correlate, the components underlying the different  $[Ca^{2+}]_{\text{cyt}}$  responses to eATP. Intracellular ROS could be visualized and quantified through staining with CM-H<sub>2</sub>DCFDA (2', 7'-dichlorodihydrofluorescein diacetate). This dye is membrane-permeable, and passively diffuses into cells. Once within the cell, it is hydrolysed to CM-H<sub>2</sub>DCF by intracellular esterases and thus trapped in the cell. CM-H<sub>2</sub>DCF rapidly reacts with a range of ROS to produce a fluorescent product, with fairly low affinity for reactive nitrogen species (Halliwell and Whiteman, 2004). The resulting fluorescence intensity can be quantified in relation to position along the root. The produced fluorescent product is stable, *i.e.* the dye is cumulative, therefore great care was taken to minimize any (oxidative) stress during the staining procedure. Furthermore, the dye is known to be photolabile, *i.e.* long light exposure might induce artifactual photochemical oxidation yielding a fluorescent product (Halliwell and Whiteman, 2004). Hence, exposure time was kept to a minimum.

Wild type *Arabidopsis* plants were grown on growth medium with varying levels of P and Fe, including full P\_full Fe, zero P\_full Fe, full P\_zero Fe, zero P\_zero Fe, full free P\_full free Fe and full P\_excess Fe (see Chapter 2, section 2.2.3, for more details on growth conditions, and Chapter 3, section 3.2.14 onwards for corresponding aequorin assays).

Bright field images of roots grown on these different growth conditions for 10 to 11 days showed root architectural differences (on the left of Figure 46). Nutrient-sufficient roots had few root hairs emerging within the field imaged, *i.e.* 1 – 2 mm from the root tip (Figure 46A). In contrast, zero P\_full Fe grown roots showed increased root hair outgrowth (Figure 46B), which is a phenotype conclusively reported for P-starved roots (also see Chapter 5). Excluding Fe, as well as P, from the growth medium (Figure 46C), rescued this dramatic root hair response back to what was observed for nutrient-sufficient roots. Decreasing or increasing Fe levels in a P-replete background led to little differences

compared to nutrient-sufficient roots (Figure 46D, F). Adjusting the free ionic availability of P and Fe to resemble that of zero P\_full Fe growth medium (Figure 46E), produced a root phenotype comparable to nutrient-sufficient conditions.

Capturing the fluorescence signal of roots grown on varying P and Fe conditions and stained with 20  $\mu\text{M}$  CM-H<sub>2</sub>DCFDA revealed strong differences of intracellular ROS levels (on the right of Figure 46). Nutrient-sufficient roots showed very low fluorescence levels in the apical root tip, increasing slightly to low fluorescence levels, evenly spread along the upper parts of the roots (Figure 46A). In stark contrast, P-starved but Fe-replete roots (zero P\_full Fe) showed much higher fluorescence levels, with a hotspot occurring approximately 0.5 to 1.5 mm away from the root tip (Figure 46B). All other variations in P and Fe showed low fluorescence levels, overall comparable to nutrient-sufficient conditions (Figure 46C-F). This included roots grown on zero P\_zero Fe (Figure 46C), indicating that excluding P did not necessarily lead to higher fluorescence through *e.g.* more porous membranes and thus higher uptake of dye.

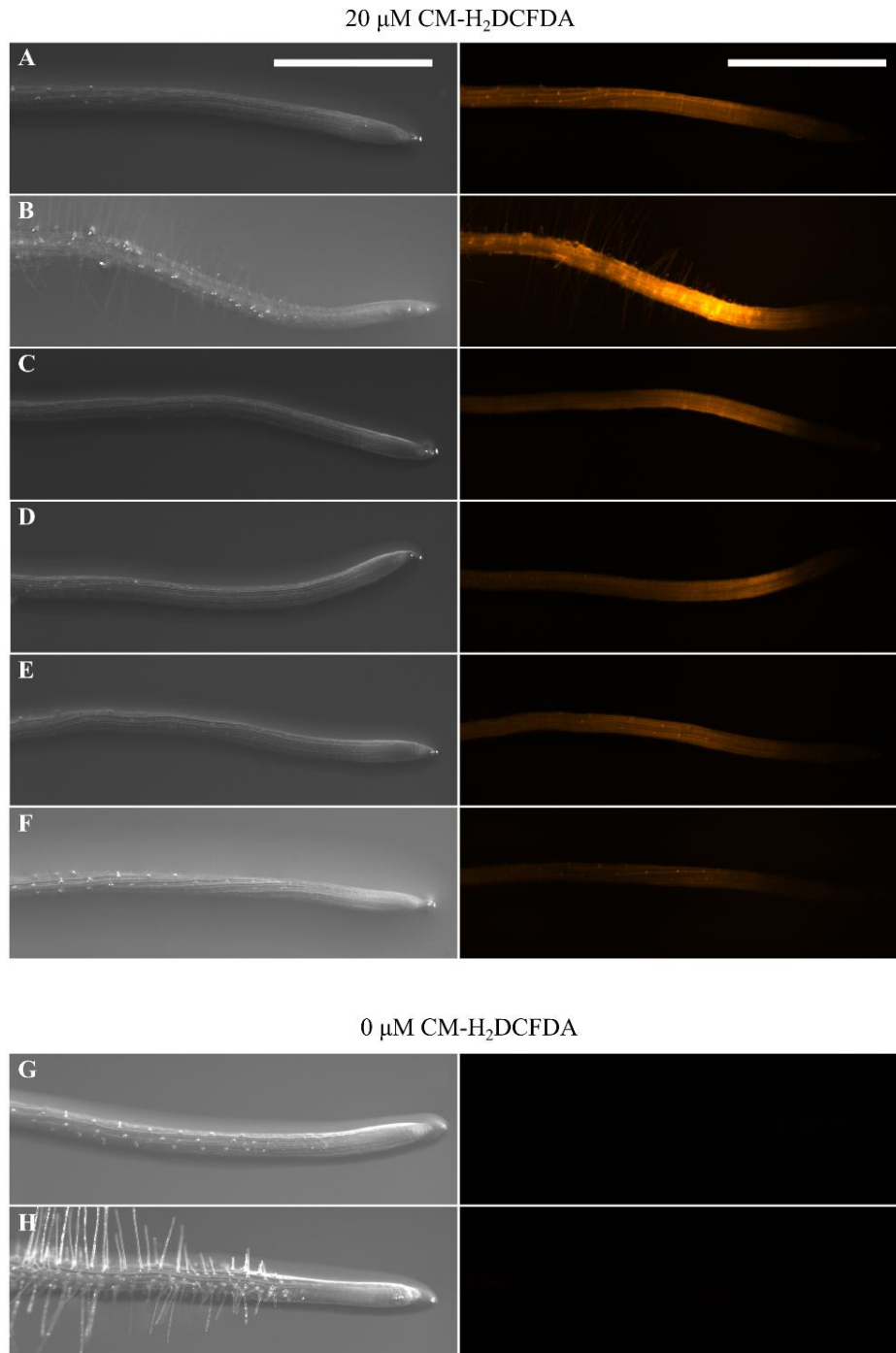
Roots that had undergone the same staining procedure, except including the CM-H<sub>2</sub>DCFDA dye, showed no fluorescence signal, independent of growth condition (Figure 46G, H). This indicates that any fluorescence signal quantified is due to fluorescence of CM-H<sub>2</sub>DCFDA, background fluorescence can be excluded as a confounding factor.

To quantify the observed differences in fluorescence, the fluorescence signal of individual roots was analysed (according to Reyt *et al.*, 2015, see Chapter 2, section 2.2.9.1, for analysis details). Mean fluorescence intensities were then plotted along the length of the root (data from 3 independent trials, with  $n = 14 - 16$  individual roots per growth condition, Figure 47). Quantification allowed localization of the intracellular ROS hotspot observed in zero P\_full Fe roots, showing maximal intensity approximately 1 mm from the root tip (blue trace in Figure 47). Extracting the fluorescence signal intensities at designated distances from the root tip (100  $\mu\text{m}$ , 1000  $\mu\text{m}$  and 2000  $\mu\text{m}$  from the root tip, Table 4) allowed statistical comparison between the different growth conditions (Analysis of variance (ANOVA) with *post-hoc* Tukey test). This revealed that at the apical root tip (position: 100  $\mu\text{m}$ ), zero P\_full P roots already showed a higher fluorescence signal compared to all other growth conditions, however this difference was not significant ( $p \geq 0.18$ ). All other growth conditions showed highly similar fluorescence levels ( $p = 0.999$  for all comparisons). At 1000  $\mu\text{m}$  from the root tip, roots of all growth conditions showed increased fluorescence intensities. However, zero P\_full Fe roots

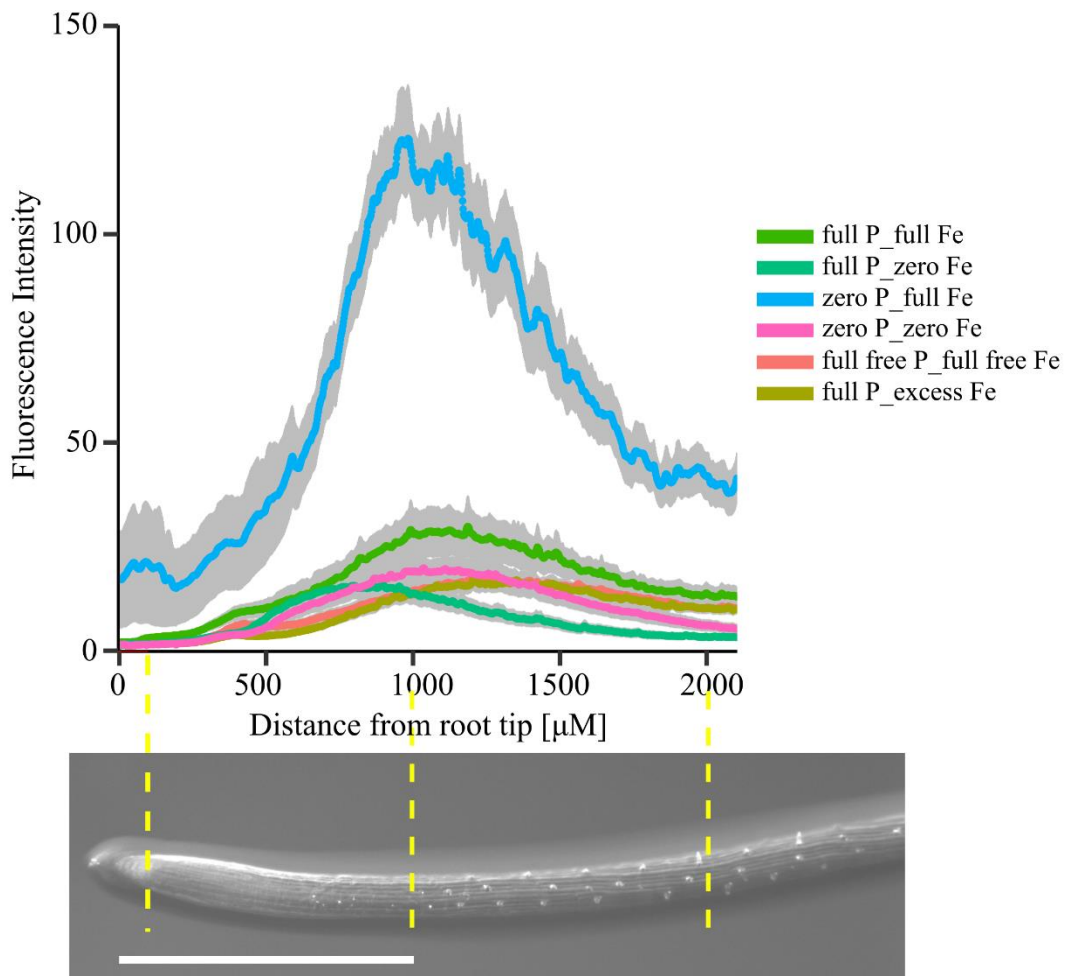
showed a significantly higher fluorescence intensity in contrast to all other growth conditions ( $p < 0.001$ ). As was seen for the apical root tip, all other growth conditions showed comparable signal intensities ( $p \geq 0.45$ ). Further up the root, 2000  $\mu\text{m}$  from the root tip, zero P\_full Fe roots showed a decreased signal compared to 1000  $\mu\text{m}$  from the root tip, however still significantly higher than all other growth conditions ( $p < 0.001$ ). Again, comparing all other growth conditions except zero P\_full Fe did not show any significant differences in signal intensity at 2000  $\mu\text{m}$  from the tip ( $p \geq 0.12$ ).

Taken together, using a dye that stained intracellular ROS, it could be shown that roots grown without P but standard levels of Fe showed a higher ROS load. A ROS hotspot was found to be localized approximately 1 mm from the root tip, which spatially correlated with a much dampened  $[\text{Ca}^{2+}]_{\text{cyt}}$  response in the same region (see kymograph in Figure 38). Excluding Fe, as well as P, from growth medium, reduced this ROS overload back to roots grown on optimal nutrient conditions. Only excluding Fe from growth medium (as in full P\_zero Fe) did not lead to any changes in intracellular ROS levels, indicating that the interplay of P starvation and Fe availability is necessary to induce intracellular ROS accumulation within the root tip of *Arabidopsis*.





**Figure 46:** Distribution of intracellular reactive oxygen species in phosphate- and iron-starved primary root tips. *Arabidopsis* Col-0 were grown on growth medium with different P and Fe levels: (A, G) full P\_full Fe, (B, H) zero P\_full Fe, (C) zero P\_zero Fe, (D) full P\_zero Fe, (E) full free P\_full free Fe and (F) full P\_excess Fe. Ten- to 11-day old seedlings were stained with 20  $\mu$ M CM-H<sub>2</sub>DCFDA (A-F), or incubation solution without CM-H<sub>2</sub>DCFDA as control for any background fluorescence (G-H), for 1 hour before bright field (on the left) and GFP fluorescence images (on the right) were captured. CM-H<sub>2</sub>DCFDA stains intracellular ROS. Three independent trials were conducted, representative images per growth condition are shown, false colour-coded. Scale bar in (A): 1 mm.



**Figure 47:** Fluorescence intensity from intracellular reactive oxygen species staining along phosphate- and iron-starved primary roots. *Arabidopsis* Col-0 were grown on medium with different P and Fe levels: full P\_full Fe (green), full P\_zero Fe (turquoise), zero P\_full Fe (blue), zero P\_zero Fe (pink), full free P\_full free Fe (magenta) and full P\_excess Fe (brown). Ten- to 11-day old seedlings were stained for intracellular ROS with 20  $\mu$ M CM-H<sub>2</sub>DCFDA for 1 hour before fluorescence images were captured. Fluorescence intensity was quantified, background subtracted and averaged along the root length. Mean values (coloured lines)  $\pm$  SEM (grey shading) are shown, data from 3 independent trials, with n = 14 - 16 roots analysed per growth condition. Root micrograph (bottom) aligns with root tip regions quantified (yellow dashed lines), scale bar: 1 mm.

**Table 4:** Mean signal intensities of phosphate- and iron-starved primary root tips stained for intracellular reactive oxygen species. Roots were incubated with 20  $\mu\text{M}$  CM-H<sub>2</sub>DCFDA stain (20  $\mu\text{M}$  dye) or control solution without dye (no dye). Primary data are shown in Figure 47 (analysed root tip regions are marked by yellow dashed line). Fluorescence intensities were averaged at 100  $\mu\text{m}$ , 1000  $\mu\text{m}$  and 2000  $\mu\text{m}$  from the root tip (means  $\pm$  SEM), n – number of individual root tips averaged, from 3 independent trials.

Incubation	Growth condition	100 $\mu\text{M}$ from tip		1000 $\mu\text{M}$ from tip		2000 $\mu\text{M}$ from tip		n
		mean	$\pm$ SEM	mean	$\pm$ SEM	mean	$\pm$ SEM	
20 $\mu\text{M}$ dye	full P_full Fe	3.25	0.44	28.30	6.39	13.70	2.57	15
20 $\mu\text{M}$ dye	full P_zero Fe	1.74	0.19	13.95	2.61	3.45	0.85	14
20 $\mu\text{M}$ dye	zero P_full Fe	21.28	14.44	115.93	11.06	42.01	5.78	15
20 $\mu\text{M}$ dye	zero P_zero Fe	1.69	0.19	19.05	3.19	6.22	1.37	16
20 $\mu\text{M}$ dye	full free P_full free Fe	2.00	0.18	14.58	2.02	10.51	0.97	14
20 $\mu\text{M}$ dye	full P_100 $\mu\text{M}$ Fe	1.91	0.16	13.71	1.91	10.41	1.33	15
no dye	full P_full Fe	0.43	0.20	0.09	0.04	-0.18	0.02	2
no dye	zero P_full Fe	0.82	0.05	0.26	0.17	0.35	0.01	2

#### 4.2.5 The secondary $[Ca^{2+}]_{cyt}$ response to extracellular ATP is sensitive to pharmacological alterations of cellular redox status

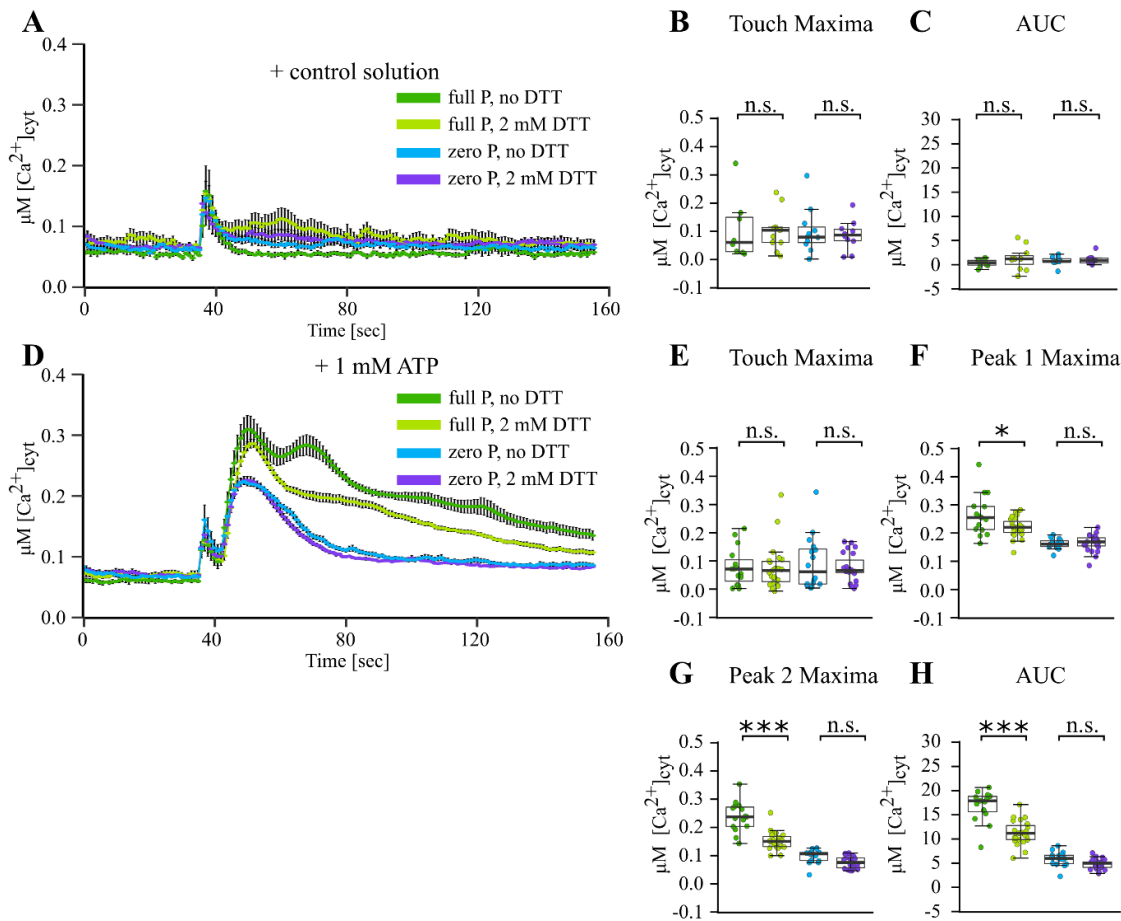
To further test the role of ROS in the  $[Ca^{2+}]_{cyt}$  signal generation upon eATP treatment, pharmacological inhibitors known to affect cellular redox state or impair ROS production were employed. First, sample tissue in a more reduced state was used for experimentation. To this end, aequorin-expressing *Arabidopsis* plants were grown on full or zero P (both including standard Fe levels). Excised root tips (1 cm) of 11-day old seedlings were incubated for 30 minutes with 2 mM 1,4 – dithiothreitol (DTT) prior to running the assay. DTT is known as a potent reducing agent, maintaining accessible protein thiol groups in reduced states (Carmack and Kelley, 1968; Demidchik *et al.*, 2009).

DTT pre-treated roots were then challenged with 1 mM eATP treatment (in control solution background), or control solution alone, to control for the mechanical stimulation due to treatment application (Figure 48). Application of control solution led to immediate and monophasic increases in  $[Ca^{2+}]_{cyt}$  (data from 3 independent trials,  $n = 8 - 11$  individual root tips per pre-treatment and growth condition, Figure 48A). Even though 2 mM DTT pre-treatment led to a more unsteady  $[Ca^{2+}]_{cyt}$  behaviour in full P root tips (see light green trace in Figure 48A), there was no significant difference in magnitude of touch maxima or derived area under the curve between any P growth regime or pre-treatment condition (mean peak maxima  $\pm$  SEM: full P + 2 mM DTT:  $0.10 \pm 0.02$ , full P no DTT:  $0.11 \pm 0.04$ , zero P + 2 mM DTT:  $0.09 \pm 0.02$ , zero P no DTT:  $0.10 \pm 0.02$ ,  $p \geq 0.970$  for all comparisons involving touch maxima and area under the curve, Figure 48B and C).

However, DTT pre-treatment altered the response to 1 mM ATP treatment (data from 3 independent trials,  $n = 15 - 23$  individual root tips per pre-treatment and growth condition, Figure 48D). Whereas full P grown root tips *without* DTT pre-treatment showed the characteristic multi-phasic  $[Ca^{2+}]_{cyt}$  response (dark green trace in Figure 48D), root tips pre-treated *with* DTT showed a much lower secondary ATP-specific response (light green trace in Figure 48D). Zero P grown root tips showed an overall dampened  $[Ca^{2+}]_{cyt}$  response to ATP treatment, as has been described in detail before (see Chapter 3), but without any obvious effect of DTT pre-treatment (blue and purple trace, Figure 48D). Analysis of the time-course data showed no difference between touch maxima, regardless of P regime or DTT pre-treatment (full P + 2 mM DTT:  $0.08 \pm 0.02$   $\mu$ M, full P no DTT:  $0.08 \pm 0.02$   $\mu$ M, zero P + 2 mM DTT:  $0.08 \pm 0.01$   $\mu$ M, zero P no DTT:  $0.09 \pm 0.02$   $\mu$ M,

$p \geq 0.997$ , Figure 48E). DTT pre-treatment led to a slight but significant dampening of peak 1 maxima in full P root tips (full P + 2 mM DTT:  $0.22 \pm 0.01 \mu\text{M}$ , full P no DTT:  $0.26 \pm 0.02 \mu\text{M}$ ,  $p = 0.023$ , Figure 48F). Peak 1 in zero P root tips was not affected by DTT (zero P + 2 mM DTT:  $0.17 \pm 0.01 \mu\text{M}$ , zero P no DTT:  $0.16 \pm 0.004 \mu\text{M}$ ,  $p = 0.999$ , Figure 48F). The effect of DTT was even stronger on peak 2 maxima in full P root tips, significantly dampening the  $[\text{Ca}^{2+}]_{\text{cyt}}$  increase (full P + 2 mM DTT:  $0.15 \pm 0.01 \mu\text{M}$ , full P no DTT:  $0.24 \pm 0.01 \mu\text{M}$ ,  $p < 0.001$ ), but again showed no effect on zero P root tips (zero P + 2 mM DTT:  $0.08 \pm 0.004 \mu\text{M}$ , zero P no DTT:  $0.09 \pm 0.001 \mu\text{M}$ ,  $p = 0.406$ , Figure 48G). Overall, DTT pre-treatment led to a significantly lower mobilization of  $[\text{Ca}^{2+}]_{\text{cyt}}$  in full P root tips, compared to DMSO pre-treatment alone ( $p < 0.001$ , Figure 48H). The area under the curve of zero P root tips was not affected by DTT pre-treatment ( $p = 0.624$ , Figure 48H).

Taken together, the reducing agent DTT altered the  $[\text{Ca}^{2+}]_{\text{cyt}}$  signature in full P grown root tips, with particularly peak 2 being dampened upon eATP treatment. In zero P root tips, which already exhibited a dampened  $[\text{Ca}^{2+}]_{\text{cyt}}$  signature regardless of DTT treatment, DTT had no further impact on the  $[\text{Ca}^{2+}]_{\text{cyt}}$  response to eATP.



**Figure 48:** The effect of a more reduced cellular redox state on the  $[\text{Ca}^{2+}]_{\text{cyt}}$  response of phosphate-starved root tips to extracellular ATP. Aequorin-expressing, *Arabidopsis Col-0* plants were grown on full or zero P growth medium (green traces, blue-purple traces, respectively). Root tips (1 cm) of 11-day old seedlings were pre-incubated for 30 minutes with the reducing agent DTT (2 mM DTT) or no DTT, before challenging root tips with treatments applied at 35 seconds, and measuring  $[\text{Ca}^{2+}]_{\text{cyt}}$  for 155 seconds. (A) Application of control solution; time course trace represents mean  $\pm$  standard error of mean (SEM) from 3 independent trials, with  $n = 8 - 11$  individual root tips averaged per data point. Time course data were analysed for (B) touch maxima and (C) area under the curve (AUC), all baseline-subtracted, with each dot representing an individual data point (see Figure 6 for details). Boxplot middle line denotes median. (D-H) Responses to 1 mM eATP (3 independent trials,  $n = 15 - 23$  individual root tips per growth condition). Analysis of variance (ANOVA) with *post-hoc* Tukey Test was used to assess statistical differences. Significance levels ( $p$ -values): \*\*\* ( $<0.001$ ), \*\* ( $<0.01$ ), \* ( $<0.05$ ), n.s. (not significant).

However, DTT has been reported to have rather unspecific side-effects in both plant and animal cells. As it disrupts disulphide bond formation, it is also known to *e.g.* induce ER stress through the accumulation of unfolded proteins in the endoplasmic reticulum (Martinez and Chrispeels, 2003). Therefore, another pharmacological agent described to affect redox signalling in cells was trialled. Diphenyleneiodonium chloride (DPI) is a cell membrane-permeable, irreversible inhibitor of NADPH-oxidases and other flavin-containing enzymes (Bolwell and Wojtaszek, 1997; Demidchik *et al.*, 2009; Sun *et al.*, 2012). NADPH-oxidases are the major producers of ROS within cells (Desikan *et al.*, 1996; Foreman *et al.*, 2003).

The effect of NADPH-oxidase inhibition was tested on 11-day old, aequorin-expressing *Arabidopsis* root tissue. Full and zero P grown excised root tips (1 cm) were pre-incubated for 30 minutes with a 100  $\mu\text{M}$  DPI solution (dissolved in DMSO, and further diluted to working concentration in control solution background; maintaining full and zero P growth conditions during the incubation). To account for any effects of DMSO as the solvent, control roots were incubated with DMSO in control solution alone. As DPI irreversibly inhibits NADPH-oxidases, DPI could be washed off prior to the assay, hence all roots were washed prior to application of 1 mM eATP treatment or mechanical stimulation (control solution application).

Application of control solution led to an immediate and monophasic  $[\text{Ca}^{2+}]_{\text{cyt}}$  response (data from 3 independent trials,  $n = 5 - 7$  individual root tips per growth condition and pre-treatment, Figure 49A). This touch response did not depend on P growth conditions or DMSO or DPI pre-treatment (mean touch maxima  $\pm$  SEM: full P + 100  $\mu\text{M}$  DPI:  $0.09 \pm 0.01$   $\mu\text{M}$ , full P no DPI:  $0.15 \pm 0.07$   $\mu\text{M}$ , zero P + 100  $\mu\text{M}$  DPI:  $0.09 \pm 0.02$   $\mu\text{M}$ , zero P no DPI:  $0.03 \pm 0.01$   $\mu\text{M}$ ,  $p \geq 0.918$ , Figure 49B). Accordingly, the area under the curve was similar between all treatments ( $p = 0.999$ , Figure 49C).

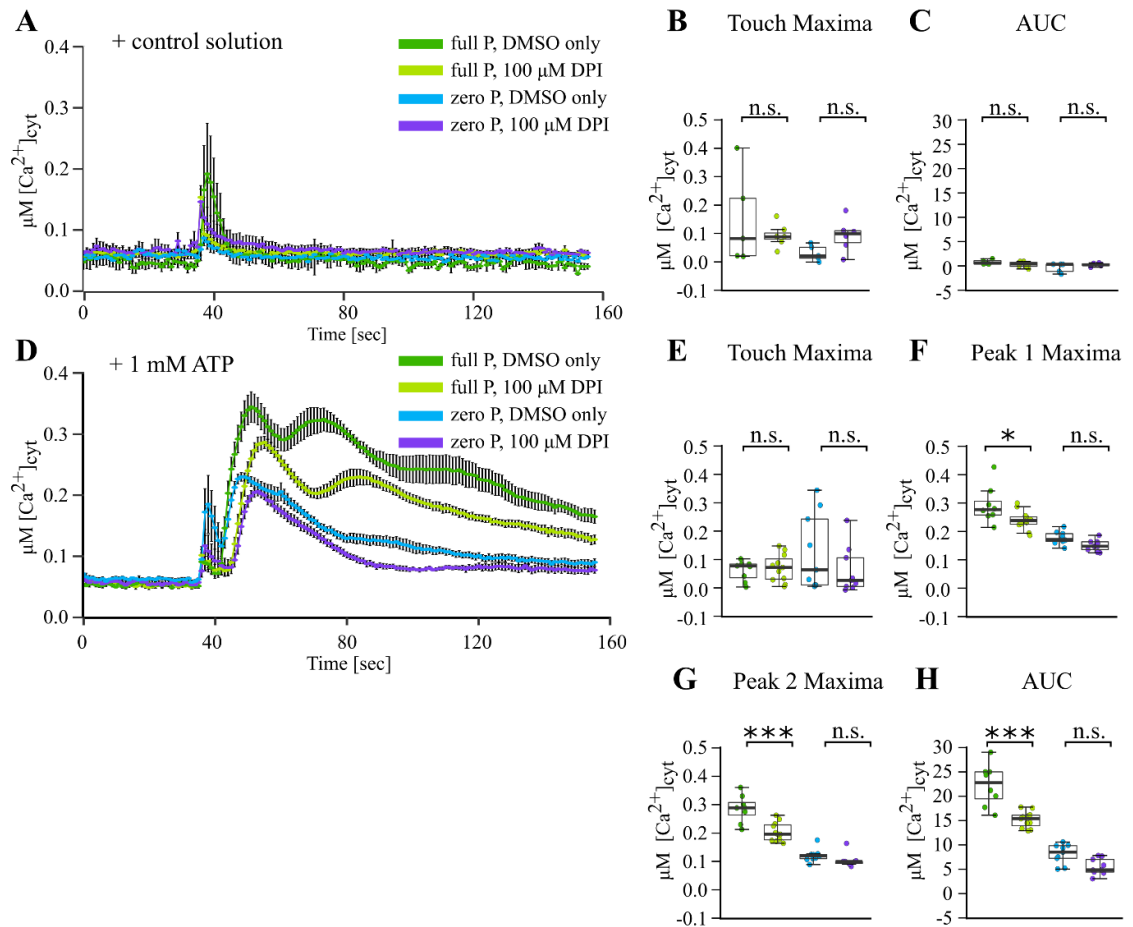
In contrast, DPI pre-treatment had a distinct effect on the  $[\text{Ca}^{2+}]_{\text{cyt}}$  signature in response to 1 mM eATP (data from 3 independent trials,  $n = 8 - 11$  individual root tips per growth condition and pre-treatment, Figure 49D). Full P grown root tips showed the characteristic multi-phasic  $[\text{Ca}^{2+}]_{\text{cyt}}$  response (traces show higher variation than what has been reported before in this thesis, likely due to lower sample size, see error bars of dark green trace in Figure 49D). However, DPI pre-treated full P root tips showed a  $[\text{Ca}^{2+}]_{\text{cyt}}$  response that, after the initial touch response, showed a time-lag of approximately three to five seconds and was severely dampened (Figure 49D). Zero P grown root tips equally showed a delayed response of peak 1. However, DPI pre-treatment did not dampen the  $[\text{Ca}^{2+}]_{\text{cyt}}$

response of zero P grown root tips nearly as severely (Figure 49D). Analysis of the response showed no difference between touch maxima (full P + 100  $\mu$ M DPI:  $0.07 \pm 0.02$   $\mu$ M, full P no DPI:  $0.06 \pm 0.01$   $\mu$ M, zero P + 100  $\mu$ M DPI:  $0.06 \pm 0.03$   $\mu$ M, zero P no DPI:  $0.13 \pm 0.05$   $\mu$ M,  $p \geq 0.706$ , Figure 49E). Peak 1 maxima were (just about) significantly lower in full P roots treated with DPI compared to no DPI treatment (full P + 100  $\mu$ M DPI:  $0.24 \pm 0.01$   $\mu$ M, full P no DPI:  $0.29 \pm 0.02$   $\mu$ M,  $p = 0.046$ , Figure 49F). Zero P roots showed lower peak 1 maxima compared to full P root tips, but no significant difference with regards to DPI treatment (zero P + 100  $\mu$ M DPI:  $0.15 \pm 0.01$   $\mu$ M, zero P no DPI:  $0.18 \pm 0.01$   $\mu$ M,  $p \geq 0.774$ , Figure 49F). The effect of DPI pre-treatment was even more pronounced for full P grown root tips peak 2 maxima, where DPI led to a highly significantly reduction of peak amplitude (full P + 100  $\mu$ M DPI:  $0.20 \pm 0.01$   $\mu$ M, full P no DPI:  $0.29 \pm 0.02$   $\mu$ M,  $p < 0.001$ , Figure 49G). DPI again did not affect the amplitude of peak 2 in zero P root tips (zero P + 100  $\mu$ M DPI:  $0.10 \pm 0.01$   $\mu$ M, zero P no DPI:  $0.12 \pm 0.01$   $\mu$ M,  $p \geq 0.903$ , Figure 49G). Overall, DPI pre-treatment led to significantly less  $[\text{Ca}^{2+}]_{\text{cyt}}$  being mobilized in response to eATP in full P root tips ( $p < 0.001$ ), without affecting zero P root tips ( $p = 0.148$ , Figure 49H).

Taken together, DPI pre-treatment led to an overall dampened  $[\text{Ca}^{2+}]_{\text{cyt}}$  response of full P root tips to eATP, particularly of peak 2. Zero P root tips did not show a DPI-dependent dampening of the  $[\text{Ca}^{2+}]_{\text{cyt}}$  response. In both full and zero P grown root tips, DPI pre-treatment led to a delayed onset of  $[\text{Ca}^{2+}]_{\text{cyt}}$  increase.

In summary, both DTT and DPI, pharmacological agents interfering with cellular redox status and ROS production, showed an effect on the  $[\text{Ca}^{2+}]_{\text{cyt}}$  response of P-replete root tips to eATP treatment. Both a more reduced cellular redox state as well as inhibition of ROS-production through NADPH-oxidases dampened peak 1, and particularly peak 2  $[\text{Ca}^{2+}]_{\text{cyt}}$  increases in full P roots. P-starved root tips were not affected by neither a more reduced cellular state or inhibition of ROS production with regards to amplitude of response. Both P-replete and -starved root tips however showed a distinct lag of ATP-specific  $[\text{Ca}^{2+}]_{\text{cyt}}$  response (peak 1) when ROS production was inhibited by DPI. No delay in response occurred when the root tissue was pushed towards a more reduced state using DTT.





**Figure 49:** The effect of inhibiting ROS production on the  $[\text{Ca}^{2+}]_{\text{cyt}}$  response of phosphate-starved root tips to extracellular ATP. Aequorin-expressing, *Arabidopsis* Col-0 plants were grown on full or zero P growth medium (green traces, blue-purple traces, respectively). Root tips (1 cm) of 11-day old seedlings were pre-incubated for 30 minutes with an inhibitor of NADPH-oxidases: 100  $\mu\text{M}$  DPI (in DMSO) or no DPI (DMSO only), before challenging root tips with treatments applied at 35 seconds, and measuring  $[\text{Ca}^{2+}]_{\text{cyt}}$  for 155 seconds. (A) Application of control solution; time course trace represents mean  $\pm$  standard error of mean (SEM) from 3 independent trials, with  $n = 5 - 7$  individual root tips averaged per data point. Time course data were analysed for (B) touch maxima and (C) area under the curve (AUC), all baseline-subtracted, with each dot representing an individual data point (see Figure 6 for details). Boxplot middle line denotes median. (D-H) Responses to 1 mM eATP (3 independent trials,  $n = 8 - 11$  individual root tips per growth condition). Analysis of variance (ANOVA) with *post-hoc* Tukey Test was used to assess statistical differences. Significance levels ( $p$ -values): \*\*\* ( $<0.001$ ), \*\* ( $<0.01$ ), \* ( $<0.05$ ), n.s. (not significant).

#### 4.2.6 Callose deposition is dependent on iron, but not phosphate, availability

To investigate the previously reported link between high ROS load and callose deposition (Müller *et al.*, 2015; Hoehenwarter *et al.*, 2016), and if a resulting loss of symplastic communication might play a role in the observed dampening of the  $[Ca^{2+}]_{cyt}$  response to eATP, it was of interest to visualize and quantify callose depositions. This was achieved by staining callose deposits with aniline blue solution (0.1 % (w/v) aniline blue). Callose-bound aniline blue emits fluorescence within the UV-light range, which was captured using a stereomicroscope. Callose deposits are known to occur as distinct small spots. To control for any unspecific staining, a few control roots were subjected to the staining procedure, without including aniline blue in the incubation solution. After staining samples for 1.5 with or without aniline blue, samples were embedded in 60 % glycerol, to prevent formation of air bubbles close to the samples and optimise imaging (see Chapter 2, section 2.9.2, for more details).

Ten- to 11-day old *Arabidopsis* wild type plants, grown on half MS growth medium containing varying P and Fe levels, were used for aniline blue staining. The growth conditions were as described for intracellular ROS staining (see Figure 46) and included: full P\_full Fe (= standard half MS growth medium, including both standard levels of P and Fe; mostly labelled ‘full P’ in this thesis), zero P\_full Fe (= half MS without P, but with standard Fe levels; mostly labelled ‘zero P’ in this thesis), full P\_zero Fe (= half MS containing standard P levels, but no Fe), zero P\_zero Fe (= half MS without P and Fe), full free P\_full free Fe (half MS with levels of P and Fe adjusted to give ionic free concentrations comparable to ionic free concentrations of zero P\_full Fe medium), or full P\_excess Fe (half MS containing standard levels of P, and double-strength (100  $\mu$ M) Fe levels).

Bright field images of the prepared root samples revealed drastic differences in root architecture between the different growth conditions (on the left of Figure 50). As described for ROS-stained root samples (Figure 46), P-starvation increased the outgrowth of long root hairs, close to the root tip and along the root (compare Figure 50A and B). Excluding Fe, as well as P from the growth medium, rescued this root hair phenotype, resulting in much less and shorter root hairs (Figure 50C). This root hair phenotype was not influenced by increasing or decreasing Fe levels, in a P-replete background (Figure 50D, E, F). It was observed that some samples suffered from air inclusion close to the

sample. This was particularly apparent in P-starved roots, where air bubbles seemed to easily become trapped between the dense root hairs (Figure 50B, H).

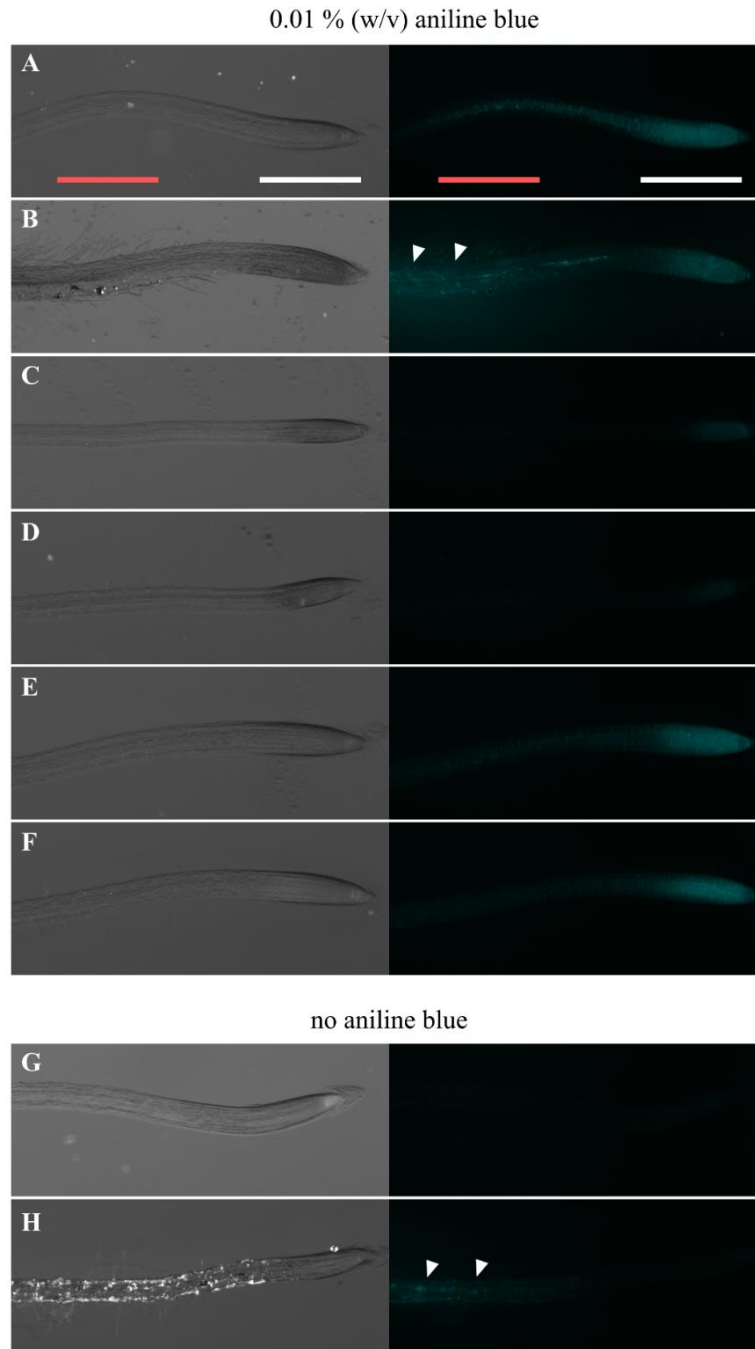
Capturing aniline blue-specific fluorescent emission revealed a strong and distinct pattern of callose deposition in most samples (on the right of Figure 50). As a stereomicroscope was used to image the samples, and thus all cell layers were superimposed per image, localization of callose deposits could only be distinguished with regards to their longitudinal position along the root, but not attributed to specific cell types.

Nutrient-replete roots showed small, but distinct fluorescence emissions, spread out over the apical root tip, and centring more to the stele further up the root (Figure 50A). P-starved, but Fe-replete, root tips showed a signal comparable to nutrient-replete plants (Figure 50B). Strikingly, the fluorescence emission was much lower in roots that were grown without Fe, regardless of whether P was included or excluded from the medium (Figure 50C and D). Some fluorescence could be detected in the apical tips of Fe-starved roots, however few samples showed any emission further up the root (Figure 50C and D). Increasing the free P and Fe levels (Figure 50E), or doubling the Fe concentration in a P-replete background (Figure 50F) led to a distribution of fluorescence emission comparable to nutrient-replete plants.

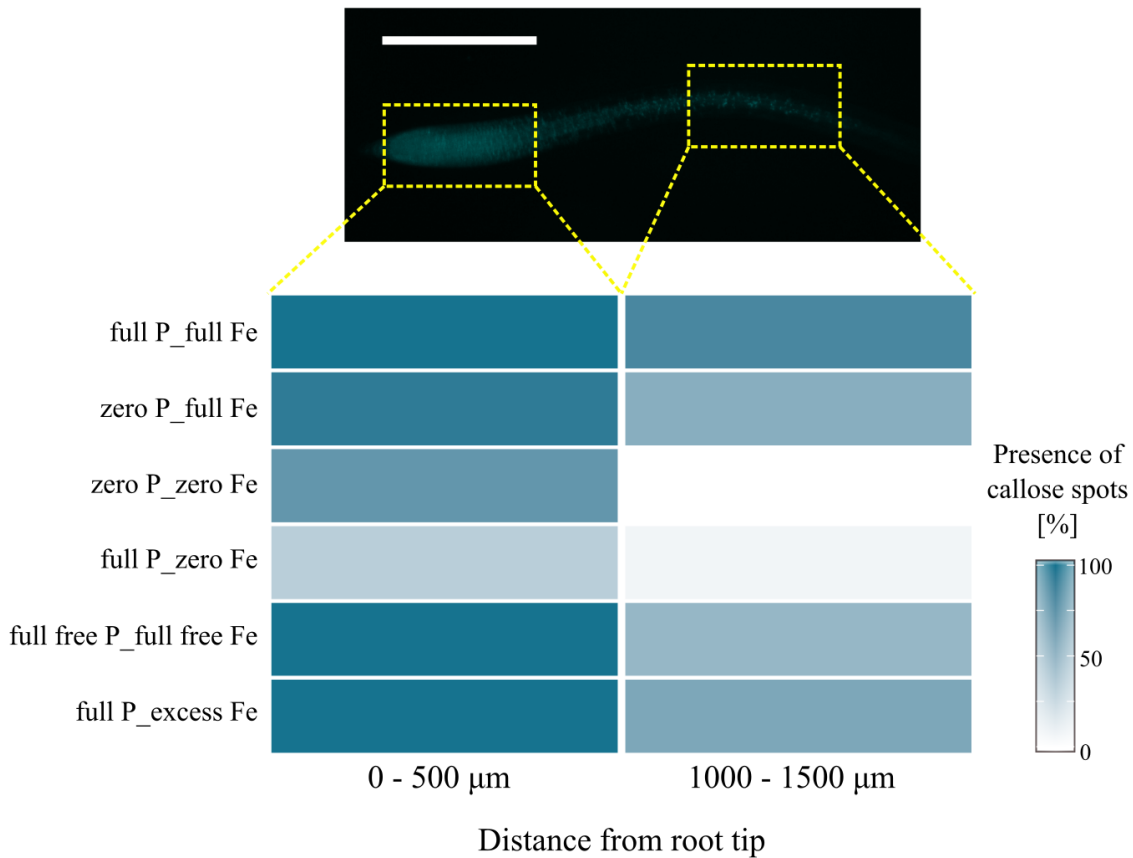
To control for any potential background noise, some roots were subjected to the staining procedure without including the aniline blue dye. None of these control plants showed the distinct fluorescence emissions described above (Figure 50G, H). However, some roots showed a more diffuse fluorescence emission, mostly observed in P-starved roots (annotated by white triangles in Figure 50B for aniline blue stained, and Figure 50H for non-aniline blue stained control root). These diffuse blotches always co-localized with air bubbles, which occurred more often in the root hair dense areas of P-starved roots. Thus, particular care was taken to distinguish between distinct, sharp callose spots, and diffuse background noise blotches.

As callose-specific fluorescence ‘spots’ were small in size, and the employed stereomicroscope limited in resolution, a qualitative approach was taken to analyse the occurrence of callose deposits. Rather than counting individual spots, overall callose presence was scored within regions of the root (callose present = 1, callose not present = 0). This was done to prevent analysis error, whilst being able to distinguish between clear phenotypes. Root regions used for scoring were designed to be comparable to ROS-staining data (Figure 46). Hence, presence or absence of callose spots was scored in the

range of 0 to 500  $\mu\text{m}$  from the root tip, and 1000 to 1500  $\mu\text{m}$  from the root tip (see yellow dashed boxes in root micrograph in Figure 51). A heat map was generated to visualise the average occurrence pattern of callose deposits in roots grown on different P and Fe medium (data from 3 independent trials,  $n = 13 - 16$  individual roots per growth condition, Figure 51). This allowed quantification of the pattern that had been described above: nutrient-replete plants, as well as P-starved plants showed similar levels of callose occurrence, both in the root tip and further up within the stele (Figure 51). The single variable correlating with less callose in the root tip, and almost no callose deposits further up the root, was the availability of Fe in the medium. Both full P<sub>zero</sub> Fe and zero P<sub>zero</sub> Fe roots showed this pattern of low callose occurrence (colour-coded with light blue, Figure 51).



**Figure 50:** Callose distribution in phosphate- and iron-starved primary root tips. *Arabidopsis Col-0* were grown on growth medium with different P and Fe levels: (A, G) full P\_full Fe, (B, H) zero P\_full Fe, (C) zero P\_zero Fe, (D) full P\_zero Fe, (E) full free P\_full free Fe and (F) full P\_excess Fe. Ten- to 11-day old seedlings were stained with 0.01 % (w/v) aniline blue (A-F), or incubation solution without aniline blue as control for any background signal (G-H), for 1.5 hours before bright field (on the left) and UV fluorescence images (on the right) were captured. Aniline blue stains callose depositions. (A) Scale bar: 0.5 mm, white and red scale bar indicate regions scored for callose presence. (B, H) White triangles indicate unspecific background signal. Three independent trials were conducted, representative and false colour-coded images per growth condition are shown.



**Figure 51:** Quantification of callose distribution in phosphate- and iron-starved primary root tips. *Arabidopsis Col-0* were grown on growth medium with different P and Fe levels as labelled above. Ten- to 11-day old seedlings were stained with 0.01 % (w/v) aniline blue for 1.5 hours before UV-emission of the aniline-specific signal was captured using a stereo microscope. Root micrograph (top) indicates regions analysed for presence of distinct callose spots: 0 – 500  $\mu\text{m}$  from the root tip, or 1000 – 1500  $\mu\text{m}$  from the root tip (yellow dashed boxes), scale bar: 0.5 mm. Heat map (bottom) colour-codes percentage of roots scored for presence of callose depositions (darker colour indicates more callose deposition). Three independent trials were conducted, n = 13 – 16 individual roots per growth condition.

## 4.3 Discussion

### 4.3.1 On whole plant level, root tip tissue responds most strongly to eATP

Most studies investigating the  $[Ca^{2+}]_{\text{cyt}}$  response to eATP used whole seedlings as test tissue (Jeter *et al.*, 2004; Tanaka *et al.*, 2010; J. Choi, Tanaka, Cao, *et al.*, 2014; Chen *et al.*, 2017). To dissect the eATP-induced response, true leaves, whole roots or apical root tips (1 cm) of aequorin-expressing *Arabidopsis* were assayed, and the strongest  $[Ca^{2+}]_{\text{cyt}}$  response to eATP was found to originate from the root tip tissue. This confirmed previous findings (Tanaka *et al.*, 2010, who did however not show shoot-derived data). All three types of tissue monitored showed an initial touch response, due to treatment application (Knight *et al.*, 1991). In leaves, the touch response was followed by a delayed and small, but sustained  $[Ca^{2+}]_{\text{cyt}}$  increase. Root tissue on the other hand responded with distinct, multi-phasic modulations of  $[Ca^{2+}]_{\text{cyt}}$ , agreeing with previous studies (Demidchik, Nichols, *et al.*, 2003; Tanaka *et al.*, 2010; J. Choi, Tanaka, Cao, *et al.*, 2014) and findings reported in this thesis. In Chapter 3, (Figure 10 and accompanying analysis) it was found that the initial touch response is a response to mechanical stimulation only, and the subsequent response (peak 1 and peak 2) were specific to eATP treatment. Therefore, to deconstruct the eATP-induced  $[Ca^{2+}]_{\text{cyt}}$  signature further, the root tip tissue was of major importance.

### 4.3.2 On root tip level, eATP triggers distinct $[Ca^{2+}]_{\text{cyt}}$ responses that vary in time and space

It is important to stress the implications of the thus far reported multi-phasic  $[Ca^{2+}]_{\text{cyt}}$  response upon eATP perception. In the aequorin assays, applied eATP solution would in an instant be in direct contact with all (outer) cells of the tissue monitored. However, two temporarily distinct  $[Ca^{2+}]_{\text{cyt}}$  increases occur when monitoring aequorin-expressing root tips, the first increase peaking 10 to 15 seconds after treatment application (= peak 1), the second increase peaking *circa* 35 seconds after treatment application (= peak 2). The difference between peak 1 and peak 2 maxima amounts to approximately 20 to 25 seconds. Both timing and amplitude of response agree with a previous study using excised root tissue (Demidchik, Nichols, *et al.*, 2003). Aequorin allowed a high-throughput assay, resulting in consistent  $[Ca^{2+}]_{\text{cyt}}$  responses. However, aequorin necessitated a prolonged incubation time in coelenterazine-containing solution and excision of sample tissue if a

specific region were to be monitored instead of whole seedlings. Furthermore, the plate reader set-up required injection of treatment solution, triggering a response to mechanical stimulation, which complicated downstream analysis.

The reporter NES-YC3.6 did not necessitate any reconstitution or light-tight photon-counting set-up. Using NES-YC3.6 in a superfusion set-up allowed application of treatment solution without mechanical stimulus (Behera and Kudla, 2013). As a ratiometric reporter, NES-YC3.6 would be expected to be very reliable in conditions that might change reporter protein expression levels, *e.g.* nutrient starvation conditions (P. Koldenkova and Nagai, 2013). However, a sophisticated microscopy set-up is necessary to record the two emitted wavelengths from the YFP and CFP fluorophore separately. Using the NES-YC3.6 reporter in a superfusion set-up, which would envelop the imaged root tissue quickly, a slight bi-phasic response to 1 mM eATP could be observed when quantifying the ratio increases in the first 2.5 mm of apical root tip. However, as it was not measured how quickly the treatment solution would reach the perfusion chamber, 'time point of treatment reaching the sample tissue' to 'maximal response' could not be unambiguously determined as was possible in the aequorin assay. However, the difference between first peak and second peak observed was *circa* 30 to 40 seconds, which is a larger delay than what was observed in aequorin trials, but within the same range. The difference could likely be explained by the different experimental set-ups. In aequorin assays, a double-strength eATP treatment is injected, which only in the well mixes to give the final concentration of 1 mM eATP, implying that some tissue might perceive eATP concentrations above 1 mM. In comparison, the superfusion system would more gently deliver the eATP treatment, already at the final concentration, to the root.

NES-YC3.6 further allowed spatial mapping of the  $[Ca^{2+}]_{cyt}$  increases to root tip regions. The first  $[Ca^{2+}]_{cyt}$  response was localized mainly to the root tip apex, followed by a secondary response further up the root. This was reminiscent of 'peak 1' and 'peak 2' observed using the aequorin reporter. Furthermore, it fully agrees with a recent study which trialled different fluorescent reporter constructs, including YC3.6, and used eATP treatment as a tool to elicit robust  $[Ca^{2+}]_{cyt}$  changes (Waadt *et al.*, 2017). In addition, the data presented here showed that P-starved root tips responded with a similarly strong response in the apical root tip, however little or no ratio change was observed within the elongation zone. This in turn was reminiscent of peak 2's being absent in P-starved aequorin-expressing root tips.



Interestingly, using NES-YC3.6 it could be clearly monitored that the  $[Ca^{2+}]_{\text{cyt}}$  response died down *before* the eATP treatment was switched back to control solution. This was also observed in aequorin experiments, for both standard ATP and non-hydrolyzable ATP (see Chapter 3, Figure 10 and Figure 11). This indicated that the eATP response is terminated not due to ATP hydrolysis, but due to de-sensitization of the molecular players involved. It remains to be determined if this de-sensitization occurs on the level of eATP receptor DORN1, or downstream of DORN1 through altered signal transduction.

For YC3.6 imaging, a sophisticated microscopy set-up is necessary to record the two emitted wavelengths from the YFP and CFP fluorophore separately. To bypass the need for such a set-up, the intensimetric reporter GCaMP3 was trialled. Being based on the conformational  $Ca^{2+}$ -induced changes of *one* fluorophore only, a simple fluorescence stereomicroscopy set-up was sufficient for imaging. In common with NES-YC3.6, GCaMP3 did not require any prior reconstitution step. In contrast to NES-YC3.6, and similar to aequorin, its signal read-out depended on the initial amount of reporter protein, sounding a note of caution when comparing between *e.g.* roots grown on different nutrient conditions. Advantages of GCaMP3 include its photostability and greater dynamic range, *i.e.* strong increase in fluorescence upon  $Ca^{2+}$  binding (Tian *et al.*, 2009; P. Koldenkova and Nagai, 2013; Vincent *et al.*, 2017). Using GCaMP3-expressing plants in a straight-forward set-up (imaging plants on their gel-based growth medium plates), allowed minimal handling and the possibility to manipulate the samples easily. Using the GCaMP3 reporter, and manual treatment application, the application time could be again tracked exactly. Analysing and averaging the response in the first 2.5 mm of apical root tips showed a first  $[Ca^{2+}]_{\text{cyt}}$  peak *circa* 20 seconds after treatment application, followed by a secondary peak in  $[Ca^{2+}]_{\text{cyt}}$  55 to 60 seconds after treatment application. Thus, the two maximal responses were approximately 35 to 40 seconds apart, agreeing with the NES-YC3.6 derived data. GCaMP3 further corroborated NES-YC3.6 in the spatial occurrences of the two responses. P-replete grown root tips responded first in the root tip apex, followed by a response in the elongation zone. P-starved root tips showed a defined response in the root tip, but only a weak response in the elongation zone. As the treatment solutions were not perfused over the sample, but instead applied using a pipette, a drawback of the system was a slight decrease of signal upon treatment application (due to slight shift out of focus).

GCaMP3 had a large response magnitude, as had been reported previously (Tian *et al.*, 2009; Kleist *et al.*, 2017; Vincent *et al.*, 2017), making it visually easy to detect changes

in fluorescence whilst running the experiments. However, this also complicated matters as the change between baseline and eATP-stimulated fluorescence was so great that in order to not oversaturate the camera and bias downstream analysis, exposure time had to be lowered, resulting in overall low baseline fluorescence levels. Considering that recorded raw fluorescence intensities are normalized for pre-stimulus baseline levels (after Vincent *et al.*, 2017), downstream data analysis would be much affected by even slight inaccuracies in baseline levels.

Taken together, all three  $[Ca^{2+}]_{cyt}$  reporters employed (aequorin, NES-YC3.6, GCaMP3) painted similar pictures overall of the immediate root tip response to eATP. All three constructs reported two distinct  $[Ca^{2+}]_{cyt}$  responses to eATP, peaking approximately 20 to 40 seconds apart from each other. Using NES-YC3.6 and GCaMP3, the primary response could be mapped to the apical root tips of *Arabidopsis*, followed by a secondary response in the distal root tip. All constructs reported a dampened  $[Ca^{2+}]_{cyt}$  response in P-starved roots.

#### 4.3.3 The $Ca^{2+}$ reporters paint an overall similar picture, but differ in sensitivity

Aequorin, NES-YC3.6 and GCaMP3 were all ubiquitously expressed in the cytosol of all cell types. For aequorin assays, assayed tissue was slightly larger (1 cm apical root tip for most assays) than the field of view analysed in microscopy-based YC3.6 and GCaMP3 experiments (2.5 mm apical root tip). However, derived data would in all cases report an averaged signal from all monitored tissue, as widefield- and stereomicroscopy would illuminate all tissue layers in view. Hence, none of the reporter set-ups allowed resolution of the  $[Ca^{2+}]_{cyt}$  response down to specific cell types, or intracellular organellar  $Ca^{2+}$  fluxes.

A calibration formula, to convert bioluminescence counts into  $[Ca^{2+}]_{cyt}$ , has been empirically determined for aequorin (Knight *et al.*, 1997). Both NES-YC3.6 and GCaMP3 currently lack a calibrated conversion from raw fluorescence intensities into absolute  $[Ca^{2+}]_{cyt}$  concentrations. Recently, the first *in vivo* calibration of a fluorescent genetically encoded  $Ca^{2+}$  indicator in plants has been reported for another single-wavelength construct, R-GECO1 (Waadt *et al.*, 2017). However, as  $[Ca^{2+}]_{cyt}$  dynamics rather than absolute  $[Ca^{2+}]_{cyt}$  increases only are thought to encode stress-specific information (Whalley *et al.*, 2011; J. Liu *et al.*, 2015; Lenzoni *et al.*, 2017), the NES-

YC3.6 and GCaMP3 employed here are useful tools to follow dynamic fluxes in  $[Ca^{2+}]_{cyt}$ . What *is* known about GCaMP3 and YC3.6 are their varying  $Ca^{2+}$ -binding affinities. GCaMP3 has been described to have a comparably lower affinity for free  $Ca^{2+}$  (with a dissociation constant,  $K_D$ , reported to be in the range of 405 nM to 660 nM, (Tian *et al.*, 2009; Akerboom *et al.*, 2012)) compared to YC3.6 ( $K_D = 250$  nM, (Nagai *et al.*, 2004)). Put differently, this indicates that YC3.6 is more sensitive to smaller changes in  $[Ca^{2+}]_{cyt}$  compared to GCaMP3. Thus, the *presence* of  $[Ca^{2+}]_{cyt}$  fluxes reported by the different reporters can be taken as proof of their existence, the *absence* of reported  $[Ca^{2+}]_{cyt}$  fluxes might however be biased by the reporter's being too insensitive (further discussed below).

#### 4.3.4 The two distinct increases in $[Ca^{2+}]_{cyt}$ can be generated independently of each other – a ‘wave’ component is likely but requires further analysis

Physical separation of apical and distal root tip revealed that generation of an eATP-response still proceed in both apex and distal parts of the root, and that the two  $[Ca^{2+}]_{cyt}$  responses could indeed occur independently of each other, *i.e.* an increase in the elongation zone in response to eATP could occur even though the apical root tip was removed. However, physical manipulation would have induced a serious wounding response. Furthermore, it did not allow testing for any component that might indeed be triggered by local eATP perception and propagate systemically. For salt stress, it had been shown that salt application triggered an increase in  $[Ca^{2+}]_{cyt}$  at the site of treatment application, which rapidly propagated into tissue outside the treated area (W.-G. Choi *et al.*, 2014). However, Choi *et al.* (2014) did not test for eATP's triggering a systemic response, and all published eATP-focussed studies submerged all root tissue in treatment solution (Demidchik, Nichols, *et al.*, 2003; Tanaka *et al.*, 2010; J. Choi, Tanaka, Cao, *et al.*, 2014; Loro *et al.*, 2016). It was therefore unknown if local eATP perception would trigger a systemic ‘ $Ca^{2+}$  wave’. To test any systemic component, easy-to-handle GCaMP3-expressing roots were prepared in such a way that enabled localized treatment application. It was found that local application of 1 mM eATP to either apical root tip or elongation zone triggered a steep, local increase in  $[Ca^{2+}]_{cyt}$ . Most interestingly, a gradual increase in  $[Ca^{2+}]_{cyt}$  was also found to occur in non-treated tissue, quickly traversing a distance of up to 2 mm (maximum distance analysed). Propagation of such a  $Ca^{2+}$  wave has been described to occur rapidly (approximately 400  $\mu$ m per seconds, as quantified by W.-G. Choi *et al.*, 2014), which would be below the temporal resolution of the data presented here (with images taken every 5 seconds). However, the data presented here

would indeed indicate that eATP perception triggered a systemically propagating  $[Ca^{2+}]_{cyt}$  response. As the GCaMP3 reporter employed here is comparably insensitive to subtle changes in  $[Ca^{2+}]_{cyt}$ , the data presented likely underestimate the extent of any systemic  $[Ca^{2+}]_{cyt}$  signal propagation compared to the more sensitive reporter used in the salt-wave study (YCnano-65, (W.-G. Choi *et al.*, 2014)).

Furthermore, local application of treatment is not trivial, if entire root tissue were to be kept in the same conditions. In this thesis, local application of treatment solution was made possible by placing roots across a gap in the underlying agar medium. Previous studies used roots embedded in gelled medium, with a window cut out on top into which treatment solution was administered (W.-G. Choi *et al.*, 2014). In both cases, parameters such as humidity would vary along the root, possibly biasing any downstream response.

Intriguingly, the  $[Ca^{2+}]_{cyt}$  response in the elongation zone always showed a delay in maximal response compared to the response in the apical root tip, even when the apical root tip was removed or treatment was locally applied to the elongation zone. The underlying cause is unclear. It could possibly be explained by a quicker diffusion of eATP treatment solution into PM vicinity in apical root tip cells, compared to a slower diffusion to the more mature cells in distal parts of the root. Another (more enticing) explanation could possibly be different modes of eATP perception in the different root regions. For example, in leaves of *Arabidopsis* it has recently been shown that the eATP receptor DORN1 interacts with, and phosphorylates, NADPH-oxidase RBOHD upon eATP perception (Chen *et al.*, 2017). Whether this interaction also occurs in root cells remains to be determined. However, it is intriguing to hypothesize that DORN1 could interact with different effector proteins, depending on *e.g.* cell type, cell context or developmental stage, leading to differential signalling output. Publicly available protein-protein interaction data (MIND database, (Jones *et al.*, 2014)) revealed few interaction partners of DORN1, as only one uncharacterized leucine-rich repeat receptor kinase, At3g02880, was found to reliably interact with DORN1. It did not report DORN1 interaction with RBOHD. This is unsurprising, as interaction would highly depend on cellular conditions, and be transient. Accordingly, Chen *et al.* (2017) reported that in total 23 peptides were phosphorylated by DORN1 upon eATP perception, one of which was RBOHD (the remaining 22 peptides were not further identified in the study).

#### 4.3.5 The secondary response is linked to ROS signalling, and lost when the root tissue is primed by ROS overload

To determine which other signalling molecules might modulate the  $[Ca^{2+}]_{cyt}$  response to eATP, and possibly explain the difference in timing, the link to ROS was tested. ROS had already been firmly established in signal transduction upon eATP perception (S.-Y. Kim *et al.*, 2006; Song *et al.*, 2006; Demidchik *et al.*, 2009; Sun *et al.*, 2012; Chen *et al.*, 2017). ROS have also been described to increase in P starvation conditions, as well as excess Fe conditions (Shin *et al.*, 2005; Müller *et al.*, 2015; Reyt *et al.*, 2015). Thus, it was of interest to test (i) how initial ROS levels might alter any downstream  $[Ca^{2+}]_{cyt}$  response to eATP, and further, (ii) how manipulation of ROS production and cellular redox status would immediately affect the  $[Ca^{2+}]_{cyt}$  response to eATP.

Staining of intracellular ROS was done using the membrane-permeable dye CM-H<sub>2</sub>DCFDA. This dye has been described to be particularly efficient in detecting ROS production that is reliant on transition metal catalysis (Halliwell and Whiteman, 2004). Furthermore, the dye does not detect specific ROS species, but rather is a general marker for oxidative stress in cells (Halliwell and Whiteman, 2004). Staining roots grown on varying levels of P and Fe showed a striking pattern of ROS distribution dependent on nutrient levels. P-starved, but Fe-replete root tips showed strongly elevated intracellular ROS levels, with a particular ROS hotspot's being localized to the elongation zone (1 – 1.5 mm from the apical root tip). This pattern is in agreement with previous studies using the same ROS stain (Shin *et al.*, 2005; Müller *et al.*, 2015; Balzergue *et al.*, 2017). A previous study further showed that the ROS increase in the elongation zone was mediated through NADPH-oxidase RBOHC (Shin *et al.*, 2005). In the data reported here, excluding Fe as well as P rescued this ROS overload back to lower levels, comparable to what was seen in nutrient-replete root tips (also tested and reported similarly by Balzergue *et al.*, 2017). Fe exclusion only did not alter the ROS levels significantly (not tested in any of the mentioned studies).

Most intriguingly, the ROS overload spatially correlated with the impaired  $[Ca^{2+}]_{cyt}$  response to eATP in P-starved roots, as visualized using the NES-YC3.6 reporter. This indicated that ROS priming, *i.e.* tissue being pre-exposed to high ROS levels, could impair the  $[Ca^{2+}]_{cyt}$  influx upon eATP treatment. To validate this link to ROS signalling further, pharmacological inhibitors known to manipulate cellular redox status (DTT) or

ROS production (DPI) were employed. And indeed, the multiphasic  $[Ca^{2+}]_{cyt}$  response to eATP was sensitive to both DTT as well as DPI.

DTT particularly dampened the secondary response to eATP (peak 2) in nutrient-replete root tips. This corroborates previous findings, where DTT impaired the  $Ca^{2+}$  conductance in root epidermal protoplasts in response to 20  $\mu$ M eATP (Demidchik *et al.*, 2009). On the other hand, the  $[Ca^{2+}]_{cyt}$  response of P-starved root tips (peak 1 only, peak 2 being absent) was not influenced by DTT. However, DTT is known to have unspecific side-effects, such as induction of ER-stress. Another inhibitor, DPI, has been described to have greater target specificity. DPI inhibits NADPH-oxidases, and thus major players involved in ROS production. DPI pre-treatment overall dampened the  $[Ca^{2+}]_{cyt}$  response of nutrient-replete root tips to eATP, affecting both peak 1 and peak 2. This indicates that NADPH-oxidases are involved in the signalling cascade upon eATP perception. This agrees with previous findings, identifying the NADPH-oxidase RBOHC as responsible for eATP-induced ROS production in *Arabidopsis* roots (Demidchik *et al.*, 2009). DPI treatment of P-starved root tips did not further dampen their  $[Ca^{2+}]_{cyt}$  response to eATP.

Overall, eATP perception induces ROS production through NADPH-oxidases, which in turn trigger  $[Ca^{2+}]_{cyt}$  influx. Particularly the secondary response to eATP (peak 2) was impaired if (i) root tissue was already primed with an ROS overload before the eATP pulse was perceived, (ii) ROS production through NADPH-oxidases was inhibited or (iii) tissue was pushed towards a more reduced state. As DPI and DTT did not impair all of the  $[Ca^{2+}]_{cyt}$  response, it is very likely that other signalling molecules / events co-occur and further promote  $[Ca^{2+}]_{cyt}$  influx.

For further discussion of oxidative stress triggered  $[Ca^{2+}]_{cyt}$  responses, please see Chapter 5, section 5.2.

#### 4.3.6 Absolute levels of callose deposition do not correlate with the secondary response to eATP

Callose deposition has recently been reported to occur due to P starvation-induced Fe accumulation, and resulting ROS overload, in *Arabidopsis* primary roots (Müller *et al.*, 2015; Hoehenwarter *et al.*, 2016; Balzergue *et al.*, 2017). Callose deposition was suggested to block plasmodesmata, and as such inhibit symplastic communication, leading to impaired movement of *e.g.* a transcription factor essential for stem cell niche maintenance (SHORT ROOT), and thus suggested to explain the stunted primary root

growth as observed in P-starved roots (Müller *et al.*, 2015). Using aniline blue staining, Müller *et al.* (2015) imaged approximately the first apical 1 mm of *Arabidopsis* roots, and reported P-starvation to increase callose deposition in meristematic cells as well as cortex cells. Further, callose deposition reportedly did *not* occur if Fe as well as P was excluded from the growth medium (Müller *et al.*, 2015).

It was therefore intriguing to hypothesize that increased callose deposition due to P starvation conditions would correlate with a dampened  $[Ca^{2+}]_{cyt}$  response to eATP. To test this hypothesis, *Arabidopsis* roots grown on varying levels of P and Fe were stained for callose deposits using aniline blue dye.

In the data presented here, callose deposits in the apical root tip (first 0.5 mm) were detectable at similar levels and not strongly influenced by P and Fe availability. Callose deposits further up the root (1 – 1.5 mm) were found to *only* be influenced by Fe, but not P availability: roots grown without Fe showed very weak callose staining in the elongation zone. This contradicts the result of Müller *et al.*, who reported increased callose deposition under P starvation. Instead, findings presented here agree with a more recent study, which could not replicate the findings of Müller *et al.*, but instead reported that *meristematic* callose levels were mostly unchanged regardless of P and Fe nutrition (O’Lexy *et al.*, 2018). Furthermore, increasing Fe availability led to higher accumulation of callose in phloem cells in the *elongation zone*, which was reversed when plants were transferred and grown on Fe-free medium (O’Lexy *et al.*, 2018). Again, this would agree with the data presented here: low Fe levels led to low levels of callose accumulation in the elongation zone, increased Fe levels led to higher levels of callose accumulation in the elongation zone, independent of P levels in the growth medium. However, Müller *et al.*, O’Lexy *et al.* and data reported in this thesis used different growth conditions (nutrient composition and length of nutrient starvation differ), which could further explain the observed differences as callose deposition has been described as a dynamic, reversible process (Kauss, 1985; Xu *et al.*, 2017).

Superimposing the pattern of callose deposition with the  $[Ca^{2+}]_{cyt}$  response to eATP with regards to P and Fe nutrition (also see Chapter 3, section 3.2.14 onwards), did not show any correlation between presence of callose and  $[Ca^{2+}]_{cyt}$  response to eATP. For example, P-starved (and Fe-replete) root tips showed a dampened  $[Ca^{2+}]_{cyt}$  response to eATP with peak 2’s being absent, but showed no difference in callose abundance compared to nutrient replete roots. And the other way around, P- and Fe-starved root tips showed a

multi-phasic  $[Ca^{2+}]_{cyt}$  response to eATP, but showed much lower levels of callose deposition in the corresponding root region.

Taking this reasoning a step further, the following could be deduced: if callose deposits did *not* correlate with the observed variations in  $[Ca^{2+}]_{cyt}$  signatures in response to eATP, it could be hypothesized that callose dependent cell-to-cell transmission of  $[Ca^{2+}]_{cyt}$  or other signal in response to eATP does not play a major role in dampening peak 2.

It should be considered that the callose quantification employed in this thesis and in the previous studies (Müller *et al.*, 2015; Balzergue *et al.*, 2017) only very roughly estimated presence or absence of callose. It is however likely that not absolute callose levels, but specific localization of callose might influence cell-to-cell communication. Ideally, callose levels and localization would be manipulated to infer function. This is however technically challenging, as treatments aimed to digest callose or inhibit callose formation quickly led to harmful side effects (Parre and Geitmann, 2005). A callose inhibitor reported recently specifically inhibits callose deposits during cell plate formation, but not stress-induced callose deposits (Park *et al.*, 2014). The recent development of an estradiol-inducible system to overproduce callose in specific tissues is promising (Yadav *et al.*, 2014), and if coupled with a  $[Ca^{2+}]_{cyt}$  reporter, could elegantly dissect if callose deposition were to affect cell-to-cell dependent  $[Ca^{2+}]_{cyt}$  signalling.

#### 4.3.7 Conclusions and Future work

It was confirmed that the root tip region of *Arabidopsis* responds strongly to eATP, more strongly compared to the overall response of leaf and whole root tissue. Dissecting the root tip response to eATP showed two distinct increases in  $[Ca^{2+}]_{cyt}$  which were separated in time and space. The first response could be mainly localized to the apical root tip, the secondary response localized mainly to the elongation zone. The two responses could be generated upon eATP perception even in tissue that was not physically connected, indicating that these two responses can be generated independently of each other. A  $Ca^{2+}$  wave component, propagating into tissue which was not in direct contact with eATP treatment, was observed. Particularly the secondary response in the elongation zone was inhibited if this region showed an initially high ROS load, such as in P-starved root tips. As the secondary response in the elongation zone was also strongly affected by pharmacological manipulation of cellular redox status and ROS generation, this suggests that particularly the secondary response is based on ROS production / signalling upon



eATP perception. Callose deposition did not correlate with the spatially observed variation in  $[Ca^{2+}]_{cyt}$  response. Callose involvement in modulating cell-to-cell communication can however not be dismissed, but necessitates study at higher resolution. In summary, the presented work dissects the spatial origin of eATP induced  $[Ca^{2+}]_{cyt}$  increases in the *Arabidopsis* root tip which has recently also been shown by another group (Waadt *et al.*, 2017). Furthermore, the data presented here indicate that local eATP perception is necessary to evoke independent  $[Ca^{2+}]_{cyt}$  responses in both apical root tip and elongation zone, with  $[Ca^{2+}]_{cyt}$  changes propagating into areas of untreated root tissue. As ubiquitously expressed  $[Ca^{2+}]_{cyt}$  reporters were employed, no deduction with regards to the origin of  $Ca^{2+}$  (apoplast or organellar stores) could be made and requires further research. It further remains to be elucidated why and how cells of the apical root tip and elongation zone showed a response to eATP that is separated in time. To investigate any systemic propagation of eATP-induced  $[Ca^{2+}]_{cyt}$  changes, higher resolution imaging techniques such as confocal microscopy or current advances in light-sheet microscopy (inducing less photodamage on live samples) are to be employed (Costa *et al.*, 2013b; Candeo *et al.*, 2017).

As the multiphasic  $[Ca^{2+}]_{cyt}$  signature upon eATP perception was strongly altered in P starvation conditions, it would be very interesting to quantify downstream consequences. One such marker could be to monitor gene expression changes, and how an altered  $[Ca^{2+}]_{cyt}$  signature results in different expression outputs. This would advance the field of  $Ca^{2+}$  signalling, as well as the field of P starvation research.

## 5 DISCUSSION

### 5.1 Phosphate starvation dampens root tips' $[Ca^{2+}]_{\text{cyt}}$ response to abiotic stresses

Dynamic changes of  $[Ca^{2+}]_{\text{cyt}}$  translate extracellular stresses into intracellular events, and enable plants to perceive environmental fluctuations. In this thesis, P starvation was shown to significantly dampen the  $[Ca^{2+}]_{\text{cyt}}$  response of *Arabidopsis* root tips to mechanical, oxidative, salt and general osmotic stress, as well extracellular nucleotides. Nutrient-replete root tips in all cases showed a pronounced  $[Ca^{2+}]_{\text{cyt}}$  response to these abiotic stresses, which was gradually dampened when decreasing P availability in the growth medium. P resupply (2-3 days) could rescue the dampened  $[Ca^{2+}]_{\text{cyt}}$  response (tested for eATP-elicited response). Most intriguingly, this dampened  $[Ca^{2+}]_{\text{cyt}}$  signature was only observed under P starvation conditions, as severe N starvation did not lead to a dampening of response. This suggests that not nutrient deficiency in general, but P starvation in particular influences the use of  $[Ca^{2+}]_{\text{cyt}}$  as a signal transducer: P starved root tips respond to the world differently.

The versions of the genetically encoded  $Ca^{2+}$  reporters used in this thesis – aequorin, YC3.6 and GCaMP3 - were ubiquitously expressed in the cytosol of all cell types (Knight *et al.*, 1997; Krebs *et al.*, 2012; Vincent *et al.*, 2017). Thus, observed  $[Ca^{2+}]_{\text{cyt}}$  modulations were based on the averaged response of all underlying cells and cell types. Thus, similar kinetics and amplitude of response do not allow the inference of similar underlying mechanisms. For example, salt and osmotic stress were reported to show similar responses when averaging the response from all cell types (aequorin expressed ubiquitously, Knight *et al.*, 1997), but cell-type specific expression showed different

$[Ca^{2+}]_{cyt}$  modulations between osmotic and salt stress perception (Kiegle, C. A. Moore, *et al.*, 2000). What follows is that comparing amplitude and kinetics of two  $[Ca^{2+}]_{cyt}$  signatures does not allow any inference of the underlying mechanisms. Similar  $[Ca^{2+}]_{cyt}$  signatures could be composed of very different individual events, just as two dissimilar  $[Ca^{2+}]_{cyt}$  signatures could very well have all underlying components in common, only activated to a different degree.

What was however striking was that P starvation led to a dampening of the  $[Ca^{2+}]_{cyt}$  response for *all* stresses tested. As this was not specific to a type of stress, it can be deduced that this  $[Ca^{2+}]_{cyt}$  dampening is not effected through changes in the level of stress-specific receptors (exemplified for the eATP receptor DORN1 in more detail below), but rather occurs upstream or downstream of receptor-specific stress recognition. As different stresses induce overlapping signalling components (besides  $Ca^{2+}$  fluxes *e.g.*, ROS and lipid signalling molecules), it could be envisaged that common components might be generally downregulated in an overall P-limited cellular environment. The changes occurring under P limitation are numerous, but a few of the most striking connections are discussed in the following.

For example, it is well studied that P starvation quickly leads to remodelling of membranes, *i.e.*, substituting P-rich phospholipids with glycol- and sulpholipids (Andersson *et al.*, 2005; Tjellstrom *et al.*, 2010; Nakamura, 2013). This did reportedly not alter the membrane resting potential in *Chara* and *Arabidopsis* root hairs (Mimura *et al.*, 1998; Dindas *et al.*, 2018), indicating an unchanged context for the activation of membrane-localized channels. However, it is unknown how membrane re-composition would influence organization of protein domains, and protein-protein or protein-lipid interaction. Both oxidative stress and osmotic stress are known to affect the membrane, the first through ROS-induced peroxidation of membrane lipids, the latter through increased mechanical tension (Rudolphi-Skórska and Sieprawska, 2016). It is however unclear how an altered membrane composition might relay oxidative or osmotic stress differently.

A drop in intracellular nucleotides, particularly ATP, is also well documented to occur under P starvation (Shimano and Ashihara, 2006; Gout *et al.*, 2014). In a breakthrough study, ATP has recently been described as a hydrotrope, *i.e.*, being essential in maintaining protein solubility and preventing protein aggregates (Patel *et al.*, 2017). A decrease in intracellular ATP would strongly influence the cellular milieu to become more viscous (Patel *et al.*, 2017). Considering that the  $Ca^{2+}$  ion has been described to be a rather slow

and short-distance signal (Allbritton *et al.*, 1992), it is intriguing to speculate that a more viscous cellular state would further slow signalling processes and perception by specific binding partners. In addition, intracellular ATP has recently been described to act as a voltage-dependent channel blocker; the higher the ATP concentration the higher the rate of channel closure (De Angeli *et al.*, 2016). Interestingly, the study delineated ATP's action as a pore blocker for ALMT9 (De Angeli *et al.*, 2016). ALMT9 localizes to the tonoplast (De Angeli *et al.*, 2016), but is of the same family as ALMT1, the PM-localized malate transporter recently identified to regulate root growth under P starvation (Balzergue *et al.*, 2017; Mora-Macías *et al.*, 2017). It is intriguing to speculate that a decrease in intracellular ATP would relieve blockage of ALMT's other than ALMT9, and explain a higher efflux of malate under P starvation conditions.

Increased malate efflux has been described as a strategy to solubilize P in the rhizosphere (Raghothama, 1999; Diatloff *et al.*, 2004). This acidification of the rhizosphere also solubilizes Fe, leading to Fe overaccumulation as an effect of P starvation (Grillet *et al.*, 2014; Balzergue *et al.*, 2017). It had been reasoned that some or all of *Arabidopsis* P starvation responses would really be Fe toxicity responses (Ward *et al.*, 2008). However, a number of studies have since shown that mere Fe overload is not sufficient, but an interaction between P starvation and Fe availability necessary to trigger downstream responses such as inhibition of root growth (Ticconi *et al.*, 2009; Müller *et al.*, 2015; Balzergue *et al.*, 2017). In this thesis, altering Fe as well as P availability replicated what had been reported before with regards to primary root growth: P-replete plants grew the longest primary roots if Fe levels were adequate (50  $\mu\text{M}$ ), and shorter roots if the growth medium lacked Fe (0  $\mu\text{M}$ ). Excess Fe (100  $\mu\text{M}$ ) did not affect primary root growth much if P levels were adequate. In a P starvation background however, 50  $\mu\text{M}$  Fe led to severely shorted primary roots, which were rescued back to nutrient-replete root lengths when Fe was lowered (10  $\mu\text{M}$ ) or excluded (0  $\mu\text{M}$ ).

The link between P and Fe is fascinating, as it is unclear why plant roots would not circumvent excess Fe accumulation. P and Fe have been described to form complexes since the dawn of plant evolution, when ancient oceans were Fe-rich and therefore P-scarce (Bjerrum and Canfield, 2002; Poulton, 2017). Thus, it could be speculated that P and Fe uptake co-evolved and are linked. Molecular evidence suggests that P and Fe nutrition are indeed linked (Bournier *et al.*, 2013; Li and Lan, 2015). However, although well-studied in *Arabidopsis*, it is currently unknown if this pattern of Fe accumulation

under P starvation conditions is a common feature across the phylogenetic tree, as ionic data are (surprisingly) scarce.

In this thesis, all experiments quantifying  $[Ca^{2+}]_{cyt}$  dynamics employed the *Arabidopsis* ecotype Col-0. Care should be taken not to extrapolate from one accession to the whole plant field. Col-0 is an ecotype of poorly annotated origin, but it is most closely related to an accession from Western Germany (Nordborg *et al.*, 2005; Somssich, 2018) and likely collected there. However, exact soil conditions of its adaptation history are unknown. Members of the *Brassicaceae* family have been described to be ‘calcicol’ (White and Broadley, 2003). Calcicoles can tolerate high external  $Ca^{2+}$  conditions whilst managing to keep  $[Ca^{2+}]_{cyt}$  levels low (White and Broadley, 2003), suggesting *Arabidopsis* to have a (comparably) well-developed  $Ca^{2+}$  transport and effector machinery. However, it remains to be determined if the P starvation induced dampening of the  $[Ca^{2+}]_{cyt}$  signature reported here is a conserved response, within *Arabidopsis* ecotypes and in more distantly related plant species.

For example, considering natural variation underlying a P starvation response (the elongated root hair phenotype), Col-0 was described to have a rather intermediate – ‘not short, not long’ – root hair phenotype compared to another 165 natural accessions (Stetter *et al.*, 2015). Thus, P use and/or sensing displayed a high genetic diversity. It is intriguing to speculate that accessions displaying a more extreme P starvation root hair phenotype might similarly show an even stronger P-dependent modulation of the  $[Ca^{2+}]_{cyt}$  signature. For example, the accession Cvi-0 showed comparably short root hairs under both P-replete and deplete conditions, whereas *e.g.*, Ler-1, Sha and C24 showed much longer root hairs (Stetter *et al.*, 2015). If not considering the priming stress (P starvation) but rather the acute stress (*e.g.*, oxidative stress mimicked by application of  $H_2O_2$ ), natural variation reported for  $H_2O_2$ -affected root growth should be considered when interpreting Col-0-based data. In a recent study employing 133 natural accessions, Col-0 was found to be relatively tolerant to  $H_2O_2$ , whereas *e.g.*, Ler-1 and Sha were found to be sensitive to  $H_2O_2$  (Sadhukhan *et al.*, 2017).

Besides of considering natural variation within *Arabidopsis*, the real deal would be to extend findings reported here into other plant species. Agriculturally relevant crops such as rice, wheat and tomato have been transformed with  $Ca^{2+}$  reporters such as aequorin and YC3.6 (Moyen *et al.*, 1998; Nagel-Volkman *et al.*, 2009; Behera *et al.*, 2015; Y. Zhang *et al.*, 2015). The transformed plants have been tested for  $[Ca^{2+}]_{cyt}$  response to stresses such as cooling, salt and oxidative stress. However, plants in all cases were grown

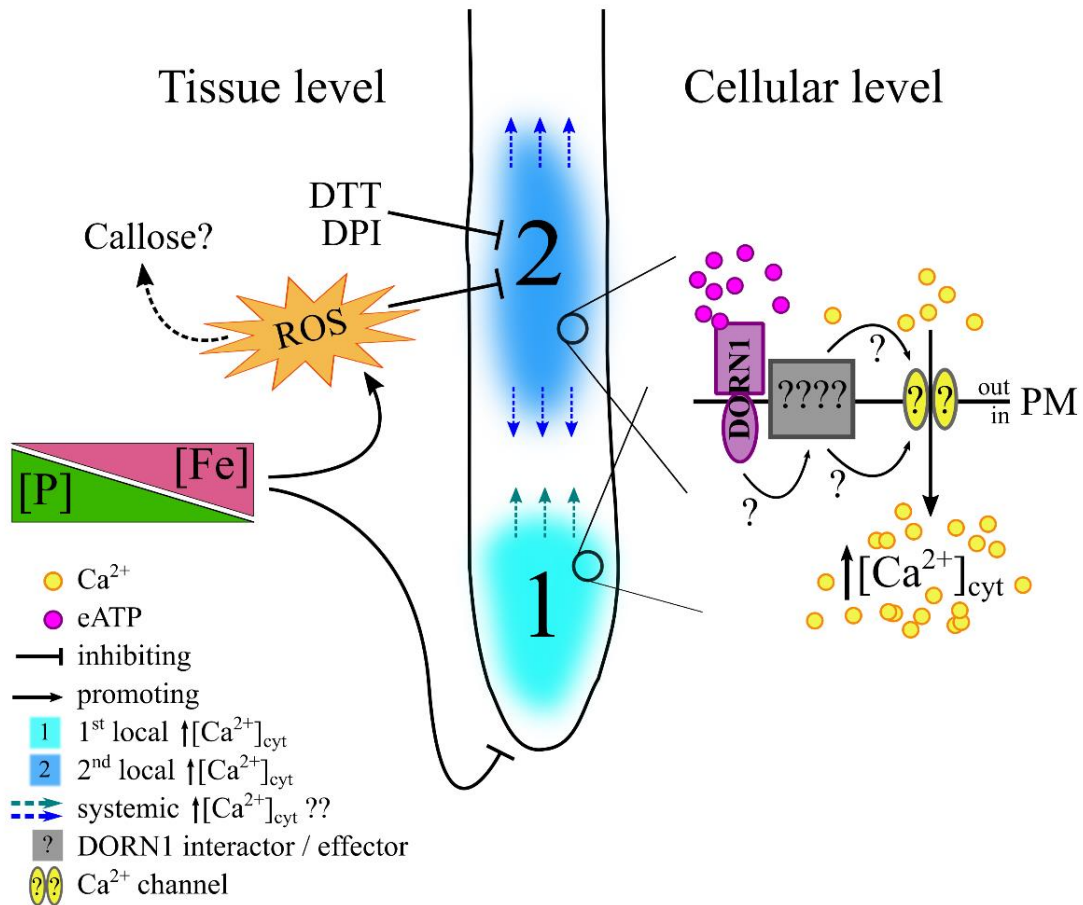
under optimal nutrient conditions, a scenario unlikely to occur in the field. It would be interesting to test how a nutritional priming stress, such as P starvation, would alter the  $[Ca^{2+}]_{cyt}$  signalling output.

## 5.2 Phosphate-starved root tips lack the response to extracellular ATP in the distal root tip

In the data reported here, the most pronounced P starvation-induced changes of the  $[Ca^{2+}]_{cyt}$  signature were observed for the root tips' response to extracellular nucleotides, ATP and ADP. Particularly eATP has been characterized to increase outside cells upon wounding or pathogen attack, and in general to function as a danger signal (Tanaka *et al.*, 2014). eATP has also been shown to increase upon mechanical stress or salt stress (Weerasinghe *et al.*, 2009; Dark *et al.*, 2011), implying eATP at the cross-road of stress perception. eATP perception at the PM has been described to trigger robust  $[Ca^{2+}]_{cyt}$  increases, as well as the generation of other signalling molecules such as ROS (Demidchik, Nichols, *et al.*, 2003; Demidchik *et al.*, 2009; Tanaka *et al.*, 2010). These initial studies employed the ubiquitously expressed  $Ca^{2+}$  reporter aequorin, and eATP treatment was described to trigger multiple distinct  $[Ca^{2+}]_{cyt}$  increases in whole seedlings, and particularly root tissue (Demidchik, Nichols, *et al.*, 2003; Tanaka *et al.*, 2010; J. Choi, Tanaka, Cao, *et al.*, 2014). A schematic overview of signalling events occurring at the root tip as investigated in this thesis is depicted in Figure 52, and will be put into perspective in the following.

In nutrient-replete plants, 1 mM eATP triggered an immediate and strong increase in  $[Ca^{2+}]_{cyt}$  in the apical root tip, followed by a delayed  $[Ca^{2+}]_{cyt}$  response in the elongation zone (delayed by 20 to 40 seconds, depending on  $Ca^{2+}$  reporter and experimental set-up used, responses are numbered '1' and '2' in Figure 52). P starvation led to a dampened  $[Ca^{2+}]_{cyt}$  response to eATP. P starvation also inhibited primary root growth, as had been described before (Svistoonoff *et al.*, 2007; Ticconi *et al.*, 2009; Balzergue *et al.*, 2017). Both  $[Ca^{2+}]_{cyt}$  signature and primary root length were found to depend on Fe availability in a P starvation background. However, primary root length *per se* was not predictive of a dampened  $[Ca^{2+}]_{cyt}$  response, as *e.g.*, P-replete and Fe-starved primary roots were as short as P-starved and Fe-replete roots, but showed the full  $[Ca^{2+}]_{cyt}$  response to eATP. Similarly, N-starved primary roots were as stunted as P-starved primary roots, but still sustained the full  $[Ca^{2+}]_{cyt}$  response to eATP.

Under P starvation, particularly the secondary  $[Ca^{2+}]_{cyt}$  response to eATP in the elongation zone was strongly dampened, whilst the  $[Ca^{2+}]_{cyt}$  response in the apical root tip was comparable to nutrient-replete root tips. Incorporating the finding that P-starved roots still accumulated low, but nonetheless detectable levels of eATP into bathing medium surrounding their roots, it can be deduced that P-starved roots were not in general impaired in sensing eATP, but that the eATP signalling machinery was maintained.



**Figure 52:** Components involved in signalling extracellular ATP in the root tip of *Arabidopsis* as investigated in this thesis. For a description of the model see text. [P] – phosphate levels in the growth medium, [Fe] – iron levels in the growth medium, ROS – reactive oxygen species, DTT – cellular reductant, DPI – NADPH-oxidase inhibitor, DORN1 – plant receptor for eATP, PM – plasma membrane, out – extracellular space, in – intracellular space, dashed lines indicate hypothetical links.

Previous studies reported an increased ROS load of P-starved, and Fe-replete, roots (Müller *et al.*, 2015; Balzergue *et al.*, 2017), which was also observed in this thesis.

Further, the ROS hotspot in the elongation zone correlated with a dampened  $[Ca^{2+}]_{cyt}$  response to eATP. As pharmacological manipulation of cellular redox status as well as inhibition of NADPH-oxidases (using DTT and DPI) particularly dampened the secondary, elongation zone-localized  $[Ca^{2+}]_{cyt}$  response to eATP, this strongly suggests that ROS generation through NADPH-oxidases is necessary to elicit the full  $[Ca^{2+}]_{cyt}$  response. ROS-primed tissue, as observed in P-starved roots, was not able to perceive any newly generated ROS signal. NADPH-oxidases are described as generating extracellular ROS, whereas the ROS hotspot reported here was intracellular (using an intracellular ROS reporter dye). How extracellular ROS generation would influence intracellular ROS status had been puzzling for some time. Only recently this apparent gap has been bridged by the finding that aquaporins could facilitate transport of  $H_2O_2$  across membranes, and thus from extracellular to intracellular space, demonstrated for *Arabidopsis* guard cells and leaf tissue (Tian *et al.*, 2016; Rodrigues *et al.*, 2017). Aquaporin distribution in root membranes has been shown to be dynamic, as both 0.5 mM  $H_2O_2$  as well as 100 mM salt stress were shown to quickly internalize and re-distribute aquaporins (Luu *et al.*, 2012; Wudick *et al.*, 2015). In addition, P starvation has been shown to alter phosphorylation status of many aquaporins (di Pietro *et al.*, 2013). It has further been reported that aquaporins were excluded from sites of auxin maxima (Péret *et al.*, 2012). A recent surge of work showed P starvation-induced root hair outgrowth to rely on increased auxin transport from the root apex to the differentiation zone in both *Arabidopsis* and rice (Bhosale *et al.*, 2018; Giri *et al.*, 2018). Taken together, it is intriguing to speculate that aquaporins might be involved in facilitating (and terminating) any ROS-triggered  $[Ca^{2+}]_{cyt}$  response upon eATP treatment, and be differently regulated and/or distributed under P starvation conditions.

ROS action has further been mentioned as a major component for the wave-like propagation of systemic  $[Ca^{2+}]_{cyt}$  signals (Evans *et al.*, 2016). Data presented here showed that local eATP application to either apical root tip or elongation zone was sufficient to elicit a  $[Ca^{2+}]_{cyt}$  increase in the respective tissue, and as such the first report dissecting local from systemic eATP action. However, some  $[Ca^{2+}]_{cyt}$  increase upon eATP treatment was also observed in tissue outside the treated area (indicated by blue dashed arrows in Figure 52). As these sets of experiments were done using the  $Ca^{2+}$  reporter GCaMP3 which is comparably insensitive to subtle changes in  $[Ca^{2+}]_{cyt}$ , the extent of this propagating  $[Ca^{2+}]_{cyt}$  signal might be underestimated and warrants further research. It does however suggest that eATP triggers a systemic  $[Ca^{2+}]_{cyt}$  response as had been



reported for salt stress in roots (W.-G. Choi *et al.*, 2014) and wounding of leaves (Kiep *et al.*, 2015; Nguyen *et al.*, 2018; Toyota *et al.*, 2018). The moss *Physcomitrella patens* was recently described as propagating a 'Ca<sup>2+</sup> wave' when challenged with osmotic stress, however treatments were not explicitly applied locally but perfused over the whole sample tissue (Storti *et al.*, 2018). As stressed before, care should be taken to discern between systemic signals occurring simply because treatment comes into contact with all (outer) cell layers, or due to true cell-to-cell propagation.

It further remains to be determined if free ATP or rather Mg-complexed ATP (MgATP) were the active binding partner of DORN1. In animals, ATP or MgATP add another level of complexity to eATP receptor activation (Li *et al.*, 2013). In sycamore cell culture, cytosolic ATP has been described to mainly occur complexed with Mg<sup>2+</sup> (Gout *et al.*, 2014). Which ligand actually activates DORN1 is further hampered by so far unsuccessful attempts to crystallize the extracellular domain of *Arabidopsis*' DORN1 (Li *et al.*, 2016). Adding to the conundrum is the fact that ADP elicited a [Ca<sup>2+</sup>]<sub>cyt</sub> signature very similar to what was observed upon eATP treatment (data presented in this thesis, also reported by Demidchik *et al.*, 2003, 2011; J. Choi *et al.*, 2014). P starvation dampened the root tip [Ca<sup>2+</sup>]<sub>cyt</sub> response to ADP similarly to what was observed upon ATP perception. As ATP-hydrolysis was not necessary to trigger the full [Ca<sup>2+</sup>]<sub>cyt</sub> response upon eATP perception, it is unlikely that ADP is perceived merely as part of an ATP-hydrolysis event, but might rather be a discrete signalling molecule (Demidchik *et al.*, 2011). A thorough study by Gout *et al.* (2014) reported cytosolic ADP levels to be tightly regulated and stable over a range of fluctuating conditions, whilst cytosolic ATP levels varied greatly depending on cellular conditions. An alluring hypothesis would be that extracellular ADP could be read-out in a more linear fashion than fluctuating eATP, thus carrying more precise information about *e.g.*, the extent of wounding.

In the data reported in this thesis, all [Ca<sup>2+</sup>]<sub>cyt</sub> influx upon eATP perception was dependent on DORN1, corroborating previous findings of DORN1's being *Arabidopsis*' major eATP receptor (J. Choi, Tanaka, Cao, *et al.*, 2014). DORN1 was not differentially regulated under P starvation (Lin *et al.*, 2011; Lan *et al.*, 2012), or N or K<sup>+</sup> deficiency for that matter (Kellermeier *et al.*, 2014), suggesting DORN1 to be unfazed by nutrient shortages. As mentioned above, this agrees with the idea that the P starvation-induced dampening of the [Ca<sup>2+</sup>]<sub>cyt</sub> signature did not occur on the stress-specific receptor level, and further supports that the eATP signalling machinery is maintained even when P is limited. Besides *Arabidopsis*, removal or addition of eATP have been shown to trigger

responses in a number of plant species, including bean, maize, *Medicago*, poplar, tobacco and tomato (Demidchik, Nichols, *et al.*, 2003; S. a Kim *et al.*, 2006; Sueldo *et al.*, 2010; Sun *et al.*, 2012; Chivasa *et al.*, 2013). However, eATP receptors outside of *Arabidopsis* are currently unknown, as are the molecular identities of K<sup>+</sup> and Ca<sup>2+</sup> channels activated downstream of DORN1 (L. Wang *et al.*, 2018). As discussed in Chapter 4, DORN1 has been shown to interact with NADPH-oxidase RBOHD in leaves (Chen *et al.*, 2017). It is unclear if this interaction also occurs in root cells upon eATP perception (illustrated by grey box in Figure 52). RBOHD would be expressed in root cells (Birnbaum *et al.*, 2003), and was recently found to be involved in systemic propagation of the salt-induced [Ca<sup>2+</sup>]<sub>cyt</sub> wave there (Evans *et al.*, 2016). Besides this, RBOHC has been implied as a major root NADPH-oxidase (Foreman *et al.*, 2003; Shin and Schachtman, 2004; Demidchik *et al.*, 2009). No experimental protein-protein interaction data are available for RBOHC, but *in silico* mining has recently described RBOHC to have unique partners, most of which are annotated to function in root hair development (Kaur and Pati, 2018).

### 5.3 Molecular identities of plasma membrane Ca<sup>2+</sup> channels and transporters remain largely unknown

It is well established, and corroborated by data shown in this thesis, that a range of abiotic stresses induce immediate and distinct [Ca<sup>2+</sup>]<sub>cyt</sub> fluxes. Almost surprisingly, the genetic identity of the Ca<sup>2+</sup> channels underlying these fluxes remains largely elusive (summarized by Wilkins *et al.*, 2016). Even though non-functional versions of individual putative Ca<sup>2+</sup> genes are available for *Arabidopsis*, investigated single mutants mostly showed mild or no Ca<sup>2+</sup> phenotypes, likely due to large gene families and genetic redundancy.

The here reported altered [Ca<sup>2+</sup>]<sub>cyt</sub> signature was shown to be linked to P and Fe availability, as well as ROS homeostasis, and possibly did not depend on stress-specific receptors. What has not been discussed is the potential differential regulation of proteins mediating the actual Ca<sup>2+</sup> fluxes. Considering previous studies reporting the effect of P starvation on *Arabidopsis* roots, the only putative Ca<sup>2+</sup> channel found to be significantly transcriptionally downregulated after 6 hours of P starvation was *CNGC15*, with the effect being lost after 24 hours of P starvation (Lin *et al.*, 2011). No putative Ca<sup>2+</sup> channel was picked up to be downregulated at the protein level (Lan *et al.*, 2012; Hoehenwarter *et al.*, 2016; Z. Q. Wang *et al.*, 2018).

Some putative  $\text{Ca}^{2+}$  channels were found to be significantly *upregulated* at the protein level, including ANN1, GLR2.3 and GLR2.9 (Lan *et al.*, 2012; Hoehenwarter *et al.*, 2016; Z. Q. Wang *et al.*, 2018), which however is counterintuitive if these were to explain a *dampened*  $[\text{Ca}^{2+}]_{\text{cyt}}$  signature. Particularly with regards to channel proteins, which already in low numbers can have a dramatic impact on ion fluxes, global studies reporting protein level changes in homogenized tissue might not detect slight changes in abundance. Particularly for membrane-integral proteins, protein extraction methods would strongly determine the level of resolution (Niu *et al.*, 2018). Besides, rather than absolute levels, post-translational modifications might influence channel sensitivity. A previous study considering phosphorylation patterns under nutrient deficiencies did indeed report changes in phosphorylation pattern as a consequence of P limitation and resupply in 14-day old P-starved *Arabidopsis*, but no putative  $\text{Ca}^{2+}$  channel was detected (Duan *et al.*, 2013).

As part of this PhD project, a library of putative  $\text{Ca}^{2+}$  channel mutants was compiled, with focus on genes annotated to be root expressed and PM localized. These were screened for aberrant root hair growth under P starvation. Root hair growth has been demonstrated to rely on oscillatory PM  $\text{Ca}^{2+}$  fluxes (Bibikova *et al.*, 1997; Very and Davies, 2000; Monshausen *et al.*, 2008; Candeo *et al.*, 2017), and any mutant essential for these  $\text{Ca}^{2+}$  fluxes was hypothesized to be particularly sensitive to conditions that provoked elongated root hair outgrowth. However, none of the mutants tested grew root hairs considerably different to their respective wild type. This could be due to genetic redundancy or  $\text{Ca}^{2+}$  channels that so far have not been annotated and thus escaped the screen. Recently, another group reported CNGC14 to be necessary for root hair growth under nutrient-replete conditions (Zhang *et al.*, 2017). CNGC14 has also been described to govern auxin-induced  $[\text{Ca}^{2+}]_{\text{cyt}}$  elevations (Shih *et al.*, 2015; Dindas *et al.*, 2018). However, root hair growth of the *cngc14* mutant was only impaired when roots grew into the gelled medium (Zhang *et al.*, 2017). This could explain why the *same* mutant line did not show a root hair phenotype in the growth conditions tested in this thesis, and elongated root hairs just as wild type, even under P starvation. Root hair growth appears a highly conditional phenotype, potentially involving not one, but different  $\text{Ca}^{2+}$  channel proteins.

It should also be considered that any dampened  $[\text{Ca}^{2+}]_{\text{cyt}}$  signature could not be the effect of a downregulated  $\text{Ca}^{2+}$  influx channel, but rather a highly upregulated  $\text{Ca}^{2+}$  efflux transporter. As it has recently been reported that determination of the  $[\text{Ca}^{2+}]_{\text{cyt}}$  signal carried information and affected the level of downstream gene expression (Lenzoni *et al.*,

2017), alterations in  $\text{Ca}^{2+}$  efflux proteins would strongly affect the transduced message. Early work in tomato indeed reported a strong upregulation of *LCA1*, a root  $\text{Ca}^{2+}$ -ATPase, under P starvation (Muchhal *et al.*, 1997), which however remained a maverick. In *Arabidopsis*, upregulation of  $\text{Ca}^{2+}$  exchanger3 (*CAX3*), *CAX7* and  $\text{Ca}^{2+}$ -ATPases13 (*ACA13*) were detected on the transcriptional level (Misson *et al.*, 2005; Lin *et al.*, 2011; Kellermeier *et al.*, 2014). However, *CAX3* was not only upregulated by P starvation, but also N and  $\text{K}^+$  imbalances (Kellermeier *et al.*, 2014). Furthermore, the transcriptional upregulation did not translate into higher protein levels, where only a downregulation of *ACA7* and *ACA12* was detected (Lan *et al.*, 2012; Hoehenwarter *et al.*, 2016).

Overall, mining previous studies provided little evidence to draw a strong connection between P starvation responses and  $\text{Ca}^{2+}$  regulating machinery, a ‘ $\text{Ca}^{2+}$  fingerprint’ seems to be absent.

#### 5.4 Linking P and $\text{Ca}^{2+}$ is difficult, and direct links are scarce

P and  $\text{Ca}^{2+}$  have an extraordinary relationship, with  $\text{Ca}^{2+}$ 's being cytotoxic to a P-based metabolism, as P and  $\text{Ca}^{2+}$  easily form tight complexes. In contrast to animals, plants rarely ‘waste’ precious P to complex with  $\text{Ca}^{2+}$  for structural biomineralization purposes. Only recently, the first ever Ca-P complexes were reported in plants, stabilizing trichomes in a variety of plant species including *Arabidopsis* (Ensikat *et al.*, 2016; Mustafa *et al.*, 2018). The mechanism underlying Ca-P formation is unknown (Weigend *et al.*, 2017). Recently it has been shown that plant pathogenic *Pseudomonas* bacteria precipitate Ca-P intra- and extracellularly, and that this process is dependent on virulence genes (Fishman *et al.*, 2018). The authors hypothesize that  $\text{Ca}^{2+}$  precipitation could be a mechanism to disrupt pathogen-induced  $\text{Ca}^{2+}$  signalling necessary for the full plant immune response (Fishman *et al.*, 2018). Taken together, the special relationship between P and  $\text{Ca}^{2+}$  seems to be involved in many scenarios relevant for plant development and physiology.

In the data reported here, the dampened  $[\text{Ca}^{2+}]_{\text{cyt}}$  signature observed under P starvation could indicate a downregulation of the use of  $\text{Ca}^{2+}$  as a signalling ion when P is limited. Little evidence however exists with regards to how this would be regulated through differential  $\text{Ca}^{2+}$  influx or efflux (as discussed above). Besides the  $[\text{Ca}^{2+}]_{\text{cyt}}$  signature's being differentially regulated under P starvation conditions,  $\text{Ca}^{2+}$  could signal P availability. The involvement of  $\text{Ca}^{2+}$  in signalling nutrient availability has been the focus of many recent studies, most prominently for sensing nitrate (Riveras *et al.*, 2015; Liu *et*

*al.*, 2017). The use of  $\text{Ca}^{2+}$  to signal P availability has been hypothesized (Chiou and Lin, 2011; Chien *et al.*, 2018), but so far remains elusive.

Data reported in this thesis did not show modulations of  $[\text{Ca}^{2+}]_{\text{cyt}}$  upon P resupply. However, resolution might be too limited as only ubiquitously expressed aequorin was used to monitor  $[\text{Ca}^{2+}]_{\text{cyt}}$  changes. Particularly the finding that P uptake predominantly occurred during the night and as such seems to be under circadian control (Terabayashi *et al.*, 1991; Yamawaki *et al.*, 2011), is intriguing. As  $[\text{Ca}^{2+}]_{\text{cyt}}$  has also been described to be under circadian control, and most recently to also control circadian rhythms in *Arabidopsis* (Martí Ruiz *et al.*, 2018), it might be a question of monitoring the right time window in which P uptake and  $[\text{Ca}^{2+}]_{\text{cyt}}$  oscillations are linked. Considering any interaction of the P uptake system and putative  $\text{Ca}^{2+}$  channels, only one interaction between a root-expressed P transporter (PHT1;9) and a putative  $\text{Ca}^{2+}$  channel (OSCA2.1) could be found (Jones *et al.*, 2014a). However, OSCA2.1 was found to interact with in total 234 protein partners according to the same database, and is furthermore mainly expressed in guard cells (mined from araport.org).

Downstream read-out of any potential  $[\text{Ca}^{2+}]_{\text{cyt}}$  signal upon P uptake is equally difficult to mine from previous studies. Considering the multitude of proteins potentially involved in  $\text{Ca}^{2+}$ -binding and -recognition (approximately 2 percent of all expressed *Arabidopsis* genes are annotated to be involved in  $\text{Ca}^{2+}$  binding; Vaz Martins *et al.*, 2013) occurrence of some  $\text{Ca}^{2+}$ -binding proteins within studies is likely stochastic. An enriched ‘ $\text{Ca}^{2+}$  fingerprint’ in previous P starvation / resupply studies is missing. Investigating plant species capable of forming mutual symbiosis (which *Arabidopsis* is not capable of), any link between P nutrition and  $\text{Ca}^{2+}$  might be indirect, as  $[\text{Ca}^{2+}]$  oscillations are necessary to establish symbiosis and thus any downstream beneficial P-uptake through associated mycorrhiza (Gutjahr and Paszkowski, 2013; Campos *et al.*, 2018). For example, a recent study reported a CDPK, annotated to be involved in symbiosis signalling, to be consistently upregulated under P starvation in rice, wheat and oat (Z. Q. Wang *et al.*, 2018).

## 5.5 Concluding remarks and future work

This is the first report of P starvation influencing  $[\text{Ca}^{2+}]_{\text{cyt}}$ . As  $[\text{Ca}^{2+}]_{\text{cyt}}$  transduces external into internal signals, any alteration of its use likely affects how plants perceive their environment, even though downstream read-outs do not necessarily correspond

quantitatively. Considering that previous studies mostly aimed at elucidating signalling components in plants grown under optimal, nutrient-replete laboratory conditions, the insight reported here should add to the understanding of how plants cope in less optimal conditions as are occurring in the field. It is intriguing to hypothesize that an altered  $[Ca^{2+}]_{\text{cyt}}$  signature could integrate information of internal nutrient status *and* external stress, potentially adding another layer of complexity to the significance of  $[Ca^{2+}]_{\text{cyt}}$  signatures.

Next steps to take should involve testing if the altered  $[Ca^{2+}]_{\text{cyt}}$  signature under P starvation is conserved across the *Arabidopsis* genus, and translates into other plant species of interest. Moving into plant species that establish mycorrhizal symbiosis will add a layer of complexity to any observed  $Ca^{2+}$  signal in response to P availability, as both symbiotic  $[Ca^{2+}]_{\text{cyt}}$  oscillations and the fungal membrane as another component of P uptake will need to be considered. Furthermore, this thesis focussed on the stress response to abiotic stresses. It remains to be determined if *biotic* stress perception would show a similar, P-starvation dependent regulation of  $[Ca^{2+}]_{\text{cyt}}$  signatures. As eATP has been described to also signal in biotic stress interactions (Tripathi *et al.*, 2017), the dissection of the eATP-induced  $[Ca^{2+}]_{\text{cyt}}$  signature reported here is a first step in elucidating components of biotic stress perception under P starvation.

To elucidate the underlying molecular components, advances in targeted mutagenesis (such as the CRISPR/Cas9 system being developed for *Arabidopsis*, Miki *et al.*, 2018) promise to efficiently circumvent the problem of genetic redundancy posed by large gene families, as found for putative  $Ca^{2+}$  channels. The downstream consequence of the altered  $[Ca^{2+}]_{\text{cyt}}$  signature in response to P starvation remains to be determined. Determining the read-out of transient  $[Ca^{2+}]_{\text{cyt}}$  modulations is often achieved by quantifying gene expression changes, which will gain greatly through increasingly higher tissue resolution. For example, single cell RNAseq is becoming economically and technically feasible in plants (Yuan *et al.*, 2018).

Nutrient deficiencies (or toxicities) are a complex field to investigate, as altering availability of one nutrient likely influences availability of all other nutrients, making causal relationships difficult to dissect. Little attention has been given to any circadian regulation of nutrient uptake, likely due to its being technically challenging. An expanding toolkit of  $Ca^{2+}$  reporters, as well as genetically encoded reporters for pH, intracellular P and ATP (Mukherjee *et al.*, 2015; De Col *et al.*, 2017; Martinière *et al.*, 2018), might greatly enhance our understanding of stress-triggered signalling networks.

## 6 REFERENCES

**Abel S** (2017) ‘Phosphate scouting by root tips’, *Current Opinion in Plant Biology*. Elsevier Ltd, 39, pp. 168–177. doi: 10.1016/j.pbi.2017.04.016.

**Abràmoff MD, Hospitals I, Magalhães PJ and Abràmoff M** (2004) ‘Image Processing with ImageJ’, *Biophotonics International*.

**Akerboom J, Chen T-W, Wardill TJ, Tian L, Marvin JS, Mutlu S, Calderon NC, Esposti F, Borghuis BG, Sun XR, et al.** (2012) ‘Optimization of a GCaMP calcium indicator for neural activity imaging’, *Journal of Neuroscience*, 32, pp. 13819–13840. doi: 10.1523/JNEUROSCI.2601-12.2012.

**Allbritton NL, Meyer T and Stryer L** (1992) ‘Range of messenger action of calcium ion and inositol 1,4,5- trisphosphate’, *Science*, 258, pp. 1812–1815.

**Alonso JM, Stepanova AN, Lisse TJ, Kim CJ, Chen H, Shinn P, Stevenson DK, Zimmerman J, Barajas P, Cheuk R, et al.** (2003) ‘Genome-wide insertional mutagenesis of *Arabidopsis thaliana*’, *Science*, 301, pp. 653–657.

**Andersen TG, Naseer S, Ursache R, Wybouw B, Smet W, De Rybel B, Vermeer JEM and Geldner N** (2018) ‘Diffusible repression of cytokinin signalling produces endodermal symmetry and passage cells’, *Nature*. doi: 10.1038/nature25976.

**Andersson MX, Larsson KE, Tjellström H, Liljenberg C and Sandelius AS** (2005) ‘Phosphate-limited oat: The plasma membrane and the tonoplast as major targets for phospholipid-to-glycolipid replacement and stimulation of phospholipases in the plasma membrane’, *Journal of Biological Chemistry*, 280, pp. 27578–27586. doi: 10.1074/jbc.M503273200.

**De Angeli A, Thomine S and Frachisse JM** (2016) ‘Anion channel blockage by ATP as a means for membranes to perceive the energy status of the cell’, *Molecular Plant*, 9, pp. 320–322. doi: 10.1016/j.molp.2016.01.004.

**Aouini A, Hernould M, Ariizumi T, Matsukura C, Ezura H and Asamizu E** (2012) ‘Overexpression of the tomato glutamate receptor-like genes SIGLR1.1 and SIGLR3.5 hinders Ca<sup>2+</sup> utilization and promotes hypersensitivity to Na<sup>+</sup> and K<sup>+</sup> stresses’, *Plant Biotechnology*, 29, pp. 229–235. doi: 10.5511/plantbiotechnology.12.0213a.

**Arpat AB, Magliano P, Wege S, Rouached H, Stefanovic A and Poirier Y** (2012) ‘Functional expression of PHO1 to the Golgi and trans-Golgi network and its role in export of inorganic phosphate’, *Plant Journal*, 71, pp. 479–491. doi: 10.1111/j.1365-313X.2012.05004.x.

**Aslam R, Williams LE, Bhatti MF and Virk N** (2017) ‘Genome-wide analysis of wheat calcium ATPases and potential role of selected ACAs and ECAs in calcium stress’, *BMC Plant Biology*, 17. doi: 10.1186/s12870-017-1112-5.

**Ayadi A, David P, Arrighi J-F, Chiarenza S, Thibaud M-C, Nussaume L and Marin E** (2015) ‘Reducing the genetic redundancy of *Arabidopsis* PHOSPHATE TRANSPORTER1 transporters to study phosphate uptake and signaling’, *Plant Physiology*, 167, pp. 1511–1526. doi: 10.1104/pp.114.252338.

**Bai H, Murali B, Barber K and Wolverton C** (2013) ‘Low phosphate alters lateral root setpoint angle and gravitropism’, *American Journal of Botany*, 100, pp. 175–182. doi: 10.3732/ajb.1200285.

**Balergue C, Dartevelle T, Godon C, Laugier E, Meisrimler C, Teulon J-M, Creff A, Bissler M, Bouchoud C, Hagège A, et al.** (2017) ‘Low phosphate activates STOP1-ALMT1 to rapidly inhibit root cell elongation’, *Nature Communication*, doi: 10.1038/ncomms15300.

**Barberon M and Geldner N** (2014) ‘Radial transport of nutrients: The plant root as a polarized epithelium’, *Plant Physiology*, 166, pp. 528–537. doi: 10.1104/pp.114.246124.

**Bari R, Pant BD, Stitt M and Golm SP** (2006) ‘PHO2, microRNA399 and PHR1 define a phosphate signaling pathway in plants’, *Plant Physiology*, 141, pp. 988–999. doi: 10.1104/pp.106.079707.988.

**Bates TR and Lynch JP** (1996) ‘Stimulation of root hair elongation in *Arabidopsis thaliana* by low phosphorus availability’, *Plant, Cell & Environment*, 19, pp. 529–538. doi: 10.1111/j.1365-3040.1996.tb00386.x.



- Baxter I, Hosmani PS, Rus A, Lahner B, Borevitz JO, Muthukumar B, Mickelbart M V., Schreiber L, Franke RB and Salt DE** (2009) 'Root suberin forms an extracellular barrier that affects water relations and mineral nutrition in *Arabidopsis*', *PLoS Genetics*, 5. doi: 10.1371/journal.pgen.1000492.
- Becker JD, Takeda S, Borges F, Dolan L and Feijó JA** (2014) 'Transcriptional profiling of *Arabidopsis* root hairs and pollen defines an apical cell growth signature', *BMC Plant Biology*, 14, p. 197. doi: 10.1186/s12870-014-0197-3.
- Behera S, Wang N, Zhang C, Schmitz-Thom I, Strohkamp S, Schültke S, Hashimoto K, Xiong L and Kudla J** (2015) 'Analyses of Ca<sup>2+</sup> dynamics using a ubiquitin-10 promoter-driven Yellow Cameleon 3.6 indicator reveal reliable transgene expression and differences in cytoplasmic Ca<sup>2+</sup> responses in *Arabidopsis* and rice (*Oryza sativa*) roots', *New Phytologist*, 206, pp. 751–760. doi: 10.1111/nph.13250.
- Behera S, Long Y, Schmitz-Thom I, Wang X-P, Zhang C, Li H, Steinhorst L, Manishankar P, Ren X-L, Offenborn JN, et al.** (2017) 'Two spatially and temporally distinct Ca<sup>2+</sup> signals convey *Arabidopsis thaliana* responses to K<sup>+</sup> deficiency', *New Phytologist*, 213, pp. 739–750. doi: 10.1111/nph.14145.
- Behera S and Kudla J** (2013) 'High-Resolution Imaging of Cytoplasmic Ca<sup>2+</sup> Dynamics in *Arabidopsis* Roots', *Cold Spring Harbor Protocols*, 8, pp. 670–674. doi: 10.1101/pdb.prot073023.
- Bender KW, Zielinski RE and Huber SC** (2018) 'Revisiting paradigms of Ca<sup>2+</sup> signaling protein kinase regulation in plants', *Biochemical Journal*, 475, pp. 207–223. doi: 10.1042/BCJ20170022.
- Bhosale R, Giri J, Pandey BK, Giehl RFH, Hartmann A, Traini R, Truskina J, Leftley N, Hanlon M, Swarup K, et al.** (2018) 'A mechanistic framework for auxin dependent *Arabidopsis* root hair elongation to low external phosphate', *Nature Communications*, 9. doi: 10.1038/s41467-018-03851-3.
- Bibikova TN, Zhigilei A and Gilroy S** (1997) 'Root hair growth in *Arabidopsis thaliana* is directed by calcium and an endogenous polarity', *Planta*, 203, pp. 495–505. doi: 10.1007/s004250050219.
- Bielecki RL** (1973) 'Phosphate pools, phosphate transport, and phosphate availability', *Annual Review of Plant Physiology*, 24, pp. 225–252. doi: 10.1146/annurev.pp.24.060173.001301.
- Birnbaum K, Shasha DE, Wang JY, Jung JW, Lambert GM, Galbraith DW and Benfey PN** (2003) 'A gene expression map of the *Arabidopsis* root', *Science*, 302, pp. 1956–1961. doi: 10.1126/science.1090022.

**Bjerrum CJ** and **Canfield DE** (2002) ‘Ocean productivity before about 1.9 Gyr ago limited by phosphorus adsorption onto iron oxides’, *Nature*, 417, pp. 159–162. doi: 10.1038/417159a.

**Bolwell GP** and **Wojtaszek P** (1997) ‘Mechanisms for the generation of reactive oxygen species in plant defence – a broad perspective’, *Physiological and Molecular Plant Pathology*, 51, pp. 347–366. doi: 10.1006/pmpp.1997.0129.

**Bonza MC**, **Loro G**, **Behera S**, **Wong A**, **Kudla J** and **Costa A** (2013) ‘Analyses of Ca<sup>2+</sup> accumulation and dynamics in the endoplasmic reticulum of *Arabidopsis* root cells using a genetically encoded cameleon sensor’, *Plant Physiology*, 163, pp. 1230–41. doi: 10.1104/pp.113.226050.

**Bouguyon E**, **Brun F**, **Meynard D**, **Kubeš M**, **Pervent M**, **Leran S**, **Lacombe B**, **Krouk G**, **Guiderdoni E**, **Zažímalová E**, *et al.* (2015) ‘Multiple mechanisms of nitrate sensing by *Arabidopsis* nitrate transceptor NRT1.1’, *Nature Plants*. doi: 10.1038/nplants.2015.15.

**Bouillon R** and **Suda T** (2014) ‘Vitamin D: calcium and bone homeostasis during evolution’, *BoneKey Reports*, pp. 1–10. doi: 10.1038/bonekey.2013.214.

**Bournier M**, **Tissot N**, **Mari S**, **Boucherez J**, **Lacombe E**, **Briat JF** and **Gaymard F** (2013) ‘*Arabidopsis* ferritin 1 (AtFer1) gene regulation by the phosphate starvation response 1 (AtPHR1) transcription factor reveals a direct molecular link between iron and phosphate homeostasis’, *Journal of Biological Chemistry*, 288, pp. 22670–22680. doi: 10.1074/jbc.M113.482281.

**Boursiac Y** and **Harper JF** (2007) ‘The origin and function of calmodulin regulated Ca<sup>2+</sup> pumps in plants’, *Journal of Bioenergetics and Biomembranes*, 39, pp. 409–414. doi: 10.1007/s10863-007-9104-z.

**Bouwman AF**, **Beusen AHW**, **Lassaletta L**, **Van Apeldoorn DF**, **Van Grinsven HJM**, **Zhang J** and **Ittersum Van MK** (2017) ‘Lessons from temporal and spatial patterns in global use of N and P fertilizer on cropland’, *Scientific Reports*, 7. doi: 10.1038/srep40366.

**Bouwmeester K**, **de Sain M**, **Weide R**, **Gouget A**, **Klamer S**, **Canut H** and **Govers F** (2011) ‘The lectin receptor kinase LecRK-I.9 is a novel Phytophthora resistance component and a potential host target for a RXLR effector’, *PLoS Pathogens*, 7. doi: 10.1371/journal.ppat.1001327.

**Braam J** and **Davis RW** (1990) ‘Rain-, wind-, and touch-induced expression of calmodulin and calmodulin-related genes in *Arabidopsis*’, *Cell*, 60, pp. 357–364.

- Brady SM, Orlando DA, Lee J-Y, Wang JY, Koch J, Dinneny JR, Mace D, Ohler U and Benfey PN** (2007) 'A high-resolution root spatiotemporal map reveals dominant expression patterns', *Science*, 318, pp. 801–806.
- Briat J-F, Rouached H, Tissot N, Gaymard F and Dubos C** (2015) 'Integration of P, S, Fe, and Zn nutrition signals in *Arabidopsis thaliana*: potential involvement of PHOSPHATE STARVATION RESPONSE 1 (PHR1)', *Frontiers in Plant Science*, 6, pp. 1–16. doi: 10.3389/fpls.2015.00290.
- Brini M, Marsault R, Bastianutto C, Alvarez J, Pozzan T and Rizzuto R** (1995) 'Transfected aequorin in the measurement of cytosolic Ca<sup>2+</sup> concentration. A critical evaluation', *Journal of Biological Chemistry*, pp. 9896–9903. doi: 10.1074/jbc.270.17.9896.
- Brini M** (2008) 'Calcium-sensitive photoproteins', *Methods*, 46, pp. 160–166. doi: 10.1016/j.ymeth.2008.09.011.
- Bruex A, Kainkaryam RM, Wieckowski Y, Kang YH, Bernhardt C, Xia Y, Zheng X, Wang JY, Lee MM, Benfey P, et al.** (2012) 'A gene regulatory network for root epidermis cell differentiation in *Arabidopsis*', *PLoS Genetics*, 8. doi: 10.1371/journal.pgen.1002446.
- Burnstock G** (1972) 'Purinergetic nerves', *Pharmacological Reviews*, 24, pp. 509–581. doi: 10.1016/S0140-6736(78)90513-5.
- Bustos R, Castrillo G, Linhares F, Puga MI, Rubio V, Pérez-Pérez J, Solano R, Leyva A and Paz-Ares J** (2010) 'A central regulatory system largely controls transcriptional activation and repression responses to phosphate starvation in *Arabidopsis*', *PLoS Genetics*, 6. doi: 10.1371/journal.pgen.1001102.
- Campos P, Borie F, Cornejo P, Lopez Ruez JA, López-García Á and Seguel A** (2018) 'Phosphorus acquisition efficiency related to root traits: Is mycorrhizal symbiosis a key factor to wheat and barley cropping?', *Frontiers in Plant Science*, 9. doi: 10.3389/FPLS.2018.00752.
- Candéo A, Doccia FG, Valentini G, Bassi A and Costa A** (2017) 'Light Sheet Fluorescence Microscopy quantifies calcium oscillations in root hairs of *Arabidopsis thaliana*', *Plant & Cell Physiology*. doi: 10.1093/pcp/pcx045.
- Capoen W, Sun J, Wysham D, Otegui MS, Venkateshwaran M and Hirsch S** (2011) 'Nuclear membranes control symbiotic calcium signaling of legumes', *PNAS*, 108. doi: 10.1073/pnas.1107912108.

**Cárdenas L, Martínez A, Sánchez F and Quinto C** (2008) 'Fast, transient and specific intracellular ROS changes in living root hair cells responding to Nod factors (NFs)', *Plant Journal*, 56, pp. 802–813. doi: 10.1111/j.1365-313X.2008.03644.x.

**Carmack M and Kelley CJ** (1968) 'Synthesis of optically active Cleland's reagent [( -)-1,4-dithio-L-threitol]', *The Journal of Organic Chemistry*, 33, pp. 2171–2173. doi: 10.1021/jo01269a123.

**Castrillo G, Teixeira PJPL, Paredes SH, Law TF, De Lorenzo L, Feltcher ME, Finkel OM, Breakfield NW, Mieczkowski P, Jones CD, et al.** (2017) 'Root microbiota drive direct integration of phosphate stress and immunity', *Nature*, 543, pp. 513–518. doi: 10.1038/nature21417.

**Cederholm HM and Benfey PN** (2015) 'Distinct sensitivities to phosphate deprivation suggest that RGF peptides play disparate roles in *Arabidopsis thaliana* root development', *New Phytologist*. doi: 10.1111/nph.13405.

**Chaiwongsar S, Strohm AK, Roe JR, Godiwalla RY and Chan CWM** (2009) 'A cyclic nucleotide-gated channel is necessary for optimum fertility in high-calcium environments', *New Phytologist*, 183, pp. 76–87. doi: 10.1111/j.1469-8137.2009.02833.x.

**Chan CWM, Wohlbach DJ, Rodesch MJ and Sussman MR** (2008) 'Transcriptional changes in response to growth of *Arabidopsis* in high external calcium', *FEBS Letters*, 582, pp. 967–976. doi: 10.1016/j.febslet.2008.02.043.

**Charpentier M, Sun J, Martins TV, Radhakrishnan G V, Findlay K, Soumpourou E, Thouin J, Véry A, Sanders D, Morris RJ, et al.** (2016) 'Nuclear-localized cyclic nucleotide-gated channels mediate symbiotic calcium oscillations', *Science*, 352, pp. 1102–1105. doi: 10.1126/science.aae0109.

**Chen C-Y, Wu K and Schmidt W** (2015) 'The histone deacetylase HDA19 controls root cell elongation and modulates a subset of phosphate starvation responses in *Arabidopsis*', *Nature Scientific Reports*, 5. doi: 10.1038/srep15708.

**Chen D, Cao Y, Li H, Kim D, Ahsan N, Thelen J and Stacey G** (2017) 'Extracellular ATP elicits DORN1-mediated RBOHD phosphorylation to regulate stomatal aperture', *Nature Communications*, 8. doi: 10.1038/s41467-017-02340-3.

**Chen J, Jing Y, Zhang X, Li L, Wang P, Zhang S, Zhou H and Wu J** (2016) 'Evolutionary and expression analysis provides evidence for the plant glutamate-like receptors family is involved in woody growth-related function', *Scientific Reports*, 6. doi: 10.1038/srep32013.

- Cheng N-H, Pittman JK, Shigaki T, Lachmansingh J, LeClere S, Lahner B, Salt DE and Hirschi KD** (2005) 'Functional association of *Arabidopsis* CAX1 and CAX3 is required for normal growth and ion homeostasis', *Plant Physiology*, 138, pp. 2048–2060. doi: 10.1104/pp.105.061218.
- Cheng Y, Tian Q and Zhang WH** (2016) 'Glutamate receptors are involved in mitigating effects of amino acids on seed germination of *Arabidopsis thaliana* under salt stress', *Environmental and Experimental Botany*, 130, pp. 68–78. doi: 10.1016/j.envexpbot.2016.05.004.
- Cheong YH, Pandey GK, Grant JJ, Batistic O, Li L, Kim BG, Lee SC, Kudla J and Luan S** (2007) 'Two calcineurin B-like calcium sensors, interacting with protein kinase CIPK23, regulate leaf transpiration and root potassium uptake in *Arabidopsis*', *The Plant Journal*, 52, pp. 223–239. doi: 10.1111/j.1365-313X.2007.03236.x.
- Chien P-S, Chiang C-P, Leong SJ and Chiou T-J** (2018) 'Sensing and signaling of phosphate starvation – from local to long distance', *Plant and Cell Physiology*, 59. doi: 10.1093/pcp/pcy148.
- Chinchilla D, Zipfel C, Robatzek S, Kemmerling B, Nu T, Jones JDG, Felix G and Boller T** (2007) 'A flagellin-induced complex of the receptor FLS2 and BAK1 initiates plant defence', *Nature*, 448, pp. 497–501. doi: 10.1038/nature05999.
- Chiou T-J and Lin S-I** (2011) 'Signaling network in sensing phosphate availability in plants', *Annual Review of Plant Biology*, 62, pp. 185–206. doi: 10.1146/annurev-arplant-042110-103849.
- Chiu JC, Brenner ED, DeSalle R, Nitabach MN, Holmes TC and Coruzzi GM** (2002) 'Phylogenetic and expression analysis of the glutamate-receptor-like gene family in *Arabidopsis thaliana*', *Molecular Biology and Evolution*, 19, pp. 1066–1082.
- Chiu TY, Christiansen K, Moreno I, Lao J, Loqué D, Orellana A, Heazlewood JL, Clark G and Roux SJ** (2012) 'AtAPY1 and AtAPY2 function as golgi-localized nucleoside diphosphatases in *Arabidopsis thaliana*', *Plant and Cell Physiology*, 53, pp. 1913–1925. doi: 10.1093/pcp/pcs131.
- Chivasa S, Ndimba BK, Simon WJ, Lindsey K and Slabas AR** (2013) 'Extracellular ATP functions as an endogenous external metabolite regulating plant cell viability', *The Plant Cell*, 17, pp. 3019–3034. doi: 10.1105/tpc.105.036806.osmotic.
- Choi J, Tanaka K, Liang Y, Cao Y, Lee SY and Stacey G** (2014) 'Extracellular ATP, a danger signal, is recognized by DORN1 in *Arabidopsis*', *The Biochemical Journal*, 463, pp. 429–437. doi: 10.1042/BJ20140666.

- Choi J, Tanaka K, Cao Y, Qi Y, Qiu J, Liang Y, Lee SY and Stacey G** (2014) ‘Identification of a plant receptor for extracellular ATP’, *Science*, 343, pp. 290–294. doi: 10.1126/science.343.6168.290.
- Choi J, Summers W and Paszkowski U** (2018) ‘Mechanisms underlying establishment of arbuscular mycorrhizal symbioses’, *Annual Review of Phytopathology*, 56, pp. 135–160. doi: 10.1146/annurev-phyto-080516.
- Choi W-G, Toyota M, Kim S-H, Hilleary R and Gilroy S** (2014) ‘Salt stress-induced Ca<sup>2+</sup> waves are associated with rapid, long-distance root-to-shoot signaling in plants’, *Proceedings of the National Academy of Sciences*, 111, pp. 6497–6502. doi: 10.1073/pnas.1319955111.
- Clark G, Wu M, Wat N, Onyirimba J, Pham T, Herz N, Ogoti J, Gomez D, Canales AA, Aranda G, et al.** (2010) ‘Both the stimulation and inhibition of root hair growth induced by extracellular nucleotides in *Arabidopsis* are mediated by nitric oxide and reactive oxygen species’, *Plant Molecular Biology*, 74, pp. 423–435. doi: 10.1007/s11103-010-9683-7.
- Clough SJ, Fengler KA, Yu I, Lippok B, Smith RK and Bent AF** (2000) ‘The *Arabidopsis* dnd1 “defense, no death” gene encodes a mutated cyclic nucleotide-gated ion channel’, *Proceedings of the National Academy of Sciences*, 97, pp. 9323–9328. doi: 10.1073/pnas.150005697.
- De Col V, Fuchs P, Nietzel T, Voon CP, Candeo A, Seeliger I, Fricker MD, Grefen C, Bassi A, Lim BL, et al.** (2017) ‘ATP sensing in living plant cells reveals tissue gradients and stress dynamics of energy physiology’, *eLIFE*, pp. 1–53. doi: 10.1101/153163.
- Cole CV, Olsen SR, Scott CO** (1953) ‘The nature of phosphate sorption by calcium carbonate’, *Proceedings of the Soil Science Society of America*, 135, pp. 352-356.
- Conn S and Gilliam M** (2010) ‘Comparative physiology of elemental distributions in plants’, *Annals of Botany*, 105, pp. 1081–1102. doi: 10.1093/aob/mcq027.
- Conn SJ, Gilliam M, Athman A, Schreiber AW, Baumann U, Moller I, Cheng N-H, Stancombe MA, Hirschi KD, Webb AAR, et al.** (2011) ‘Cell-specific vacuolar calcium storage mediated by CAX1 regulates apoplastic calcium concentration, gas exchange, and plant productivity in *Arabidopsis*’, *Plant Cell*, 23, pp. 240–257. doi: 10.1105/tpc.109.072769.
- Cordell D, Drangert JO and White S** (2009) ‘The story of phosphorus: Global food security and food for thought’, *Global Environmental Change*, 19, pp. 292–305. doi: 10.1016/j.gloenvcha.2008.10.009.

- Costa A, Candeo A, Fieramonti L, Valentini G and Bassi A** (2013) ‘Calcium dynamics in root cells of *Arabidopsis thaliana* visualized with selective plane illumination microscopy’, *PloS one*, 8. doi: 10.1371/journal.pone.0075646.
- Costa A, Luoni L, Marrano CA, Hashimoto K, Köster P, Giacometti S, De Michelis MI, Kudla J and Bonza MC** (2017) ‘Ca<sup>2+</sup>-dependent phosphoregulation of the plasma membrane Ca<sup>2+</sup>-ATPase ACA8 modulates stimulus-induced calcium signatures’, *Journal of Experimental Botany*, 68, pp. 3215–3230. doi: 10.1093/jxb/erx162.
- Costa A and Kudla J** (2015) ‘Colorful insights: Advances in imaging drive novel breakthroughs in Ca<sup>2+</sup> signaling’, *Molecular Plant*, 8, pp. 352–355. doi: 10.1016/j.molp.2014.11.020.
- Costa A, Navazio L and Szabo I** (2018) ‘The contribution of organelles to plant intracellular calcium signalling’, *Journal of Experimental Botany*. doi: 10.1093/jxb/ery185/4996169.
- Covington MF and Harmer SL** (2007) ‘The circadian clock regulates auxin signaling and responses in *Arabidopsis*’, *PLoS Biology*, 5, pp. 1773–1784. doi: 10.1371/journal.pbio.0050222.
- Dark A, Demidchik V, Shabala S and Davies JM** (2011) ‘Release of extracellular purines from plant roots and effect on ion fluxes’, *Plant Signaling & Behavior*, 6, pp. 1855–1857. doi: 10.1093/jxb/ern242.5.
- Darwin C and Darwin F** (1880) *The power of movement in plants*. doi: 10.1016/S0169-5347(97)01324-4.
- Datta S, Prescott H and Dolan L** (2015) ‘Intensity of a pulse of RSL4 transcription factor synthesis determines *Arabidopsis* root hair cell size’, *Nature Plants*, 1. doi: 10.1038/nplants.2015.138.
- Davies J** (2014) ‘Annexin-mediated calcium signalling in plants’, *Plants*, 3, pp. 128–140. doi: 10.3390/plants3010128.
- Deal RB and Henikoff S** (2010) ‘A simple method for gene expression and chromatin profiling of individual cell types within a tissue’, *Developmental Cell*, 18, pp. 1030–1040.
- Demidchik V, Bowen HC, Maathuis FJM, Shabala SN, Tester MA, White PJ and Davies JM** (2002) ‘*Arabidopsis thaliana* root non-selective cation channels mediate calcium uptake and are involved in growth’, *The Plant Journal*, 32, pp. 799–808.
- Demidchik V, Shabala SN, Coutts KB, Tester MA and Davies JM** (2003) ‘Free oxygen radicals regulate plasma membrane Ca<sup>2+</sup>- and K<sup>+</sup>-permeable channels in plant root cells’, *Journal of Cell Science*, 116, pp. 81–88. doi: 10.1242/jcs.00201.

**Demidchik V, Nichols C, Oliynyk M, Dark A, Glover BJ and Davies JM** (2003) 'Is ATP a signaling agent in plants?', *Plant Physiology*, 133, pp. 456–461. doi: 10.1104/pp.103.024091.1978.

**Demidchik V, Shang Z, Shin R, Thompson E, Rubio L, Laohavisit A, Mortimer JC, Chivasa S, Slabas AR, Glover BJ, et al.** (2009) 'Plant extracellular ATP signalling by plasma membrane NADPH oxidase and Ca<sup>2+</sup> channels', *Plant Journal*, 58, pp. 903–913. doi: 10.1111/j.1365-313X.2009.03830.x.

**Demidchik V, Shang Z, Shin R, Colaço R, Laohavisit A, Shabala S and Davies JM** (2011) 'Receptor-like activity evoked by extracellular ADP in *Arabidopsis* root epidermal plasma membrane', *Plant Physiology*, 156, pp. 1375–1385. doi: 10.1104/pp.111.174722.

**Demidchik V, Shabala S, Isayenkov S, Cuin TA and Pottosin I** (2018) 'Calcium transport across plant membranes: mechanisms and functions', *New Phytologist*. doi: 10.1111/nph.15266.

**Demidchik V, Shabala SN and Davies JM** (2007) 'Spatial variation in H<sub>2</sub>O<sub>2</sub> response of *Arabidopsis thaliana* root epidermal Ca<sup>2+</sup> flux and plasma membrane Ca<sup>2+</sup> channels', *Plant Journal*, 49, pp. 377–386. doi: 10.1111/j.1365-313X.2006.02971.x.

**Desikan R, Hancock JT, Coffey MJ and Neill SJ** (1996) 'Generation of active oxygen in elicited cells of *Arabidopsis thaliana* is mediated by a NADPH oxidase-like enzyme', *FEBS Letters*, 382, pp. 213–217.

**Devireddy AR, Zandalinas SI, Gómez-Cadenas A, Blumwald E and Mittler R** (2018) 'Coordinating the overall stomatal response of plants: Rapid leaf-to-leaf communication during light stress', *Science Signaling*, 11. doi: 10.1126/scisignal.aam9514.

**Diatloff E, Roberts M, Sanders D and Roberts SK** (2004) 'Characterization of anion channels in the plasma membrane of *Arabidopsis* epidermal root cells and the identification of a citrate-permeable channel induced by phosphate starvation', *Plant Physiology*, 136, pp. 4136–4149. doi: 10.1104/pp.104.046995.

**Dindas J, Scherzer S, Roelfsema MRG, Meyer K Von, Müller HM, Palme K, Dietrich P, Becker D, Bennett MJ and Hedrich R** (2018) 'AUX1-mediated root hair auxin influx governs SCF TIR1/AFP-type Ca<sup>2+</sup> signaling', *Nature Communications*, 9. doi: 10.1038/s41467-018-03582-5.

**Ding JP and Pickard BG** (1993) 'Mechanosensory calcium-selective cation channels in epidermal cells', *The Plant Journal*, 3, pp. 83–110.



- Dodd AN, Jakobsen MK, Baker AJ, Telzerow A, Hou SW, Laplaze L, Barrot L, Scott Poethig R, Haseloff J and Webb AAR** (2006) ‘Time of day modulates low-temperature Ca<sup>2+</sup> signals in *Arabidopsis*’, *Plant Journal*, 48, pp. 962–973. doi: 10.1111/j.1365-313X.2006.02933.x.
- Dodd AN, Kudla J and Sanders D** (2010) ‘The language of calcium signaling’, *Annual review of Plant Biology*, 61, pp. 593–620. doi: 10.1146/annurev-arplant-070109-104628.
- Dong B, Ryan PR, Rengel Z and Delhaize E** (1999) ‘Phosphate uptake in *Arabidopsis thaliana*: Dependence of uptake on the expression of transporter genes and internal phosphate concentrations’, *Plant, Cell and Environment*, 22, pp. 1455–1461. doi: 10.1046/j.1365-3040.1999.00500.x.
- Duan G, Walther D and Schulze WX** (2013) ‘Reconstruction and analysis of nutrient-induced phosphorylation networks in *Arabidopsis thaliana*’, *Frontiers in Plant Science*, 4. doi: 10.3389/fpls.2013.00540.
- Duan K, Yi K, Dang L, Huang H, Wu W and Wu P** (2008) ‘Characterization of a sub-family of *Arabidopsis* genes with the SPX domain reveals their diverse functions in plant tolerance to phosphorus starvation’, *Plant Journal*, 54, pp. 965–975. doi: 10.1111/j.1365-313X.2008.03460.x.
- Dubeaux G, Neveu J, Zelazny E and Vert G** (2018) ‘Metal sensing by the IRT1 transporter-receptor orchestrates its own degradation and plant metal nutrition’, *Molecular Cell*, 69. doi: 10.1016/j.molcel.2018.02.009.
- Duff SM, Moorhead GB, Lefebvre DD and Plaxton WC** (1989) ‘Phosphate starvation inducible “Bypasses” of adenylate and phosphate dependent glycolytic enzymes in *Brassica nigra* suspension cells’, *Plant Physiology*, 90, pp. 1275–1278. doi: 10.1104/pp.90.4.1275.
- Dunlop J and Gardiner S** (1993) ‘Phosphate uptake, proton extrusion and membrane electropotentials of phosphorus-deficient *Trifolium repens* L.’, *Journal of Experimental Botany*, 44, pp. 1801–1808. doi: 10.1093/jxb/44.12.1801.
- Eason WR, Newman EI and Chuba PN** (1991) ‘Specificity of interplant cycling of phosphorus: The role of mycorrhizas’, *Plant and Soil*, 137, pp. 267–274. doi: 10.1007/BF00011205.
- Edel KH and Kudla J** (2015) ‘Increasing complexity and versatility: how the calcium signaling toolkit was shaped during plant land colonization’, *Cell Calcium*, 57, pp. 231–46. doi: 10.1016/j.ceca.2014.10.013.
- Ensikat H-J, Geisler T and Weigend M** (2016) ‘A first report of hydroxylated apatite as structural biomineral in Loasaceae-plants’ teeth against herbivores’, *Scientific Reports*, 6. doi: 10.1038/srep26073.

- Evans MJ, Choi W-G, Gilroy S and Morris RJ** (2016) 'A ROS-assisted calcium wave dependent on AtRBOHD and TPC1 propagates the systemic response to salt stress in *Arabidopsis* roots', *Plant Physiology*, 171, pp. 1771–1784. doi: 10.1104/pp.16.00215.
- Evans NH, McAinsh MR, Hetherington AM and Knight MR** (2005) 'ROS perception in *Arabidopsis thaliana*: The ozone-induced calcium response', *The Plant Journal*, 41, pp. 615–626. doi: 10.1111/j.1365-313X.2004.02325.x.
- Falciatore A, Ribeira D'Alcalà M, Croot P and Bowler C** (2000) 'Perception of environmental signals by a marine diatom', *Science*, 288, pp. 2363–2366. doi: 10.1126/science.288.5475.2363.
- Felle H** (1988) 'Cytoplasmic free calcium in *Riccia fluitans* L. and *Zea mays* L.: Interaction of  $\text{Ca}^{2+}$  and pH?', *Planta*, 176, pp. 248–255.
- Felle HH and Hepler PK** (1997) 'The cytosolic  $\text{Ca}^{2+}$  concentration gradient of *Sinapis alba* root hairs as revealed by  $\text{Ca}^{2+}$ -selective microelectrode tests and Fura-Dextran ratio imaging', *Plant Physiology*, 114, pp. 39–45. doi: 10.1104/pp.124.4.1844.
- Ferguson I and Clarkson D** (1976) 'Simultaneous uptake and translocation of magnesium and calcium in barley (*Hordeum vulgare* L.) roots', *Planta*, 128, pp. 267–269.
- Fernández-García C, Coggins AJ and Powner MW** (2017) 'A chemist's perspective on the role of phosphorus at the origins of life', *Life*, 7. doi: 10.3390/life7030031.
- Fink S** (1991) 'The micromorphological distribution of bound calcium in needles of Norway spruce [*Picea abies* (L.) Karst.]', *New Phytologist*, 119, pp. 33–40. doi: 10.1111/j.1469-8137.1991.tb01005.x.
- Finka A, Cuendet AFH, Maathuis FJM, Saidi Y and Goloubinoff P** (2012) 'Plasma membrane cyclic nucleotide gated calcium channels control land plant thermal sensing and acquired thermotolerance', *The Plant Cell*, 24, pp. 3333–3348. doi: 10.1105/tpc.112.095844.
- Fishman MR, Giglio K, Fay D and Filiatrault MJ** (2018) 'Physiological and genetic characterization of calcium phosphate precipitation by *Pseudomonas* species', *Scientific Reports*, 8. doi: 10.1038/s41598-018-28525-4.
- Foehse D and Jungk A** (1983) 'Influence of phosphate and nitrate supply on root hair formation of rape, spinach and tomato plants', *Plant and Soil*, 74, pp. 359–368. doi: 10.1007/BF02181353.
- Food and Agriculture Organization of the United Nations** (2017) 'The state of food security and nutrition in the world', available at <http://www.fao.org/3/a-I7695e.pdf>.

**Food and Agriculture Organization of the United Nations STAT (FAO STAT)**, available at <http://www.fao.org/faostat/en/>, accessed June 2018.

**Foreman J, Demidchik V, Bothwell JHF, Mylona P, Miedema H, Torresk MA, Linstead P, Costa S, Brownlee C, Jonesk JDG, et al.** (2003) ‘Reactive oxygen species produced by NADPH oxidase regulate plant cell growth’, *Nature*, 422, pp. 442–446.

**Foresi NP, Laxalt AM, Tonón C V, Casalengué CA and Lamattina L** (2007) ‘Extracellular ATP induces nitric oxide production in tomato cell suspensions’, *Plant Physiology*, 145, pp. 589–592. doi: 10.1104/pp.107.106518.

**Franceschi VR and Nakata PA** (2005) ‘Calcium oxalate in plants: Formation and function’, *Annual Review of Plant Biology*, 56, pp. 41–71. doi: 10.1146/annurev.arplant.56.032604.144106.

**Gahoonia TS, Care D and Nielsen NE** (1997) ‘Root hairs and phosphorus acquisition of wheat and barley cultivars’, *Plant and Soil*, 191, pp. 181–188. doi: 10.1023/A:1004270201418.

**Gilbert N** (2009) ‘The disappearing nutrient’, *Nature*, 461, pp. 716–718. doi: 10.1038/461716a.

**Giri J, Bhosale R, Huang G, Pandey BK, Parker H, Zappala S, Yang J, Dievart A, Bureau C, Ljung K, et al.** (2018) ‘Rice auxin influx carrier OsAUX1 facilitates root hair elongation in response to low external phosphate’, *Nature Communications*, 9. doi: 10.1038/s41467-018-03850-4.

**Gobert A, Park G, Amtmann A, Sanders D and Maathuis FJM** (2006) ‘*Arabidopsis thaliana* cyclic nucleotide gated channel 3 forms a non-selective ion transporter involved in germination and cation transport’, *Journal of Experimental Botany*, 57, pp. 791–800. doi: 10.1093/jxb/erj064.

**Gomez-Gomez L and Boller T** (2000) ‘FLS2 : An LRR receptor-like kinase involved in the perception of the bacterial elicitor flagellin in *Arabidopsis*’, *Molecular Cell*, 5, pp. 1003–1011.

**Gonzalez-Fontes A, Navarro-Gochicoa MT, Camacho-Cristobal JJ, Herrera-Rodriguez MB, Quiles-Pando C and Rexach J** (2014) ‘Is Ca<sup>2+</sup> involved in the signal transduction pathway of boron deficiency? New hypotheses for sensing boron deprivation’, *Plant Science*, 217–218, pp. 135–139. doi: 10.1016/j.plantsci.2013.12.011.

**González A, Trebotich J, Vergara E, Medina C, Morales B and Moenne A** (2010) ‘Copper-induced calcium release from ER involves the activation of ryanodine-sensitive and IP3-sensitive channels in *Ulva compressa*’, *Plant Signaling and Behavior*, 5, pp. 1647–1649. doi: 10.1111/j.1365-3040.2010.02169. x.

**Gonzalez E, Solano R, Rubio V, Leyva A and Paz-Ares J** (2005) ‘PHOSPHATE TRANSPORTER TRAFFIC FACILITATOR1 is a plant-specific SEC12-related protein that

enables the endoplasmic reticulum exit of a high-affinity phosphate transporter in *Arabidopsis*', *The Plant Cell*, 17, pp. 3500–3512. doi: 10.1105/tpc.105.036640.

**Gordon-Weeks R, Tong Y, Davies TGE and Leggewie G** (2003) 'Restricted spatial expression of a high-affinity phosphate transporter in potato roots', *Journal of Cell Science*, 116, pp. 3135–3144. doi: 10.1242/jcs.00615.

**Gout E, Rebeille F, Douce R and Bligny R** (2014) 'Interplay of Mg<sup>2+</sup>, ADP, and ATP in the cytosol and mitochondria: Unravelling the role of Mg<sup>2+</sup> in cell respiration', *Proceedings of the National Academy of Sciences*, 111. doi: 10.1073/pnas.1406251111.

**Gout E, Bligny R and Douce R** (1992) 'Regulation of intracellular pH values in higher plant cells', *The Journal of Biological Chemistry*, 267, pp. 13903–13909. doi: 10.1111/j.1600-0587.2010.06669.x.

**Grillet L, Ouerdane L, Flis P, Hoang MTT, Isaure MP, Lobinski R, Curie C and Mari S** (2014) 'Ascorbate efflux as a new strategy for iron reduction and transport in plants', *Journal of Biological Chemistry*, 289, pp. 2515–2525. doi: 10.1074/jbc.M113.514828.

**Gruber BD, Giehl RFH, Friedel S and von Wirén N** (2013a) 'Plasticity of the *Arabidopsis* root system under nutrient deficiencies', *Plant Physiology*, 163, pp. 161–79. doi: 10.1104/pp.113.218453.

**Grynkiewicz G, Poenie M and Tsien RY** (1985) 'A new generation of Ca<sup>2+</sup> indicators with greatly improved fluorescence properties', *Journal of Biological Chemistry*, 260, pp. 3440–3450. doi: 3838314.

**Guo J, Zeng W, Chen Q, Lee C, Chen L, Yang Y, Cang C, Ren D and Jiang Y** (2016) 'Structure of the voltage-gated two-pore channel TPC1 from *Arabidopsis thaliana*', *Nature*, 531, pp. 196–201. doi: 10.1038/nature16446.

**Guo J, Islam MA, Lin H, Ji C, Duan Y, Liu P, Zeng Q, Day B, Kang Z and Guo J** (2018) 'Genome-wide identification of cyclic nucleotide-gated ion channel gene family in wheat and functional analyses of TaCNGC14 and TaCNGC16', *Frontiers in Plant Science*, 9. doi: 10.3389/fpls.2018.00018.

**Gutjahr C and Paszkowski U** (2013) 'Multiple control levels of root system remodeling in arbuscular mycorrhizal symbiosis', *Frontiers in Plant Science*, 4. doi: 10.3389/fpls.2013.00204.

**Haling RE, Brown LK, Bengough a. G, Young IM, Hallett PD, White PJ and George TS** (2013) 'Root hairs improve root penetration, root-soil contact, and phosphorus acquisition in soils

of different strength', *Journal of Experimental Botany*, 64, pp. 3711–3721. doi: 10.1093/jxb/ert200.

**Halliwell B and Whiteman M** (2004) 'Measuring reactive species and oxidative damage in vivo and in cell culture: How should you do it and what do the results mean?', *British Journal of Pharmacology*, 142, pp. 231–255. doi: 10.1038/sj.bjp.0705776.

**Hamburger D, Rezzonico E, Somerville C and Poirier Y** (2002) 'Identification and characterization of the *Arabidopsis PHO1* gene involved in phosphate loading to the xylem', *The Plant Cell*, 14, pp. 889–902. doi: 10.1105/tpc.000745.the.

**Hamilton ES, Jensen GS, Maksaev G, Katims A, Sherp AM and Haswell ES** (2015) 'Mechanosensitive channel MSL8 regulates osmotic forces during pollen hydration and germination', *Science*, 350, pp. 438–41. doi: 10.1126/science.aac6014.

**Hammond JP and White PJ** (2011) 'Sugar signaling in root responses to low phosphorus availability.', *Plant Physiology*, 156, pp. 1033–1040. doi: 10.1104/pp.111.175380.

**Haruta M and Sussman MR** (2012) 'The effect of a genetically reduced plasma membrane protonmotive force on vegetative growth of *Arabidopsis*.', *Plant Physiology*, 158, pp. 1158–71. doi: 10.1104/pp.111.189167.

**Haswell ES, Peyronnet R, Barbier-Brygoo H, Meyerowitz EM and Frachisse J-M** (2008) 'Two MscS homologs provide mechanosensitive channel activities in the *Arabidopsis* root', *Current Biology*, 18, pp. 730–4. doi: 10.1016/j.cub.2008.04.039.

**Haswell ES and Meyerowitz EM** (2006) 'MscS-like proteins control plastid size and shape in *Arabidopsis thaliana*', *Current Biology*, 16. doi: 10.1016/j.cub.2005.11.044.

**Haydon MJ, Bell LJ and Webb AAR** (2011) 'Interactions between plant circadian clocks and solute transport', *Journal of Experimental Botany*, 62, pp. 2333–2348. doi: 10.1093/jxb/err040.

**Haydon MJ, Román Á and Arshad W** (2015) 'Nutrient homeostasis within the plant circadian network', *Frontiers in Plant science*, 6. doi: 10.3389/fpls.2015.00299.

**Hepler PK and Wayne RO** (1985) 'Calcium and plant development', *Annual Review of Plant Physiology*, 36, pp. 397–439. doi: 10.1146/annurev.pp.36.060185.002145.

**Hetherington AM, Gray JE, Leckie CP, McAinsh MR, Ng C, Pical C, Priestley AJ, Staxen I, Webb AAR** (1998) 'The control of specificity in guard cell signal transduction', *Philosophical Transactions of the Royal Society*, 353, pp.1489-1494.

**Hilson P, Allemeersch J, Altmann T, Aubourg S, Avon A, Beynon J, Bhalerao RP, Bitton F, Caboche M, Cannoot B, et al.** (2004) 'Versatile gene-specific sequence tags for *Arabidopsis* functional genomics : Transcript profiling and reverse genetics applications', *Genome Research*, pp. 2176–2189. doi: 10.1101/gr.2544504.

**Hirsch J, Marin E, Floriani M, Chiarenza S, Richaud P, Nussaume L and Thibaud MC** (2006) 'Phosphate deficiency promotes modification of iron distribution in *Arabidopsis* plants', *Biochimie*, 88, pp. 1767–1771. doi: 10.1016/j.biochi.2006.05.007.

**Hirschi KD, Zhen RG, Cunningham KW, Rea P a and Fink GR** (1996) 'CAX1, an H<sup>+</sup>/Ca<sup>2+</sup> antiporter from *Arabidopsis*', *Proceedings of the National Academy of Sciences*, 93, pp. 8782–8786. doi: 10.1073/pnas.93.16.8782.

**Hirschi KD** (2004) 'The calcium conundrum. Both versatile nutrient and specific signal', *Plant Physiology*, 136, pp. 2438–2442. doi: 10.1104/pp.104.046490.

**Hiruma K, Gerlach N, Sacristán S, Nakano RT, Hacquard S, Kracher B, Neumann U, Ramírez D, Bucher M, O'Connell RJ, et al.** (2016) 'Root endophyte *Colletotrichum tofieldiae* confers plant fitness benefits that are phosphate status dependent', *Cell*, 165, pp. 464–474. doi: 10.1016/j.cell.2016.02.028.

**Ho CH, Lin SH, Hu HC and Tsay YF** (2009) 'CHL1 functions as a nitrate sensor in plants', *Cell*, 138, pp. 1184–1194. doi: 10.1016/j.cell.2009.07.004.

**Hodgkin AL and Keynes RD** (1957) 'Movements of labeled calcium in squid giant axons', *The Journal of Physiology*, 138, pp. 253–281. doi: 10.1113/jphysiol.1957.sp005850.

**Hoehenwarter W, Mönchgesang S, Neumann S, Majovsky P, Abel S and Müller J** (2016) 'Comparative expression profiling reveals a role of the root apoplast in local phosphate response', *BMC Plant Biology*, 16. doi: 10.1186/s12870-016-0790-8.

**Horikawa K, Yamada Y, Matsuda T, Kobayashi K, Hashimoto M, Matsu-ura T, Miyawaki A, Michikawa T, Mikoshiba K and Nagai T** (2010) 'Spontaneous network activity visualized by ultrasensitive Ca<sup>2+</sup> indicators, yellow Cameleon-Nano', *Nature Methods*, 7, pp. 729–732. doi: 10.1038/nmeth.1488.

**Hou C, Tian W, Kleist T, He K, Garcia V, Bai F, Hao Y, Luan S and Li L** (2014) 'DUF221 proteins are a family of osmosensitive calcium-permeable cation channels conserved across eukaryotes', *Cell Research*, 24, pp. 632–635. doi: 10.1038/cr.2014.14.

**Hua D, Wang C, He J, Liao H, Duan Y, Zhu Z, Guo Y, Chen Z and Gong Z** (2012) 'A plasma membrane receptor kinase, GHR1, mediates abscisic acid- and hydrogen peroxide-regulated

stomatal movement in *Arabidopsis*', *The Plant Cell*, 24, pp. 2546–2561. doi: 10.1105/tpc.112.100107.

**Huang F, Luo J, Ning T, Cao W, Jin X, Zhao H, Wang Y and Han S** (2017) 'Cytosolic and nucleosolic calcium signaling in response to osmotic and salt stresses are independent of each other in roots of *Arabidopsis* seedlings', *Frontiers in Plant Science*, 8. doi: 10.3389/fpls.2017.01648.

**Huang G, Liang W, Sturrock CJ, Pandey BK, Giri J, Mairhofer S, Wang D, Muller L, Tan H, York LM, et al.** (2018) 'Rice actin binding protein RMD controls crown root angle in response to external phosphate', *Nature Communications*, 9. doi: 10.1038/s41467-018-04710-x.

**Huang L, Shi X, Wang W, Ryu KH and Schiefelbein J** (2017) 'Diversification of root hair development genes in vascular plants', *Plant Physiology*, 174, pp. 1697–1712. doi: 10.1104/pp.17.00374.

**Hunter T** (2012) 'Why nature chose phosphate to modify proteins', *Philosophical Transactions of the Royal Society*, 367, pp. 2513–2516. doi: 10.1098/rstb.2012.0013.

**Inoue H, Kudo T, Kamada H, Kimura M, Yamaguchi I and Hamamoto H** (2005) 'Copper elicits an increase in cytosolic free calcium in cultured tobacco cells', *Plant Physiology and Biochemistry*, 43, pp. 1089–1094. doi: 10.1016/j.plaphy.2005.09.003.

**Jami SK, Clark GB, Ayele BT, Ashe P and Kirti PB** (2012) 'Genome-wide comparative analysis of annexin superfamily in plants', *PLoS ONE*, 7, p. e47801. doi: 10.1371/journal.pone.0047801.

**Janes G, von Wangenheim D, Cowling S, Kerr ID, Band LR, French AP and Bishopp A** (2018) 'Cellular patterning of *Arabidopsis* roots under low phosphate conditions', *Frontiers in Plant Science*, 9. doi: 10.3389/FPLS.2018.00735.

**Jäpelt RB and Jakobsen J** (2013) 'Vitamin D in plants: a review of occurrence, analysis, and biosynthesis.', *Frontiers in Plant Science*, 4. doi: 10.3389/fpls.2013.00136.

**Javot H, Penmetsa RV, Terzaghi N, Cook DR and Harrison MJ** (2007) 'A *Medicago truncatula* phosphate transporter indispensable for the arbuscular mycorrhizal symbiosis', *PNAS*, 104, pp. 1720–1725. doi: 10.1073/pnas.0608136104.

**Jeter CR, Tang W, Henaff E, Butterfield T and Roux SJ** (2004) 'Evidence of a novel cell signaling role for extracellular adenosine triphosphates and diphosphates in *Arabidopsis*', *The Plant Cell*, 16, pp. 2652–2664. doi: 10.1105/tpc.104.023945.include.

**Jia F, Wan X, Zhu W, Sun D, Zheng C, Liu P and Huang J** (2015) ‘Overexpression of mitochondrial phosphate transporter 3 severely hampers plant development through regulating mitochondrial function in *Arabidopsis*’, *PLoS ONE*, 10. doi: 10.1371/journal.pone.0129717.

**Jin Y, Jing W, Zhang Q and Zhang W** (2014) ‘Cyclic nucleotide gated channel 10 negatively regulates salt tolerance by mediating Na<sup>+</sup> transport in *Arabidopsis*’, *Journal of Plant Research*, 128, pp. 211–220. doi: 10.1007/s10265-014-0679-2.

**Johnson CH, Knight MR, Kondo T, Masson P, Sedbrook J, Haley A and Trewavas A** (1995) ‘Circadian oscillations of cytosolic and chloroplastic free calcium in plants’, *Science*, 269, pp. 1863–1865. doi: 10.1126/science.7569925.

**Jones AM, Xuan Y, Xu M, Wang R-S, Ho C-H, Lalonde S, You CH, Sardi MI, Parsa SA, Smith-Valle E, et al.** (2014) ‘Border control—a membrane-linked interactome of *Arabidopsis*’, *Science*, 344, pp. 711–716. doi: 10.1126/science.1251358.

**Jones MA, Raymond MJ and Smirnov N** (2006) ‘Analysis of the root-hair morphogenesis transcriptome reveals the molecular identity of six genes with roles in root-hair development in *Arabidopsis*’, *The Plant Journal*, 45, pp. 83–100. doi: 10.1111/j.1365-3113X.2005.02609.x.

**Kamano S, Kume S, Iida K, Lei KJ, Nakano M, Nakayama Y and Iida H** (2015) ‘Transmembrane topologies of Ca<sup>2+</sup>-permeable mechanosensitive channels MCA1 and MCA2 in *Arabidopsis thaliana*’, *Journal of Biological Chemistry*, 290, pp. 30901–30909. doi: 10.1074/jbc.M115.692574.

**Kanno S, Arrighi JF, Chiarenza S, Bayle V, Berthomé R, Péret B, Javot H, Delannoy E, Marin E, Nakanishi TM, et al.** (2016) ‘A novel role for the root cap in phosphate uptake and homeostasis’, *eLife*, 5. doi: 10.7554/eLife.14577.

**Kanno S, Cuyas L, Javot H, Bligny R, Gout E, Darteville T, Hanchi M, Nakanishi TM, Thibaud MC and Nussaume L** (2016) ‘Performance and limitations of phosphate quantification: Guidelines for plant biologists’, *Plant and Cell Physiology*, 57, pp. 690–706. doi: 10.1093/pcp/pcv208.

**Kapulnik Y, Delaux PM, Resnick N, Mayzlish-Gati E, Wininger S, Bhattacharya C, Séjalon-Delmas N, Combier JP, Bécard G, Belausov E, et al.** (2011) ‘Strigolactones affect lateral root formation and root-hair elongation in *Arabidopsis*’, *Planta*, 233, pp. 209–216. doi: 10.1007/s00425-010-1310-y.

**Kapulnik Y, Resnick N, Mayzlish-Gati E, Kaplan Y, Wininger S, Hershenhorn J and Koltai H** (2011) ‘Strigolactones interact with ethylene and auxin in regulating root-hair elongation in *Arabidopsis*’, *Journal of Experimental Botany*, 62, pp. 2915–2924. doi: 10.1093/jxb/erq464.



- Kaur G** and **Pati PK** (2018) ‘In silico insights on diverse interacting partners and phosphorylation sites of respiratory burst oxidase homolog (Rboh) gene families from *Arabidopsis* and rice’, *BMC Plant Biology*, 18. doi: 10.1186/s12870-018-1378-2.
- Kauss H** (1985) ‘Callose biosynthesis as a  $\text{Ca}^{2+}$ -regulated process and possible relations to the induction of other metabolic changes’, *Journal of Cell Science*, 2, pp. 89–103.
- Kehrer JP** (2000) ‘The Haber – Weiss reaction and mechanisms of toxicity’, *Toxicology*, 149, pp. 43–50.
- Kellermeier F**, **Armengaud P**, **Seditas TJ**, **Danku J**, **Salt DE** and **Amtmann A** (2014) ‘Analysis of the root system architecture of *Arabidopsis* provides a quantitative readout of crosstalk between nutritional signals’, *Plant Cell*, 26, pp. 1480–1496. doi: 10.1105/tpc.113.122101.
- Kendall JM**, **Sala-Newby G**, **Ghalaut V**, **Dormer RL** and **Cambell AK** (1992) ‘Engineering the  $\text{Ca}^{2+}$ -activated photoprotein aequorin with reduced affinity for calcium’, *Biochemical and Biophysical Research Communications*, 187, pp. 1091–1097. doi: 10.1016/0006-291X(92)91309-E.
- Ketelaar T**, **Galway ME**, **Mulder BM** and **Emons a. MC** (2008) ‘Rates of exocytosis and endocytosis in *Arabidopsis* root hairs and pollen tubes’, *Journal of Microscopy*, 231, pp. 265–273. doi: 10.1111/j.1365-2818.2008.02031.x.
- Kiegle E**, **Moore CA**, **Haseloff J**, **Tester MA** and **Knight MR** (2000) ‘Cell-type-specific calcium responses to drought, salt and cold in the *Arabidopsis* root’, *The Plant Journal*, 23, pp. 267–278.
- Kiegle E**, **Moore C**, **Haseloff J**, **Tester M** and **Knight M** (2000) ‘Cell-type specific calcium responses to drought, salt and cold in the *Arabidopsis* root’, *The Plant Journal*, 23, pp. 267–278.
- Kiep V**, **Vadassery J**, **Lattke J**, **Maaß JP**, **Boland W**, **Peiter E** and **Mithöfer A** (2015) ‘Systemic cytosolic  $\text{Ca}^{2+}$  elevation is activated upon wounding and herbivory in *Arabidopsis*’, *New Phytologist*, 207, pp. 996–1004. doi: 10.1111/nph.13493.
- Kim S-Y**, **Sivaguru M** and **Stacey G** (2006) ‘Extracellular ATP in plants. Visualization, localization, and analysis of physiological significance in growth and signaling’, *Plant Physiology*, 142, pp. 984–992. doi: 10.1104/pp.106.085670.
- Kim S a**, **Punshon T**, **Lanzirotti A**, **Li L**, **Alonso JM**, **Ecker JR**, **Kaplan J** and **Guerinot M Lou** (2006) ‘Localization of iron in *Arabidopsis* seed requires the vacuolar membrane transporter VIT1.’, *Science*, 314, pp. 1295–1298. doi: 10.1126/science.1132563.

**Kimbrough JM, Salinas-Mondragon R, Boss WF, Brown CS and Sederoff HW** (2004) ‘The fast and transient transcriptional network of gravity and mechanical stimulation in the *Arabidopsis* root apex’, *Plant Physiology*, 136, pp. 2790–2805. doi: 10.1104/pp.104.044594.

**Kinzel H** (1989) ‘Calcium in the vacuoles and cell walls of plant tissue’, *Flora*, 182, pp. 99–125. doi: 10.1016/S0367-2530(17)30398-5.

**Kleinboelting N, Huep G, Kloetgen A, Viehoveer P and Weisshaar B** (2012) ‘GABI-Kat SimpleSearch: New features of the *Arabidopsis thaliana* T-DNA mutant database’, *Nucleic Acids Research*, 40, pp. 1211–1215. doi: 10.1093/nar/gkr1047.

**Kleist TJ, Cartwright HN, Perera AM, Christianson ML, Lemaux PG and Luan S** (2017) ‘Genetically encoded calcium indicators for fluorescence imaging in the moss *Physcomitrella*: GCaMP3 provides a bright new look’, *Plant Biotechnology Journal*, 15, pp. 1235–1237. doi: 10.1111/pbi.12769.

**Knappe S** (2003) ‘Analysis of the plastidic phosphate translocator gene family in *Arabidopsis* and identification of new phosphate translocator-homologous transporters, classified by their putative substrate-binding site’, *Plant Physiology*, 131, pp. 1178–1190. doi: 10.1104/pp.016519.

**Knight H, Trewavas AJ and Knight MR** (1996) ‘Cold calcium signaling in *Arabidopsis* involves two cellular pools and a change in calcium signature after acclimation’, *Plant Cell*, 8, pp. 489–503. doi: 10.1105/tpc.8.3.489.

**Knight H, Trewavas AJ and Knight MR** (1997) ‘Calcium signalling in *Arabidopsis thaliana* responding to drought and salinity’, *The Plant Journal*, 12, pp. 1067–1078.

**Knight H, Trewavas AJ and Knight MR** (1997) ‘Recombinant aequorin methods for measurement of intracellular calcium in plants’, *Plant Molecular Biology Manual*, pp. 1-22.

**Knight MR, Campbell AK, Smith SM and Trewavas AJ** (1991) ‘Transgenic plant aequorin reports the effects of touch and cold-shock and elicitors on cytoplasmic calcium’, *Nature*, 352, pp. 524–526. doi: 10.1038/352524a0.

**Knight MR, Smith SM and Trewavas a J** (1992) ‘Wind-induced plant motion immediately increases cytosolic calcium’, *Proceedings of the National Academy of Sciences of the United States of America*, 89, pp. 4967–4971. doi: 10.1073/pnas.89.11.4967.

**Knoll AAH** (2003) ‘Biomineralization and evolutionary history’, *Reviews in Mineralogy and Geochemistry*, 54, pp. 329–356. doi: 10.2113/0540329.

- Kobae Y and Hata S** (2010) ‘Dynamics of periarbuscular membranes visualized with a fluorescent phosphate transporter in arbuscular mycorrhizal roots of rice’, *Plant and Cell Physiology*, 51, pp. 341–353. doi: 10.1093/pcp/pcq013.
- Kobayashi NI, Iwata N, Saito T, Suzuki H, Iwata R, Tanoi K and Nakanishi TM** (2013) ‘Different magnesium uptake and transport activity along the rice root axis revealed by  $^{28}\text{Mg}$  tracer experiments’, *Soil Science and Plant Nutrition*, 59, pp. 149–155. doi: 10.1080/00380768.2012.751554.
- Kochian LV** (2012) ‘Rooting for more phosphorus’, *Nature*, 488, pp. 466–467.
- Kohlen C, Merkle T and Neuhaus G** (1999) ‘Characterisation of a novel gene family of putative cyclic nucleotide- and calmodulin-regulated ion channels in *Arabidopsis thaliana*’, *Plant Journal*, 18, pp. 97–104.
- Kohlen W, Charnikhova T, Liu Q, Bours R, Domagalska MA, Beguerie S, Verstappen F, Leyser O, Bouwmeester H and Ruyter-Spira C** (2011) ‘Strigolactones are transported through the xylem and play a key role in shoot architectural response to phosphate deficiency in nonarbuscular mycorrhizal host *Arabidopsis*.’, *Plant Physiology*, 155, pp. 974–987. doi: 10.1104/pp.110.164640.
- Kong D, Hu H-C, Okuma E, Lee Y, Lee HS, Munemasa S, Cho D, Ju C, Pedoeim L, Rodriguez B, et al.** (2016) ‘L-Met activates *Arabidopsis* GLR  $\text{Ca}^{2+}$  channels upstream of ROS production and regulates stomatal movement’, *Cell Reports*, 17, pp. 2553–2561. doi: 10.1016/j.celrep.2016.11.015.
- Koshiba T, Kobayashi M, Ishihara A and Matoh T** (2010) ‘Boron nutrition of cultured Tobacco BY-2 Cells. VI. Calcium is involved in early responses to Boron deprivation’, *Plant and Cell Physiology*, 51, pp. 323–327. doi: 10.1093/pcp/pcp179.
- Krebs M, Held K, Binder A, Hashimoto K, Den Herder G, Parniske M, Kudla J and Schumacher K** (2012) ‘FRET-based genetically encoded sensors allow high-resolution live cell imaging of  $\text{Ca}^{2+}$  dynamics’, *Plant Journal*, 69, pp. 181–192. doi: 10.1111/j.1365-313X.2011.04780.x.
- Kung C, Martinac B and Sukharev S** (2010) ‘Mechanosensitive channels in microbes.’, *Annual Review of Microbiology*, 64, pp. 313–29. doi: 10.1146/annurev.micro.112408.134106.
- Kurusu T, Yamanaka T, Nakano M, Takiguchi A, Ogasawara Y, Hayashi T, Iida K, Hanamata S, Shinozaki K, Iida H, et al.** (2012) ‘Involvement of the putative  $\text{Ca}^{2+}$ -permeable mechanosensitive channels, NtMCA1 and NtMCA2, in  $\text{Ca}^{2+}$  uptake,  $\text{Ca}^{2+}$ -dependent cell

proliferation and mechanical stress-induced gene expression in tobacco (*Nicotiana tabacum*) BY-2 cells', *Journal of Plant Research*, 125, pp. 555–568. doi: 10.1007/s10265-011-0462-6.

**Kurusu T, Kuchitsu K, Nakano M, Nakayama Y and Iida H** (2013) 'Plant mechanosensing and Ca<sup>2+</sup> transport', *Trends in Plant Science*, 18, pp. 227–233. doi: 10.1016/j.tplants.2012.12.002.

**Kurusu T, Nishikawa D and Yamazaki Y** (2012) 'Plasma membrane protein OsMCA1 is involved in regulation of hypo-osmotic shock-induced Ca<sup>2+</sup> influx and modulates generation of reactive oxygen species in cultured rice', *BMC Plant Biology*, 12. doi: 10.1186/1471-2229-12-11.

**Kwaaitaal M, Huisman R, Maintz J, Reinstädler A and Panstruga R** (2011) 'Ionotropic glutamate receptor (iGluR)-like channels mediate MAMP-induced calcium influx in *Arabidopsis thaliana*', *Biochemical Journal*, 440, pp. 355–373. doi: 10.1042/BJ20111112.

**Lam H-M, Chiu J, Hsieh M-H, Meisel L, Oliveira IC, Shin M and Coruzzi G** (1998) 'Glutamate-receptor genes in plants', *Nature*, 396, pp. 125–126. doi: 10.1038/24066.

**Lambers H, Martinoia E and Renton M** (2015) 'Plant adaptations to severely phosphorus-impooverished soils', *Current Opinion in Plant Biology*, 25, pp. 23–31. doi: 10.1016/j.pbi.2015.04.002.

**Lan P, Li W, Lin W-D, Santi S and Schmidt W** (2013) 'Mapping gene activity of *Arabidopsis* root hairs', *Genome Biology*, 14. doi: 10.1186/gb-2013-14-6-r67.

**Lan P, Li W and Schmidt W** (2012) 'Complementary proteome and transcriptome profiling in phosphate-deficient *Arabidopsis* roots reveals multiple levels of gene regulation', *Molecular & Cellular Proteomics*, 11, pp. 1156–1166. doi: 10.1074/mcp.M112.020461.

**Laohavisit A, Mortimer JC, Demidchik V, Coxon KM, Stancombe MA, Macpherson N, Brownlee C, Hofmann A, Webb AAR, Miedema H, et al.** (2009) '*Zea mays* annexins modulate cytosolic free Ca<sup>2+</sup> and generate a Ca<sup>2+</sup>-permeable conductance', *The Plant Cell*, 21, pp. 479–493. doi: 10.1105/tpc.108.059550.

**Laohavisit A, Shang Z, Rubio L, Cubin TA, Very A-A, Wang A, Mortimer JC, Macpherson N, Coxon KM, Battey NH, et al.** (2012) '*Arabidopsis* Annexin1 mediates the radical-activated plasma membrane Ca<sup>2+</sup> - and K<sup>+</sup>-permeable conductance in root cells', *Plant Cell*, 24, pp. 1522–1533. doi: 10.1105/tpc.112.097881.

**Laohavisit A, Richards SL, Shabala L, Chen C, Colaco RDDR, Swarbreck SM, Shaw E, Dark A, Shabala S, Shang Z, et al.** (2013) 'Salinity-induced calcium signaling and root

adaptation in *Arabidopsis* require the calcium regulatory protein annexin 1', *Plant Physiology*, 163, pp. 253–262. doi: 10.1104/pp.113.217810.

**Lee CP, Maksaev G, Jensen GS, Murcha MW, Wilson ME, Fricker M, Hell R, Haswell ES, Millar AH and Sweetlove L** (2016) 'MSL1 is a mechanosensitive ion channel that dissipates mitochondrial membrane potential and maintains redox homeostasis in mitochondria during abiotic stress', *Plant Journal*, 88. doi: 10.1016/j.bbi.2015.08.015.Chronic.

**Lee SK, Eom JS, Voll LM, Prasch CM, Park Y II, Hahn TR, Ha SH, An G and Jeon JS** (2014) 'Analysis of a triose phosphate/phosphate translocator-deficient mutant reveals a limited capacity for starch synthesis in rice leaves', *Molecular Plant*, 7, pp. 1705–1708. doi: 10.1093/mp/ssu082.

**Legati A, Giovannini D, Nicolas G, López-Sánchez U, Quintáns B, Oliveira JRM, Sears RL, Ramos EM, Spiteri E, Sobrido MJ, et al.** (2015) 'Mutations in XPR1 cause primary familial brain calcification associated with altered phosphate export', *Nature Genetics*, 47, pp. 579–581. doi: 10.1038/ng.3289.

**Legué V, Blancaflor E, Wymer C, Perbal C, Fantin D, Cilroy S, Pierre U, Jussieu P, Cedex P and France VL** (1997) 'Cytoplasmic free  $Ca^{2+}$  in *Arabidopsis* roots changes in response to touch but not gravity', *Plant Physiology*, 114, pp. 789–800.

**Legué V, Blancaflor E, Wymer C, Perbal G, Fantin D and Gilroy S** (1997) 'Cytoplasmic free  $Ca^{2+}$  in *Arabidopsis* roots changes in response to touch but not gravity', *Plant Physiology*, 114, pp. 789–800. doi: 10.1104/pp.114.3.789.

**Leng Q, Mercier RW, Yao W and Berkowitz GA** (1999) 'Cloning and first functional characterization of a plant cyclic nucleotide-gated cation channel', *Plant Physiology*, 121, pp. 753–761.

**Lenzoni G, Liu J and Knight MR** (2017) 'Predicting plant immunity gene expression by identifying the decoding mechanism of calcium signatures', *New Phytologist*. doi: 10.1111/nph.14924.

**Lew RR and Dearnaley JDW** (2000) 'Extracellular nucleotide effects on the electrical properties of growing *Arabidopsis thaliana* root hairs', *Plant Science*, 153. doi: 10.1016/S0168-9452(99)00242-3.

**Li B, Kamiya T, Kalmbach L, Yamagami M, Yamaguchi K, Shigenobu S, Sawa S, Danku JMC, Salt DE, Geldner N, et al.** (2017) 'Role of LOTR1 in nutrient transport through organization of spatial distribution of root endodermal barriers', *Current Biology*, 27, pp. 758–765. doi: 10.1016/j.cub.2017.01.030.

**Li J, Long Y, Qi G-N, Li J, Xu Z-J, Wu W-H and Wang Y** (2014) ‘The Os-AKT1 channel is critical for K<sup>+</sup> uptake in rice roots and is modulated by the rice CBL1-CIPK23 complex’, *The Plant Cell*, 26, pp. 3387–3402. doi: 10.1105/tpc.114.123455.

**Li M, Silberberg SD and Swartz KJ** (2013) ‘Subtype-specific control of P2X receptor channel signaling by ATP and Mg<sup>2+</sup>’, *Proceedings of the National Academy of Sciences*, 110. doi: 10.1073/pnas.1308088110.

**Li W and Lan P** (2015) ‘Re-analysis of RNA-seq transcriptome data reveals new aspects of gene activity in *Arabidopsis* root hairs’, *Frontiers in Plant Science*, 6. doi: 10.3389/fpls.2015.00421.

**Li Y, Yuan F, Wen Z, Li Y, Wang F, Zhu T, Zhuo W, Jin X, Wang Y, Zhao H, et al.** (2015) ‘Genome-wide survey and expression analysis of the OSCA gene family in rice’, *BMC Plant Biology*, 15. doi: 10.1186/s12870-015-0653-8.

**Li Z, Chakraborty S and Xu G** (2016) ‘X-ray crystallographic studies of the extracellular domain of the first plant ATP receptor, DORN1, and the orthologous protein from *Camelina sativa*’, *Structural Biology Communications*, 72, pp. 782–787. doi: 10.1107/S2053230X16014278.

**Lim MH, Wu J, Yao J, Gallardo IF, Dugger JW, Webb LJ, Huang J, Salmi ML, Song J, Clark G, et al.** (2014) ‘Apyrase suppression raises extracellular ATP levels and induces gene expression and cell wall changes characteristic of stress responses’, *Plant Physiology*, 164, pp. 2054–2067. doi: 10.1104/pp.113.233429.

**Lin W-D, Liao Y-Y, Yang TJW, Pan C-Y, Buckhout TJ and Schmidt W** (2011) ‘Coexpression-based clustering of *Arabidopsis* root genes predicts functional modules in early phosphate deficiency signaling’, *Plant Physiology*, 155, pp. 1383–1402. doi: 10.1104/pp.110.166520.

**Lin WY, Huang TK, Leong SJ and Chiou TJ** (2014) ‘Long-distance call from phosphate: Systemic regulation of phosphate starvation responses’, *Journal of Experimental Botany*, 65, pp. 1817–1827. doi: 10.1093/jxb/ert431.

**Linn J, Ren M, Berkowitz O, Ding W, van der Merwe MJ, Whelan J and Jost R** (2017) ‘Root cell-specific regulators of phosphate-dependent growth’, *Plant Physiology*, 174, pp. 1969–1989. doi: 10.1104/pp.16.01698.

**Liu J, Ishitani M, Halfter U, Kim CS and Zhu JK** (2000) ‘The *Arabidopsis thaliana* SOS2 gene encodes a protein kinase that is required for salt tolerance’, *Proceedings of the National Academy of Science*, 97, pp. 3730–3734. doi: 10.1073/pnas.060034197.

- Liu J, Yang L, Luan M, Wang Y, Zhang C, Zhang B, Shi J, Zhao F-G, Lan W and Luan S** (2015) ‘A vacuolar phosphate transporter essential for phosphate homeostasis in *Arabidopsis*’, *Proceedings of the National Academy of Sciences*, 112. doi: 10.1073/pnas.1514598112.
- Liu J, Whalley HJ and Knight MR** (2015) ‘Combining modelling and experimental approaches to explain how calcium signatures are decoded by calmodulin-binding transcription activators (CAMTAs) to produce specific gene expression responses’, *New Phytologist*, 208, pp. 174–187. doi: 10.1111/nph.13428.
- Liu K, Niu Y, Konishi M, Wu Y, Du H, Sun Chung H, Li L, Boudsocq M, McCormack M, Maekawa S, et al.** (2017) ‘Discovery of nitrate–CPK–NLP signalling in central nutrient–growth networks’, *Nature*. doi: 10.1038/nature22077.
- Liu N, Shang W, Li C, Jia L, Wang X and Xing G** (2018) ‘Evolution of the SPX gene family in plants and its role in the response mechanism to phosphorus stress’, *Open Biology*, 8. doi: 10.1098/rsob.170231.
- Liu T-Y, Aung K, Tseng C-Y, Chang T-Y, Chen Y-S and Chiou T-J** (2011) ‘Vacuolar  $\text{Ca}^{2+}/\text{H}^{+}$  transport activity is required for systemic phosphate homeostasis involving shoot-to-root signaling in *Arabidopsis*’, *Plant Physiology*, 156, pp. 1176–1189. doi: 10.1104/pp.111.175257.
- Liu T-Y, Huang T-K, Yang S-Y, Hong Y-T, Huang S-M, Wang F-N, Chiang S-F, Tsai S-Y, Lu W-C and Chiou T-J** (2016) ‘Identification of plant vacuolar transporters mediating phosphate storage’, *Nature Communications*, 7, p. 11095. doi: 10.1038/ncomms11095.
- Loro G, Drago I, Pozzan T, Schiavo F Lo, Zottini M and Costa A** (2012) ‘Targeting of Cameleons to various subcellular compartments reveals a strict cytoplasmic/mitochondrial  $\text{Ca}^{2+}$  handling relationship in plant cells’, *Plant Journal*, 71, pp. 1–13. doi: 10.1111/j.1365-313X.2012.04968.x.
- Loro G, Wagner S, Doccula FG, Behera S, Weigl S, Kudla J, Schwarzländer M, Costa A and Zottini M** (2016) ‘Chloroplast-specific in vivo  $\text{Ca}^{2+}$  imaging using Yellow Cameleon fluorescent protein sensors reveals organelle-autonomous  $\text{Ca}^{2+}$  signatures in the stroma’, *Plant Physiology*. doi: 10.1104/pp.16.00652.
- Luu DT, Martinière A, Sorieul M, Runions J and Maurel C** (2012) ‘Fluorescence recovery after photobleaching reveals high cycling dynamics of plasma membrane aquaporins in *Arabidopsis* roots under salt stress’, *Plant Journal*, 69, pp. 894–905. doi: 10.1111/j.1365-313X.2011.04841.x.
- Lynch JP** (2007) ‘Roots of the second Green Revolution’, *Australian Journal of Botany*, 55, pp. 493–512. doi: 10.1071/BT06118.

**Lynch JP and Brown KM** (2001) ‘Topsoil foraging – an architectural adaptation of plants to low phosphorus availability’, *Plant and Soil*, 237, pp. 225–237.

**Ma L, Zhang H, Sun L, Jiao Y, Zhang G, Miao C and Hao F** (2012) ‘NADPH oxidase AtrbohD and AtrbohF function in ROS-dependent regulation of Na<sup>+</sup>/K<sup>+</sup> homeostasis in *Arabidopsis* under salt stress’, *Journal of Experimental Botany*, 63, pp. 305–317. doi: 10.1093/jxb/err280.

**Ma Z, Bielenberg DG, Brown KM and Lynch JP** (2001) ‘Regulation of root hair density by phosphorus availability in *Arabidopsis thaliana*’, *Plant, Cell and Environment*, 24, pp. 459–467. doi: 10.1046/j.1365-3040.2001.00695.x.

**Maathuis FJM** (2014) ‘Sodium in plants: Perception, signalling, and regulation of sodium fluxes’, *Journal of Experimental Botany*, 65, pp. 849–858. doi: 10.1093/jxb/ert326.

**Magnani F, Nenci S, Millana Fananas E, Ceccon M, Romero E, Fraaije MW and Mattevi A** (2017) ‘Crystal structures and atomic model of NADPH oxidase’, *Proceedings of the National Academy of Sciences*. doi: 10.1073/pnas.1702293114.

**Malhotra A and Habibovic P** (2016) ‘Calcium phosphates and angiogenesis: Implications and advances for bone regeneration’, *Trends in Biotechnology*, 34, pp. 983–992. doi: 10.1016/j.tibtech.2016.07.005.

**Marschner H** (2012) ‘Mineral nutrition of higher plants, 3<sup>rd</sup> edition’, *Elsevier Ltd.*, ISBN: 978-0-12-384905-2

**Marti MC, Stancombe MA and Webb AAR** (2013) ‘Cell- and stimulus type-specific intracellular free Ca<sup>2+</sup> signals in *Arabidopsis*’, *Plant Physiology*, 163, pp. 625–634. doi: 10.1104/pp.113.222901.

**Martí Ruiz MC, Hubbard KE, Gardner MJ, Jung HJ, Aubry S, Hotta CT, Mohd-Noh NI, Robertson FC, Hearn TJ, Tsai Y-C, et al.** (2018) ‘Circadian oscillations of cytosolic free calcium regulate the *Arabidopsis* circadian clock’, *Nature Plants*, 4. doi: 10.1038/s41477-018-0224-8.

**Martinez IM and Chrispeels MJ** (2003) ‘Genomic analysis of the unfolded protein response in *Arabidopsis* shows its connection to important cellular processes’, *Plant Cell*, 15, pp. 561–576. doi: 10.1105/tpc.007609.

**Martinière A, Gibrat R, Sentenac H, Dumont X, Gaillard I and Paris N** (2018) ‘Uncovering pH at both sides of the root plasma membrane interface using noninvasive imaging’, *Proceedings of the National Academy of Sciences*. doi: 10.1073/pnas.1721769115.



- Mäser P, Thomine S, Schroeder JI, Ward JM, Hirschi K, Sze H, Talke IN, Amtmann A, Maathuis FJM, Sanders D, et al.** (2001) ‘Phylogenetic relationships within cation transporter families of *Arabidopsis*’, *Plant Physiology*, 126, pp. 1646–1667.
- McAinsh MR and Pittman JK** (2009) ‘Shaping the calcium signature’, *New Phytologist*, 181, pp. 275–292. doi: 10.1111/j.1469-8137.2005.01543.x.
- Medici A, Marshall-Colon A, Ronzier E, Szponarski W, Wang R, Gojon A, Crawford NM, Ruffel S, Coruzzi GM and Krouk G** (2015) ‘AtNIGT1/HRS1 integrates nitrate and phosphate signals at the *Arabidopsis* root tip’, *Nature Communications*, 6. doi: 10.1038/ncomms7274.
- Mehlmer N, Parvin N, Hurst CH, Knight MR, Teige M and Vothknecht UC** (2012) ‘A toolset of aequorin expression vectors for in planta studies of subcellular calcium concentrations in *Arabidopsis thaliana*’, *Journal of Experimental Botany*, 63, pp. 1751–1761. doi: 10.1093/jxb/err406.
- Meijering E, Jacob M, Sarria JF, Steiner P, Hirling H and Unser M** (2004) ‘Design and validation of a tool for neurite tracing and analysis in fluorescence microscopy images’, *Cytometry*, 58, pp. 167–176.
- Michard E, Lima PT, Borges F, Silva AC, Portes MT, Carvalho JE, Gilliam M, Liu L-H, Obermeyer G and Feijó J a** (2011) ‘Glutamate receptor-like genes form Ca<sup>2+</sup> channels in pollen tubes and are regulated by pistil D-serine’, *Science*, 332, pp. 434–437. doi: 10.1126/science.1201101.
- Miki D, Zhang W, Zeng W, Feng Z and Zhu J** (2018) ‘CRISPR / Cas9-mediated gene targeting in *Arabidopsis* using sequential transformation’, *Nature Communications*. doi: 10.1038/s41467-018-04416-0.
- Miller G, Schlauch K, Tam R, Cortes D, Torres MA, Shulaev V, Dangl JL and Mittler R** (2009) ‘The plant NADPH oxidase RBOHD mediates rapid systemic signaling in response to diverse stimuli’, *Science Signaling*, 2. doi: 10.1126/scisignal.2000448.
- Mimura T, Reid RJ and Smith FA** (1998) ‘Control of phosphate transport across the plasma membrane of *Chara corallina*’, *Journal of Experimental Botany*, 49, pp. 13–19. doi: 10.1093/jexbot/49.318.13.
- Mimura T, Sakano K and Shimmen T** (1996) ‘Studies on the distribution, re-translocation and homeostasis of inorganic phosphate in barley leaves’, *Plant, Cell and Environment*, 19, pp. 311–320.

**Misson J, Raghothama KG, Jain A, Jouhet J, Block M a, Bligny R, Ortet P, Creff A, Somerville S, Rolland N, et al.** (2005) 'A genome-wide transcriptional analysis using *Arabidopsis thaliana* Affymetrix gene chips determined plant responses to phosphate deprivation', *Proceedings of the National Academy of Sciences*, 102, pp. 11934–11939. doi: 10.1073/pnas.0505266102.

**Miyawaki A, Llopis J, Heim R, McCaffery JM, Adams J a, Ikura M and Tsien RY** (1997) 'Fluorescent indicators for Ca<sup>2+</sup> based on green fluorescent proteins and calmodulin.', *Nature*, 388, pp. 882–887. doi: 10.1038/42264.

**Młodzińska E and Zboińska M** (2016) 'Phosphate uptake and allocation – a closer look at *Arabidopsis thaliana* L. and *Oryza sativa* L.', *Frontiers in Plant Science*, 7. doi: 10.3389/fpls.2016.01198.

**Monshausen GB, Bibikova TN, Weisenseel MH and Gilroy S** (2009) 'Ca<sup>2+</sup> regulates reactive oxygen species production and pH during mechanosensing in *Arabidopsis* roots', *The Plant Cell*, 21, pp. 2341–56. doi: 10.1105/tpc.109.068395.

**Monshausen GB, Messerli M a and Gilroy S** (2008) 'Imaging of the Yellow Cameleon 3.6 indicator reveals that elevations in cytosolic Ca<sup>2+</sup> follow oscillating increases in growth in root hairs of *Arabidopsis*', *Plant Physiology*, 147, pp. 1690–1698. doi: 10.1104/pp.108.123638.

**Moore CA, Bowen HC, Scrase-Field S, Knight MR and White PJ** (2002) 'The deposition of suberin lamellae determines the magnitude of cytosolic Ca<sup>2+</sup> elevations in root endodermal cells subjected to cooling', *Plant Journal*, 30, pp. 457–465. doi: 10.1046/j.1365-313X.2002.01306.x.

**Mora-Macías J, Ojeda-Rivera JO, Gutiérrez-Alanís D, Yong-Villalobos L, Oropeza-Aburto A, Raya-González J, Jiménez-Domínguez G, Chávez-Calvillo G, Rellán-Álvarez R and Herrera-Estrella L** (2017) 'Malate-dependent Fe accumulation is a critical checkpoint in the root developmental response to low phosphate', *Proceedings of the National Academy of Sciences*. doi: 10.1073/pnas.1701952114.

**Mori K, Renhu N, Naito M, Nakamura A, Shiba H, Yamamoto T, Suzaki T, Iida H and Miura K** (2018) 'Ca<sup>2+</sup>-permeable mechanosensitive channels MCA1 and MCA2 mediate cold-induced cytosolic Ca<sup>2+</sup> increase and cold tolerance in *Arabidopsis*', *Scientific Reports*, 8. doi: 10.1038/s41598-017-17483-y.

**Moyen C, Hammond-Kosack KE, Jones J, Knight MR and Johannes E** (1998) 'Systemin triggers an increase of cytoplasmic calcium in tomato mesophyll cells: Ca<sup>2+</sup> mobilization from intra- and extracellular compartments', *Plant, Cell and Environment*, 21, pp. 1101–1111. doi: 10.1046/j.1365-3040.1998.00378.x.

- Muchhal US, Liu CM and Raghothama KG** (1997) 'Ca<sup>2+</sup>-ATPase is expressed differentially in phosphate-starved roots of tomato', *Physiologia Plantarum*, 101, pp. 540–544. doi: 10.1034/j.1399-3054.1997.1010313.x.
- Muchhal US, Pardo JM and Raghothama KG** (1996) 'Phosphate transporters from the higher plant *Arabidopsis thaliana*', *Proceedings of the National Academy of Sciences*, 93, pp. 10519–23. doi: 10.1073/pnas.93.19.10519.
- Mueller M and Schmidt W** (2004) 'Environmentally induced plasticity of root hair development in *Arabidopsis*', *Plant Physiology*, 134, pp. 409–419. doi: 10.1104/pp.
- Mueller ND, Gerber JS, Johnston M, Ray DK, Ramankutty N and Foley J** (2012) 'Closing yield gaps through nutrient and water management', *Nature*, 490, pp. 254–7. doi: 10.1038/nature11420.
- Mühling KH, Wimmer M and Goldbach HE** (1998) 'Apoplastic and membrane associated Ca<sup>2+</sup> in leaves and roots as affected by boron deficiency', *Physiologia Plantarum*, 102, pp. 179–184.
- Mukherjee P, Banerjee S, Wheeler A, Ratliff L a, Irigoyen S, Garcia LR, Lockless SW and Versaw WK** (2015) 'Live imaging of inorganic phosphate in plants with cellular and subcellular resolution', *Plant Physiology*, 167, pp. 628–38. doi: 10.1104/pp.114.254003.
- Müller J, Toev T, Heisters M, Teller J, Moore KL, Hause G, Dinesh DC, Bürstenbinder K and Abel S** (2015) 'Iron-dependent callose deposition adjusts root meristem maintenance to phosphate availability', *Developmental Cell*, 33, pp. 216–230. doi: 10.1016/j.devcel.2015.02.007.
- Mustafa A, Ensikat H-J and Weigend M** (2018) 'Mineralized trichomes in Boraginales: complex microscale heterogeneity and simple phylogenetic patterns', *Annals of Botany*. doi: 10.1093/aob/mcx191.
- Nachtergaele F, Velthuisen H van, Verelst L, Batjes N, Dijkshoorn K, Engelen V van, Fischer G, Jones A, Montanarella L, Petri M, et al.** (2009) 'Harmonized world soil database', *Food and Agriculture Organization*. doi: 3123.
- Nacry P, Canivenc G, Muller B, Azmi A, Onckelen H Van, Nacry P, Rossignol M and Doumas P** (2005) 'A role for auxin redistribution in the responses of the root system architecture to phosphate starvation in *Arabidopsis*', *Plant Physiology*, 138, pp. 2061–2074. doi: 10.1104/pp.105.060061.explored.
- Nagai T, Yamada S, Tominaga T, Ichikawa M and Miyawaki A** (2004) 'Expanded dynamic range of fluorescent indicators for Ca<sup>2+</sup> by circularly permuted yellow fluorescent proteins', *Proceedings of the National Academy of Sciences*, 101, pp. 10554–10559.

**Nagarajan VK, Jain A, Poling MD, Lewis AJ, Raghothama KG and Smith AP** (2011) ‘*Arabidopsis* Pht1;5 mobilizes phosphate between source and sink organs and influences the interaction between phosphate homeostasis and ethylene signaling’, *Plant Physiology*, 156, pp. 1149–1163. doi: 10.1104/pp.111.174805.

**Nagel-Volkmann J, Plieth C, Becker D, Lüthen H and Dörffling K** (2009) ‘Cold-induced cytosolic free calcium ion concentration changes in wheat’, *Journal of Plant Physiology*, 166, pp. 1955–1960. doi: 10.1016/j.jplph.2009.05.002.

**Nakagawa Y, Katagiri T, Shinozaki K, Qi Z, Tatsumi H and Furuichi T** (2007) ‘*Arabidopsis* plasma membrane protein crucial for Ca<sup>2+</sup> influx and touch sensing in roots’, *PNAS*, 104, pp. 3639–3644.

**Nakamura Y** (2013) ‘Phosphate starvation and membrane lipid remodeling in seed plants’, *Progress in Lipid Research*, 52, pp. 43–50. doi: 10.1016/j.plipres.2012.07.002.

**Napolitano MJ and Shain DH** (2005) ‘Quantitating adenylate nucleotides in diverse organisms’, *Journal of Biochemical and Biophysical Methods*, 63, pp. 69–77. doi: 10.1016/j.jbbm.2005.03.001.

**Nawy T, Lee J-Y, Colinas J, Wang JY, Thongrod SC, Malamy JE, Birnbaum K and Benfey PN** (2005) ‘Transcriptional profile of the *Arabidopsis* root quiescent center’, *Science*, 17, pp. 1908–1925. doi: 10.1105/tpc.105.031724.1.

**Nguyen CT, Kurenda A, Stolz S, Chételat A and Farmer EE** (2018) ‘Identification of cell populations necessary for leaf-to-leaf electrical signaling in a wounded plant’, *Proceedings of the National Academy of Sciences*. doi: 10.1073/pnas.1807049115.

**Niu L, Yuan H, Gong F, Wu X and Wang W** (2018) ‘Protein extraction methods shape much of the extracted proteomes’, *Frontiers in Plant Science*, 9. doi: 10.3389/fpls.2018.00802.

**Nordborg M, Hu TT, Ishino Y, Jhaveri J, Toomajian C, Zheng H, Bakker E, Calabrese P, Gladstone J, Goyal R, et al.** (2005) ‘The pattern of polymorphism in *Arabidopsis thaliana*’, *PLoS Biology*, 3, pp. 1289–1299. doi: 10.1371/journal.pbio.0030196.

**Nussaume L, Kanno S, Javot H, Marin E, Pochon N, Ayadi A, Nakanishi TM and Thibaud M-C** (2011) ‘Phosphate import in plants: focus on the PHT1 transporters’, *Frontiers in Plant Science*, 2. doi: 10.3389/fpls.2011.00083.

**O’Lexy R, Kasai K, Clark N, Fujiwara T, Sozzani R and Gallagher KL** (2018) ‘Exposure to heavy metal stress triggers changes in plasmodesmatal permeability via deposition and

breakdown of callose', *Journal of Experimental Botany*, 69, pp. 3715–3728. doi: 10.1093/jxb/ery171.

**Obayashi T, Okamura Y, Ito S, Tadaka S, Aoki Y, Shirota M and Kinoshita K** (2014) 'ATTED-II in 2014: Evaluation of gene coexpression in agriculturally important plants', *Plant and Cell Physiology*, 55. doi: 10.1093/pcp/pct178.

**Obersteiner M, Peñuelas J, Ciais P, van der Velde M and Janssens I a.** (2013) 'The phosphorus trilemma', *Nature Geoscience*, 6, pp. 897–898. doi: 10.1038/ngeo1990.

**Okazaki Y, Otsuki H, Narisawa T, Kobayashi M, Sawai S, Kamide Y, Kusano M, Aoki T, Hirai MY and Saito K** (2013) 'A new class of plant lipid is essential for protection against phosphorus depletion', *Nature Communications*, 4. doi: 10.1038/ncomms2512.

**P. Koldenkova V and Nagai T** (2013) 'Genetically encoded Ca<sup>2+</sup> indicators: Properties and evaluation', *Biochimica et Biophysica Acta*, 1833, pp. 1787–1797. doi: 10.1016/j.bbamcr.2013.01.011.

**Pant B-D, Pant P, Erban A, Huhman D, Kopka J and Scheible W-R** (2015) 'Identification of primary and secondary metabolites with phosphorus status-dependent abundance in *Arabidopsis*, and of the transcription factor PHR1 as a major regulator of metabolic changes during phosphorus-limitation', *Plant, Cell and Environment*, 38, pp. 172–187. doi: 10.1111/pce.12378.

**Pant BD, Buhtz A, Kehr J and Scheible WR** (2008) 'MicroRNA399 is a long-distance signal for the regulation of plant phosphate homeostasis', *Plant Journal*, 53, pp. 731–738. doi: 10.1111/j.1365-313X.2007.03363.x.

**Park E, Diaz-Moreno SM, Davis DJ, Wilkop TE, Bulone V and Drakakaki G** (2014) 'Endosidin 7 specifically arrests late cytokinesis and inhibits callose biosynthesis, revealing distinct trafficking events during cell plate maturation', *Plant Physiology*, 165, pp. 1019–1034. doi: 10.1104/pp.114.241497.

**Park J, Gu Y, Lee YY, Yang Z and Lee YY** (2004) 'Phosphatidic acid induces leaf cell death in *Arabidopsis* by activating the Rho-related small G protein GTPase-mediated pathway of reactive oxygen species generation', *Plant Physiology*, 134, pp. 129–136. doi: 10.1104/pp.103.031393.

**Parre E and Geitmann A** (2005) 'More than a leak sealant: The mechanical properties of callose in pollen tubes', *Plant Physiology*, 137, pp. 274–286. doi: 10.1104/pp.104.050773.

**Paszkowski U, Kroken S, Roux C and Briggs SP** (2002) 'Rice phosphate transporters include an evolutionarily divergent gene specifically activated in arbuscular mycorrhizal symbiosis',

*Proceedings of the National Academy of Sciences*, 99, pp. 13324–13329. doi: 10.1073/pnas.202474599.

**Patel AA, Malinowska L, Saha S and Wang J** (2017) ‘ATP as a biological hydrotrope’, *Science*, 356, pp. 753–756. doi: 10.1126/science.aaf6846.

**Pei Z-M, Murata Y, Benning G, Thomine S, Klu B, Allen GJ, Grill E and Schroeder JI** (2000) ‘Calcium channels activated by hydrogen peroxide mediate abscisic acid signalling in guard cells’, *Nature*, 406, pp. 731–734. doi: 10.1007/978-1-4939-1261-2.

**Peiter E, Maathuis FJM, Mills LN, Knight H, Pelloux J, Hetherington AM and Sanders D** (2005) ‘The vacuolar Ca<sup>2+</sup>-activated channel TPC1 regulates germination and stomatal movement’, *Nature*, 434, pp. 404–408. doi: 10.1038/nature03440.

**Peret B, Desnos T, Jost R, Kanno S, Berkowitz O and Nussaume L** (2014) ‘Root architecture responses: In search of phosphate’, *Plant Physiology*, 166, pp. 1713–1723. doi: 10.1104/pp.114.244541.

**Péret B, Li G, Zhao J, Band LR, Voß U, Postaire O, Luu DT, Da Ines O, Casimiro I, Lucas M, et al.** (2012) ‘Auxin regulates aquaporin function to facilitate lateral root emergence’, *Nature Cell Biology*, 14, pp. 991–998. doi: 10.1038/ncb2573.

**Pérez V, Wherrett T, Shabala S, Muñiz J, Dobrovinskaya O and Pottosin I** (2008) ‘Homeostatic control of slow vacuolar channels by luminal cations and evaluation of the channel-mediated tonoplast Ca<sup>2+</sup> fluxes in situ’, *Journal of Experimental Botany*, 59, pp. 3845–3855. doi: 10.1093/jxb/ern225.

**di Pietro M, Vialaret J, Li G-W, Hem S, Prado K, Rossignol M, Maurel C and Santoni V** (2013) ‘Coordinated post-translational responses of aquaporins to abiotic and nutritional stimuli in *Arabidopsis* roots’, *Molecular & Cellular Proteomics*, 12, pp. 3886–3897. doi: 10.1074/mcp.M113.028241.

**Plattner H and Verkhatsky A** (2015) ‘The ancient roots of calcium signalling evolutionary tree’, *Cell Calcium*, 57, pp. 123–132. doi: 10.1016/j.ceca.2014.12.004.

**Plaxton WC and Tran HT** (2011) ‘Metabolic adaptations of phosphate-starved plants’, *Plant Physiology*, 156, pp. 1006–1015. doi: 10.1104/pp.111.175281.

**Poirier Y, Thoma S, Somerville C and Schiefelbein J** (1991) ‘Mutant of *Arabidopsis* deficient in xylem loading of phosphate’, *Plant Physiology*, 97, pp. 1087–1093. doi: 10.1104/pp.97.3.1087.

**Popova Y, Thayumanavan P, Lonati E, Agrochao M and Thevelein JM** (2010) ‘Transport and signaling through the phosphate-binding site of the yeast Pho84 phosphate transceptor’,

*Proceedings of the National Academy of Sciences*, 107, pp. 2890–2895. doi: 10.1073/pnas.0906546107.

**Poulton SW** (2017) ‘Biogeochemistry: Early phosphorus redigested’, *Nature Geoscience*, 10, pp. 75–76. doi: 10.1038/ngeo2884.

**Pratt J, Boisson A-M, Gout E, Bligny R, Douce R and Aubert S** (2009) ‘Phosphate (Pi) starvation effect on the cytosolic Pi concentration and Pi exchanges across the tonoplast in plant cells: an in vivo <sup>31</sup>P-nuclear magnetic resonance study using methylphosphonate as a Pi analog’, *Plant Physiology*, 151, pp. 1646–57. doi: 10.1104/pp.109.144626.

**Price AH, Taylor A, Ripley SJ, Griffiths A, Trewavas AJ and Knight MR** (1994) ‘Oxidative signals in tobacco increase cytosolic calcium’, *The Plant Cell*, 6, pp. 1301–1310. doi: 10.1105/tpc.6.9.1301.

**Price MB and Okumoto S** (2013) ‘Inter-subunit interactions between Glutamate-Like Receptors in *Arabidopsis*’, *Plant Signaling and Behavior*, 8. doi: 10.4161/psb.27034.

**Puga MI, Mateos I, Charukesi R, Wang Z, Franco-Zorrilla JM, de Lorenzo L, Irigoyen ML, Masiero S, Bustos R, Rodriguez J, et al.** (2014) ‘SPX1 is a phosphate-dependent inhibitor of PHOSPHATE STARVATION RESPONSE 1 in *Arabidopsis*’, *Proceedings of the National Academy of Sciences*, 111, pp. 14947–14952. doi: 10.1073/pnas.1404654111.

**Quiles-Pando C, Rexach J, Navarro-Gochicoa MT, Camacho-Cristóbal JJ, Herrera-Rodríguez MB and González-Fontes A** (2013) ‘Boron deficiency increases the levels of cytosolic Ca<sup>2+</sup> and expression of Ca<sup>2+</sup>-related genes in *Arabidopsis thaliana* roots’, *Plant Physiology and Biochemistry*, 65, pp. 55–60. doi: 10.1016/j.plaphy.2013.01.004.

**Quintero FJ, Martínez-Atienza J, Villalta I, Jiang X, Kim W-Y, Ali Z, Fujii H, Mendoza I, Yun D-J, Zhu J-K, et al.** (2011) ‘Activation of the plasma membrane Na/H antiporter Salt-Overly-Sensitive 1 (SOS1) by phosphorylation of an auto-inhibitory C-terminal domain’, *Proceedings of the National Academy of Sciences*, 108, pp. 2611–2616. doi: 10.1073/pnas.1018921108.

**Ragel P, Ródenas R, García-Martín E, Andrés Z, Villalta I, Nieves-Cordones M, Rivero RM, Martínez V, Pardo JM, Quintero FJ, et al.** (2015) ‘The CBL-interacting protein kinase CIPK23 regulates HAK5-mediated high-affinity K<sup>+</sup> uptake in *Arabidopsis* roots’, *Plant Physiology*, 169. doi: 10.1104/pp.15.01401.

**Raghothama KG** (1999) ‘Phosphate acquisition’, *Annual Review Plant Physiology and Plant Molecular Biology*, 50, pp. 665–93.

**Ranf S, Wuennenberg P, Lee J, Becker D, Dunkel M, Hedrich R, Scheel D and Dietrich P** (2008) 'Loss of the vacuolar cation channel, AtTPC1, does not impair Ca<sup>2+</sup> signals induced by abiotic and biotic stresses', *Plant Journal*, 53, pp. 287–299. doi: 10.1111/j.1365-313X.2007.03342.x.

**Ravet K, Touraine B and Boucherez J** (2009) 'Ferritins control interaction between iron homeostasis and oxidative stress in *Arabidopsis*', *The Plant Journal*, 57, pp. 400–412. doi: 10.1111/j.1365-313X.2008.03698.x.

**Rebeille F, Bligny R, Martin JB and Douce R** (1983) 'Relationship between the cytoplasm and the vacuole phosphate pool in *Acer pseudoplatanus* cells', *Archives of Biochemistry and Biophysics*, 225, pp. 143–148. doi: 10.1016/0003-9861(83)90017-6.

**Rentel MC and Knight MR** (2004) 'Oxidative stress-induced calcium signaling in *Arabidopsis*', *Plant Physiology*, 135, pp. 1471–1479. doi: 10.1104/pp.104.042663.1.

**Reyt G, Boudouf S, Boucherez J, Gaymard F and Briat JF** (2015) 'Iron- and ferritin-dependent reactive oxygen species distribution: Impact on *Arabidopsis* root system architecture', *Molecular Plant*, 8, pp. 439–453. doi: 10.1016/j.molp.2014.11.014.

**Richards SL, Laohavisit A, Mortimer JC, Shabala L, Swarbreck SM, Shabala S and Davies JM** (2014) 'Annexin 1 regulates the H<sub>2</sub>O<sub>2</sub>-induced calcium signature in *Arabidopsis thaliana* roots', *The Plant Journal*, 77, pp. 136–45. doi: 10.1111/tpj.12372.

**Richards SL, Wilkins KA, Swarbreck SM, Anderson AA, Habib N, Smith AG, McAinsh M and Davies JM** (2015) 'The hydroxyl radical in plants: From seed to seed', *Journal of Experimental Botany*, 66. doi: 10.1093/jxb/eru398.

**Rieder B and Neuhaus HE** (2011) 'Identification of an *Arabidopsis* plasma membrane–located ATP transporter important for anther development', *The Plant Cell*, 23, pp. 1932–1944. doi: 10.1105/tpc.111.084574.

**Riveras E, Alvarez JM, Vidal EA, Oses C, Vega A and Gutiérrez RA** (2015) 'The calcium ion is a second messenger in the nitrate signaling pathway of *Arabidopsis*', *Plant Physiology*, 169, pp. 1397–404. doi: 10.1104/pp.15.00961.

**Rodrigo-Moreno A, Andrés-Colás N, Poschenrieder C, Gunsé B, Peñarrubia L and Shabala S** (2013) 'Calcium- and potassium-permeable plasma membrane transporters are activated by copper in *Arabidopsis* root tips: Linking copper transport with cytosolic hydroxyl radical production', *Plant, Cell and Environment*, 36, pp. 844–855. doi: 10.1111/pce.12020.



- Rodrigues O, Reshetnyak G, Grondin A, Saijo Y, Leonhardt N, Maurel C and Verdoucq L** (2017) ‘Aquaporins facilitate hydrogen peroxide entry into guard cells to mediate ABA- and pathogen-triggered stomatal closure’, *Proceedings of the National Academy of Sciences*. doi: 10.1073/pnas.1704754114.
- Rubio V, Linhares F, Solano R, Martín AC, Iglesias J, Leyva A and Paz-Ares J** (2001) ‘A conserved MYB transcription factor involved in phosphate starvation signaling both in vascular plants and in unicellular algae’, *Genes & Development*, 15, pp. 2122–2133. doi: 10.1101/gad.204401.availability.
- Rudolphi-Skórska E and Sieprawska A** (2016) ‘Physicochemical techniques in description of interactions in model and native plant membranes under stressful conditions and in physiological processes’, *Acta Physiologiae Plantarum*, 38. doi: 10.1007/s11738-015-2034-1.
- Saand MA, Xu YP, Munyampundu JP, Li W, Zhang XR and Cai XZ** (2015) ‘Phylogeny and evolution of plant cyclic nucleotide-gated ion channel (CNGC) gene family and functional analyses of tomato CNGCs’, *DNA Research*, 22, pp. 471–483. doi: 10.1093/dnares/dsv029.
- Sadhukhan A, Kobayashi Y, Nakano Y, Iuchi S, Kobayashi M, Sahoo L and Koyama H** (2017) ‘Genome-wide association study reveals that the aquaporin NIP1;1 contributes to variation in hydrogen peroxide sensitivity in *Arabidopsis thaliana*’, *Molecular Plant*, 10, pp. 1082–1094. doi: 10.1016/j.molp.2017.07.003.
- Sakano K, Yazaki Y and Mimura T** (1992) ‘Cytoplasmic acidification induced by inorganic phosphate uptake in suspension cultured *Catharanthus roseus* cells: Measurement with fluorescent pH indicator and P-nuclear magnetic resonance.’, *Plant Physiology*, 99, pp. 672–80. doi: 10.1104/pp.99.2.672.
- Sánchez-Calderón L, López-Bucio J, Chacón-López A, Cruz-Ramírez A, Nieto-Jacobo F, Dubrovsky JG and Herrera-Estrella L** (2005) ‘Phosphate starvation induces a determinate developmental program in the roots of *Arabidopsis thaliana*’, *Plant and Cell Physiology*, 46, pp. 174–184. doi: 10.1093/pcp/pci011.
- Sanders D, Brownlee C and Harper JF** (1999) ‘Communicating with calcium’, *The Plant Cell*, 11, pp. 691–706.
- Sawers RJH, Svane SF, Quan C, Grønlund M, Wozniak B, Gebreselassie MN, González-Muñoz E, Chávez Montes RA, Baxter I, Goudet J, et al.** (2017) ‘Phosphorus acquisition efficiency in arbuscular mycorrhizal maize is correlated with the abundance of root-external hyphae and the accumulation of transcripts encoding PHT1 phosphate transporters’, *New Phytologist*, 214, pp. 632–643. doi: 10.1111/nph.14403.

- Schenk ST and Schikora A** (2015) ‘Staining of callose depositions in root and leaf tissues’, *Bio-Protocol*, 5. doi: 10.1017/CBO9781107415324.004.
- Schiller M, Massalski C, Kurth T and Steinebrunner I** (2012) ‘The *Arabidopsis* apyrase AtAPY1 is localized in the Golgi instead of the extracellular space’, *BMC Plant Biology*, 12. doi: 10.1186/1471-2229-12-123.
- Schönknecht G** (2013) ‘Calcium signals from the vacuole’, *Plants*, 2, pp. 589–614. doi: 10.3390/plants2040589.
- Secco D, Wang C, Shou H, Schultz MD, Chiarenza S, Nussaume L, Ecker JR, Whelan J and Lister R** (2015) ‘Stress induced gene expression drives transient DNA methylation changes at adjacent repetitive elements’, *eLife*, 4. doi: 10.7554/eLife.09343.001.
- Sello S, Moscatiello R, Mehlmer N, Leonardelli M, Carraretto L, Cortese E, Zanella FG, Baldan B, Szabò I, Vothknecht UC, et al.** (2018) ‘Chloroplast Ca<sup>2+</sup> fluxes into and across thylakoids revealed by thylakoid-targeted aequorin probes’, *Plant Physiology*. doi: 10.1104/pp.18.00027.
- Seta A, Tabara M, Nishibori Y, Hiraguri A, Ohkama-Ohtsu N, Yokoyama T, Hara S, Yoshida K, Hisabori T, Fukudome A, et al.** (2017) ‘Post-translational regulation of the dicing activities of *Arabidopsis* DICER-LIKE 3 and 4 by inorganic phosphate and the redox state’, *Plant and Cell Physiology*, 58, pp. 485–495. doi: 10.1093/pcp/pcw226.
- Shaff JE, Schultz B a., Craft EJ, Clark RT and Kochian L V.** (2010) ‘GEOCHEM-EZ: A chemical speciation program with greater power and flexibility’, *Plant and Soil*, 330, pp. 207–214. doi: 10.1007/s11104-009-0193-9.
- Shi H, Ishitani M, Kim C and Zhu J-K** (2000) ‘The *Arabidopsis thaliana* salt tolerance gene SOS1 encodes a putative Na<sup>+</sup>/H<sup>+</sup> antiporter’, *Proceedings of the National Academy of Sciences*, 97, pp. 6896–6901. doi: 10.1073/pnas.120170197.
- Shih H-W, Miller ND, Dai C, Spalding EP and Monshausen GB** (2014) ‘The receptor-like kinase FERONIA is required for mechanical signal transduction in *Arabidopsis* seedlings’, *Current Biology*, 24, pp. 1887–1892. doi: 10.1016/j.cub.2014.06.064.
- Shih H-W, DePew CL, Miller ND and Monshausen GB** (2015) ‘The cyclic nucleotide-gated channel CNGC14 regulates root gravitropism in *Arabidopsis thaliana*’, *Current Biology*, 25. doi: 10.1016/j.cub.2015.10.025.

- Shimano F** and **Ashihara H** (2006) ‘Effect of long-term phosphate starvation on the levels and metabolism of purine nucleotides in suspension-cultured *Catharanthus roseus* cells’, *Phytochemistry*, 67, pp. 132–141. doi: 10.1016/j.phytochem.2005.10.013.
- Shimomura O**, **Inouye S**, **Musicki B** and **Kishi Y** (1990) ‘Recombinant aequorin and recombinant semi-synthetic aequorins’, *The Biochemical Journal*, 270, pp. 309–312.
- Shimomura O** (1995) ‘A short story of aequorin’, *Biological Bulletin*, 189.
- Shimomura O**, **Johnson FH** and **Saiga Y** (1962) ‘Extraction, purification and properties of aequorin, a bioluminescent protein from the luminous hydromedusan, *Aequorea*’, *Journal of Cellular and Comparative Physiology*, 59, pp. 223–239. doi: 10.1002/jcp.1030590302.
- Shin H**, **Shin HS**, **Dewbre GR** and **Harrison MJ** (2004) ‘Phosphate transport in *Arabidopsis*: Pht1;1 and Pht1;4 play a major role in phosphate acquisition from both low- and high-phosphate environments’, *Plant Journal*, 39, pp. 629–642. doi: 10.1111/j.1365-313X.2004.02161.x.
- Shin R**, **Berg RH** and **Schachtman DP** (2005) ‘Reactive oxygen species and root hairs in *Arabidopsis* root response to nitrogen, phosphorus and potassium deficiency’, *Plant and Cell Physiology*, 46, pp. 1350–1357. doi: 10.1093/pcp/pci145.
- Shin R** and **Schachtman DP** (2004) ‘Hydrogen peroxide mediates plant root cell response to nutrient deprivation’, *Proceedings of the National Academy of Sciences*, 101, pp. 8827–32. doi: 10.1073/pnas.0401707101.
- Singh A**, **Bhatnagar N**, **Pandey A** and **Pandey GK** (2015) ‘Plant phospholipase C family: Regulation and functional role in lipid signaling’, *Cell Calcium*, 58, pp. 139–146. doi: 10.1016/j.ceca.2015.04.003.
- Somssich M** (2018) ‘A short history of *Arabidopsis thaliana* (L.) Heynh. Columbia-0’, *PeerJ Preprints*, 6. doi: 10.7287/peerj.preprints.26931v3.
- Song CJ**, **Steinebrunner I**, **Wang X**, **Stout SC** and **Roux SJ** (2006) ‘Extracellular ATP induces the accumulation of superoxide via NADPH oxidases in *Arabidopsis*’, *Plant Physiology*, 140, pp. 1222–1232. doi: 10.1104/pp.105.073072.et.
- Srivastava S**, **Upadhyay M**, **Srivastava A**, **Abdelrahman M**, **Suprasanna P** and **Tran L-S** (2018) ‘Cellular and subcellular phosphate transport machinery in plants’, *International Journal of Molecular Sciences*, 19. doi: 10.3390/ijms19071914.
- Stael S**, **Wurzinger B**, **Mair A**, **Mehlmer N**, **Vothknecht UC** and **Teige M** (2012) ‘Plant organellar calcium signalling: An emerging field’, *Journal of Experimental Botany*, 63, pp. 1525–1542. doi: 10.1093/jxb/err394.

**Stetter MG, Schmid K and Ludewig U** (2015) ‘Uncovering genes and ploidy involved in the high diversity in root hair density, length and response to local scarce phosphate in *Arabidopsis thaliana*’, *Plos ONE*, 10. doi: 10.1371/journal.pone.0120604.

**Storti M, Costa A, Golin S, Zottini M, Morosinotto To and Alboresi A** (2018) ‘Systemic calcium wave propagation in *Physcomitrella patens*’, *Plant and Cell Physiology*. doi: 10.1093/pcp/pcy104/5033790.

**Straub T, Ludewig U and Neuhäuser B** (2017) ‘The kinase CIPK23 inhibits ammonium transport in *Arabidopsis thaliana*’, *The Plant Cell*, 29, pp. 409–422. doi: 10.1105/tpc.16.00806.

**Sueldo DJ, Foresi NP, Casalongue CA and Laxalt AM** (2010) ‘Phosphatidic acid formation is required for extracellular ATP-mediated nitric oxide production in suspension- cultured tomato cells’, *New Phytologist*, 185, pp. 909–916.

**Sugita R, Kobayashi NI, Hirose A, Saito T, Iwata R, Tanoi K and Nakanishi TM** (2016) ‘Visualization of uptake of mineral elements and the dynamics of photosynthates in *Arabidopsis* by a newly developed Real-Time Radioisotope Imaging System (RRIS)’, *Plant and Cell Physiology*, 57, pp. 743–753. doi: 10.1093/pcp/pcw056.

**Sun J, Zhang X, Deng S, Zhang C, Wang M, Ding M, Zhao R, Shen X, Zhou X, Lu C, et al.** (2012) ‘Extracellular ATP signaling is mediated by H<sub>2</sub>O<sub>2</sub> and cytosolic Ca<sup>2+</sup> in the salt response of *Populus euphratica* cells’, *PLoS ONE*, 7. doi: 10.1371/journal.pone.0053136.

**Sun L, Song L, Zhang Y, Zheng Z and Liu D** (2016) ‘*Arabidopsis* PHL2 and PHR1 act redundantly as the key components of the central regulatory system controlling transcriptional responses to phosphate starvation’, *Plant Physiology*, 170, pp. 499–514. doi: 10.1104/pp.15.01336.

**Svistonoff S, Creff A, Reymond M, Sigoillot-Claude C, Ricaud L, Blanchet A, Nussaume L and Desnos T** (2007) ‘Root tip contact with low-phosphate media reprograms plant root architecture’, *Nature Genetics*, 39, pp. 792–796. doi: 10.1038/ng2041.

**Swaminathan M** (2000) ‘Sustainable agriculture: towards an Evergreen Revolution’, *Bulleting of the Nutrition Foundation of India*, 21.

**Swarbreck SM, Colaco R and Davies JM** (2013) ‘Plant calcium-permeable channels’, *Plant Physiology*, 163, pp. 514–522. doi: 10.1104/pp.113.220855.

**Sylvester-Bradley R, Withers P, Rollett A, Talboys P, Walker R, Edwards T, Payvandi S, Heppell J, Roose T and Jones D** (2016) *Improving the sustainability of phosphorus use in arable*

*farming* – ‘Targeted P’. Agriculture and Horticulture Development Board, Project Report No. PR569.

**Takahashi N, Udagawa N and Suda T** (2014) ‘Vitamin D endocrine system and osteoclasts’, *BoneKey Reports*, 3. doi: 10.1038/bonekey.2013.229.

**Talke IN, Blaudez D, Maathuis FJ and Sanders D** (2003) ‘CNGCs: prime targets of plant cyclic nucleotide signalling?’, *Trends in Plant Science*, 8, pp. 286–293. doi: 10.1016/S1360-1385(03)00099-2.

**Tanaka K, Swanson SJ, Gilroy S and Stacey G** (2010) ‘Extracellular nucleotides elicit cytosolic free calcium oscillations in *Arabidopsis*’, *Plant Physiology*, 154, pp. 705–19. doi: 10.1104/pp.110.162503.

**Tanaka K, Choi J, Cao Y and Stacey G** (2014) ‘Extracellular ATP acts as a damage-associated molecular pattern (DAMP) signal in plants’, *Frontiers in Plant Science*, 5, pp. 1–9. doi: 10.3389/fpls.2014.00446.

**Tang R-J, Zhao F-G, Garcia VJ, Kleist TJ, Yang L, Zhang H-X and Luan S** (2015) ‘Tonoplast CBL-CIPK calcium signaling network regulates magnesium homeostasis in *Arabidopsis*’, *Proceedings of the National Academy of Sciences*, 112, pp. 3134–3139. doi: 10.1073/pnas.1420944112.

**Tang R-J and Luan S** (2017) ‘Regulation of calcium and magnesium homeostasis in plants: from transporters to signaling network’, *Current Opinion in Plant Biology*, 39, pp. 97–105. doi: 10.1016/j.pbi.2017.06.009.

**Tang W, Brady SR, Sun Y, Muday GK and Roux SJ** (2003) ‘Extracellular ATP inhibits root gravitropism at concentrations that inhibit polar auxin transport.’, *Plant Physiology*, 131, pp. 147–154. doi: 10.1104/pp.013672.

**Teardo E, Formentin E, Segalla A, Giacometti GM, Marin O, Zanetti M, Lo Schiavo F, Zoratti M and Szabò I** (2011) ‘Dual localization of plant glutamate receptor AtGLR3.4 to plastids and plasmamembrane’, *Biochimica et Biophysica Acta - Bioenergetics*, 1807, pp. 359–367. doi: 10.1016/j.bbabi.2010.11.008.

**Teardo E, Carraretto L, De Bortoli S, Costa A, Behera S, Wagner R, Lo Schiavo F, Formentin E and Szabo I** (2015) ‘Alternative splicing-mediated targeting of the *Arabidopsis* GLUTAMATE RECEPTOR3.5 to mitochondria affects organelle morphology’, *Plant Physiology*, 167, pp. 216–227. doi: 10.1104/pp.114.242602.

**Teardo E, Carraretto L, Wagner S, Formentin E, Behera S, De Bortoli S, Larosa V, Fuchs P, Lo Schiavo F, Raffaello A, et al.** (2017) 'Physiological characterization of a plant mitochondrial calcium uniporter in vitro and in vivo', *Plant Physiology*, 173, pp. 1355–1370. doi: 10.1104/pp.16.01359.

**Tedersoo L, May TW and Smith ME** (2010) 'Ectomycorrhizal lifestyle in fungi: Global diversity, distribution, and evolution of phylogenetic lineages', *Mycorrhiza*, 20, pp. 217–263. doi: 10.1007/s00572-009-0274-x.

**Terabayashi S, Takii K and Namiki T** (1991) 'Variations in diurnal uptake of water and nutrients by tomato plants grown hydroponically', *Journal of the Japanese Society for Horticultural Science*, 60, pp. 547–553.

**Terrile MC, Tonón CV, Iglesias MJ, Lamattina L and Casalengué CA** (2010) 'Extracellular ATP and nitric oxide signaling pathways regulate redox-dependent responses associated to root hair growth in etiolated *Arabidopsis* seedlings', *Plant Signaling & Behavior*, 5, pp. 698–701. doi: 10.1016/j.jplph.2009.11.002.xtracellular.

**Thibaud MC, Arrighi JF, Bayle V, Chiarenza S, Creff A, Bustos R, Paz-Ares J, Poirier Y and Nussaume L** (2010) 'Dissection of local and systemic transcriptional responses to phosphate starvation in *Arabidopsis*', *Plant Journal*, 64, pp. 775–789. doi: 10.1111/j.1365-313X.2010.04375.x.

**Thomas C, Sun Y, Naus K, Lloyd A and Roux S** (1999) 'Apyrase functions in plant phosphate nutrition and mobilizes phosphate from extracellular ATP', *Plant Physiology*, 119, pp. 543–552. doi: 10.1104/pp.119.2.543.

**Thor K and Peiter E** (2014) 'Cytosolic calcium signals elicited by the pathogen-associated molecular pattern flg22 in stomatal guard cells are of an oscillatory nature', *New Phytologist*, 204, pp. 873–881.

**Tian L, Hires SA, Mao T, Huber D, Chiappe ME, Chalasani SH, Petreanu L, Akerboom J, McKinney SA, Schreiter ER, et al.** (2009) 'Imaging neural activity in worms, flies and mice with improved GCaMP calcium indicators', *Nature Methods*, 6, pp. 875–881. doi: 10.1038/nmeth.1398.

**Tian S, Wang X, Li P, Wang H, Ji H, Xie J, Qiu Q, Shen D and Dong H** (2016) 'Plant aquaporin AtPIP1;4 links apoplastic H<sub>2</sub>O<sub>2</sub> induction to disease immunity pathways', *Plant Physiology*, 171, pp. 1635–1650. doi: 10.1104/pp.15.01237.

**Ticconi CA, Lucero RD, Sakhonwasee S, Adamson AW, Creff A, Nussaume L, Desnos T and Abel S** (2009) 'ER-resident proteins PDR2 and LPR1 mediate the developmental response

of root meristems to phosphate availability', *Proceedings of the National Academy of Sciences*, 106, pp. 14174–14179. doi: 10.1073/pnas.0901778106.

**Ticconi CA, Delatorre CA and Abel S** (2001) 'Attenuation of phosphate starvation responses by phosphite in *Arabidopsis*', *Plant Physiology*, 127, pp. 963–972. doi: 10.1104/pp.010396.availability.

**Till BJ, Reynolds SH, Greene E a, Codomo C a, Enns LC, Johnson JE, Burtner C, Odden a R, Young K, Taylor NE, et al.** (2003) 'Large scale discovery of induced point mutations with high throughput TILLING', *Genome Research*, 13, pp. 524–530. doi: 10.1101/gr.977903.

**Tjellstrom H, Hellgren LI, Wieslander A and Sandelius AS** (2010) 'Lipid asymmetry in plant plasma membranes: phosphate deficiency-induced phospholipid replacement is restricted to the cytosolic leaflet', *The FASEB Journal*, 24, pp. 1128–1138. doi: 10.1096/fj.09-139410.

**Toyota M, Spencer D, Sawai-toyota S, Jiaqi W and Zhang T** (2018) 'Glutamate triggers long-distance, calcium-based plant defense signaling', *Science*, 361, pp. 1112–1115.

**Tracey F, Gilliham M, Dodd A, Webb A and Tester M** (2008) 'NaCl-induced changes in cytosolic free Ca<sup>2+</sup> in *Arabidopsis thaliana* are heterogeneous and modified by external ionic composition', *Plant, Cell and Environment*, 31, pp. 1063–1073. doi: 10.1111/j.1365-3040.2008.01817.x.

**Tran D, Galletti R, Neumann ED, Dubois A, Sharif-Naeini R, Geitmann A, Frachisse J-M, Hamant O and Ingram GC** (2017) 'A mechanosensitive Ca<sup>2+</sup> channel activity is dependent on the developmental regulator DEK1', *Nature Communications*, 8. doi: 10.1038/s41467-017-00878-w.

**Traut TW** (1994) 'Physiological concentrations of purines and pyrimidines', *Molecular and Cellular Biochemistry*, 140. doi: 10.1007/BF00928361.

**Tripathi D, Zhang T, Koo AJ, Stacey G and Tanaka K** (2017) 'Extracellular ATP acts on jasmonate signaling to reinforce plant defense', *Plant Physiology*. doi: 10.1104/pp.17.01477.

**Tsien RW, Hess P, McCleskey EW and Rosenberg RL** (1987) 'Calcium channels: Mechanisms of selectivity, permeation, and block', *Annual Review of Biophysics and Biomolecular Structure*, 16, pp. 265–290. doi: 10.1146/annurev.biophys.16.1.265.

**Tsien RY, Pozzan T and Rink TJ** (1982) 'Calcium homeostatis in intact lymphocytes: Cytoplasmic free calcium monitored with a new, intracellularly trapped fluorescent indicator', *Journal of Cell Biology*, 94, pp. 325–334.

**Ullrich-Eberius CI, Novacky A, Fischer E and Lüttge U** (1981) 'Relationship between energy-dependent phosphate uptake and the electrical membrane potential in *Lemna gibba* G1', *Plant Physiology*, 67, pp. 797–801. doi: 10.1104/pp.67.4.797.

**Ullrich CI and Novacky AJ** (1990) 'Extra- and intracellular pH and membrane potential changes induced by  $K^+$ ,  $Cl^-$ ,  $H_2PO_4^-$ , and  $NO_3^-$  uptake and fusicoccin in root hairs of *Limnium stoloniferum*', *Plant Physiology*, 94, pp. 1561–1567. doi: 10.1104/pp.94.4.1561.

**Umehara M, Hanada A, Magome H, Takeda-Kamiya N and Yamaguchi S** (2010) 'Contribution of strigolactones to the inhibition of tiller bud outgrowth under phosphate deficiency in rice', *Plant and Cell Physiology*, 51, pp. 1118–1126. doi: 10.1093/pcp/pcq084.

**United States Geological Survey** (2018) 'Mineral commodity summaries - Phosphate rock', accessed at: [https://minerals.usgs.gov/minerals/pubs/commodity/phosphate\\_rock/mcs-2018-phosp.pdf](https://minerals.usgs.gov/minerals/pubs/commodity/phosphate_rock/mcs-2018-phosp.pdf)

**Vadassery J, Ranf S, Drzewiecki C, Mithöfer A, Mazars C, Scheel D, Lee J and Oelmüller R** (2009) 'A cell wall extract from the endophytic fungus *Piriformospora indica* promotes growth of *Arabidopsis* seedlings and induces intracellular calcium elevation in roots', *The Plant Journal*, 59, pp. 193–206. doi: 10.1111/j.1365-313X.2009.03867.x.

**Vaz Martins T, Evans M, Woolfenden H and Morris R** (2013) 'Towards the physics of calcium signalling in plants', *Plants*, 2, pp. 541–588. doi: 10.3390/plants2040541.

**Vega MA, Santamaria EC, Morales A and Boland RL** (1985) 'Vitamin D3 affects growth and  $Ca^{2+}$  uptake by *Phaseolus vulgaris* roots cultured in vitro', *Physiologia Plantarum*, 65, pp. 423–426. doi: 10.1111/j.1399-3054.1985.tb08667.x.

**Vega MA and Boland RL** (1986) 'Vitamin D3 induces the de novo synthesis of calmodulin in *Phaseolus vulgaris* root semnets growing in vitro', *Biochimica et Biophysica Acta*, 881, pp. 364–374.

**Verkhatsky A and Parpura V** (2015) 'Calcium signalling and calcium channels: Evolution and general principles', *European Journal of Pharmacology*. doi: 10.1016/j.ejphar.2013.11.013.Calcium.

**Versaw WK and Garcia LR** (2017) 'Intracellular transport and compartmentation of phosphate in plants', *Current Opinion in Plant Biology*, 39, pp. 25–30. doi: 10.1016/j.pbi.2017.04.015.

**Very A-A and Davies JM** (2000) 'Hyperpolarization-activated calcium channels at the tip of *Arabidopsis* root hairs', *Proceedings of the National Academy of Science*, 97, pp. 9801–9806.



- Vincent TR, Canham J, Toyota M, Avramova M, Mugford ST, Gilroy S, Miller AJ, Hogenhout S and Sanders D** (2017) 'Real-time in vivo recording of *Arabidopsis* calcium signals during insect feeding using a fluorescent biosensor', *Journal of Visualized Experiments*. doi: 10.3791/56142.
- Vincill ED, Bieck AM and Spalding EP** (2012) 'Ca<sup>2+</sup> conduction by an amino acid-gated ion channel related to glutamate receptors', *Plant Physiology*, 159, pp. 40–46. doi: 10.1104/pp.112.197509.
- Vörösmarty CJ, McIntyre PB, Gessner MO, Dudgeon D, Prusevich A, Green P, Glidden S, Bunn SE, Sullivan CA, Liermann CR, et al.** (2010) 'Global threats to human water security and river biodiversity', *Nature*, 467, pp. 555–561. doi: 10.1038/nature09440.
- Waadt R, Krebs M and Schumacher K** (2017) 'Multiparameter imaging of calcium and abscisic acid and high-resolution quantitative calcium measurements using R-GECO1-mTurquoise in *Arabidopsis*', *New Phytologist*, 216, pp. 303–320. doi: 10.1111/nph.14706.
- Wagner S, Behera S, De Bortoli S, Logan DC, Fuchs P, Carraretto L, Teardo E, Cendron L, Nietzel T, Fussl M, et al.** (2015) 'The EF-hand Ca<sup>2+</sup> binding protein MICU choreographs mitochondrial Ca<sup>2+</sup> dynamics in *Arabidopsis*', *The Plant Cell*. doi: 10.1105/tpc.15.00509.
- Wang L, Ruiz-Agudo E, Putnis C V., Menneken M and Putnis A** (2012) 'Kinetics of calcium phosphate nucleation and growth on calcite: Implications for predicting the fate of dissolved phosphate species in alkaline soils', *Environmental Science and Technology*, 46, pp. 834–842. doi: 10.1021/es202924f.
- Wang L and Liu D** (2018) 'Functions and regulation of phosphate starvation-induced secreted acid phosphatases in higher plants', *Plant Science*, 271, pp. 108–116. doi: 10.1016/j.plantsci.2018.03.013.
- Wang L, Wilkins KA and Davies JM** (2018) '*Arabidopsis* DORN1 extracellular ATP receptor; activation of plasma membrane K<sup>+</sup>- and Ca<sup>2+</sup>-permeable conductances', *New Phytologist*. doi: 10.1111/nph.15111.
- Wang ZQ, Zhou X, Dong L, Guo J, Chen Y, Zhang Y, Wu L and Xu M** (2018) 'iTRAQ-based analysis of the *Arabidopsis* proteome reveals insights into the potential mechanisms of anthocyanin accumulation regulation in response to phosphate deficiency', *Journal of Proteomics*. doi: 10.1016/j.jprot.2018.06.006.
- Ward JT, Lahner B, Yakubova E, Salt DE and Raghothama KG** (2008) 'The effect of iron on the primary root elongation of *Arabidopsis* during phosphate deficiency', *Plant Physiology*, 147, pp. 1181–1191. doi: 10.1104/pp.108.118562.

**Waters BM and Armbrust LC** (2013) ‘Optimal copper supply is required for normal plant iron deficiency responses’, *Plant Signaling & Behavior*, 8. doi: 10.4161/psb.26611.

**Weerasinghe RR, Swanson SJ, Okada SF, Garrett MB, Kim S-Y, Stacey G, Boucher RC, Gilroy S and Jones AM** (2009) ‘Touch induces ATP release in *Arabidopsis* roots that is modulated by the heterotrimeric G-protein complex’, *FEBS Letters*, 583, pp. 2521–2526. doi: 10.1016/j.febslet.2009.07.007.

**Weigend M, Mustafa A and Ensikat H-J** (2017) ‘Calcium phosphate in plant trichomes: the overlooked biomineral’, *Planta*. doi: 10.1007/s00425-017-2826-1.

**Werner F, Mueller CW, Thieme J, Gianoncelli A, Rivard C, Höschel C and Prietzel J** (2017) ‘Micro-scale heterogeneity of soil phosphorus depends on soil substrate and depth’, *Scientific Reports*, 7. doi: 10.1038/s41598-017-03537-8.

**Westheimer FH** (1987) ‘Why nature chose phosphates’, *Science*, 235, pp. 1173–1178.

**Whalley HJ, Sargeant AW, Steele JFC, Lacoere T, Lamb R, Saunders NJ, Knight H and Knight MR** (2011) ‘Transcriptomic analysis reveals calcium regulation of specific promoter motifs in *Arabidopsis*’, *The Plant Cell*, 23, pp. 4079–4095. doi: 10.1105/tpc.111.090480.

**Whalley HJ and Knight MR** (2013) ‘Calcium signatures are decoded by plants to give specific gene responses’, *New Phytologist*, 197, pp. 690–693. doi: 10.1111/nph.12087.

**White PJ** (2001) ‘The pathways of calcium movement to the xylem’, *Journal of Experimental Botany*, 52, pp. 891–899. doi: 10.1093/jexbot/52.358.891.

**White PJ and Broadley MR** (2003) ‘Calcium in plants’, *Annals of Botany*, 92, pp. 487–511. doi: 10.1093/aob/mcg164.

**Wild R, Gerasimaite R, Jung JY, Truffault V, Pavlovic I, Schmidt A, Saiardi A, Jacob Jessen H, Poirier Y, Hothorn M, et al.** (2016) ‘Control of eukaryotic phosphate homeostasis by inositol polyphosphate sensor domains’, *Science*, 352, pp. 986–990. doi: 10.1126/science.aad9858.

**Wilkins K, Matthus E, Swarbreck S and Davies J** (2016) ‘Calcium-mediated abiotic stress signaling in roots’, *Frontiers in Plant Science*. doi: 10.3389/fpls.2016.01296.

**Williamson LC, Ribrioux SP, Fitter a H and Leyser HM** (2001) ‘Phosphate availability regulates root system architecture in *Arabidopsis*’, *Plant physiology*, 126, pp. 875–882. doi: 10.1104/pp.126.2.875.

- Williamson RE** and **Ashley CC** (1982) 'Free  $\text{Ca}^{2+}$  and cytoplasmic streaming in the alga *Chara*', *Nature*, 296, pp. 647–651. doi: 10.1038/296647a0.
- Woody ST**, **Austin-Phillips S**, **Amasino RM** and **Krysan PJ** (2007) 'The WiscDsLox T-DNA collection: An *Arabidopsis* community resource generated by using an improved high-throughput T-DNA sequencing pipeline', *Journal of Plant Research*, 120, pp. 157–165. doi: 10.1007/s10265-006-0048-x.
- Wu J**, **Steinebrunner I**, **Sun Y**, **Butterfield T**, **Torres J**, **Arnold D**, **Gonzalez A**, **Jacob F**, **Reichler S** and **Roux SJ** (2007) 'Apyrases (nucleoside triphosphate-diphosphohydrolases) play a key role in growth control in *Arabidopsis*', *Plant Physiology*, 144, pp. 961–975. doi: 10.1104/pp.107.097568.
- Wu SJ**, **Siu KC** and **Wu JY** (2011) 'Involvement of anion channels in mediating elicitor-induced ATP efflux in *Salvia miltiorrhiza* hairy roots', *Journal of Plant Physiology*, 168, pp. 128–132. doi: 10.1016/j.jplph.2010.07.015.
- Wu SJ** and **Wu JY** (2008) 'Extracellular ATP-induced NO production and its dependence on membrane  $\text{Ca}^{2+}$  flux in *Salvia miltiorrhiza* hairy roots', *Journal of Experimental Botany*, 59, pp. 4007–4016. doi: 10.1093/jxb/ern242.
- Wu Y**, **Xun Q**, **Guo Y**, **Zhang J**, **Cheng K**, **Shi T**, **He K**, **Hou S**, **Gou X** and **Li J** (2016) 'Genome-wide expression pattern analyses of the *Arabidopsis* leucine-rich repeat receptor-like kinases', *Molecular Plant*, 9, pp. 289–300. doi: 10.1016/j.molp.2015.12.011.
- Wudick MM**, **Li X**, **Valentini V**, **Geldner N**, **Chory J**, **Lin J**, **Maurel C** and **Luu DT** (2015) 'Subcellular redistribution of root aquaporins induced by hydrogen peroxide', *Molecular Plant*, 8, pp. 1103–1114. doi: 10.1016/j.molp.2015.02.017.
- Xu B**, **Cheval C**, **Laohavisit A**, **Hocking B**, **Chiasson D**, **Olsson TSG**, **Shirasu K**, **Faulkner C** and **Gilliham M** (2017) 'A calmodulin-like protein regulates plasmodesmal closure during bacterial immune responses', *New Phytologist*, 215, pp. 77–84. doi: 10.1111/nph.14599.
- Yadav SR**, **Yan D**, **Sevilem I** and **Helariutta Y** (2014) 'Plasmodesmata-mediated intercellular signaling during plant growth and development', *Frontiers in Plant Science*, 5. doi: 10.3389/fpls.2014.00044.
- Yamanaka T**, **Nakagawa Y**, **Mori K**, **Nakano M**, **Imamura T**, **Kataoka H**, **Terashima A**, **Iida K**, **Kojima I**, **Katagiri T**, *et al.* (2010) 'MCA1 and MCA2 that mediate  $\text{Ca}^{2+}$  uptake have distinct and overlapping roles in *Arabidopsis*', *Plant Physiology*, 152, pp. 1284–1296. doi: 10.1104/pp.109.147371.

**Yamawaki BM, Kanno S, Ishibashi H, Noda A, Hirose A, Tanoi K and Nakanishi TM** (2011) 'A study of <sup>32</sup>phosphate uptake in a plant by a real-time imaging system', *Proceedings Radiochimica Acta*, 293, pp. 289–293. doi: 10.1524/rcpr.2011.0050.

**Yang S-Y, Huang T-K, Kuo H-F and Chiou T-J** (2017) 'Role of vacuoles in phosphorus storage and remobilization', *Journal of Experimental Botany*. doi: 10.1093/jxb/erw481.

**Yang X, Wang B, Farris B, Clark G and Roux SJ** (2015) 'Modulation of root skewing in *Arabidopsis* by apyrases and extracellular ATP', *Plant and Cell Physiology*, 56, pp. 2197–2206. doi: 10.1093/pcp/pcv134.

**Ye Q, Wang H, Su T, Wu W-H and Chen Y-F** (2018) 'The ubiquitin E3 ligase PRU1 regulates WRKY6 degradation to modulate phosphate homeostasis in response to low-Pi stress in *Arabidopsis*', *The Plant Cell*. doi: 10.1105/tpc.17.00845.

**Yi K, Menand B, Bell E and Dolan L** (2010) 'A basic helix-loop-helix transcription factor controls cell growth and size in root hairs', *Nature Genetics*, 42, pp. 264–267. doi: 10.1038/ng.529.

**Yong-Villalobos L, González-Morales SI, Wrobel K, Gutiérrez-Alanis D, Cervantes-Peréz SA, Hayano-Kanashiro C, Oropeza-Aburto A, Cruz-Ramírez A, Martínez O and Herrera-Estrella L** (2015) 'Methylome analysis reveals an important role for epigenetic changes in the regulation of the *Arabidopsis* response to phosphate starvation', *Proceedings of the National Academy of Sciences*, 112. doi: 10.1073/pnas.1522301112.

**Yoshioka K, Moeder W, Kang HG, Kachroo P, Masmoudi K, Berkowitz G and Klessig DF** (2006) 'The chimeric *Arabidopsis* CYCLIC NUCLEOTIDE-GATED ION CHANNEL11/12 activates multiple pathogen resistance responses', *The Plant Cell*, 18, pp. 747–763. doi: 10.1105/tpc.105.038786.

**Yu IC, Parker J and Bent AF** (1998) 'Gene-for-gene disease resistance without the hypersensitive response in *Arabidopsis* dnd1 mutant', *Proceedings of the National Academy of Sciences*, 95, pp. 7819–7824. doi: 10.1073/pnas.95.13.7819.

**Yuan F, Yang H, Xue Y, Kong D, Ye R, Li C, Zhang J and Theprungsirikul L** (2014) 'OSCA1 mediates osmotic-stress-evoked Ca<sup>2+</sup> increases vital for osmosensing in *Arabidopsis*', *Nature*, 514, pp. 367–371. doi: 10.1038/nature13593.

**Yuan J, Zhang Y, Dong J, Sun Y, Lim BL, Liu D and Lu ZJ** (2016) 'Systematic characterization of novel lncRNAs responding to phosphate starvation in *Arabidopsis thaliana*', *BMC Genomics*, 17. doi: 10.1186/s12864-016-2929-2.

- Yuan Y, Lee HT, Hu H, Scheben A and Edwards D** (2018) 'Single-cell genomic analysis in plants', *Genes*, 9. doi: 10.3390/genes9010050.
- Yuen CCY and Christopher DA** (2013) 'The group IV-A cyclic nucleotide-gated channels, CNGC19 and CNGC20, localize to the vacuole membrane in *Arabidopsis thaliana*', *AoB Plants*, 5. doi: 10.1093/aobpla/plt012.
- Zepeda-Jazo I, Velarde-Buendia AM, Enriquez-Figueroa R, Bose J, Shabala S, Muniz-Murguía J and Pottosin II** (2011) 'Polyamines interact with hydroxyl radicals in activating Ca<sup>2+</sup> and K<sup>+</sup> transport across the root epidermal plasma membranes', *Plant Physiology*, 157, pp. 2167–2180. doi: 10.1104/pp.111.179671.
- Zhang S, Pan Y, Tian W, Dong M, Zhu H, Luan S and Li L** (2017) '*Arabidopsis* CNGC14 mediates calcium influx required for tip-growth in root hairs', *Molecular Plant*. doi: 10.1016/j.molp.2017.02.007.
- Zhang X, Shen Z, Sun J, Yu Y, Deng S, Li Z, Sun C, Zhang J, Zhao R, Shen X, et al.** (2015) 'NaCl-elicited, vacuolar Ca<sup>2+</sup> release facilitates prolonged cytosolic Ca<sup>2+</sup> signaling in the salt response of *Populus euphratica* cells', *Cell Calcium*, 57, pp. 348–365. doi: 10.1016/j.ceca.2015.03.001.
- Zhang Y, Wang Y, Taylor JL, Jiang Z, Zhang S, Mei F, Wu Y, Wu P and Ni J** (2015) 'Aequorin-based luminescence imaging reveals differential calcium signalling responses to salt and reactive oxygen species in rice roots', *Journal of Experimental Botany*, 66, pp. 2535–2545. doi: 10.1093/jxb/erv043.
- Zhao P, Wang L and Yin H** (2018) 'Transcriptional responses to phosphate starvation in *Brachypodium distachyon* roots', *Plant Physiology and Biochemistry*, 122, pp. 113–120. doi: 10.1016/j.plaphy.2017.11.010.
- Zhu R, Dong X, Hao W, Gao W, Zhang W, Xia S, Liu T and Shang Z** (2017) 'Heterotrimeric G protein-regulated Ca<sup>2+</sup> influx and PIN2 asymmetric distribution are involved in *Arabidopsis thaliana* roots' avoidance response to extracellular ATP', *Frontiers in Plant Science*, 8. doi: 10.3389/fpls.2017.01522.
- Zipfel C and Oldroyd GED** (2017) 'Plant signalling in symbiosis and immunity', *Nature*, 543, pp. 328–336. doi: 10.1038/nature22009.

## 7 APPENDICES

Appendix I.....	277
Appendix II.....	282
Appendix III.....	287
Appendix IV.....	289
Appendix V.....	292
Appendix VI.....	295

## APPENDIX I

List of putative *Arabidopsis* Ca<sup>2+</sup> channel mutants and annotation details (see following pages).

Descriptions are as follows:

‘**Gene**’: Gene name as commonly abbreviated;

‘**AGI**’: Arabidopsis Genome Initiative (AGI) unique locus identifier;

‘**R / PT exp**’: Root and/or pollen tube expressed, R – root expressed, PT – pollen tube expressed, no – not expressed in root or pollen tube, NA – no annotation, expression data sourced from araport.org, supplemented with expression studies by (T) -Talke *et al.* (2003), (G) - Gobert *et al.* (2006) or (K) - Kellermeier *et al.* (2014);

‘**RH exp**’: details on root hair (RH) expression, small letter – RH expressed, capital letter – RH enriched/involved in RH morphogenesis, (-) expression specifically downregulated in RH, based on studies by A - Jones *et al.* (2006), B - Brady *et al.* (2007), C – Deal and Henikoff (2010), D – Bruex *et al.* (2012), E – Lan *et al.* (2013), F – Becker *et al.* (2014), G – Huang *et al.* (2017).

‘**T**’: Transcriptional expression changes under phosphate starvation, after Lin *et al.* (2011); +/+/+/+++ upregulated after 1/6/24 hours of starvation, -/-/- downregulated after 1/6/24 hours of starvation, noted is earliest timepoint, based on relative expression, NC – no change;

‘**P**’ Changes in protein abundance under phosphate starvation after Lan *et al.* (2012), up – upregulation, NC – no change; ‘**Co-exp**’: Co-expressed genes (other putative Ca<sup>2+</sup> channels, genes related to RH growth), sourced from atted.jp, connected on network by up to 2 edges; NA – no annotation;

‘**P-P-I**’: Protein-protein-interaction, sourced from MIND database (Jones *et al.*, 2014), given in brackets is interaction score (out of 4 replicates, how many were positive), manual curation of all protein partners that were putative Ca<sup>2+</sup> channels, involved in Ca<sup>2+</sup> transport, nutrition.

Gene	AGI	R / PT exp	RH exp	T	P	Co-exp	P-P-I
ANN1	AT1G35720	R	F, g	---	up	ANN2	CNGC17, RBOHD, PIN5, NRT1.8 (++++), CHX6, CPK15, NRT1.1 (+++), OSCA2.2, GLR2.9, CHX10, NRT1.7 (++)
ANN2	AT5G65020	R	F, g	+++	NC	ANN1, ANN3	
ANN3	AT2G38760	R	F, g	---	NC	ANN4	
ANN4	AT2G38750	R	g	NC	NC	ANN3	
ANN5	AT1G68090	R, P		NC		/	
ANN6	AT5G10220	no				/	
ANN7	AT5G10230	R		NC	NC	/	
ANN8	AT5G12380	no				/	
TPC1	AT4G03560	R, P	B, f, g	NC	NC	/	
CNGC1	AT5G53130	R	g	+		/	
CNGC2	AT5G15410	R		NC		/	
CNGC3	AT2G46430	R (T, G)		NC	NA	NA	
CNGC4	AT5G54250	no			/	/	
CNGC5	AT5G57940	R		NC	/	/	
CNGC6	AT2G23980	R	g	++	/	/	
CNGC7	AT1G15990	R (T), P			ACA7, CHX27		
CNGC8	AT1G19780	R (T), P			CHX15, CPK17, CPK34		
CNGC9	AT4G30560	R	A, B, C, d, E, F, G	NC	RHS10, RHS12		GLR2.9 (++)
CNGC10	AT1G01340	R	A	NC			
CNGC11	AT2G46440	no		NC	NC	NA	
CNGC12	AT2G46450	R		NC	NC	/	NRT1.1 (+++), CPK15, CNGC17, CHX10 (++)
CNGC13	AT4G01010	R (K)		+		/	
CNGC14	AT2G24610	R		--		MSL9	
CNGC15	AT2G28260	R	e (-)	-		/	GLR2.9 (+++)



Gene	AGI	R / PT exp	RH exp	T	P	Co-exp	P-P-J
CNGC16	AT3G48010	P				CHX14, CHX27	
CNGC17	AT4G30360	R	g			/	ANN1 (++++)
CNGC18	AT5G14870	no				/	
CNGC19	AT3G17690	R		++		CML39	
CNGC20	AT3G17700	R		NC		/	
GLR1.1	AT3G04110	R		---		/	
GLR1.2	AT5G48400	R	f			GLR1.3, GLR2.5	
GLR1.3	AT5G48410	R	f	NC		GLR1.2, GLR2.5, PHT3;2	
GLR1.4	AT3G07520	no				/	
GLR2.1	AT5G27100	R	B, f, G	NC		/	
GLR2.2	AT2G24720	NA				/	
GLR2.3	AT2G24710	NA		---	up	/	
GLR2.4	AT4G31710	R	f			/	
GLR2.5	AT5G11210	no		++		GLR1.3	
GLR2.6	AT5G11180	NA		NC		/	
GLR2.7	AT2G29120	no				LPR2	
GLR2.8	AT2G29110	R				/	
GLR2.9	AT2G29100	R (K)			up	/	CNGC15 (+++), CNGC9 (++) , ANNI (++)
GLR3.1	AT2G17260	R		NC		GLR3.6	
GLR3.2	AT4G35290	no				/	
GLR3.3	AT1G42540	R		NC		/	
GLR3.4	AT1G05200	no	g			/	
GLR3.5	AT2G32390	R	f, g	NC		/	
GLR3.6	AT3G51480	R		NC		GLR3.1	
GLR3.7	AT2G32400	R		NC		/	

Gene	AGI	R / PT exp	RH exp	T	P	Co-exp	P-P-I
MSL1	AT4G00290	no	g			NA	
MSL2	AT5G10490	R	g	NC		/	
MSL3	AT1G58200	R, P	f, g	NC	NC	/	
MSL4	AT1G53470	no	g			NA	
MSL5	AT3G14810	no			NC	NA	
MSL6	AT1G78610	R	g	++		CPK15	
MSL7	AT2G17000	no				/	
MSL8	AT2G17010	NA				NA	
MSL9	AT5G19520	R	e (-)	--		CNGC14	
MSL10	AT5G12080	R, P	f, g	-	NC	/	
OSCA1.1	AT4G04340	R	g	-	NC	/	
OSCA1.2	AT4G22120	R	g	NC	NC	/	
OSCA1.3	AT1G11960	R		NC		OSCA2.2, OSCA3.1	
OSCA1.4	AT1G62320	P	A, C, E, G	NC		RHS10, RHS12, RHS16	
OSCA1.5	AT3G21620	no		-		/	
OSCA1.6	AT4G15430	R, P		-		/	
OSCA1.7	AT4G02900	R, P		NC		/	
OSCA1.8	AT1G32090	R	C, g	NC	NC	ACA8	
OSCA2.1	AT1G58520	no	g	---		NA	
OSCA2.2	AT1G10090	R	F, g	NC		OSCA1.3, OSCA3.1	ANN1 (++)
OSCA2.3	AT3G01100	R, P	A, f, g	NC		/	RHD2, CPK13 (++)
OSCA2.4	AT1G69450	R, P	F, G	++	NC	SPX-domain containing protein (At1g63010)	
OSCA2.5	AT3G54510	R, P	f	++		/	
OSCA3.1	AT1G30360	R	C, g	+	NC	OSCA2.2	CaS (At5g23060) (++++), GLR2.9 (++)
OSCA4.1	AT4G35870	R, P	f, g	NC		/	

Gene	AGI	R / PT exp	RHexp	T	P	Co-exp	P-P-I
MCA1	At4G35920	R	g	-		/	
MCA2	At2G17780	R				/	
Piezo	At2G48060	no	g			PAP28	
calcium uniporter-like protein (DUF607)	At1g09575	R		+ - - - -		/	
calcium uniporter (DUF607)	At2g23790	no				/	
calcium uniporter (DUF607)	At4g36820	NA			up	/	ATIPS2 (At5g03545) (++++)
ACA1	At1g27770	R		NC	NC	/	
calcium uniporter (DUF607)	At1g57610	no				/	
calcium uniporter (DUF607)	At5g42610	NA				/	
calcium uniporter (DUF607)	At5g66650	R		+		/	

## APPENDIX II

Library of putative *Arabidopsis* Ca<sup>2+</sup> channel mutants as assembled in this thesis, including origin of seed stock, mutant details and genotyping details (see following pages, including table with multiple mutant lines, mutant lines that were genotyped to be wild typical for the mutation, mutant lines that did not germinate). Descriptions are as follows:

‘**Allele name**’: Abbreviated mutant line name, dash indicates more than one allele for the mutation was processed. Bold print – genotyped homozygous in this thesis and/or previously in our laboratory. Superscript letters indicate origin of seed stock and further resources, A – gift from Lee et al. (2004); B – see J. Mortimer PhD thesis, University of Cambridge, for further details; C – gift from Edgar Peiter group; D – gift from (and genotyped, if not stated otherwise) by Keiko Yoshioka group; E – gift from and genotyped by Gerald Berkowitz group; F – gift from Zhonglin Shang group; G – gift from and genotyped by Alex Costa group (seed originally from José Feijo, published in Michard *et al.*, 2011); H – gift from Elisasbeth Hasell / Elliot Meyerowitz group; I – gift from Hidetoshi Iida group; J – triple mutant generated by Adeeba Dark, Julia Davies group; / - not genotyped in this thesis, ? – line likely homozygous for the mutation but genotyping during this PhD project was troublesome / could not repeat previous results / line needs to be sequenced (refer to laboratory books by EM for further information).

‘**AGI**’: *Arabidopsis* Genome Initiative (AGI) unique locus identifier;

‘**Mutant details**’: Unique identifier for mutant line

‘**Paired WT**’: Paired wild type *Arabidopsis*, as was used for mutagenesis background; used as control wild type in this thesis,

‘**WT size**’: Wild type amplicon band size in number of base pairs, as predicted by Signal Salk Primer Design Tool, when using LP + RP primer

‘**M size**’: Mutant amplicon band size in number of base pairs, as predicted by Signal Salk Primer Design Tool, when using LP/RP primer together with LBb1.3 SALK T-DNA-specific primer (ATTTTGCCGATTTCCGAAC).

‘**LP**’: Left genomic primer used for genotyping

‘**RP**’: Right genomic primer used for genotyping

Allele name	AGI	Mutant details	Paired WT	WT size	Msize	LP	RP
<b>ann1</b> <sup>A</sup>	AT1G35720	SALK_015426	Col-0	1227	598-898	TGTTGTTGGTCTCCCTTTTGG	AATCTTTGGGCTCACAGAA GTGC
<b>ann2</b>	AT5G65020	SALK_054223	Col-0	/	/		
<b>ann3</b>	AT2G38760	SALK_082344C	Col-0	1010	455-755	TCCTCAAAAACGAAAAA TCTCG	CATA GCCGCCTCAA TAGTAGC
<b>ann4</b>	AT2G38750	SALK_019725	Col-0	/	/		
<b>ann5</b> <sup>B</sup>	AT1G68090	AgricolaRNAi	Col-9	/	/		
<b>ann7</b>	AT5G10230	SAIL_253_F05	Col-3	1278	542-942	CGTTGGCTATTGIGGGAATAG	ACGCTATGACCCAA CCAAACTG
<b>ann8-1</b>	AT5G12380	SALK_056246C	Col-0	1062	440-740	AACA GAGGATGATCTGGGTC	GCTTCTCTGGAACA AATTCC
<b>ann8-2</b>	AT5G12380	SALK_062276C	Col-0	1135	448-748	AGGATGATCTGGGTCCTTGG	CAAAAATTGCCAGAGAGCTCAG
<b>tpc1-2</b> <sup>C</sup>	AT4G03560	SALK_145413	Col-0	/	/		
<b>engc1-2</b>	AT5G53130	SALK_047403	Col-0	1133	505-805	TTGATTTGATCCCATAA CCAAAC	TGCTTCA TGTGTCTTCTTCAAC
<b>engc1-3</b> <sup>D</sup>	AT5G53130	SAIL_443_B11	Col-3	/	/		
<b>engc2-1</b> <sup>E</sup>	AT5G15410	EMS	Col-0	/	/		
<b>engc2-2</b> <sup>D</sup>	AT5G15410	SALK_066908 ?		1229	550-850	ATA TCCA A CTGTCTGTTCGG	CTTTCCA TTCA A CTAGCTGGG
<b>engc3-1</b> <sup>D,F</sup>	AT2G46430	SALK_066634	Col-0	1097	530-830	CTGTTGCGCTTTA GCCCTTGG	CAC TCGTCTTCAA A GTTTTGGC
<b>engc3-2</b> <sup>D,F</sup>	AT2G46430	SALK_056832	Col-0	1027	499-799	AAA TCA GA ACCTTTAA GCGGC	TACCAA AAGTTGAAA A A CCGTCCG
<b>engc5-1</b>	AT5G57940	SALK_053354C	Col-0	1217	561-861	TCGATA AACACCGAA A CCAAAG	GAGACTGGAGGTTGGA A TTCC
<b>engc5-2</b> <sup>D,F</sup>	AT5G57940	SALK_149893	Col-0	1017	433-733	GAGCTTTCTGGTTA A GCCGTC	CACGCTCCCTA A GATCTTGTG
<b>engc5-3</b> <sup>D</sup>	AT5G57940	SAIL_215_F04	Col-3	1104	525-825	CAGCGTGTGTTA CGTCTAAG	TCTTTCA GTGTTTGTGGACCC
<b>engc6</b> <sup>F</sup>	AT2G23980	SALK_042207	Col-0	1080	443-743	TCCAGGATA TGTGCTGGTTC	TCCGTTGATCTCTCTTCTTGG
<b>engc8</b>	AT1G19780	SALK_004230C		1110	527-827	ACTTGA CCGCTA A A CCA GCGTC	TCAA CCAATCAAAA A CCAAAGC
<b>engc9-1</b> <sup>D</sup>	AT4G30560	SAIL_736_D02	Col-3	1124	447-747	TGACCGCA GAGAGAGAGAG	CTTCA GGA AAAA A CTGCTCGTG
<b>engc9-2</b> <sup>F</sup> , <b>engc9-3</b> <sup>D</sup>	AT4G30560	SALK_026086	Col-0	1109	580-880	ATTTGCA GCAA A CTTTGAAGC	TGTTTATGGTGGGACTTTCAG
<b>engc10-1</b> <sup>F</sup>	AT1G01340	SALK_015952	Col-0	1191	556-865	CCTGTGCTCTACA CCGAGAAC	AGCA TTCTCCCTCA GGTTC
<b>engc12-2</b> <sup>D</sup>	AT2G46450	SALK_092657	Col-0	??	??		
<b>engc13-1</b> <sup>F</sup>	AT4G01010	SALK_057742	Col-0	1130	546-846	TTTTGGTCAA A ACACACACATG	CAGCTATGCAA A TTCGAGAA GG
<b>engc13-2</b>	AT4G01010	SALK_013536C	Col-0	1123	509-809	CCTTCTCGAA TTGCATA GCTG	TGGCATA GTTACTGAA A CCCC

Allele name	AGI	Mutant details	Paired WT	WT size	Msize	LP	RP
<b>engc14-1</b> ,	AT2G24610	SALK_206460C	Col-0	1105	546-846	TCGGAACAATTGGCGAATAAC	CACCTGCTTGTAAAGCAAAGG
<b>engc14-2</b> <sup>D</sup>				??	??		
<b>engc14-3</b> <sup>D</sup>	AT2G24610	WisDsLox437E09	Col-0	??	??	GCAACAATAATAAAGAAAACAATCAAACTCAAAAC	AGTATTACTCTTTTCACTCGGTFTT TACCC
<b>engc15-3</b>	AT2G28260	N93704	Col-0 er-105	/	/		
<b>engc16-1</b> <sup>D</sup>	AT3G48010	SALK_065792C	Col-0	/	/		
<b>engc16-2</b> <sup>D</sup>	AT3G48010	SAIL_232_B12	Col-3	/	/		
<b>engc17</b> <sup>F</sup>	AT4G30360	SALK_041923	Col-0	1125	555-855	CAGCAGCTTAGGTAAATGGCAG	ATTGATTCAAATCGCAGTGAAG
<b>engc19</b> <sup>F</sup>	AT3G17690	SALK_027306	Col-0	1114	474-774	CGCGGATCTCTTTATTTCACAC	ATGAGGATTCAATTAATCCCGGG
<b>engc20-1</b>	AT3G17700	SALK_129133C	Col-0	1055	467-767	AAACACAGITACCTGGAAAGCC	TGCCCTTACACCACTTTTGTG
<b>engc20-2</b>	AT3G17700	SALK_074919C	Col-0	1614	697-1197	TTGCATTGATTGGCATACTTG	TAAATTTACCGAGCACACCG
<b>glr1.1</b>	AT3G04110	SALK_065031	Col-0	1185	508-808	TTCGAAACTCACCGTGTATTC	TACATTCCAAACACCCGAGGAAG
<b>glr1.3</b>	AT5G48410	GK-507D11	Col-0	1246	581-881	GAGGTAAACGGGTTCAGATCC	TGGCCAGATTAATGGTCTCAAAG
<b>glr2.1</b>	AT5G27100	SAIL_439_B09	Col-3	1112	525-825	TATTGACTACCGATGGAAGCG	ATCGCAAGATTGCTTTGTGAG
<b>glr2.2-1</b>	AT2G24720	SALK_036453C	Col-0	1220	564-864	ATGAAATGCTGATTTGGCTAAG	AAACAAGAAACGGGAAGAAGCC
<b>glr2.2-3</b>	AT2G24720	SALK_060913	Col-0	1270	589-889	GAGAACTCGAGAGGAAAGAGG	AAACGGAACGAGAAAGAAGAGG
<b>glr2.4</b>	AT4G31710	SALK_010571	Col-0	1115	478-778	AGGAAACAATGTGATTGTGC	TCCAAATAATGCCCTTGTCAAAG
<b>glr2.6-1</b>	AT5G11180	SALK_046023	Col-0	1095	575-875	TGTCTCAACATCCGAGATTC	AATGGTCTTGCATTGAATTC
<b>glr2.6-2</b>	AT5G11180	SALK_132296C	Col-0	1111	575-875	TCTACGGTGAACCAAAGTTGG	TTTTTCAACAAGGGTCTTGTGG
<b>glr2.8-1</b>	AT2G29110	SALK_111659	Col-0	1129	452-752	CGCCATAGACATCTTTGAAGC	ACAATGGCATAATTCGAGCCAG
<b>glr2.9</b>	AT2G29100	SALK_125496	Col-0	1097	495-795	TGACAAAGGTGCTCCCATTAATC	AGAATTCATGGTGAACGGTTG
<b>glr3.1</b>	AT2G17260	SALK_063873C	Col-0	1161	595-895	AGATGAACAAACGTGACCAAC	TGGCTTTTGTGGTCTGATC
<b>glr3.3-2</b>	AT1G42540	SALK_082194	Col-0	1060	505-805	CAGCTCTCTTCACCCATCAAG	ACCAACCTTTATGGTCCCAAC
<b>glr3.5</b>	AT2G32390	SALK_035264	Col-0	1165	534-834	TGAAGTTGCTGCAAAATGTGAG	TGTCGACATGTCCACAGCTAG
<b>glr3.6</b>	AT3G51480	SALK_091801C	Col-0	990	437-737	TTCGTTCAAAAGGTGGCATAAC	CGACTATGAGGAAAGACCGCAG
<b>glr3.7-1</b>	AT2G32400	SALK_103942	Col-0	1169	509-809	TCCCCACTGTTGAAAATAATTG	TTGGAAGGTAACCGTGAACGTGTC
<b>(glr3.7)</b>							
<b>glr3.7-2</b> <sup>G</sup>	AT2G32400	SALK_103942.25.55.x	Col-0	1169	509-809	TCCCCACTGTTGAAAATAATTG	TTGGAAGGTAACCGTGAACGTGTC

Allele name	AGI	Mutant details	Paired WT	WT size	Msize	LP	RP
ms12	AT5G10490	SALK_032627C	Col-0	1113	480-780	TTCTTCAAGCCATTTGGATTG	GCGTGCCATATTCATTAACAG
ms13-1	AT1G58200	SALK_113015	Col-0	979	440-740	ATCCAAGAGAGATCCGAAGC	CCACCAATCCGATAATGTGAC
ms13-2	AT1G58200	SALK_125490	Col-0	1103	480-780	TAATGAGGCTGAGGTGGACAC	CTTTGCTTTGATTCACCTTGG
ms16 <sup>H</sup>	AT1G78610	SALK_067711	Col-0	1164	519-819	TCCCTTTGTTTTCTCCCTCCTC	CGAAGCTGATTTGGTCAAGTTTC
ms18	AT2G17010	SALK_142172C	Col-0	1067	492-792	AAGA CGAAGAAAGAA CCGAAC	TGTGTTGTTGTTGTTGGTGA TG
ms19 <sup>H</sup>	AT5G19520	SALK_114626	Col-0	1231	582-882	CGGTGCAAGCATGTGTTATG	AGGTCCCAGAGAGTCTGAAG
ms110 <sup>H</sup>	AT5G12080	SALK_076254	Col-0	1123	483-783	GTGGTTTCTGGGTTTAA GCC	TACTTGGAGTAA CCGGTGCTG
osca1.1-1	AT4G04340	SALK_038633C	Col-0	1265	585-885	CGTTGTTGTCCAAATTAACCG	CTCAAGAGA CTGGGTCA GGC
osca1.1-2	AT4G04340	SALK_129692C	Col-0	977	461-761	GGTTTAAACA AA CTTCATGTCCG	TGCCTCGAGATTCATA TGAAG
osca1.2-1	AT4G22120	SALK_064396	Col-0	1144	549-849	TTTCA C C C T T G T T C C T C C T T C	CGTTATGAGCCAGCTTTCATC
osca1.3	AT1G11960	SALK_092990C	Col-0	1073	473-773	TTTTACCGAA AAGGAAATTGG	GTGACATTTCTCCAGA AGCTCG
osca1.4-1	AT1G62320	SALK_021370C	Col-0	1206	608-908	TTTTATCTCCA AAATAAGCATGGG	TGAAAGTAAATGCAATCGGACC
osca1.4-2	AT1G62320	SALK_135698C	Col-0	1115	543-843	AGCGATGTGCAATTAACAATC	AATGTCGAA CGTGGATCAGAC
osca1.6	AT4G15430	SALK_015653C	Col-0	1157	474-774	AATGCCTTAACCGATCCAATC	CCAGACAAAATCCAAA AAGCTC
osca1.8-1	AT1G32090	SALK_091368C	Col-0	1122	602-902	GAA GA A G G G A A G T G G A A T T G	TCCTTCA CCAATCA CCACTCTC
osca1.8-2	AT1G32090	SALK_081479C	Col-0	1034	502-802	TTTGGTTCTTGTCTCTGTGGG	CTCTTTGCTTCA CCA C C T T T G
osca2.2-1	AT1G10090	SALK_122773C	Col-0	1050	476-776	CAGCCAA C A T C T C T C C T C A G	TTGCAAAGTTTAA GAA C C C G A G
osca2.2-2	AT1G10090	SALK_131951C	Col-0	1134	526-826	ATGCA G G G A C A A T C A G A C A A C	CAAGATCCGTATA GTCCGAGG
osca2.3-2	AT3G01100	SALK_141893C	Col-0	1129	607-907	GAAATCCCTCCCAATCTTGGC	CTATTGCA GCA CCA TGTCTTG
osca3.1-1	AT1G30360	SALK_026942C	Col-0	1140	449-749	TGAGTTTGGTACCAAGTGGC	GGTCAAAGAAGCTTGGTACCC
osca3.1-2	AT1G30360	SALK_078537C	Col-0	1154	575-875	AGCTACCTCGAGAGCTGTGTG	GGCAGAATCTCAA CATCAAGC
osca4.1-1	AT4G35870	SALK_059492C	Col-0	1214	588-888	AATTGTGTCGGATTA TCACG	CATCGTTTTCGAAAGCTCA TC
osca4.1-2	AT4G35870	SALK_139226C	Col-0	1190	555-855	CGA GA A G C A A A T T C G A A C A G	TCCCATTTCCCATCTCTAAACC
mca1 <sup>I</sup>	AT4G35920	T-DNA-tag Kazusa DNA Research Institute	Col-0	??	??	??	CAGCAGCAGCAGCTTGTGTGTAACA CCAAATTA AAC
mca2 <sup>I</sup>	AT2G17780	SALK_129208	Col-0	??	??	ATGGCTAAATTCA TGGGATCAGTTA G	GAGGTGTGGTGGAGCTCA TTTCTCT TATTAC
DUF.1	At4g36820	SALK_020393C	Col-0	1201	607-907	TCA CCA T C A A A T T T G A A T C A G C	CTCCTTCGGATGAGAAAGTCC
DUF.2	At5g66650	SALK_037347C	Col-0	1170	512-812	CGAACTGTATTCTCCCGCAGAC	A C C G T C A T C A C C A T T T A G G T G
DUF.3	At1g09575	SALK_102327C	Col-0	1274	598-898	A G C T T C A T C G G G A G A T C T A G C	TCTCAA G G A G A G A A A A G G G C

Multiple mutants		Paired WT						
Name	Paired WT							
ann1ann2ann4	Col-0							
mca1mca2 <sup>1</sup>	Col-0							
ms19ms110 <sup>H</sup>	Col-0							
ms14ms15ms16ms19ms110 <sup>H</sup>	Col-0							
WT instead of mutant		AGI	Mutant details	Paired WT	LP	RP		
Allele name	AGI	Mutant details	Paired WT	LP	RP			
cngc1-1	AT5G53130	SALK_047401	Col-0	TTGTTGTGAGCCTGTGAAATTC	GTTTGATCCTTGCA GAGCTTG			
cngc10-2	AT1G01340	SALK_071112C	Col-0	TGGTTGGTTTGTCTTGTATTTTC	CAAGTGATTTCTGCGGAGAAG			
gfr1.2-1	AT5G48400	SALK_053535C	Col-0	CGTTGGCTCAATGGAACTAAC	ATCGGTTGTGTA TGGAA GCTG			
gfr1.2-2	AT5G48400	SALK_136614C	Col-0	TTCCCTTCTAGCAACGAGTTC	GATGGAAAGAGTTTGTGGTCC			
cngc15-1	AT2G28260	SALK_017995	Col-0	TCCGTTGATGTTTTTGTATCTTG	AACCA TTTAAGCCA ACTTGGG			
gfr2.3-1	AT2G24710	SALK_113206	Col-0	TCACA CTCGAA GGTGICATG	GGAGTCTTCGTA CGTA GCAAG			
gfr2.8-2	AT2G29110	SALK_111661	Col-0	CGCCATAGACATCTTTGAAAGC	ACAATGGCATATTTGGAGCAG			
osca1.7	AT4G02900	SALK_050602C	Col-0	GCA TTTGTTCAGTCTCTTGCC	AAATTTTGAGAA GCCCGATTTC			
osca2.3-1	AT3G01100	SALK_014068C	Col-0	ATTCTTCAAAGCTCTCGAAGCC	AAGAGAA GCCTGCCAAGAATC			
osca2.4	AT1G69450	SALK_070743C	Col-0	TGGAAAGGTA TGCCTCTGATG	GTAATCCCAA GAA GCCCAAAG			
osca2.5	AT3G54510	SALK_055548C	Col-0	TTGAGTGGCTGCTGTGTTGAG	CTTGA TGGCTCTCGTCTCATC			
Germination problems		AGI	Mutant details	Paired WT	LP	RP		
Allele name	AGI	Mutant details	Paired WT	LP	RP			
osca1.2-2	AT4G22120	SALK_152349	Col-0	TTTAGGAACA A A ACCCCACAC	ATGTCACCAATCGTTACGC			
cngc15-2	AT2G28260	N93280	Col-0 er-105					
gfr2.3-2	AT2G24710	SALK_128660	Col-0	GGATTCCGGCTTTGTAA GTTCC	TGGGTCTGAA TGGAA GAACAG			
gfr2.2-2	AT2G24720	SALK_060908	Col-0	AATGAA GATCAAAGCAGCAGG	AACCGAAACGAGAAAGAAAGG			



## APPENDIX III

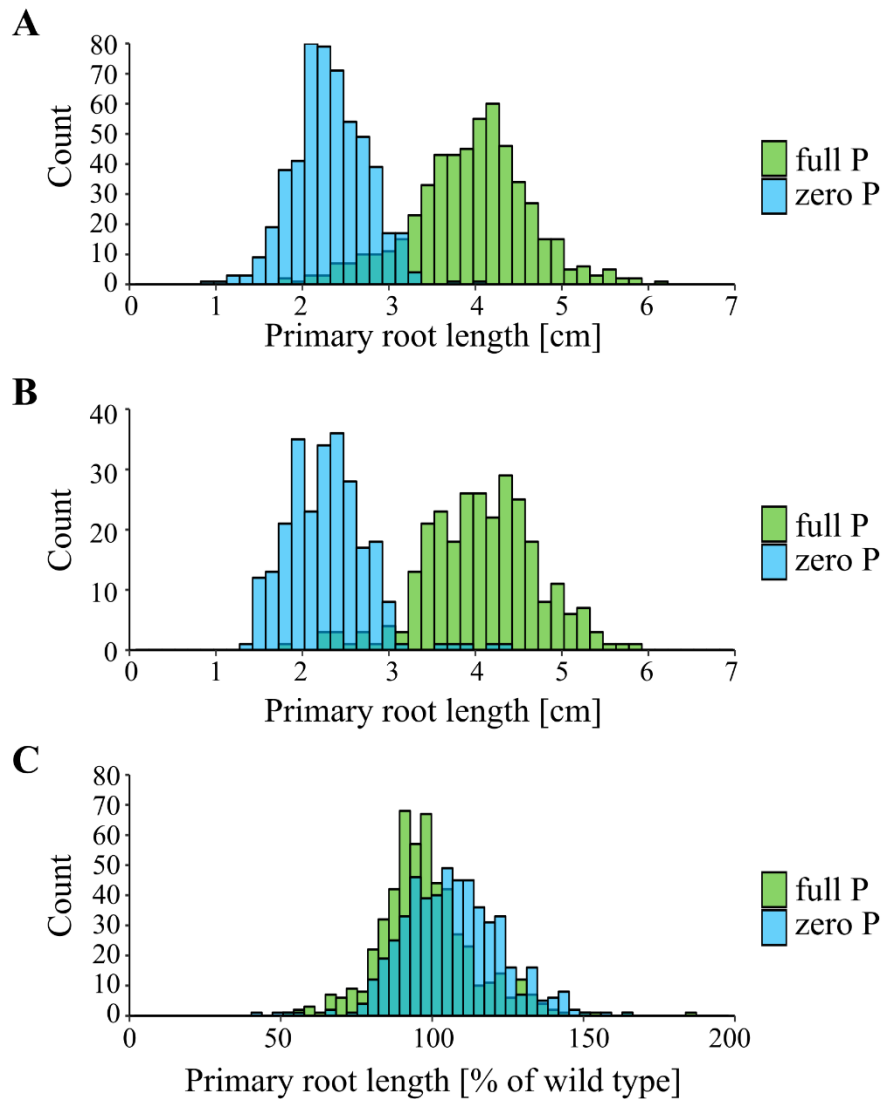
Growth conditions and quantification parameters used in previous studies reporting root hair phenotypes of *Arabidopsis*. RH – root hairs, d – days, MS – Murashige and Skoog growth medium, ATS – *Arabidopsis thaliana* salts.

Laboratory Study	Davies	Schmidt	Ludewig	Bates & Lynch	Gilroy	Dolan	Raghothama	Koltai
	Véry & Davies, 2000	Chandrika <i>et al.</i> , 2013; Li <i>et al.</i> , 2010	Stetter <i>et al.</i> , 2015	Bates <i>et al.</i> , 1996; Ma <i>et al.</i> , 2001	Bibikova <i>et al.</i> , 1997	Yi <i>et al.</i> , 2010; Datta <i>et la.</i> , 2015	Jain <i>et al.</i> , 2007; Karthikeyan <i>et al.</i>	Mayzlish-Cati <i>et al.</i> , 2012; Kapulnik <i>et al.</i> ,
Phosphate study?	no	yes	yes	yes	no	yes	yes	yes
Growth medium	0.1 mM KCl, 0.1 mM CaCl <sub>2</sub>	ATS	ATS	Half Johnson	Half Johnson	Half Johnson	Half MS	Half MS
Gelling agent	Agar	Phytigel	Phytoagar	Phytigel	Phytigel	Phytigel	Agar	Gelzan
% (w/v) gelling agent	1	0.3 - 0.4	1.2	0.2	1	0.5	1.2	0.5
% (w/v) sucrose	0	1.5	1.5	1	1	1	1.5	1.5
pH	5.6	5.5	5.7	5.7	5.7	5.7	5.7	?
Plate position	vertical	?	vertical	inclined	vertical	vertical	vertical	inclined
Light condition	16 h light/8 h	continuous	continuous	continuous	continuous	continuous	16 h light/8 h	16 h light/8 h
Plant age	3 d	14 d	10 - 20 d	8 - 16 d	4 - 7 d	4 or 7 d	7 d	2 / 4 / 6 d
RH length quantification	no quantification	2-6 mm away from tip	1 cm of tip, measuring 5 straight hairs on either side	10 randomly selected RHs in 1mm of main axis containing fully	no quantification	3 mm from tip, counting all RH with clear ends	5 mm from tip	no quantification (RH density only)

Components of growth conditions trialed to phenotype root hairs of *Arabidopsis*. ‘Inclined’ plate orientation indicates roots would need to penetrate growth medium, then grow between bottom of plastic plate and medium, whereas with ‘vertical’ plate orientation, roots will not penetrate but grow on surface of growth medium (between growth medium and air). N – nitrogen, P – phosphate, RH – root hair, RSA – root system architecture, MES - 2-(N-morpholino)ethanesulfonic.

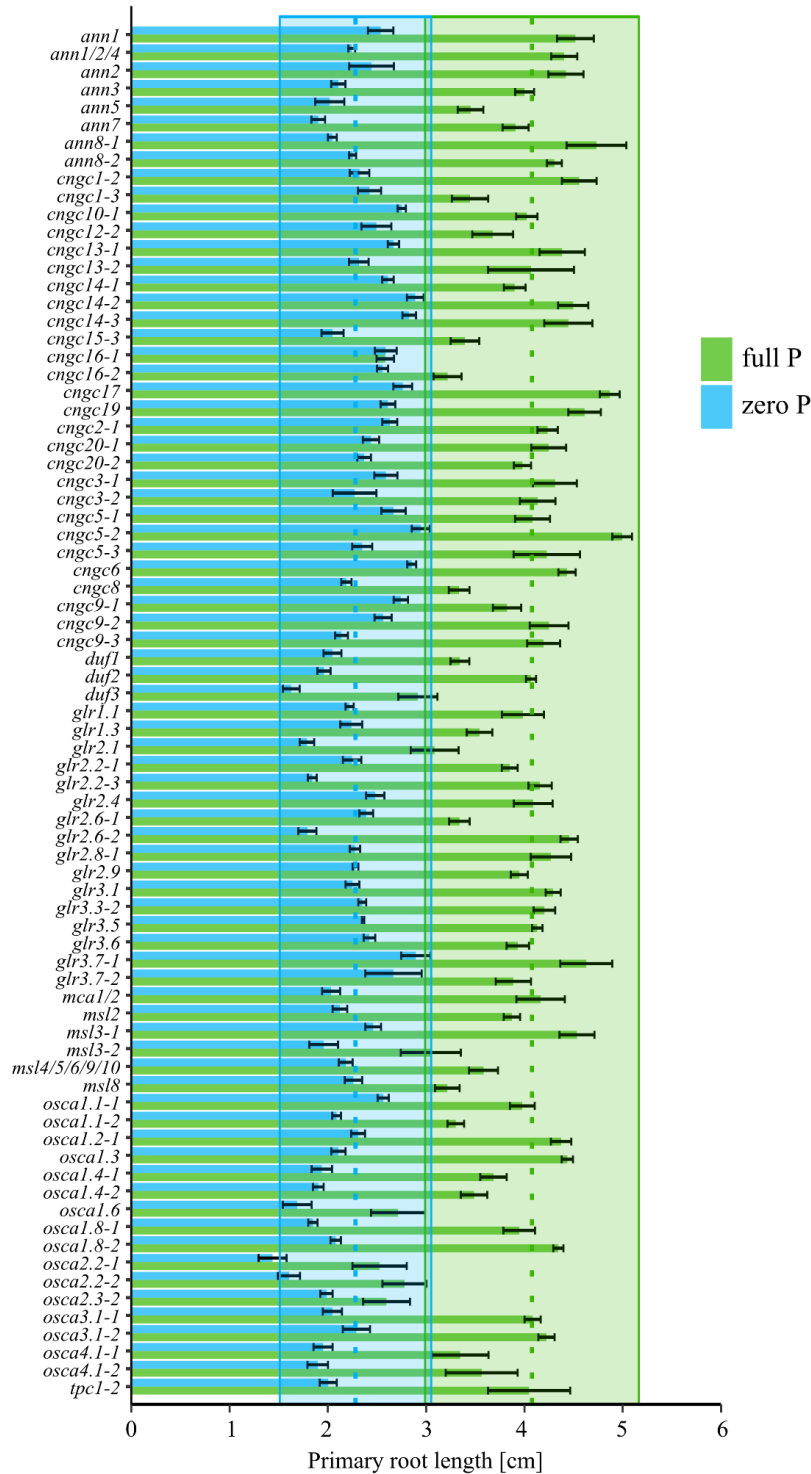
		Pro	Contra
Gelling agent	Bactoagar (BD)	no sucrose needed	RHs grow heterogeneously
		low ash content (3.6 %, with < 0.005 % P) solidifies all medium	not ideal for imaging (opaque)
	Phytigel (Sigma)	ideal for imaging (transparent) homogeneous RH growth (if +sucrose)	Sucrose required for good growth higher ash content (9.5%, with 0.15% P) doesn't solidify in low cationic medium
Plate orientation	Inclined (45°)	strong RH phenotype	roots will need to penetrate medium not space efficient
			no RSA measurements possible (scan, biomass)
			no manipulation of seedlings (e.g. add treatment)
			weak contrast under microscope
			many RHs impede correct quantification
	Vertical (90°)	space efficient RSA quantification possible manipulation of seedlings possible	RH phenotype under zero P not as pronounced
Nutrient medium	Half MS	easy preparation lab standard	high nutrient (especially N) content masks root growth
	Half Johnson	reported for many P deficiency studies MES background (pH stable)	individual component medium - more error prone

## APPENDIX IV

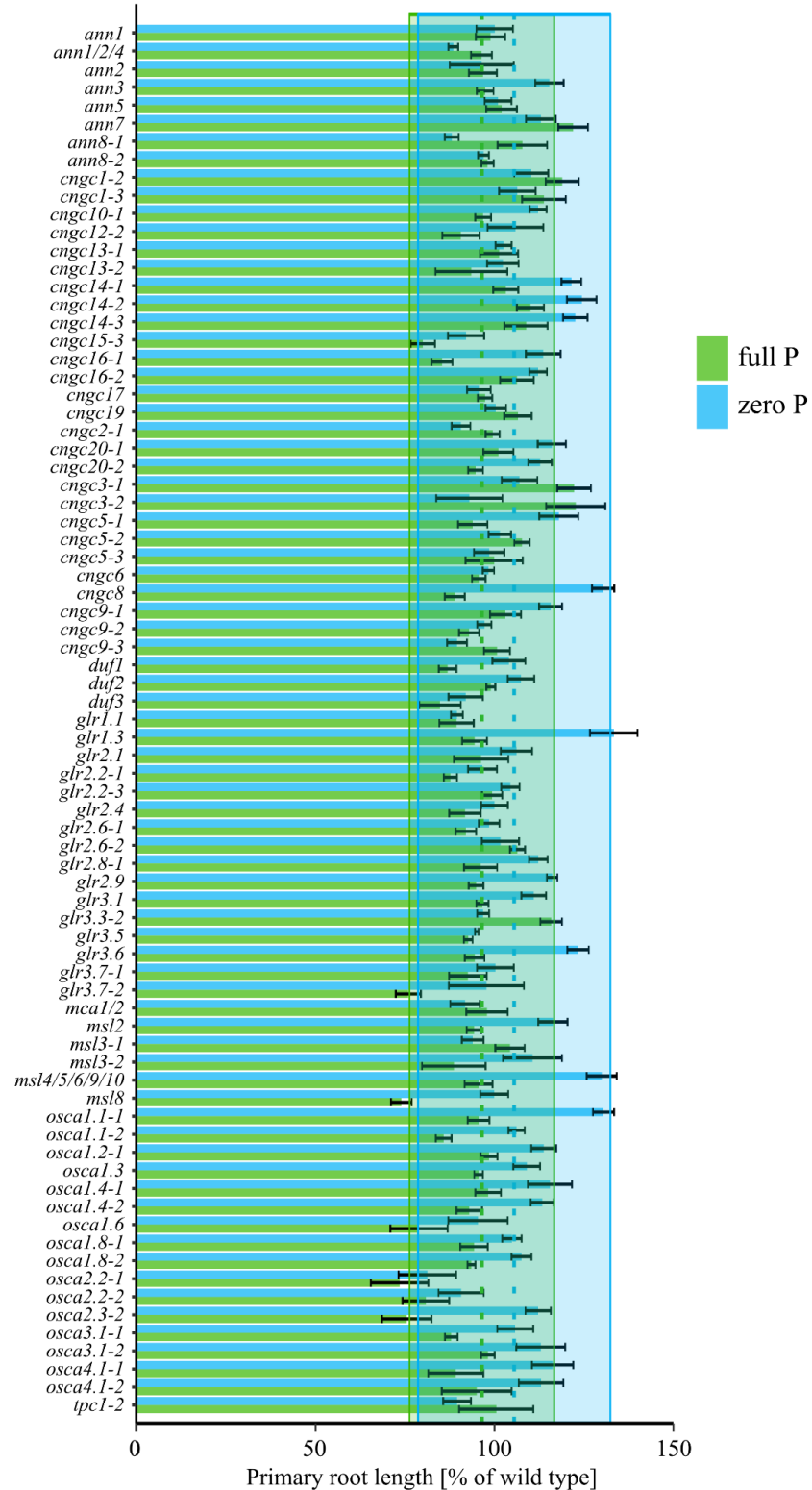


Distribution of primary root length of putative *Arabidopsis* Ca<sup>2+</sup> channel mutants. Lines were grown for six days on full P (green) or zero P (blue) growth medium, and primary root length was measured using the ImageJ NeuronJ plugin. Y-axis displays the absolute frequency of observations. (A) Histogram of primary root lengths in cm of individual roots of putative *Arabidopsis* Ca<sup>2+</sup> channel mutants, (B) and their paired wild type backgrounds. (C) Histogram of primary root lengths of putative mutants given as percent of growth compared to their respective wild type backgrounds. Data from 6 independent trials, with n = 532 / 527 (mutants grown on full / zero P, respectively) and 278 / 252 (wild types grown on full / zero P respectively).

Phosphate Starvation alters Calcium Signalling in Roots of *Arabidopsis thaliana*

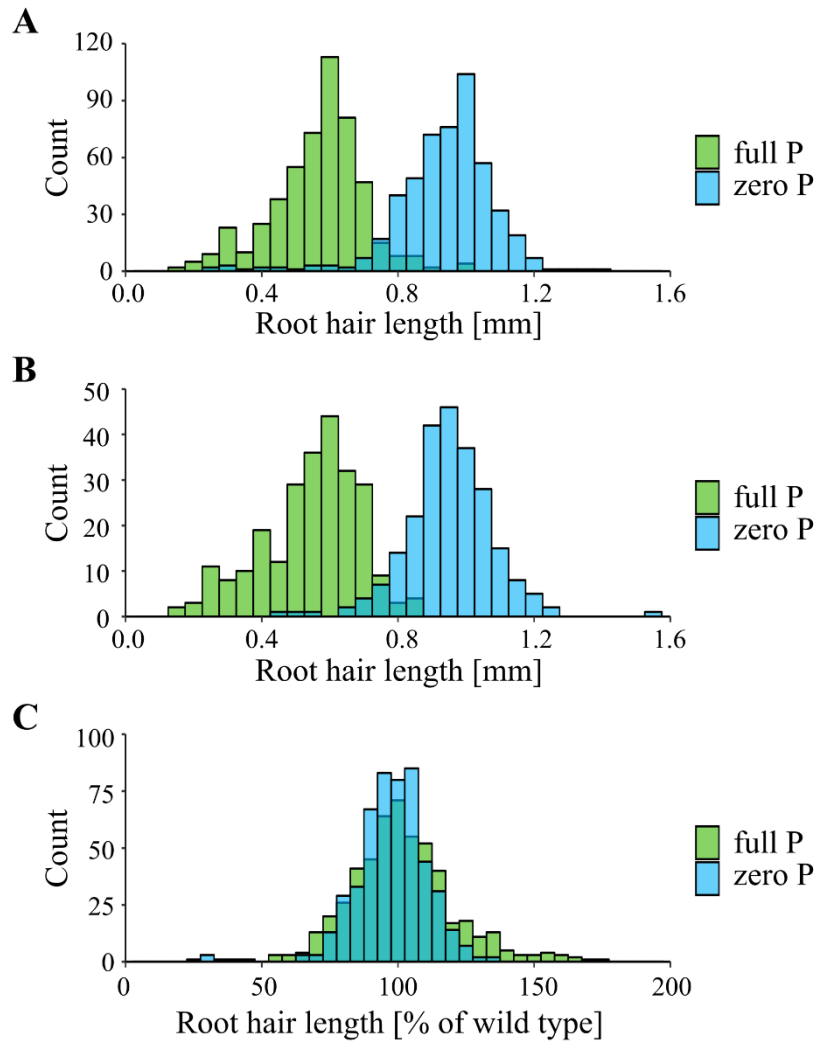


Primary root lengths of putative *Arabidopsis* Ca<sup>2+</sup> channel mutants. Lines were grown for six days on full P (green) or zero P (blue) growth medium, and primary root length was measured using the ImageJ NeuronJ plugin. Means of primary root length ( $\pm$  SEM, in cm) of 4 – 22 roots analysed per mutant per growth condition are shown, data from 6 independent trials. Each mutant line was grown with its respective paired wild type. Median primary root length of wild types across all experiments is shown as dashed line for full and zero P (green / blue respectively),  $\pm$  2.5 fold MAD (median absolute deviation, light green and blue boxes).

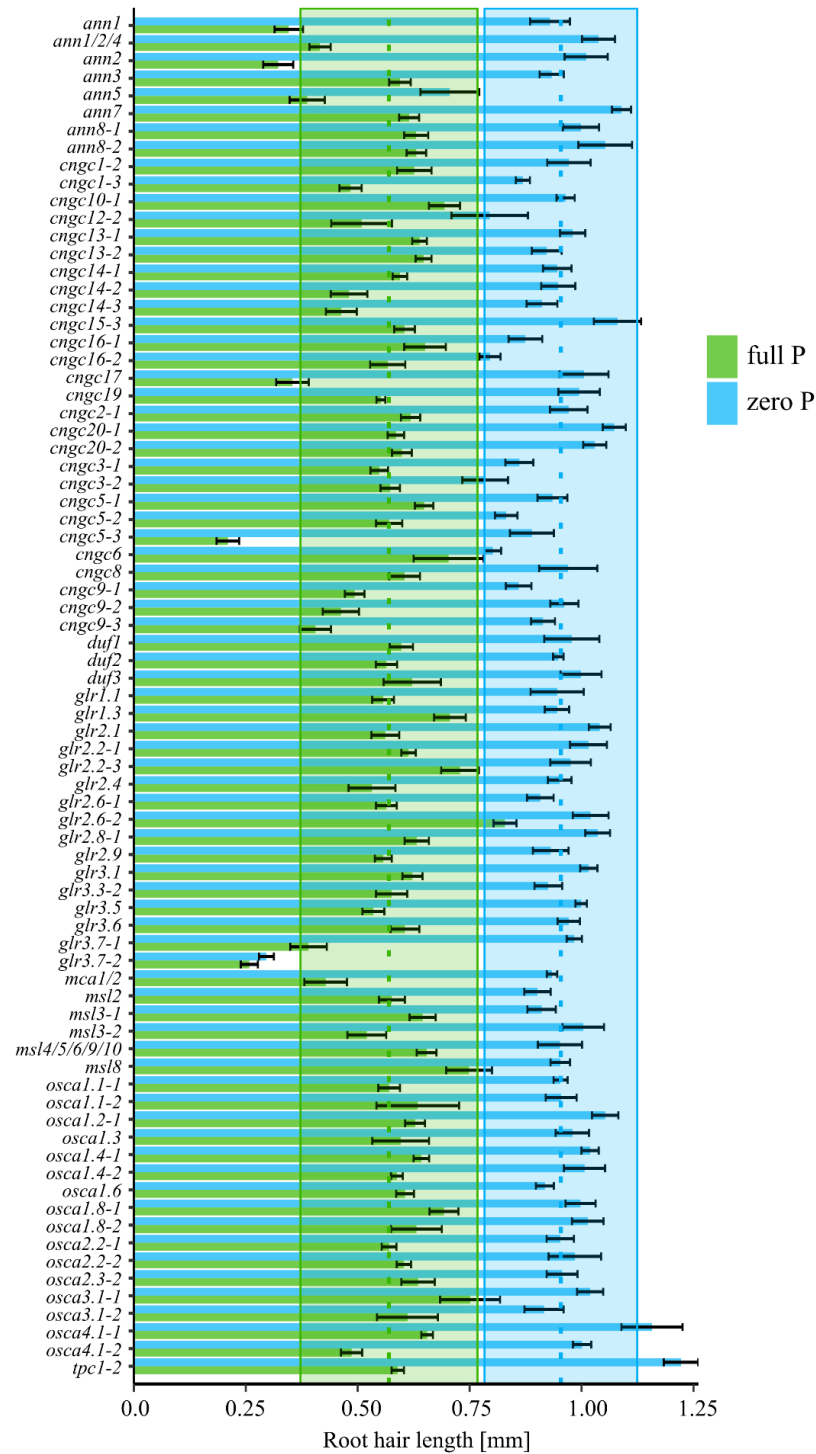


Primary root length of putative *Arabidopsis* Ca<sup>2+</sup> channel mutants as percent of paired wild type primary root length. Median primary root length of mutants across all experiments is shown as dashed line for full and zero P (green / blue respectively),  $\pm 2.5$  fold MAD (median absolute deviation, light green and blue boxes).

## APPENDIX V

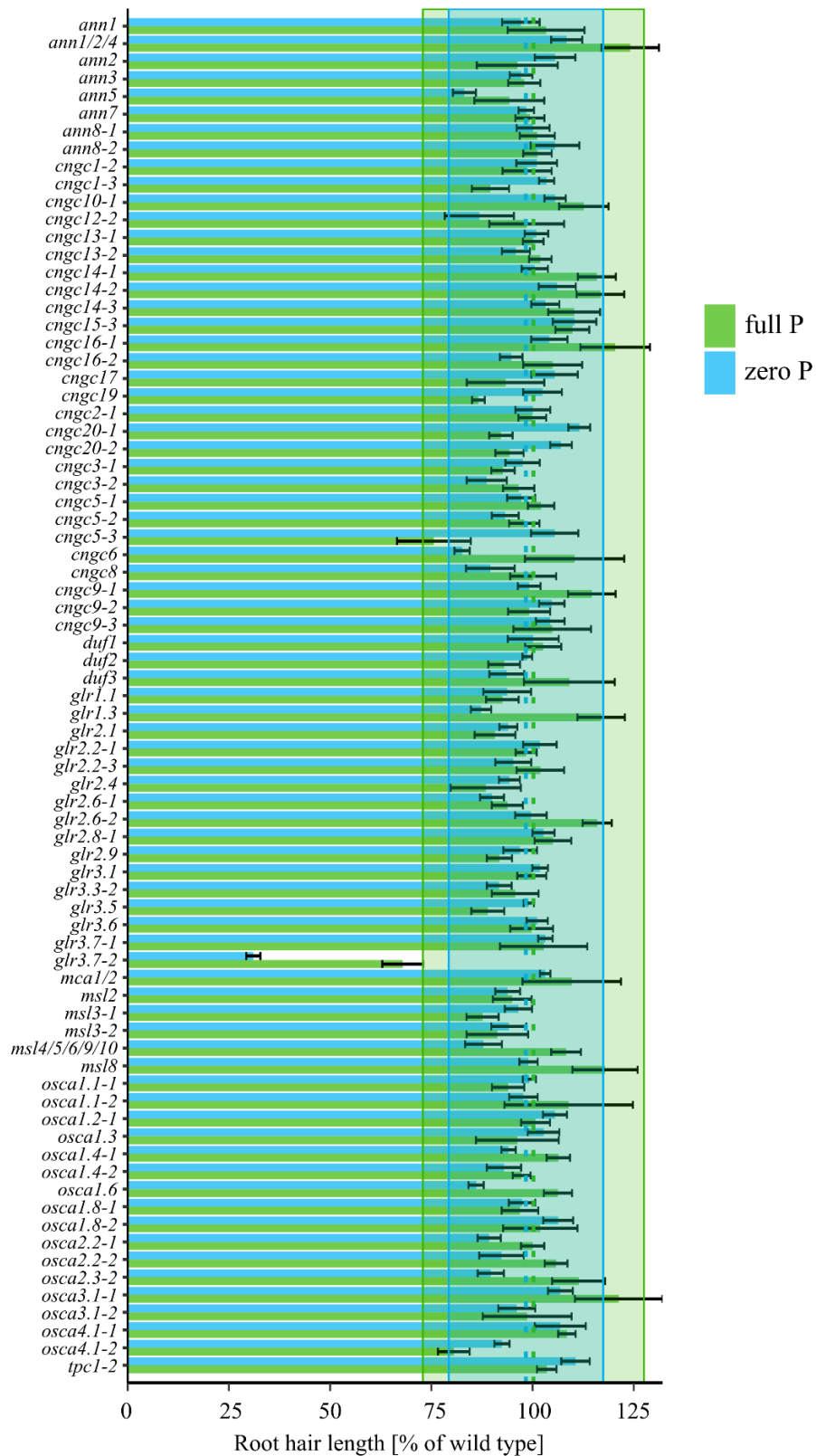


Distribution of measured root hair lengths of putative *Arabidopsis*  $\text{Ca}^{2+}$  channel mutants. Lines were grown for six days on full P (green) or zero P (blue) growth medium, and root hair lengths of the 10 longest root hairs (5 per side of the root) within a 1 mm segment, 4 – 5 mm from the root tip, were quantified and averaged. Y-axis displays the absolute frequency of observations. (A) Histogram of average root hair length in mm of individual roots of putative *Arabidopsis*  $\text{Ca}^{2+}$  channel mutants, (B) and their paired wild type backgrounds. (C) Histogram of root hair length averages of putative mutants given as percent of growth compared to their respective wild type backgrounds. Data from 6 independent trials, with  $n = 518 / 503$  (mutants grown on full / zero P, respectively) and  $251 / 236$  (wild types grown on full / zero P, respectively).



Root hair lengths of putative *Arabidopsis* Ca<sup>2+</sup> channel mutants. Lines were grown for six days on full P (green) or zero P (blue) growth medium, and root hair lengths of the 10 longest root hairs within a 1 mm segment, 4 – 5 mm from the root tip, were quantified using the ImageJ NeuronJ plugin. Shown are averages of 4 -22 analysed roots per mutant per growth condition, ± SEM, data from 6 independent trials. Each mutant line was grown with its respective paired wild type. Median root hair length of wild types across all experiments is shown as dashed line for full and zero P (green / blue, respectively), ± 2.5 fold MAD (median absolute deviation, light green and blue boxes).

Phosphate Starvation alters Calcium Signalling in Roots of *Arabidopsis thaliana*



Root hair lengths of putative *Arabidopsis*  $\text{Ca}^{2+}$  channel mutants as percent of paired wild type root hair lengths. Median root hair length of mutants across all experiments is shown as dashed line for full and zero P (green / blue, respectively),  $\pm 2.5$  fold MAD (median absolute deviation, light green and blue boxes).



## APPENDIX VI

[see attached CD]

**Movie 1** – Ratiometric false-colour movie from a representative time series of a P-replete Col-0 root expressing NES-YC3.6, response to 1 mM extracellular ATP. A 10-day old seedling was superfused with control solution before 1 mM eATP (in control solution background) was superfused at 3 minutes after start of image acquisition. Scale bar: 1 mm.

**Movie 2** - Ratiometric false-colour movie from a representative time series of a P-starved Col-0 root expressing NES-YC3.6, response to 1 mM extracellular ATP. A 10-day old seedling was superfused with control solution before 1 mM eATP (in control solution background) was superfused at 3 minutes after start of image acquisition. Scale bar: 1 mm.

**Movie 3** – Intensiometric false-colour movie from a representative time series of a P-replete Col-0 root expressing GCaMP3, response to application of control solution. The root tip of a 10-day old seedling was treated with control solution at 20 seconds after start of image acquisition. Scale bar: 1 mm.

**Movie 4** - Intensiometric false-colour movie from a representative time series of a P-replete Col-0 root expressing GCaMP3, response to application of 1 mM eATP treatment. The root tip of a 10-day old seedling was treated with 1 mM eATP (in control solution background) at 20 seconds after start of image acquisition. Scale bar: 1 mm.

**Movie 5** - Intensiometric false-colour movie from a representative time series of a P-starved Col-0 root expressing GCaMP3, response to application of control solution. The root tip of a 10-day old seedling was treated with control solution at 20 seconds after start of image acquisition. Scale bar: 1 mm.

**Movie 6** - Intensiometric false-colour movie from a representative time series of a P-starved Col-0 root expressing GCaMP3, response to application of 1 mM eATP treatment. The root tip of a 10-day old seedling was treated with 1 mM eATP (in control solution background) at 20 seconds after start of image acquisition. Scale bar: 1 mm.

**Movie 7** - Intensiometric false-colour movie from a representative time series of a P-replete Col-0 root expressing GCaMP3 with cut off apical root tip, response to application of 1 mM eATP treatment. The apical root tip (~ 0.8 mm) of a 10-day old seedling was cut off, and apical root tip and distal root stump were treated simultaneously with 1 mM eATP (in control solution background) at 20 seconds after start of image acquisition. Scale bar: 1 mm.